DEVELOPMENT OF A DEMOUNTABLE PRECAST CONCRETE FRAME BUILDING SYSTEM FOR SEISMIC REGIONS

A thesis submitted in partial fulfilment of the requirements for the degree of
Doctor of Philosophy in Civil Engineering

By

PAVAN KUMAR ANINTHANENI

Supervised by
Professor Rajesh Dhakal

Associate supervisors
John Marshall
Jitendra Bothara

DEPARTMENT OF CIVIL AND NATURAL RESOURCES ENGINEERING

UNIVERSITY OF CANTERBURY

CHRISTCHURCH, NEW ZEALAND

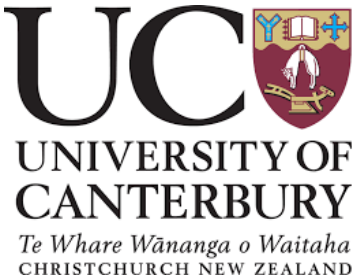

MARCH 2017

Dedicated to my parents

Kamala.A & Kodanda Naidu.A

Abstract

Present generation reinforced concrete (RC) and precast concrete buildings are mostly monolithic. As a result, these buildings have to be demolished when they are either obsolete in function or irreparably damaged in an earthquake shaking. Demolition leads to irrecoverable wastage of non-renewable building materials, which is against the philosophy of a sustainable building. The demolition process is environmentally unfriendly, requires careful planning to avoid any danger to nearby structures, and consumes a large amount of energy. Because of its monolithic nature, upgrading a concrete building to accommodate for any future changes is not easy. At the same time, a monolithic concrete building has a very limited structural flexibility (i.e. allowance to remove/replace existing building components or to add new building components). Because of this, a damaged monolithic concrete building which is in a repairable state requires considerable time and money to restore its full functionality. This induces substantial seismic losses contributed by direct repair cost, and more significantly by the downtime (i.e. occupancy interruption). In this research, a conceptual layout of a next generation seismically robust precast concrete frame building system which uses "dry" and removable steel connections is developed. The proposed demountable building system is structurally flexible as it allows repair/replacement of existing building components or addition of new building components.

Experimental investigation is carried out in this research to identify the most suitable "dry" connection configuration to join the precast concrete beams and columns in the proposed demountable building system. Structural performance of the tested frame sub-assemblies with three different connection configurations are evaluated by comparing the test results with analytically predicted responses and conclusions are drawn with respect to their structural performance. To investigate whether emulation of structural behaviour of a wet jointed/monolithic concrete frame system can be achieved with the use of precast concrete beams and columns connected by using the proposed "dry" connections, experimentally obtained hysteretic plots of the tested frame sub-assemblies are compared with the hysteresis behaviour of a "wet jointed" or "ductile connectors" precast concrete frame sub-assembly available in the literature. Also, the feasibility of demounting a damaged beam and replacing with a new beam of the same (or higher) capacity and achieving the same (or better) performance compared to the original sub-assembly is assessed through this test programme. Qualitative analyses are performed on the proposed connections, and based on the comparison the connection which is easy to erect and dismantle is identified.

Numerical macro models are developed to simulate the hysteretic behaviour of the tested frame sub-assemblies with the proposed "dry" connections. Numerically simulated results with different hysteresis rules and different input backbone curves are compared, and issues with the macro models in capturing strength degradation are highlighted. The accuracy of the simulated cyclic behaviour of the sub-assemblies is assessed by comparing with the experimental test results and conclusions are drawn with regard to the reliability of the macro models. To eliminate any possible damage to the ground storey columns and to avoid the need to replace the damaged columns, feasibility of pin base (instead of fixed base) columns for unbraced lateral load moment resisting frames is investigated. Different lateral load resisting frame options that render the proposed demountable building system a "low downtime" building system are then ranked in an increasing order of "structural flexibility".

A simple hand calculation method to estimate lateral stiffness and fundamental period of a frame building (braced or unbraced) with either fixed or pin bases is theoretically derived in this thesis. To verify the reliability of the developed equations, the estimated lateral stiffness and fundamental periods are compared with the corresponding values obtained from pushover and Eigenvalue analyses (and also Rayleigh method) for a wide range of low to medium rise buildings with varying cross-sectional and geometrical configurations. Suitability of the proposed equation for frames with linear variation of section properties along the building height and simple/pin beam-column connections is also scrutinized. Reliability of the developed equation to estimate the fundamental period is also verified using the experimental test and numerical analysis results available in the literature. Since the developed equations are found to closely predict the lateral stiffness and fundamental period of a frame building, they are recommended to be used in everyday design practice.

Keywords

Precast concrete, demountable; designed to dismantle; deconstruction; structurally flexible, dry connections, hand calculation method, simple equation, lateral stiffness, fundamental period, frame building

Deputy Vice-Chancellor's Office
Postgraduate Office

UNIVERSITY OF CANTERBURY
Te Whare Wānanga o Waitaha
CHRISTCHURCH NEW ZEALAND

Co-Authorship Form

This form is to accompany the submission of any thesis that contains research reported in co-authored work that has been published, accepted for publication, or submitted for publication. A copy of this form should be included for each co-authored work that is included in the thesis. Completed forms should be included at the front (after the thesis abstract) of each copy of the thesis submitted for examination and library deposit.

Please indicate the chapter/section/pages of this thesis that are extracted from co-authored work and provide details of the publication or submission from the extract comes:

Chapter 2:

Aninthaneni, P. K., and Dhakal, R. P. (2017). "Demountable precast concrete frame building system for seismic regions: conceptual development." Journal of Architectural Engineering (accepted).

Aninthaneni, P. K., and Dhakal, R. P. (2015). "Demountable Precast RC frame building system for seismic regions." International Conference on Earthquake Engineering and Seismology (IZIIS-50) Kiel, Germany.

Aninthaneni, P. K., and Dhakal, R. P. (2014). "Conceptual development: Low loss precast concrete frame building system with steel connections." NZSEE Conference Auckland, New Zealand, Paper No 44.

Chapter 4:

Aninthaneni, P. K., Dhakal, R. P., Marshall, J., and Bothara, J. (2016). "Experimental investigation of dry beam-column moment connections for demountable precast concrete RC frame buildings." New Zealand Society for Earthquake Engineering Annual Conference (NZSEE 2016) Christchurch, 10pp.

Chapter 5:

Aninthaneni, P. K., Dhakal, R. P., Marshall, J., and Bothara, J. (2017). "Seismic performance of beam-column sub-assemblies of a demountable precast concrete frame building." *16th World Conference on Earthquake Engineering, 16WCEE 2017* Santiago Chile, January 9th to 13th 2017.

Aninthaneni, P. K., Dhakal, R. P., Marshall, J., and Bothara, J. (2016). "Experimental investigation of dry beam-column moment connections for demountable precast concrete RC frame buildings." New Zealand Society for Earthquake Engineering Annual Conference (NZSEE 2016) Christchurch, 10pp.

Aninthaneni, P. K., Dhakal, R. P., Marshall, J., and Bothara, J. (2015). "Seismic performance of sub-assembly of a demountable precast concrete frame building" Tenth Pacific Conference on Earthquake Engineering: Building an Earthquake-Resilient Pacific Sydney, Australia, Paper 189.

Chapter 6:

Aninthaneni, P. K., Dhakal, R. P., and Marshall, J. (2014). "Feasibility of pinned-base connections for demountable precast frame building systems." 23rd Australasian Conference on Mechanics of Structures and Materials (ACMSM 23) Byron Bay, Australia, 9-12 Dec 2015.

Chapter 7:

Aninthaneni, P. K., and Dhakal, R. P. (2016). "Prediction of fundamental period of regular frame buildings." Bulletin of the New Zealand Society for Earthquake Engineering, 49(2).

Chapter 8:

Aninthaneni, P. K., and Dhakal, R. P. (2017). "Prediction of lateral stiffness and fundamental period of concentrically braced frame buildings." Bulletin of Earthquake Engineering, 1-30, DOI 10.1007/s10518-016-0081-7

Please detail the nature and extent (%) of contribution by the candidate:
The candidate did all the work (100%) under our supervision.

Certification by Co-authors:

If there is more than one co-author then a single co-author can sign on behalf of all
The undersigned certifys that:

- The above statement correctly reflects the nature and extent of the PhD candidate's contribution to this co-authored work
- In cases where the candidate was the lead author of the co-authored work he or she wrote the text

Name: *Rajesh Dhakal* Signature:  Date: 30/03/2017

Acknowledgments

This research would not have been possible without the help, technical guidance and support of Prof. Rajesh Dhakal, who is the principal supervisor. I am grateful to him for his advice at critical times and teaching me how to really write a technical paper. I am also thankful to Prof. Dhakal for setting an example; how to invent different ways of enjoying life. He helped in many technical aspects to flourish my mind into what is required to become an independent researcher. Completion of this research would have not been possible without the financial support provided by the University of Canterbury and other project funds provided by Prof. Dhakal.

I am deeply grateful to Mr. John Marshall, who is one of the associate supervisors for this research for his time and valuable feedback. His advice on the practical aspects of the research are really helpful. I am also grateful to him for his help in supporting me to obtain financial support from Precast NZ and allowing me to fabricate the specimens at the Stalhton precast yard (where he was Design Manager). Another associate supervisor for this research is Mr. Jitendra Bothara, I am extremely thankful to him for his feedback at various stages of this research. The technical discussions with him were extremely useful in improving the analytical models. This project would not have been completed on time without the help of Mr. Alan Thrilwell, who is the main technician, I am very thankful for his time, technical advice and on the spot decisions. Special thanks to Mosese Fifita, who helped me to get things done before the start of the project. I am also grateful to David MacPherson, Gavin Keats, John Maley, Peter Coursey, Stuart Toase, and Russell McConchie for their support and advice at different stages of the project.

I am indebted to my Christchurch family; Tushar, Rachana, and Neel for their unconditional love and support at difficult times. The time I spent with Neel is the definitely the most happy time during my stay in Christchurch. I am also indebted to all E321 roommates for their support and friendship which made my life memorable; Tushar Chaudhari, Helmy Tjahjanto, Mayank Tripathi, and Saul Colunga. I am also thankful to other fellow postgraduate friends for sharing and discussing many technical and non-technical stuff; Reza Sedgh, Farhad Dashti, Sandip Saha (former post-doc fellow), Royce Liu, Robin Xie, Atefeh Pourali, Salina Poudyal, and many others.

I would not have come this long way without the support of Prof. Ravi Sinha and Prof. C. Shashidhar, who are former supervisors, I am extremely lucky to have such wonderful persons in my life. Finally, I wish to express my deepest gratitude to my family. To my parents Kamala and Kodanda Naidu; and my sister Saritha for all their love, understanding and encouragement during this research.

List of publications

The following papers have been published based on some of the work reported in this thesis.

Journals

1. Aninthaneni, P. K., and Dhakal, R. P. (2017). "Prediction of lateral stiffness and fundamental period of concentrically braced frame buildings." Bulletin of Earthquake Engineering, 1-30, DOI 10.1007/s10518-016-0081-7.
2. Aninthaneni, P. K., and Dhakal, R. P. (2017). "Demountable precast concrete frame building system for seismic regions: conceptual development." Journal of Architectural Engineering (accepted).
3. Aninthaneni, P. K., and Dhakal, R. P. (2016). "Prediction of fundamental period of regular frame buildings." Bulletin of the New Zealand Society for Earthquake Engineering, 49(2).

Conference proceedings

1. Aninthaneni, P. K., Dhakal, R. P., Marshall, J., and Bothara, J. (2017). "Seismic performance of beam-column sub-assemblies of a demountable precast concrete frame building." *16th World Conference on Earthquake, 16WCEE 2017 Santiago* Chile, January 9th to 13th 2017.
2. Aninthaneni, P. K., Dhakal, R. P., Marshall, J., and Bothara, J. (2016). "Experimental investigation of dry beam-column moment connections for demountable precast concrete RC frame buildings." New Zealand Society for Earthquake Engineering Annual Conference (NZSEE 2016) Christchurch, 10pp.
3. Aninthaneni, P. K., Dhakal, R. P., Marshall, J., and Bothara, J. (2015). "Seismic performance of sub-assembly of a demountable precast concrete frame building" Tenth Pacific Conference on Earthquake Engineering: Building an Earthquake-Resilient Pacific Sydney, Australia, Paper 189.
4. Aninthaneni, P. K., and Dhakal, R. P. (2015). "Demountable Precast RC frame building system for seismic regions." International Conference on Earthquake Engineering and Seismology (IZIIS-50) Kiel, Germany.
5. Aninthaneni, P. K., Dhakal, R. P., and Marshall, J. (2014). "Feasibility of pinned-base connections for demountable precast frame building systems." 23rd Australasian Conference on Mechanics of Structures and Materials (ACMSM23) Byron Bay, Australia, 9-12 Dec 2015.
6. Aninthaneni, P. K., and Dhakal, R. P. (2014). "Conceptual development: Low loss precast concrete frame building system with steel connections." NZSEE Conference Auckland, New Zealand, Paper No 44.

Table of Contents

Table of Appendices

Chapter 1: Introduction

1.1 Introduction and literature review

1.1.1 *Background*

Present generation buildings are planned, designed and built without any consideration to deconstruction; as a result, most buildings need to be demolished either at the end of their life span or when a building is obsolete in function. Also, buildings in seismic regions that have suffered irreparable damage after an earthquake have to be demolished well before the end of their intended/designed life span. The demolition process of a building is environmentally unfriendly, requires careful planning to avoid any danger to people and nearby structures, and causes extensive wastage of non-renewable building materials [1]. In the European Union, the total production of Construction and Demolition Waste (CDW) is about 180 million tonnes per year [2]. CDW amounts to 17% (this percentage will be more after incorporating the demolition data following the 2010 and 2011 Canterbury earthquakes) and 40% of total landfill waste in New Zealand and Australia respectively [3, 4]. Concrete buildings are a major contributor to CDW as they represent the majority of the multi-storey building environment in many countries. Also, demolition of concrete buildings requires enormous amount of energy; demolition of one tonne of concrete from a building requires 275 MJ of energy and crushing of one tonne of concrete requires 85 MJ of energy, which means to demolish a six storey building with plan area of 400 m^2 requires approximately $1/75^{th}$ of the energy of fat man atomic bomb [1].

The challenges and complications pertinent to concrete building construction process has significantly eased with the advent of prefabricated/precast concrete building components when compared to cast-in-situ concrete construction methods. Nevertheless, precast concrete building construction still involves a lot of site intensive activities [5]. Also, precast concrete building construction is comparatively a more sustainable building technology and it has a much reduced carbon emission when compared to cast-in-situ concrete building construction [6, 7]. The main attributes of sustainable design and construction are less energy consumption and usage of materials, reuse of components, and reduction and recycling the waste materials. It is recognized that the prefabrication of concrete building components results in the reduction of wastage of building materials during the construction phase, but produces larger amount of waste during demolition [8]. To minimize the wastage of building materials,

design and construction techniques should incorporate a "*closed-loop*" building material strategy, which basically means re-use of the building components rather than disposal [9].

1.1.2 *Precast concrete frame building systems*

Precast concrete frame buildings designed and built to resist lateral seismic forces can be classified into two broad categories such as; "equivalent monolithic" and "jointed" systems [10]. Also, these buildings can be categorized based on the construction technique adopted in connecting the building components as; (i) "wet" jointed system, (ii) "dry" jointed system, and (iii) "partial dry" jointed system. The difference between these systems lies in the type of connections/joints between the precast concrete components/elements and inertial load transfer mechanism from floor slabs to the foundations. Structural dynamic properties and expected seismic performance of these systems are quite different. Generally, "equivalent monolithic" frame systems are achieved either using wet/cast-in-situ joints or bonded pre-stressed tendons between the precast concrete components [10, 11]. A ''wet joint" to connect the precast concrete elements uses cast-in-place concrete or grout to fill the splicing closures, and the location of the splicing can be either at the beam column junctions or mid span of the beam. Precast concrete frame buildings with wet connections will then comply with design requirements applicable to monolithic concrete frame buildings. Also, the performance of these buildings in a design basis earthquake will be similar to monolithic concrete frame buildings. In New Zealand and Japan many precast concrete frame buildings with "wet joints" have been built in last three decades [10, 12, 13].

Four ways of achieving an equivalent monolithic frame system behaviour with the use of the precast concrete elements connected by "wet joints" are shown in Figure 1.1. In System-1 [10, 14], the beams are placed between the columns and seated onto cover concrete of the cast-in-place or precast concrete columns as shown in Figure 1.1a. Precast concrete floor slabs are seated on the top of the beams and reinforcement is placed on top of the beams and over the floor slabs. Thereafter, cast-in-situ concrete is poured into the beam-column joints and over the precast concrete floor slabs to form a diaphragm topping slab. In System-2 [14], beams are passed on top of the bottom storey columns and connected at mid span using wet joints as shown in Figure 1.1b. The protruding rebars of the bottom storey columns are passed through the beams and inserted into the ducts of the upper storey columns and grouted. In System-3 [12, 14], T–shaped or cruciform precast concrete elements as shown in Figure 1.1c are fabricated. Joints between precast concrete columns and beams for this system are identical to those employed for System-2. In System-4 [13], pre-tensioned precast concrete beam shell (i.e. U-shaped) units are used as permanent formwork for the cast-in-situ

beams as shown in Figure 1.1d. The precast concrete shell beams act compositely with the cast-in-situ beams when subjected to loading. It is important to note that U beams are not connected to the cast-in-place beams by the reinforcement, and the composite action comes from the bond between the roughened inner surface of the precast concrete U shaped beam and the cast-in-place concrete [13].

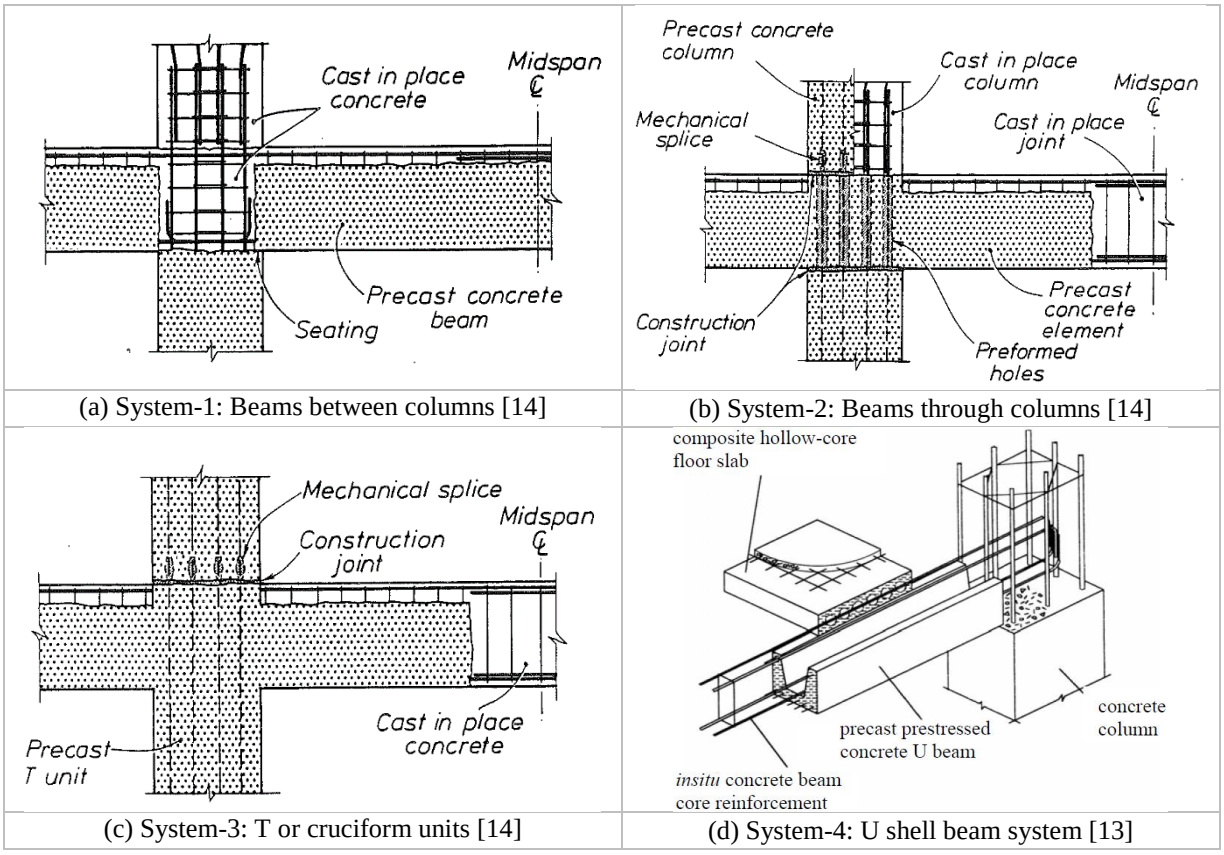

(a) System-1: Beams between columns [14]

(b) System-2: Beams through columns [14]

(c) System-3: T or cruciform units [14]

(d) System-4: U shell beam system [13]

Figure 1.1. Equivalent monolithic precast concrete frame systems with use of wet joints

Precast concrete frame systems developed using bonded pre-stressed tendons can also emulate the behaviour of the monolithic concrete frame system, and the two systems which are in practice are shown in Figure 1.2. These systems come under the "partial dry" jointed category [12]. In System-1, precast concrete beams are supported over temporary supports and tendons are passed through ducts as shown in Figure 1.2a. Gaps between the beam ends and the column faces and the ducts are grouted followed by post-tensioning of the tendons. System-2 is very similar to System-1 except that there is no need of temporary supports as the precast concrete beams permanently sits on the column corbels as shown in Figure 1.2b. In these systems, plastic hinges develop at beam-column interfaces due to yielding of the tendons. It has been reported these systems have less energy dissipation but still their behaviour is close to monolithic concrete frame systems. System-1 can be designed as a fully ductile moment resisting frame, whereas System-2 has to be designed as a nominal elastic frame system because of the complex shear interaction at higher drift levels [10].

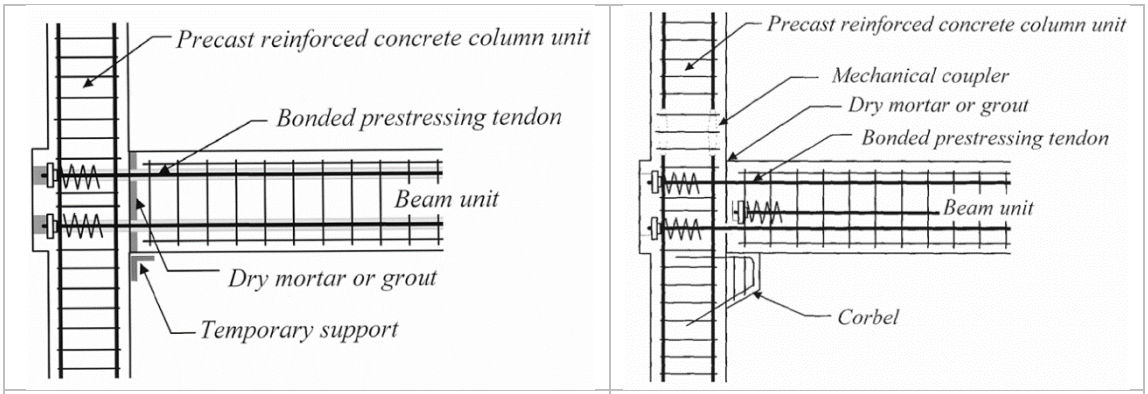

(a) System-1: Beams between columns | (a) System-2: Beams supported on corbels

Figure 1.2. Equivalent monolithic precast frame systems with use of bonded pre-stressed tendons [10]

In jointed frame building systems, the precast concrete beams and columns are connected either by using un-bonded post-tensioned tendons or steel connections made out of components such as steel billets, steel plates, steel angles and dowels or threaded rods, and come under "partial dry" category due to a mix of dry and wet joints [15-20]. The jointed frame building system with post-tensioned tendons shown in Figure 1.3a (also called as pre-stressed structural system (PRESSS), rocking frame system, low damage system, and damage avoidance design (DAD) system) do not emulate the structural behaviour of a monolithic concrete frame building system, but the overall structural system behaviour is ductile [20-22]. The post-tensioned tendons connecting the precast concrete beams and columns are either straight or draped along the beam. As there is no monolithic connection between the beams and the columns, the shear force is transferred from the beams to the columns through concrete corbels or shear keys or friction and dowel action. Due to the gap opening between the frame components under the lateral load, this frame system exhibits low damage (mostly concentrated to the beam edges) compared to a monolithic concrete frame system. The damage to the beam edges due to concentrated contact forces between the beam ends and column faces is further minimized by providing steel armouring [23, 24]. Also, this jointed frame system offers the distinct advantage of self-centering with minimal residual deformation after removal of the lateral load, this is due to the post-tensioned tendons which are in elastic state enforce the building system to return to its initial position [20, 21].

As the jointed frame system with only post-tensioned tendons possess negligible hysteretic energy dissipation characteristics. Therefore, additional internal or external devices are required to provide the damping to the overall building system. The jointed frame system with the post-tensioned tendons and the damping devices is called as a hybrid jointed frame system. The internal damping devices are made up of mild steel rebars connecting the beams and the columns as shown in Figure 3a, which are designed to yield after certain drift level

and provide the required damping to the system. The disadvantage with the internal damping device is that they cannot be replaced once they are yielded. Therefore, to facilitate the addition or removal, many variants of external damping devices have been developed and implemented; (i) hysteretic damping devices (mild steel rods), (ii) frictional damping devices, (iii) viscous damping devices, and (iv) coil spring damping devices [10, 25, 26]. The damage avoidance design philosophy is also applied to the bridges by post-tensioning the piers and armouring the pier ends [27]. The limitations of the jointed frame systems developed using post-tensioned tendons are; (i) it requires additional devices to provide damping to the building, (ii) not structurally adaptable as it is not possible to replace the damaged frame components due to global pre-stressed tendons, (iii) because of the cast-in-situ diaphragm floor slabs it is not possible/easy to dismantle all building components, and (iv) non-emulative frame systems as it is not possible to replicate structural behaviour (in every aspect) of the monolithic concrete frame system due to different load transfer mechanism.

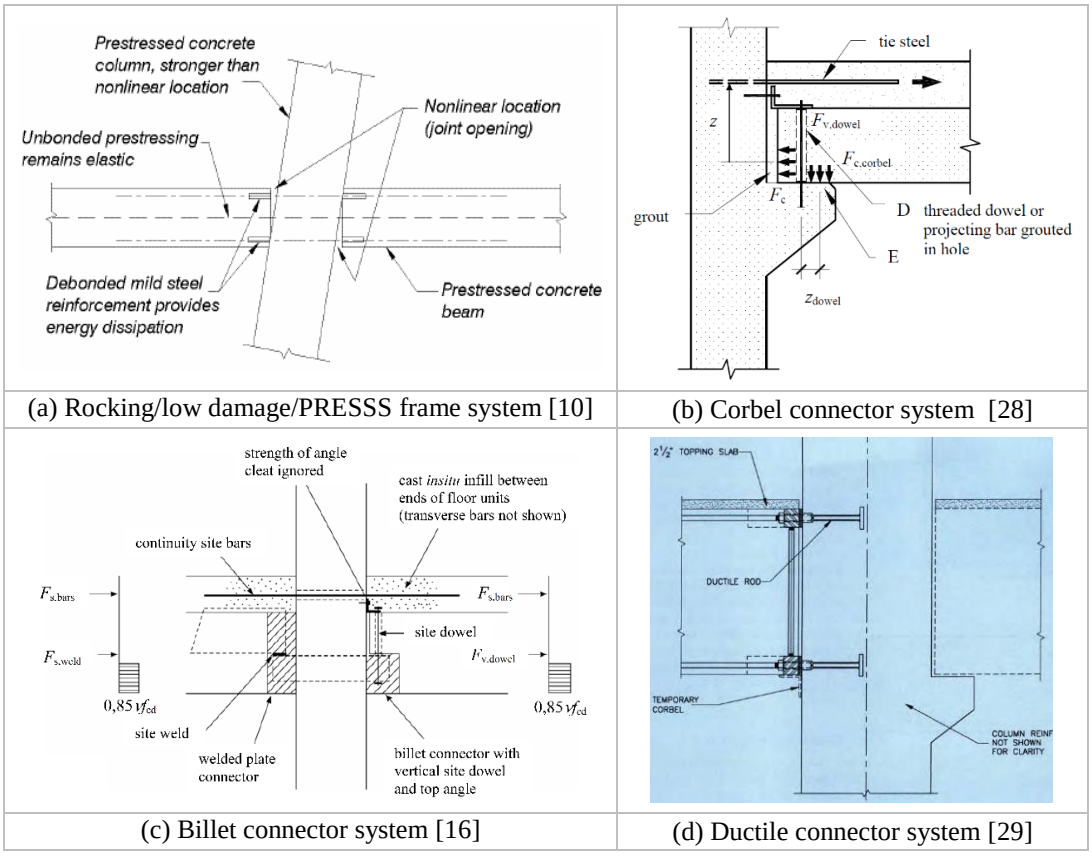

(a) Rocking/low damage/PRESSS frame system [10]

(b) Corbel connector system [28]

(c) Billet connector system [16]

(d) Ductile connector system [29]

Figure 1.3. Jointed precast frame systems with use of un-bonded tendons or steel connections

As mentioned before, another class of jointed frame building systems is developed by connecting precast concrete elements using steel connections. In the past three decades, researchers have developed many steel connection configurations and most of them rely on dowel action for the force transfer between beams and columns, and it has been reported that the most of these connection configurations can be considered as semi-rigid or nominal pin

connections [15, 16, 18, 28, 30, 31]. Schematic representations of a concrete corbel connection using steel angle and dowels, and a steel connection using a steel billet and dowels or welded plate are shown in Figures 1.3b and 1.3c, respectively. To the author knowledge, frame building systems with the existing steel connection configurations alone will not emulate the behaviour of monolithic concrete frame buildings, hence they need to rely on other lateral load resisting options such as braces or shear walls [10, 12, 28]. As it can be seen from Figures 1.3b and 1.3c, these connections require concreting or grouting to fill the ducts and gaps, thereby turning the connection into monolithic form and eliminating any possibility of easy removal of the connections. There is another category of jointed frame building systems in which the precast concrete elements are connected using "ductile connectors", which is shown in Figure 1.3d. The cyclic behaviour of the precast concrete frame with this connection is characterized by severe pinching hysteresis with less energy dissipation, and this system has a poorer seismic performance compared to the monolithic concrete frame system [29].

Based on the literature available and previous discussions, the easiest way to achieve an equivalent monolithic system in precast concrete frame buildings is by connecting the building components using "wet joints". Because of the "wet joints", the inherent advantages of precast concrete building construction in-terms of construction speed are limited; mainly because of the requirement and setting up of formwork and the curing time required before erecting other precast concrete elements. Also, the building structural system with wet/existing steel connections turns into either fully or partially monolithic in form, requiring these buildings to be demolished either at the end of the building's life span or when it is decided to construct a new building at the site or the building has suffered irreparable damage after an earthquake or for any other reasons. The environmental and sustainability issues associated with the demolition of a concrete building have already been highlighted. Because of the monolithic form of conventional precast concrete buildings, when these buildings are in a reparable damage state after an earthquake, they require considerable downtime to repair in addition to the repair cost to restore their functionality. These buildings require more time to bring back the damaged building to the usable state because of the; (i) decision taking time to decide whether the components are structurally damaged or not, (ii) time required to identify an appropriate strengthening/retrofit technique for that building, (iii) time required to re-design and review the retrofitted building, (iv) time required to develop a specific execution plan to implement the identified strengthening technique, and (v) project execution time which involves ordering materials, scaffolding, removing facades and partitions, installation of the retrofit specimens, and many other case specific activities. This will induce

substantial seismic losses contributed by the direct repair cost, and more significantly by the downtime (i.e. occupancy interruption) [32-34]. The issues with a precast concrete frame building with "wet or existing steel joints" can be summarized as; (i) to a certain extent construction speed is limited, (ii) the building needs to be demolished and cannot be deconstructed and reused, and (iii) damaged building components in an earthquake cannot be quickly repaired/replaced. These issues in precast concrete frame buildings in seismic regions can be addressed by incorporating the philosophy of the "Next Generation Building" system into the design and construction process.

1.1.3 *Next-generation/demountable concrete building systems*

1.1.1.1 Philosophy and definition of NGB systems

The concept of next generation building (NGB) systems emerged with the primary objective of achieving "sustainable buildings". The basic philosophy of the NGB system is to build buildings in shorter time and in a flexible manner so that they can cater for the changes in functionality, and be dismantled and reused rather than demolished. The definition of different components, design criteria, and construction techniques of the NGB system are listed in Table 1.1. NGB systems in different parts of the world are identified by different names as; industrialized, flexible, and demountable (IFD) system, design for deconstruction or disassembly (DfD), industrialized building system (IBS), and open building (OB) system [5, 35-39]. The difference between these building systems lies in the extent of covering different aspects of the NGB system requirements defined in Table 1.1. There is a major gap in the definition of flexibility of existing NGB systems. The functional flexibility of the building is explicitly defined and addressed, whereas structural flexibility/adaptability is not identified as a requirement. For completeness, the definition of structural adaptability has been added to the specifications of the NGB system reported in Table 1.1.

Table 1.1. Definitions of different components of the Next Generation Building (NGB) system

NGB system requirements		**Definition**	**Ref**
Industrialized		Standard building components of high quality and durability are mass produced in a controlled environment and transported to the site.	[5, 8]
Flexible/ Adaptable/ Open	*Functional*	Buildings are built to adapt to future functional changes by using interchangeable non-structural elements (i.e. partitions and facades).	[5, 40-42]
	Structural	Building structural layout is flexible/changeable to cater for the change in the loads in the future. Also, in seismic regions structural layout allows replacement of damaged building components with new ones or addition of new components to the original building system.	
Demountable/ Dismantle/Deconstruction		Building components can be dismantled without major damage and can be reused.	[5, 43]
Design criteria/ Construction techniques		Design should clearly define the process of erection and dismantling of building components upfront before construction. On site construction involves only erection and assembly of the building components.	[44, 45]

1.1.1.2 Development and implementation of NGB systems

The discussion on development and implementation of existing NGB systems is limited to concrete buildings in this thesis. Few concrete buildings have been constructed in the world by utilizing some of the concepts of NGB system. The very few efforts available in literature deal with gravity loaded building systems, mostly in non-seismic regions [43, 46, 47]. When it comes to removable and interchangeable non-structural elements (i.e. internal partition walls and external facades), many configurations have been developed and implemented to facilitate "functional flexibility" even in non-demountable buildings [48-50].

By utilizing the concept of IFD, five demountable concrete building systems were developed and implemented in Netherlands, namely; MXB-5, SMT, CD-20, Bestcon-30, and Moducon-2000 [2, 35, 46]. All these building systems consist of prefabricated building components like slabs, columns, and walls; the only difference among them is the connection configurations. In MXB-5 system, columns are embedded with steel plates on both ends and floor slab units are cast with steel ducts (on each corner) as shown in Figure 1.4a. The columns and the floor slabs are connected by using bolts, and the on-site assembly process of the building components can be identified from Figure 1.4a. In case of SMT system, upper and lower ends of the column are cast with steel fitting pieces into which dowels are inserted through the slotted holes of the floor slabs (on each corner) and finally the holes are grouted, the schematic view of the connection and construction process of the SMT system is shown in Figure 1.4b. The CD-20 system shown in Figure 1.5 consists of the columns embedded with dowels/pins on both sides and floor slabs are armoured on corners with slotted holes. The on-site assembly process of the building components of the CD-20 system is very much similar to that of the SMT system.

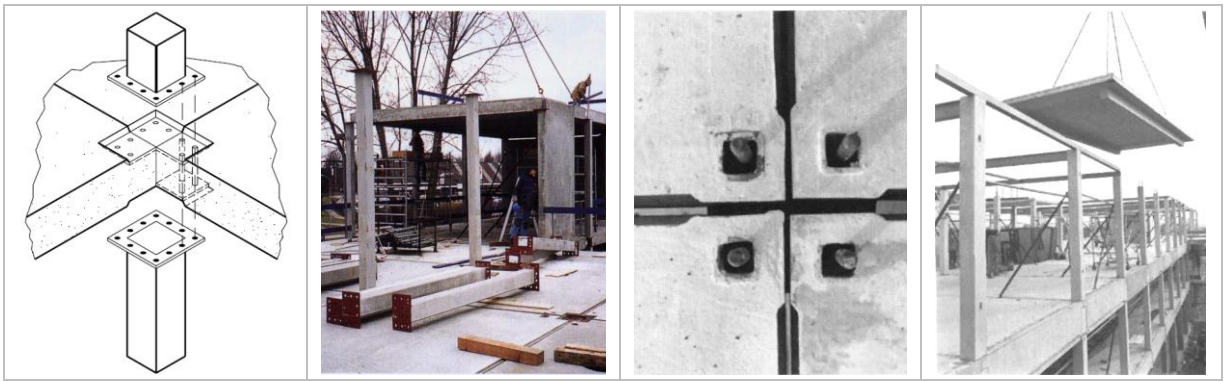

(a) Connections and onsite assembly of the MXB-5 | (b) Connections and onsite assembly of the SMT

Figure 1.4. Connections of the MXB-5 and SMT system and on-site assembly process [1, 28]

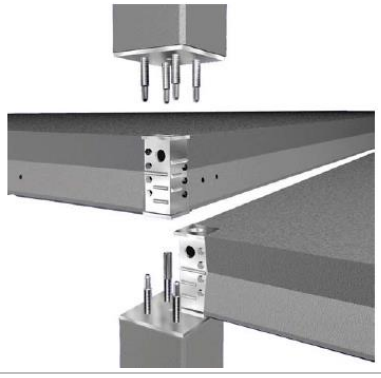

(a) Schematic view of the connection

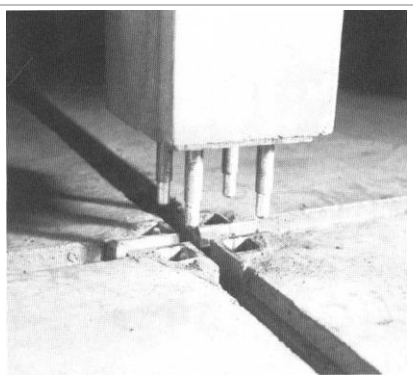

(b) Actual view of the connection

(c) CD-20 building

Figure 1.5. Connections of the CD-20 system and on-site assembly process [1, 28]

In the Bestcon-30 system, four threaded rods on the upper end of the columns are inserted into steel ducts located on the corners of the floor slabs, and the bottom storey column is connected to the upper storey column through massive steel cylinder to form the connection shown in Figure 1.6. At first, the building components are assembled and then the connections are sealed with non-shrink mortar/grout. In the case of Moducon-2000 system, four embedded rods on the upper end of the bottom storey column pass through the openings in the floor slabs and fitted into the four ducts on the lower end of the upper storey column and the openings are grouted to form the structural connection as shown in Figure 1.7. The Moducon-2000 system is very much similar to the Bestcon-30 system except that the steel cylinder is not provided.

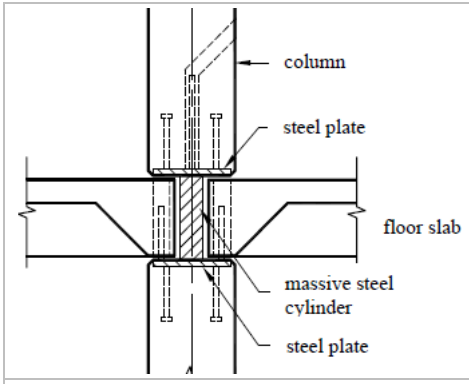

(a) Schematic view of the connection

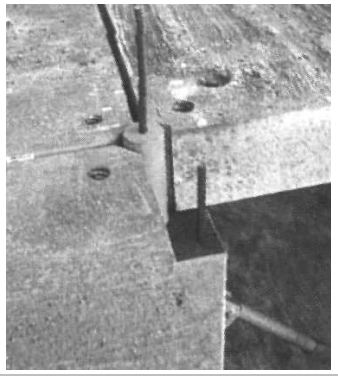

(b) Actual view

(c) Bestcon-30 building

Figure 1.6. Connections of the Bestcon-30 system and on-site assembly process [1, 28]

In Japan, by using the concept of the “open building” system, the “NOHS” housing project with a flexible floor plan, replaceable non-structural components and a long life of 200 years was developed and implemented, and the “NEXT21” housing project was implemented as a highly functional flexible building system [38, 51, 52]. The “NOHS” housing project comes under the category of jointed frame building system with use of un-bonded post-tensioned tendons. The pre-stressed columns and beams, and the actual “NOHS” housing project during construction are shown in Figure 1.8. It is important to note that the “NOHS” building is not

a pure rocking frame because the building is base isolated, and the "NEXT21" is not a demountable building but it is a highly functional flexible building with movable partitions and many other green building features.

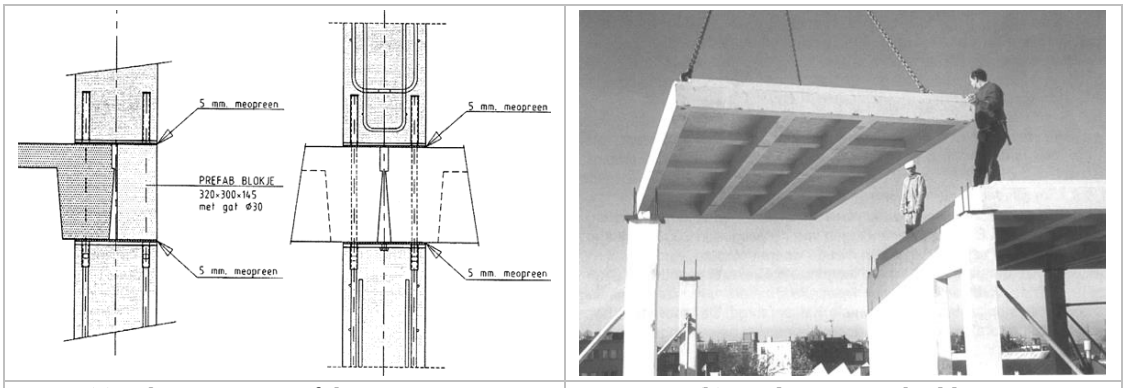

(a) Schematic view of the connection (b) Moducon-2000 building

Figure 1.7. Connections of the Moducon-2000 system and on-site assembly process [1, 28]

(a) Post-tensioned column (b) Post-tensioned beam (c) NOHS during construction

Figure 1.8. Connections of "NOHS" housing project and building during construction [52]

In New Zealand, concept of deconstruction of a building is very much in its infancy and education and research is needed to develop the concept and awareness of benefits [54]. Nevertheless, a few partially demountable car park buildings (i.e. some components of the building need to be demolished) have been designed and built [53, 55]. The structural frame system of one of the car park building is developed by placing the precast concrete spandrels into the rebates of the slender columns and welding the steel plates of the spandrels and columns as shown in Figure 1.9a. The precast concrete T-floor slabs are connected to the spandrels using bolts, and the connections between the floor slabs are knob and plate connections. Steel braces are also added to the frame system to resist the lateral loads as shown in Figure 1.9b. The connections of this building are patented and this is one of the reasons for not extensive use of this kind of building in practice.

(a) Spandrels to slender column connections

(b) Actual building during construction

Figure 1.9. Car parking building using spandrels and slender columns at Auckland Airport [53]

Another car parking building uses cast-in-situ L-shaped shear walls on all corners of the building and an internal precast concrete gravity frame system. The layout of the building is shown in Figure 1.10a. The internal gravity frame system consists of precast concrete columns with corbels to support the precast concrete beams. The flanges of T-floor slab are connected to the precast beam using the embedded bolts as shown in the Figure 1.10b. The internal beam-column connections were made by welding the steel plate at the bottom of the beam to the steel plate on top of the corbel which can be cut at the time of deconstruction. The floor slabs are welded to L-shaped walls for transfer of diaphragm forces as shown in Figure 1.10c. It was estimated that recovery of the structural components will be in the order of 85% of the total [3]. It was shown with this project that it is feasible to design a building for deconstruction in a seismic region without significant increase in cost.

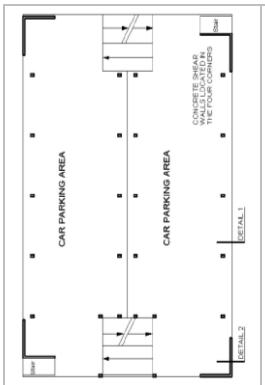

(a) Layout of plan

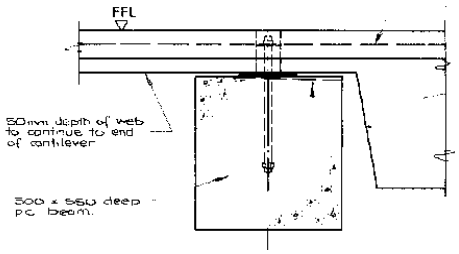

(b) Floor to beam connection

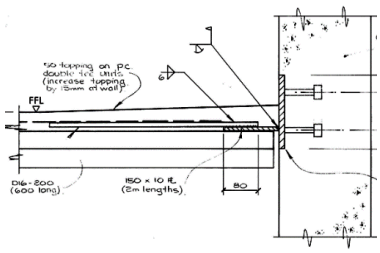

(c) Floor to wall connection

Figure 1.10. Layout of ANZAC car parking building, floor to slab, and floor to wall connections [3]

Recently, four point bending tests were conducted on a partially demountable steel end plate connection (which involves breaking of the grout through embedded anchors and cutting of bolts) between the protruded corbel of the precast concrete column and the precast concrete beam [56, 57]. It has been noticed that the precast concrete beam with this connection cannot be removed in a real building because of its monolithic joint with the floor slabs.

1.1.4 *Observations, drawbacks, and barriers for mass implementation of NGB systems*

The main observations and drawbacks with respect to existing NGB systems (with reference to concrete buildings) are listed below:

1. Most concrete NGB buildings adhere to only some requirements of NGB systems.
2. Existing concrete NGB systems have to be demounted as a whole (i.e. from top to bottom of the building), and some systems require partial demolition or removal of grout before dismantling.
3. Existing concrete NGB systems are not structurally flexible. Removal of structural elements is not possible either because of constrained degree of movement or global pre/post-tensioning of tendons.
4. No technical information is available on seismic performance of most existing concrete NGB systems.
5. Lack of guidelines to design removable dry connections in the building codes for seismic and wind loads.
6. Lack of development of connection configurations that can be applied to custom-made buildings with different layouts and loads to meet client's requirements (i.e. modular building construction).

Even though many NGB building systems have been developed, the implementation is limited to very few projects [9, 58-61]. The primary barriers for the mass implementation of NGB systems are listed below:

1. Building codes do not define and include "sustainable building technologies", nor do they use the life cycle cost as a design criteria for a building or require building components to be dismantled and reused at the end of the building life.
2. Lack of familiarity about these concepts among the architects and engineers.
3. Absence of tools to assess the cost, quality and construction time of NGB systems.
4. Absence of specifications and drawings of dry connections between different building components.
5. Absence of a tool to estimate structural properties of NGB systems.
6. Lack of demonstration of benefits of these building systems to the clients.

To estimate the lateral stiffness and fundamental period of the proposed demountable with different lateral load resisting options (i.e. braced or unbraced with either fixed or pin bases), the available analytical formulations/simple hand calculation methods and their limitations are explored as detailed in the next section.

1.1.5 *Existing analytical methods to estimate lateral stiffness and the fundamental period of frame buildings*

The most vital structural parameter required in the seismic design of a frame building (braced or unbraced) is its period of fundamental mode of vibration, which controls the seismic demand and subsequently its structural member dimensions. The fundamental period of a frame building depends on its lateral stiffness and seismic mass and cannot be precisely calculated for a building yet to be designed. A frame building lateral stiffness is a function of material properties, sectional properties, geometric configuration of its frames, and also the base boundary conditions. In reality, it is very difficult to predict the actual period of vibration of a building under real earthquake shaking because of many uncertain parameters (i.e. actual material properties, seismic mass of a building during an earthquake shaking, soil condition, contribution of secondary elements such as infill walls to the lateral stiffness of a building, actual base fixity condition etc.). Therefore, it is a common practice to use approximate empirical and analytical methods to estimate the fundamental period for design of a new building as well in the assessment of an existing building.

The empirical equations prescribed in most of the building codes to predict the fundamental period are developed using an actual database of recorded periods of real buildings in earthquakes [62, 63]. Most of the empirical equations relate the fundamental period of a building to the height of the building H; usually in the form $T_a = C_t H^x$ [64]. In the Japanese building code [65], the fundamental period is a linear function of the building height which is given as $T_a = (0.02 + 0.01\varphi)H$ [66], where the value of φ for concrete and steel buildings are 0 and 1 respectively. The fundamental period of braced frame buildings is also calculated by $T_a = C_t\ H/\sqrt{D}$, where D is the length of the braced bay [67]. The full compilation of existing empirical equations and seismic demand prediction using the equivalent static procedure in different building codes can be found in the literature [67-70]. The empirical equations prescribed in the building codes are simple, and very approximate. In most cases, they underestimate the fundamental period, which is conservative (hence acceptable) in design of a new building, but are unsuitable for assessment of an existing building as they underestimate seismic displacement [71]. The empirical equations to predict the fundamental period developed using database from high seismic regions results in overly conservative

seismic demand for the buildings in low to moderate seismic regions [63]. Also, the empirical equations prescribed in the building codes do not recognize the effect of base fixity (i.e. fixed or pin base) on the fundamental period [65, 72, 73].

Table 1.2. Values to be used in the empirical equation $T_a = C_t H^x$ in different building codes

Country	Limit state	Concrete		Steel		Building code
		C_t	x	C_t	x	
US/Chile	ULS	0.0466	0.9	0.0724	0.8	ASCE7-10 and NCh433-11
NZ	ULS and (SLS=ULS/1.25)	0.0937	0.75	0.1375	0.75	NZS1170.5-04
Europe/India	SLS	0.075	0.75	0.085	0.75	EN1998-1-04 and IS1893-02
Japan*	ULS	0.02	1	0.03	1	BLEO-1981
* Though the empirical equation in Japanese code is in a different form, the coefficient values given in the table are derived after converting the expression into $T_a = C_t H^x$, thereby resulting in the same period.						

Building codes in different countries prescribe different empirical equations to estimate the fundamental period at ultimate and serviceability limit states. The values of the coefficients to be used in those empirical equations (i.e. $T_a = C_t H^x$) in different building codes are shown in Table 1.2. Obviously, the different values of the coefficients result in different fundamental periods, and hence different seismic demands for the same building. It is important to note that some building codes (e.g. New Zealand) prescribe the periods at different limit states, whereas most of the other building codes define the period at only one limit state, and then the seismic demand for other limit state is scaled up or down [74]. The fundamental period of typical 3 and 10 storey concrete and steel frame buildings (at ULS) calculated using empirical equations given in the Japanese, American and New Zealand building seismic design standards [65, 72, 73] are shown in Figure 1.11. It is clear that there is significant variation in the estimated fundamental periods from one building code to another.

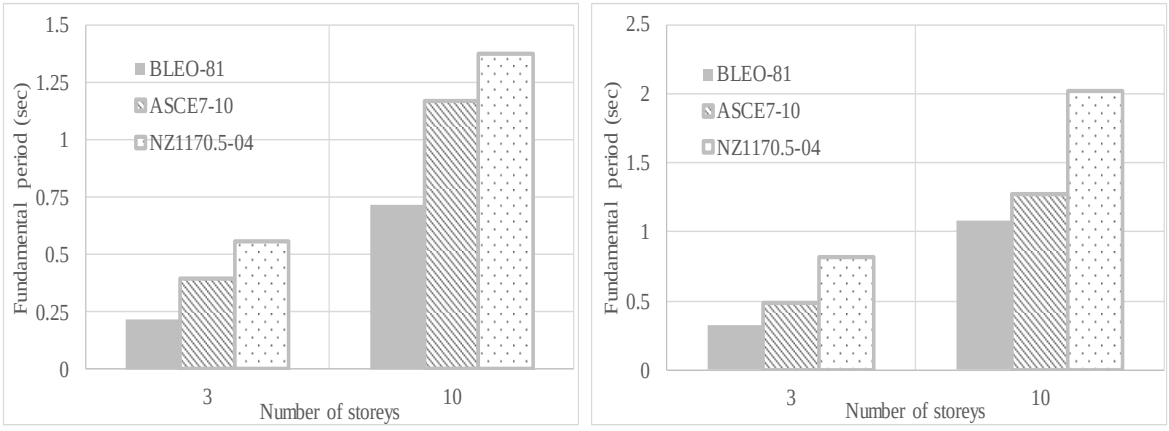

(a) Concrete moment resisting frame building (b) Steel moment resisting frame building

Figure 1.11. Fundamental period calculated using empirical equations in different standards.

The building codes allow the use of analytical methods (Eigenvalue analysis, and Rayleigh method, etc.) to predict the fundamental period, but limit to a certain value more than the fundamental period calculated using empirical equations prescribed in the building code. This

upper bound limit is to protect the buildings against un-conservative estimate of seismic demand because of unreasonable assumptions in finite element modelling. It is important to note that some building codes specify an upper bound limit on the predicted period obtained from analytical methods only for capacity design (i.e. sizing the structural members), but not for calculating lateral displacement at serviceability limit state [73]. On the other hand, some building codes do not impose any upper limit on the period calculated from analytical methods in strength and displacement checks [72, 74]. Building codes also differ from each other in the calculation of the gross or effective section properties (i.e. moment of inertia) in the estimation of the fundamental period by using analytical methods [75, 76]. Existing analytical methods like Eigenvalue analysis and Rayleigh method take into account most of the parameters that affect the period of a building. These methods are able to predict the fundamental period with reasonable accuracy, but require considerable effort in computer modelling of a building and expertise in using structural analysis software. In most cases, the fundamental periods predicted using analytical methods will be higher than those predicted using empirical equations [77].

There has been little effort towards the development of simple theoretical equations to predict the fundamental period of a frame building which accounts for all structural parameters that are likely to affect and can be used both in design of new buildings as well as in the assessment of existing buildings. Approximate hand calculation methods for the estimation of the fundamental period of frame buildings reported so far in literature are derived by solving the fourth order differential equation of cantilever column under free vibration [78, 79]. In these methods, a frame building is idealized as an equivalent cantilever column with separate flexural and shear mode of deformation. The periods of shear and flexural mode of vibration are combined using Dunkerley's combination rule to obtain the period of a building [79].

1.2 Research objectives and scope

Based on the literature review on existing precast concrete frame building systems and the next generation/demountable concrete building systems, there is a need to develop a building system which is structurally efficient and seismically robust. The developed building system should be similar to the existing conventional frame system, but does not require cast-in-situ joints and involves simple assemblage of the building components. Also, the developed building system has to be demountable, and structurally flexible (i.e. any component can be removed and replaced with a well-defined process). The objectives of this research are set such that they address some of these gaps. The project it is conducted in four stages; (i)

conceptual development, (ii) experimental test programme, (iii) numerical analysis, and (iv) analytical methods.

1.2.1 *Conceptual development*

The research objectives related to the conceptual development are;

1. To develop a schematic layout of a seismically robust and demountable precast concrete frame structural system that can be applied to any custom-made building.
2. To develop possible removable dry connections between different building components; either by utilizing and modifying some of the existing connections or developing new connection configurations that suit the proposed demountable building system.
3. To demonstrate the process of demountability and structural flexibility of a hypothetical building and assess the features of the proposed demountable precast concrete building system against the next generation building (NGB) requirements.

1.2.2 *Experimental test programme*

The research objectives related to the experimental test programme are outlined below;

1. To experimentally investigate seismic performance of proposed dry beam-column connections developed for the demountable concrete frames under quasi-static cyclic loading tests.
2. To understand the failure modes in the precast concrete beam with different proposed connection configurations at different stages of cyclic lateral loading.
3. To check whether the structural performance of the beam-column sub-assemblies with the proposed dry and demountable connections can be compared with the "wet jointed" precast concrete frame system or the monolithic concrete frame system.
4. To investigate the feasibility of demounting a damaged beam and replacing it with a new beam of the same (or higher) capacity and achieving the same (or better) performance compared to the original sub-assembly system.
5. To identify the best steel beam-column connection configuration with superior structural performance and ease to construct and remove.

1.2.3 *Numerical and analytical investigation of proposed demountable building system*

The research objectives related to the numerical analysis and development of theoretical equations with regard to the proposed demountable building system are listed below;

1. To develop theoretical/analytical equations/methods to evaluate the ultimate capacity of the proposed dry beam column connections considering all possible modes of failure.
2. To identify the design parameters of the proposed beam column connections that dictate the lateral strength and stiffness of the precast concrete frame sub-assemblies.
3. To develop numerical macro-models that can reliably simulate the hysteresis behaviour of the beam column sub-assemblies with the proposed dry connection configurations.
4. To identify the hysteresis rules and associated parameters with different dry beam column connections that can be used in analysis and design.
5. To investigate the feasibility of pin base connections (to avoid the damage to the columns) and identify the possible lateral load resisting frame options that are suitable for the proposed demountable building system.

1.2.4 *Analytical method to evaluate stiffness and fundamental period of frame buildings*

This research objective applies not only to the proposed demountable building system, but also to the conventional braced or unbraced frame building systems with rigid or pin beam column connections and fixed or pin bases. The specific aims under this objective are listed below;

1. To develop a simple theoretical model and generic equation (which takes into account most structural parameters that are known to affect the period) to predict the lateral stiffness and the fundamental period of a frame building (unbraced or braced).
2. To study the limitations of the empirical equations prescribed in building codes in predicting the fundamental period of frame buildings.

1.3 Organization of the thesis

The thesis has been organized into nine chapters. Chapter 1 presents the background/motivation for this research work. The issues associated with the present generation of buildings and the need for the next generation/demountable concrete buildings are highlighted. In seismic regions the requirement of NGB systems which can facilitate quick replacement of damaged building components is emphasized. A literature review on

different types of precast concrete frame building systems and existing demountable concrete building systems is covered. The main observations and drawbacks of the existing NGB systems with regard to their application in active seismic regions, and barriers for the mass implementation are presented. Need for simple and reliable analytical equations to estimate the lateral stiffness and fundamental period of frame buildings is emphasized. The objectives of this research and organization of the thesis are presented.

In Chapter 2, the schematic layout of the demountable concrete building system that is suitable for seismic regions is presented. The possible removable dry connections between different building components are reported in detail. Different possible options of lateral load resisting frames within the proposed building demountable system are explored. The process of demounting building components from a two storey building structural system is pictorially demonstrated. The "structural flexibility/adaptability" of the proposed building structural system is also demonstrated for two scenarios. Features of the proposed demountable building system are evaluated against the technical requirements of NGB systems. Finally, the advantages of the proposed building system in seismic regions are summarized in brief.

The objectives that are assessed through the test programme are reported in Chapter 3. The design details of a benchmark building whose cross sections are taken as the basis for the tested specimens sizes are summarized. Thereafter, an overview of the experiments, including the details of the test setup, number of tests and the applied loading protocol, is presented. Types and locations of instruments that are mounted on the specimens to record various responses are explained. Details of tests performed on various materials to evaluate and validate their mechanical properties and the summary of the test results is reported. The process of fabrication of the specimens in the precast concrete yard is explained. The component details of three types of removable beam column connections are elaborated. The basic philosophy of the load transfer mechanism between the precast concrete beam and column for different types of the proposed connections is explained. The possible modes of failure within the connection and in the beam (in the connection region) are identified. Thereafter, analytical equations developed to evaluate the capacities of the proposed connections are presented. A summary of the tested connection configurations along with their ultimate capacities is reported. The process of erection and demounting the precast concrete beam with the proposed connections is summarized. Subjective and qualitative analysis (SQA) and comparison of the proposed connections is performed, and the connection which is easy to erect and connect to the frame members, and also easy to

dismantle is reported.

In Chapter 4, design and cyclic test results of two beam column sub-assemblies with the proposed dry end plate connection are reported in detail. A summary of the capacities of the precast concrete specimens and the proposed connection is reported. Structural performance of the sub-assemblies are evaluated by comparing the experimental test results with analytically predicted values and with the hysteresis results of the "wet jointed" and "ductile connector" sub-assemblies taken from the literature. Cyclic behaviour of the sub-assemblies are numerically simulated using lumped plasticity models in finite element analysis software SAP 2000 and Opensees [80, 81]. Numerically simulated results with two different hysteresis rules and with different input backbone curves are compared, and the issues with the macro models in capturing strength degradation are highlighted. Also, the numerically developed hysteresis plots, stiffness degradation, and energy dissipation are compared with experimental results and conclusions are drawn. Finally, the primary question *"whether emulation of the behaviour of a monolithic concrete frame system or a precast concrete frame system with "wet joints" can be achieved with the use of precast concrete beams and columns connected by using the proposed end plate connection is possible or not"* is answered.

The scope of Chapter 5 includes a full description of the proposed dry angle and tube connections between precast concrete beams and columns. The experimental response of the precast concrete specimens along with the ultimate capacities are reported. Experimental test results are compared with analytically predicted values, and the reliability of the existing analytical equations is investigated. Two modelling approaches that can simulate the cyclic behaviour of the sub-assemblies with proposed connections are introduced. Numerically simulated hysteresis results of the sub-assemblies are compared with experimental hysteresis plots and conclusions are drawn based on the findings. Also, other simulated structural performance parameters such as equivalent viscous damping, stiffness degradation, and slip envelopes are compared with experimental values. Also, the experimentally obtained hysteresis plots of the sub-assemblies are compared with hysteresis plots of the sub-assemblies with "wet joints" and "ductile connectors". Finally, the primary question *"whether emulation of the behaviour of a wet jointed or monolithic concrete frame system can be achieved with the use of precast concrete beams and columns connected by using proposed angle and tube connections is possible or not"* is answered.

In Chapter 6, three types of lateral load resisting frames for the proposed demountable concrete frame building system are reported. Pros and cons of each type from the perspective of possible locations of the damage in an earthquake and the challenges involved in replacing

the damaged components are detailed. To eliminate any possible damage to the ground storey columns and to avoid the need to replace the damaged columns, feasibility of pin base connections instead of fixed base connections for an unbraced lateral load resisting frame is investigated. Pushover analysis is carried out on a wide range of low to medium rise frames to capture the effect of base fixity (i.e. fixed to pin) on structural performance parameters. Thereafter, different options to increase the base shear capacity and lateral stiffness of a pin base frame to match a fixed base frame are explored. Also, issues such as the soft storey mechanism and secondary effects in an unbraced frame with pin bases are highlighted. The design parameters that need to be explicitly considered to avoid the soft storey mechanism in an unbraced frame with pin bases are identified. The lateral load resisting frame options with increasing order of structural flexibility/adaptability that are suitable for the proposed demountable building system are reported. The reasons for an unbraced frame with pin bases that cannot be suitable for the proposed demountable building system are identified and reported.

In Chapter 7, a generic method is developed to estimate the fundamental period of regular unbraced frame buildings with fixed bases and a simple yet reliable equation is proposed. To verify the reliability and versatility of the developed equation, the fundamental periods predicted are compared with the periods obtained from an Eigenvalue analysis of large number of low to medium rise concrete frame buildings. The predicted fundamental period using the proposed equation is also verified using the period obtained using the Rayleigh method and measured in experimental tests. The results obtained from the proposed equation and Eigenvalue analysis are used to study the limitations of the empirical equations prescribed in building codes.

The primary objective of Chapter 8 is to develop a simple theoretical model and derive a generic equation to predict the lateral stiffness and the fundamental period of concentrically braced frame buildings with either fixed or pin bases. Applicability of the developed equation to unbraced frame buildings is also verified. In the basic formulation of the theoretical model, X and chevron brace configurations are explicitly considered, and its applicability to other types of brace configurations is also investigated. The predicted lateral stiffness and fundamental period values using developed equations are compared with actual lateral stiffness and fundamental period obtained from pushover analysis and Eigenvalue analysis respectively for a wide range of low to medium rise frame buildings. The range of errors with original equation is reported, reasons for the error are identified and a correction factor as a function of key structural parameters is introduced to neutralize the error. Thereafter, the

predicted lateral stiffness and fundamental period in conjunction with the correction factor are again compared with the actual values, and the amount of reduction in error is reported. By utilizing the results obtained from the developed equation, systematic interpretation of the parameters affecting the fundamental period is carried out. Also, the fundamental periods predicted by the proposed method are compared with the fundamental periods obtained from experimental tests and numerical analysis reported in literature.

Chapter 9 presents the summary of conclusions arrived at based on the developed demountable precast concrete frame system (at the conceptual level), experimental test results, numerical and analytical investigation. Also, scope for future research work related to the demountable precast concrete building system that is suitable for seismic regions is presented.

1.4 References

1. Reinhardt, H.W., *Demountable concrete structures - an energy and material saving building concept.* Int. J. Sustainable Materials and Structural Systems, 2012. **Vol. 1**(No. 1): p. pp.18–28.
2. Dorsthorst, B.J.H.t. and T. Kowalczyk, *Report 5 - state of deconstruction in the Netherlands*, in *Deconstruction and Materials Reuse - an International Overview*. 2005, in - house publishing: Rotterdam (Netherlands). p. approx. 19 p.
3. Storey, J.B., M. Gjerde, A. Charleson, and M. Pedersen, *Report 6 - The state of deconstruction in New Zealand*, in *Deconstruction and Materials Reuse - an International Overview*. 2005, in - house publishing: Rotterdam (Netherlands). p. approx. 92 p.
4. Crowther, P., *Report 1 - the state of building deconstruction in Australia*, in *Deconstruction and Materials Reuse - an International Overview*. 2005, in - house publishing: Rotterdam (Netherlands). p. approx. 32.
5. Richard, R.B., *Industrialized, flexible and demountable building systems: quality, economy and sustainability* in *CRIOCM 2006 International Research Symposium on Advancement of Construction Management and Real Estate*. 2006, in-house publishing: Rotterdam (Netherlands). p. approx. 11 p.
6. Dong, Y.H., L. Jaillon, P. Chu, and C. Poon, *Comparing carbon emissions of precast and cast-in-situ construction methods–A case study of high-rise private building.* Construction and Building Materials, 2015. **99**: p. 39-53.
7. Charlson, A., *Recycling and reuse of waste in the construction industry*. The Structural Engineer, 2008. **86**(4): p. 32-7.
8. Jaillon, L. and C. Poon, *Life cycle design and prefabrication in buildings: A review and case studies in Hong Kong.* Automation in Construction, 2014. **39**: p. 195-202.
9. Kibert, C.J., *Sustainable construction: green building design and delivery*. 2008: John Wiley & Sons.
10. fib, *Seismic design of precast concrete building structures.State-of-the-art report*. 2003, Lausanne, Switzerland. 262.
11. Restrepo, J.I., R. Park, and A.H. Buchanan, *Seismic behaviour of connections between precast concrete elements*. 1993: University of Canterbury, Department of Civil Engineering.
12. Park, R. *The fib state-of-the-art report on the seismic design of precast concrete building structures*. in *2003 Pacific Conference on Earthquake Engineering in Auckland, New Zealand,*

Paper. 2003.

13. Bull, D. and R. Park, *Seismic resistance of frames incorporating precast prestressed concrete beam shells.* PCI JOURNAL, 1986. **31**(4): p. 54-93.
14. Restrepo, P.J., *Seismic behaviour of connections between precast concrete elements.* 1992.
15. Elliott, K.S. and C. Jolly, *Multi-storey Precast Concrete Framed Structures*. 2013: Wiley Online Library.
16. Elliott, K.S., G. Davies, M. Ferreira, H. Gorgun, and A. Mahdi, *Can precast concrete structures be designed as semi-rigid frames? Pt. 1: the experimental evidence.* Structural Engineer, 2003. **81**(16): p. 14-27.
17. Negro, P. and G. Toniolo, *Design guidelines for connections of precast structures under seismic actions*. 2012: Publications Office.
18. Mohamed, S.A.M., *Behaviour of sleeved bolt connections in precast concrete building frames*. 1992, University of Southampton.
19. Bournas, D.A., P. Negro, and F.J. Molina, *Pseudodynamic tests on a full-scale 3-storey precast concrete building: behavior of the mechanical connections and floor diaphragms.* Engineering Structures, 2013. **57**: p. 609-627.
20. Priestley, M.N., S. Sritharan, J.R. Conley, and S. Pampanin, *Preliminary results and conclusions from the PRESSS five-story precast concrete test building.* PCI journal, 1999. **44**(6): p. 42-67.
21. Pampanin, S., *Emerging solutions for high seismic performance of precast/prestressed concrete buildings.* Journal of Advanced Concrete Technology, 2005. **3**(2): p. 207-223.
22. MacRae, G. and M. Priestley, *Precast post-tensioned ungrouted concrete beam-column subassemblage tests*. Vol. 94. 1994: Dept. of Applied Mechanics & Engineering Sciences, University of California, San Diego.
23. Li, L., J.B. Mander, and R.P. Dhakal, *Bidirectional cyclic loading experiment on a 3D beam–column joint designed for damage avoidance.* Journal of structural engineering, 2008. **134**(11): p. 1733-1742.
24. Solberg, K., R.P. Dhakal, B. Bradley, J.B. Mander, and L. Li, *Seismic performance of damage-protected beam-column joints.* 2008.
25. Stone, W.C., G.S. Cheok, and J.F. Stanton, *Performance of hybrid moment-resisting precast beam-column concrete connections subjected to cyclic loading.* ACI Structural Journal, 1995. **92**(2): p. 229-249.
26. Rodgers, G.W., K.M. Solberg, J.G. Chase, J.B. Mander, B.A. Bradley, R.P. Dhakal, and L. Li, *Performance of a damage‐protected beam–column subassembly utilizing external HF2V energy dissipation devices.* Earthquake Engineering & Structural Dynamics, 2008. **37**(13): p. 1549-1564.
27. Mander, J.B. and C.-T. Cheng, *Seismic resistance of bridge piers based on damage avoidance design.* 1997.
28. fib, *Structural connections for precast concrete buildings*. 2008, Lausanne, Switzerland,. 262.
29. Englekirk, R., *Development and testing of a ductile connector for assembling precast concrete beams and columns.* PCI journal, 1995. **40**(2): p. 36-51.
30. Zoubek, B., M. Fischinger, and T. Isakovic, *Seismic response of dowel connections in RC structures*, in *NZSEE Conference*. 2016: Christchurch, New Zealand.
31. Zoubek, B., T. Isakovic, Y. Fahjan, and M. Fischinger, *Cyclic failure analysis of the beam-to-column dowel connections in precast industrial buildings.* Engineering Structures, 2013. **52**: p. 179-191.
32. Mary, C. and B. Howard, *Estimating Downtime from Data on Residential Buildings after the Northridge and Loma Prieta Earthquakes.* Earthquake Spectra, 2010. **26**(4): p. 951-965.
33. Almufti, I. and M. Willford, *REDiTM Rating System: Resilience-based Earthquake Design*

Initiative for the Next Generation of Buildings. ARUP Co, 2013.

34. Cimellaro, G.P., *Urban Resilience for Emergency Response and Recovery*. 2016, Switzerland: Springer International Publishing.
35. Westra, H. and H. Vos, *Demonstration projects "Industrial, Flexible and Demountable Building" in the Netherlands*, in *20th International Symposium on Automation and Robotics in Construction (ISARC)*. 2003, Technische Universiteit Eindhoven: Eindhoven (Netherlands). p. p.67-70.
36. Reinhardt, H.W. and J.J.B.J.J. Bouvy, *Demountable concrete structures : a challenge for precast concrete : proceedings of the international symposium, held at Rotterdam, the Netherlands, May 30-31, 1985*. 1985, Delft, Netherlands: Delft University Press. 351 p.
37. Crowther, P., *Design for Disassembly-Themes and principles.* BDP Environment Design Guide, 2005. **2005**.
38. Osakagas. *Osaka gas experimental residental complex*. 1993; Available from: http://www.osakagas.co.jp.
39. Badir, Y.F., M.A. Kadir, and A.H. Hashim, *Industrialized building systems construction in Malaysia.* Journal of Architectural Engineering, 2002. **8**(1): p. 19-23.
40. Habraken, N.J., *Supports: an alternative to mass housing.* London: Architectural Press(1972), 97 PP.(General), 1972.
41. Blok, R. and F. Van Herwijnen, *Quantifying Structural Flexibility for performance based life cycle design of buildings*, in *Adaptables'06 "Adaptability in Design and Construction" on July 2006 in Eindhoven, The Netherlands*. 2006, in-house publishing: Rotterdam (Netherlands). p. p.1/16-1/20.
42. Tiuri, U. and E. Kahri, *Characteristics of Open Building in Experimental Housing*, in *CIB TG26 Open Building Implementation - 3-5 November 1997, Washington, USA*. 1998, in-house publishing: Rotterdam (Netherlands). p. approx. 8 p.
43. Reinhardt, H.W., *Demountable concrete structures? Inaugural lecture at Delft University of Technology (in German).* Cement, 1976. **28**(No 6): p. 266-273.
44. Zeegers, A., M. Hermans, and G. Ang, *In search for design criteria for the delivery of industrialized, flexible and demountable buildings; a performance based model*, in *CIB World Building Congress*. 2001, CIB: in-house publishing (Netherlands). p. approx. 10 p.
45. Durmisevic, E. and J. Brouwer, *Building deconstruction demountable building connections, a key to sustainable c onstruction*, in *Agile Architecture*. 2001, OBOM, Delft University of Technology: Delft (Netherlands). p. p.61-74.
46. Rijksgebouwendienst, M.V.V., *Demontabele bouwsystemen in beton*. 1996: RGD.
47. Herwijnen, F., *Development of a new adaptable and demountable structural system for utility buildings*, in *International Conference Sustainable Building 2000, 22-25 October 2000, Maastricht, The Netherlands*. 2000, In-house publishing: Rotterdam (Netherlands). p. approx. 3 p.
48. Sadafi, N., M.F.M. Zain, and M. Jamil. *Industrial and adaptable components for building waste reduction*. in *Clean Energy and Technology (CET), 2011 IEEE First Conference on*. 2011.
49. Sadafi, N., M. Zain, and M. Jamil, *Assessment of industrial and adaptable building components for a residential layout.* International Journal of Physical Sciences, 2012. **7**(2): p. 338-348.
50. Park, J.H., *Demountable and Interchangeable Construction System: R. M. Schindler's Panel Post Construction*, in *Open Building Implementation - The 11th Annual Conference, September 30, 2005*. 2005, in-house publishing: Rotterdam (Netherlands). p. approx. 18 p.
51. Kim, J., R. Brouwer, and J. Kearney, *NEXT 21: A Prototype Multi-Family Housing Complex.* Ann Arbor, Michigan: University of Michigan, College of Architecture and Urban Planning, 1993.

52. Okamoto, S., T. Yashiro, M. Matsuie, M. Hayashi, R. Tanaka, and Y. Watanabe. *Design and construction of first skeleton-rent apartment in the private sector*. in *Building for the Future: The 16th CIB World Building Congress 2004*. 2004. Rotterdam (Netherlands): in-house publishing.

53. Worldwideparkinggroup. *Demountable cark park building built in Auckland*. 2006; Available from: www.worldwideparkinggroup.com.

54. Storey, J.B. and M. Pedersen, *Overcoming the barriers to deconstruction and materials reuse in New Zealand*, in *Deconstruction and Materials Reuse*. 2003, in-house publishing: Rotterdam (Netherlands). p. approx. 15 p.

55. Gjerde, M., J. Storey, and M. Pedersen, *A deconstructable car parking building. In an active seismic zone*, in *Deconstruction and Materials Reuse*. 2003, in-house publishing: Rotterdam (Netherlands). p. approx. 8 p.

56. Ong, K., Z.S. Lin, L.R. Chandra, C.T. Tam, and S. Dai Pang, *Experimental investigation of a DfD moment-resisting beam–column connection.* Engineering Structures, 2013. **56**: p. 1676-1683.

57. Zhisheng, L., *Designing Moment-resisting Connection for Disassembly for Implementation in Precast Reinforced Concrete Buildings*. 2013.

58. Sadafi, N., M. Zain, and M. Jamil, *Adaptable Industrial Building System: Construction Industry Perspective.* Journal of Architectural Engineering, 2012. **18**(2): p. 140-147.

59. Geraedts, R., *Success and failure in flexible building; Flexible input leads to flexible output*, in *16th International Conference on*. 2010, Labein Tecnalia Derio: Bilbao (Spain). p. p.73-83.

60. fib, *The fib Model Code for Concrete Structures 2010*. 2010: Fédération Internationale du Béton fib/International Federation for Structural Concrete.

61. Van Gassel, F., *Experiences with the Design and Production. of an Industrial, Flexible and Demountable (IFD) Building System*, in *20th International Symposium on Automation and Robotics in Construction (ISARC)*. 2003, Technische Universiteit Eindhoven: Eindhoven (Netherlands). p. p.209-214.

62. Goel, R.K. and A.K. Chopra, *Period formulas for moment-resisting frame buildings.* Journal of Structural Engineering, 1997. **123**(11): p. 1454-1461.

63. Günaydın, E. and C. Topkaya, *Fundamental periods of steel concentrically braced frames designed to Eurocode 8.* Earthquake Engineering & Structural Dynamics, 2013. **42**(10): p. 1415-1433.

64. Crowley, H. and R. Pinho, *Period-height relationship for existing European reinforced concrete buildings.* Journal of Earthquake Engineering, 2004. **8**(spec01): p. 93-119.

65. JapanBLEO, *Part 1, Earthquake Resistant Design of Structures and Part 2, Earthquake Resistant Design of Buildings*. 1981: Tokyo, Japan.

66. Aoyama, H., *Outline of earthquake provisions in the recently revised Japanese building code*. Tokyo University, Japan, 1981.

67. Bangash, M., *Earthquake resistant buildings: dynamic analyses, numerical computations, codified methods, case studies and examples*. 2011: Springer Science & Business Media.

68. Kelly, C.Y., *An Investigation of the Fundamental Period of Vibration of Irregular Steel Structures*. 2011, Master's Thesis, The Ohio State University.

69. Günaydn, E., *Natural periods of braced steel frames designed to EC8*. 2012, Master's Thesis, Middle East Technical University.

70. Shon, B.A., *Study on the fundamental period of vibration for buildings with different configurations*. 2015, Atilim University.

71. Chopra, A.K. and R.K. Goel, *Building period formulas for estimating seismic displacements.* Earthquake Spectra, 2000. **16**(2): p. 533-536.

72. NZS1170, *NZS1170: Structural design actions. Part 5: Earthquake actions - New Zealand*. 2004: Wellington, NZ.

73. ASCE, *Minimum Design Loads for Buildings and Other Structures*. Standards. 2013: American Society of Civil Engineers. -1.

74. EN1998, *Eurocode 8: Design of structures for earthquake resistance-Part 1: General rules, seismic actions and rules for buildings*, in *London: BSi*. 2004. p. 10-12.

75. ACI, *Building code requirements for structural concrete (ACI 318-08) and commentary*. 2008, American Concrete Institute.

76. NZS3101, *NZS3101: The Design of Concrete Structures*. 2006, Standards New Zealand Wellington.

77. Di Sarno, L. and A.S. Elnashai, *Bracing systems for seismic retrofitting of steel frames.* Journal of Constructional Steel Research, 2009. **65**(2): p. 452-465.

78. Adeli, H., *Approximate formulae for period of vibrations of building systems.* Civil Engineering for practicing and design engineers, 1985. **4**(1): p. 93-128.

79. Chrysanthakopoulos, C., N. Bazeos, and D. Beskos, *Approximate formulae for natural periods of plane steel frames.* Journal of Constructional Steel Research, 2006. **62**(6): p. 592-604.

80. SAP, *Computers and Structures Inc*. 2013: Berkeley, CA, USA.

81. Mazzoni, S., F. McKenna, M.H. Scott, and G.L. Fenves, *OpenSees command language manual.* Pacific Earthquake Engineering Research (PEER) Center, 2006.

Chapter 2: Demountable precast concrete frame building system for seismic regions: Conceptual development

Aninthaneni, P. K., and Dhakal, R. P. (2017). "Demountable precast concrete frame building system for seismic regions: conceptual development." Journal of Architectural Engineering (accepted).

Aninthaneni, P. K., and Dhakal, R. P. (2015). "Demountable Precast RC frame building system for seismic regions." International Conference on Earthquake Engineering and Seismology (IZIIS-50) Kiel, Germany.

Aninthaneni, P. K., and Dhakal, R. P. (2014). "Conceptual development: Low loss precast concrete frame building system with steel connections." NZSEE Conference Auckland, New Zealand, Paper No 44.

2.1 Introduction

2.1.1 *Overview*

In this chapter, a demountable precast concrete frame building system suitable for seismic regions is developed by applying the concepts of a next generation building (NGB) system which incorporates sustainability into the process of building design and construction. The schematic details of the structural frame system and the possible dry steel connections between different building components are reported. The three structural frame options that can be considered for resisting the lateral loads, the possible locations of the damage in an earthquake shaking, and the advantages and disadvantages of each type of frame system in-terms of structural robustness and redundancy, demountability, and structural flexibility/adaptability are reported. The process of demounting/dismantling the building components of a two storey building structural frame system is demonstrated. The structural flexibility/adaptability of the proposed demountable building system is also demonstrated for two possible scenarios during the building's life span. Also, features of the proposed demountable building system are evaluated against the technical requirements of the NGB system. Finally, the advantages of the proposed demountable precast concrete frame building system in seismic regions are reported.

2.1.2 *Background*

Present generation buildings are planned, designed and built without any due consideration to deconstruction; as a result, most buildings need to be demolished either at the end of their life or when a building is obsolete in function. Also, buildings in seismic regions that have suffered irreparable damage after an earthquake have to be demolished well before the end of their intended/designed life. The demolition process of a building is environmentally unfriendly, requires careful planning to avoid any danger to nearby structures, and causes extensive wastage of non-renewable building materials [1]. In European union, the total production of Construction and Demolition Waste (CDW) is about 180 million tonnes per year [2]. The CDW amounts to 17% (this will increase after the demolition data following the 2010 and 2011 Canterbury earthquakes are accounted for) and 40% of total landfill waste in New Zealand and Australia respectively [3, 4]. Concrete buildings are major contributor to the CDW as they represent majority of the built environment in many countries. Also, demolition of concrete buildings requires enormous amount of energy; e.g. demolition of one tonne of concrete from a building requires 275 Mega Joules of energy and crushing of one tonne of concrete requires 85 Mega Joules of energy [1].

The challenges and complications pertinent to concrete building construction process have significantly eased with the advent of prefabricated/precast concrete building components when compared to cast-in-situ concrete building construction methods. Nevertheless, precast concrete building construction still involves a lot of site intensive activities [5]. Also, precast concrete building construction is comparatively a more sustainable building technology and it has a much reduced carbon emission when compared to cast-in-situ concrete building construction [6, 7]. It is recognized that the prefabrication of concrete building components results in the reduction of wastage of building materials during construction phase, but produces larger amount of waste during demolition [8]. To minimize the wastage of building materials, design and construction techniques should incorporate closed-loop building material strategy, which basically means re-use of the building components rather than disposal [9].

2.1.3 *Precast concrete building systems in seismic regions*

In seismic regions, precast concrete building systems designed to resist the lateral loads due to earthquake induced shakings fall into two broad categories; “equivalent monolithic” and “jointed” systems [10, 11]. The difference between these two systems lies in the type of connections/joints between the precast concrete building components/elements of the lateral

load resisting system. The equivalent monolithic systems are achieved with the use of "wet joints" (i.e. cast in-situ joints) between precast concrete building components [12]. In jointed systems, the precast concrete building components are connected using global un-bonded post-tensioned tendons throughout the building dimensions [13]. The jointed systems do not emulate the behaviour of the monolithic systems, but the overall building system can be designed as "ductile". Also, the jointed building systems offer the distinct advantage of self-centering with minimal residual deformation after a design level earthquake. There is another category of jointed system in which the precast concrete elements are connected using ductile steel connectors, and the behaviour is classified as "ductile" with lesser seismic performance compared to monolithic systems [14]. In the past two decades, many researchers have tried to develop an equivalent monolithic precast concrete building systems with the use of "dry joints" (i.e. similar to the connections in the steel buildings), and to the authors' knowledge this has not been very successful [15, 16]. Because of this, the structural elements in an equivalent monolithic precast concrete frame buildings are still being connected using "wet joints" to resist the lateral loads, which limits the inherent advantage of precast concrete building construction in-terms of construction speed (i.e. due to the requirement of formwork and curing time before erecting other precast concrete elements).

The precast concrete building structural system with "wet joints" turns into either fully or partially monolithic in form, enforcing these buildings to be demolished when they enter into irreparable damage after an earthquake. At the same time, monolithic precast concrete buildings which are in a reparable damage state after an earthquake, require considerable downtime to repair in addition to the repair cost to restore its functionality. This may induce substantial seismic losses contributed by direct repair cost, and more significantly by the downtime (i.e. occupancy interruption) [17]. The issues with a precast concrete building with "wet joints" can be summarized to; to a certain extent construction speed is limited, building needs to be demolished (rather than dismantled and reused), and damaged building components in an earthquake cannot be replaced. These issues in precast concrete buildings in seismic regions can be addressed by incorporating the philosophy of "Next Generation Building" system into building design and construction process.

2.1.4 *Philosophy and definition of next generation building systems*

The concept of next generation building (NGB) systems emerged with the primary objective of achieving "sustainable buildings". The basic philosophy of the NGB system is to build buildings in shorter time and in a flexible manner so that they can cater for the changes in functionality, and be dismantled and reused rather than demolished. The definition of

different components, design criteria, and construction techniques of the NGB system are listed in Table 2.1. NGB systems in different parts of the world are identified by different names as; Industrialized, Flexible, and Demountable (IFD) system, Design for Deconstruction or Disassembly (DfD), Industrialized Building System (IBS), and Open building (OB) system [5, 18-22]. The difference between these building systems lies in the extent of covering different aspects of the NGB system requirements defined in Table 2.1. There is a major gap in the definition of flexibility of existing NGB systems. The "functional flexibility" of the building is explicitly defined and addressed, whereas "structural flexibility/adaptability" is not identified as a requirement. For completeness, the definition of "structural flexibility/adaptability" to the specifications of the NGB system is reported in Table 2.1.

Table 2.1. Definitions of different components of the Next Generation Building (NGB) system

NGB system requirements		**Definition**	**Ref**
Industrialized		Standard building components of high quality and durability are mass produced in a controlled environment and transported to the site.	[5, 8]
Flexible/ Adaptable/ Open	*Functional*	Buildings are built to adapt to future functional changes by using interchangeable non-structural elements (i.e. partitions and facades).	[5, 23-25]
	Structural	Building structural layout is flexible/changeable to cater for the change in the loads in the future. Also, in seismic regions structural layout allows replacement of damaged building components with new ones.	
Demountable/Disassembly/ Deconstruction		Building components can be dismantled without major damage and can be reused.	[5, 26]
Design criteria/ Construction techniques		Design should clearly define the process of erection and dismantle of building components up front before construction. On site construction involves only erection and assembly of the building components and connections.	[27, 28]

2.1.5 *Development, implementation and barrier of NGB systems*

In this chapter, discussions on development and implementation of existing NGB systems are limited to concrete buildings. Few concrete buildings have been constructed the world by utilizing some of the concepts of NGB system. Based on the concept of IFD, five demountable concrete building systems were developed and implemented in Netherlands, namely; Mxb-5, CD-20, Bestcon-30, Moducon-2000 and SMT [2, 18, 29]. All these building systems consist of prefabricated building components like slabs, columns, and walls; the only difference among them is the connection configurations. In Japan, by using the concept of "open building" system, "NEXT21" housing project was implemented as a highly functional flexible building system, and "NOHS" housing project with a flexible floor plan, replaceable non-structural components and a long life of 200 years was developed and implemented [21, 30, 31]. In New Zealand, few partially demountable concrete car park buildings have been

designed and built [32, 33]. Also, demountable and interchangeable non-structural elements (i.e. internal partition walls and external facades) were developed and implemented to facilitate "functional flexibility" of buildings [34-36]. The main observations with existing NGB systems with reference to concrete buildings are listed below:

1. Most concrete NGB buildings adhere to only some of the requirements of NGB systems.
2. Existing concrete NGB systems have to be demounted as a whole (i.e. from top to bottom of the building), and some systems require partial demolition or removal of grout before dismantle.
3. Existing concrete NGB systems are not structurally flexible. Removal of structural elements is not possible either because of constrained degree of movement or global pre-stressing of tendons.
4. No technical information on the seismic performance of the existing concrete NGB systems.
5. Lack of guidelines to design removable dry connections in the building codes for seismic and wind loads.
6. Lack of development of connection configurations that can be applied to custom-made buildings with different layouts and loads to meet client's requirements (i.e. modular building construction).

Even though many NGB building systems have been developed, the implementation is limited to very few projects [9, 37-40]. The primary reasons identified for this are listed below:

1. Building codes do not define and include "sustainable building technologies", nor do they use the life cycle cost as a design criteria for a building or require building components to be dismantled and reused at the end of the building life.
2. Lack of familiarity about these concepts among the architects and engineers. Absence of tools to assess the cost, quality and construction time of NGB systems.
3. Absence of specifications and drawings of dry connections between different building components.
4. Lack of demonstration of benefits of these building systems to the clients.

2.1.6 *Objectives and research significance*

This chapter conceptually introduces a demountable concrete building system which not only satisfies all the requirements of NGB system but is also suitable for seismic regions. The

schematic layout of the building structural system and possible removable dry connections/joints between the building components are reported in detail. Different possible options of lateral load resisting mechanisms within the proposed building system are explored. The process of demounting of building components from the two storey building structural system is pictorially demonstrated. The "structural flexibility/adaptability" of the proposed building structural system is also demonstrated for two scenarios: (i) demounting of the damaged building components after an earthquake and replacing with a new one, and (ii) upgrading the building structural system at any stage of the building's life span by the addition of new building components (steel braces) to the lateral load resisting system. Also, features of the proposed building system are evaluated against the technical requirements of NGB systems. Finally, the advantages of the proposed building system in seismic regions are summarized in brief.

2.2 Proposed demountable precast concrete frame building system

The overall schematic layout of the proposed building structural system is shown in Figure 2.1. The structural system is comprised of standard precast concrete elements (i.e. foundations, columns, beams, and floor slabs) and removable steel connections. The proposed building system falls into "Post and Beam" modular grid building system according to architectural engineering terminology [5]. To avoid any visible projections to enhance the architecture of the building; (i) the steel connections can be flush by providing recess/rebates in the precast concrete building components, (ii) the steel connections can be covered with easily removable screed or grout. In this chapter, some steel connections between the building components are shown projecting on to precast concrete building components for better schematic representation/visualization.

The load resisting elements of the proposed building system are similar to a conventional frame building system with perimeter frames resisting lateral loads either due to wind or an earthquake and internal frames primarily resisting gravity loads due to self-weight of the building and live load (depending on occupancy class). Steel braces can also be easily added (as part of the initial design or upgrade of an existing demountable building) to the lateral load resisting frames utilizing the steel connections between the precast concrete beams and columns as shown in Figure 2.1. The schematic details of the possible types of removable steel connections between precast concrete elements are elaborated in the following sections.

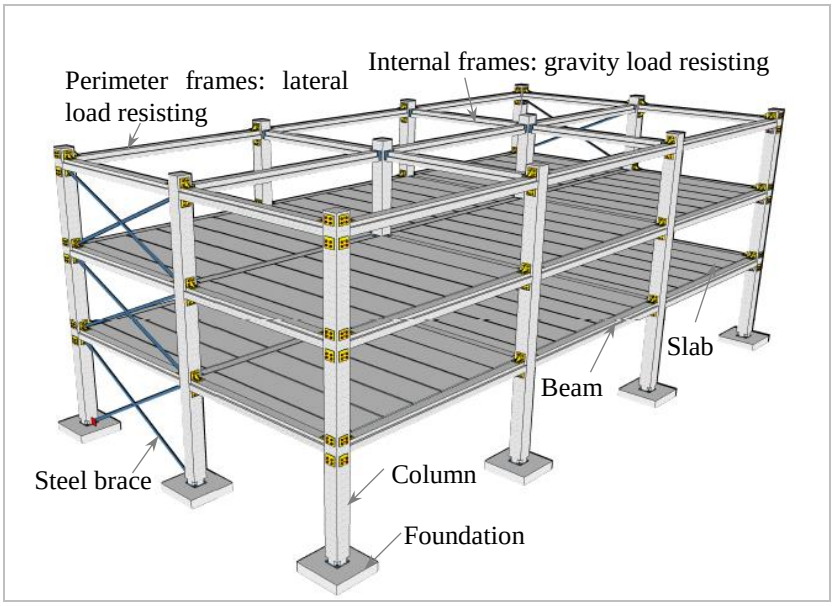

Figure 2.1. Schematic layout of the proposed demountable precast concrete frame building system

2.2.1 *Floor to floor connections*

The proposed building system can accommodate any type of precast concrete floor slabs (i.e. flat slab, ribbed slab, hollow core slab, and T shaped slab). The type of floor slab is selected based upon the grid dimensions (i.e. distance between the columns) and building occupancy class (i.e. live load). The floor slab between the grids can be a single unit or multiple units depending on the available fabrication, transportation and erection facilities. For buildings with larger grid dimensions, the depth of the floor slabs can be reduced by using pre-stressed tendons. The number of floor to floor connections can be minimized by fabricating larger size floor slab units, and can be completely eliminated by using a single floor slab unit between each modular grid, which is shown in Figure 2.2a.

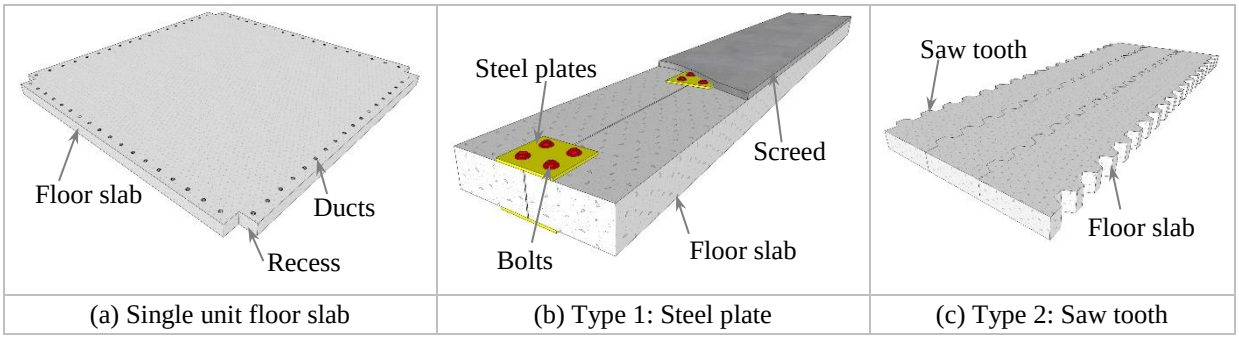

(a) Single unit floor slab | (b) Type 1: Steel plate | (c) Type 2: Saw tooth

Figure 2.2. Schematic layout of possible types of removable floor to floor connections

Type 1 floor slab to floor slab connection is made up of steel plates and threaded rods/bolts as shown in Figure 2.2b. The top surface of the floor slab is levelled with an easily removable screed to avoid visibility of the connections. In Type 2 floor to floor connection, the floor slabs are saw toothed as shown in Figure 2.2c. The saw toothed floor slabs are connected to each other by embedding projected ends of one floor slab into recessed ends of another floor

slab. The ducts in the floor slabs can be either un-grouted or filled with easily removable grout. The connections are designed to transfer the earthquake induced lateral loads from one floor slab to another.

2.2.2 *Floor to beam connections*

The schematic details of the two possible types of removable floor to beam connections are shown in Figure 2.3. In the Type 1 connection, the floor slabs are positioned on top of the beam and connected to the beam using steel angles. The bolts connecting the floor slabs to steel angles are removable, whereas the bolts connecting steel angles to the beam are embedded into the beam. The holes in the steel angle leg on the beam side is slotted in the vertical direction to accommodate any relative vertical movement between the beams and the floor slabs during an earthquake shaking, thereby eliminating damage to the floor slabs. In the Type 2 connection, threaded sleeves are embedded into the beam and the floor slabs are provided with ducts. The bolts pass through the ducts in the floor slab and clamped to the embedded sleeves in the beam. The size and spacing of the connections are designed to transfer all possible loads from the floor slab to the beam during the building's life span.

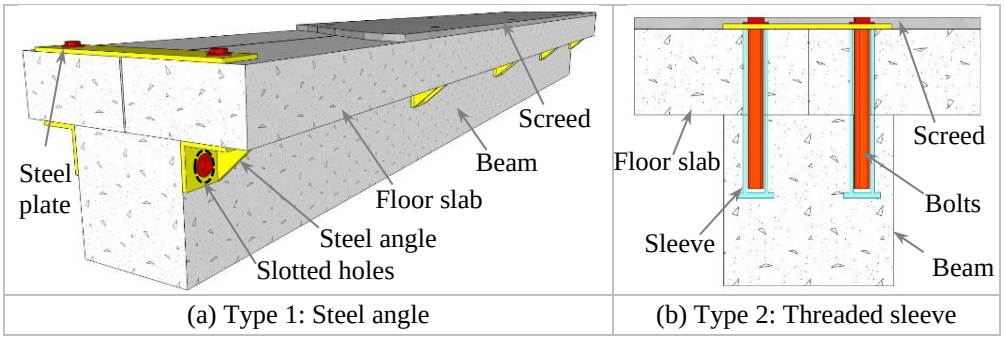

(a) Type 1: Steel angle (b) Type 2: Threaded sleeve

Figure 2.3. Schematic layout of possible types of removable floor to beam connections

2.2.3 *Beam to column connections*

The structural behaviour of a frame building predominantly relies on the performance of beam to column connections. In the proposed building structural system, the beam to column connections in the perimeter frames (i.e. lateral load resisting frames) are moment connections (i.e. rigid) whereas in the internal frames (gravity load resisting frames) are shear connections (i.e. pin). Three possible types of moment connections, and two types of shear connections which make the overall building system demountable are explored herein. The connections are designed and sized based upon the fabrication and erection tolerance requirements and the magnitude of the load/moment to be transferred from the beam to the column. The connections are designed using the capacity design principle to ensure "weak beam-strong connection-strong column" strength hierarchy.

2.2.3.1 Perimeter frames: lateral load resisting

The component details of three possible types of steel connections between precast concrete beams and columns in the perimeter lateral load resisting frame are illustrated in Figure 2.4. The Type 1 connection consists of a steel end plate and two embedded steel plates with gussets into the precast concrete beam as shown in Figure 2.4a. The steel rebars in the beam are welded to the embedded steel plates or passed through the slotted holes in the embedded steel plates before fabrication of the precast concrete beam. The steel end plate is then connected to the precast concrete column by using threaded rods/bolts as shown in Figure 2.4a. In Type 2 connections, the precast concrete beam and column are connected using stiffened steel angles as shown in Figure 2.4b. In Type 3 connections, the precast concrete beam is encased in a stiffened steel tube which is then connected to the precast concrete column, as depicted in Figure 2.4c. The only difference between Type 2 and Type 3 connections is that the Type 3 connection has extra two side plates to form a steel tube as shown in Figure 2.4c.

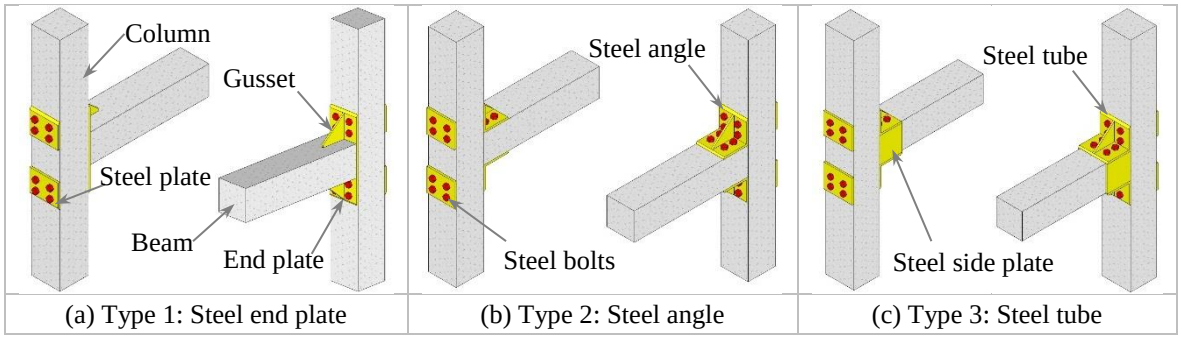

(a) Type 1: Steel end plate (b) Type 2: Steel angle (c) Type 3: Steel tube

Figure 2.4. Schematic layout of possible types of removable rigid beam column connections

The precast concrete beams and columns are cast with steel ducts through which the threaded rods/bolts are passed and bolted. In Type 1 connections, only columns are cast with steel ducts, whereas in Types 2 and 3 connections both beams and columns are provided with steel ducts as shown in Figure 2.4. To eliminate the requirement of temporary support during the erection of the beams, the precast concrete columns can be rebated (i.e. either small lug angle or concrete corbel). The threaded rods across the column can also be accommodated beside the beam side faces if the column is at least 200 mm wider than the beam, otherwise the bolts have to be provided above and below the beam.

2.2.3.2 Internal frames: gravity load resisting

The two types of possible shear connections between precast concrete beams and columns in the internal frames, which render the whole building demountable, are shown in Figure 2.5a. In Type 1 connections, the precast concrete beams and columns are embedded with steel web plates which are connected by using steel bolts. The holes in the steel web plates are slotted

in horizontal direction to allow free rotation under lateral loads, thereby not transferring any moment from beam to the column until the designed rotation ability of the connection is reached. In Type 2 connections, precast concrete beams and columns are embedded with steel inserts and connected by using a steel pin. These two types of connections allow free rotation between the beams and columns of internal frames, thereby transferring only shear and axial forces. The internal frames beam to column connections are designed to transfer the vertical loads (i.e. dead and live loads).

2.2.4 *Column to column connections*

The column to column connections can be completely avoided in case of low rise buildings (i.e. up to 4 storeys) by fabricating single unit columns of the required building height. The column to column connections that facilitate easy removal of precast concrete columns from a medium rise building are shown in Figure 2.5b. The connection is comprised of steel end plates which are embedded on both sides of the column within the column dimensions and the column ends are recessed to accommodate the bolts. Where required, the connections are to be positioned at mid height of a storey (i.e. location of less lateral load demand). The size of steel plates of the connection, and the number of bolts are designed to transfer the vertical and lateral loads, and are fabricated within erection tolerance limits.

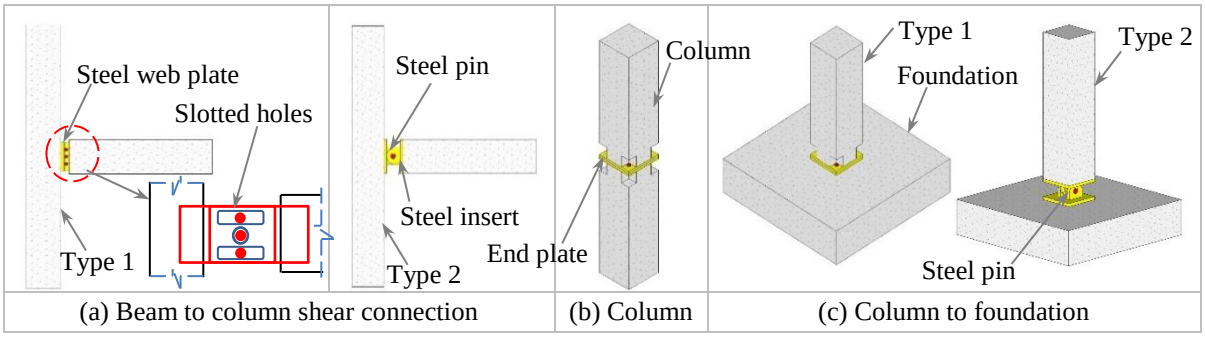

Figure 2.5. Removable beam to column pin, column to column and column to foundation connections

2.2.5 *Column to foundation connections*

The connections between precast concrete columns and foundations in the perimeter and internal frames can be either moment (i.e. rigid) or shear (i.e. pin) connections as shown in Figure 2.5c. In the figure, Type 1 connection is a rigid connection, which can be developed by using column to column connection configuration. The foundation is cast with the threaded sleeves, and the bolts are inserted through the steel end plate at the base of the column and threaded into the sleeves embedded in the foundation. The column to foundation pin connection can be achieved in two ways; (i) by using rigid column-foundation connection configuration with bolts on column center lines (this is not a perfect pin connection, but can

be classified as a nominal pin connection), and (ii) by embedding steel inserts at the end of the column and on the top of the foundation, and connecting both steel inserts by using a standard steel pin as shown in Figure 2.5c (Type 2). The column to foundation connection can be eliminated by fabricating foundation together with a pedestal which can be transported to the site and connected to the precast concrete column.

2.3 Structural frame options to resist lateral loads

In the proposed building system, the perimeter frames can be either unbraced or braced and the column to foundation connections can be either fixed or pinned depending on the magnitude of lateral loads. The three structural frame options for resisting lateral loads are: (i) unbraced frame with fixed base, (ii) braced frame with a pin base (pin or rigid beam column connections), and (iii) unbraced frame with a pin base as shown in Figure 2.6. In case of unbraced frames, the lateral load is resisted by flexural resistance of frame elements. In pin base braced frames with rigid beam column connections, the lateral load is resisted by a combination of flexural resistance of frame elements and axial resistance of braces, whereas with pin beam column connections the lateral load is transferred to the foundation only through strut and tie action provided by the braces. The load paths and possible locations of plastic hinges (i.e. damage) under lateral load with different structural frame options are shown in Figure 2.6. In case of fixed base frames, the ground storey columns will be damaged along with beams in a design level earthquake, whereas with pin base frame the damage will be limited to the beams (provided the weak beam strong column hierarchy is ensured) as shown in Figures 2.6a and 2.6c.

The unbraced fixed base frame offers higher strength, stiffness and robustness compared to the unbraced pin base frame. However strength and stiffness of the unbraced pin base frame can be considerably increased either with increase of strength of frame elements or with the addition of steel braces (which can be adopted as an option for new design or strengthening/upgrade) or both as shown in Figure 2.6b. The choice of designing a frame with or without bracing can be left to the designer and the owner depending on the desired damage mechanism in a design level earthquake and availability of bays for bracing without disrupting the planned use of the building. As the proposed building system is similar to the conventional frame building system, the capacity design principle should be followed in designing the building structural system.

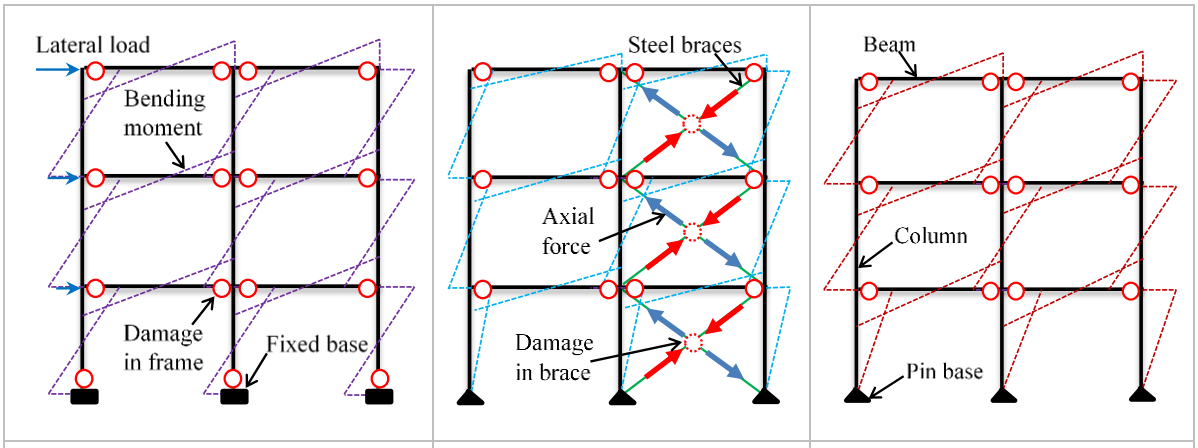

(a) Unbraced fixed base frame | (b) Braced pin base frame | (c) Unbraced pin base frame

Figure 2.6. Lateral load resisting frame options within the proposed demountable building system

2.4 Demonstration of demountability of the proposed building system

As the connections between the components of the proposed precast concrete building system are fully dry and removable, technically the building can be dismantled at any stage of its life span. The process of dismantling/deconstructing a building is exactly opposite (i.e. in terms of the erection sequence of components) of the construction of the building. To demonstrate the demountability of the proposed building system, a two storey building is chosen as an example, which is shown in Figure 2.7.

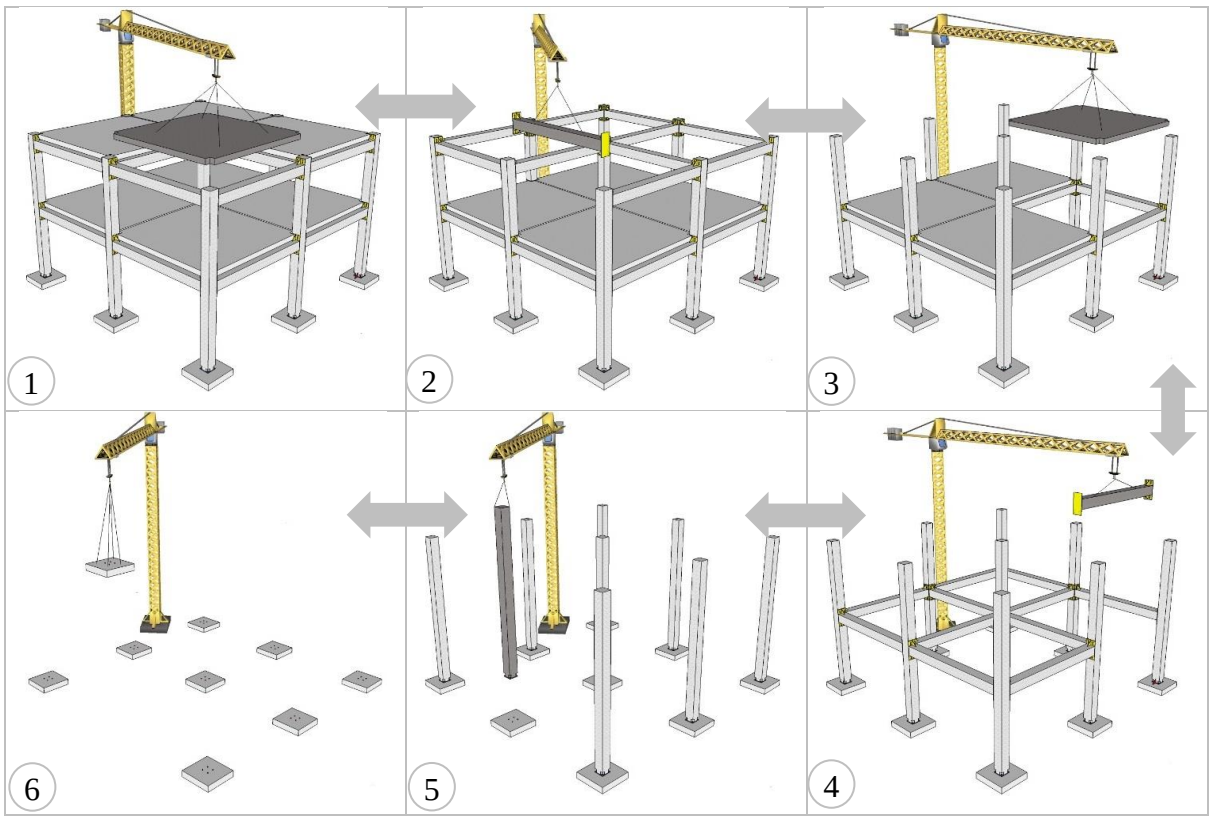

Figure 2.7. Demounting and erection process of building components of a two storey building

The sequence of demounting of the building components from top to bottom of two storey building is pictorially demonstrated in Figure 2.7 and is as follows; (i) disconnecting and removal of the second storey floor slabs, (ii) unbolting and removal of the second storey beams, (iii) disconnecting and removal of the first storey floor slabs, (iv) unbolting and removal of the first storey beams, (v) unbolting and removal of the columns, and (vi) removal of foundations. In the figure, the sequence numbering from 1 to 6 represents the deconstruction process of a building and the reverse sequence (i.e. 6 to 1) represents the construction process of a building.

2.5 Demonstration of structural adaptability of the proposed building system

As stated earlier, structural flexibility/adaptability is defined here as the ability of the building structural system to cater for future changes. Structural flexibility/adaptability can be demonstrated by the replacement of old building components with new ones or with the addition of new building components to the existing building structural system. The necessity of a structurally flexible building arises in the following situations; (i) the strength of the building components need to be increased to cater for an increase in loads or seismic demand, and (ii) the building components are damaged in an earthquake and need to be replaced.

2.5.1 *Replaceability of building components*

The replaceability feature of the proposed building system is demonstrated with a scenario of a repairable damaged building after an earthquake. Generally in frame buildings damage is concentrated in lower storey perimeter beams and ground storey columns. The damaged columns are challenging to replace, but with use of column to column connections at mid height of the first storey, only the damaged precast column element at the base needs to be replaced. Also, the damage to the columns can be avoided with use of pin base connections which eliminate the need to replace the columns after an earthquake. The downtime assessment of the proposed demountable building system with different damage states and repair/replacement options is carried out and compared with the downtime of monolithic concrete frame building, which is reported in Appendix A.

For demonstration, it is assumed that only corner beams in the first storey of the two storey building are damaged as shown in Figure 2.8a. At a system level, the replacement process of damaged beams with new ones can be summarized as; (i) first storey floor slabs supported on the damaged beams are to be temporarily supported with shores, (ii) unbolt the connections between the damaged beams, floor slabs and columns, (iii) remove the damaged beams by using a crane or forklift, (iv) erect the new beams of same size and connection configuration,

(v) connect new beam to the columns and slabs, and (vi) remove the temporary shores. At an elemental level, the process of removal of damaged beam involves unbolting the beam connections with the floor slabs and the columns, and installation of new beam involves bolting new beam to the floor slabs and the columns, which is schematically shown in Figure 2.8b. As no decision on the extent of damage and the type of repair needs to be made, the process of replacing the damaged building components is straight forward and the proposed building system can be brought back to a functional state in quick time; thereby minimizing the seismic loss especially due to occupancy interruption.

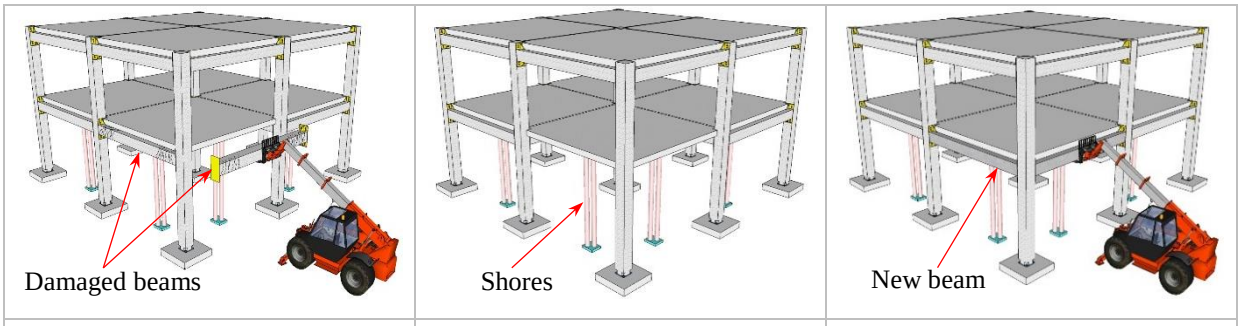

(i) Removing damaged beams	(ii) Building with removed beams	(iii) Building with new beams

(a) At system level, the process of replacement of first storey damaged beams with new one

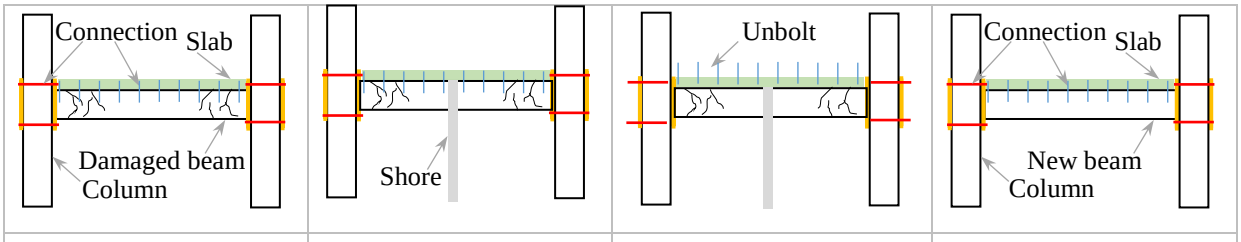

(i) Damaged beam	(ii) Shore the slabs	(iii) Unbolt connections	(iv) Bolt connections

(b) At an elemental level, process of unbolting and bolting the connections (simplified for the demonstration)

Figure 2.8. Demonstration of replaceability scenario: replacing damaged beams with new one

2.5.2 *Upgradability of building system*

The proposed building structural system can be upgraded or strengthened at any stage of a building's life span. To demonstrate the upgradability of the proposed building system, procedure to strengthen an existing two storey building by adding steel braces is shown in Figure 2.9. The addition of steel braces to the lateral load resisting frame is easier because the beam to column connections are already provided with steel gussets to which steel braces can be easily connected as shown in Figure 2.9b. The process of upgrading the building with the addition of steel braces is as follows: (i) decide the location and configuration of the steel braces to be added without affecting the functionality of the building, (ii) install steel inserts at the base of the columns (if not planned in the initial design), (iii) erect the steel braces by using a crane, and (iv) connect the steel braces to the steel gussets of the beam to column connection.

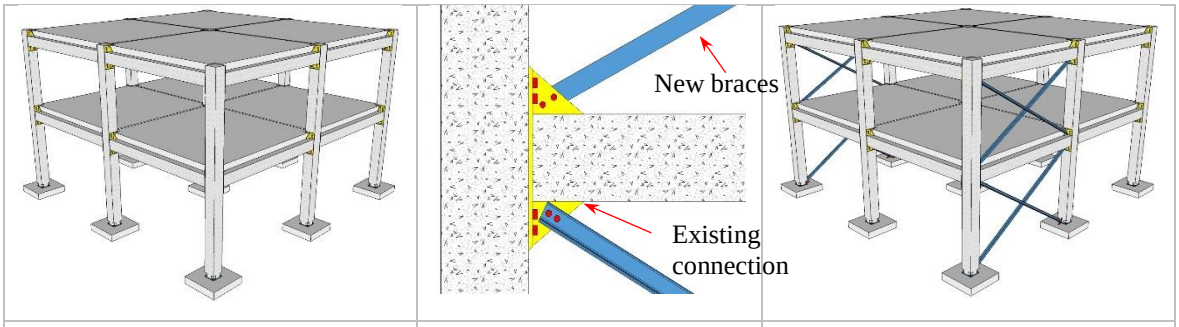

(a) Existing building | (b) Existing connection | (c) Upgrdaded building

Figure 2.9. Demonstration of upgradability scenario: addition of steel braces to lateral load resisting frame

The seismic capacity of the proposed building system can also be upgraded by replacing the existing beams (i.e. the weakest element on the strength hierarchy) with new beams of similar dimensions (for ensuring the connectivity) but larger capacity. The procedure to upgrade the building system in this way is same as the process explained earlier for replacing damaged beams. In this approach, care should be taken to maintain the strength hierarchy "weak beam strong column"; hence the extent of achievable upgrade may be limited if the difference between the beam and column strengths in the existing building system is small. To provide this option for future upgrade, it may be advisable to go for stronger columns in the initial design (than the minimum required by capacity design).

Table 2.2. Assessment of the proposed building system against requirements of NGB system

NGB system criteria		**Features of the proposed building system**
Industrialized	Standard components	Precast concrete building components and the steel connections are manufactured in a factory and then transported to the building site.
	Modular configuration	The building structural system can be easily planned and designed to meet individual client's requirements.
	Process of erection	Most of the details of the connections are quite familiar to building construction industry, which makes the erection process easy to understand and implement.
	Tolerance limits	The components of the proposed building system can be fabricated within the code specified tolerance limits.
Flexible	Functional flexibility	The proposed building system can demonstrate functional flexibility by using interchangeable non-structural elements.
	Structural flexibility	Structural flexibility of the proposed building system is demonstrated with examples of two scenarios, and can be easily demonstrated for other scenarios as well.
Demountable	Dry connections	All building components are connected with dry and removable steel connections.
	Minimal damage	Since all connections are removable, the building components can be demounted with minimal damage.
	Reuse of components	Precast concrete building components can be designed to have a longer life than the building's design life span, so the components can still be used after the building is obsolete in function.

2.6 Assessment of the proposed building system

The features of the proposed building system is evaluated against the specifications of NGB system. Generally, the assessment of the NGB system has to be carried out in two stages; initial theoretical assessment and real building prototype assessment. Here, only the theoretical assessment of the proposed system against NGB system requirements is carried out. The key design parameters considered are; industrialization, flexibility/adaptability, and demountability, which are reported in Table 2.2.

2.7 Advantages of the proposed building system

General advantages of NGB systems are already known to architects and engineers, but the proposed building system provides additional advantages in seismic regions, which are summarized below.

1. **Sustainable:** The proposed system can be demounted easily by avoiding demolition, thereby contributing towards sustainable building technology. It reduces a substantial amount of non-renewable building material waste and also saves the energy otherwise required in demolition of concrete buildings.
2. **Quick to construct:** The proposed building system does not need any cast-in-situ concrete; hence no formwork is needed. Because of the dry connections, the building system can be erected in quick time, which leads to significant reduction in the project overhead cost and greater financial return due to earlier occupancy of the building.
3. **Simple system:** No specialist knowledge is required in the design and construction of the proposed building system. As the building components and the connections to be used in the building system are simple, general builders can easily erect the proposed system without much difficulty.
4. **Demountable:** The connections between the precast concrete building components/elements are made such that the building can be easily demounted when/if needed without damaging the components. The proposed system enables financial savings through dismantle and reuse (rather than demolish).
5. **Upgradable:** The proposed building system can be upgraded if higher strength is required due to change of building occupancy or change in design code/demand. Higher strength can be achieved by replacing the weak building components with bigger/stronger ones or by adding steel braces with little intervention (as the steel connections can be predesigned to accommodate the bracing elements when/if needed in future).

6. **Easy to repair and compliant to insurance policy "like for like as when new":** Any frame elements damaged in a design level earthquake can be easily replaced with new one within a short time (which leads to significantly less downtime loss); thereby rendering it a definitely repairable and low downtime building system. The damaged building can be recovered exactly to the original state (or stronger, if needed) in a short time, which leaves no room for ambiguity in terms of compliance to the common insurance policy of "like for like as when new".

2.8 Concluding remarks

A demountable concrete building system appropriate for seismic regions has been introduced at a conceptual level in this chapter. The proposed building system is simple, can be quickly erected, and satisfies all requirements of the "Next Generation Building" (NGB) system. All building components of the building structural system are interconnected using removable dry steel connections/joints. The building system can be designed to achieve the desired level of lateral load resistance through moment resisting frames or truss actions provided by steel braces. The proposed building structural system is structurally flexible and the building components can be easily demounted whenever needed. Consequently, a building with the proposed structural system does not need to be demolished at the end of its life. The building can be sequentially demounted and its components can be reused; thereby saving a huge amount of non-renewable building waste, and energy associated with demolition of concrete buildings. Compared to traditional concrete buildings and normal NGB systems, the proposed building system offers several additional advantages in seismic regions. In addition to its fast construction/erection, simplicity, sustainability, demountability, the proposed building system is also able to be upgraded (i.e. strengthened) whenever needed. Also, following a damaging earthquake the proposed building system can be quickly and fully repaired to the satisfaction of all stakeholders by replacing the damaged building components with new building components, which significantly reduces the building downtime and makes it a low loss building system in terms of earthquake induced losses.

2.9 References

1. Reinhardt, H.W., *Demountable concrete structures - an energy and material saving building concept.* Int. J. Sustainable Materials and Structural Systems, 2012. **Vol. 1**(No. 1): p. pp.18–28.
2. Dorsthorst, B.J.H.t. and T. Kowalczyk, *Report 5 - state of deconstruction in the Netherlands*, in *Deconstruction and Materials Reuse - an International Overview*. 2005, in - house publishing: Rotterdam (Netherlands). p. approx. 19 p.
3. Storey, J.B., et al., *Report 6 - The state of deconstruction in New Zealand*, in *Deconstruction and*

Materials Reuse - an International Overview. 2005, in - house publishing: Rotterdam (Netherlands). p. approx. 92 p.

4. Crowther, P., *Report 1 - the state of building deconstruction in Australia*, in *Deconstruction and Materials Reuse - an International Overview*. 2005, in - house publishing: Rotterdam (Netherlands). p. approx. 32.
5. Richard, R.B., *Industrialized, flexible and demountable building systems: quality, economy and sustainability* in *CRIOCM 2006 International Research Symposium on Advancement of Construction Management and Real Estate*. 2006, in-house publishing: Rotterdam (Netherlands). p. approx. 11 p.
6. Dong, Y.H., et al., *Comparing carbon emissions of precast and cast-in-situ construction methods–A case study of high-rise private building.* Construction and Building Materials, 2015. **99**: p. 39-53.
7. Charlson, A., *Recycling and reuse of waste in the construction industry.* The Structural Engineer, 2008. **86**(4): p. 32-7.
8. Jaillon, L. and C. Poon, *Life cycle design and prefabrication in buildings: A review and case studies in Hong Kong.* Automation in Construction, 2014. **39**: p. 195-202.
9. Kibert, C.J., *Sustainable construction: green building design and delivery*. 2008: John Wiley & Sons.
10. fib, *Seismic design of precast concrete building structures.State-of-the-art report*. 2003, Lausanne, Switzerland. 262.
11. Park, R. *The fib state-of-the-art report on the seismic design of precast concrete building structures*. in *2003 Pacific Conference on Earthquake Engineering in Auckland, New Zealand, Paper*. 2003.
12. Restrepo, J.I., R. Park, and A.H. Buchanan, *Seismic behaviour of connections between precast concrete elements*. 1993: University of Canterbury, Department of Civil Engineering.
13. Priestley, M.N., et al., *Preliminary results and conclusions from the PRESSS five-story precast concrete test building.* PCI journal, 1999. **44**(6): p. 42-67.
14. Englekirk, R., *Development and testing of a ductile connector for assembling precast concrete beams and columns.* PCI journal, 1995. **40**(2): p. 36-51.
15. fib, *Structural connections for precast concrete buildings*. 2008, Lausanne, Switzerland,. 262.
16. Elliott, K.S., et al., *Can precast concrete structures be designed as semi-rigid frames? Pt. 1: the experimental evidence.* Structural Engineer, 2003. **81**(16): p. 14-27.
17. Mary, C. and B. Howard, *Estimating Downtime from Data on Residential Buildings after the Northridge and Loma Prieta Earthquakes.* Earthquake Spectra, 2010. **26**(4): p. 951-965.
18. Westra, H. and H. Vos, *Demonstration projects "Industrial, Flexible and Demountable Building" in the Netherlands*, in *20th International Symposium on Automation and Robotics in Construction (ISARC)*. 2003, Technische Universiteit Eindhoven: Eindhoven (Netherlands). p. p.67-70.
19. Reinhardt, H.W. and J.J.B.J.J. Bouvy, *Demountable concrete structures : a challenge for precast concrete : proceedings of the international symposium, held at Rotterdam, the Netherlands, May 30-31, 1985*. 1985, Delft, Netherlands: Delft University Press. 351 p.
20. Crowther, P., *Design for Disassembly-Themes and principles.* BDP Environment Design Guide, 2005. **2005**.
21. Osakagas. *Osaka gas experimental residental complex*. 1993; Available from: http://www.osakagas.co.jp/csr_e/charter02/technology.html.
22. Badir, Y.F., M.A. Kadir, and A.H. Hashim, *Industrialized building systems construction in Malaysia.* Journal of Architectural Engineering, 2002. **8**(1): p. 19-23.
23. Habraken, N.J., *Supports: an alternative to mass housing.* London: architectural press(1972), 97

PP.(General), 1972.

24. Blok, R. and F. Van Herwijnen, *Quantifying Structural Flexibility for performance based life cycle design of buildings*, in *Adaptables'06 "Adaptability in Design and Construction" on July 2006 in Eindhoven, The Netherlands*. 2006, in-house publishing: Rotterdam (Netherlands). p. p.1/16-1/20.

25. Tiuri, U. and E. Kahri, *Characteristics of Open Building in Experimental Housing*, in *CIB TG26 Open Building Implementation - 3-5 November 1997, Washington, USA*. 1998, in-house publishing: Rotterdam (Netherlands). p. approx. 8 p.

26. Reinhardt, H.W., *Demountable concrete structures? Inaugural lecture at Delft University of Technology (in German).* Cement, 1976. **28** (No 6): p. 266-273.

27. Zeegers, A., M. Hermans, and G. Ang, *In search for design criteria for the delivery of industrialized, flexible and demountable buildings; a performance based model*, in *CIB World Building Congress*. 2001, CIB: in-house publishing (Netherlands). p. approx. 10 p.

28. Durmisevic, E. and J. Brouwer, *Building deconstruction demountable building connections, a key to sustainable c onstruction*, in *Agile Architecture*. 2001, OBOM, Delft University of Technology: Delft (Netherlands). p. p.61-74.

29. Rijksgebouwendienst, M.V.V., *Demontabele bouwsystemen in beton*. 1996: RGD.

30. Kim, J., R. Brouwer, and J. Kearney, *NEXT 21: A Prototype Multi-Family Housing Complex.* Ann Arbor, Michigan: University of Michigan, College of Architecture and Urban Planning, 1993.

31. Okamoto, S., et al. *Design and construction of first skeleton-rent apartment in the private sector*. in *Building for the Future: The 16th CIB World Building Congress 2004*. 2004. Rotterdam (Netherlands): in-house publishing.

32. Gjerde, M., J. Storey, and M. Pedersen, *A deconstructable car parking building. In an active seismic zone*, in *Deconstruction and Materials Reuse*. 2003, in-house publishing: Rotterdam (Netherlands). p. approx. 8 p.

33. Worldwideparkinggroup. *Cark park buildings in Auckland*. 2006; Available from: http://www.worldwideparkinggroup.com/projects/index.html.

34. Sadafi, N., M.F.M. Zain, and M. Jamil. *Industrial and adaptable components for building waste reduction*. in *Clean Energy and Technology (CET), 2011 IEEE First Conference on*. 2011.

35. Sadafi, N., M. Zain, and M. Jamil, *Assessment of industrial and adaptable building components for a residential layout.* International Journal of Physical Sciences, 2012. **7**(2): p. 338-348.

36. Park, J.H., *Demountable and Interchangeable Construction System: R. M. Schindler's Panel Post Construction*, in *Open Building Implementation - The 11th Annual Conference, September 30, 2005*. 2005, in-house publishing: Rotterdam (Netherlands). p. approx. 18 p.

37. Sadafi, N., M. Zain, and M. Jamil, *Adaptable Industrial Building System: Construction Industry Perspective.* Journal of Architectural Engineering, 2012. **18**(2): p. 140-147.

38. Geraedts, R., *Success and failure in flexible building; Flexible input leads to flexible output*, in *16th International Conference on*. 2010, Labein Tecnalia Derio: Bilbao (Spain). p. p.73-83.

39. fib, *The fib Model Code for Concrete Structures 2010*. 2010: Fédération Internationale du Béton fib/International Federation for Structural Concrete.

40. Van Gassel, F., *Experiences with the Design and Production. of an Industrial, Flexible and Demountable (IFD) Building System*, in *20th International Symposium on Automation and Robotics in Construction (ISARC)*. 2003, Technische Universiteit Eindhoven: Eindhoven (Netherlands). p. p.209-214.

Chapter 3: Experimental test programme

3.1 Introduction

3.1.1 *Overview*

This chapter reports the details of the experimental test programme conducted in this research including its primary objectives. The design details of a benchmark frame building, from which the lateral load resisting frame is taken as the basis for the precast concrete specimen's sizes to be tested are summarized. Thereafter, overview of the experiments along with the details of the tested sub-assemblies, the test setup, and the loading protocol applied to the sub-assemblies to assess their cyclic performance are elaborated. Types and locations of instruments mounted on the specimens to record the linear and radial movements, strains, and relative slip between the connection and precast concrete members during the quasi-static cyclic testing is reported. Secondary tests performed on the materials such as concrete, threaded rods/bolts, and infill materials (i.e. rubber, grout etc.) to evaluate and validate their mechanical properties and the test results are also reported in detail. Also, the material properties used for the design and evaluation of capacities of the precast concrete specimens and the steel connections in the different tests are summarized. The reasons for the revision of initially designed precast concrete specimens sizes to fit with the connection sizes are reported. The process of fabrication/construction of the specimens in the precast concrete yard, including the procedure adopted to position and align the steel ducts within the tolerance limits (almost zero tolerance) is also explained.

The component details of the proposed removable dry beam-column connections, namely; (i) Type-1: end plate connection (EP), (ii) Type-2: angle connection (A), and (iii) Type-3: tube connection (T) are elaborated. The basic philosophy of the load transfer mechanism between the precast concrete beam and column with different types of proposed connections is explained. Based on the preliminary understanding of the load transfer mechanism, the expected cyclic behaviour of the sub-assemblies with proposed steel connections is reported. Also, the possible modes of failures within the connection and in the beam (in the connection region) are identified. Thereafter, mechanics based analytical models, idealized stress diagrams, and equations are developed to evaluate the ultimate capacities of the proposed connections. A summary of the tested steel connection configurations along with ultimate capacities on beam and column sides at various stages of loading are reported. The

fabrication process along with identified issues for the proposed steel connections is explained. The process of erection and demounting of the precast concrete beam with the three types of steel connections is summarized. Also, the challenges identified during erection and dismantle of the sub-assemblies with different connection configurations are reported. Ease of removing the damaged beam and the connection, and replacing with new beam with different connection configurations is assessed. Finally, subjective and qualitative analyses are performed on the proposed connections, and based on the comparison the connection which is easy to connect to the frame members and also easy to erect and dismantle is identified and recommended.

3.1.2 *Objectives of the test programme*

The main aim of the research study is to demonstrate that the proposed demountable precast concrete frame building has a seismic performance similar to that of a "wet jointed" precast concrete or monolithic concrete frame building. So, the primary objective of the experimental test programme is to investigate the cyclic performance of beam-column sub-assemblies with the proposed dry and removable connections under quasi-static cyclic loading. Also, the other objectives which are investigated through this test program are;

(i) to check if the precast concrete frame system with the proposed "dry joints" can emulate the behaviour of the wet jointed/monolithic concrete frame system.

(ii) to identify the best among the proposed dry steel connections in-terms of cyclic performance, and ease to construct and remove.

(iii) to demonstrate the demountability, replaceability, and upgradability of the proposed demountable building system at the sub-assembly level.

3.1.3 *Design details of the benchmark building*

A five storey office building assumed to be located in Christchurch was selected as the benchmark building. The building structural system comprised moment resisting frames in both directions with internal frames resisting predominantly gravity loads, and perimeter frames resisting lateral forces induced by earthquake shaking or wind. The chosen building was assumed to be square in plan with four bays in both directions, with each bay of span length 6 m and storey height of 3.6 m as shown in Figures 3.1a and 3.1b. The loading and seismic design requirements considered for the analysis and design of the building's structural system were as per New Zealand loading standards, and the summary of the details is reported in Table 3.1 [1, 2].

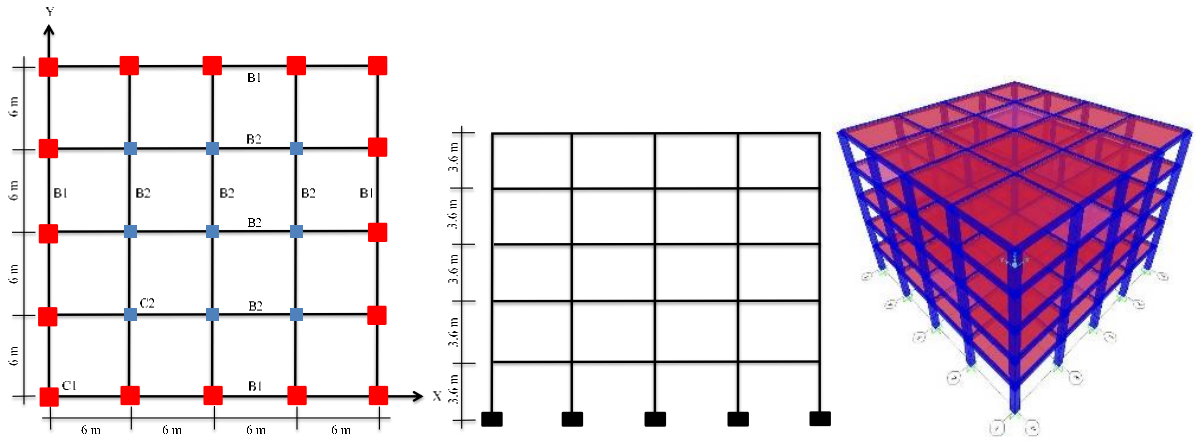

(a) Plan of the building (b) Elevation of the building (c) FE model of the building

Figure 3.1. Layout of the office building considered for the analysis and design

Table 3.1. Design requirements for the office building [1-3]

Loading requirements	**Seismic requirements**	**Material/design properties**	
Live load	Ductility at ULS: 3	Grade of concrete (f'_c)	40 N/mm^2
Roof: 2.5 kN/m^2 ; Other: 3.0 kN/m^2	Ductility at SLS: 1.25	Grade of rebar (f_y)	500 N/mm^2
Super imposed dead load	Hazard factor: 0.3	Density of concrete (γ_c)	23.5 kN/m^3
Roof: Ceilings and services: 0.25 kN/m^2; Screed to falls: 1 kN/m^2	Near fault distance : 20 KM	Modulus of elasticity of concrete (E_c)	29997 N/mm^2
Other floors: Ceilings and services: 0.25 kN/m^2; Partitions: 0.5 kN/m^2	Soil class: E	Modulus of elasticity of rebars (E_s)	2×10^5 N/mm^2

To estimate the possible combinations of the actions/demands on the structural members during the life span of the building, linear elastic analysis was performed on a finite element (FE) model constructed by using structural analysis software SAP 2000 [4], which is shown in Figure 3.1c. The load calculations (i.e. dead, live, and seismic) and load combinations used in the finite element analysis are also detailed in Appendix B. Also, the un-factored internal forces (i.e. bending moments, shear forces, and axial forces) of the perimeter lateral load resisting frame which were used for the design are reported in Appendix B. Eigenvalue analysis was performed on the building model to estimate the fundamental period, which was used to predict the seismic base shear at ultimate and serviceability limit states (ULS and SLS). In the estimation of the fundamental period at ULS, the considered effective moment of inertia was 0.55 and 0.32 times the gross moment of inertia for the columns and the beams respectively, whereas at SLS, effective moment of inertia was 0.8 and 0.7 times gross moment of inertia for the columns and the beams, respectively. The summary of estimated fundamental periods and seismic base shear calculated by using an equivalent static method at ULS and SLS are given in Table 3.2. It is clear that the ULS shear demand is more than the SLS shear demand and governs the design of the structural members.

Table 3.2. Summary of seismic design parameters and base shear at ULS and SLS

Description	ULS	SLS	Reference/Notes
Fundamental period	1.97 Sec	1.44 Sec	Eigenvalue analysis
Return period factor	1	0.25	NZS 1170.5 Eq 3.1
Seismic coefficient	0.12	0.096	NZS 1170.5 Eq 5.1
Base shear demand	2426 kN	1941 kN	ULS >SLS demand
Ductility	3	1	

The design of the structural members was carried out as per capacity design principles (strong column-weak beam) prescribed in New Zealand concrete building code [3] by using SAP 2000 along with hand calculation checks. The detailed design calculation report for a typical column and beam of the perimeter frame is reported in Appendix B. Also, the summary of the required longitudinal rebar area, stirrup area per unit length, and capacity to demand ratios in the beams and the columns of the perimeter frame is reported in Appendix B. The inter-storey lateral drift including P-Δ effects of the building was calculated at ULS and is less than 2.5%, and details of the calculations can be found in Appendix B. The summary of the member cross sections along with the reinforcement layout that meets the design requirements specified in Table 3.1 is shown in Figure 3.2. The cross section and rebar layout of the column (C1) and the beam (B1) of the perimeter frame shown in Figure 3.2 were taken as the basis for the design of precast concrete specimens which will be used in this test programme.

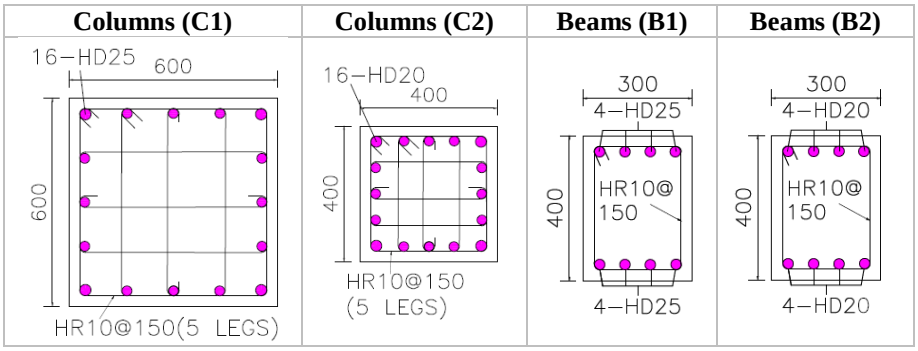

Figure 3.2. Cross sectional layout of the columns and the beams (all dimensions are in mm)

3.2 Overview of the experiments

As the main aim of the test programme was to understand the cyclic behaviour of the proposed steel connections between precast concrete beams and columns, the widely accepted and most effective protocol is a quasi-static displacement control loading regime applied to the beam column sub-assemblies (given the number of tests and types of connections). The identified locations of the external and internal beam column sub-assemblies from a typical lateral load moment resisting frame considered for the test programme are shown in Figure 3.3. Also, the point of application of incremental cyclic sway load, qualitative lateral deformation profile and boundary conditions of the sub-assemblies

are shown in Figure 3.3. The height of the column and length of the beam of the sub-assembly were chosen such that they represent the distances between points of contra-flexure. As the frame system was designed as per capacity design principles to ensure "strong column-weak beam", the lateral load capacity of the beam column sub-assembly is limited by the ultimate capacity of the beam.

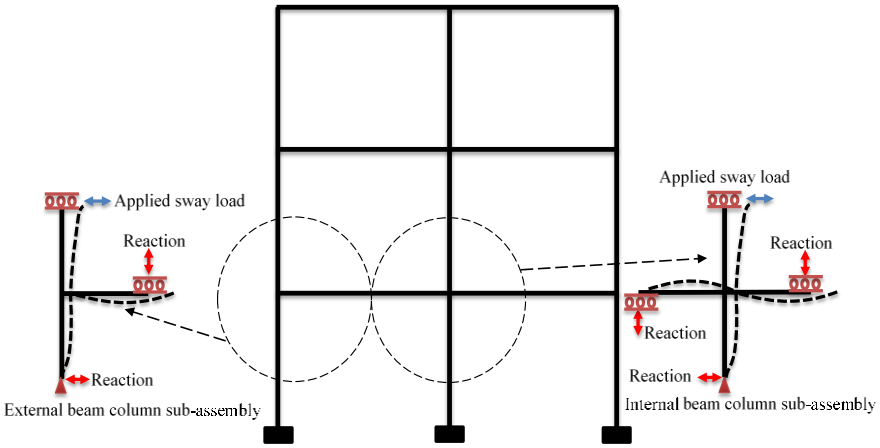

Figure 3.3. Location details of the beam column sub-assemblies of a perimeter frame

3.2.1 *Test setup details*

The overall experimental test setup with an internal beam-column subassembly including details of the location of the hydraulic actuator and the load cell is schematically shown in Figure 3.4a. For a corner beam-column assembly, the beam either on the left or right side of the column was omitted in the setup. A beam of length 3.23 m and a column of height 2.95 m were chosen so that the test sub-assembly approximately represented half of a bay length and storey height of a typical frame building (i.e. the distance between points of contra-flexure). In the figure, "negative" and "positive" represent the directions of loading (hysteresis/load-displacement plots need to be interpreted accordingly in the next chapter). Twelve quasi-static tests were carried out with different connection configurations. Out of twelve tests, the first test was conducted on an internal beam-column sub-assembly whereas all remaining tests were on corner beam-column sub-assemblies. The reason for testing more external beam column sub-assemblies is that it facilitates to investigate more number of connection parameters affecting the cyclic performance (for the same number of precast concrete beams). All the specimens were subjected to quasi-static cyclic loading as per ACI loading protocol [5], which is shown in Figure 3.4b. The sub-assemblies were subjected to three cycles of incremental lateral drift ratios of 0.1%, 0.3%, 0.5%, 0.75%, 1%, 1.5%, 2%, 2.5%, 3%, 4%, and 5%. In this way, it is possible to investigate the strength and stiffness degradation of the sub-assemblies with proposed connections and identify the connection type which can simulate the behaviour of the monolithic concrete frame system.

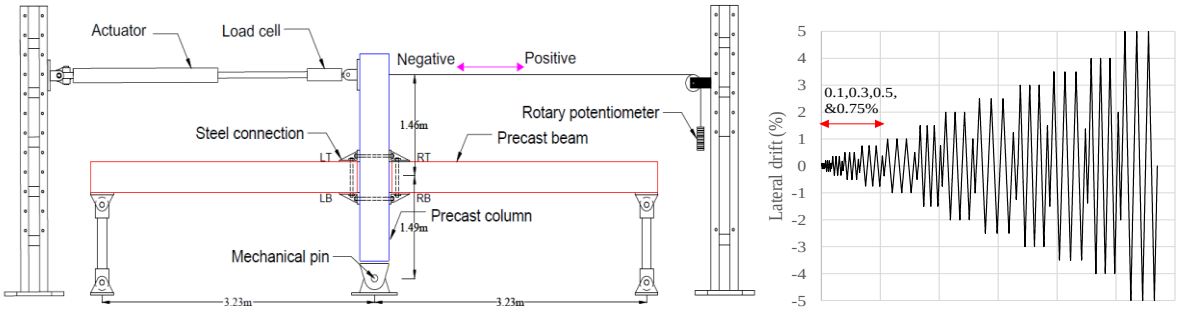

(a) Experimental test setup (b) Quasi-static loading protocol

Figure 3.4. Test setup and loading protocol to evaluate performance of beam-column sub-assemblies

3.2.2 *Instrumentation details*

Four types of instruments were mounted on the tested beam column sub-assemblies to measure the slip, strains, lateral movements, and rotations. Spring potentiometers were fixed to the precast concrete specimens near the connections on beam and column sides with its tip touching the connection to measure the relative movement/slip of the connection with respect to the precast concrete member surfaces as shown in Figure 3.5. The location details of the different spring potentiometers are schematically shown in Figure 3.4a. In the figure, the notations "LT", "LB", "RT", and "RB" represent the locations (e.g. right top, left bottom etc.) of spring the potentiometers.

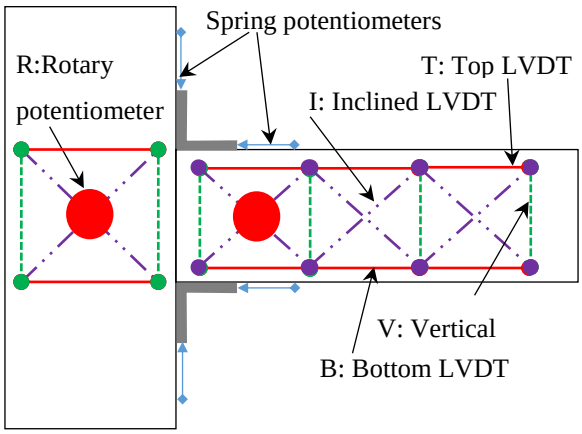

Figure 3.5. Layout of spring, linear, and rotary potentiometers on the column and beam

Linear potentiometers (i.e. LVDTs) were mounted on the precast concrete beam and column close to and away from the connection region to measure the relative stretch or compression of the zone considered between the ends of the potentiometer as shown in Figure 3.5. A rotary potentiometer along with a string was mounted on to the reaction frame at the level of the point of application of the lateral load, which is shown in Figure 3.4a to measure the lateral deformation. Also, another rotary potentiometer was mounted on the column and beam in the joint region along the beam center line to measure the rotations of the specimens under

the lateral deformation of the sub-assembly as shown in Figure 3.5. Strain gauges were glued to the longitudinal reinforcement, and vertical and horizontal stirrups to record the strains under incremental cyclic loading.

3.3 Material properties evaluation

The specified concrete design mix for the precast concrete specimens was 40 MPa grade with a slump of 120 mm. To evaluate and validate the specified compressive strength of the precast concrete specimens, concrete cylinders of 100 mm diameter and height of 200 mm (aspect ratio of 2) were cast. As the concrete attained early high strength (i.e. more than 50% of its maximum strength in one day), curing of the specimens were not done before removing from the moulds in the precast yard (generally next day of the casting). Also, the precast concrete specimens were not cured at any time, so it was decided not to cure the casted concrete cylinders as well to replicate the actual environmental conditions. At the end of each test, concrete core from the undamaged portion of the beam was taken to evaluate the actual compressive strength of the specimen.

(a) Crushing failure (b) Shear failure (c) Edge failure

Figure 3.6. Different modes of failure of concrete cylinder under compression loading

The cast and cored cylinders were tested in a compression testing machine as shown in Figure 3.6a. It was observed that there was no consistency of modes of damage of the tested concrete cylinders. Three modes of failure such as crushing, shear, and edge failure of the concrete cylinders were observed as shown in the Figure 3.6. The maximum compressive strength of cast and cored samples on the day of testing of a sub-assembly are plotted against the specified design strength in Figure 3.8a. The observed variation was ±10 MPa from specified compressive strength of 40 MPa. In general, the compressive strength of the cored samples was more than that of the cast samples. This might be because of the less exposed surface area available for evaporation compared to the cast concrete cylinders.

For connecting the steel assemblies to the precast concrete beams and the columns, threaded rods/bolts were used. For grade 8.8 bolts, the specified minimum yield and ultimate stress were 640 and 800 MPa, respectively. To cross verify their mechanical properties, tensile tests were carried out as shown Figure 3.7a. For the tensile testing, 33 mm diameter threaded rods were milled to a diameter of 27.5 mm for 75 mm length as shown in Figure 3.7b. An extensometer with a 50 mm gauge length was mounted onto the milled portion of the threaded rod to measure the elongation under tensile loading, and actual ultimate elongation of the threaded rod can be seen in Figure 3.7c. The obtained stress-strain curves for the four tested threaded rod samples (i.e. TB-1 to 4) are plotted in Figure 3.8b. Also, the values of the yield stress, yield strain, ultimate stress, and Young's modulus are reported in Table 3.3. It is clear that the actual strengths are more than the specified/required strengths and actual deformation capacity is more than required minimum deformation capacity. Hence, the behaviour of threaded rods can be categorized as "ductile" and can be used for the proposed connections under cyclic loading.

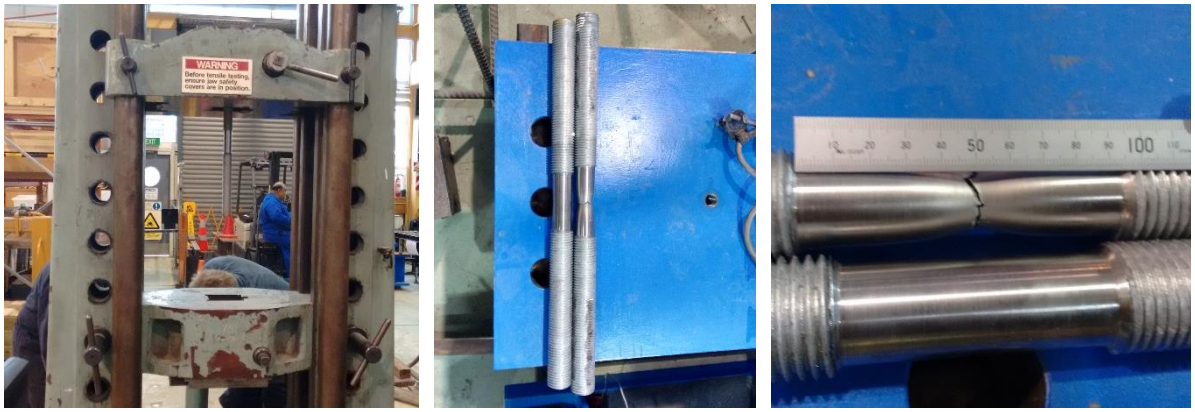

(a) Tensile testing machine (b) Milled threaded rod (c) Ultimate elongation of threaded rod

Figure 3.7. Tensile testing of the threaded rods

The specified grade for the rebars and stirrups to be used in the precast concrete specimens was 500 MPa. But, it was noticed from the manufacture's mill certificate that the yield strength of the rebars varies with diameter, which is reported in Table 3.3. For the fabrication of the steel connections, grade 350 structural steel was specified, and a summary of its mechanical properties is reported in Table 3.3. The tensile properties of the steel plates were also obtained from the manufacture's mill certificate. As the specified properties are reliable, no explicit tests were conducted.

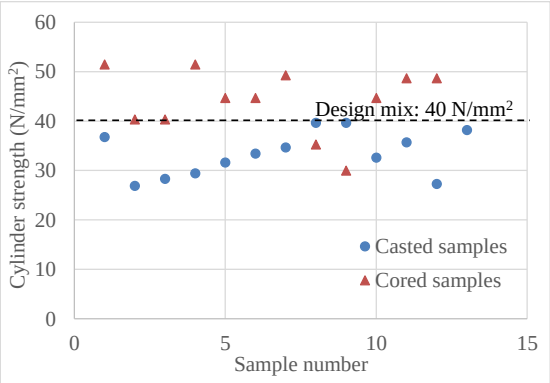

(a) Compressive strength of concrete cylinders

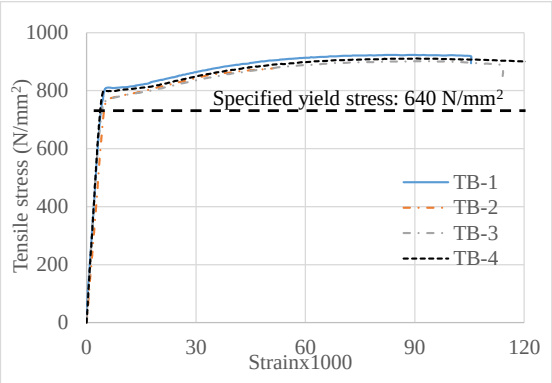

(b) Tensile properties of threaded rods

Figure 3.8. Comparison of compression strength of concrete cylinders and tensile strength of bolts

Table 3.3. Mechanical properties of threaded rods, rebars/reinforcement, and steel plates

Description	Threaded rods				Rebars			Steel plates
	TB-1	TB-2	TB-3	TB-4	R-10	R-25	R-32	S-350
Yield stress (MPa)	682.21	685.09	759.58	765.48	586	517	532	350
Yield strain x 1000	3.57	3.6	4.93	4.07	2.93	2.58	2.66	1.75
99% stress (MPa)	915.37	900.02	892.24	902.06	720	646	665	480
Young's modulus (GPa)	184.56	190	181.64	200.34	200	200	200	200

For the design and evaluation of capacities of precast concrete specimens and steel connections, the material properties summarized in Table 3.4 were used as input parameters. The previously identified variation of the material properties of concrete, threaded rods, and reinforcement was ignored as it has little effect on the ultimate capacities of the specimens and the connections. It is important to note that no material safety factors (as per building codes) were applied in the capacity evaluation of the tested specimens and the connections as it was not a real building. Also, details of the threaded rods including yield and ultimate tensile capacities are reported in Table 3.4.

Table 3.4. Summary of the material properties used in the design and tensile strength of bolts

Material properties		Threaded rod/bolt properties	
Yield stress of steel components (f_{yp})	350 N/mm^2	Grade of bolts	8.8
Ultimate stress of steel components (f_{up})	480 N/mm^2	Yield stress of bolts (f_{yb})	700 N/mm^2
Yield stress of rebars (f_{yr})	500 N/mm^2	Ultimate stress of bolts (f_{ub})	900 N/mm^2
Ultimate stress of rebars (f_{ur})	625 N/mm^2	Net area of bolt (A_{nb})	680 mm^2
Grade of the concrete beam (f'c)	40 N/mm^2	Yield capacity of bolt (T_{yb})	475 kN
Grade of the weld E48XXSP (f_{yw})	480 N/mm^2	Ultimate capacity of bolt (T_{ub})	612 kN

During the erection of the first test sub-assembly, uneven gaps were observed between the connection and the precast concrete member surfaces as shown in Figure 3.9. This was because precast specimens' finished surfaces were not perfectly level and the legs of steel angle/steel tube were not exactly perpendicular. To have a uniform contact surface between the steel connection plates and the precast member surfaces fill material was required to effectively transfer pre-tension force from the bolts to members. Also, some of the proposed

steel connections rely on the frictional resistance to transfer loads between precast concrete members, so the ideal properties that the infill material should possess are; (i) its mechanical properties are similar to the concrete (i.e. compressive strength of infill material should be at least equal to the strength of the concrete), (ii) the frictional coefficient between steel, infill material, and concrete should be equal or more than frictional coefficient between steel and concrete, and (iii) the setting time of the infill material should adequate enough to align and join the connection to the precast concrete members. As there was no direct literature on the behaviour of infill materials between steel connections and precast concrete members under cyclic loading, four types of infill materials were identified and tested, namely; rubber sheet, grout, dental plaster, and epoxy resin.

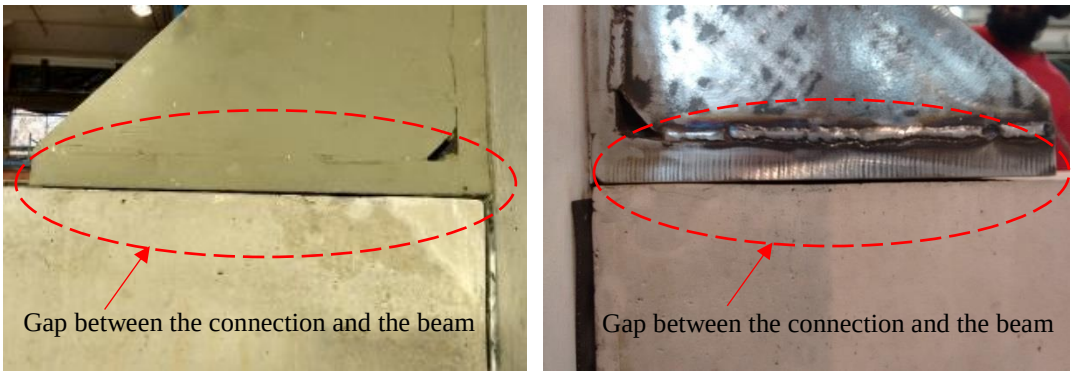

Figure 3.9. Uneven gaps between the connection and the beam

Three types of rubber sheets namely; natural rubber (NAT), ethylene propylene diene monomer (EPDM), and Nitrile rubber (NIT) of 3 mm thickness were tested to identify the one with superior compressive strength as shown in Figures 3.10a to 3.10c. The obtained stress-strain curves of three types of rubber under compressive loading is plotted in Figure 3.10d. Because of same shore hardness of D60 for the three types of rubber sheets, the obtained mechanical properties were very similar. Natural rubber sheet was selected and used as infill material because of the less cost compared to others. Another advantage with use of rubber sheet as infill material was it eliminates the damage to the column because of the bearing of the connection under lateral load. As can be observed from Figure 3.10d, the rubber sheet was highly compressible, because of this the amount of pretension in the threaded rods/bolts was limited to a value such that the compressive stress is less than 10 MPa or compressibility index is less than 0.33 whichever is less (only when rubber sheet was used as an infill material).

(a) Natural rubber b) EPDM rubber (c) Nitrile rubber (d) Comparison of stress-strain curves

Figure 3.10. Tested samples of three types of rubber material and comparison of stress strain curves

The mechanical properties of other infill materials were well reported in the manufacturer's catalogue, so no explicit tests were conducted. The obtained properties from the manufacturer's catalogue are reported in Table 3.5. Figure 3.11 shows a case where rubber sheet or grout were used as an infill material between the connection and the beam to fill the uneven gaps.

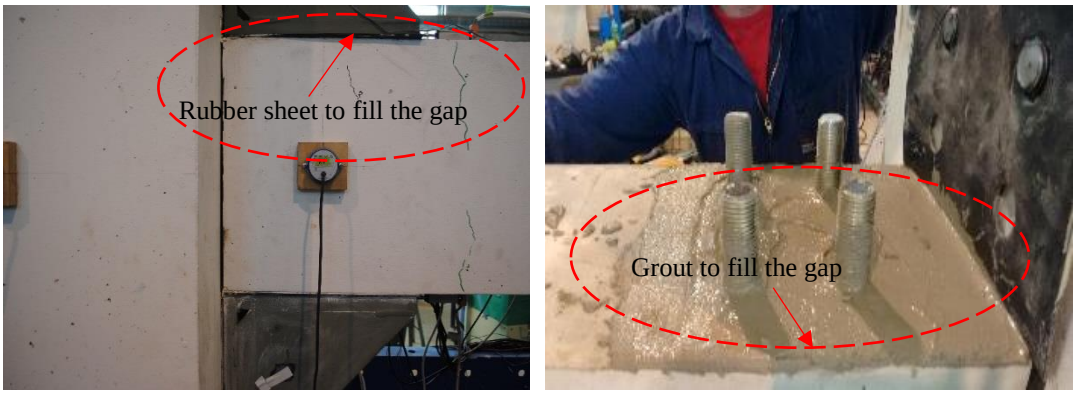

Figure 3.11. Infill materials to fill the gap between the connection and the beam

Table 3.5. Mechanical and frictional properties of infill materials

Infill materials	Compres-sive strength	Contact surfaces	Coefficient of friction			Ref
			Static (μ_s)	Kinetic (μ_k)	Design (μ_f)	
Rubber	10 MPa	Steel on concrete	0.47-0.65	-	0.4	[6, 7]
Sika grout	50 MPa	Steel or concrete on rubber	1.0	0.6-0.85	0.6	[8]
Dental plaster	60 MPa	Steel or concrete on grout	0.47-0.65	-	0.4	[7]
Hilti epoxy	82.7 MPa	Steel or concrete on resin	0.7*	-	0.4	
* Bond strength of 12.4 MPa has been converted into equivalent frictional coefficient						

As mentioned before, another important property of the infill material that dictates the capacity of the steel connection and the sub-assembly system was its frictional coefficient. The static and kinetic coefficient of friction between different contact surfaces was taken from the literature and reproduced in Table 3.5. It was observed that there was no direct literature available on dynamic/ kinetic friction coefficient between the steel and concrete surfaces. Also, a wide variation of the friction coefficient for the same contact materials was

observed depending on the contact pressure, surface roughness, sliding velocity, contact surface condition (i.e. dry and wet), and temperature. Because of this, a conservative friction coefficient was used in the design and evaluation of the connection capacity as reported in Table 3.5.

3.4 Precast concrete specimen details

3.4.1 *Details of the tested specimens*

The previously designed beam (B1) and column (C1) cross sections of the perimeter frame of a five storey building were taken as the reference for the design of precast concrete specimens used in the test programme. But, the width of the column and beams had to be increased by 100 mm and 50 mm respectively, this was required in order to cater for different bolt configurations without changing the column given the limitation of available hydraulic jack/torque wrench size in the laboratory. To investigate some of the objectives of the experimental programme (i.e. replaceability and upgradability), precast beams of different capacities (Beams-1 to 4) were designed by keeping the same cross section but with varying reinforcement ratios as shown in Figure 3.12. Also, the strength of the columns (Column-1 and 2) to be used in the test programme shown in Figure 3.12 was increased by increasing reinforcement ratio from previously designed column (C1), this was because the same column was used with beams of higher capacities as well (i.e. Beam-4).

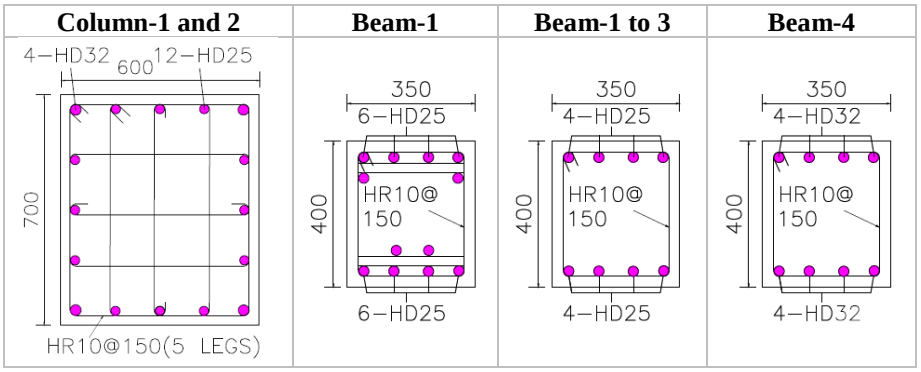

Figure 3.12. Cross sections of the tested precast concrete specimens (all dimensions are in mm)

In practice, the column size can be reduced conforming to building code provisions by ensuring “strong column-weak beam”. Also, the capacity of the beam can be increased by increasing the depth of the beam rather than increasing reinforcement ration. The detailed drawings of the cross sectional and reinforcement layouts of the tested precast concrete specimens are reported in Appendix C. For Beams-2 and 4, horizontal stirrups of 10 mm diameter were spaced at 50 mm along the beam depth near to beam edge to increase the beam edge breakout resistance under longitudinal shear force (more explanation of the mechanism

is reported in the next section).

The summary of nominal yield capacities of the tested precast concrete specimens is reported in Table 3.6. It can be observed that beam capacities were varied between 319 kN-m and 487 kN-m, and the ratios of the yield capacity of the column to over strength demand of beam varies from 1.1 to 1.74. For the estimation of the demand on the connection, "stronger column-strong connection-weak beam" concept was used. Accordingly, the yield capacities of the beams were amplified by assuming a over-strength factor of 1.4, so that the connection strength is more than the beam strength. The summary of over strength shear and moment demand on the connections for the beams of different capacities is also reported in Table 3.6.

Table 3.6. Summary of yield capacities of the specimens and the demand on the connection

Description	**Beam-1**	**Beam 2 and 3**	**Beam 4**
Nominal yield moment capacity of the beam (M_{yb})	404 kN-m	319 kN-m	487
Over strength factor for design of the connection (ϕ_o)	1.4	1.4	1.4
Over strength moment demand on the connection (M_{ob})	565 kN-m	445 kN-m	680 kN-m
Over strength shear demand on the connection (V_o)	188 kN	148 kN	225 kN
Ratio of yield capacity of column to over strength demand	1.70	2.15	1.40
Note: 40 MPa grade of concrete is considered in the calculation of yield capacity of beams, but of the actual concrete strength varied by ± 10MPa among specimens (this has been neglected because of little effect on the yield capacity).			

3.4.2 *Fabrication of the specimens*

The sequence of fabrication of precast concrete specimens for the proposed demountable concrete frame building system is explained herein, and it is very much similar to the fabrication of the components for a conventional precast concrete frame building system with the use of "wet joints". But for the proposed system, the location of the steel ducts in the beams and columns need to be positioned accurately and aligned within the tolerance limits, so that the connection process of the beams and the columns at the building site is not affected and delayed. For this project, the precast components were fabricated within tolerance limits as per New Zealand concrete construction practice [9]. Firstly, rebar caging for the precast concrete columns and beams with specified layout was prepared as shown in Figure 3.13. The rebar cage preparation for the precast concrete beam with the steel end plate connection (i.e. Type-1) is different to the precast concrete beam with the steel angle and tube connections (i.e. Type-2 and 3 respectively), and more details of the tested connection types are reported in the next section. For the Type-1 connection, the longitudinal rebars of the beam were either welded to the steel plates or passed through the slotted holes of the steel plates or both (depending on the design criteria) as shown in Figure 3.13c. For Type-2 and 3 connections, the required rebar cage for the precast concrete beams is shown in Figure 3.13c. Also, for Type-2 (only Type-2a) and 3 connections horizontal stirrups were provided at the

beam ends (in the connection region) to increase beam edge breakout resistance (mechanism is explained in the next section).

(a) Rebar cage for the beam

(b) Rebar cage for the column

(c) Rebar cage for Type-1

(d) Horizontal stirrups for Type-2 and 3

Figure 3.13. Caging of the rebars for the precast concrete specimens

Timber moulds were prepared to cast the specimens as shown in Figure 3.14. But for the mass production and long-term use, standard steel moulds of different lengths and depths can be made to increase the speed of production. To prevent the outward movement of the vertical formwork of the moulds, wooden braces were provided on either sides of the mould as shown in Figure 3.14b.

(a) Timber mould for the beam

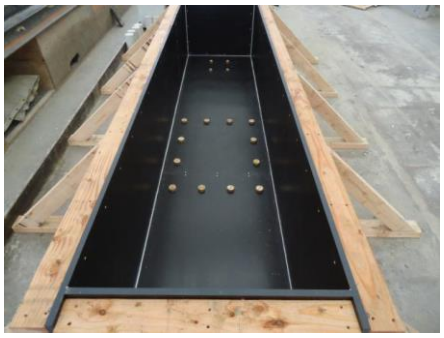

(b) Timber mould for the column

Figure 3.14. Timber moulds for the beam and the column

The Type-1 connection does not require steel ducts to be cast in the precast concrete beams, whereas the precast concrete beams with the Type-2 or 3 connection require steel ducts at both ends of the beam (in the connection region) as shown in Figure 3.15a. Also, columns were cast with steel ducts in the connection region as shown in Figure 3.14b. To position the steel ducts in the exact location and to align perpendicular to member surfaces, circular wooden rebates were cut to size and positioned such that they exactly fit inside the steel ducts as shown in Figure 3.15a. Thereafter, steel ducts were inserted on the wooden rebates and aligned perpendicular to the beam's top and bottom surfaces. At the bottom and sides of the mould, cover blocks were positioned to provide specified cover to the rebars. Thereafter, the rebar cage was positioned into the mould with the help of crane as shown in Figure 3.15b. Finally, to keep the steel ducts in specified location and position, a wooden plate with circular rebates was also positioned on top of the ducts and firmly screwed to the mould.

(a) Positioning of the steel ducts in the beam (b) Positioning of the rebar cage in the beam

Figure 3.15. Steel ducts and rebar cage positioning in the beams

Thereafter, fresh concrete was poured into the moulds and vibrated by using needle vibrator to remove air pockets as shown in Figure 3.16a. As mentioned before, it was very important to have the precast specimens' surfaces level, otherwise the steel connection will not have proper contact with specimens, resulting in non-uniform stress distribution when the threaded rods/bolts are pre-tensioned. To achieve level surface, the top surface of the specimen was levelled by using a trowel as shown in Figure 3.16b. The hardened precast concrete beam with embedded steel ducts before lifting from the mould is shown in Figure 3.17a. Once the precast concrete specimen achieved 40% of its specified maximum strength, it was lifted from the mould by connecting chains to the embedded lifting anchors and by using a crane as shown in Figure 3.17b.

(a) Pouring of the concrete into the mould (b) Finished surface of fresh concrete

Figure 3.16. Pouring of the fresh concrete into the mould and finishing the top surface

(a) Hardened precast specimen in the mould (b) Lifting and transporting of the precast beam

Figure 3.17. Hardened precast specimen in the mould and transportation of the specimen

3.5 Steel connection configuration details

3.5.1 *Components details of the connections*

Three types of removable connections between precast concrete beams and columns were identified and investigated, namely; (i) Type-1: steel end plate connection, (ii) Type-2: steel angle connection, and (iii) Type-3: steel tube connection. All are illustrated in Figure 3.18. The Type-1 connection consists of a steel end plate and two embedded steel plates into the precast concrete beam as shown in Figure 3.18a. As mentioned before, depending on the design criteria the longitudinal rebars of the beam can be either welded to the embedded steel plates or passed through the slotted holes of the embedded steel plates or both. In the Type-2 connection, the precast concrete beam and column is connected using steel angles as shown in Figure 3.18b. Two variations of the Type-2 connection were identified and tested; (i) Type-2a: without embedded steel web plates, and (ii) Type-2b: with embedded steel web plates as shown in Figure 3.18c. In the Type-3 connection, the precast concrete beam is encased in a steel tube which is then connected to precast concrete column, as depicted in Figure 3.18b. The only difference between Type-2 and Type-3 connections is that the Type-3 connection has extra two side plates to form steel tube as shown in Figure 3.18b. The Type-2

and 3 connections requires the threaded rods/bolts on beam and column sides to connect the frame members (i.e. beams and columns), whereas Type-1 connection requires only on column side. In all connection types, gussets are required to increase the capacity and stiffness as shown in Figure 3.18.

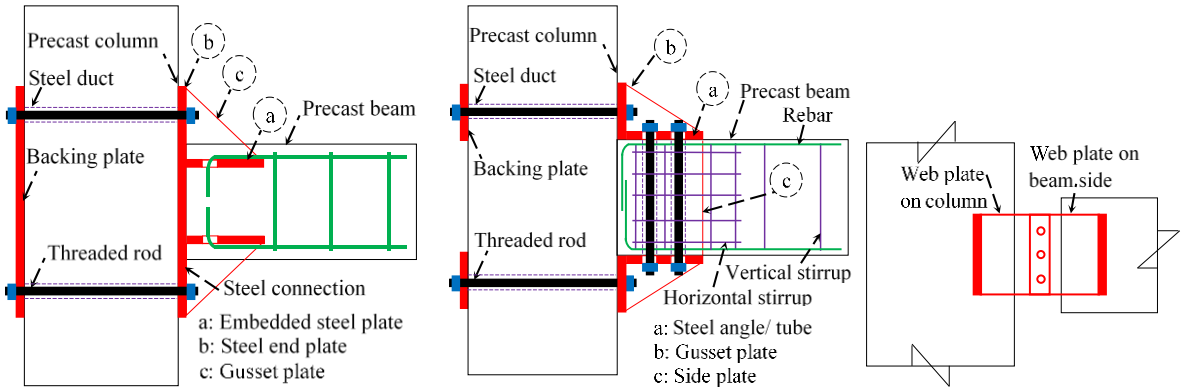

(a) Type-1 connection (b) Type-2 and 3 connection (c) Type-2b connection only

Figure 3.18. Components details for the different connection configurations

As mentioned earlier, to bolt the connection to the frame members, the precast concrete beams and columns were cast with steel ducts through which threaded rods/bolts were passed and bolted. In Type-1 connection, only columns were casted with steel ducts whereas in Type-2 and 3 connections both beams and columns were provided with steel ducts as shown in Figure 3.18. To avoid any visible projections to enhance the architecture of the frame, the backing plates can be flush into the columns. To eliminate the requirement of temporary support during erection of the beams, the precast concrete columns can be rebated (i.e. either small concrete corbel or lug angle). The threaded rods on the column side can also be accommodated beside the beam side faces if the column width is at least 200 mm more than the beam width, otherwise they have to be provided only above and below the beam.

3.5.2 *Philosophy of load transfer mechanism*

The basic philosophy of the proposed steel connections in transfer of load between the precast concrete beam and column is explained herein. The schematic representation of transfer mechanism of the internal forces (i.e. moment (M), shear (V), and axial (N)) for the three connection configurations are shown in Figures 3.19 to 3.21. The load transfer mechanism with Type-1 connection is very different when compared to Type-2 and 3 connections. In these Figures, "*P*" represents the pre-tension applied to the bolts, "*T*" is tension force either in the longitudinal rebars or embedded steel plates or in the bolts or in the horizontal stirrups, "*C*" is the total compressive force either in an idealized internal concrete stress block or on the column due to bearing of the connection or on the beam due to bearing

of the bolts or in the longitudinal rebars or embedded steel plates, *d*' represents the lever arm, "*F*" is the frictional resistance developed between the connection and the beam due to bending moment, "F_{rd}" is the reduced frictional resistance due to reduction of pre-tension in the bolts (either due to relaxation of the bolts or prying action or loss of contact area due to spalling of concrete) and frictional coefficient (i.e. kinetic/dynamic friction coefficient is less than static friction coefficient), "V_f" is frictional shear resistance between the connection and the column, and subscripts "r", "c", "p", "ci", "s", and "b" represent rebar, concrete, plate, capacity of bolt row *i*, horizontal stirrups, and bearing of bolts on to concrete, respectively.

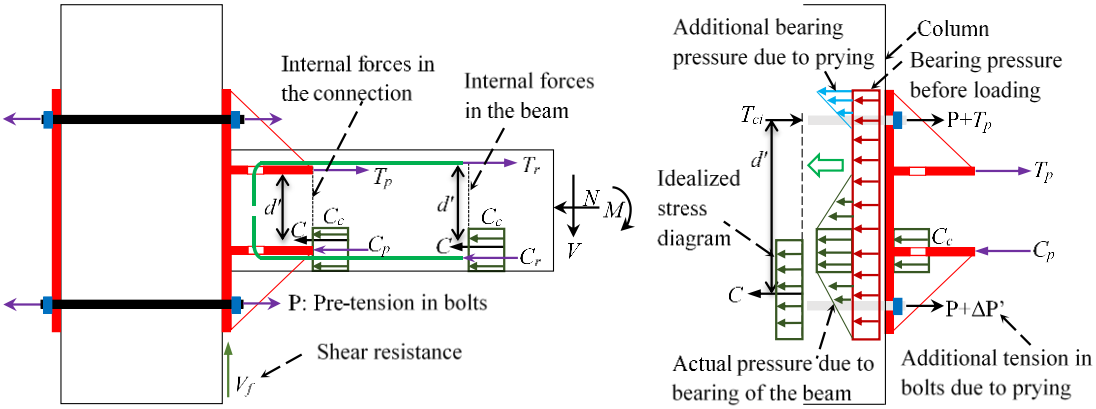

(a) Internal force diagram on beam side (b) Internal force diagram on column side

Figure 3.19. Load transfer mechanism from the beam to the column with Type-1 connection

In Type-1 connection, the bolts on the column side are pre-tensioned (P) so that the frictional resistance (V_f) is developed to resist the shear force (V) as shown in Figure 3.19a. When the shear force at the interface of the connection and the column exceeds the frictional shear resistance, the beam slips in the vertical plane and the final shear resistance (V_u) is offered through the shear or bearing failure of the bolts or bearing failure of the concrete beyond the ducts or both. Bending moment (M) generated tensile and compressive forces in the rebars of the beam are directly transferred to the embedded steel plates and concrete compressive stresses of the beam are transferred to the column as bearing pressure as shown in Figure 3.19a. The internal forces in the connection on beam side are transferred to the connection on the column side as tensile force in the bolts and bearing pressure on the column surface, which is schematically shown in Figure 3.19b. Based on the initial understanding of the behaviour of Type-1 connection, it can be categorized as "non-sliding" as long as vertical slip between the connection and the column is eliminated and the expected cyclic behaviour of the sub-assembly can be similar to the monolithic RC frame system. The different possible modes of failures within the connection and analytical equations to calculate the ultimate capacity of the connection are reported in the next section.

In Type-2 and 3 connections, there is no direct transfer of the rebar forces of the beam to the connection, hence need to rely on some other mechanisms (such as friction and beam end/edge breakout resistance) so that rebars will enter into yield/plastic state at higher drift levels before bond failure occurs in the connection region due to the slip of the connection. To achieve this, bolts are pre-tensioned on the beam side so that the frictional resistance (*F*) is developed between the connection and beam top and bottom surfaces as shown in Figure 3.20. Unlike Type-1 connection which can slip only in the vertical plane, Type-2 and 3 connections can slip simultaneously in vertical and horizontal planes. The shear resistance mechanism between the connection and the column with Type-2 and 3 connections is similar to Type-1 connection.

The bending moment (M) transfer from the beam to the connection can be treated as a two stage process. When the frictional resistance is higher than the horizontal interface force due to bending moment (i.e. beam end moment (M) divided by the beam depth (d)), then no slip occurs in the horizontal plane. In such a case, the behaviour of the frame with these connections is similar to a cast-in-situ/monolithic concrete frame system (i.e. yielding of the rebar through the development length and spread of flexural cracking along the beam length). The internal force transfer mechanism between the connection and the beam until no slip of the connection is shown in Figure 3.20a. When the induced force exceeds the frictional resistance, the behaviour of the connection comes from a combination of slip between the connection and beam and conventional frame behaviour (i.e. predominant flexural deformation). After the slip, the longitudinal shear force (V_l) from the threaded rods is transferred to the steel ducts as bearing pressure which is being resisted by the concrete beyond the ducts (V_c) and horizontal stirrups (T_s) in the connection region, which are shown in Figures 3.20b and 3.20c. For easier understanding of longitudinal shear force transfer mechanism from the threaded rods to the horizontal stirrups strut and tie model as shown in Figure 3.20b can be utilized. The capacity of the connection on the beam side can be limited to the beam end breakout resistance rather than beam's ultimate moment capacity if the connection slips at an early stage, thereby resulting in bond failure between the rebars and the concrete.

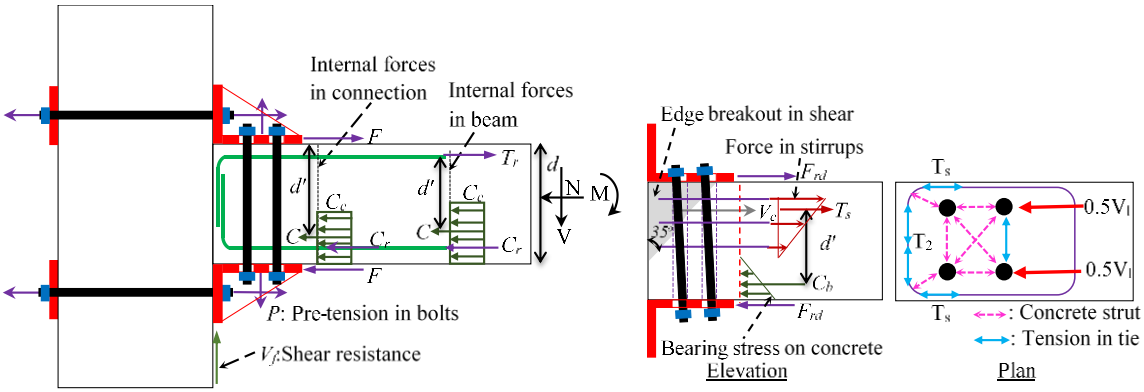

(a) Internal force diagram on beam side before slip (b) Internal force diagram on beam side-after slip

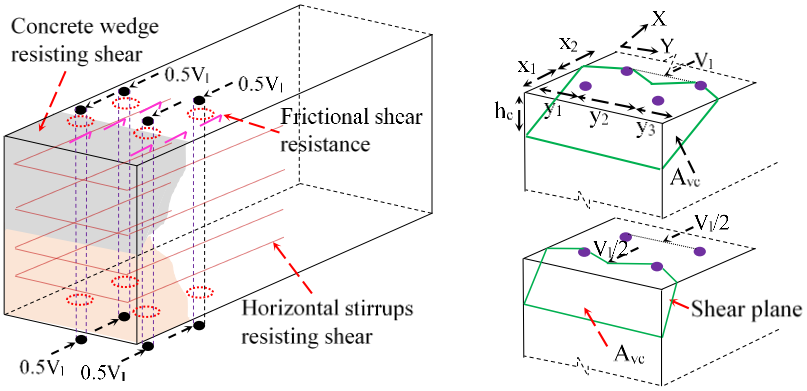

(c) Beam edge breakout mechanism (d) Analytical model to estimate V_c

Figure 3.20. Load transfer mechanism on beam side with Type-2 or 3 connection

The internal force transfer mechanism between the connection and the column depends on whether there is a gap between the beam end face and column face or not, and both mechanisms are pictorially shown in Figures 3.21a and 3.21b respectively. In case of no gap, the beam end compressive stresses are transferred to the column as bearing pressure, and when there is a gap, the compressive stresses are transferred as frictional forces (before slip) or compressive forces (after slip) through the horizontal leg of the connection. The longitudinal shear force (V_l) from the threaded rods on the beam side is transferred as either tensile or compressive forces to the horizontal leg of the connection. Based on initial understanding of the behaviour of angle and tube connections (i.e. Type-2 and 3), they can be categorized as "sliding hinge" (i.e. slip critical) connections. The expected structural performance of sub-assemblies with the proposed connections can only be close to the wet jointed concrete frame system if yielding of the rebars happens before the beam edge failure. The different possible modes of failures within the connection and analytical equations to calculate the internal resistance of the connection are reported in the next section.

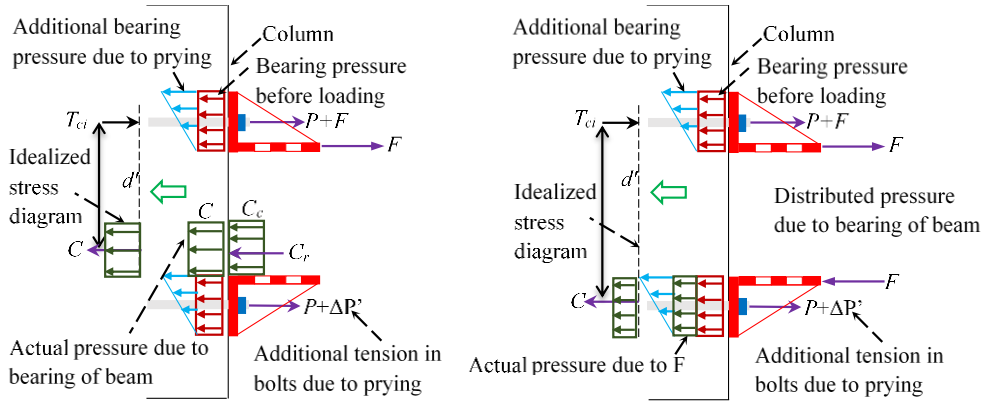

(a) Internal force diagram on column side without gap (b) Internal force diagram on column side with gap

Figure 3.21. Load transfer mechanism on column side with Type-2 or 3 connection

One of the design parameters that controls the behaviour of the proposed connections (especially Type-2 and 3) is the amount of pre-tension in the bolts and is limited to 70% of their tensile yield capacity (which depends on the grade and cross sectional area of the bolts). Also, other criteria such as grade of concrete (induced compressive stress due to pre-tension has to be less than 25% of maximum strength of concrete), and the infill material strength can also limit the pre-tension force in the bolts. As the bolts are pre-tensioned to a value depending on the design criteria, only remaining tensile capacity of the bolts need to be utilized in the evaluation of the connection capacity on the column side. For all types of connections, design criteria for the total amount pre-tension in the bolts on column side is such that vertical slip due to shear force is avoided or kept to a minimum value at the ultimate stage of loading. The required amount of pre-tension in the bolts to resist the shear force (V) is much less compared to the bending moment (M) (i.e. bending moment resistance is frictional resistance times the beam depth). Prying tensile forces (ΔP') may be developed in the bolts on the column and beam sides and additional bearing pressure can be exerted onto the column due to bending of the plates of the connections (if plates are thin) or rigid body rotation of some part of the connection as shown in Figures 3.19 and 3.21. These need to be accounted for in the design and evaluation of capacity of the connections.

3.5.3 *Evaluation of the connection capacities*

In general, the connections of the building's structural frame system are classified in three ways; (i) moment of resistance (i.e. full strength, partial strength, and nominally pinned), (ii) rotation stiffness (rigid, semi-rigid, and nominally pinned), (iii) rotation capacity (i.e. ductile, and non-ductile). The behaviour of the connection can be best understood by studying moment versus relative rotation, and the expected moment-rotation behaviour of the proposed connections is shown in Figure 3.22. In this section, analytical equations are developed to

evaluate the ultimate moment capacities of the proposed connections by utilizing the philosophy and idealized stress diagram from the previous section. The overall moment capacity of the connection is the minimum of the connection capacities on the beam and column sides.

Evaluation of the proposed connections' capacity requires identification of the possible modes of failure in the components of the connection such as; (i) weld failure between the rebars and embedded steel plate, (ii) tension/yielding failure of the embedded steel plate, (iii) weld failure between the embedded plates and the end plate, (iv) weld failure between the gussets and steel plates, (v) yielding or buckling of the gussets, (vi) yielding failure of the end plate, and (vii) bolts failure in shear or tension or both. Analytical equations to predict the strength of the components of the connection with respect to the above mentioned modes of failure are reported in Table 3.6.

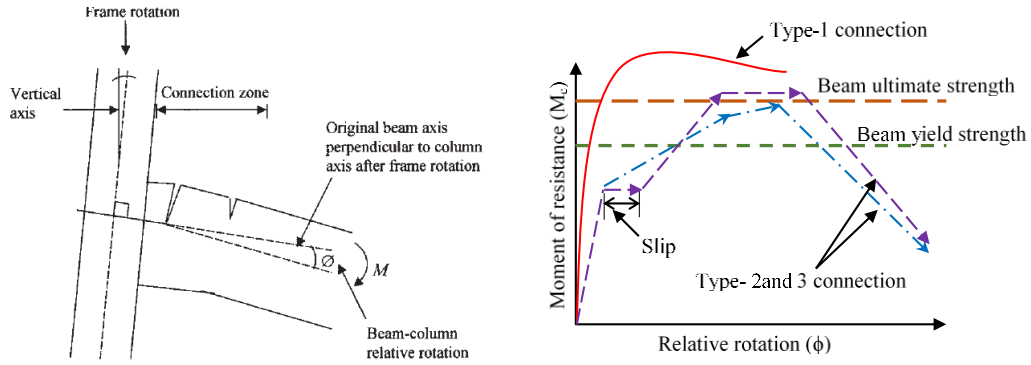

(a) Definition of connection relative rotation [10] (b) Expected moment rotation of the connections

Figure 3.22. Expected moment rotation behaviour of the proposed connections

The idealized stress diagram to evaluate the Type-1 connection's moment capacity on beam and column sides is shown in Figure 3.19. The ultimate moment capacity of the connection is minimum of the connection capacities on the beam and column sides. The moment capacity of the connection on the beam side is equal to the ultimate tensile capacity of the embedded plate times the lever arm as shown Figure 3.19a. The moment capacity of the connection on the column side requires to identify the possible combination failure modes such as; (i) mode-1: yielding of the plate, (ii) mode-2: simultaneous yielding of the plate and bolts failure, and (iii) mode-3: bolts failure, which are pictorially shown in Figure 3.23. To evaluate the capacity for failure modes 1 and 2, complex yield pattern is converted into equivalent yield line as shown in Figure 3.24a, and the formulas for the conversion can be found in the literature [11, 12]. The probable capacity of a bolt row is minimum of capacities of mode 1, 2, and 3 failures. The moment capacity of the connection on the column side is calculated as the sum of the probable capacity of each bolt row times the distance from the center of

compression as shown in Figure 3.19b. Also, the analytical equations to calculate connections moment capacities on beam side and column sides are reported in Table 3.7. As the rebar forces from the beam are directly transferred to the connection, the Type-1 connection can be designed to have more strength than the beam's ultimate capacity by directly applying capacity design principle as shown in Figure 3.21b. Also, the stiffness of the connection is more than the stiffness of the beam as there is no slip between the connection and beam and gussets will increase connection stiffness substantially (which will be cross verified in the next chapter), and the rotation capacity of the frame system will be limited by the rotation capacity of the beam as the connection will be in elastic state.

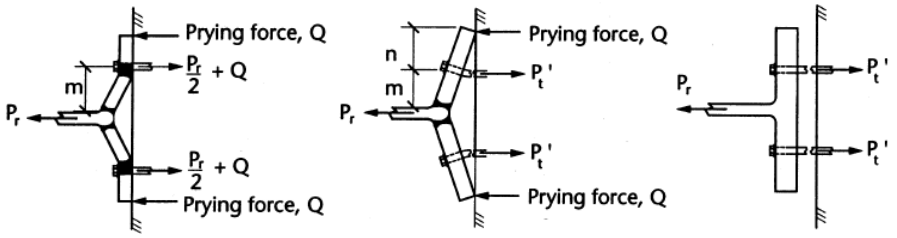

(a) Mode-1 failure (b) Mode-2 failure (c) Mode-3 failure

Figure 3.23. Possible modes of failure of the plate (depending on the plate thickness) [12]

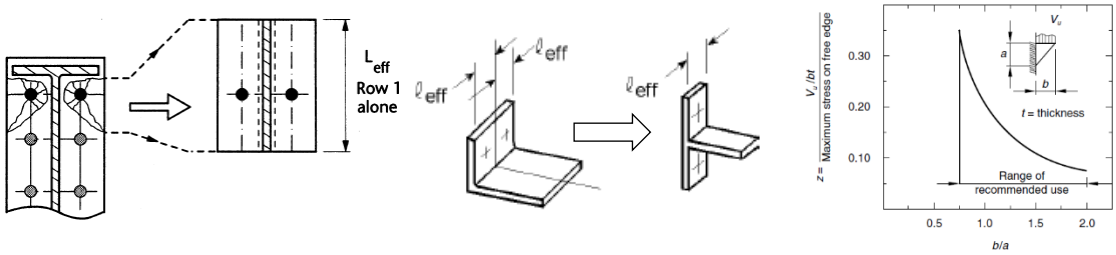

(a) Effective length for end plate (b) Effective length for steel angle (c) Gusset plate limiting stress [13]

Figure 3.24. Equivalent length of end plate and steel angle and limiting stress for gusset plate

There is no literature available on evaluation of the capacities of Type-2 and 3 connections (especially beam edge breakout resistance), but the capacities of these connections can be evaluated by taking the analogy of embedded anchors/dowel bars in concrete under shear force [3, 13-15]. The ultimate moment capacity of the connection on the beam side corresponding to beam edge mechanism is evaluated here in by using this analogy. The overall moment versus relative rotation of the connection is dictated by initiation and extent of the slip (which is controlled by the available frictional resistance) and beam edge breakout resistance, which is schematically shown in Figure 3.22b. The initiation of the slip depends on the available frictional resistance (*F*) which in turn depends on the normal force (P) (i.e. total pre-tension in the bolts) and frictional coefficient (μ_f). In general, the amount of frictional resistance required to avoid the slip between the connection and the beam before the beam reaches its ultimate moment capacity is large and it is not feasible to induce such

high pre-tension in the bolts (given the limitation of the connection size and number of bolts). So, the amount of pre-tension applied to the bolts connecting the connection and the beam is limited to a value such that the slip is avoided before the beam reaches its 2/3rd yield moment capacity (i.e. $0.67M_{yb}$). As mentioned earlier, other criteria such as tensile capacity of the bolts (i.e. amount of pre-tension in the bolts is limited to 70% of its tensile yield capacity), and grade of concrete (i.e. induced compressive bearing stress due to pre-tension has to be less than 25% of maximum compressive strength) can also limit the pre-tension force in the bolts.

The moment of resistance of the connection on the beam side up to the point of initiation of the slip is calculated as frictional resistance (F) times beam depth (gap between the beam and column faces) or frictional resistance times lever arm (no gap between the beam and column faces), which is pictorially shown in Figure 3.20a. After the slip, the ultimate moment of resistance of the connection on the beam side comes from three components; (i) reduced frictional resistance (F_{rd}), (ii) beam edge concrete breakout strength in shear (V_c), and (iii) tensile resistance from the horizontal stirrups located above the pivot point of rotation (T_s) as shown in Figure 3.20b. The ultimate moment of resistance of the connection on the beam side is equal to the sum of the reduced frictional resistance times beam depth and sum of concrete breakout resistance (V_c) and tensile resistance of horizontal stirrups (T_s) times the lever arm. The transitional and moment equilibrium equations to estimate the ultimate moment of resistance of the connection after the slip of the connection on the beam side are reported in Table 3.7. The calculation of the ultimate moment of resistance of the Type-2 and 3 connections on the column side is similar to Type-1 connection except in the calculation of the effective yield line (L_{eff}), as shown in Figure 3.24b. More details on this can be found in the literature [11].

As mentioned before, to evaluate the ultimate moment of resistance of the connection on the beam side, it was required to estimate the beam edge concrete breakout strength (V_c). For this, the analytical model showing the two possible shear failure planes and the shear area (A_{vc}) resisting the longitudinal shear force are shown in Figure 3.20d. Out of the two shear planes, the one with less capacity governs the design. Firstly, the shear capacity of the embedded anchor un-influenced by multiple nearby anchors and beam edge boundaries is computed [3, 13, 14]. Then, the estimated shear capacity is modified by a series of factors to arrive at the final beam edge breakout strength (V_c). The final form of the equations are taken from the different codes and reproduced in Table 3.7 (for detailed calculations refer to Appendix D), and more details can be found in the literature [3, 13, 14]. In Figure 3.20d, "h_c"

is the embedded depth of the threaded rod (it was assumed as half of beam depth), x_1, x_2, y_1, and y_2 represent the distance to the steel ducts from the edges. It important to note that the contribution of concrete breakout resistance (V_c) is small compared to the horizontal stirrup tensile resistance (T_s).

Table 3.7. Equations to evaluate connection's resistance for different modes of failure

Mode of failure/ connection resistance		Equation
Embedded steel plate in tension (only for Type-1 connection)		
Yield resistance of the embedded steel plate in the beam		$T_p = btf_{yp}$
		$T_p = (bt - ndt)f_{yp}$
Weld resistance between rebars and embedded plate		$T_w = \left(\frac{f_{yw}}{\sqrt{3}}\right) t_w l_w$
Weld resistance between embedded plate and end plate		$T_w = \left(\frac{f_{yw}}{\sqrt{3}}\right) 2t_w b$
Type-1 connection: Moment of resistance of the connection on beam side		
Moment of resistance of the connection		$M_c = T_p d'; C_c + C_p = T_p$
Type-2 and 3 connection: Moment of resistance of the connection on beam side		
No slip between the connection and the beam	No gap	$M_c = Fd'; C_c + C_r = F; F = \mu_f P$
	Gap	$M_c = Fd; C_c + C_r = F; F = \mu_f P$
After slip between the connection and the beam		$M_c = (T_s + V_c)d' + F_r d;$ $T_s = n_s A_s f_y; F_r + T_s + V_c = F_r + C_b$
Type-1 to 3 connection: Moment of resistance of the connection on column side		
Mode 1: Yielding of the plate before bolt failure		$P_{r1} = \frac{4M_p}{m}$; $M_p = \frac{L_{eff} t^2 f_y}{4}$
Mode 2: Yielding of the plate and bolt failure		$P_{r2} = \frac{2M_p + n\sum P_t'}{m+n}$
Mode 3: Bolt failure before yielding of the plate		$P_{r3} = \sum P_t'$
Potential resistance of each row of bolts in tension		$T_{ci} = \min(P_{r1}, P_{r2}, P_{r3})$
Bolt force distribution in the calculation of connection resistance		$T_{c1} = [Capacity\ of\ row\ 1\ alone]$ $T_{c2} = Min\begin{bmatrix} Capacity\ of\ row\ 2\ alone \\ Capacity\ of\ row\ 2\ and\ 1 - T_{c1} \end{bmatrix}$
Moment of resistance of the connection		$M_c = \sum T_{ci} d'; C = \sum T_{ci}\ ; C = (\alpha f_c')b(\beta a)$
Type-1 to 3 connection: Shear resistance of the connection		
Shear resistance of the connection until no slip		$V_f = \mu_f P$
Final shear resistance of the connection after slip		$V_u = 0.6 f_{ub} A$
Bolts resistance for combined shear and tension		$\frac{V}{V_u} + \frac{T}{1.4T_c} \leq 1$ or $V_c = \sum^x V_{cc} + 0.28\sum^y V_{ct}$
Gusset plate/stiffener		
Shear capacity of the gusset		$V_g = f_y z b t;$ $z = 1.39 - 2.2\left(\frac{b}{a}\right) + 1.27\left(\frac{b}{a}\right)^2 - 0.25\left(\frac{b}{a}\right)^3$
Gusset thickness limit to avoid buckling		$0.75 \leq \left(\frac{b}{a}\right) \leq 1; b/t \leq 250/\sqrt{f_y}$ $1 \leq \left(\frac{b}{a}\right) \leq 2;\ b/t \leq 250\left(\frac{b}{a}\right)/\sqrt{f_y}$
Concrete breakout strength for a single or multiple-stud connection in shear		
ACI 318-08, NZS 3101-06		$V_c = 0.6(l_e/d_a)^{0.2}\sqrt{d_a}\sqrt{f'_c}(C_{a1})^{1.5}$ $(\Psi_{ec,V}\Psi_{ed,V}\Psi_{c,V}\Psi_{h,V})(A_{vc}/A_{vco})$
PCI design handbook		$V_c = 16.5\lambda\sqrt{f'c}\,(BED)^{1.33}\,(C_{x3}/C_{C3})(C_{h3})(C_{ev3})(C_{vcr})$

Gusset plates were required for all tested connection types to increase the strength and stiffness. The dimensions of the each gusset plate are dictated by the size of the connection. The required number and thickness of gusset plates were designed such that buckling under ultimate compressive load and yielding under ultimate tensile load is avoided. The shear strength of the gusset is limited to factor "z" times yielding based shear strength of the plate.

The value of factor "z" is a function of aspect ratio of the plate dimensions as shown in Figure 3.24d. Also, the thickness of the plate has to be checked against anti-buckling requirement criteria. Summary of the equations to evaluate the strength of the gusset plate are reported in Table 3.7.

3.5.4 *Summary of the tested connections*

The typical layout details of the tested connection configurations are shown in Figure 3.25a, (note the dimensions are shown in millimetres). The actual size of the connection, and the arrangement and number of bolts in each test can be identified from Figure 3.25a and Table 3.8. In all tests, threaded rods were post-tensioned to the values reported in Table 3.8. The threaded rods were tightened using a torque wrench (along with torque multiplier) for the first 6 tests (Tests 1-6). As there is no direct way to measure the pre-tension in the bolts when using a torque wrench for tightening of bolts, the torque was converted to an equivalent pre-tension using the approximate formula $T=0.2PD$, where T is the torque, P is the pre-tension in bolts, and D is the diameter of the bolt [16]. For the last 6 tests (Tests 7-12), the bolts were tensioned using a hydraulic bolt tensioner as shown in Figure 3.25b (which is easy, precise, accurate in measuring the actual tension in the bolts and highly effective for these types of connections). As mentioned before, for Type-2 and Type-3 connection configurations the precast concrete member surfaces had to be level to have uniform contact between the connection and precast members and to transfer pre-tension force effectively, any likely gaps were filled using different types of fill materials. Actual fill materials that were used in different tests can be identified from Table 3.8.

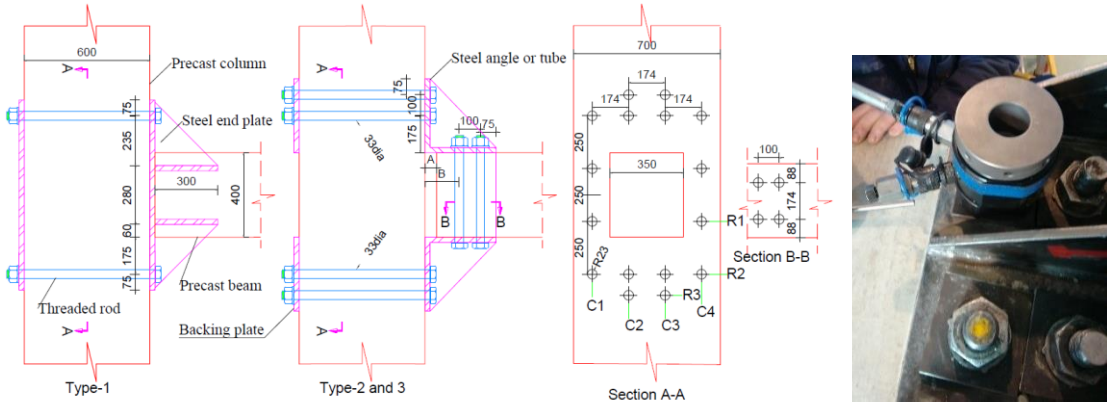

(a) Tested connection configurations (b) Bolt tensioner

Figure 3.25. Tested connections configuration details (refer along with Table 3.8) and bolt tensioner

The capacities of the proposed connections with different configurations were calculated by applying the philosophy and analytical models developed in the previous sections. For all steel connections, it was decided to use 25 mm thick plates and 33 mm diameter threaded rods, accordingly the capacity of the connections was estimated and compared against the demand. The yield and over strength demands on the connection in different tests are reported in Table 3.9. Also, the summary of ratios of connection capacities to yield and over strength demands on beam and column sides are reported in Table 3.9. It is clear from the Table, Type-1 connection's ultimate capacity with Beam-1 is more than over strength demand on both beam and column sides. For Type-2 and 3 connections, it is appropriate to compare the connection's capacity with a nominal yield capacity of the beam rather than over strength demand as the connections are designed to slip before yielding of the beam. It is expected for the sub-assembly with Type-2 or 3 connection and Beam-2 will achieve its nominal lateral strength computed based on the yield moment capacity of the beam (only if the chosen design parameters are reliable). For Beam-4, beam edge failure occurs before yielding of the beam, therefore the sub-assembly will not achieve its nominal lateral strength. The detailed calculation report of evaluation of the connection capacities can be found in the Appendix D. The actual observed behaviour of the sub-assemblies with the proposed connections is reported in the next chapter.

Table 3.8. Summary of number of tests, bolts arrangement and tensions, and fill material

Connection type	**Test no-Ref**	**Gap and location of first duct**		**Layout of bolts on column side**	**Duct on beam**	**Threaded rods**		**Fill material to provide uniform contact area**	
		A (mm)	**B (mm)**			**Torque (N-m)**	**Tension (kN)**	**Beam to connection**	**Column to connection**
Type 1: end plate	7-EP1	N/A	N/A	R1-2&C1-4	N/A	N/A	200*	N/A	N/A
	8-EP2	N/A	N/A	R1-2&C1-4	N/A	N/A	200*	N/A	N/A
Type 2a: angle	2-A1	1-2	165	R2-3&C2-3	UG	2000	300	RS+ DP	RS+ DP
	3-A2	1-2	165	R2-3&C2-3	UG	2250	340	DP	DP
	5-A3	40	125	R2&C1-4	UG	2250	340	G	RS
	6-A4	1-2	125	R2&C2-3	G	2250	340	G	RS
	12-A5	40^	125	R2-3&C2-3	G	N/A	375	G	N/A
Type 2b: angle + web plate	1-AWP1	75	90	R2-3&C2-3	UG	1600	240	RS	RS
	4-AWP2	65	90	R2-3&C2-3	UG	2250	340	DP	DP
Type 3: tube	9#-T1	1-2	125	R2&C2-3	UG	N/A	300	G	N/A
	10-T2	0	125	R1-2&C1-4	G	N/A	200*/300	G	N/A
	11#-T3	1-2	125	R2&C2-3	UG	N/A	375	ER	ER

Note: "UG", "G" represents ducts are un-grouted and grouted, tension in each bolt on beam and column sides is same unless specifically represented with "*" which represents on column side only. "#" represents steel tube without end plate made out of angles, "RS", "DP", "ER" represents rubber sheet, dental plaster, epoxy resin respectively, "^" represents gap between beam end and column face is grouted.

Table 3.9 Summary of connection capacity to demand with different connection configurations

Type	Test	Demand on the connection				Ratio of connections moment and shear capacity to demand				
						on beam side			on column side	
		Beam Id	M_y	M_o	V_o	Moment at first slip	Ultimate moment		Ultimate moment	Shear at first slip
						(M_c/M_y)	(M_c/M_y)	(M_c/M_o)	(M_c/M_o)	(V_f/V_o)
Type 1	7	Beam-1	402	565	188	NS	NA	1.31	2.17	2.55
	8	Beam-1	402	565	188	NS	NA	1.31	2.17	2.55
Type 2a	2	Beam-2	319	445	148	0.90	1.33	0.96	2.12	4.86
	3	Beam-2	319	445	148	0.68	1.10	0.79	2.12	3.68
	5	Beam-2	319	445	148	0.68	1.10	0.79	1.55	5.51
	6	Beam-2	319	445	148	0.68#	1.10	0.79	0.92	2.76
	12	Beam-4	487	680	225	0.50#	0.77	0.55	1.39	2.67
Type 2b	1	Beam-3	319	445	148	0.72	0.76	0.54	2.12	3.89
	4	Beam-3	319	445	148	0.68	>1	>1	1.58	3.68
Type 3	9	Beam-2	319	445	148	0.60	1.03	0.74	0.92	1.62
	10	Beam-2	319	445	148	0.60#	1.03	0.74	2.76	3.24
	11	Beam-4	487	680	225	0.50	0.77	0.55	0.60	1.33

Note: NS represents no slip for Type-1 connection, # represents no actual slip of the connection due to grout of the ducts on the beam side, but it is the point at which bolts start bear against the ducts and beam edge, * represents the ratio of the is evaluated against the beam ultimate moment capacity rather than yield capacity. Units: moments in kN-m, and shear force is in kN

3.5.5 *Fabrication of the connections*

The Type-1 connection was fabricated by welding the two horizontal steel plates to the steel end plate. The most important fabrication check with Type-1 connection is to ensure that the steel end plates at both ends of the beam are aligned vertically; otherwise beams and floors will not be level. The weld between the end plate and embedded plates has to be full penetration butt weld so that the capacity of the weld is more than the capacity of the embedded plates. For Type-2 connection, steel angles can be standardized (i.e. maximum available size is 300×300×25 mm) or custom made by using the steel plates. In this project, the required angle sizes vary from 250 to 350 mm, and it was decided to fabricate custom made steel angles by welding of the steel plates. The maximum size of the steel tube available for the Type-3 connection is 300 mm and in general concrete dimensions are more than 300 mm, hence custom made steel tubes were fabricated by welding the side plates to the steel angles. It is important to note that the custom made connections involve high fabrication cost and also are not easy to fabricate within tolerance limits.

3.6 Erection and demounting process, and comparison of the connections

3.6.1 *Erection process*

The erection and connection process of precast concrete beam with Type-1 connection (i.e. steel end plate) is similar to a steel beam erection process with end plate connection. Firstly, the beams were aligned to the steel ducts on the column side, then the threaded rods were

inserted through the ducts and the end plate and bolted. By using the bolt tensioner, the bolts were pre-tensioned as shown Figure 3.25b. With Type-1 connection, the required alignment of the bolts and connection was only in the horizontal plane (i.e. along beam length). To connect the precast concrete beam to the column by using Type-2 connection (i.e. steel angle), the sequence of steps to be followed in the erection process are as follows; (i) bottom steel angles were connected to the column and levelled, (ii) beams were placed on top of it and gaps were filled with infill material, (iii) top steel angles were placed and aligned so that threaded rods can pass through the steel angles and the steel ducts, and uneven gaps were filled with infill material, (iv) threaded rods were passed through the ducts and the steel angles, and tightened simultaneously on the beam and column sides by using a bolt tensioner. It is important to note that if the precast concrete specimens and the steel connections were not fabricated within the tolerance limits, then it is impossible to align the connections and the beams. The erection process for the Type-3 connection involves encasing steel tubes at the both ends of the beam followed by grouting the gap between the connection and the beam, erecting the beam along with the connections, and finally connecting to the column by using threaded rods. Type-1 and 2 connections requires alignment of the bolts and the connection in two planes (i.e. along beam length and column height) which requires more time and effort compared to the Type-1 connection.

3.6.2 *Demounting process*

One of the primary aims of the experimental investigation is to assess whether the proposed connections between precast concrete beam and column can be considered as a demountable connection so that the whole building system can also be considered as demountable. Another aspect is whether the damaged beam can be replaced with new beam of either same or higher capacity without modifying the capacity design principle of weak beam–strong column/connection within given limits. The deconstruction process of the beam and the connection followed in the lab was exactly opposite the erection sequence, which can be summarized as; (i) unbolting the connection, (ii) removing the connection components above the beam top surface, (iii) removing the damaged beam with the help of a crane, and (iv) removing the connection components below the beam surface. It was realized that the beams with Type-1 connection can be easily demounted and replaced without much effort at the sub-assembly level. With Type-2 connection, because of the sliding of the connection, the bolts on the beam side had moved away from the initial position, which resulted in some difficulty in removing the bolts and steel angles. Also, Type-2 connection configuration with grouted ducts on the beam side required extra effort in removing the steel angles (as the holes

are fully grouted). Removal of precast concrete beam with Type-3 connection (i.e. steel tube) involved unbolting on the column side and then removing the beam along with connection with the help of the crane.

If the whole building has to be demounted for any reason, then demounting of the components (slabs, beams, columns) can be undertaken from top to bottom of the building with available lifting facilities (i.e. mobile cranes or forklift). It is important to note that demounting of the components from building without structural damage is not as easy as removing beam from the sub-assembly in the lab. This is primarily due to the difficulty of access, and involves propping of the slabs and beams, relative movement between connection components, presence of non-structural elements, and other unexpected challenges. If a building is in reparable damage state after an earthquake, then the exact process of demounting of the damaged components (say beams) after an earthquake (i.e. say from 2 level) and replacing with new ones will not be the same and as easy as demounting the damaged beams and replacing with new ones in the laboratory at sub-assembly level. Before demounting the damaged beams, all the surrounding elements (i.e. precast floors) in that level need to be shored to the bottom of the building. If the damaged components (say beams) are from the perimeter lateral resisting frame, it can be replaced with little effort and available lifting facilities, whereas if the damaged beams are from the internal gravity frames then the exact process of demounting and replacing with new ones is a building specific and exact demounting process need to be worked out. More details of the demounting process of building components at building level are demonstrated in the previous chapter.

3.6.3 *Comparison of the steel connections*

Subjective and qualitative comparative analysis (*SQA*) of the proposed connections (i.e. Type-1 to 3) is performed by considering the ease of specimen's construction in the precast yard, cost of the connection, and ease of fabrication of the connection, and the summary of the analysis is reported in Tables 3.10 and 3.11. In the Table, performance indicators are defined such that the connection, which is the easiest and quickest to erect/dismantle, which poses least demanding tolerance requirements, and which can be reused gets the highest points whereas the connection at the other extreme of these spectra is assigned the lowest points. More explanation about the performance indicators is explained and reported in Table 3.10. The percentage in brackets is the weightage assigned to the different components to arrive at a final score. Based on the final scores reported in Table 3.11, it can be concluded that Type-1 connection (steel end plate) ranks first and is found to be superior in terms of ease of erection and dismantling when compared to the other two connection types.

Table 3.10 Detailed explanation for the performance indicators

Indicators		1	2	3
Specimen's construction		Involves significant level of welding in the yard.	Involves minimal welding in the precast yard.	Involves no welding in the yard.
Connection	Material cost	Relatively large amount of steel compared to other connections.	Relatively less amount of steel compared to the connection with highest steel quantity.	Relatively least amount of steel compared to other connections.
	Ease and cost of connection fabrication	Involves a lot of welding, more time to fabricate and alignment.	Involves medium amount of welding, average time to fabricate and alignment.	Involves least welding, average time to fabricate and alignment.
Erection of the sub-assembly	Ease of connection erection and alignment	Involves many connection elements to be erected and aligned separately.	Involves a minimum number of connection elements to be erected and aligned separately.	Involves no connection elements to be erected and aligned separately.
	Additional preparation	Requires gap fill material, and grouting of ducts on beam side	Requires gap fill material, and no grouting of ducts on ducts.	Requires no gap fill material, and no grouting of ducts.
	Ease of specimen's erection	Requires more tolerance to align beam at both ends and directions.	Requires an average tolerance to align beam at both ends and in one direction only.	Requires less tolerance to align beam at both ends and in one direction only.
Dismantle of sub-assembly	Ease of connection dismantle	Requires more effort to remove bolts in both directions to remove the connection.	Requires average effort to remove bolts in both directions to remove the connection.	Requires less effort to remove bolts in one direction to remove the connection.
	Ease of specimen dismantle	Requires more effort to remove the specimen	Requires average effort to remove the specimen	Requires less effort to remove the specimen
	Reusable components	Less connection components re-usable	Average connection components re-usable	More connection components re-usable

Table 3.11 Qualitative comparison of the proposed connection configurations

Description		Connection type		
		Type-1	**Type-2**	**Type-3**
Ease of precast concrete specimen's construction (30%)		2	3	3
Connection (30%)	Material cost of connection (30%)	2	3	1
	Ease and cost of fabrication (70%)	3	2	1
Erection of sub-assembly (20%)	Ease of connection erection (30%)	3	1	2
	Additional preparation (50%)	3	2	1
	Ease of specimen's erection (20%)	3	1	2
Dismantle of sub-assembly (20%)	Ease of connection dismantle (50%)	3	2	1
	Ease of specimen dismantle (30%)	2	3	2
	Reusable components (20%)	1	3	2
	Average score	2.5	2.4	1.8
	Rank	1	2	3

3.7 Conclusions

This chapter mainly covered an overview of the experimental test programme and its objectives. Component details and load transfer mechanism of the three removable beam-column connections, namely; (i) Type-1: steel end plate, (ii) Type-2: steel angle, and (iii) Type-3: steel tube between precast concrete beam and column is presented. Mechanics based

analytical models to evaluate the capacities of the proposed connections and the summary of the connection capacities with different configurations are reported. Based on the preliminary understanding of the connection behaviour, the Type-1 connection can be categorized as "non-sliding" connection, whereas Type-2 and 3 connections are "sliding" connections. Based on the subjective and qualitative comparative analysis, it can be concluded that Type-1 connection (end plate) ranks first and is found to be superior in terms of ease of erection and dismantling when compared to the other two connection types.

3.8 References

1. NZS1170, *NZS1170: Structural design actions.Part 1*. Wellington, New Zealand: Standards New Zealand, 2002.
2. NZS1170, *NZS1170: Structural design actions. Part 5: Earthquake actions - New Zealand*. 2004: Wellington, NZ.
3. NZS3101, *NZS3101: The Design of Concrete Structures*. 2006, Standards New Zealand Wellington.
4. SAP, *Computers and Structures Inc*. 2013: Berkeley, CA, USA.
5. ACI, *Acceptance Criteria for Moment Frames Based on Structural Testing*, in *Report by ACI Innovation Task Group 1 and Collaborators*. 2001.
6. Baltay, P. and A. Gjelsvik, *Coefficient of friction for steel on concrete at high normal stress.* Journal of Materials in Civil Engineering, 1990. **2**(1): p. 46-49.
7. Rabbat, B. and H. Russell, *Friction coefficient of steel on concrete or grout.* Journal of Structural Engineering, 1985. **111**(3): p. 505-515.
8. Michaels, M. *Coefficients of Friction for Concrete*. 2006; Available from: http://hypertextbook.com/facts/2006/MatthewMichaels.shtml.
9. NZS3109, *Concrete Construction,*. Standards Association of New Zeland, Wellington, New Zealand, 1997.
10. Elliott, K.S., et al., *Can precast concrete structures be designed as semi-rigid frames? Pt. 1: the experimental evidence.* Structural Engineer, 2003. **81**(16): p. 14-27.
11. Eurocode, *3: Design of steel structures, Part 1.8: Design of joints*. 2005, EN-1993-1-8. Brussels: European Committee for Standardization.
12. BCSA, *Joints in Steel Construction: Moment Connections*, in *Steel Construction Institute*. 1997.
13. PCI, *PCI Design Handbook: Precast and Prestressed Concrete*. 2010, MNL-120. 6th ed. Chicago, IL: PCI.
14. ACI, *Building code requirements for structural concrete (ACI 318-08) and commentary*. 2008, American Concrete Institute.
15. Zoubek, B., M. Fischinger, and T. Isakovic, *Seismic response of dowel connections in RC structures*, in *NZSEE Conference*. 2016: Christchurch, New Zealand.
16. http://www.efunda.com. *Torque and Tension in Bolts*, . 2015.

Chapter 4: Experimental, analytical and numerical investigation of demountable frame sub-assemblies with end plate connection

Aninthaneni, P. K., Dhakal, R. P., Marshall, J., and Bothara, J. (2016). "Experimental investigation of dry beam-column moment connections for demountable precast concrete RC frame buildings." New Zealand Society for Earthquake Engineering Annual Conference (NZSEE 2016) Christchurch, 10pp.

4.1 Introduction

4.1.1 *Overview*

This chapter presents in detail the design characteristics and performance evaluation of a dry and demountable end plate connection between precast concrete beams and columns. The load transfer mechanism of the connection as well as evolution/propagation of damage in the connection and the beam together with the sequence of failure modes are discussed in detail. Erection and demounting process of beams with the end plate connection is explained and the challenges that are likely to be encountered in real building are identified. Seismic performance and demountability of the frame sub-assemblies with the end plate connection are experimentally evaluated under quasi-static cyclic loading and the test results are compared with the response predicted using analytical equations developed herein. The hysteresis behaviour of the tested frame sub-assemblies are numerically simulated by using the hysteresis rules developed for monolithic frames, and the importance of the right combination of material models and plastic hinge length in development of moment-rotation backbone curve to rightly capture the strength degradation/capping point is highlighted. The hysteresis behaviour of the tested frame sub-assembly with the end plate connection is compared with the hysteresis behaviour of precast concrete frame sub-assemblies with "wet joints" and "ductile connectors" reported in literature. Finally, based on the test results and numerical analysis the primary question of the research; *whether the structural performance of a "wet jointed" precast concrete frame system can be achieved by a precast concrete beams and columns connected using proposed dry "end plate connection" or not* is answered.

4.1.2 *Background*

Precast concrete frame buildings designed and built to resist lateral seismic forces can be classified into two broad categories such as; “equivalent monolithic” and “jointed” systems [1]. Structural dynamic properties, inertial load transfer mechanism from floors to the foundation, and expected seismic performance of these two systems are quite different. The difference between these two systems lies in the type of connections/joints between the precast concrete components/elements of the lateral load resisting frame system. The equivalent monolithic frame building systems are achieved with the use of “wet/cast-in-situ joints” between the precast concrete components [2]. A ‘‘wet joint” to connect the precast concrete elements uses cast-in-place concrete or grout to fill the splicing closures and the location of the splicing can be either at beam column junction or mid span of the beam. Precast concrete frame buildings with wet connections will then comply with design requirements applicable to monolithic concrete frame buildings. Also, the performance of these buildings in a design basis earthquake will be similar to monolithic concrete frame buildings. For example, in New Zealand and Japan many precast concrete frame buildings with “wet joints” have been built in last three decades [1, 3, 4]. A precast concrete frame system with shell beam and wet joint at the beam column junction is shown in Figure 4.1a.

In jointed frame building systems, the precast concrete building components are connected by using either bonded/un-bonded pre-stressed tendons throughout the building dimensions or steel connections made out of components such as steel billets, steel plates, steel angles and dowels or threaded rods [6, 8-12]. The jointed systems with post-tensioned tendons (i.e. also called PRESS system) do not emulate the behaviour of a monolithic concrete frame building system, but the overall building system can be designed to behave as “ductile” in an earthquake shaking. Also, this system offers the distinct advantage of self-centering with minimal residual deformation after a design level earthquake and buildings have been built by using this technology in New Zealand [12]. As mentioned before, another class of jointed frame building systems is developed by connecting precast concrete elements with use of steel connections. In the past three decades, researchers have developed many steel connection configurations and most of them rely on dowel action for the force transfer between beams and columns, and it has been reported that the most of these connection configurations can be considered as semi-rigid or nominal pin connections [5, 6]. Schematic representations of a steel connection using a steel billet and dowels or welded plate, and a concrete corbel connection using steel angle and dowels are shown in Figures 4.1b and 4.1c, respectively.

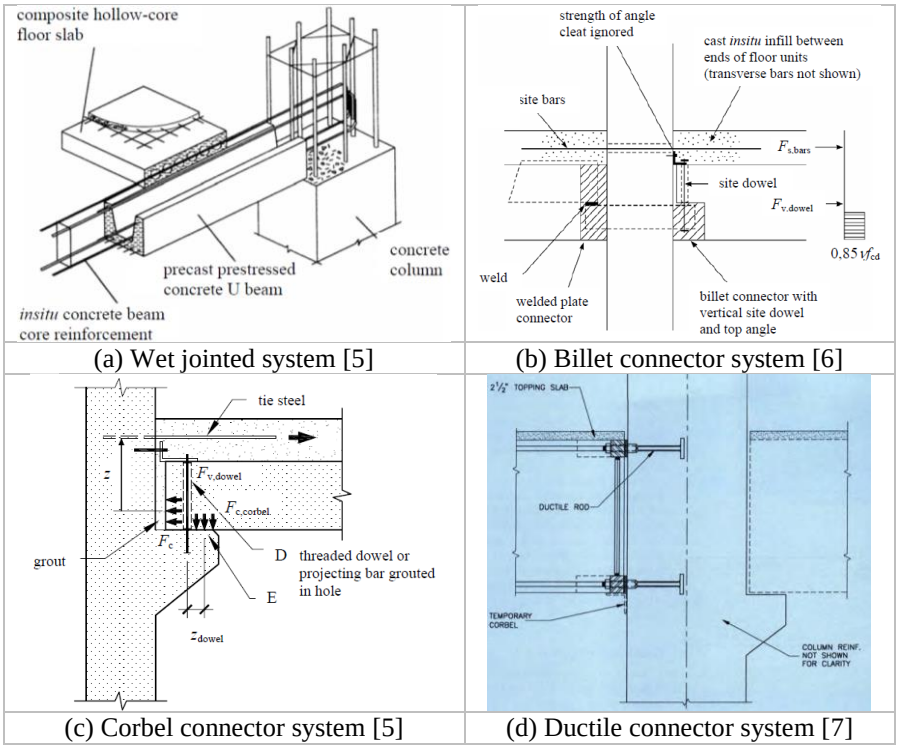

(a) Wet jointed system [5] (b) Billet connector system [6]

(c) Corbel connector system [5] (d) Ductile connector system [7]

Figure 4.1. Examples showing different beam column connection options for a precast concrete frame

To the authors' knowledge, frame building systems with the existing steel connection configurations alone will not emulate the behaviour of wet jointed/monolithic concrete frame buildings, hence they need to rely on other lateral load resisting options such as braces or shear walls [1, 3, 5]. As it can be seen from Figures 4.1b and 4.1c, these connections require concreting or grouting to fill the ducts and gaps, thereby turning the connection into monolithic form and eliminating any possibility of easy removal of the connections. There is another category of jointed frame building system in which the precast concrete elements are connected using "ductile connectors", which is shown in Figure 4.1d. The cyclic behaviour of precast concrete frame with this connection is characterized by severe pinching hysteresis with less energy dissipation, and this system has less seismic performance compared to the monolithic concrete frame system [7].

As the structural elements in precast concrete frame buildings are still being connected by using "wet joints" to resist the lateral loads, the inherent advantages of precast concrete building construction in-terms of construction speed are limited; mainly because of the requirement and setting up of formwork and curing time required before erecting other precast concrete elements. As mentioned before, the building structural system with wet/existing steel connections turns into either fully or partially monolithic in form, enforcing these buildings to be demolished either at the end of the building's life span or when it is decided to construct a new building at the site or the building has suffered irreparable damage after an earthquake or for any other reasons. The demolition process of a concrete building is

environmentally unfriendly and causes extensive wastage of building materials (i.e. concrete and steel). It is reported that Construction and Demolition Waste (CDW) amounts to 17% (this percentage will be much higher after 2010 and 2011 Canterbury earthquakes) and 40% of total landfill waste in New Zealand and Australia respectively [13, 14]. Demolition of concrete buildings requires great amount of energy, it consumes around 275 MJ/t and the crushing of concrete consumes another 85 MJ/t [15]. Demolition of a concrete building is usually time consuming as well, and requires careful planning to avoid any hazard to nearby structures. At the same time, conventional precast concrete buildings which are in a reparable damage state after an earthquake, require considerable downtime to repair in addition to the repair cost to restore its functionality. This will induce substantial seismic losses contributed by direct repair cost, and more significantly by the downtime (i.e. occupancy interruption) [16]. The issues with a precast concrete frame building with "wet or existing steel joints" can be summarized as; (i) to a certain extent construction speed is limited, (ii) building needs to be demolished rather deconstructed and reused, and (ii) damaged building components in an earthquake cannot be replaced. These issues can be addressed with a precast concrete frame building system with fully removable "dry joints", which makes the building demountable and replaceable at any stage.

4.1.3 *Demountable concrete building systems*

There has been limited research work carried out in the development of demountable concrete building systems. The very few efforts available in literature deal mostly with gravity loaded systems in non-seismic regions [17-19]. Five types of demountable concrete building systems were developed and implemented in Netherlands, namely; Mxb-5, CD-20, Bestcon-30, Moducon-2000 and SMT [18, 20, 21]. All these building systems consist of prefabricated building components like slabs, columns, and walls; the only major difference among them is the connection configurations. In Japan, by using the concept of "open building" system, "NEXT21" housing project was implemented as a highly functional flexible building system, and "NOHS" housing project with a flexible floor plan, replaceable non-structural components and a long life of 200 years was developed and implemented [22-24]. In New Zealand, few partially demountable concrete car park buildings relying on braces to resist the lateral loads have been designed and built [25, 26]. However, the main drawbacks of the existing demountable concrete building systems are [27-31]; (i) existing systems have to be demounted as a whole (i.e. from top to bottom of the building), and some systems require partial demolition or removal of grout before dismantle, (ii) existing systems are not structurally flexible (i.e. removal of structural elements is not possible either because

of constrained degree of movement or global pre-stressing of tendons), (iii) no technical information is available on the seismic performance of the existing systems as most of them are developed and built in non-seismic regions, (iv) lack of guidelines to design dry connections for seismic actions, and (v) lack of development of connection configurations that can be applied to custom-made buildings with different layouts and loads to meet client's requirements (i.e. modular building construction). Recently, four point bending tests were conducted on a partially demountable steel end plate connection (which involves breaking of the grout through embedded anchors and cutting of bolts) between protruded corbel of the precast concrete column and precast concrete beam [32, 33]. It has been noticed that the precast concrete beam with this connection cannot be removed in a real building because of its monolithically joint with the floor slabs. Extensive research has been carried out on demountable and interchangeable non-structural elements (i.e. internal partition walls and external facades). Many configurations were developed and implemented to facilitate "functional flexibility" of buildings [34-36].

For these reasons, the authors have developed a low to medium rise precast concrete frame building system which is industrialized, easy to erect/construct, demountable and structurally flexible [37-39]. This building system can also be considered as a low downtime system because it allows for a quick repair/replacement of damaged building components with new ones; thereby minimizing the seismic losses due to occupancy interruption. The building frame structural system is comprised of standard precast concrete elements (i.e. foundations, columns, beams, floor slabs, and non-structural wall panels) and "strong" steel connections. A ''strong'' connection is the one that remains elastic while designated portions of structural members (i.e. beam ends and column bases) undergo inelastic deformations under the design actions. The structural system is similar to conventional frame building system with perimeter lateral load resisting frames and internal gravity load resisting frames, except that all precast elements are removable/replaceable. Steel braces can also be easily added to the lateral load resisting frames because of the steel connections between the precast concrete beams and columns. Full details of the proposed demountable precast concrete building system, possible strong and removable connections between precast concrete building components, process of erection and demounting process of a hypothetical building, and possible advantages in seismic regions are detailed in the literature [37-39].

4.1.4 *Objectives and scope*

The primary objectives of the research study reported in this chapter include; (i) to develop the details of an end plate (EP) connection for the demountable frames and to investigate it's structural performance under quasi-static cyclic loading, (ii) to understand the failure modes of the beam and the connection at different stages of lateral drift, (iii) to check whether the structural performance of beam column sub-assemblies with the proposed EP connection can be compared with the "wet jointed" or "ductile connector" precast concrete frame system, (iv) to investigate the feasibility of replacing a damaged beam with a new beam of the same capacity and achieving the same performance of the original sub-assembly system, and (v) to develop a numerical model that can reliably simulate the cyclic behaviour of the sub-assemblies with the proposed connection. In this chapter, design and cyclic test results of two beam column sub-assemblies with the proposed dry and demountable end plate connection are reported in detail. The basic philosophy in load transfer mechanism between precast concrete beam and column with the proposed connection is explained. Based on the preliminary understanding of the load transfer mechanism, the expected cyclic behaviour of the sub-assemblies and possible modes of failure within the connection and in the beam are identified. Analytical models and idealized stress diagrams are developed to evaluate the ultimate capacity of the connection. Thereafter, overview of the experiments which includes the details of the sub-assemblies, test setup, and loading protocol is briefed. Summary of the capacities of the precast concrete specimens and the proposed connection is reported. Structural performance of the sub-assemblies are evaluated by comparing the experimental test results with analytically predicted values and with the hysteresis results of the "wet jointed" and "ductile connector" sub-assemblies taken from the literature. The cyclic behaviour of the sub-assemblies are numerically simulated using lumped plasticity models in finite element analysis softwares SAP 2000 and Opensees [40, 41]. Numerically simulated results with two different hysteresis rules and with different input backbone curves are compared, and the issues with the macro models in capturing strength degradation are highlighted. Also, the numerically developed hysteresis plots, stiffness degradation, and energy dissipation are compared with experimental results and conclusions are drawn. Finally, the primary question *"whether emulation of the behaviour of a monolithic concrete frame system or precast concrete frame system with "wet joints" can be achieved with the use of precast concrete beams and columns connected by using proposed end plate connection is possible or not"* is answered.

4.2 Description of the end plate connection

4.2.1 *Component details*

The proposed dry connection consists of a steel end plate and two embedded steel plates into the precast concrete beam. The schematic layout of the components of the connection and actual tested connection configuration are pictorially shown in Figures 4.2a and 4.2b, respectively. Depending on the design criteria, the longitudinal rebars of the beam can be either welded to the embedded steel plates or passed through the slotted holes of the embedded steel plates or both. Gussets/stiffeners are required to increase the connection's strength and stiffness and to remain elastic under design actions. To connect the beam to the column, the column was embedded with steel ducts through which threaded rods/bolts are passed and bolted to the end and backing plates. To avoid any visible projections of the connection and to enhance the architecture; (i) the connection can be flushed by providing recess/rebates in surrounding precast concrete components, and (ii) the connection can also be covered with easily removable screed or grout. For example, top gussets can be hidden by providing recess in the slab corners, and bottom gussets can be hidden by ceilings. To eliminate the requirement of temporary support during erection of the beams, the precast concrete columns can be embedded with small rebate (i.e. either small concrete corbel or lug angle). The threaded rods can also be accommodated beside the beam side faces if the column width is at least 200 mm more than the beam width, otherwise they have to be provided above and below the beam.

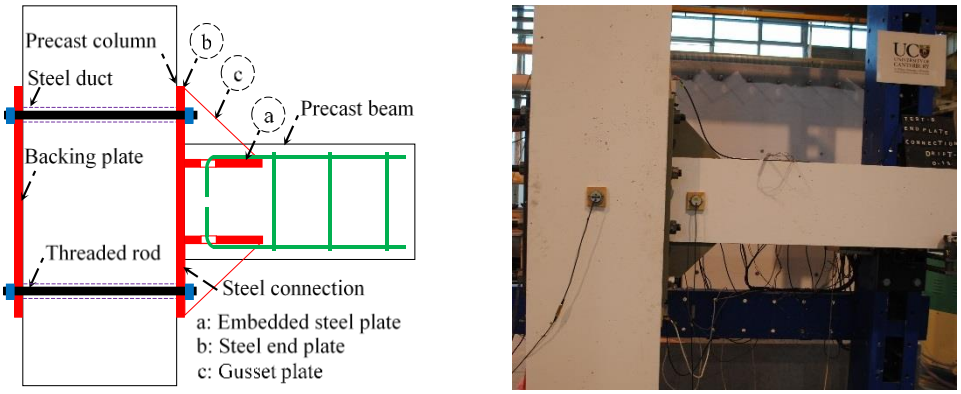

(a) Schematic layout of the components (b) Tested end plate connection configuration

Figure 4.2. Components details of the proposed end plate connection configuration

4.2.2 *Load transfer mechanism*

The basic philosophy in transfer of load between the precast concrete beam and column with the proposed end plate connection is explained herein. The bolts on the column side are pre-

tensioned (P) so that the frictional resistance (V_f) is developed to resist the shear force (V) as shown in Figure 4.3a. When the shear force at the interface of the connection and the column exceeds the frictional shear resistance, the beam slips in the vertical plane and the final shear resistance (V_u) is offered through the shear or bearing failure of the bolts or bearing failure of the concrete beyond the ducts or both. Bending moment (M) generated tensile and compressive forces in the rebars of the beam are directly transferred to the embedded steel plates and concrete compressive stresses of the beam are transferred to the column as bearing pressure as shown in Figure 4.3a. The internal forces in the connection on beam side are transferred to the connection on the column side as tensile force in the bolts and bearing pressure on the column surface, which is schematically shown in Figure 4.3b. In the figure, "*T*" represents a tensile force, "*C*" represents a compressive force, *d*' represents the lever arm, and subscripts "r", "c", "p", and "ci" indicate that the force is on the rebar, concrete, plate, and bolt row, respectively.

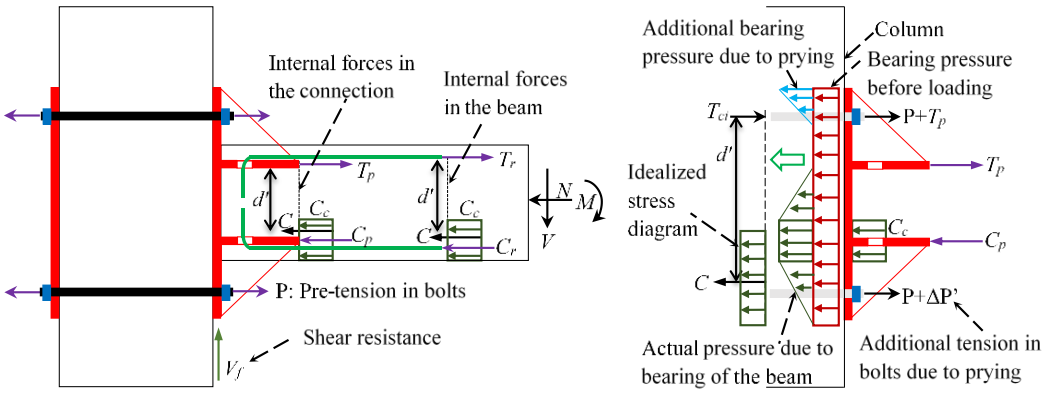

(a) Internal force transfer on beam side (b) Internal force transfer on column side

Figure 4.3. Load transfer mechanism from the beam to the column

One of the major governing design parameter that controls the behaviour of the connection is the amount of pre-tension in the bolts which is limited to 70% of its tensile yield capacity (which depends on the grade and cross sectional area of the bolts). Also, other criteria such as grade of concrete (i.e. induced compressive bearing stress due to pre-tension has to be less than 25% of maximum compressive strength) can also limit the pre-tension force in the bolts as shown in Figure 4.3b. As the bolts are pre-tensioned to a value (depending on the design criteria), only remaining available tensile capacity of the bolts need to be utilized in the evaluation of the connection capacity. The design criteria for the total amount of pre-tension in the bolts is such that vertical slip is avoided or minimal at the ultimate stage of loading. As shown in Figure 4.3b, prying tensile forces (ΔP') in the bolts and additional bearing pressure onto the column surface can be exerted due to bending of the end plate (if plate is thin) or rigid body rotation of part of the connection, which need to be accounted for in the design

and evaluation of connection capacity.

4.2.3 *Evaluation of the connection capacity*

In this section, analytical equations are developed to estimate the ultimate capacity of the end plate connection by utilizing the idealized stress diagrams from Figure 4.3. The ultimate moment capacity of the connection is minimum of the connection capacities on the beam and column sides. The moment capacity of the connection on the beam side is equal to the ultimate tensile capacity of the embedded plate times the lever arm as shown Figure 4.3a. The moment capacity of the connection on the column side requires to identify the possible combination failure modes such as; (i) mode-1: yielding of the plate, (ii) mode-2: simultaneous yielding of the plate and bolts failure, and (iii) mode-3: bolts failure, which are pictorially shown in Figure 4.4a. To evaluate the capacity for failure modes 1 and 2, complex yield pattern is converted into equivalent yield line as shown in Figure 4.4b, and the formulas for the conversion can be found in the literature [42, 43]. The probable capacity of a bolt row is minimum of capacities of mode 1, 2, and 3 failures. The moment capacity of the connection on the column side is calculated as the sum of the probable capacity of each bolt row times the distance from the center of compression as shown in Figure 4.3b. The analytical equations to calculate connection capacities on beam side and column sides are reported in Table 4.1.

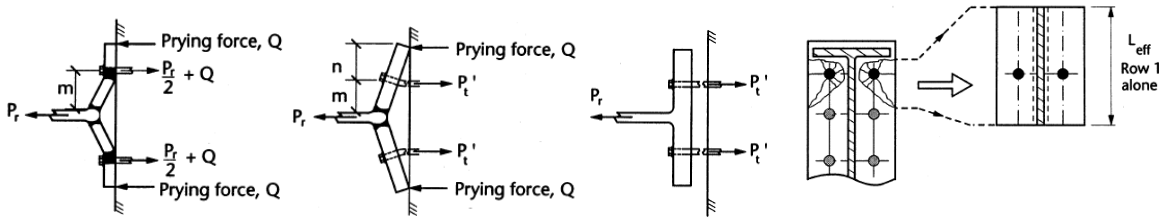

(a) Three possible modes of failure (b) Equivalent yield length

Figure 4.4. Possible modes of failure and equivalent yield length of the end plate [43]

In general, connections of a structural frame system are classified in three ways based on; (i) moment of resistance (i.e. full strength, partial strength, and nominally pinned), (ii) rotation stiffness (rigid, semi-rigid, and nominally pinned), (iii) rotation capacity (i.e. ductile, and non-ductile). The proposed end plate connection can be classified based on moment versus relative rotation as shown in Figure 4.5a. As the internal forces of the rebars in the beam are directly transferred to embedded plates of the connection, the connection can be designed to have more strength than the beam's ultimate capacity by directly applying capacity design principles, which is schematically shown in Figure 4.5b. Endplate connection is commonly deemed as rigid connection because of high relative stiffness (because of gussets) compared to

the stiffness of the beam. The actual connection stiffness can be estimated by component stiffness method detailed in the literature [42]. The rotation capacity of a structural frame system will be limited by the rotation capacity of the precast concrete components as the connection will be in elastic state. The schematic representation of the expected moment versus relative rotation of the proposed end plate connection is shown in Figure 4.5b.

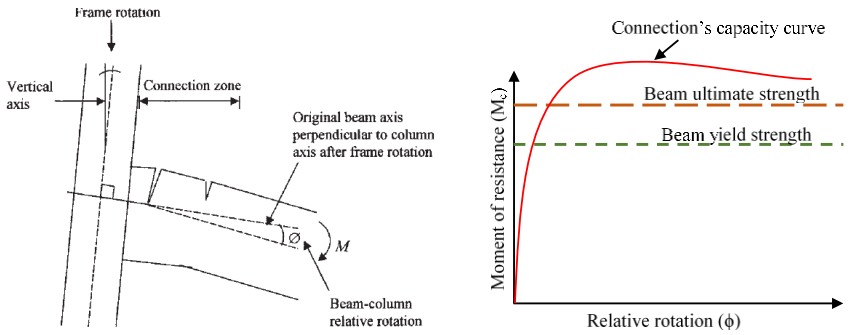

(a) Definition of relative rotation [6] (b) Expected moment rotation

Figure 4.5. Expected moment rotation behaviour of the proposed connection

Table 4.1. Analytical equations to estimate capacity of connection (refer along with Figures 4.3 & 4.4)

Mode of failure/ connection resistance	Equation	No
Moment of resistance of the connection on the beam side		
Moment of resistance of the connection	$M_c = T_p d'; C_c + C_p = T_p$	1
Moment of resistance of the connection on the column side		
Mode 1: Yielding of the plate before bolt failure	$P_{r1} = \frac{4M_p}{m}\ ; M_p = \frac{L_{eff} t^2 f_y}{4}$	2
Mode 2: Yielding of the plate and bolt failure	$P_{r2} = \frac{2M_p + n\sum P_t'}{m+n}$	3
Mode 3: Bolt failure before yielding of the plate	$P_{r3} = \sum P_t'$	4
Potential resistance of each row of bolts	$T_{ci} = \min(P_{r1}, P_{r2}, P_{r3})$	5
Bolt force distribution for calculation of connection resistance	$T_{c1} = [Capacity\ of\ row\ 1\ alone]$ $T_{c2} = Min\begin{bmatrix} Capacity\ of\ row\ 2\ alone \\ Capacity\ of\ row\ 2\ and\ 1 - T_{c1} \end{bmatrix}$	6
Moment of resistance of the connection	$M_c = \sum T_{ci} d'; C = \sum T_{ci}\ ; C = (\alpha f_c')b(\beta a)$	7
Shear resistance of the connection		
Shear resistance of the connection until no slip	$V_f = \mu_f P;\ \mu_f = 0.4$	8
Final shear resistance of the connection after slip	$V_u = 0.6 f_{ub} A$	9
Bolts resistance for combined shear and tension	$\frac{V}{V_u} + \frac{T}{1.4T_c} \leq 1$	10
Note: L_{eff} represents the effective yield length, μ_f is frictional coefficient and for steel to concrete contact it is 0.4, V and T represent the actual shear and tension demand on the bolts.		

4.3 Overview of the experiments

4.3.1 *Test setup details*

The overall experimental test setup with the external beam-column subassembly including details of location of hydraulic actuator and load cell is schematically shown in Figure 4.6a. A beam of length 3.23 m and a column of height 2.95 m were chosen so that the test sub-

assembly approximately represent half of a bay length and storey height of a typical frame building (i.e. the distance between points of contra-flexure). In the figure, "negative" and "positive" represent the directions of loading (hysteresis/load-displacement plots need to be interpreted accordingly). Beam column sub-assemblies were subjected to quasi-static cyclic loading as per ACI loading protocol, which is shown in Figure 4.6b [44]. The sub-assemblies were subjected to three cycles of incremental lateral drift ratios of 0.1%, 0.3%, 0.5%, 0.75%, 1%, 1.5%, 2%, 2.5%, 3%, 4%, and 5%. In this way, it is possible to investigate the strength and stiffness degradation of the sub-assemblies with proposed connection and compare it's response with the hysteresis behaviour of typical wet jointed/ monolithic concrete frame systems.

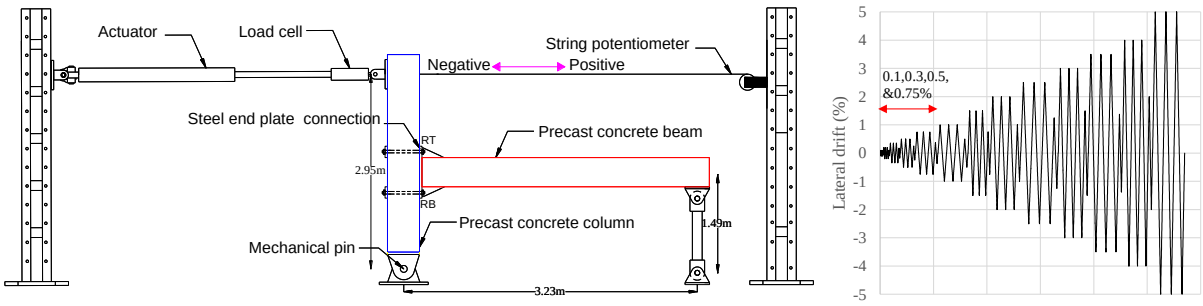

(a) Experimental test setup (b) Quasi-static loading protocol

Figure 4.6. Test setup and loading protocol to evaluate structural performance of the sub-assemblies

4.3.2 *Details of tested sub-assemblies*

Two sub-assemblies (Tests-EP1 and EP2) were designed as per capacity design principles to ensure the lateral load capacity is limited by the ultimate moment capacity of the beam. For the design and evaluation of capacities of the specimens and connection, the material properties summarized in Table 4.2 were used as input. The layout details of the tested end plate connection configuration is shown in Figure 4.7a. The connection was made up of 25 mm thick plates, 10 mm thick gussets, and 33 mm diameter threaded rods. The cross-sectional and reinforcement details of the precast concrete beam and column specimens is shown in Figure 4.7b. Each threaded rod was post-tensioned to 200 kN by using a hydraulic bolt tensioner as shown in Figure 4.7c (which is easy, precise, accurate in measuring the actual tension in the bolts and highly effective for this type of connection). For the estimation of the demand on the connection, nominal yield moment capacity of the beam was amplified by assuming a conservative over strength factor (Ω_o) of 1.4, so that the connection strength is more than the beam strength. The summary of nominal yield capacities of the precast concrete specimens and ratios of the connection capacity to over-strength demand are reported in Table 4.3.

Table 4.2. Summary of the material properties used for specimens and connection capacity evaluation

Material properties		Threaded rod/bolt properties	
Yield stress of steel components (f_{yp})	350 N/mm^2	Grade of bolts	8.8
Ultimate stress of steel components (f_{up})	480 N/mm^2	Yield stress of bolts (f_{yb})	700 N/mm^2
Yield stress of rebars (f_{yr})	500 N/mm^2	Ultimate stress of bolts (f_{ub})	900 N/mm^2
Ultimate stress of rebars (f_{ur})	625 N/mm^2	Net area of bolts (A_{nb})	680 mm^2
Grade of the concrete (f'_c)	40 N/mm^2	Yield capacity of bolts (T_{yb})	475 kN
Grade of the weld E48XXSP (f_{yw})	480 N/mm^2	Ultimate capacity of bolts (T_{ub})	612 kN

It is important to note that length of the connection had to be increased by 100 mm, and width of the column and beam had to be increased by 100 mm and 50 mm respectively than it was initially designed for, this was required in order to cater for different bolt configurations without changing the column given the limitation of available hydraulic jack size in the laboratory. Also, the strength of the column was increased by increasing reinforcement ratio than actually required, this was because the same column was used with beams of higher capacities as well as part of extensive experimental campaign. In practice, the column size can be reduced conforming to capacity design principles and satisfying "strong column-weak beam" strength hierarchy.

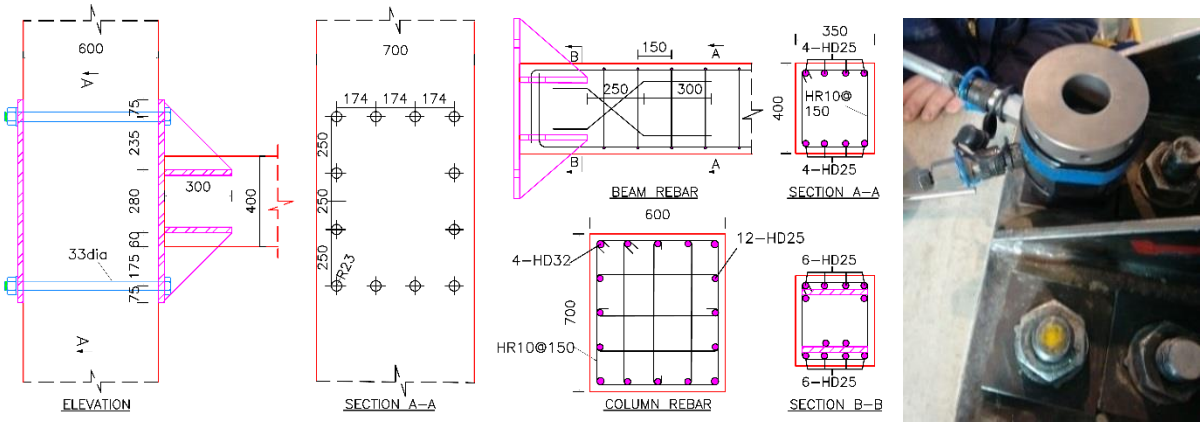

(a) Tested connection configuration (b) Rebar layout in the beam and column (c) Bolt tensioner

Figure 4.7. Layouts of the connection and rebars in the beams and column, and bolt tensioner

Table 4.3. Summary of yield capacities of the specimens and the demand on the end plate connection

S.No	Description	
1	Nominal yield moment capacity of the beam at section B-B (M_{yb})	410 kN-m
2	Nominal yield moment capacity of the beam at section A-A (M_{yb})	319 kN-m
3	Over strength moment demand on the connection (M_o)	565 kN-m
4	Over strength shear demand on the connection (V_o)	188 kN
5	Ratio of yield moment capacity of the column to moment demand (M_{yc}/M_o)	1.70
6	Ratio of moment capacity of the connection to demand on beam side (M_{ucb}/M_o)	1.31
7	Ratio of moment capacity of the connection to demand on column side (M_{ucc}/M_o)	2.17
8	Ratio of shear capacity at initiation of the slip to shear demand (V_f/V_o)	2.55

4.3.3 *Erection and demounting process*

The erection process of the precast concrete beam with end plate is similar to the erection of any steel beam with end plate. Firstly, the beam is aligned such that the holes of the end plate are in line with the steel ducts of the column, and then the threaded rods are inserted through the steel ducts and holes in the end and backing plates. By using the bolt tensioner, the threaded rods are pre-tensioned and clamped on both sides of the column as shown Figure 4.7c. In the lab, the deconstruction sequence of the beam and the connection was exactly opposite of the erection sequence, which can be summarized as; (i) unbolting the connection, (ii) removing the connection components, and (iii) removing the damaged beam with the help of a crane. In general, from this experimental test program, it was realized that the damaged beam with proposed end plate connection can be easily demounted and replaced without much effort at the sub-assembly level.

If the whole building has to be demounted for any reason, then demounting of the components (slabs, beams, columns) in a building can be done from the top to the bottom of the building with available lifting facilities (i.e. cranes or forklift). It is important to note that demounting of the components from a building without inducing any structural damage is not as easy as removing the beam from the sub-assembly in the lab. This is primarily due to the difficulty of access, and involves propping of the slabs and beams, and many other unexpected challenges. Again, if a building is in reparable damage state after an earthquake, then the exact process of demounting of the damaged components (say beams from level-2 of a multi-storey building) after an earthquake and replacing with new ones will not be as easy as demounting the damaged beams and replacing with new ones in the laboratory at sub-assembly level. Before demounting the damaged beams, all the surrounding elements (i.e. precast floors and beams in surrounding bays) in that level need to be shored to the next level down. If the damaged components (say beams) are from the perimeter lateral resisting frame, they can be replaced using available lifting facilities without much complications, whereas if the damaged beams are from the internal gravity frames then the exact process of demounting and replacing them with new ones need to be worked out by accounting for the building orientation, configuration and accessibility. More details on the demounting process of components at building level are reported elsewhere [37-39].

4.4 Experimental test results

4.4.1 *Structural performance*

The structural efficiency of the end plate connection in transfer of load is investigated through quasi-static cyclic tests of two beam column sub-assemblies (Tests-EP1 and EP2). As mentioned before, the primary aim of the test programme was to demonstrate that the structural performance of a precast concrete frame system with "wet joints" can also be achieved by "dry joints". It also investigates the feasibility of replacing a damaged beam from Test-EP1 and replacing with a new beam of the same capacity (i.e. Test-EP2) and achieving the same performance of the original sub-assembly system (i.e. Test-EP1). It is important to note that in both tests, the connection configuration and precast concrete beam layout were the same, hence the hysteresis behaviour of the sub-assemblies should be similar (if not the same). The experimentally obtained hysteresis plots of the two tested sub-assemblies (i.e. Tests-EP1 and EP2) under quasi-static cyclic loading are shown in Figure 4.8, and it is clear that the hysteresis behaviour of both sub-assemblies are similar.

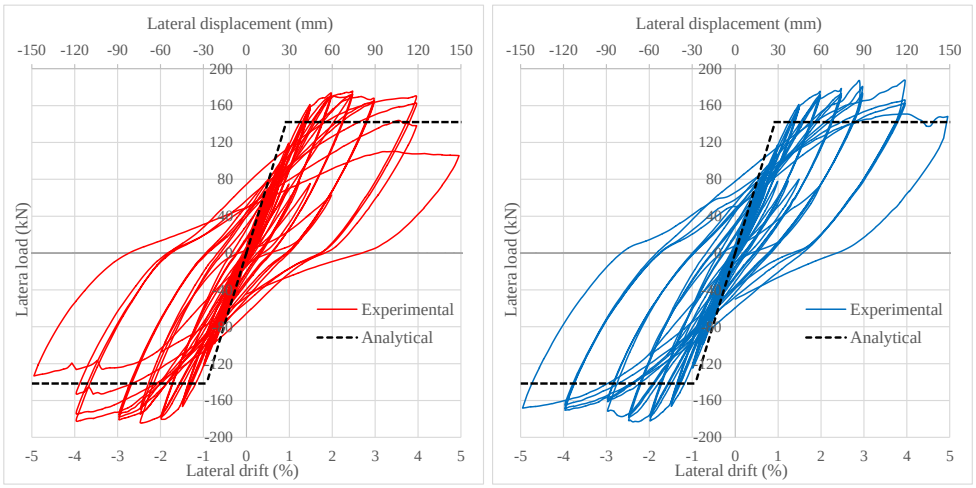

(a) Test-EP1: hysteresis behavior (b) Test-EP2: hysteresis behavior

Figure 4.8. Hysteresis behaviour of the sub-assemblies with the steel end plate connection

As mentioned before, the sub-assemblies were designed as per capacity design principles, so that the nominal lateral strength is limited by the nominal yield moment capacity of the beam. Analytically, by using section analysis method the nominal yield moment capacity of the beam can be computed and for the precast concrete beam with the layout shown in Figure 4.7b, it was 410 kN-m (refer Table 4.3), which is equivalent to the nominal lateral strength of approximately 140 kN for the corner sub-assembly with dimensions as shown in Figure 4.6a. It is evident that in both tests, the sub-assemblies were able to achieve its nominal lateral capacity of 140 kN in both directions of loading and able to sustain the nominal lateral load

up-to 4% lateral drift without much strength degradation. The analytically computed nominal lateral strength of the sub-assembly is shown as horizontal dotted lines in Figure 4.8. The lateral secant stiffness K of the sub-assembly up to the yield point can be calculated by applying any structural analysis method. For the sub-assembly shown in Figure 4.6a, the lateral displacement δ_a under a lateral load V can be estimated by Equation 11, where E is modulus of elasticity of the concrete, y_1, y_2, and y represent respectively the distances from the base of the column to the center of beam, from the center of beam to top of the column, and the total height of the column, and I_{cef} and I_{bef} are the effective moment of inertias of the column and beam, respectively. The rigidity factors are given as $\beta_1 = \frac{D}{2y_1}, \beta_2 = \frac{D}{2y_2}$, and $\alpha = \frac{0.5C+G}{l}$, where D and C are the beam and column depths respectively, and G is gusset length.

$$\delta_a = \frac{Vy_1^3(1-\beta_1)^3}{3EI_{cef}} + \frac{Vy_2^3(1-\beta_2)^3}{3EI_{cef}} + \frac{Vy^2l(1-\alpha)^3}{3EI_{bef}} \quad (11)$$

Here, the lateral secant stiffness K is estimated as the ratio of the lateral load V and lateral displacement δ_a (computed by using Equation 11) for a given lateral load V up to the yield point, which is also shown in Figure 4.8. It can be observed that analytically computed initial lateral secant stiffness of the sub-assemblies is in close agreement with the lateral secant stiffness obtained from the experimental tests. It is important to note that in the analytical formulation (for calculation of both strength and stiffness), it was assumed that the beam column connection is rigid and continuous (which is true only for wet jointed sub-assembly system). By comparison of experimental hysteresis plots with analytically predicted values, it can be concluded the same analytical formulation can also be used to evaluate the lateral strength and stiffness of the sub-assembly with the proposed "dry" end plate connection (this means strength and stiffness of "wet" and proposed "dry" jointed systems are about the same).

The comparison of load displacement backbone curves of the tested sub-assemblies (Tests-EP1 and EP2) is presented in Figure 4.9a and it is clear that the envelopes coincide/overlap up to 2.5% lateral drift. This supports the replace-ability objective of the experimental program; replacement of a damaged beam with new one of similar capacity will result in the structural frame system performing like the original building as it was before an earthquake. The above statement is only true when beams are only damaged and suffered yielding in the rebars whereas other components of the building such as columns, slabs, foundation are still in the linear elastic state. In Test-EP1, it was observed that at higher lateral drift (after 2% lateral drift) the beam was twisting along with bending, this was because of the gap between

the lateral restraint rollers and the beam side faces whereas it was not the case in Test-EP2. Because of this, the difference in load displacement envelopes after 2.5% lateral drift was observed, this difference can also be identified from Figure 4.9a. The measured relative vertical slip between the connection and the column obtained from Tests EP1 and EP2 is shown in Figure 4.9b. It is evident that the slip is less than 0.2 mm and the behaviour of the proposed end plate connection can categorized as "non-slip" as long as frictional shear resistance (V_f) is more than the over-strength shear demand (V_o) on the connection.

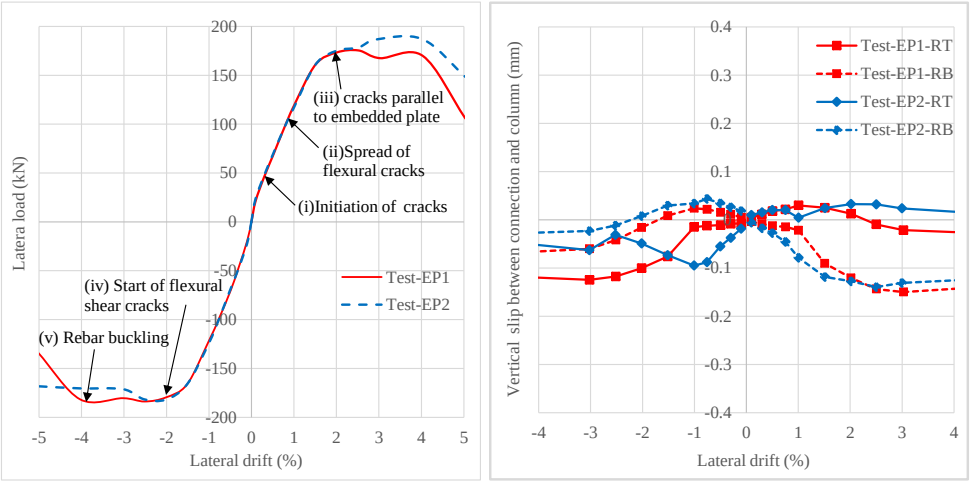

(a) Backbone envelopes (b) Slip envelopes

Figure 4.9. Comparison of backbone and slip envelopes obtained from Tests-EP1 and EP2

4.4.2 *Modes of failure*

The damage observed in the precast concrete beam of the tested sub-assemblies (i.e. Tests-EP1 and EP2) with the proposed end plate connection is similar to typical beam damage that would be observed in monolithic concrete frame or precast concrete frame with wet joints under quasi-static cyclic loading. The observed sequence of damage milestones in precast concrete beam is shown in Figure 4.10; cracking of concrete, spread of flexural cracks, yielding of longitudinal rebars, spread of flexural-shear cracks, spalling of concrete, and bucking of rebars. The detailed modes of failure of the frame sub-assemblies with end plate connections obtained from all tests can be found in Appendix E (refer Figures E.1 and E.2). The location of the maximum damage (i.e. plastic hinge region) in the beam was away from the column face (i.e. in front of the connection), this is because the connection zone is stronger than the beam ultimate capacity.

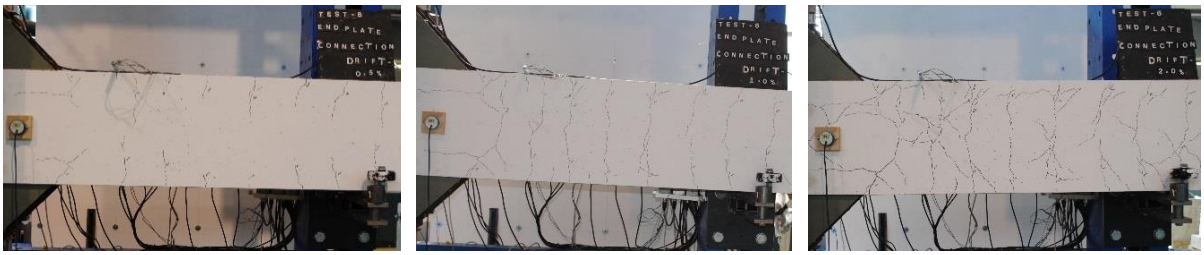

(a) 0.5% drift: initiation of cracks (b) 1.0% drift: spread of flexural cracks (c) 2.0% drift: cracks in connection

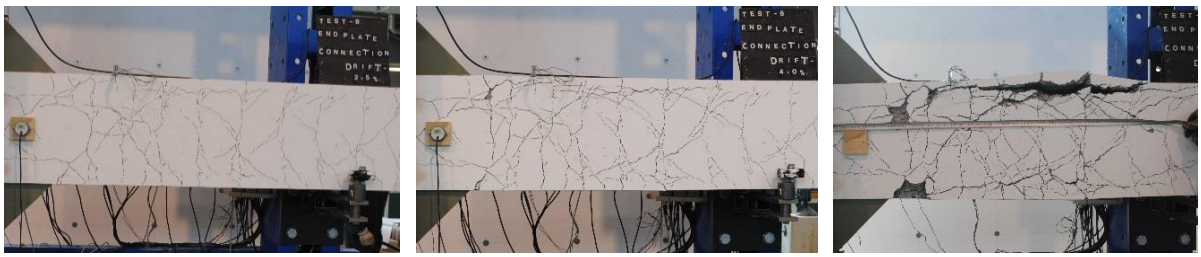

(d) 2.5% drift: flexural-shear cracks (e) 4.0% drift: initiation of rebar buckling (f) 5.0% drift: buckled rebars

Figure 4.10. Damage state of the beam at different lateral drift levels and observed crack patterns

For better representation and interpretation of the observed damage in the precast concrete beam, the actual deformed shape of the sub-assembly with the proposed connection and types of crack patterns observed in and away from the connection zone are schematically reproduced as shown in Figure 4.11. It is clear from the figure that three types of cracks were observed; (i) flexural shear cracks due to influence of shear along with the bending of beam, (ii) horizontal cracks either due to rebar buckling or splitting of cover concrete starting from in front of the gussets, and (iii) horizontal and inclined cracks in the connection zone due to pull and push of the gussets.

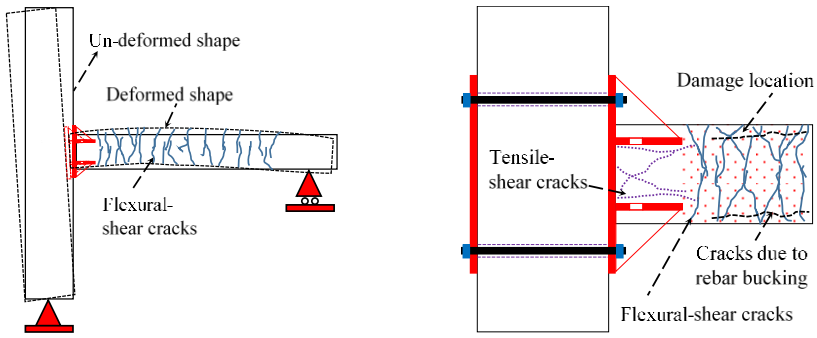

(a) Observed crack patterns (b) Typical damage location

Figure 4.11. Schematic layout of deformed shape of the sub-assembly and crack patterns in the beam

4.4.3 *Comparison of the sub-assembly behaviour with proposed dry connection with sub-assembly behaviour with "wet joints" or "ductile connectors"*

In this section, experimentally obtained hysteresis behaviour of the tested sub-assembly (Test-EP2) with the proposed "dry connection" is compared with two different precast

concrete sub-assemblies taken from the literature with; (i) wet joint, and (ii) ductile connectors. For the first type, a wet/monolithic/cast-in-situ connection that has been implemented in New Zealand for a precast concrete frame building is chosen [45]. In this wet jointed frame system, beams are passed on top of the bottom storey columns and connected at mid span. The protruded rebars of the bottom storey columns are passed through the beams and inserted into the ducts of the upper storey columns and grouted. More details of this system (referred as system-2) can be found in the literature [45]. For the second type, jointed frame system is chosen in which the precast concrete components are connected by using "ductile connectors", which are made up of anchors embedded into the columns and connected to rebars of the beam via couplers. More details of this jointed frame system can be found in the literature [7]. The normalized (with respect to theoretical strength) hysteresis plots of the tested sub-assembly (Test-EP2) and sub-assemblies with "wet joints" and "ductile connectors" are shown in Figure 4.12. It is clear that the cyclic hysteretic behaviour of the sub-assembly with the proposed end plate connection is similar to sub-assembly with "wet joints". When compared to sub-assembly with "ductile connectors", the sub-assembly with proposed connection results in better energy dissipation. This is because the proposed connection is in elastic state while damage comes mainly from the spread of flexural-shear cracks and yielding of rebars in the beam, whereas in sub-assembly with "ductile connectors" the damage is concentrated to the connection region.

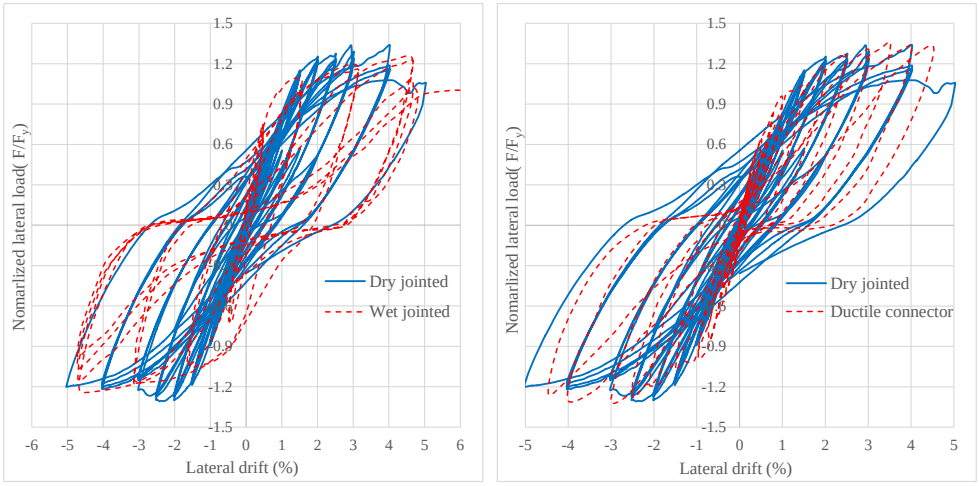

(a) Sub-assembly with "wet joint" (b) Sub-assembly with "ductile connector"

Figure 4.12. Comparison of tested sub-assembly with sub-assembly "wet joint" or "ductile connector"

4.5 Numerical analysis

As it was experimentally found that the hysteresis behaviour of the tested sub-assemblies (Tests-EP1 and EP2) is similar to monolithic frame system (with rigid beam column connections) with the predominant flexural mode of deformation and rebar buckling as the final mode of failure, this hysteresis behaviour should be reliably captured by using existing

concentrated plastic hinge (CPH)/lumped plasticity macro models. In this section, a finite element model is developed for the tested sub-assemblies and numerical analyses are conducted by using structural analysis softwares SAP 2000 and Opensees [40, 41]. A brief overview of the macro models and associated hysteresis rules along with the required input parameters is presented and the numerically simulated hysteresis loops are compared with the experimentally obtained hysteresis plots.

4.5.1 *CPH macro modelling*

The concentrated/lumped plasticity model of a frame member is comprised of an elastic element and zero length springs at both ends in series with the elastic element as shown in Figure 4.13a. For a frame system with predominant flexural nonlinear response, only the rotational spring associated with the moment and the rotational degree of freedom needs to be modelled as a nonlinear spring, whereas other springs (i.e. those associated with shear, axial, and torsion) can be treated as linear without significant error in the prediction of overall hysteresis behaviour. It is important to note that most structural analysis softwares do not account for the interaction between different springs in the nonlinear domain. To simulate the cyclic deterioration of a beam/column element as shown in Figure 4.13b, the backbone curve for the springs need to be developed. Schematic representation of a backbone input curve of the nonlinear rotational spring along with different coordinates that are to be established for a particular beam or column is shown in Figure 4.13c.

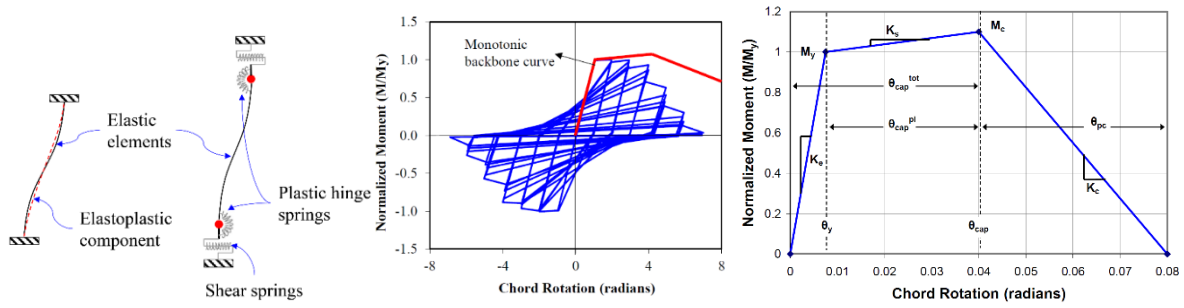

(a) CPH line element model (b) Cyclic deterioration (c) Monotonic backbone cure

Figure 4.13. Concentrated plastic hinge model and cyclic behaviour of the beam/column [46, 47]

Two approaches/methods are used to derive moment rotation backbone curve of precast concrete beams; (i) sectional/fiber analysis method, and (ii) empirical method. In the sectional analysis method, firstly moment curvature curve of the section is developed by utilizing material models of concrete and rebars as shown respectively in Figures 4.14a and 4.14b. The ultimate curvature capacity predominantly depends on the type of concrete (i.e. unconfined/confined) and rebar (i.e. buckling or no buckling) models and ultimate strain

capacity of the concrete and rebars [48, 49]. The moment curvature plots obtained by using different models are shown in Figure 4.14c. In the figure, "UC" and "C" represent respectively the unconfined and confined concrete models, "NB" and "B" represent rebar material model without buckling and with buckling respectively, "Sap" and "Cumbia" represent the plots derived by using softwares SAP2000 and Cumbia, respectively [40, 50]. The main objective of constructing different moment curvature plots is to show that by utilizing a wrong combination of material models, the ultimate curvature of the section is either over or underestimated and as a result strength deterioration cannot be rightly captured. For further study, moment-curvature plot constructed by using confined concrete model and rebar model with buckling is chosen.

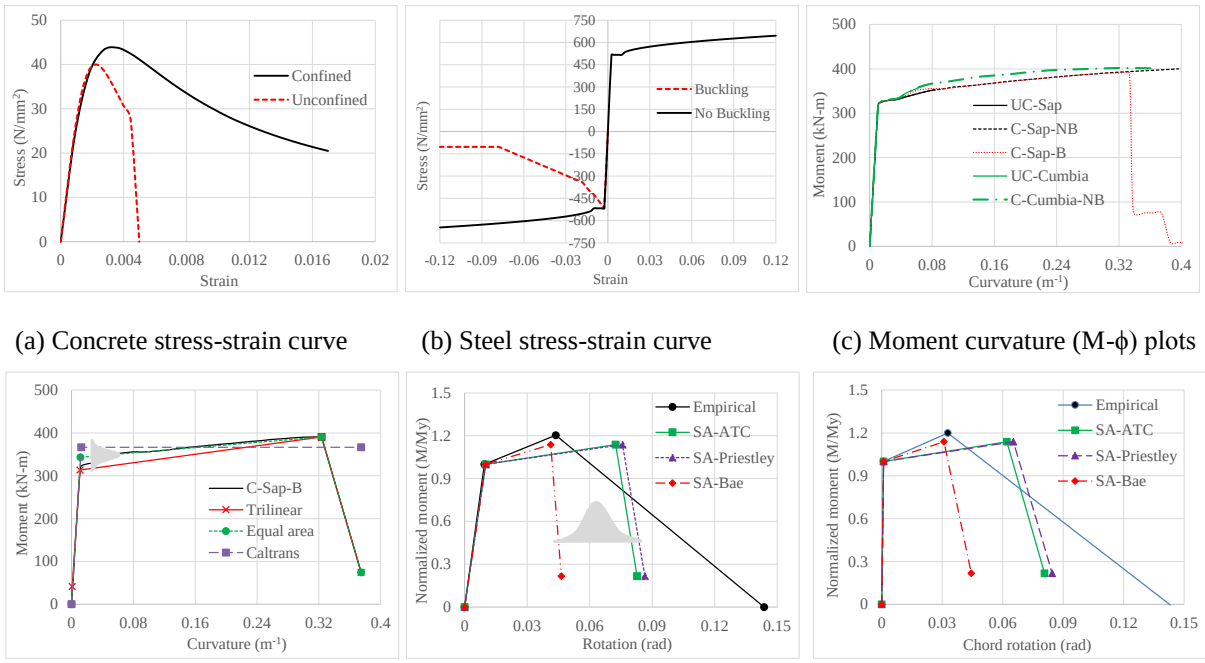

(a) Concrete stress-strain curve (b) Steel stress-strain curve (c) Moment curvature (M-ϕ) plots

(d) Idealization of M-ϕ curves (e) Moment rotation (M-θ) curves (f) Modified M-θ curves

Figure 4.14. Process for development of moment-curvature/rotation of a beam element

Thereafter, the developed moment-curvature curve is idealized either as bilinear or trilinear curves by using existing idealization techniques. Depending on the idealization technique adopted, variation in the yield point (ϕ_y, M_y) is expected. In this study, three idealization techniques are used to show variation in the yield point as shown in Figure 4.14d; (i) trilinear curve connecting cracking point (ϕ_{cr}, M_{cr}) and yield point (ϕ_y, M_y) and ultimate capacity point (ϕ^{tot}_{cap}, M_c), (ii) bilinear curve connecting yield point (ϕ_y, M_y) and ultimate capacity point (ϕ^{tot}_{cap}, M_c) such that the area of the idealized curve is equal to the area of the original M-ϕ curve and the pre-yield stiffness of the idealized curve passes through 0.67 times the yield point ($0.67\phi_y$, $0.67M_y$) of the original curve, (iii) elasto-plastic idealized curve connecting fictitious yield point (ϕ_y, M_c) and ultimate moment capacity point (ϕ^{tot}_{cap}, M_c) such that the

initial stiffness of the idealized line pass through the yield point of original M-ϕ curve and areas of the idealized curve and the original M-ϕ curve beyond the yield point of the original M-ϕ curve are equal. For further study, idealized curves obtained by using the second technique (i.e. bilinear curve with the area equal to area of the original curve) is chosen.

Once the idealized M-ϕ curve is developed, it is converted into moment rotation (M-θ) as follows; yield rotation θ_y is calculated as $\phi_y l/6$ and the plastic rotation θ^{pl}_{cap} is given as $(\phi^{tot}_{cap}-\phi_y)l_p$, where "l" is the clear span of the beam and "l_p" is the plastic hinge length which is a fictitious length over which the plastic curvature is assumed to be constant. Numerous empirical equations have been proposed to estimate the plastic hinge length l_p and till now there is no consensus among researchers [51]. For this study, three different equations; (i) ATC:l_p=0.5D [52], (ii) Priestley: $l_p=0.08l_s$ [51], and (iii) Bae: $l_p=((0.3(P/P_o)+3(A_s/A_g)-1)(l_s/D)+0.25\geq 0.25)D$ [53] are utilized to understand the variation of plastic rotation capacity θ^{pl}_{cap} and its effect on simulating hysteresis behaviour of the sub-assemblies [53]. In the above equations, "D" represents the beam depth, l_s is the shear span, "P/P_o" is the ratio of axial load to capacity, and "A_s/A_g" is the ratio of area of tensile reinforcement to the gross section area. The post yield ultimate rotation capacity $(\theta^{pl}_{cap}+\theta_{pc})$ is calculated as $(\phi^{tot}_u-\phi_y)l_p$ and it is assumed the plastic hinge length is constant even after capping rotation θ^{tot}_{cap}, where ϕ^{tot}_u is ultimate curvature of a section. The moment rotation backbone plots of the section with different plastic hinge lengths are shown in Figure 4.14e. It is clear that there is a wide variation of plastic rotation capacity and the same would be expected in hysteresis behaviour of the sub-assemblies. In the empirical method, yield moment (M_y) and rotation (θ_y) are computed by using cross sectional and dimensional properties, and other points of moment rotation backbone curve such as post yield stiffness (K_s), plastic/pre-capping rotation capacity (θ_p) and post capping stiffness (K_c) and post capping rotation capacity (θ_{pc}) are computed by using empirical equations developed based on numerous experimental tests [54, 55]. Empirically obtained moment rotation curve for the section is also shown in Figure 4.14e.

The moment rotation backbones curves shown in Figure 4.14e need to be modified to correctly simulate linear elastic behaviour of an overall line element (i.e. springs plus the interior elastic element). This modification is necessary because, the flexibilities of the springs and an elastic element are additive and the correct linear elastic solution is only obtained by considering infinite pre-yield stiffness of the spring [56, 57]. But, this will pose numerical instability and make it impossible to express post yield stiffness (K_s) and post capping stiffness (K_c) as fractions of the pre-yield stiffness (K_e) of the spring. So, elastic stiffness of the spring and an elastic element are multiplied by different factors to rightly

capture the elastic behaviour of the overall line element. It is important to note that by modifying the elastic stiffness (i.e. pre-yield stiffness) of the spring, the post yield and the post capping slopes of the spring are also modified. The modified moment rotation (M-θ) curves of the section developed by using section analysis (SA) and empirical method, which are used in the finite element models, are shown in Figure 4.14f.

4.5.2 *Hysteretic behaviour simulation*

To numerically simulate the experimental hysteresis behaviour of the tested sub-assemblies, "Pivot" and "IMK peak-oriented" hysteresis model available in structural analysis softwares SAP 2000 and Opensees respectively are utilized in this study [40, 41, 47, 58]. It is important to note that the simulated numerical line element model has a continuous joint between the beam and column elements, which means it actually represents a wet jointed/monolithic frame system. The cyclic behaviour with the "pivot" hysteresis model is controlled by unloading (α) and reloading (β) stiffness parameters which depend on axial load and longitudinal rebar ratios. For the beam with no axial load and longitudinal rebar ratio of 1.39%, α and β are 6 and 0.6, respectively. The "IMK peak oriented model" captures both strength and stiffness deterioration through two parameters; (i) normalized energy dissipation (λ), and (ii) exponent (c) to describe the rate of cyclic deterioration, and for the tested sub-assemblies λ and c turn out to be 65 and 1, respectively.

The column is modelled as an elastic line element with effective moment of inertia and beam is modelled as three components connected in series (starting from column center line); (i) rigid line element of 0.6 m (from column center line to end of embedded plate in the beam), (ii) zero length nonlinear spring with either Pivot or IMK hysteresis rules and moment rotation backbone curves as input, and (iii) elastic line element with modified effective moment of inertia. The simulated cyclic behaviour of the sub-assemblies (i.e. Tests-EP1 and EP2) with different backbone curves as input and with "Pivot" and "IMK peak oriented" hysteresis models are shown in Figure 4.15. It is clear that both the hysteresis models exhibit the same linear elastic and post yield behaviour up to the peak point. Thereafter, with "IMK peak oriented" hysteresis model post capping strength and stiffness is computed based on the deterioration parameters, whereas with "pivot" hysteresis model reloading stiffness targets previous cycle displacement and follows the backbone curve, which can be noted by comparing Figures 4.15a and 4.15c. The post yield slope of the hysteresis curve depends on the post yield slope of the moment rotation input curve and the variation can be observed in Figure 4.15. Strength degradation of the sub-assembly can only be captured with the right input backbone curve. The construction of right input backbone depends on right

combination of material models and plastic hinge length. It appears that empirically constructed moment rotation curve and moment rotation curve built by using plastic hinge length proposed by Bae [53] are able to capture the strength degradation point.

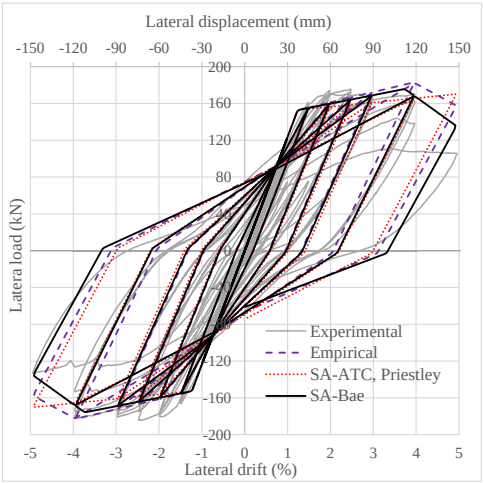

(a) Test-EP1: Pivot hysteresis model

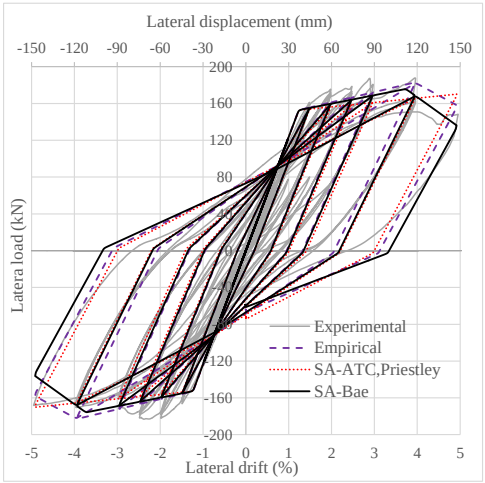

(b) Test-EP2: Pivot hysteresis model

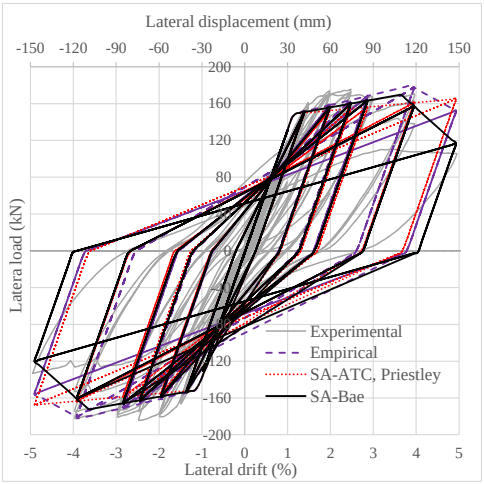

(c) Test-EP1: IMK hysteresis model

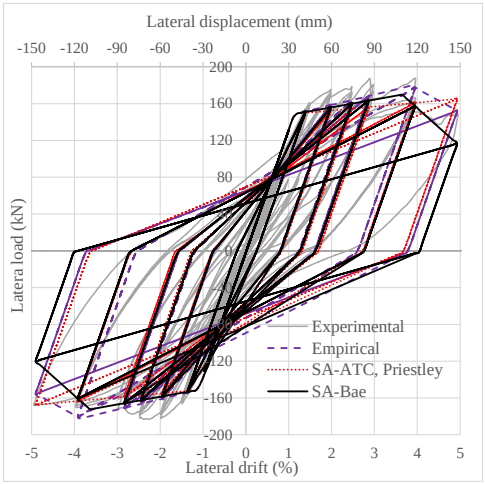

(d) Test-EP2: IMK hysteresis model

Figure 4.15. Comparison of simulated hysteresis loops with different models with test results

By comparing the numerical hysteresis plots with experimental hysteresis plots, it can be concluded that; (i) the nonlinear cyclic behaviour of the precast concrete frame system with the proposed end plate connection can be reliably captured by using zero length nonlinear rotational spring with either “Pivot” or “IMK peak oriented” hysteresis rules, and (ii) the cyclic behaviour of the sub-assembly with the proposed end plate connection is same as cyclic behaviour of a wet jointed/monolithic frame sub-assembly (this conclusion was arrived because as mentioned before in the numerical model the beam column joint was continuous and rigid). The only difference in the numerical modelling of the tested sub-assembly compared to monolithic concrete frame system is that the location of nonlinear rotational spring is shifted from the face of the column to in front of the connection (Figure 4.11b).

4.5.3 *Energy dissipation and stiffness degradation*

In this section, energy dissipation and stiffness degradation characteristics of the sub-assemblies (Tests-EP1 and EP2) are evaluated from the experimental test results and numerical analysis. The energy from each cycle was calculated from the load displacement plots shown in Figure 4.8 and converted into equivalent viscous damping to provide a better understanding of the energy dissipation and pinching characteristics of the sub-assemblies. The equivalent viscous damping ξ_{eq} is calculated as the ratio of energy dissipated E_d in each cycle to the strain energy E_s stored in the corresponding cycle which is given in Equation 12. The lateral secant stiffness is calculated as the ratio of average of peak positive and negative forces to peak positive and negative displacements of the indented drift cycle. In these equations, F_i, F_{i+1} and δ_i, δ_{i+1} represent the load and displacement at steps i and $i+1$ respectively, F_{+ve}, F_{-ve} and δ_{+ve}, δ_{-ve} represents peak load and displacement of each cycle (in the positive and negative loading directions) respectively.

$$\xi_{eq} = \frac{E_d}{4\pi E_s}; E_d = \frac{\sum_i^n (F_{i+1}+F_i)(\delta_{i+1}-\delta_i)}{2}; E_s = \frac{1}{2}\left(\frac{F_{+ve}\delta_{+ve}}{2} + \frac{F_{-ve}\delta_{-ve}}{2}\right) \quad (12)$$

$$K_l = \frac{1}{2}\left(\frac{F_{+ve}}{\delta_{+ve}} + \frac{F_{-ve}}{\delta_{-ve}}\right) \quad (13)$$

By using the above equations, the plots of equivalent viscous damping ξ_{eq} and lateral secant stiffness degradation K_l of the two sub-assemblies with increasing lateral drift are shown in Figures 4.16a and 4.16b respectively. In these figures, legend "Exp" and "Num" represent the plots are obtained from experimental tests and numerical analysis (obtained from SA-Bae hysteresis plots, refer Figure 4.15), respectively. It is evident that both tests exhibit similar damping and stiffness degradation characteristics, which support the replace-ability objective of the experimental test programme (i.e. replacing damaged beam of Test-EP1 sub-assembly with new beam of the same capacity in Test-EP2 and achieving structural performance of Test-EP1 sub-assembly). Also, it can be noticed that both models (i.e. Pivot and IMK peak oriented) have similar capabilities in capturing lateral stiffness degradation and energy dissipation characteristics. As the numerical model is also applicable for wet jointed frame system, it can be concluded that the lateral stiffness degradation and energy dissipation characteristics of the sub-assembly with the proposed end plate connection is about the same as of a wet jointed/monolithic frame system. It is clear from Figure 4.16a that numerical models have no equivalent viscous damping until 1% lateral drift, whereas there is a small amount of equivalent viscous damping obtained from the experiments. This is due to the idealization of the initial behaviour of the sub-assembly as elastic and linear in the numerical models, whereas in reality there is a small amount of energy dissipation due to the formation

and spread of flexural cracks. Also, there is a difference in actual initial lateral stiffness from the experiments and numerical analysis, this is because of idealization of the moment rotation input curve with effective secant stiffness to the yield point (which is considerably less than the initial stiffness computed based on gross sectional properties).

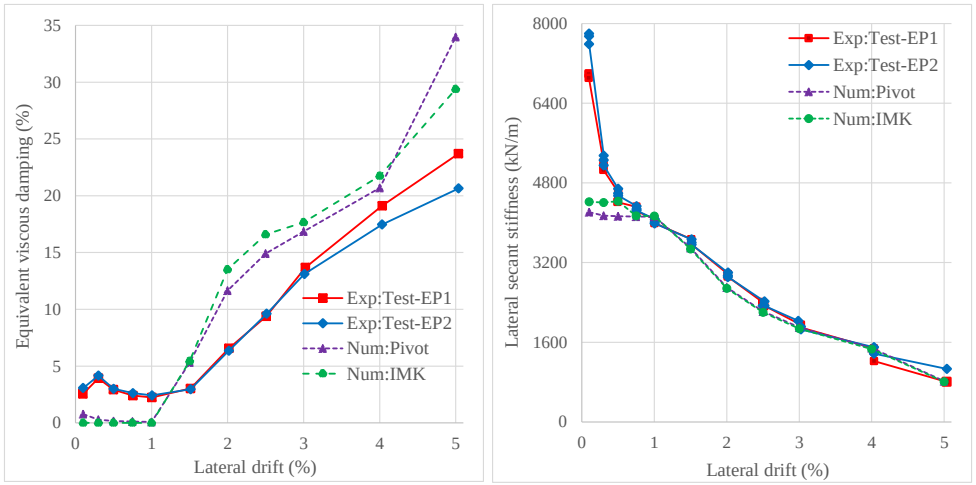

(a) Equivalent viscous damping (b) Lateral stiffness degradation

Figure 4.16. Comparison of damping and stiffness degradation of tested sub-assemblies.

4.6 Conclusions

In this chapter, a detailed description of an end plate "dry" moment resisting connection proposed to be used to connect beams and columns in demountable precast concrete frames is provided. The load transfer mechanism and analytical equations to evaluate the capacity of the connection are explained. An experimental test programme undertaken to evaluate the cyclic performance of precast concrete beam column sub-assemblies with the proposed connection is reported. Based on the experimental test findings, analytical prediction, numerical analysis, and comparison of the end plate connection sub-assemblies performance with "wet jointed" and "ductile connector" frame systems, the following important conclusions with regard to the structural behaviour of precast concrete frames with the proposed end plate connection can be made:

1. Structural performance of a frame sub-assembly with end plate connection in terms of nominal lateral strength and initial lateral stiffness is about the same as wet jointed/monolithic concrete frame system.
2. Existing analytical equations developed originally for monolithic frames can reliably predict the nominal lateral strength and stiffness of frames with the proposed end plate connection.

3. The sequence of damage and the mode of failure in a precast concrete beam with end plate connection is similar to the damage that will occur in the beam of a wet jointed/monolithic concrete frame system.
4. Cyclic behaviour of frame sub-assemblies with the proposed connection is similar to that of a wet jointed precast concrete frame system, and has better energy dissipation characteristics compared to frames with ductile connectors.
5. Existing numerical models developed for monolithic frames such as "Pivot" and "IMK peak oriented" can reliably capture the hysteresis behaviour of a frame with the proposed end plate connection.
6. Emulation of structural behaviour of wet jointed/ monolithic concrete frame system can be definitely achieved by precast concrete beams and columns connected by the proposed end plate connection.
7. Provided damage in a frame is restricted to beams only, replacement of damaged beams in a demountable precast concrete frame with new ones of the same capacity will result in the frame performing as it was in the original frame before the damage.

In the experimental test programme, the end plate connection between precast concrete beam and column was found to be demountable, and the beam could be dismantled and replaced with a new one without much effort. It is important to note that demounting of the components from a building without structural damage is not as easy as removing the beam from the sub-assembly in the lab. This is primarily due to the difficulty of access, and involves propping of the slabs and beams, and many other unexpected challenges. By using the proposed end plate connection to connect the precast concrete beams and columns in a frame building results in the following advantages compared to conventional concrete frame buildings; (i) the building does not need to be demolished; it can be demounted and the undamaged components can be reused, (ii) the damaged building components (i.e. mostly beams if the capacity design principles are followed in the building design) in an earthquake can be replaced with new ones in relatively quick time, thereby bringing the damaged building to the pre-earthquake stage, and significantly reducing seismic losses contributed by downtime required to repair and restore a damaged building.

4.7 References

1. fib, *Seismic design of precast concrete building structures.State-of-the-art report*. 2003, Lausanne, Switzerland. 262.
2. Restrepo, J.I., R. Park, and A.H. Buchanan, *Seismic behaviour of connections between precast concrete elements*. 1993: University of Canterbury, Department of Civil Engineering.
3. Park, R. *The fib state-of-the-art report on the seismic design of precast concrete building*

structures. in *2003 Pacific Conference on Earthquake Engineering in Auckland, New Zealand, Paper*. 2003.

4. Bull, D. and R. Park, *Seismic resistance of frames incorporating precast prestressed concrete beam shells.* PCI JOURNAL, 1986. **31**(4): p. 54-93.
5. fib, *Structural connections for precast concrete buildings*. 2008, Lausanne, Switzerland,. 262.
6. Elliott, K.S., et al., *Can precast concrete structures be designed as semi-rigid frames? Pt. 1: the experimental evidence.* Structural Engineer, 2003. **81**(16): p. 14-27.
7. Englekirk, R., *Development and testing of a ductile connector for assembling precast concrete beams and columns.* PCI journal, 1995. **40**(2): p. 36-51.
8. Elliott, K.S. and C. Jolly, *Multi-storey Precast Concrete Framed Structures*. 2013: Wiley Online Library.
9. Negro, P. and G. Toniolo, *Design guidelines for connections of precast structures under seismic actions*. 2012: Publications Office.
10. Mohamed, S.A.M., *Behaviour of sleeved bolt connections in precast concrete building frames*. 1992, University of Southampton.
11. Bournas, D.A., P. Negro, and F.J. Molina, *Pseudodynamic tests on a full-scale 3-storey precast concrete building: behavior of the mechanical connections and floor diaphragms.* Engineering Structures, 2013. **57**: p. 609-627.
12. Priestley, M.N., et al., *Preliminary results and conclusions from the PRESSS five-story precast concrete test building.* PCI journal, 1999. **44**(6): p. 42-67.
13. Storey, J.B., et al., *Report 6 - The state of deconstruction in New Zealand*, in *Deconstruction and Materials Reuse - an International Overview*. 2005, in - house publishing: Rotterdam (Netherlands). p. approx. 92 p.
14. Crowther, P., *Report 1 - the state of building deconstruction in Australia*, in *Deconstruction and Materials Reuse - an International Overview*. 2005, in - house publishing: Rotterdam (Netherlands). p. approx. 32.
15. Reinhardt, H.W., *Demountable concrete structures - an energy and material saving building concept.* Int. J. Sustainable Materials and Structural Systems, 2012. **Vol. 1**(No. 1): p. pp.18–28.
16. Mary, C. and B. Howard, *Estimating Downtime from Data on Residential Buildings after the Northridge and Loma Prieta Earthquakes.* Earthquake Spectra, 2010. **26**(4): p. 951-965.
17. Reinhardt, H.W., *Demountable concrete structures? Inaugural lecture at Delft University of Technology (in German).* Cement, 1976. **28**(No 6): p. 266-273.
18. Rijksgebouwendienst, M.V.V., *Demontabele bouwsystemen in beton*. 1996: RGD.
19. Herwijnen, F., *Development of a new adaptable and demountable structural system for utility buildings*, in *International Conference Sustainable Building 2000, 22-25 October 2000, Maastricht, The Netherlands*. 2000, In-house publishing: Rotterdam (Netherlands). p. approx. 3 p.
20. Dorsthorst, B.J.H.t. and T. Kowalczyk, *Report 5 - state of deconstruction in the Netherlands*, in *Deconstruction and Materials Reuse - an International Overview*. 2005, in - house publishing: Rotterdam (Netherlands). p. approx. 19 p.
21. Westra, H. and H. Vos, *Demonstration projects "Industrial, Flexible and Demountable Building" in the Netherlands*, in *20th International Symposium on Automation and Robotics in Construction (ISARC)*. 2003, Technische Universiteit Eindhoven: Eindhoven (Netherlands). p. p.67-70.
22. Kim, J., R. Brouwer, and J. Kearney, *NEXT 21: A Prototype Multi-Family Housing Complex.* Ann Arbor, Michigan: University of Michigan, College of Architecture and Urban Planning, 1993.

23. Okamoto, S., et al. *Design and construction of first skeleton-rent apartment in the private sector*. in *Building for the Future: The 16th CIB World Building Congress 2004*. 2004. Rotterdam (Netherlands): in-house publishing.

24. Osakagas. *Osaka gas experimental residental complex*. 1993; Available from: http://www.osakagas.co.jp/csr_e/charter02/technology.html.

25. Gjerde, M., J. Storey, and M. Pedersen, *A deconstructable car parking building. In an active seismic zone*, in *Deconstruction and Materials Reuse*. 2003, in-house publishing: Rotterdam (Netherlands). p. approx. 8 p.

26. Worldwideparkinggroup. *Cark park buildings in Auckland*. 2006; Available from: http://www.worldwideparkinggroup.com/projects/index.html.

27. Kibert, C.J., *Sustainable construction: green building design and delivery*. 2008: John Wiley & Sons.

28. Sadafi, N., M. Zain, and M. Jamil, *Adaptable Industrial Building System: Construction Industry Perspective.* Journal of Architectural Engineering, 2012. **18**(2): p. 140-147.

29. Geraedts, R., *Success and failure in flexible building; Flexible input leads to flexible output*, in *16th International Conference on*. 2010, Labein Tecnalia Derio: Bilbao (Spain). p. p.73-83.

30. fib, *The fib Model Code for Concrete Structures 2010*. 2010: Fédération Internationale du Béton fib/International Federation for Structural Concrete.

31. Van Gassel, F., *Experiences with the Design and Production. of an Industrial, Flexible and Demountable (IFD) Building System*, in *20th International Symposium on Automation and Robotics in Construction (ISARC)*. 2003, Technische Universiteit Eindhoven: Eindhoven (Netherlands). p. p.209-214.

32. Ong, K., et al., *Experimental investigation of a DfD moment-resisting beam–column connection.* Engineering Structures, 2013. **56**: p. 1676-1683.

33. Zhisheng, L., *Designing Moment-resisting Connection for Disassembly for Implementation in Precast Reinforced Concrete Buildings*. 2013.

34. Sadafi, N., M.F.M. Zain, and M. Jamil. *Industrial and adaptable components for building waste reduction*. in *Clean Energy and Technology (CET), 2011 IEEE First Conference on*. 2011.

35. Sadafi, N., M. Zain, and M. Jamil, *Assessment of industrial and adaptable building components for a residential layout.* International Journal of Physical Sciences, 2012. **7**(2): p. 338-348.

36. Park, J.H., *Demountable and Interchangeable Construction System: R. M. Schindler's Panel Post Construction*, in *Open Building Implementation - The 11th Annual Conference, September 30, 2005*. 2005, in-house publishing: Rotterdam (Netherlands). p. approx. 18 p.

37. Aninthaneni, P.K. and R.P. Dhakal, *Demountable concrete building system for seismic regions: conceptual development.* Journal of Architectural Engineering 2016. **(under review)**

38. Aninthaneni, P.K. and R.P. Dhakal, *Conceptual development: Low loss precast concrete frame building system with steel connections*, in *NZSEE Conference*. 2014: Auckalnd, New Zealand. p. Paper No 44.

39. Aninthaneni, P.K. and R.P. Dhakal, *Demountable precast RC frame building system for seismic regions*, in *International Conference on Earthquake Engineering and Seismology (IZIIS-50).* 2015: Kiel, Germany.

40. SAP, *Computers and Structures Inc*. 2013: Berkeley, CA, USA.

41. Mazzoni, S., et al., *OpenSees command language manual.* Pacific Earthquake Engineering Research (PEER) Center, 2006.

42. Eurocode, *3: Design of steel structures, Part 1.8: Design of joints*. 2005, EN-1993-1-8. Brussels: European Committee for Standardization.

43. BCSA, *Joints in Steel Construction: Moment Connections*, in *Steel Construction Institute*. 1997.

44. ACI, *Acceptance Criteria for Moment Frames Based on Structural Testing*, in *Report by ACI Innovation Task Group 1 and Collaborators*. 2001.

45. Restrepo, P.J., *Seismic behaviour of connections between precast concrete elements.* 1992.

46. Moharrami Gargari, M., *Development of Novel Computational Simulation Tools to Capture the Hysteretic Response and Failure of Reinforced Concrete Structures under Seismic Loads*. 2016, Virginia Tech.

47. Ibarra, L.F., R.A. Medina, and H. Krawinkler, *Hysteretic models that incorporate strength and stiffness deterioration.* Earthquake engineering & structural dynamics, 2005. **34**(12): p. 1489-1511.

48. Mander, J.B., M.J. Priestley, and R. Park, *Theoretical stress-strain model for confined concrete.* Journal of structural engineering, 1988. **114**(8): p. 1804-1826.

49. Dhakal, R.P. and K. Maekawa, *Path-dependent cyclic stress–strain relationship of reinforcing bar including buckling.* Engineering Structures, 2002. **24**(11): p. 1383-1396.

50. Montejo, L.A. and M.J. Kowalsky, *CUMBIA—Set of codes for the analysis of reinforced concrete members.* CFL Technical Rep. No. IS-07, 2007. **1**.

51. Zhao, X., et al., *Plastic hinge length in reinforced concrete flexural members.* Procedia Engineering, 2011. **14**: p. 1266-1274.

52. ATC40, *Seismic evaluation and retrofit of concrete buildings.* Applied Technology Council, report ATC-40. Redwood City, 1996.

53. Bae, S. and O. Bayrak, *Plastic hinge length of reinforced concrete columns.* ACI Structural Journal, 2008. **105**(3): p. 290.

54. Park, R. and T. Paulay, *Reinforced concrete structures*. 1975: John Wiley & Sons.

55. Haselton, C.B. and G.G. Deierlein, *Assessing seismic collapse safety of modern reinforced concrete moment frame buildings*. 2006, Stanford University.

56. Ibarra, L.F. and H. Krawinkler, *Global collapse of frame structures under seismic excitations*. 2005: Pacific Earthquake Engineering Research Center Berkeley, CA.

57. Lignos, D.G. and H. Krawinkler, *Deterioration modeling of steel components in support of collapse prediction of steel moment frames under earthquake loading.* Journal of Structural Engineering, 2010. **137**(11): p. 1291-1302.

58. Dowell, R.K., F. Seible, and E.L. Wilson, *Pivot hysteresis model for reinforced concrete members.* Structural Journal, 1998. **95**(5): p. 607-617.

Chapter 5: Experimental, analytical and numerical investigation of demountable frame sub-assemblies with angle and tube connections

Aninthaneni, P. K., Dhakal, R. P., Marshall, J., and Bothara, J. (2017). "Seismic performance of beam-column sub-assemblies of a demountable precast concrete frame building." *16th World Conference on Earthquake Engineering, 16WCEE 2017* Santiago Chile, January 9th to 13th 2017.

Aninthaneni, P. K., Dhakal, R. P., Marshall, J., and Bothara, J. (2016). "Experimental investigation of dry beam-column moment connections for demountable precast concrete RC frame buildings." New Zealand Society for Earthquake Engineering Annual Conference (NZSEE 2016) Christchurch, 10pp.

Aninthaneni, P. K., Dhakal, R. P., Marshall, J., and Bothara, J. (2015). "Seismic performance of sub-assembly of a demountable precast concrete frame building" Tenth Pacific Conference on Earthquake Engineering: Building an Earthquake-Resilient Pacific Sydney, Australia, Paper 189.

5.1 Introduction

5.1.1 *Overview*

This chapter presents a full description of two types of dry and removable beam column connections for a lateral load resisting frame, namely; angle and tube connections. The basic philosophy in the load transfer mechanism within the frame components with the proposed connections is explained in detail. Also, the possible modes of failure within the connection region which will limit the lateral strength of the frame sub-assembly are identified. Details of the analytical models and equations developed to evaluate the ultimate capacity of the connection on beam and column sides are also reported. Also, a method is introduced to evaluate the ultimate capacity of the connection on beam side corresponding to beam edge failure due to slip of the connection. Details of the overall test programme which includes test setup and number of tests, loading protocol, cross sectional dimensions and rebar layout of the tested specimens, tested connection configuration layouts, parameters varied in each test, summary of the over strength demands on the connections, and capacities of the specimens and connections are reported. Structural performance of the tested frame sub-assemblies with proposed angle or tube connection is evaluated by means of the test results and analytical predictions. The observed sequence of failure modes, schematic representation of the crack

patterns in the beam, and location of severe damage in the beam are reported. The hysteresis behaviour of the frame sub-assemblies are numerically simulated by using two macro modelling approaches. The basis for the two macro modelling approaches, assumptions involved, the process of construction of backbone input envelopes for the nonlinear springs, and parameters required for simulating hysteretic behaviour are summarized. The efficacy of the numerical models is assessed by comparing the structural performance parameters with the test results. Also, the results of the tested sub-assemblies with proposed dry angle or tube connection are compared with the hysteresis plots of the sub-assemblies with "wet joints" and "ductile connectors" taken from the literature. Feasibility of demounting a damaged beam and replacing with a new beam of the same (or higher) capacity and achieving the same (or better) performance compared to the original frame sub-assembly is assessed. Finally, based on the test results and numerical analysis the primary question of the research; *whether the structural performance of a "wet jointed" precast concrete frame system can be achieved by a precast concrete frame system with proposed "dry" angle or tube connection or not* is answered.

5.1.2 *Objectives and scope*

The primary objectives and scope of the research work presented in this chapter are; to investigate the performance of the frame sub-assemblies with proposed angle or tube connection under quasi-static cyclic loading, (ii) to understand the failure modes in the beam and connection at different stages of lateral drift, (iii) to check whether the structural performance of the sub-assemblies with the proposed connection can be compared with the "wet jointed" or "ductile connector" precast concrete frame system, (iv) to investigate the feasibility of replacing a damaged beam with a new beam of the same or higher capacity and achieving the same or better performance compared to the original sub-assembly system, and (v) to develop a numerical model that can reliably simulate the cyclic behaviour of the sub-assemblies with the proposed angle and tube connections. The scope of this chapter includes experimental, analytical and numerical investigation of demountable frame sub-assemblies with angle or tube connection. It is important to note that another variant of angle connection; angle and web plate (AWP) connection was also tested in this research and the test results are not combined with angle connection test results. The summarized details of the frame sub-assemblies with angle and web plate connection (i.e. Test-AWP1 and AWP2), test results, cyclic slip plots, comparison of the structural performance parameters, and numerical simulation results are reported in Section 5.8.

5.2 Description of angle and tube connection configurations

5.2.1 *Component details*

The schematic layout of precast concrete frame sub-assembly with steel angle connection is shown in Figure 5.1a. Gussets were welded to steel angles to increase the connection's capacity and stiffness and to remain elastic under design actions. Steel tube connection was fabricated by welding side plates to top and bottom steel angles shown in Figure 5.1a. Actual tested precast concrete beam-column sub-assemblies with angle and tube connection configuration is shown in Figures 5.1b and 5.1c respectively. To connect the beam to the column, the precast concrete beam and column were embedded with steel ducts through which threaded rods/bolts were passed through and bolted. The ends of precast concrete beam are cast with horizontal stirrups in the connection region to increase beam edge resistance to longitudinal shear force from the bolts and to delay the beam edge failure (which will be explained in detail in the next section), which is also pictorially shown in Figure 5.1a. To avoid any visible projections of the connection and to enhance the architecture; (i) the connection can be flush by providing recess/rebates in surrounding precast concrete components, and (ii) the connection can also be covered with easily removable screed or grout. To eliminate the requirement of temporary support during erection of the beams, the precast concrete columns can be rebated (i.e. either concrete corbel or lug angle).

(a) Layout of the connection (b) Sub-assembly with angle connection (c) Sub-assembly with tube connection

Figure 5.1. Layout of the connection and tested sub-assemblies with angle and tube connections

5.2.2 *Load transfer mechanism*

The basic philosophy in transfer of load between the precast concrete beam and column with the proposed angle and tube connection is explained herein. The bolts on the column side are pre-tensioned (P) so that the frictional resistance (V_f) is developed to resist the shear force (V) as shown in Figure 5.2a. When the shear force at the interface of the connection and the column exceeds the frictional shear resistance, the beam slips in the vertical plane and the

final shear resistance (V_u) is offered through the shear or bearing failure of the bolts or bearing failure of the concrete beyond the ducts or both. The design criteria for the total amount of pre-tension in the bolts on the column side is such that vertical slip is avoided or minimal at the ultimate stage of loading. In these type of connections, there is no direct transfer of the rebar forces of the beam to the connection, hence need to rely on some other mechanisms (such as friction and beam end/edge breakout resistance) so that rebars will enter into yield/plastic state at higher drift levels before bond failure occurs in the connection region due to slip of the connection. To achieve this, bolts are pre-tensioned on the beam side so that the frictional resistance (*F*) is developed between the connection and beam top and bottom surfaces as shown in Figure 5.2a. In the Figures 5.2 and 5.3, "*T*" is tension force either in the longitudinal rebars or steel plates or in the bolts, "*C*" is the total compressive force of either idealized concrete stress block in the beam or due to bearing of the connection on to the column or the longitudinal rebars or steel plates, *d*' represents the lever arm, V_l is longitudinal shear force, and subscripts "r", "c", "p", "ci", s", and "b" represent rebar, concrete, plate, bolt row number, horizontal stirrups, and bearing of bolts on to concrete, respectively.

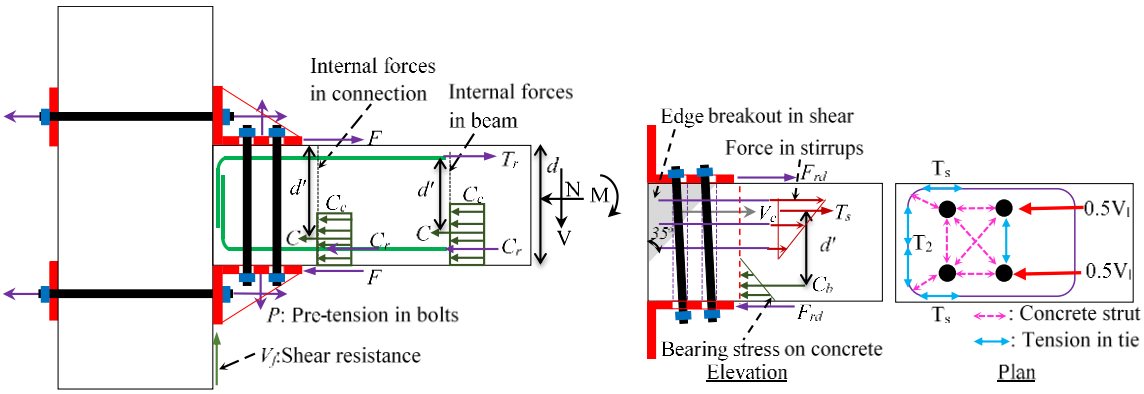

(a) Internal force diagram on beam side before slip (b) Internal force diagram on beam side-after slip

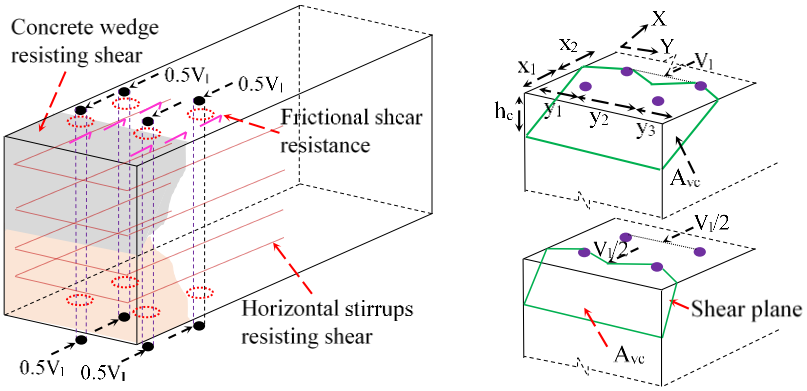

(c) Beam edge breakout mechanism (d) Analytical model to estimate V_c

Figure 5.2. Load transfer mechanism from beam to the connection on beam side

The bending moment (M) transfer from the beam to the connection can be treated as a two stage process. When the frictional resistance is higher than the horizontal interface force due to bending moment (i.e. beam end moment (M) divided by the beam depth (d)), then no slip occurs in the horizontal plane. In such case, the behaviour of the frame with these connections is similar to a cast-in-situ/monolithic concrete frame system (i.e. yielding of the rebar through the development length and spread of flexural cracking along the beam length). The internal force transfer mechanism as the frictional force between the connection and the beam until no slip of the connection is shown in Figure 5.2a. When the induced force exceeds the frictional resistance, the behaviour of the connection comes from a combination of slip between the connection and beam and conventional frame behaviour (i.e. predominant flexural deformation). After the slip, the longitudinal shear force (V_l) from the threaded rods is transferred to the steel ducts as bearing pressure which is being resisted by the concrete beyond the ducts (V_c) and horizontal stirrups (T_s) in the connection region, which are shown in Figures 5.2b and 5.2c. For easier understanding of longitudinal shear force transfer mechanism from the threaded rods to the horizontal stirrups strut and tie model as shown in Figure 5.2b can be utilized. The capacity of the connection on the beam side can be limited to the beam end breakout resistance rather than beam's ultimate moment capacity if the connection slips at an early stage, thereby resulting in bond failure between the rebars and the concrete.

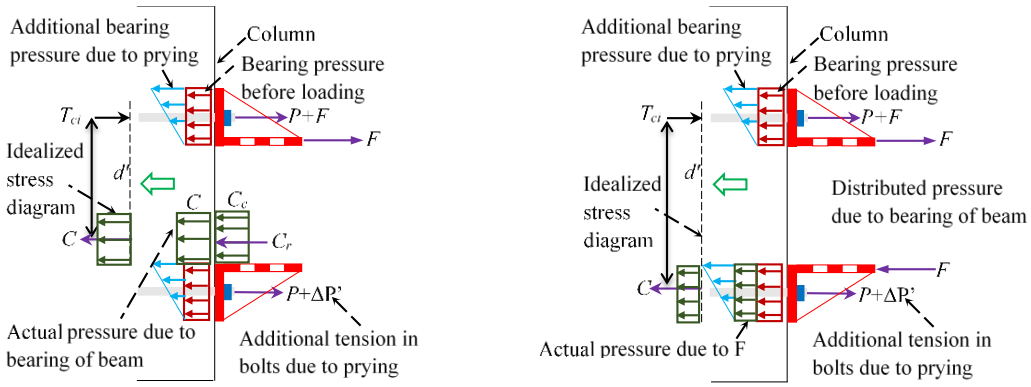

(a) Internal force diagram on column side without gap (b) Internal force diagram on column side with gap

Figure 5.3. Load transfer mechanism from connection to column on column side

The internal force transfer mechanism between the connection and the column depends on whether there is a gap between the beam end face and column face or not, and both mechanisms are pictorially shown in Figures 5.3a and 5.3b respectively. In case of no gap, the beam end compressive stresses are transferred to the column as bearing pressure, and when there is a gap, the compressive stresses are transferred as frictional forces (before slip) or compressive forces (after slip) through the horizontal leg of the connection. The

longitudinal shear force (V_l) from the threaded rods on the beam side is transferred as either tensile or compressive forces to the horizontal leg of the connection. Based on initial understanding of the behaviour of angle and tube connections, they can be categorized as "sliding hinge" (i.e. slip critical) connections. The expected structural performance of sub-assemblies with the proposed connections can only be close to the wet jointed concrete frame system if yielding of the rebars happens before the beam edge failure.

5.2.3 *Evaluation of the connection's capacities*

In this section, analytical equations are developed to estimate the ultimate capacity of the angle and tube connections by utilizing the idealized stress diagrams Figures 5.2 and 5.3. There is no literature available on evaluation of the capacities of such connections (especially beam edge breakout resistance), but the capacities of these connections can be evaluated by taking the analogy of embedded anchors/dowel bars in concrete under shear force [1-4]. The ultimate moment capacity of the connection on the beam side corresponding to beam edge mechanism is evaluated here in by using this analogy. The overall moment versus relative rotation of the connection is dictated by initiation and extent of the slip (which is controlled by the available frictional resistance) and beam edge breakout resistance, which is schematically shown in Figure 5.4.

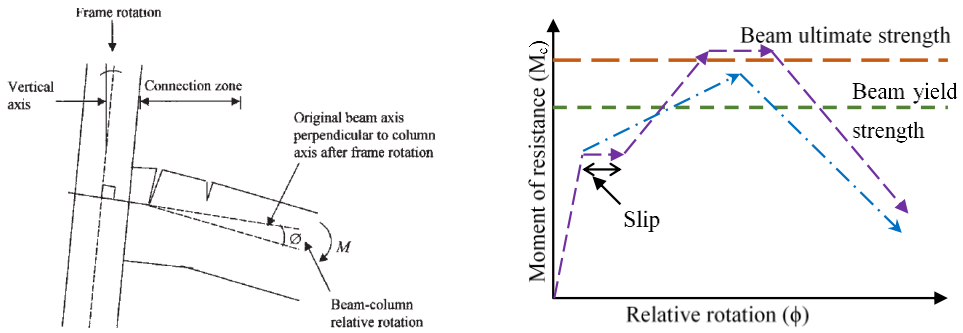

(a) Definition of relative rotation [5] (b) Expected moment rotation

Figure 5.4. Expected moment rotation behaviour of the proposed connection

The initiation of the slip depends on the available frictional resistance (F) which in turn depends on the normal force (P) (i.e. total pre-tension in the bolts) and frictional coefficient (μ_f). In general, the amount of frictional resistance required to avoid the slip between the connection and the beam before the beam reaches its ultimate moment capacity is large and it is not feasible to induce such high pre-tension in the bolts (given the limitation of the connection size and number of bolts). So, the amount of pre-tension applied to the bolts connecting the connection and the beam is limited to a value such that the slip is avoided before the beam reaches its 2/3rd yield moment capacity (i.e. $0.67M_{yb}$). Also, other criteria

such as tensile capacity of the bolts (i.e. amount of pre-tension in the bolts is limited to 70% of its tensile yield capacity), and grade of concrete (i.e. induced compressive bearing stress due to pre-tension has to be less than 25% of maximum compressive strength) can also limit the pre-tension force in the bolts. As the bolts are pre-tensioned to a value (depending on the design criteria), only remaining available tensile capacity of the bolts need to be utilized in the evaluation of the connection capacity. Prying tensile forces (ΔP') in the bolts and additional bearing pressure can be exerted onto the column surface due to bending of end plate (if plate is thin) or rigid body rotation of part of the connection as shown in Figure 5.3, which need to be accounted for in the design and evaluation of connection capacity.

The moment of resistance of the connection on the beam side up to the point of initiation of the slip is calculated as frictional resistance (F) times beam depth (gap between the beam and column faces) or frictional resistance times lever arm (no gap between the beam and column faces), which is pictorially shown in Figure 5.2a. After the slip, the ultimate moment of resistance of the connection on the beam side comes from three components; (i) reduced frictional resistance (F_{rd}), (ii) beam edge concrete breakout strength in shear (V_c), and (iii) tensile resistance from the horizontal stirrups located above the pivot point of rotation (T_s) as shown in Figure 5.2b. The ultimate moment of resistance of the connection on the beam side is equal to the sum of the reduced frictional resistance times beam depth and sum of concrete breakout resistance (V_c) and tensile resistance of horizontal stirrups (T_s) times the lever arm. The transitional and moment equilibrium equations to estimate the ultimate moment of resistance of the connection after the slip of the connection on the beam side are reported in Table 5.1. As mentioned before, to evaluate the ultimate moment of resistance of the connection on the beam side, it was required to estimate the beam edge concrete breakout strength (V_c). For this, the analytical model showing the two possible shear failure planes and the shear area (A_{vc}) resisting the longitudinal shear force is shown in Figure 5.2d. Out of the two shear planes, the one with less capacity governs the design. Firstly, the shear capacity of the embedded anchor un-influenced by multiple nearby anchors and beam edge boundaries is computed [1-3]. Then, the estimated shear capacity is modified by a series of factors to arrive at the final beam edge breakout strength (V_c). The final form of the equations are taken from the different codes and reproduced in Table 5.1, more details can be found in the literature [1-3]. In Figure 5.2d, "h_c" is the embedded depth of the threaded rod (it was assumed as half of beam depth), x_1, x_2, y_1, and y_2 represent the distance to the steel ducts from the edges. It important to note that the contribution of concrete breakout resistance (V_c) is small compared to the horizontal stirrup tensile resistance (T_s), and hence can be ignored.

Table 5.1. Analytical equations to estimate capacity of connection (refer with Figures 5.2 and 5.3)

Mode of failure/ connection resistance		Equation	No
Moment of resistance of the connection on the beam side			
No slip between the connection and the beam	No gap	$M_{fc} = Fd'; C_c + C_r = T_r = F; F = \mu_f P; \mu_f = 0.4$	1
	Gap	$M_{fc} = Fd; C_c + C_r = T_r = F; F = \mu_f P; ; \mu_f = 0.4$	2
After slip between the connection and the beam		$M_{uc} = (T_s + V_c)d' + F_r d;$ $T_s = n_s A_s f_y; F_r + T_s + V_c = F_r + C_b$	3
Concrete breakout strength for a single or multiple-stud connection in shear			
ACI 318-08, NZS 3101-06		$V_c=0.6(l_e/d_a)^{0.2}\sqrt{d_a}\sqrt{f'_c}(C_{a1})^{1.5}$ $(\Psi_{ec,V}\Psi_{ed,V}\Psi_{c,V}\Psi_{h,V})(A_{vc}/A_{vco})$	4
PCI design handbook		$V_c=16.5\lambda\sqrt{f'c}\,(BED)^{1.33}(C_{x3}/Cc_3)(C_{h3})(C_{ev3})(C_{vcr})$	5
Moment of resistance of the connection on the column side			
Mode 1: Yielding of the plate before bolt failure		$P_{r1} = \frac{4M_p}{m}$; $M_p = \frac{L_{eff}t^2 f_y}{4}$	6
Mode 2: Yielding of the plate and bolt failure		$P_{r2} = \frac{2M_p + n\sum P'_t}{m+n}$	7
Mode 3: Bolt failure before yielding of the plate		$P_{r3} = \sum P'_t$	8
Potential resistance of each row of bolts		$T_{ci} = \min(P_{r1}, P_{r2}, P_{r3})$	9
Bolt force distribution for calculation of connection resistance		$T_{c1} = [Capacity\ of\ row\ 1\ alone]$ $T_{c2} = Min\begin{bmatrix} Capacity\ of\ row\ 2\ alone \\ Capacity\ of\ row\ 2\ and\ 1 - T_{c1} \end{bmatrix}$	10
Moment of resistance of the connection		$M_c = \sum T_{ci} d'; C = \sum T_{ci}$; $C = (\alpha f'_c) b(\beta a)$	11
Shear resistance of the connection on column side			
Shear resistance of the connection until no slip		$V_f = \mu_f P;\ \mu_f = 0.4$	12
Final shear resistance of the connection after slip		$V_u = 0.6 f_{ub} A$	13
Bolts resistance for combined shear and tension		$\frac{V}{V_u} + \frac{T}{1.4T_c} \leq 1$	14

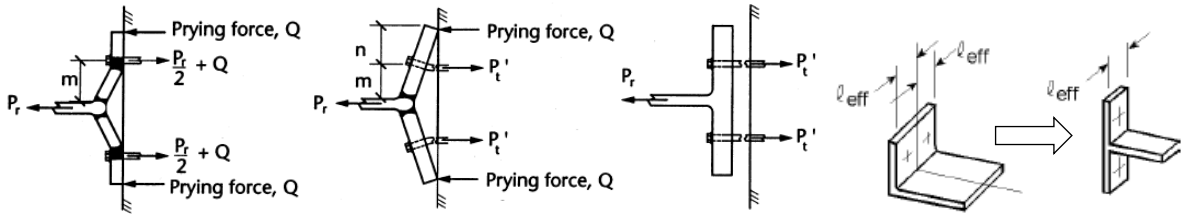

(a) Mode-1 failure (b) Mode-2 failure (c) Mode-3 failure (d) Effective length

Figure 5.5. Modes of failure of the plate and effective length (depending on the plate thickness) [7]

The ultimate moment capacity of the connection on the column side requires to identify the possible combination failure modes such as; (i) mode-1: yielding of the plate, (ii) mode-2: simultaneous yielding of the plate and bolts failure, and (iii) mode-3: bolts failure, which are pictorially shown in Figures 5.5a to 5.5c. To evaluate the capacity for failure modes 1 and 2, complex yield pattern is converted into equivalent yield line as shown in Figure 5.5d, the equations to convert the yield line can be found in the literature [6, 7]. The probable capacity of a bolt row is the minimum of the capacities of the failure modes 1, 2, and 3. The moment capacity of the connection on the column side is calculated as the sum of the probable capacity of each bolt row times the distance to the bolt row from the center of compression as shown in Figure 5.3. The analytical equations to calculate the connection capacities on the

beam and column sides are also listed in Table 5.1. The actual connection stiffness can be estimated by component stiffness method detailed in the literature [6].

5.3 Overview of the experiments

5.3.1 *Test programme and setup details*

The experimental programme includes five quasi-static cyclic tests on sub-assemblies with angle connection (Tests-A1 to A5) and three quasi-static cyclic tests on sub-assemblies with tube connections (Tests-T1 to T3). The overall test setup with external beam-column subassembly including the locations of the hydraulic actuator and load cell is shown in Figure 5.6a. Beam of length 3.23 m and column of height 2.95 m is chosen such that the test setup results in a loading pattern approximately representing half of the bay length and storey heights of typical concrete frame buildings (i.e. the distance between points of contra-flexure). In the figure, "negative" and "positive" represent the directions of loading and hysteresis plots need to be interpreted accordingly. As mentioned before, the sub-assemblies were subjected to quasi-static cyclic loading as per ACI loading protocol, which is shown in Figure 5.6b [8]. The sub-assemblies were subjected to three cycles of incremental lateral drift ratios of 0.1%, 0.3%, 0.5%, 0.75%, 1%, 1.5%, 2%, 2.5%, 3%, 4%, and 5%. In this way, it is possible to investigate the strength and stiffness degradation of the sub-assemblies with proposed connections and can be compared with the hysteresis behaviour of the monolithic concrete frame system or precast concrete frame system "wet joints".

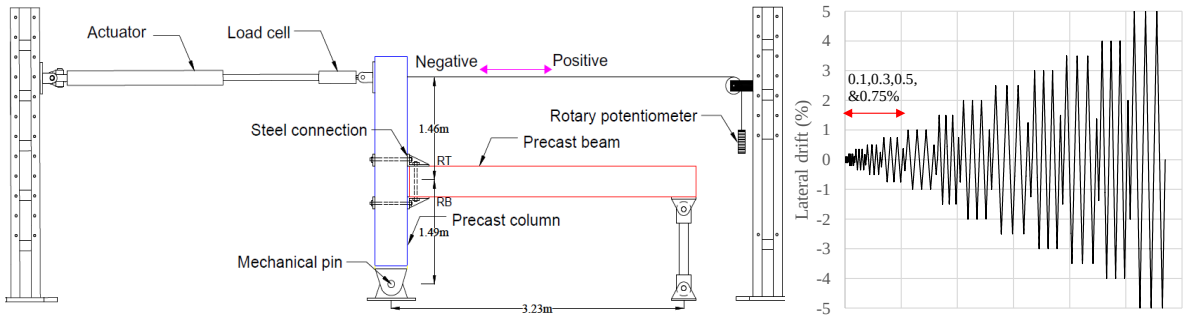

(a) Experimental test setup (b) Quasi-static loading protocol

Figure 5.6. Test setup and loading protocol to evaluate performance of the sub-assemblies

5.3.2 *Details of tested sub-assemblies*

Sub-assemblies were designed as per capacity design principles to ensure the lateral load capacity of the sub-assembly is limited by the ultimate moment capacity of the beam. For the design and evaluation of capacities of the specimens and connections, the material properties summarized in Table 5.2 were used as input. To investigate feasibility of replacing damaged beam with a new beam of the same capacity and upgrading the sub-assembly with a beam of higher capacity, precast concrete beams of two different capacities were designed by keeping the same cross section but with different reinforcement ratios (Beam-1 with 4 numbers of 25 mm diameter rebars top and bottom (ρ_s=1.55%) as shown in Figure 5.7d, and Beam-2 with 4 numbers of 32 mm diameter top and bottom (ρ_s=2.55%) but with the same layout as Beam-1). It is important to note that the beam identification numbers (i.e. Beam-1 and Beam-2) in this chapter are actually Beam-2 and Beam-4 in Chapter 3. Horizontal stirrups of 10 mm diameter were spaced at 50 mm along the beam depth (for both Beam-1 and 2) in the connection region to increase the beam edge breakout resistance (refer Figures 5.7d and 5.7f for the layout). As mentioned before, precast concrete specimens were cast with steel ducts of 50 mm diameter with 2 mm wall thickness to accommodate the 33 mm diameter threaded rods as shown in Figure 5.7a. The cross-sectional and reinforcement details of the beam-column sub-assemblies with angle and tube connections are shown in Figure 5.7b. It is important to note that the length of the connection had to be increased by 100 mm, and the widths of the column and beam had to be increased by 100 mm and 50 mm respectively than it was initially designed for. This was required in order to cater for different bolt configurations without changing the column given the limitation of available hydraulic jack size in the laboratory. In practice the column and connection size can be reduced to conform to building code provisions.

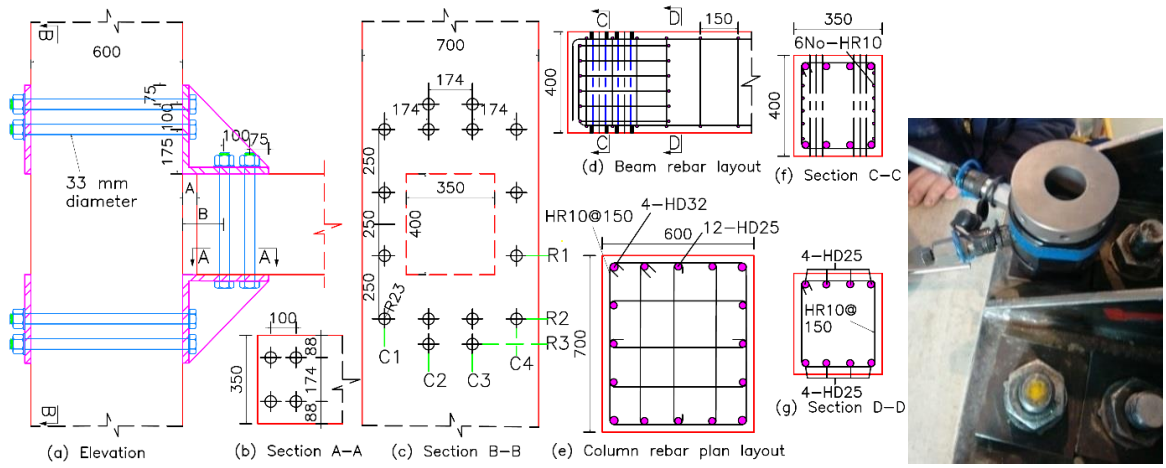

(a) Tested connection configuration (b) Rebar layout of Beam-1 and column (c) Bolt tensioner

Figure 5.7. Layouts of the connection and rebars in the beams and column, and bolt tensioner

Table 5.2. Summary of the material properties for specimens and connections capacity evaluation

Material properties		**Threaded rod/bolt properties**	
Yield stress of steel components (f_{yp})	350 N/mm^2	Grade of bolts	8.8
Ultimate stress of steel components (f_{up})	480 N/mm^2	Yield stress of bolts (f_{yb})	700 N/mm^2
Yield stress of rebars (f_{yr})	500 N/mm^2	Ultimate stress of bolts (f_{ub})	900 N/mm^2
Ultimate stress of rebars (f_{ur})	625 N/mm^2	Net area of bolts (A_{nb})	680 mm^2
Grade of the concrete (f'c)	40 N/mm^2	Yield capacity of bolts (T_{yb})	475 kN
Grade of the weld E48XXSP (f_{yw})	480 N/mm^2	Ultimate capacity of bolts (T_{ub})	612 kN

The angle and tube connections were made up of 25 mm thick plates, 10 mm thick gussets, 10 mm thick side plates, and 33 mm diameter threaded rods. The layout details of the varied connection configurations in different tests can be identified in Figure 5.7a and Table 5.3. The threaded rods were pre-tensioned to the values reported in Table 5.3 by using a torque wrench for the first four tests (i.e. Tests-A1 to A4) and for the last four tests (i.e. Tests-A5, and T1 to T3) the bolts were tensioned using a hydraulic bolt tensioner shown in Figure 5.7c. As there is no direct way to measure the pre-tension in the bolts when using a torque wrench for tightening of bolts, the torque was converted to an equivalent pre-tension using the approximate formula $T=0.2PD$, where T is the applied torque, P is the pre-tension in the bolt, and D is the diameter of the bolt.

Table 5.3. Summary of tests, bolts arrangement and tensions, and fill material (refer Figure 5.7a)

Type	**Test**	**Gap and location of first duct**		**Layout of bolts on column side**	**Duct on beam**	**Threaded rods**		**Fill material to provide uniform contact area**	
		A (mm)	**B (mm)**			**Torque (N-m)**	**Tension (kN)**	**Beam to connection**	**Column to connection**
Angle	A1	1-2	165	R2-3&C2-3	UG	2000	300	RS+ DP	RS+ DP
	A2	1-2	165	R2-3&C2-3	UG	2250	340	DP	DP
	A3	40	125	R2&C1-4	UG	2250	340	G	RS
	A4	1-2	125	R2&C2-3	G	2250	340	G	RS
	A5	40^	125	R2-3&C2-3	G	N/A	375	G	N/A
Tube	T1#	1-2	125	R2&C2-3	UG	N/A	300	G	N/A
	T2	0	125	R1-2&C1-4	G	N/A	200*/300	G	N/A
	T3#	1-2	125	R2&C2-3	UG	N/A	375	ER	ER
Note: "UG", "G" represents ducts are un-grouted and grouted, tension in each bolt on beam and column sides is same unless specifically represented with "*" which represents on column side only. "#" represents steel tube without end plate made out of angles, "^" represents gap between beam and column is grouted.									

During the erection of the first test sub-assembly (i.e. Test-A1), uneven gaps were observed between the connection and the precast concrete member surfaces as shown in Figure 5.8a. This was because of uneven finished surfaces in the precast concrete specimens and the legs of the steel angle/ tube not being exactly perpendicular. To have a uniform contact surface between the steel connection plates and the precast member surfaces a fill material was required to effectively transfer pre-tension force from the bolts to the members. As there was no direct literature on the behaviour of infill materials between steel connections and precast

concrete members under cyclic loading, four types of infill materials were identified and tested, namely; rubber sheet (RS), grout (G), dental plaster (DP), and epoxy resin (ER). Figures 5.8b and 5.8c show cases where rubber sheet and grout were used as an infill material between the connection and the beam to fill the uneven gaps. Actual fill materials that were used in different tests can be identified from Table 5.3 and the mechanical and frictional properties of the infill materials are reported in Table 5.4.

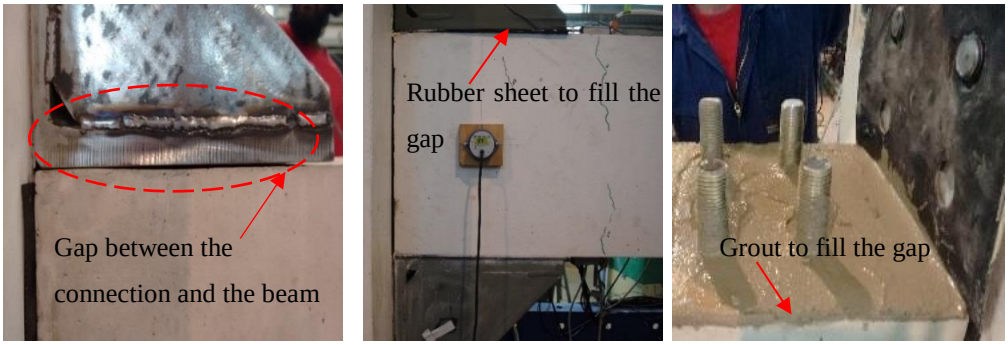

(a) Uneven gaps (b) Rubber sheet as infill (c) Grout as infill

Figure 5.8. Uneven gaps between the connection and the beam, and infill materials to fill the gap

Table 5.4. Mechanical and frictional properties of infill materials

Infill materials	Compressive strength	Contact surfaces	Coefficient of friction			Ref
			Static (μ_s)	Kinetic (μ_k)	Design (μ_f)	
Rubber sheet	10 MPa	Steel on concrete	0.47-0.65	-	0.4	[9, 10]
Sika grout	50 MPa	Steel or concrete on rubber	1.0	0.6-0.85	0.6	[11]
Dental plaster	60 MPa	Steel or concrete on grout	0.47-0.65	-	0.4	[10]
Hilti epoxy	82.7 MPa	Steel or concrete on resin	0.7*	-	0.4	
* Bond strength of 12.4 MPa was taken from catalogue and converted into equivalent frictional coefficient.						

The capacities of the proposed angle and tube connections with different configurations as listed in Table 5.3 were calculated by applying the previously developed analytical equations. The nominal yield moment capacities (M_{yb}) of Beam-1, Beam-2, and the column obtained from the section analysis are 319 kN-m, 487 kN-m, 960 kN-m respectively. The yield and over strength demands on the connections, and summary of ratios of the connection capacities to yield and over strength demands on beam and column sides are reported in Table 5.5. It is important to note that in Table 5.5 ultimate moment capacity of the connection on beam side corresponds to the ultimate moment of resistance of the beam due to edge failure (refer Figure 5.2) rather than the ultimate moment capacity of steel angle/tube components (which were designed to be in elastic state). It is clear from the table that the sub-assemblies with Beam-1 will achieve its nominal lateral strength computed based on the yield moment capacity of the beam (M_{yb}), whereas sub-assemblies with Beam-2 will not achieve its nominal lateral strength because of beam edge failure before yielding of rebars (this was

because the layout of horizontal stirrups in the connection region of Beam-2 was the same as Beam-1, thereby altering the strength hierarchy and this fact was actually realized after the test). The experimentally observed behaviour of the sub-assemblies with the proposed connections is reported in the next section.

Table 5.5. Summary of connection capacity to demand with different connection configurations

Type	Test	Demand on connection				Ratio of connection's capacity to demand				
						on beam side			on column side	
		Beam Id	M_{yb}	M_{oc}	V_{oc}	Moment at slip	Ultimate moment – beam edge failure		Ultimate moment	Shear at first slip
						(M_{fc}/M_{yb})	(M_{uc}/M_{yb})	(M_{uc}/M_{oc})	(M_{uc}/M_o)	(V_f/V_o)
Angle	A1	1	319	445	148	0.90	1.33	0.96	2.12	4.86
	A2	1	319	445	148	0.68	1.10	0.79	2.12	3.68
	A3	1	319	445	148	0.68	1.10	0.79	1.55	5.51
	A4	1	319	445	148	0.68#	1.10	0.79	0.92	2.76
	A5	2	487	680	225	0.50#	0.77	0.55	1.39	2.67
Tube	T1	1	319	445	148	0.60	1.03	0.74	0.92	1.62
	T2	1	319	445	148	0.60#	1.03	0.74	2.76	3.24
	T3	2	487	680	225	0.50	0.77	0.55	0.60	1.33
Note: # represents no actual slip of the connection due to grout of the ducts on the beam side, but it is the point at which bolts start bear against the ducts and beam edge, Units: moments in kN-m, and shear force is in kN.										

5.4 Experimental test results and observations

As mentioned before, eight experimental tests (Tests-A1 to A5 and T1 to T3) were carried out to evaluate the structural efficiency of sub-assemblies with different angle and tube connection configurations. The parameters that were varied in these tests are beam strength (Beam-1 and 2), beam edge distance (i.e. distance from the first duct location to beam edge), the gap between the beam end and column, fill material between the connection and precast concrete members, arrangement and number of bolts on column side, and the condition of the ducts on beam side. Actual details of the connection configuration in different tests can be identified using Figure 5.7a and Table 5.3.

5.4.1 *Slip/movement of the connection*

In all tests, the cyclic behaviour of the sub-assemblies was predominantly governed by the initiation and extent of slip/movement of the connection from the initial position. It is important to note that the recorded slip is the actual movement of the connection from the initial position. In case of un-grouted connection, it is a combination of the actual slip until bolts do not bear against the ducts and deformation of the steel ducts (due to transfer of shear from the bolts to the ducts), whereas in grouted connection it is only due to the deformation of the steel ducts. The measured cyclic slip of the connection obtained from Test-A1 on beam and column sides is shown in Figures 5.9a and 5.9b respectively, and cyclic slip plots for other tests are reported in Appendix F (refer Figures F.1 and F.2). Backbone slip envelopes

with angle and connections on beam and column sides are shown in Figures 5.9c to 9f. In these figures, for clarity the legend only included right top (RT) slip envelopes (refer along with Figure 5.6a), and the right bottom (RB) slip envelopes can be easily identified by dotted lines and with the corresponding right top (RT) legend symbol. It can be observed from the envelope plots that the initiation and rate of slip depends on the type of fill material; this is because of different friction coefficients for different fill materials. It was observed that the rate of movement of the connection on the beam side increases rapidly at higher lateral drift. This was due to; (i) loss of pre-tension in the bolts (because of loss of contact area), (ii) the reduction of friction coefficient (i.e. kinetic friction is less than static friction), and (iii) easy deformation of the ducts after the beam edge failure.

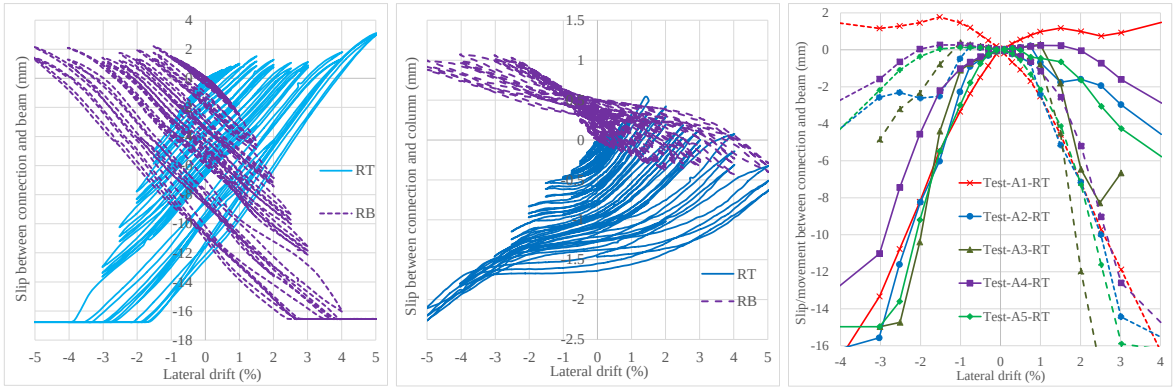

(a) Test-A1:slip on beam side (b) Test-A1: slip on column side (c) Test-A: envelopes on beam side

(d) Test-A: envelopes on column side (e) Test-T:envelopes on beam side (f) Test-T: envelopes on column side

Figure 5.9. Cyclic slip from Test-A1 and comparison of envelopes from Tests-A1 to A5 and T1 to T3

It can be concluded that initial rate of slip of the connection was high with rubber sheet infill material (refer Test-A1 plots) which was quite opposite to the initial assumption of high friction coefficient (μ_f of 0.6 is not valid under cyclic loading). The rate of slip of the connection with epoxy resin as infill material (refer Test-T3 plots) was less until bond failure, and thereafter the rate of slip of the connection increased rapidly. This indicates that the epoxy resin surface is smooth, which results in very less frictional resistance at higher drift levels. The rate of slip of the connection with grout and dental plaster as infill materials is

very much similar, which can be seen from the Tests-A2, A3, and A5 plots. In sub-assemblies with grouted ducts on beam side (refer Test-A4 and T2 plots), the rate is similar but the slip is less compared to sub-assemblies with un-grouted ducts on beam side. By comparing Figures 5.9c to 9f, it can be concluded that slip of the connection on the column side was much lesser compared to the slip of the connection on the beam side. Also, it was observed that with different arrangements and number of bolts on the column side, there was no major difference in the measured slip between the connection and the column. This was because in all tests the frictional shear resistance was higher than the shear force developed at the column and the connection interface.

5.4.2 *Structural performance*

5.4.2.1 General observations

The experimentally obtained hysteresis plots of the sub-assemblies with angle and tube connections under quasi-static cyclic loading is shown in Figures 5.10 and 5.11 respectively. It is clear from the figures that the hysteresis behaviours of the sub-assemblies were very much dependent on the varied connection parameters. In general, the overall hysteresis loop of the sub-assemblies with angle and tube connections can be classified close to "pinching" type with the extent of pinching varying in different tests. The pinching behaviour is due to slip of the connection (as discussed in the previous section) and the subsequent concentrated damage in the beam edge, which results in less energy dissipation when compared to monolithic/wet jointed concrete frame sub-assembly. Analytically computed lateral strength of the sub-assemblies corresponding to yield moment capacity of the beam (M_{yb}) and ultimate moment capacity of the connection corresponding to beam edge failure (M_{uc}) are also plotted in Figures 5.10 and 5.11. It is clear that sub-assemblies with Beam-1 (i.e. Tests-A1 to A4, and T1 and T2) were able to reach nominal lateral strength of 108 kN (corresponding to M_{yb}) at different drift levels, whereas sub-assemblies with Beam-2 (i.e. Tests-A5 and T3) were not able to achieve its nominal lateral strength of 165 kN (corresponding to M_{yb}). This was because, in sub-assemblies with Beam-2 the ultimate moment capacity of the connection corresponding to beam edge mechanism (M_{uc}) is less than the yield moment capacity of beam (M_{yb}), therefore the lateral strength of the sub-assembly is limited to beam edge failure strength.

The lateral secant stiffness of a sub-assembly up to the yield point can be calculated by applying any structural analysis method. For the corner sub-assembly shown in Figure 5.6a, the analytical equation to estimate the lateral displacement δ_a under lateral load V is given by

Equation 15, where E is modulus of elasticity of the concrete, y_1, y_2, and y represent the distances from the column base to the center of beam, from the beam center to the column top, and the total height of the column, respectively. Similarly, I_{cef} and I_{bef} are effective moment of inertias of the column and beam, respectively. The rigidity factors are given as $\beta_1 = \frac{D}{2y_1}; \beta_2 = \frac{D}{2y_2}; \alpha = \frac{0.5C}{l}$, where D and C are beam and column depths respectively.

$$\delta_a = \frac{Vy_1^3(1-\beta_1)^3}{3EI_{cef}} + \frac{Vy_2^3(1-\beta_2)^3}{3EI_{cef}} + \frac{Vy^2l(1-\alpha)^3}{3EI_{bef}} \quad (15)$$

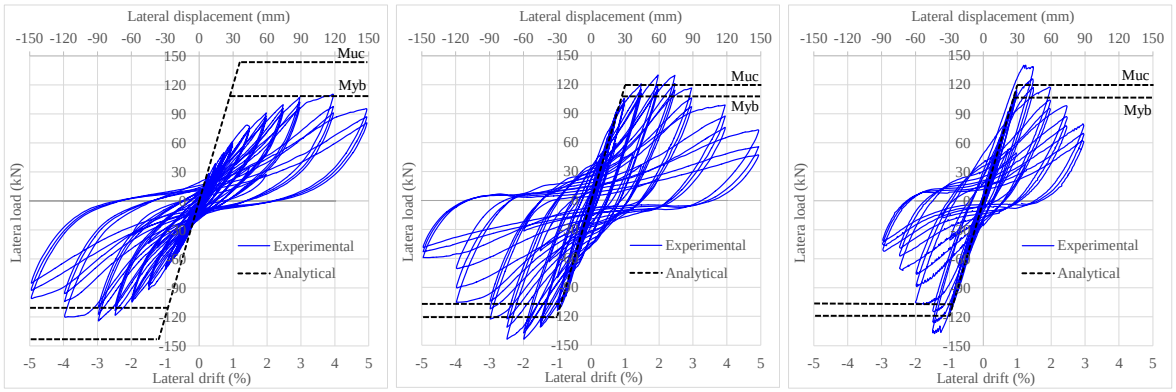

(a) Test-A1 (b) Test-A2 (c) Test-A3

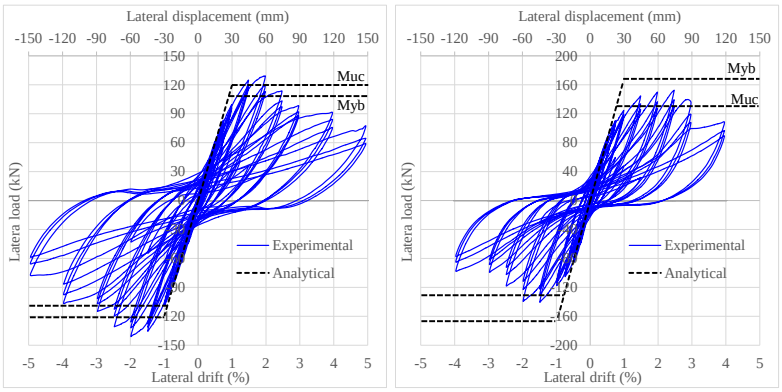

(d) Test-A4 (e) Test-A5

Figure 5.10. Hysteresis behaviour of the sub-assemblies with the angle connection

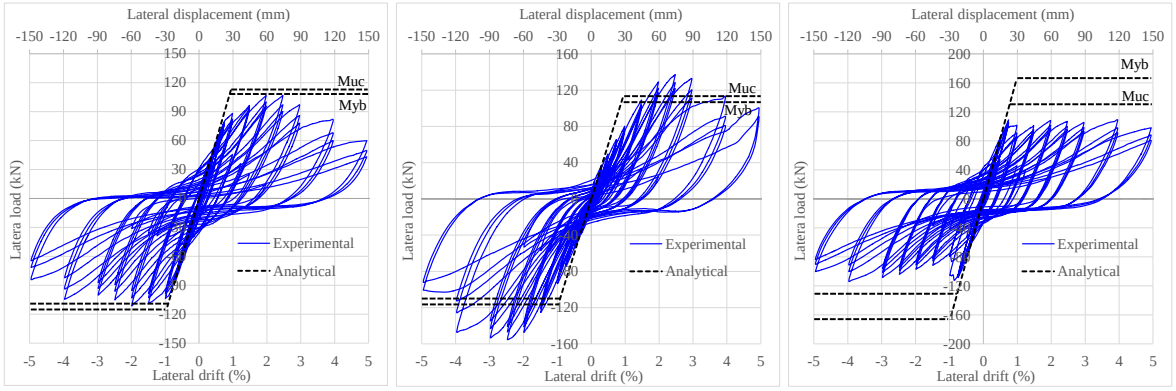

(a) Test-T1 (b) Test-T2 (c) Test-T3

Figure 5.11. Hysteresis behaviour of the sub-assemblies with tube connection

It can be observed from Figures 5.10 and 5.11 that lateral secant stiffness computed by using Equation 15 is in close agreement with the lateral secant stiffness obtained from all tests except in Test-A1. This was because in Test-A1, the connection started to slide from very low drift levels (as identified in the previous section), the slip of the connection resulted in additional flexibility (i.e. less stiffness) to the sub-assembly (refer Figure 5.10a). By comparison of experimental hysteresis and analytical load displacement plots, it can be concluded that the nominal lateral strength and stiffness of the sub-assembly is very much dependent on connection properties. It can be concluded that the overall hysteresis behaviour of the sub-assemblies depends on the sequence of modes of failure; rebar yielding after beam edge failure or beam edge failure after rebar yielding. Lateral strength of sub-assembly with proposed connections can be reasonably estimated only if the connection capacity calculation includes beam edge mechanism (refer Figure 5.2).

5.4.2.2 Effect of varied parameters on the structural performance

The comparison of load displacement backbone envelopes of the tested sub-assemblies with angle and tube connections is shown in Figures 5.12a and 5.12b respectively. By comparing the envelope plots from Figure 5.12a, it is clear that the lateral stiffness of the Test-A1 sub-assembly is smaller than that of other tested sub-assemblies (which was also evident from analytical comparison). As mentioned before, this was because in Test-A1 the connection started to slip from low drift levels and also the rubber sheet between the connection and members deformed and isolated the connection. Stiffness of the sub-assemblies obtained from Tests-A5 and T3 is higher compared to other sub-assemblies, this was because Beam-2's flexural rigidity (i.e. EI_{bef}) is higher compared to Beam-1's flexural rigidity. Initial lateral stiffness of the sub-assemblies (Tests-A2, A4, T1, and T2) with grout and dental plaster as infill material is of the same magnitude, and it can be concluded that both infill materials have similar material and frictional properties. For practical use, the dental plaster is not suitable as infill material as it sets too quickly (its setting time is around 5 minutes), and the recommended fill material, if required to be used between the connection and precast concrete members, is "non-shrink grout". Lateral strength of the sub-assemblies with Beam-1 is of similar magnitude, whereas lateral strength of sub-assemblies with Beam-2 (Tests-A5 and T3) are different because the connection strength dictates the sub-assembly capacity.

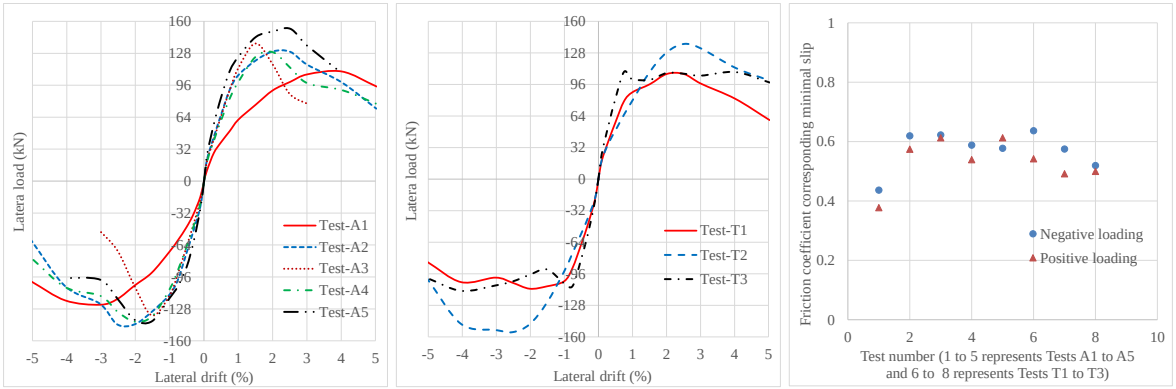

(a) Tests: A1 to A5 (b) Tests:T1 to T3 (c) Experimental: frictional coefficient (μ_e)

Figure 5.12. Backbone envelopes of sub-assemblies with angle and tube connection

The beam edge distance provided in specimens-A1 and A2 was approximately "6d", whereas in other tests it was "5d", where "d" is the rebar diameter. By comparing the backbone envelopes, it can be concluded that beam edge distance affects the strength degradation rather than the nominal lateral strength. It would have also affected the nominal lateral strength if the horizontal stirrups were not provided in the connection zone to resist the shear transfer from the bolts. By comparing the backbone envelope of Test-A3 with other tests, it appears that the sub-assembly with gap between the beam and the column suffers a faster strength degradation (resulting in low ductility) compared to the sub-assemblies without gap between the beam and the column. This was because the gap between the beam and the column allows for an early failure of beam edge¸ thereby resulting in loss of bond between the rebar and surrounding concrete, which eventually leads to strength degradation. In Tests-A4, A5 and T2, the steel ducts on the beam side were grouted, whereas it was not in other tests. By comparing the backbone envelopes, it can be concluded that the condition of the ducts on beam side does not have a major effect on load-displacement behaviour as long as the amount of pre-tension in the bolts is the same. This was because the ultimate mode of failure in both cases was the beam edge failure.

The frictional coefficient between the connection with different infill materials and precast concrete specimens was experimentally evaluated as the ratio of bending moment at the beam end corresponding to minimal recoverable slip to the product of the beam depth and the amount of pre-tension induced into bolts, mathematically represented as $\mu_e = M/(d \times P)$. The two criteria for deciding the bending moment corresponding to the minimal recoverable linear slip was; (i) slip should be less than 2 mm, and (ii) load-displacement behaviour should be linear (in most tests it was found be the case until 1.0% lateral drift). Thus obtained friction coefficients in different tests are plotted in Figure 5.12c. It is clear from the figure that the lower bound friction coefficient μ_e is around 0.5 for all tests except in Test-A1, and

this μ_e value is higher than the initially assumed friction coefficient μ_f (refer Table 5.4). In the numerical simulation, frictional coefficient μ_e of 0.5 is used for all tests except Test-A1, in which μ_e of 0.44 is used.

5.4.3 *Modes of failure*

In all tests with both angle and tube connections, similar modes of failure (damage) were observed in the beam. The damage to the beam at different drift levels obtained from Tests-A2, A4, and T1 is shown in Figures 5.13, 5.14 and 5.15 respectively. The detail modes of failures of the sub-assemblies with angle and tube connections obtained from all tests can be found in Appendix G (refer Figures G.1 to G.8). The initial damage to the beam was due to the spread of flexural shear cracks until the slip of the connection was minimal (no contact between the bolts and the ducts) as shown in Figures 5.13a, 5.14a, and 5.15a. Thereafter, when the slip of the connection exceeded the clearance between the bolts and ducts, the bolts started to bear against the ducts which induced bearing stress (i.e. bursting stress) into the beam edge concrete resulting in bursting cracks and spalling of concrete in the connection zone, which is shown in Figures 5.13b, 5.14b, and 5.15b. Also, the beam wedge failure due to the slip of the connection can be clearly identified in these figures. At higher drifts (around 4%), vertical shear crack in front of the connection was observed; this was due to simultaneous ingress of the connection into the beam and horizontal slip of the connection, which can be identified from Figures 5.13c, 5.14c, and 5.15c. By comparing Figures 5.13 and 5.14, it can be concluded that the ultimate damage to the beam with either un-grouted or grouted ducts (Tests-A2 and A4) is similar, and this was because in both cases the ultimate failure mode was beam edge damage due to slip of the connection.

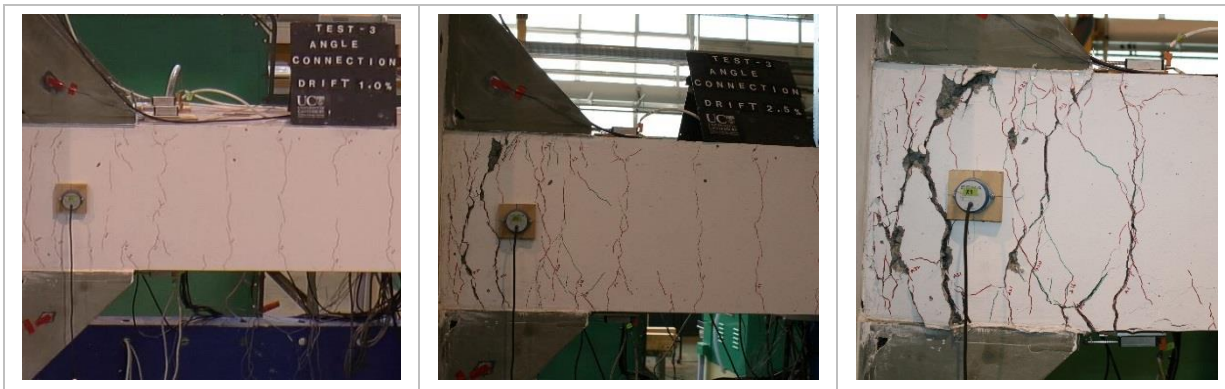

(a) 1.0% drift: flexural cracks | (b) 2.5% drift: beam edge cracks | (c) 4.0% drift: beam edge failure

Figure 5.13. Typical damage states to the beam with angle connection at different drifts (Test-A2)

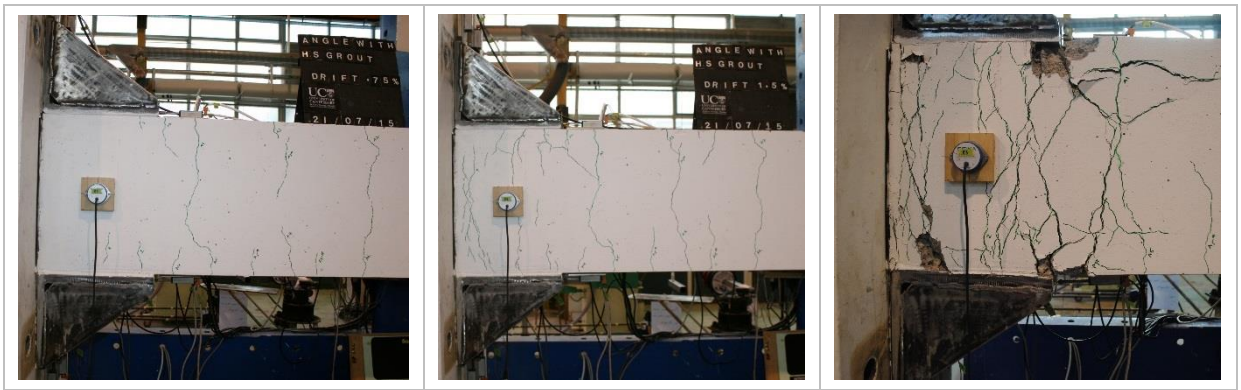

(a) 0.75% drift: flexural cracks	(b) 1.5% drift: beam edge cracks	(c) 4.0% drift: beam edge failure

Figure 5.14. Typical damage states to the beam with angle connection at different drifts (Test-A4)

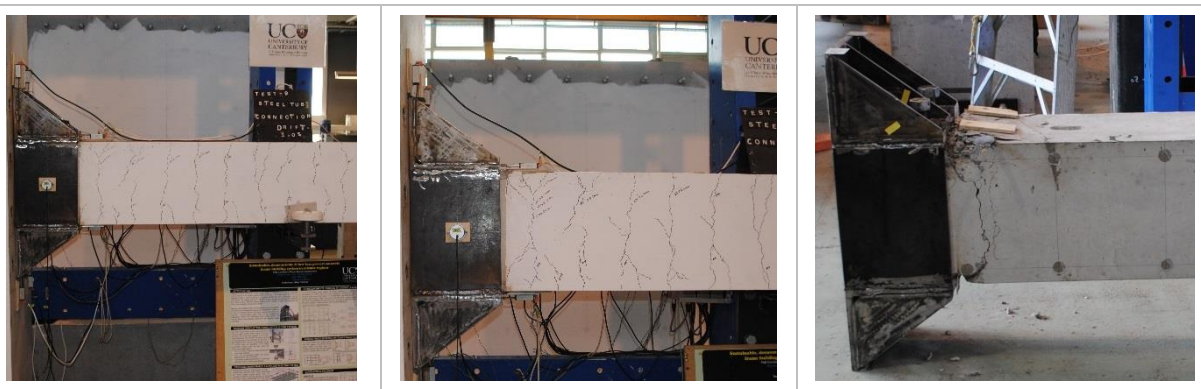

(a) 1.0% drift: flexural cracks	(b) 1.5% drift: beam edge cracks	(c) 4.0% drift: beam edge failure

Figure 5.15. Typical damage states to the beam with tube connection at different drifts (Test-T1)

For better representation and interpretation of the observed damage in the precast concrete beam, the actual deformed shape of the sub-assembly and types of crack patterns observed in and away from the connection zone are schematically reproduced in Figure 5.16. As shown in figure, three distinct types of cracks were observed; (i) flexural shear cracks due to influence of shear along with the bending of beam, (ii) bursting/beam edge cracks due to slip of the connection, and (iii) vertical tensile shear crack.

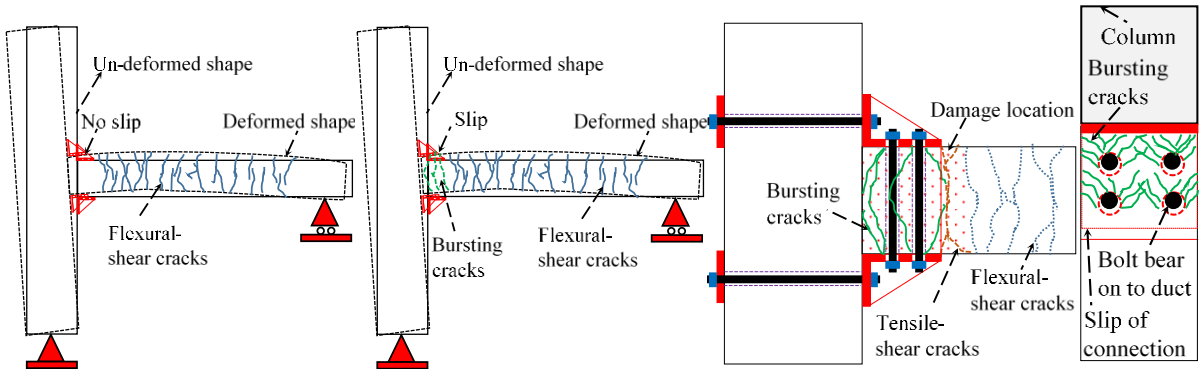

(a) Damage to beam until no slip (b) Damage to beam after slip (c) Typical damage location

Figure 5.16. Schematic layout of deformed shape of the sub-assembly and crack patterns in the beam

5.4.4 *Summary of test results and observations*

It can be concluded from the experimental test results that the hysteresis behaviour of the sub-assemblies with angle and tube connection depends on the type of fill material between the connection and members, the gap between the beam and the column, the amount of pre-tension in the bolts, and to certain extent on the beam edge distance. The slip between the steel connection and members is crucial in deciding the hysteresis behaviour. The slip can be delayed by increasing the amount of pre-tension in the bolts or by increasing the number of bolts, thereby allowing the beam to develop its nominal capacity. The strength and stiffness degradation can be delayed by delaying the beam edge failure by increasing the beam edge distance or by providing beam edge protection using steel armour plates, and eliminating any gap between the beam and column; thereby making the behaviour close to the monolithic/wet jointed concrete frame. To summarize, the sub-assemblies with angle and tube connection (i.e. grouted or un-grouted) is able to achieve its hysteresis behaviour similar to the monolithic concrete frame behaviour only if other modes of failure such as failure of the steel connection, beam edge failure in the beam due to the slip between the connection and the beam are delayed until longitudinal rebars in the beam yield (more conclusions will be drawn from the numerical analysis and comparison with existing wet jointed/ductile connector systems towards the end of the chapter).

5.5 Numerical simulation of the tested sub-assemblies

As it was experimentally found that the cyclic behaviour of the sub-assemblies governed was by a combination of slip of the connection associated with beam edge failure and flexural mode of deformation of the beam, the hysteresis behaviour of the sub-assemblies can be numerically simulated by two nonlinear springs in series. In this section, a brief overview of the macro models and associated hysteresis rules along with the model input parameters required is presented. Also, the assumptions involved in development of the backbone input envelopes are reported. Finally, the numerically simulated hysteresis loops of the sub-assemblies are compared with the experimental test results.

5.5.1 *Macro modelling approach*

The column is modelled as an elastic line element with effective moment of inertia and beam is modelled as four components connected in series (starting from the column center line); (i) rigid line element of 0.3 m (half of column depth to account for the finite size joint effect), (ii) zero length connection rotational spring (to model nonlinear behaviour of the connection), (iii) zero length beam spring (to model nonlinear flexural deformation of the beam), and (iv)

elastic line element with modified effective moment of inertia and spring flexibility in the elastic range. The overall scheme of the modelling approach is schematically shown in Figures 5.17a and 5.17b. Nonlinear behaviour of the connection can be modelled by using two approaches; (i) two parallel translation (F-S) springs separated by beam depth (d) as shown in Figure 5.17a, and (ii) rotational (M-θ) connection spring as shown in Figure 5.17b.

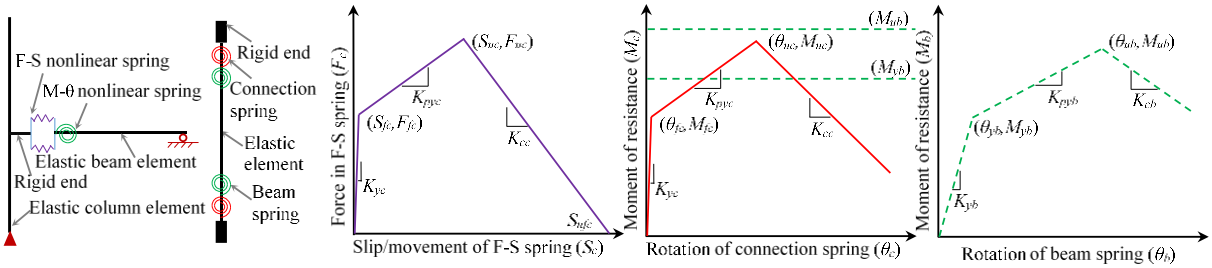

(a) Approach-1 (b) Approach-2 (c) F-S spring envelope (d) M-θ connection spring (e) M-θ beam spring

Figure 5.17. Schematic representation of nonlinear springs of line element and backbone input plots

5.5.1.1 Assumptions

In order to simplify the numerical modelling of the sub-assemblies with angle and tube connections, the following important assumptions were made with regard to backbone envelopes of the connection and beam springs:

1. The vertical slip between the connection and column was ignored (as it was found from the experiments that the vertical slip is very small compared to the horizontal slip), thereby no need to model vertical shear spring.
2. After initiation of the slip, the frictional coefficient linearly reduces to 80% of experimentally evaluated friction coefficient (μ_e) when the connection spring reaches its maximum capacity (i.e. S_{uc} or M_{uc}).
3. The initial stiffness of the connection spring (i.e. $K_{yc}= F_{fc}/ S_{fc}= M_{fc}/ \theta_{fc}$) is rigid (except in Test-A1). In the numerical model, it was assumed that the connection spring's initial stiffness is ten times of the beam spring's initial stiffness (i.e. $K_{yc}=10\ K_{yb}$).
4. The lever arm (equal to beam depth d) between the two translational springs shown in Figure 5.17a is assumed to be constant at all times. In reality after slip of the connection, lever arm (d') (distance between center of tensile forces in horizontal stirrups and center of bearing forces, refer Figure 5.2b) is less than the beam depth (d). The reduction in the moment capacity due to this assumption is indirectly accounted by reducing the longitudinal shear capacity (i.e. $F_{uc}=0.8\times\mu_e\times P+ ((T_s+V_c) \times d')/d$).
5. It is assumed that the connection spring reaches its ultimate capacity (S_{uc} or M_{uc}) when the first horizontal stirrup (refer Figure 5.2b) reaches its yield strain.

6. Concrete wedge resistance (V_c) is only effective in tube connection because of confinement whereas in angle connection it is neglected in the capacity calculation.
7. In computation of the capping rotation of the connection spring θ_{uc}, it is assumed that the pivot of rotation of the connection is either at the bottom or top beam surface. This is in agreement with the slip envelopes obtained from experiments (refer Figure 5.9).
8. In computation of θ_{uc}, strain in the horizontal stirrup linearly varies from ε_y at one end to zero at another end.

5.5.1.2 Connection and beam springs input envelopes

The input envelope of the connection spring either in-terms of longitudinal shear force and slip/deformation (F-S) or moment and rotation (M-θ) (shown in Figures 5.17c and 5.17d) need to be constructed before developing numerical model of the sub-assembly. The slip critical longitudinal shear resistance (F_{fc}) or moment (M_{fc}) can be computed by using Equations 1 and 2, but with the experimentally evaluated frictional coefficient. Ultimate longitudinal shear resistance (S_{uc}) or moment (M_{uc}) can be evaluated by using Equations 3 and 4 (or 5) but with reduced frictional coefficient (μ_r). For the numerical model, the slip critical deformation (S_{fc}) or rotation (θ_{fc}) shall be assigned a very small value rather than zero (which will induce numerical instability in the model). The slip/deformation of the translation spring (S_{uc}) or the rotation of rotational spring (θ_{uc}) can be evaluated by using Equation 16.

$$\theta_{uc} = \frac{\left(\frac{0.5\varepsilon_y l_s * d}{d_1} + d_b\right)}{d};\ S_{uc} = 0.5 d\theta_{uc} \tag{16}$$

where ε_y is the yield strain of the horizontal stirrup (in this case e_y is 0.00293), l_s is length of horizontal stirrup (340 mm), d_1 is location of the farthest horizontal stirrup from the pivot point (340 mm), d is the beam depth (400 mm), d_b is the bolt clearance. The actual bolt clearance d_b can vary for each duct and this can be between 0 to ±6.5 mm. For the numerical study, d_b was assumed to be 5 mm and by using Equation 16, θ_{uc} comes to 0.014 radians. Numerical analysis results indicated that the θ_{uc} value deviates with actual capping point, the possible reasons for the deviation are detailed in the next section. So, for the cases with large difference, θ_{uc} is adjusted to match with experimental results which is reported in Table 5.6. The post-capping slope (K_{cc}) or the ultimate slip/deformation (S_{ufc}) or rotation (θ_{ufc}) of the connection spring is evaluated based on experimental test results; e.g. θ_{ufc} was evaluated as 0.08 radians, which is conservative in most cases. A summary of the connection spring's backbone inputs used for modelling the sub-assemblies in different tests are provided in Table 5.6.

The different points on the beam spring envelope shown in Figure 5.17e can be evaluated by applying well known mechanics principles. Two approaches/methods can be adopted to arrive at a moment rotation backbone curve of the beam spring are; (i) sectional/fiber analysis method, and (ii) empirical method. Here, the first approach has been adopted to arrive at the moment-rotation backbone curve for the beam spring. The process of construction of moment rotation is not reported here (details of the process are reported in Chapter 4). A couple of important things that are to be noted in the process are; (i) bi-linearization of the moment curvature plot is based on the equal area method, and (ii) plastic hinge length calculation is based on the formulae proposed by Bae [12]. Summary of the beam spring inputs for Beam-1 and 2 are also reported in Table 5.6.

Table 5.6. Modelling parameters of connection and beam springs

Connection spring modelling parameters											
Test ref	**Approach-1**					**Approach-2**					**Hysteretic parameter**
	Slip critical		**Capping**		**Final**	**Slip critical**		**Capping**		**Final**	
	S_{fc} *(mm)*	F_{fc} *(kN)*	S_{uc} *(mm)*	F_{uc} *(kN)*	S_{ufc} *(mm)*	θ_{fc} *(rad)*	M_{fc} *(kN-m)*	θ_{uc} *(rad)*	M_{uc} *(kN-m)*	θ_{ufc} *(rad)*	
A1	1.4	576	5.6	763	16	0.007	230	0.028	305	0.08	P_x=0.67; P_y=0.3; D_1=0; D_2=0.035; β =0.67*
A2/A4	1.8×10^{-2}	680	2.8	845	16	9.2×10^{-5}	272	0.014	338	0.08	
A3	1.8×10^{-2}	680	1.4	845	8	9.2×10^{-5}	272	0.007	338	0.04	
A5	1.8×10^{-2}	750	2.8	902	16	9.2×10^{-5}	300	0.014	360	0.08	
T1/T2	1.8×10^{-2}	600	2.8	819	16	9.2×10^{-5}	240	0.014	327	0.08	
T3	1.8×10^{-2}	750	5.6	789	16	9.2×10^{-5}	300	0.028	315	0.08	

Beam spring modelling parameters								
Beam ref	**Yield point**		**Capping**		**Final**	**IMK cyclic parameters**		
	θ_{yb}	M_{yb}	θ_{ub}	M_{ub}	θ_{ufb}	α_s	λ	C
1	9.2×10^{-4}	313	0.030	391	0.08	0.0079	710	1
2	1.1×10^{-3}	511	0.023	627	0.08	0.011	710	1

Note: *for Test-A1, the calibrated β was 0.067, and θ_{fc} was estimated from slip corresponding to 1.5% lateral drift obtained from experimental test.

5.5.2 *Simulation of hysteretic behaviour*

To model nonlinear behavior of concrete elements, numerous hysteresis rules are available. For this study, "hysteretic material" and "IMK peak-oriented" hysteresis models available in OpenSees are utilized to model the behaviour of the connection and beam springs respectively [13, 14]. The cyclic behaviour of the hysteretic material is controlled by five parameters as reported in Table 5.6; (i) P_x and P_y are the target points on the load displacement plot parameters to control the pinching behaviour, (ii) D_1 and D_2 are parameters to represent damage associated with ductility and energy respectively, and (iii) β is the power factor that controls unloading stiffness. IMK peak oriented hysteretic model captures both strength and stiffness deterioration of the beam spring through two parameters; (i) normalized energy dissipation (λ), and (ii) exponent (c) to describe the rate of cyclic deterioration, and

for the tested sub-assemblies "λ" and "c" turn out to be 65 and 1, respectively.

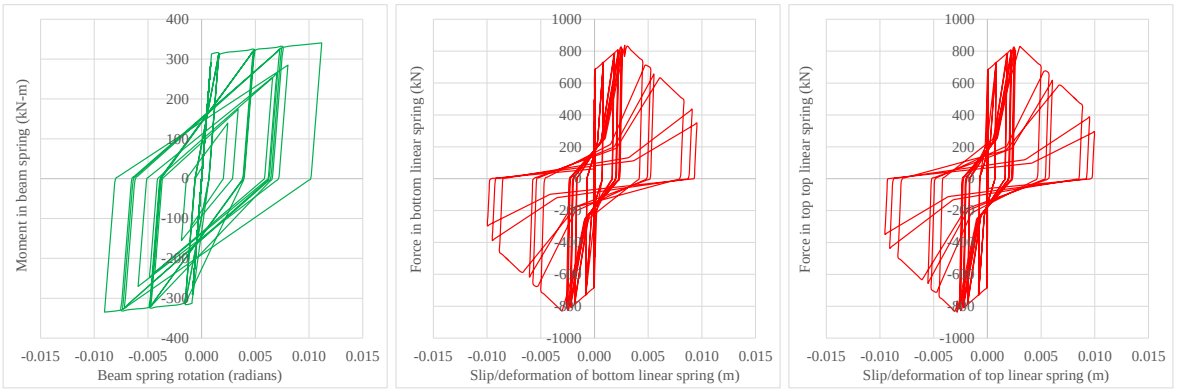

(a) Approach-1:Beam spring (b) Approach-1:F-S bottom spring (c) Approach-1:F-S top spring

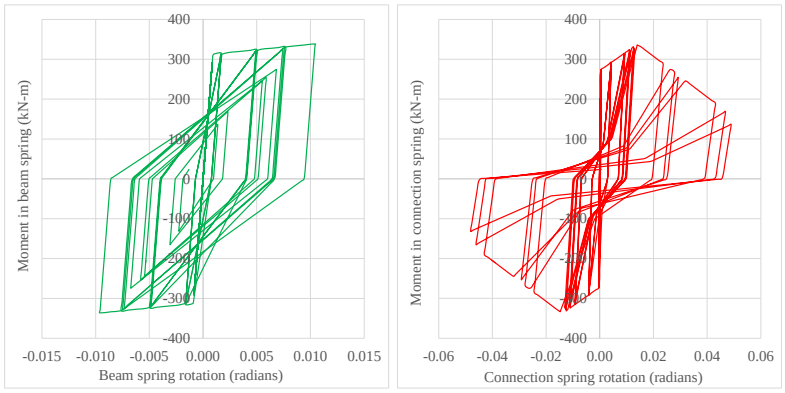

(d) Approach-2: Beam spring (e) Approach-2:Connection spring

Figure 5.18. Responses of connection and beam springs of Tests-A2 and A4 sub-assemblies

The simulated cyclic behaviour of the connection and beam springs for specimens-A2 and A4 by using the two approaches-1 and 2 are shown in Figure 5.18, and it is obvious that the beam spring doesn't reach its capping point. This is because the connection spring starts to degrade and to satisfy equilibrium the moment in the beam spring has to come down, but the reduction in reloading and unloading stiffness of the beam spring is captured, which is shown in Figures 5.19a and 5.19d. The simulated nonlinear response of the connection and beam springs for all tests are reported in Appendix H (refer Figures H.2 to H.13). Also, behaviour of the beam spring in a wet jointed sub-assembly system is reported in Appendix H (refer Figure H.1). The simulated hysteresis behaviours of the sub-assemblies with angle and tube connections by using approaches-1 and 2 are shown in Figures 5.20 to 5.23. In these figures, the legend "FD/MRSS" and "MRSS" represent numerically simulated hysteresis plots by using approaches-1 and 2, respectively. By comparing the simulated plots, it can be concluded that both approaches results in very much similar hysteresis behaviour. This was because, analytically there is no difference between these two approaches and only the backbone envelopes are represented in different form (i.e. moment in the approach-2 is represented as couple force at distance "d" in approach-1, and rotation in approach-2 is

represented as displacement at distance 0.5d in approach-1). In the first approach, the actual mechanisms happening in the connection (i.e. slip of the connection and bearing of the bolts on the beam edge) can be easily visualized whereas in the second approach all mechanisms in the connection need to be treated together as a flexible connection (i.e. semi-rigid) with nonlinear behaviour.

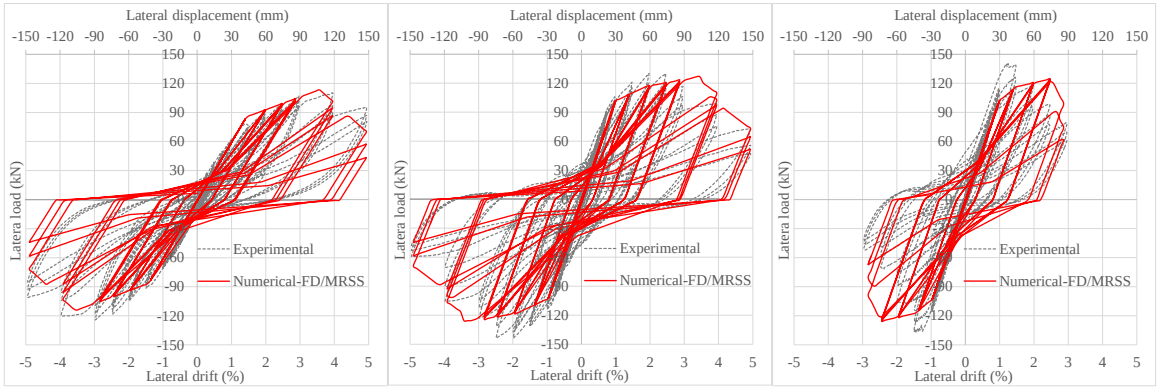

(a) Test-A1 (b) Test-A2 (c) Test-A3

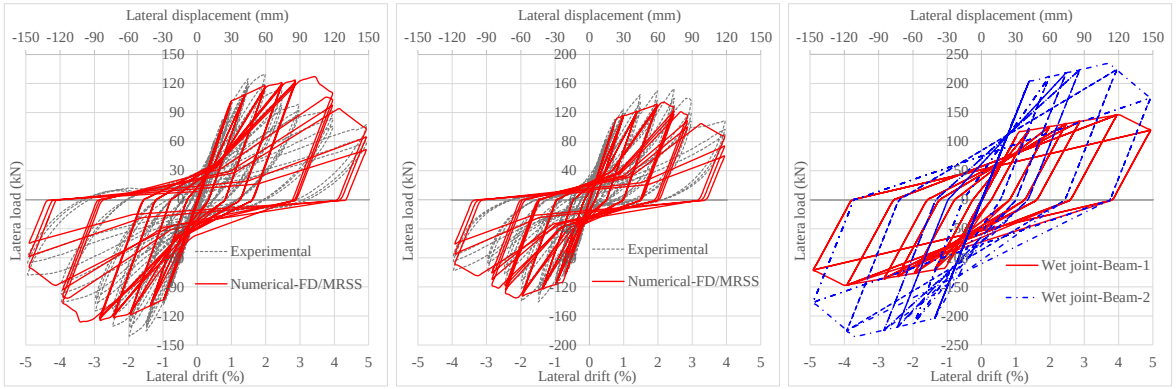

(d) Test-A4 (e) Test-A5 (f) Wet joint system

Figure 5.19. Simulated hysteresis loops of sub-assemblies with angle connection by using approach-1

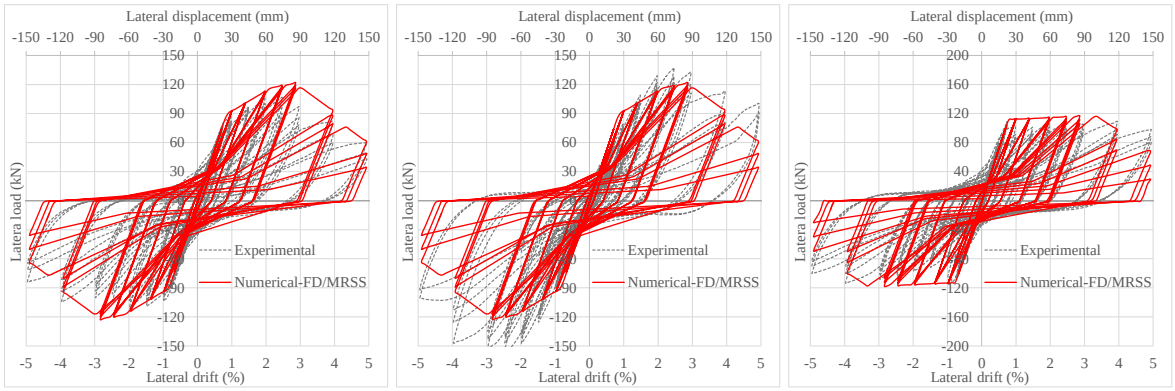

(a) Test-T1 (b) Test-T2 (c) Test-T3

Figure 5.20. Simulated hysteresis loops of sub-assemblies with tube connection by using approach-1

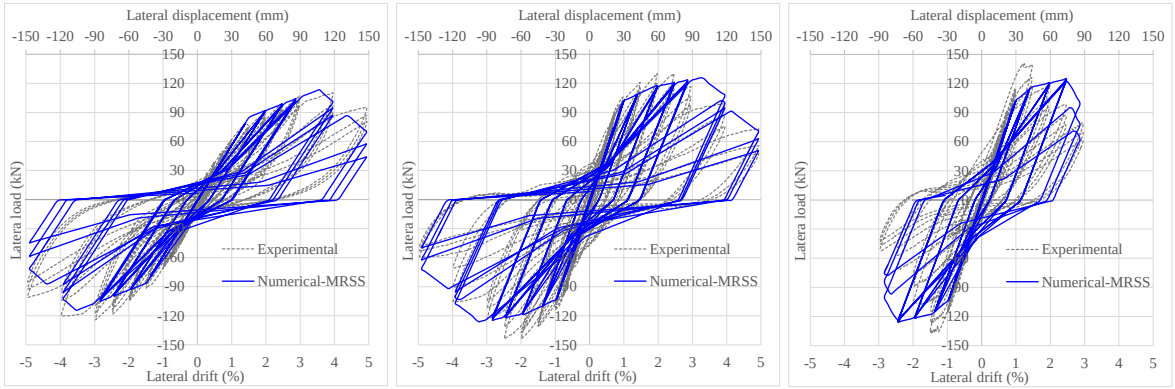

(a) Test-A1 (b) Test-A2 (c) Test-A3

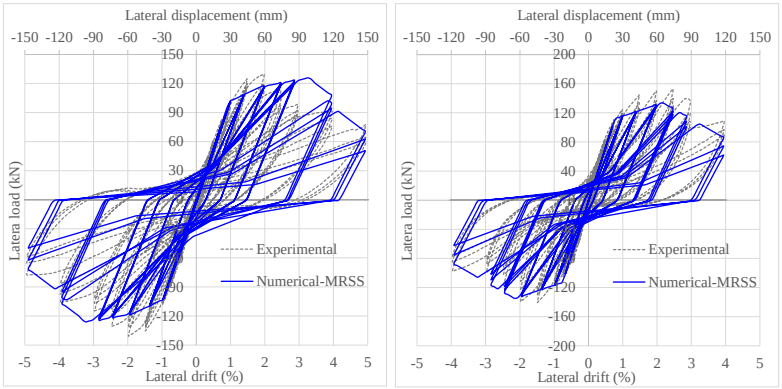

(d) Test-A4 (e) Test-A5

Figure 5.21. Simulated hysteresis loops of sub-assemblies with angle connection by using approach-2

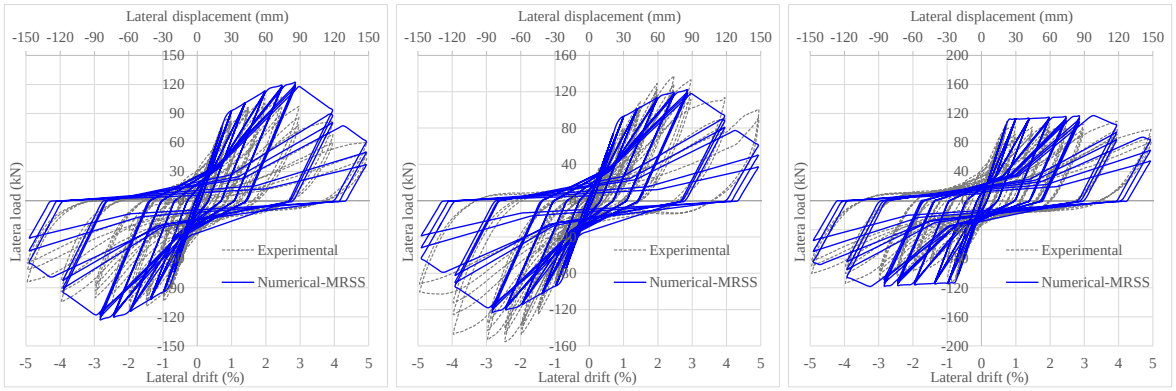

(a) Test-T1 (b) Test-T2 (c) Test-T3

Figure 5.22. Simulated hysteresis loops of sub-assemblies with tube connection by using approach-2

In general, the simulated overall hysteresis behaviour of the sub-assemblies with angle and tube connection are in close agreement with experimental results. But, the important modifications that are made to the original connection spring backbone envelope input are; (i) to match initial stiffness of Test-A1, the connection spring slip critical rotation θ_{fc} is computed from the slip corresponding to 1.5% lateral drift obtained from the experimental test and rounded to 0.007 radians, (ii) In Tests-A1, A3, and T3, θ_{uc} is computed from slip corresponding to the maximum lateral load obtained in the experimental tests, and (iii) in

Test-A3, ultimate rotation of the connection spring θ_{ufc} is modified to 0.04 radians based on the observed experimental hysteresis plot, and the final values used in the numerical analysis are reported in Table 5.6. By comparing the numerically simulated hysteresis of wet jointed sub-assembly (refer Figure 5.19f) with hysteresis behaviour of the tested sub-assemblies, it is clear that the tested sub-assemblies with proposed connections exhibit less energy dissipation.

5.5.3 *Comparison of simulated structural performance parameters with test results*

In this section, equivalent viscous damping (ξ_{eq}) and lateral stiffness degradation (K_l) characteristics of the sub-assemblies are numerically evaluated and compared with the experimental test results. Also, slip envelopes of the translational springs (approach-1) are plotted as a function of lateral drift and the accuracy of the numerical approach is evaluated by comparing with experimentally recorded slip plots. The energy from each cycle was calculated from the hysteresis plots and converted into equivalent viscous damping ξ_{eq} to provide a better understanding of the energy dissipation and pinching characteristics of the sub-assemblies. The equivalent viscous damping ξ_{eq} is calculated as the ratio of energy dissipated E_d in each cycle to the strain energy E_s stored in the corresponding cycle which is given in Equation 17. The lateral secant stiffness is calculated as the ratio of average of peak positive and negative forces to peak positive and negative displacements of the indented drift cycle which is given in Equation 18. In these equations, F_i, F_{i+1} and δ_i, δ_{i+1} represent the load and displacement at steps i and $i+1$ respectively, F_{+ve}, F_{-ve} and δ_{+ve}, δ_{-ve} represent the peak load and displacement of each cycle respectively.

$$\xi_{eq} = \frac{E_d}{4\pi E_s}; E_d = \frac{\sum_i^n (F_{i+1}+F_i)(\delta_{i+1}-\delta_i)}{2}; E_s = \frac{1}{2}\left(\frac{F_{+ve}\delta_{+ve}}{2} + \frac{F_{-ve}\delta_{-ve}}{2}\right) \quad (17)$$

$$K_l = \frac{1}{2}\left(\frac{F_{+ve}}{\delta_{+ve}} + \frac{F_{-ve}}{\delta_{-ve}}\right) \quad (18)$$

By using Equation 17, the plots of equivalent viscous damping ξ_{eq} obtained from the experimental and numerical (approach-1) hysteresis loops for the sub-assemblies with angle and tube connections are shown in Figures 5.23a and 5.23b, and Figures 5.23c and 5.23d respectively. The plots of equivalent viscous damping ξ_{eq} obtained by using approach-2 can be found in Appendix H (refer Figure H.14).

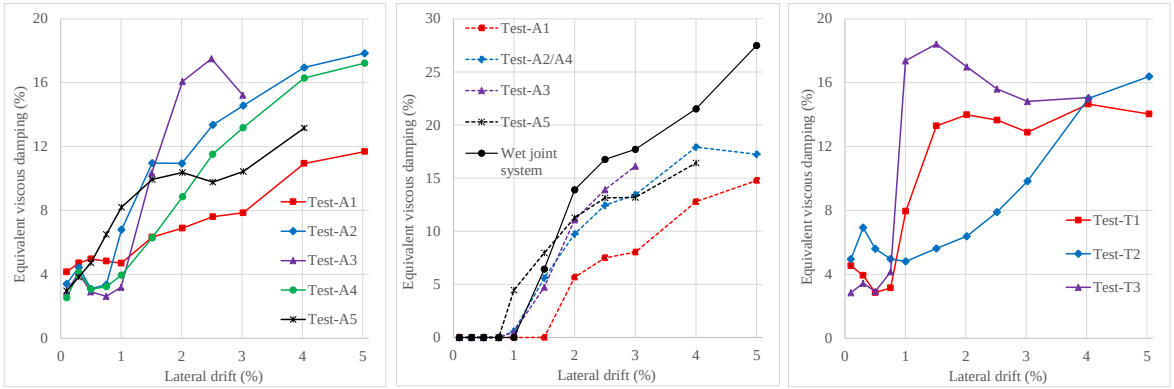

(a) Experiment: ξ_{eq} of Tests:A1 to A5 (b) Numerical: ξ_{eq} of Tests:A1 to A5 (c) Experiment: ξ_{eq} of Tests:T1 to T3

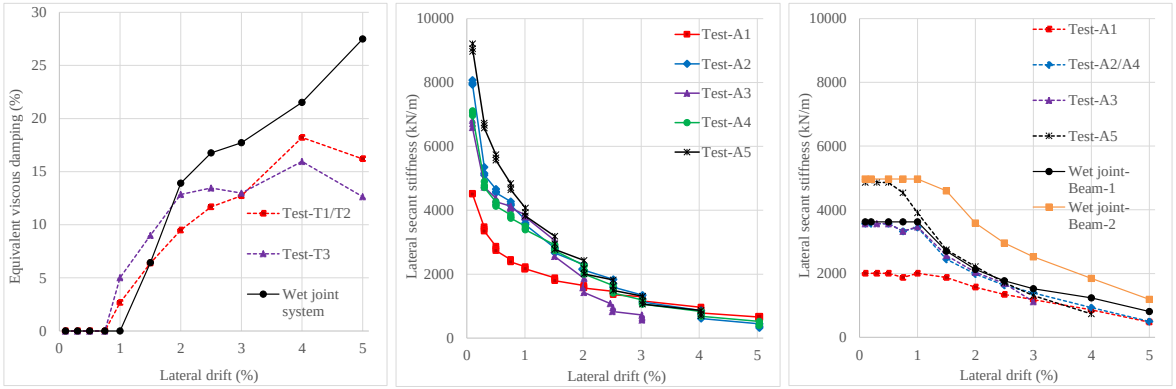

(d) Numerical: ξ_{eq} of Tests:T1 to T3 (e) Experiment: K_l of Tests:A1 to A5 (f) Numerical:K_l of Tests:A1 to A5

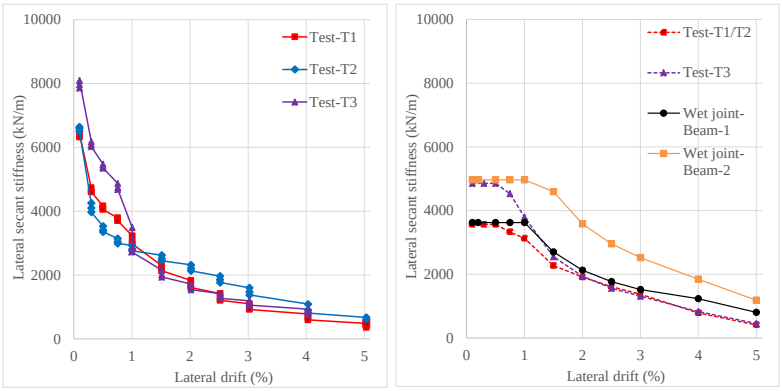

(g) Experimental: K_l of Tests:T1 to T3 (h) Numerical: K_l of Tests:T1 to T3

Figure 5.23. Equivalent viscous damping and stiffness degradation of sub-assemblies

By comparing the numerical plots with experimental plots, it can be concluded that the numerical approach is able to reliably replicate the pinching characteristics of the sub-assemblies associated with slip of the connection. It can be observed that the hysteretic damping increases with increase in lateral drift and the rate of increase of equivalent viscous damping ξ_{eq} varies primarly because of different rate of strength degradation and slip of the connection. For example, in Tests-A3 and T3 the abrupt increase in equivalent viscous damping is due to an abrupt decrease in strain energy E_s and a sudden increase in slip of the connection, respectively (refer Figures 5.10c and 5.9e). In general, equivalent viscous

damping ξ_{eq} of the sub-assemblies with angle and tube connections is less compared to wet jointed concrete frame sub-assembly (ξ_{eq} is usually more than 20% which can inferred from Figures 5.23b and 5.23d). This was due to concentrated beam edge damage in the tested sub-assemblies unlike the spread of damage that occurs in the plastic hinge region of monolithic concrete frame sub-assembly. It is clear from Figures 5.23b and 5.23d that numerical models have no equivalent viscous damping converted from hysteresis energy dissipation, whereas there is a small amount of equivalent viscous damping obtained from experiments. This is due to the idealization of the initial behaviour of the sub-assembly as elastic and linear, whereas in reality there is a small amount of energy dissipation due to the formation and spread of flexural cracks and slip of the connection.

By using Equation 18, lateral stiffness degradation K_l of the sub-assemblies with angle and tube connections obtained from experimental test results and numerical analysis (approach-1) are plotted in in Figures 5.23e and 5.23f, and Figures 5.23g and 5.23h respectively. The lateral stiffness degradation of the sub-assemblies obtained by using approach-2 is reported in Appendix H (refer Figure H.14). It is clear that the sub-assemblies with Beam-2 (Tests-A5 and T3) exhibit high lateral stiffness compared to sub-assemblies with Beam-1, and this was due to high effective flexural rigidity. In general, the rate of lateral stiffness degradation of the sub-assemblies with angle and tube connections with increasing drift of similar order, this is because of similar beam edge damage mechanism in all tests. Also, there is a difference in actual initial lateral stiffness from the experiments and numerical analysis, this is because of idealization of the moment rotation input curve with effective secant stiffness to yield point (which is considerably less than the initial stiffness computed based on gross sectional properties). In general, the rate of stiffness degradation of the sub-assemblies with angle and tube connections is higher compared to wet jointed sub-assembly, and this was due slip of the connection.

The slip envelopes of the sub-assemblies with angle and tube connections obtained by using numerical analysis (approach-1) are shown in Figure 5.24a and 5.24b, respectively. By comparing the simulated slip envelopes with experimentally obtained slip plots, it can be concluded that in general the behaviour of the connection associated with slip can be reasonably captured by the analysis but the rate of the slip/ movement of the connection deviates to some extent from the experimental plots. Also, there is an error in simulating residual slip of the connection and this is due to symmetrical F-S connection spring backbone envelope, but in reality the slip of the connection will not be symmetrical in both directions of the loading.

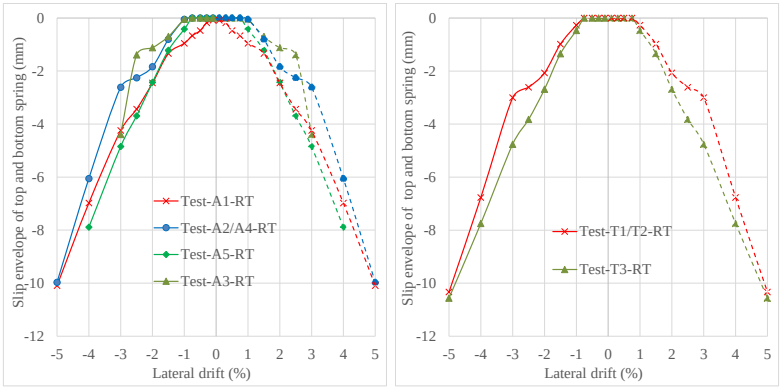

(a) Slip envelopes of Tests:A1 to A5 (b) Slip envelopes of Tests:T1 to T3

Figure 5.24. Numerically simulated slip envelopes of right top (RT) and right bottom (RB) springs

5.6 Comparison of tested sub-assemblies performance with "wet jointed" and "ductile connectors" sub-assemblies performance

In this section, experimentally obtained hysteresis behaviour of the tested sub-assembly with the proposed "dry connections" is compared with two different precast concrete sub-assemblies taken from the literature with; (i) wet joint, and (ii) ductile connectors. For the first type, a wet/monolithic/cast-in-situ connection that has been implemented in New Zealand for a precast concrete frame buildings is chosen [15]. In this wet jointed frame system, beams are passed on top of the bottom storey columns and connected at mid span. The protruded rebars of the bottom storey columns are passed through the beams and inserted into the ducts of the upper storey columns and grouted. More details of this system (referred as system-2) can be found in the literature [15]. For the second type, jointed frame system is chosen in which the precast concrete components are connected by using "ductile connectors", which are made up of anchors embedded into the columns and connected to rebars of the beam via couplers. More details of this jointed frame system can be found in the literature [16].

In this section, experimentally obtained hysteresis behaviour of the sub-assemblies with the proposed "dry" connections is compared with hysteresis behaviour of precast concrete sub-assemblies with; (i) wet joints, and (ii) ductile connectors. For this study, one of the wet/monolithic connection (referred as system-2) for a precast concrete frame buildings that has been implemented in New Zealand is chosen [15]. The frame system is made of beams passing on top of bottom storey columns and with "wet joints" at mid span of the beams, and protruded rebars of bottom storey columns are passed through beams and inserted into ducts of the upper storey columns and grouted, and more details of this system can be found in the literature [15]. As mentioned before, another class of jointed system was made by connecting

precast concrete components with use of “ductile connectors”, which are made up of anchors embedded into the columns and connected to rebars of the beam with use of couplers and more details can be found in the literature [16].

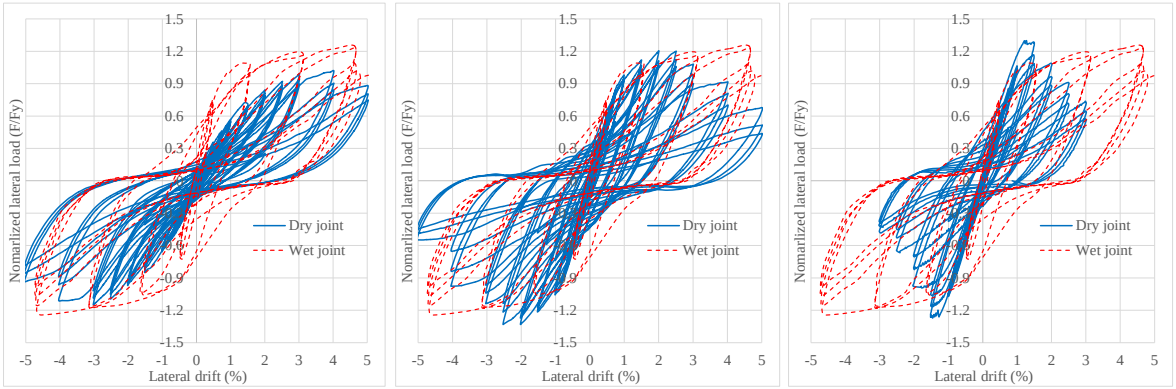

(a) Test-A1 (b) Test-A2 (c) Test-A3

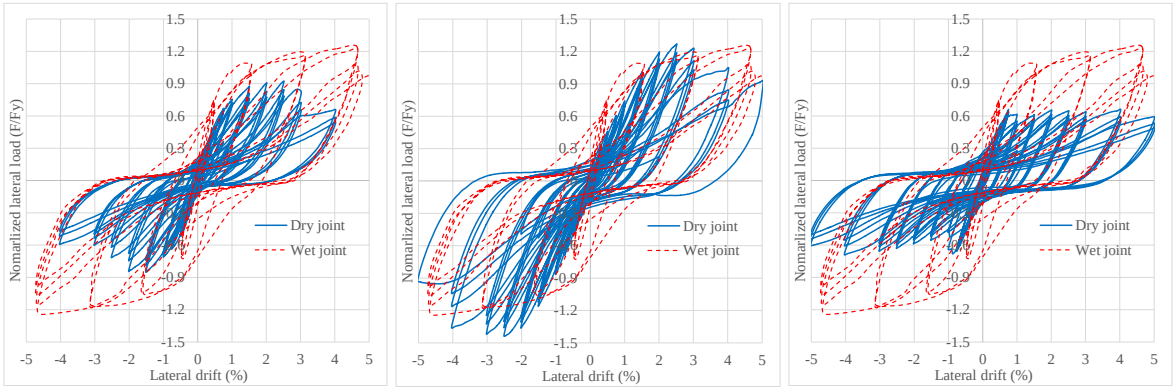

(d) Test-A5 (e) Test-T2 (f) Test-T3

Figure 5.25. Hysteresis behaviour of sub-assemblies with proposed dry connections and “wet joints”

The normalized (with respect to theoretical strength) hysteresis plots of the tested sub-assemblies and sub-assemblies with “wet joints” and “ductile connectors” are shown in Figures 5.25 and 5.26 respectively. The important conclusions that can be made from the comparison are; (i) the sub-assemblies with proposed connections exhibit more pinching behaviour compared to the wet jointed system, (ii) initial stiffness of the sub-assembly with the proposed connections can be less than the wet jointed/ductile connector system as there is an inevitable slackness in the system because it includes several interconnected elements(refer Figure 5.25a and 5.26a), (iii) nominal lateral strength of the sub-assembly with angle and tube connections can be less than wet joint/ductile connector system if the connection fails (i.e. beam edge failure) before yielding of rebars of the beam (refer Figures 5.25d and 5.25f, 5.26d and 5.26f), (iv) rate of strength degradation of the sub-assembly with proposed connections can be higher than monolithic/ductile sub-assembly system (refer Figures 5.25c and 5.26c), (v) ductility of the sub-assembly with angle and tube connections can be much less than wet/ductile jointed system (refer Figures 5.25c and 5.26c), and (vi)

initial stiffness and nominal lateral strength of the sub-assembly with angle and tube connections can be matched with wet jointed/ductile connector system (refer Figures 5.25b and 5.26b) by properly designing and delaying the beam edge failure.

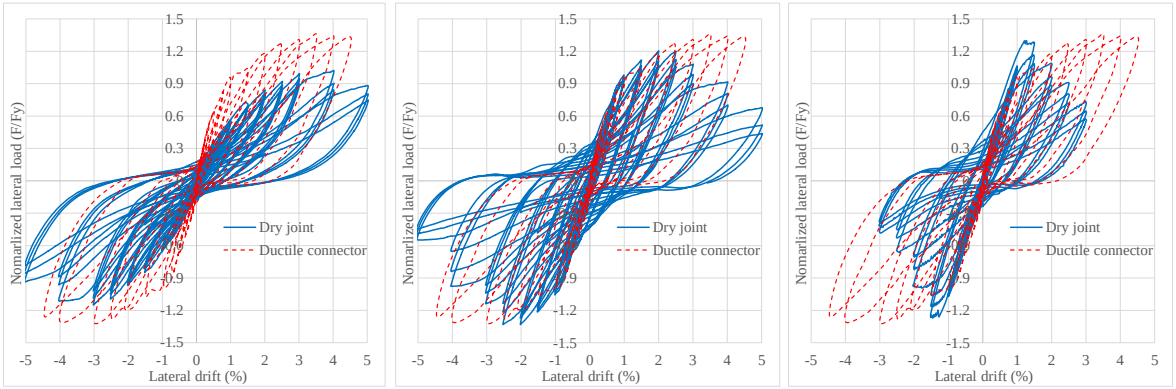

(a) Test-A1 (b) Test-A2 (c) Test-A3

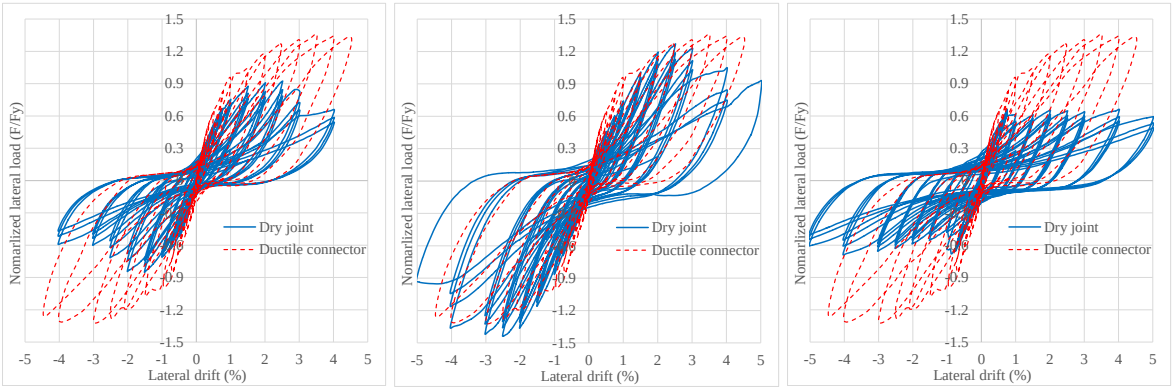

(d) Test-A5 (e) Test-T2 (f) Test-T3

Figure 5.26. Hysteresis behaviour of sub-assemblies with dry connections and "ductile connectors"

5.7 Demountability, replaceability, and upgradability assessment of the sub-assembly

One of the primary aims of the research work is to assess whether the proposed angle and tube connections between the precast concrete beam and column can be treated as demountable connections or not, thereby making the whole building frame system demountable. Another aspect of the research work is to investigate whether the damaged beam can be replaced with a new beam of either the same or a higher capacity without disrupting the weak beam–strong column/connection hierarchy and achieving the same or better structural performance compared to the original sub-assembly system. In the lab, the deconstruction sequence of the beam and the angle connection was exactly opposite of the erection sequence, which can be summarized as; (i) unbolting the connection, (ii) removing the connection components above the beam top surface, (iii) removing the damaged beam with the help of a crane, and (iv) removing the connection components below the beam

surface. It was noticed that because of the sliding of the angle connection, the bolts on the beam side had moved from their initial position, which resulted in some difficulties in removing the bolts and steel angles. Also, for the angle connection configuration with grouted ducts on the beam side may require extra effort in removing the steel angles (as the holes are fully grouted). Removal of precast concrete beam with tube connection involved unbolting on the column side and then removing the beam along with connection with the help of crane. In general, from this experimental test program, it was realized that the beams can be demounted and replaced with reasonable effort at the sub-assembly level.

It was demonstrated through the experimental programme that the structural performance of the original sub-assembly can be achieved after replacing the damaged beam of the original sub-assembly with a new beam of the same capacity (refer Tests-A2/A4 results). It is important to note that replacing a damaged beam in a real building will not be as easy as replacing a damaged beam in the laboratory. The possible challenges in demounting a damaged beam and replacing with a new beam are identified and reported in Chapter 2. Another objective of the test programme was to upgrade the structural performance of original sub-assembly by replacing the damaged beam with a new beam of higher capacity. By comparing experimental test results of Test-A2 (Beam-1) and Test-A5 (Beam-2), it is clear that this objective was not achieved. The reason for this was in Test-A5, ultimate capacity of the connection corresponding to beam edge mechanism rather than yield moment capacity of the beam governed the lateral strength of the sub-assembly (same horizontal stirrups layout was used in Beam-1 and Beam-2). The important finding from this study was that the strength hierarchy including the capacity of the connection corresponding to beam edge failure need to be considered explicitly in the design process (i.e. yield moment capacity of the beam should be less than the ultimate connection capacity corresponding to the beam edge failure), otherwise lateral strength of the frame system will be limited to the capacity of the connection.

5.8 Summarized results of sub-assemblies with angle and web plate connection

In this section, experimental test and numerical analysis results of the two tested sub-assemblies with angle and web plate connections (Tests-AWP1 and AWP2), including the cyclic slip plots of the connection on beam and column sides, and the damage state of the beam at various drift levels are presented. The details of the infill material, the amount of pre-tension in the bolts, and the connection capacity is reported in Chapter 3 (refer Table 3.8 and Table 3.9).

5.8.1 *Test-AWP1: Internal frame sub-assembly*

Test-AWP1 is carried out on the internal precast concrete frame sub-assembly with angle and web plate (AWP) connections. The cross sectional details of the AWP connection is shown in Figure 5.27a, and the tested internal frame sub-assembly configuration is shown in Figure 5.27b. The 16 mm thick web plate on the column side and beam side are connected using four 16 mm diameter (grade 8.8) bolts. As the steel web plate was embedded at the precast concrete beam end, it is not possible to have closed loop horizontal stirrups (unlike a precast concrete beam for the angle connection), so U-shaped horizontal stirrups were provided. The layout details of the precast concrete beam with the embedded web plate is reported in Appendix C.

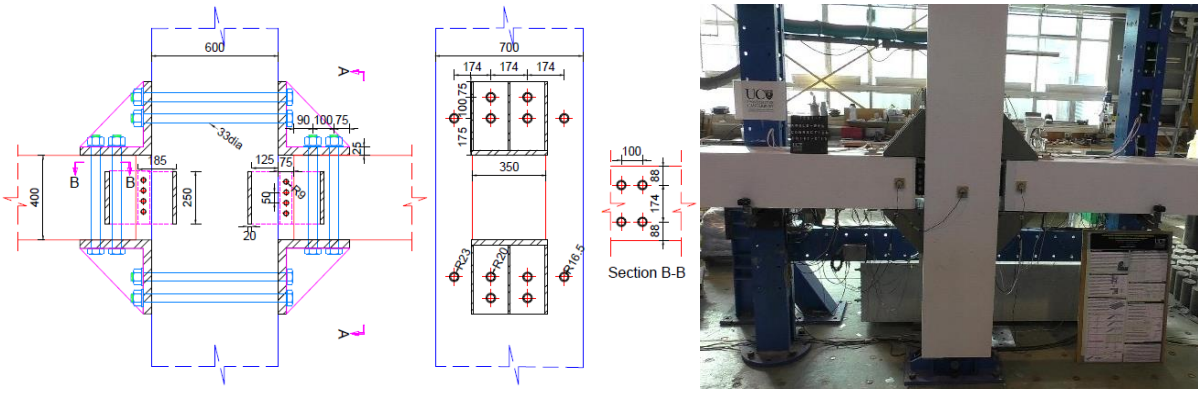

(a) Layout of the WP connection (b) Tested sub-assembly configuration

Figure 5.27. Layout of the AWP connection and tested sub-assembly configuration

The hysteretic behaviour of the internal frame sub-assembly with the AWP connection under quasi-static cyclic loading is shown in Figure 5.28a. It is clear that the tested sub-assembly did not achieve its nominal lateral strength of 210 kN computed based on the yield moment capacity of the beam (M_{yb}). The maximum lateral load that the sub-assembly could reach was only 165 kN, this was because the lateral capacity of the sub-assembly is dictated by the capacity of the connection (M_{uc}). The overall hysteresis loop of the tested sub-assembly with AWP connection is close to "pinching behaviour". The hysteretic behaviour of the sub-assembly is predominantly governed by the slip of the connection, and the experimentally obtained slip plots of the connection on beam and column sides are shown in Figures 5.28b and 5.28c. It is clear that the vertical slip between the connection and the column is of similar magnitude of the horizontal slip between the connection and the beam. This is because of the prying effect (i.e. lift off/rigid body rotation of the steel angles), which reduced the contact area and the amount of pre-tension in the bolts, thereby reducing the available frictional shear resistance.

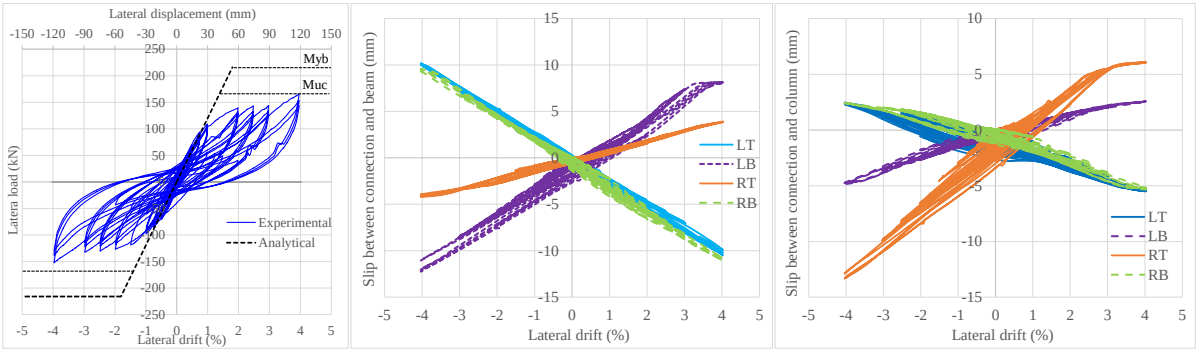

(a) Hysteresis plot (b) Slip on beam side (c) Slip on column side

Figure 5.28. Hysteresis plot of the sub-assembly and slip of the connection obtained from Test-AWP1

The initial damage to the precast concrete beam with the AWP connection (i.e. up to 0.5% lateral drift) was the spread of flexural cracks, which is shown in Figure 5.29a. It was realized that the U-shaped horizontal stirrups were not effective in resisting the longitudinal shear demand, as a result, early direct split tensile/bursting cracks were formed (when the connection slipped away from its initial position), which is shown in Figures 5.29b and 5.29c. The detail modes of failure occurred in the precast concrete beam with the AWP connection at different drift levels is reported in Appendix I.

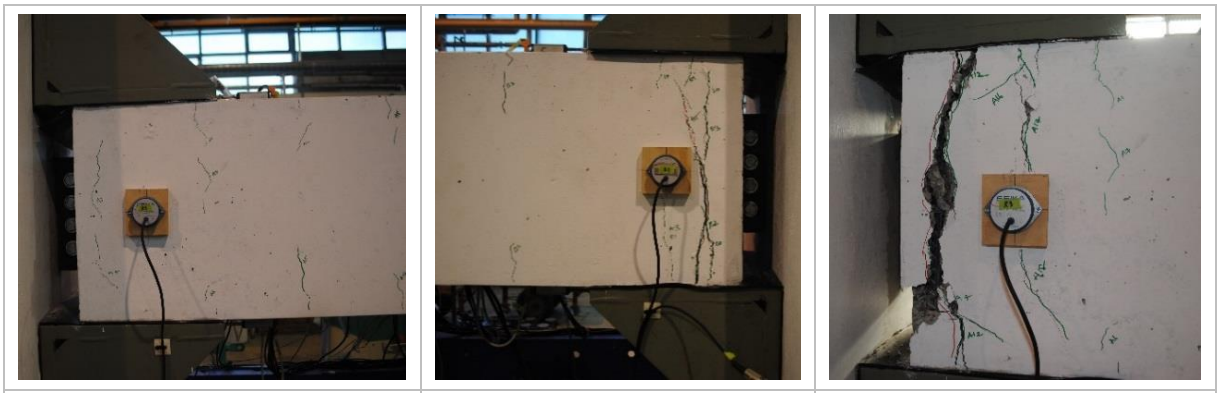

(a) 0.5% drift: flexural cracks (b) 1.5% drift: split tensile cracks (c) 2.5% drift: wide split cracks

Figure 5.29. Damage state of the precast concrete beam obtained from Test-AWP1

5.8.2 *Test-AWP2: Corner frame sub-assembly with repaired beam from Test-AWP1*

The aim of the Test-AWP2 was to prove that the sub-assembly with AWP connection in Test-AWP1 was not able to achieve its nominal lateral strength because of the early beam edge failure, which is due to no effective beam edge protection (i.e. absence of closed loop horizontal stirrups). To prove this, the damaged beam from the sub-assembly of Test-AWP1 (shown in Figure 5.30a) was repaired by armouring with steel plates on all sides of the beam end as shown in Figure 5.31a. The steel armour was anchored to the beam by welding the steel studs connecting the steel plates and longitudinal bars at beam end and side faces, and also by welding beam end face steel plate around the embedded web-plate as shown in Figure

5.31b. Thereafter, the damaged portion of the beam is filled up with high early strength (HES) grout as shown in Figure 5.31c. The corner beam column sub-assembly with the repaired beam is shown in Figure 5.30b.

(a) Damaged beam from Test-AWP1

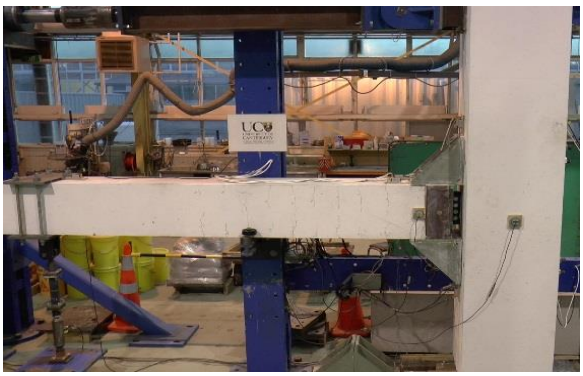

(b) Test-AWP2: with repaired beam

Figure 5.30. Damaged beam from Test-AWP1 and sub-assembly with repaired beam (Test-AWP2)

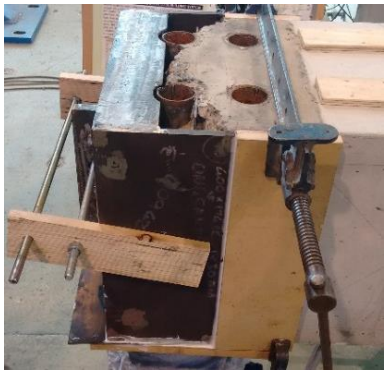

(a) Armoured beam edge

(b) Armour welded to web plate

(c) Grouted beam edge

Figure 5.31. Armouring and grouting of the damaged beam from Test-AWP1

It is clear from Figure 5.32a that the sub-assembly with the beam end protection with steel armour was able to achieve its nominal lateral strength of 108 kN. Since the beam was already damaged in the previous test (i.e. Test-AWP1), the sub-assembly showed significant strength degradation after 2.5% lateral drift. It is clear that the cyclic behaviour of the Test-AWP2 sub-assembly is a "fat" hysteresis loop (i.e. more energy dissipation) when compared to Test-AWP1 sub-assembly behaviour (refer Figures 5.28a and 5.32a). The slip between the connection and the beam under quasi-static cyclic loading is similar to other corner sub-assemblies (refer Test-A series), which is shown in Figures 5.32b and 5.32c. Comparing Figures 5.28 and 5.32 indicates that the connection's cyclic slip of the corner and internal sub-assemblies under quasi-static cyclic loading is quite different. In case of the internal frame sub-assembly, the connections being symmetrical with respect to the column, and connected to each other by the threaded rods on the column side, when the column is returned to the initial position, the connections on both sides of the column have to move equally and

have to return to the initial position as well. In case of the corner sub-assembly when the column is drifted, because of the slip between the connection and the beam has exceeded the clearance between the bolts and the ducts, which results in change of shape of the duct from circular to oblong (i.e. oval shape), and when the column returned to the initial position, the connection will equilibrate at another position which is not the initial position.

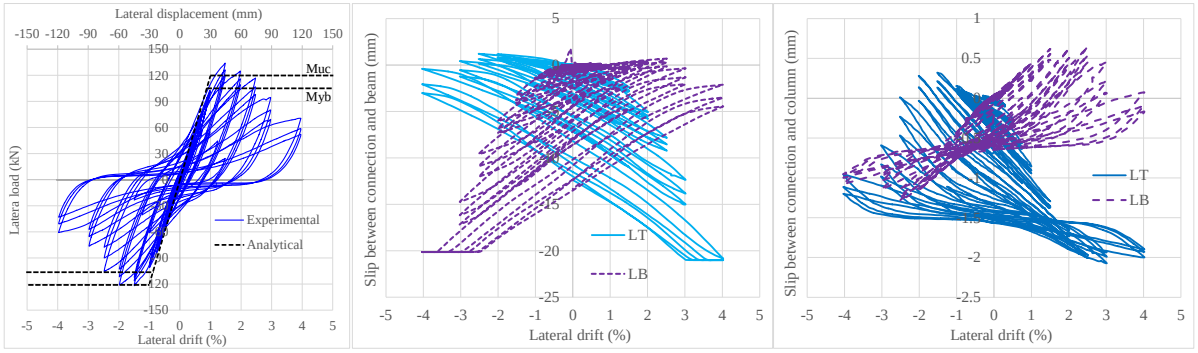

(a) Hysteresis plot (b) Slip on beam side (c) Slip on column side

Figure 5.32. Hysteresis plot of the sub-assembly and slip of the connection obtained from Test-AWP2

The major damage states of the repaired precast concrete beam in Test-AWP2 is shown in Figure 5.33. New flexural cracks were formed along with the existing cracks extending along the beam depth, which is shown in Figure 5.33a, this is due to further flexural bending of the repaired beam. Due to the ingress of the connection on the beam top and bottom surfaces, spalling of the concrete was observed as shown in Figure 5.33b. The final damage state of the beam was associated with the spalling of the concrete and the formation of edge cracks as shown in Figure 5.33c. The detail modes of failures occurred in the repaired precast concrete beam with the AWP connection in Test-AWP2 at different drift levels is also reported in Appendix I.

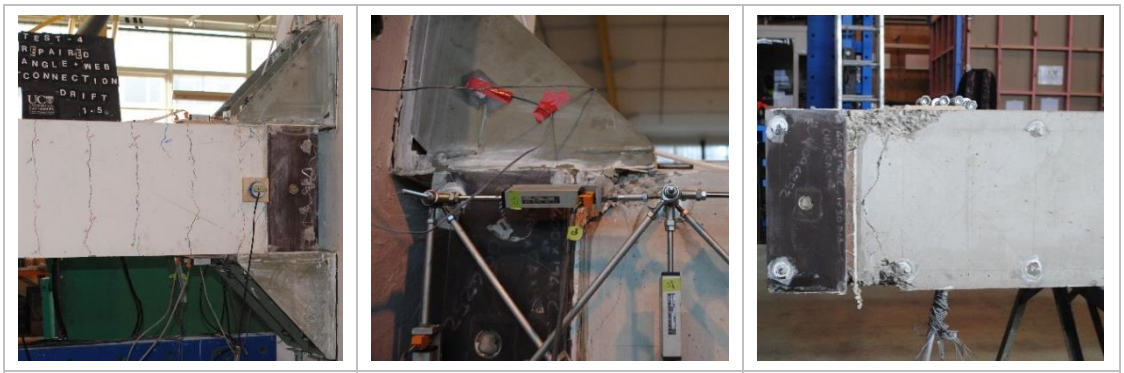

(a) 1.5% drift: new cracks (b) 2.5% drift: spalled concrete (c) Beam edge cracks

Figure 5.33. Damage state of the repaired beam with angle and web plate connection at different drifts

Comparison of the equivalent viscous damping ξ_{eq} and lateral stiffness degradation K_l of the Test-AWP1 and Test-AWP2 sub-assemblies are shown in Figure 5.34. Because of the early slip of the connection, the initial damping of the Test-AWP1 sub-assembly is high compared

to the damping of the Test-AWP2 sub-assembly. At higher drift, the damping of the Test-AWP1 sub-assembly reduces because of the concentrated beam edge failure, whereas with the Test-AWP2 sub-assembly the damping increases because of yielding of the rebars. It is clear from Figure 5.34b that the initial lateral stiffness of the Test-AWP1 frame sub-assembly is approximately twice that of the Test-AWP2 sub-assembly lateral stiffness, this is because Test-AWP1 sub-assembly is an internal frame sub-assembly whereas Test-AWP2 sub-assembly is a corner frame sub-assembly. After 0.75% lateral drift, the rate of lateral stiffness degradation of the Test-AWP1 and AWP2 sub-assemblies are similar. This is because in both cases the lateral stiffness degradation is predominantly governed by the rate of slip of the connection.

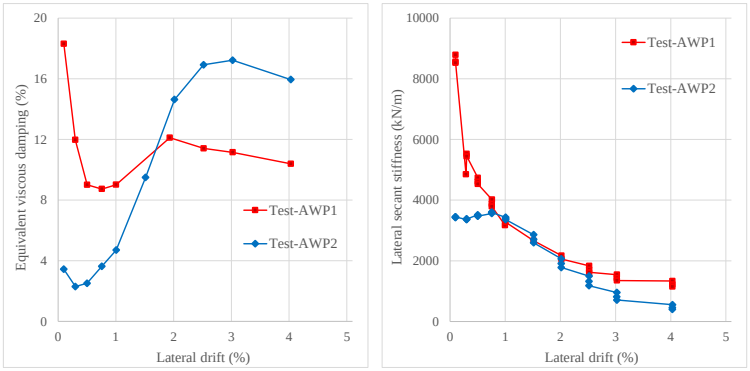

(a) Equivalent viscous damping ξ_{eq} (b) Lateral stiffness degradation K_l

Figure 5.34. Damping and stiffness degradation of the sub-assemblies with AWP connection

By using the two approaches developed and described in section 1.5, the cyclic behaviour of the corner frame sub-assembly with AWP connection (i.e. Test-AWP2) is numerically simulated and compared with experimentally obtained hysteresis plots, which is shown in Figure 5.35. It is clear that the numerical model (developed for angle and tube connections) is able to reliably simulate the cyclic behaviour of a frame sub-assembly with the angle and web plate connections. This is because the mode of deformation in a frame sub-assembly with either angle and web plate connections or angle connections alone is similar. The nonlinear response of the beam and connection springs of the frame sub-assembly (Test-AWP2) with the AWP connection under quasi-static cyclic loading is reported in Appendix I.

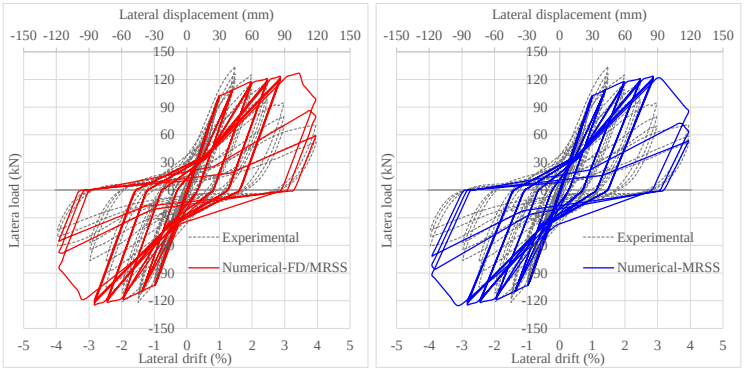

(a) Approach 1 (b) Approach 2

Figure 5.35. Simulated hysteresis behaviour of the Test-AWP2 sub-assembly

5.9 Conclusions

In this chapter, full details of design and experimental as well as analytical performance evaluation of two types of dry beam-column connections for a demountable concrete frame building system, namely; (i) angle connection, and (ii) tube connection are reported. Also, summarized results of the frame sub-assemblies with angle and web plate connection are presented. Based on the experimental test results, it can be concluded that the cyclic performance of the sub-assemblies with proposed connections predominantly depends on the fill material between the connection plates and the member surfaces, beam edge distance beyond the ducts, the gap between beam end face and column face, and the amount of pre-tension in the bolts. Also, it can be concluded that the cyclic behaviour of the sub-assemblies can be categorized to “pinching” behaviour due to slip of the connection and concentrated beam edge failure. The proposed analytical model is able to reliably estimate the ultimate moment capacity of the connection on beam side corresponding to beam edge failure. Analytically predicted initial lateral stiffness and nominal lateral strength of the sub-assemblies with angle and tube connections match well with experimental results. It was evident from the test results that the sub-assembly with proposed connections may or may not achieve the initial lateral stiffness and nominal lateral strength of a wet jointed sub-assembly depending on the connection behaviour. Also, it can be concluded that the sub-assembly with the proposed connections can underperform in-terms of ductility, energy dissipation, and strength and stiffness degradation when compared to wet jointed precast concrete sub-assembly if the beam edge failure mechanism is not delayed until full yielding of the beam.

The behaviour of the sub-assemblies associated with slip of the connection can be simulated by using two macro modelling approaches; (i) approach-1; two parallel translation connection springs in series with beam rotational spring, and (ii) approach-2: connection rotational spring in series with beam spring. Comparison of the tested sub-assemblies performance with

existing precast concrete sub-assemblies with “wet joints” and “ductile connectors” proved that performance of sub-assemblies with proposed connections can be very uncertain depending on design and detailing of the beam edge, infill material properties, and strength hierarchy. It can be concluded that precast concrete frame sub-assembly with proposed angle and tube connections cannot completely emulate the behaviour of wet jointed precast concrete frame sub-assembly in every aspect. Nevertheless, the initial lateral stiffness and nominal lateral strength of the sub-assembly with proposed connections can be close to wet jointed precast concrete frame systems. Finally, it was demonstrated through the experimental programme that the structural performance of the original sub-assembly can be regained after the beam is damaged and replaced with a new beam of the same capacity. Upgradation of the sub-assembly by replacing the damaged beam with a new beam of higher capacity was not achieved, and this was due to alteration in the strength hierarchy (connection strength corresponding to beam edge failure turned out to be less than yield moment capacity of the beam).

5.10 References

1. ACI, *Building code requirements for structural concrete (ACI 318-08) and commentary*. 2008, American Concrete Institute.
2. NZS3101, *NZS3101: The Design of Concrete Structures*. 2006, Standards New Zealand Wellington.
3. PCI, *PCI Design Handbook: Precast and Prestressed Concrete*. 2010, MNL-120. 6th ed. Chicago, IL: PCI.
4. Zoubek, B., M. Fischinger, and T. Isakovic, *Seismic response of dowel connections in RC structures*, in *NZSEE Conference*. 2016: Christchurch, New Zealand.
5. Elliott, K.S., et al., *Can precast concrete structures be designed as semi-rigid frames? Pt. 1: the experimental evidence.* Structural Engineer, 2003. **81**(16): p. 14-27.
6. Eurocode, *3: Design of steel structures, Part 1.8: Design of joints*. 2005, EN-1993-1-8. Brussels: European Committee for Standardization.
7. BCSA, *Joints in Steel Construction: Moment Connections*, in *Steel Construction Institute*. 1997.
8. ACI, *Acceptance Criteria for Moment Frames Based on Structural Testing*, in *Report by ACI Innovation Task Group 1 and Collaborators*. 2001.
9. Baltay, P. and A. Gjelsvik, *Coefficient of friction for steel on concrete at high normal stress.* Journal of Materials in Civil Engineering, 1990. **2**(1): p. 46-49.
10. Rabbat, B. and H. Russell, *Friction coefficient of steel on concrete or grout.* Journal of Structural Engineering, 1985. **111**(3): p. 505-515.
11. Michaels, M. *Coefficients of Friction for Concrete*. 2006; Available from: http://hypertextbook.com/facts/2006/MatthewMichaels.shtml.
12. Bae, S. and O. Bayrak, *Plastic hinge length of reinforced concrete columns.* ACI Structural Journal, 2008. **105**(3): p. 290.
13. Ibarra, L.F., R.A. Medina, and H. Krawinkler, *Hysteretic models that incorporate strength and stiffness deterioration.* Earthquake engineering & structural dynamics, 2005. **34**(12): p. 1489-

1511.

14. Mazzoni, S., et al., *OpenSees command language manual*. Pacific Earthquake Engineering Research (PEER) Center, 2006.
15. Restrepo, P.J., *Seismic behaviour of connections between precast concrete elements.* PhD thesis, University of Canterbury, 1992.
16. Englekirk, R., *Development and testing of a ductile connector for assembling precast concrete beams and columns.* PCI journal, 1995. **40**(2): p. 36-51.

Chapter 6: Feasibility assessment of pin base connections for the lateral load resisting frame of the proposed demountable building system

Aninthaneni, P. K., Dhakal, R. P., and Marshall, J. (2014). "Feasibility of pinned-base connections for demountable precast frame building systems." 23rd Australasian Conference on Mechanics of Structures and Materials (ACMSM23) Byron Bay, Australia, 9-12 Dec 2015.

6.1 Introduction

6.1.1 *Overview*

In this chapter, three types of lateral load resisting frames along with pros and cons of each type are discussed in detail, and out of these three types the frame options that are structurally robust, flexible/adaptable, and suitable for the proposed demountable building system are reported. In order to avoid damage to the columns and eliminate the need to replace them, and to make the proposed demountable building system to be considered as quickly repairable/replaceable (i.e. low downtime) building system (by forcing the damage to occur in easily replaceable components such as beams and braces), the column to foundation connections have to be pin instead of fixed. Because of the base connection changing from fixed to pin, the lateral strength and stiffness of an unbraced frame are reduced, and the primary aim of the numerical study is to quantify the average reduction of these parameters. Pushover analysis is carried out on a wide range of low to medium rise (i.e. up to 10 storeys) unbraced frames with fixed and pin bases to estimate the lateral strength and stiffness. The affected structural performance parameters of the unbraced frames due to change of base fixity are plotted against the column to beam capacity ratio β, and number of storeys n_s. The options to increase the lateral strength and stiffness of an unbraced frame with pin bases to match with the pushover capacity curve of the fixed base frame are explored. Moreover, issues such as soft storey mechanism (i.e. damage to the columns), secondary (i.e. *P-Δ*) and higher mode effects in an unbraced frame with pin bases are also highlighted. In cases where pin base connections are inevitable to avoid damage to the columns, the lateral load resisting frame options that can be considered for the proposed demountable building system are reported. Finally, lateral load resisting frame options with increasing order of structural flexibility/adaptability (i.e. the system which requires less time to replace the damaged

components is more structurally flexible) that render the proposed demountable building system a “low downtime” building system are reported.

6.1.2 *Background*

Structural frames of any building are classified based on the load transfer mechanism from the floors to the foundations; (i) an “unbraced” frame with predominant flexural behaviour, and (ii) a “braced” frame with predominant strut and tie behaviour. Another way to classify the structural frame of a building is based on the amount of expected lateral deformation and whether second order effects can be neglected or not; (i) a “sway” frame with predominant lateral deformation where second order effects cannot be neglected, and (ii) a “non-sway” frame with minimal lateral deformation and second order effects can be ignored. The common assumption is that all “braced” frames are “non-sway” frames, whereas all “unbraced” frames are “sway” frames. It is possible to design a braced frame with flexible braces that can be a “sway” frame, and an unbraced frame with sufficient flexural rigidity so that it can be categorized as a “non-sway” frame. The actual classification of a frame should be based on both load transfer mechanism and the amount of expected lateral deformation under design lateral load.

The column to foundation connections of a frame building are classified as either fixed/rigid or semi-rigid or pin/simple depending on the rotational stiffness and moment carrying capacity [1]. In the analysis and design, pin base connections with low rotational stiffness are also considered as pin connections as long as they are able to transfer the internal forces to the base and the distribution of internal forces in the frame are not significantly altered because of the partial fixity at the base. With the use of pin base connections, the cost of the connections and the size of the foundations are substantially reduced. The building codes allow pin base connections as long as the overall structural frame system satisfies the strength and stability requirements at ultimate and serviceability limit states. Pin base connections are quite common in single storey unbraced portal frame structures (like storage sheds, and warehouse, etc.) because of the light roof and very small design lateral load, whereas they are considered to be uneconomical and not feasible in unbraced multi-storey frame buildings. Also, pin base connections are apt for multi-storey braced frame buildings (i.e. generally designed as non-sway frames) because of the nature of the load transfer mechanism (i.e. strut and tie action).

Most of the time, concrete frame buildings are unbraced because it is easy to achieve the required flexural rigidity, and the column to foundation connections are monolithic

connections (i.e. fixed) which can transfer moment along with shear and axial forces to the foundations. The proposed demountable building system (which is made of precast concrete elements and steel connections, refer Chapter 2 for details) is structurally flexible to accommodate either fixed or pin base connections depending on whether damage to the columns is allowed or not [2-4]. Also, the schematic layout of the proposed fixed and pin base connections, and the load transfer mechanism between precast concrete columns and foundations is reported in Chapter 2.

The damage to the ground storey columns of the proposed demountable building system can be eliminated by having pin base connections instead of fixed base connections. Therefore, the need to replace the damaged columns (if it was fixed base connections) can be completely avoided, and only other damaged components (mostly beams and braces (if the frame was braced)) can be replaced with new ones (which is less challenging compared to replacing the damaged columns) to bring back the damaged building to its original state as it was before the earthquake. The lateral load resisting frame of the proposed demountable building system can be either unbraced or braced (as part of initial design or later upgradation). If the lateral load resisting frame is braced with pin bases then beam-column connections can be either rigid or pin. In seismic regions, braced frame buildings with rigid beam column connections are also being constructed in order to improve reserve strength and to reduce maximum and residual drift demands after an earthquake [5]. In case of a braced frame with pin bases and rigid beam column connections the damage occurs in beams and braces, whereas with pinned beam column connections the damage can be limited to only braces which is relatively very easy to replace. More detailed explanation on possible locations of the damage in different lateral load resisting frame options is reported in the following sections.

6.1.3 *Objectives and scope*

In this chapter, three types of lateral load resisting frames for the proposed demountable concrete frame building system are reported. Pros and cons of each type from the perspective of possible locations of the damage in an earthquake and the challenges involved in replacing the damaged components (such as columns, beams, and braces) are detailed. As mentioned before, to eliminate any possible damage to the ground storey columns and avoid the need to replace the damaged columns, feasibility of pin base (instead of fixed base) connections for the unbraced lateral load resisting frame is investigated. Because of change of the base fixity from fixed to pin, the lateral strength (i.e. base shear capacity) and initial lateral stiffness of an unbraced frame reduce. In this study, pushover analysis is carried out on a wide range of

low to medium rise frames to; (i) identify the governing parameters that dictate the base shear capacity and to understand variation of the base shear capacity with the identified parameters, (ii) quantify average range of reduction in base shear capacity and initial lateral stiffness, (iii) quantify average range of increase in fundamental period, and (iv) quantify average range of decrease in seismic demand.

Thereafter, the options to increase the base shear capacity and lateral stiffness of a pin base frame to match with the fixed base frame are explored, which include; (i) increasing the rebar percentage or cross-section sizes or both, and (ii) adding the steel braces. To identify the pros and cons of each option, capacity curves of the upgraded and original pin base frames are compared to the fixed base frames' pushover capacity curves. Also, issues such as soft storey mechanism and secondary effects in an unbraced frame with pin bases are highlighted. Design parameters that need to be explicitly considered to avoid soft storey mechanism in an unbraced frame with pin bases are identified. The lateral load resisting frame options with increasing order of structural flexibility/adaptability (i.e. decreasing order of downtime required to replace the damaged components) that are suitable for the proposed demountable building system are reported. Finally, the reasons for an unbraced frame with pin bases that cannot be part of the proposed demountable building system are identified and reported.

6.2 Lateral load resisting frame options for the demountable building system

As mentioned before in Chapter 2, in the proposed demountable concrete building system the perimeter lateral load resisting frames can be either un-braced or braced with fixed or pin base connections. With the above mentioned criteria, the possible lateral load resisting frame options to transfer the lateral load from the floors to the foundations are shown in Figure 6.1; (i) an unbraced frame with fixed bases, (ii) a braced frame with either pin or rigid beam-column connections and pin bases, and (iii) an unbraced frame with pin bases. Hereafter, an *"unbraced frame"* means the beam column connections of that frame are *"rigid"*, and a *"braced frame"* means the column to foundation connections are *"pin"*. Also, a *"frame"* means it is actually an *"unbraced frame"*. An unbraced frame with fixed bases is chosen as the base frame, and is hereafter called as the "*reference frame"*.

In the case of an unbraced frame with fixed bases (refer Figure 6.1a), the lateral load is predominantly resisted by flexural resistance of frame elements, and frame components (i.e. beams and mostly ground storey columns) that are expected to get damaged to varying extents in a moderate level earthquake. If the building is in a reparable damage state, then

both damaged beams and columns need to be replaced with new ones to bring back the damaged building to its original state as it was before the earthquake. Replacing the damaged columns will be challenging as compared to replacing the damaged beams. This is because, replacing the damaged columns requires shoring of all the floors and beams around the damaged columns and it may encounter a lot of unexpected challenges due to tolerance limits and space restrictions, whereas replacing the damaged beams will require shoring to the slabs around the damaged beams and ensuring that the floor slabs below the damaged floor level have enough capacity for the additional loads. As mentioned before, the damage to the columns can be avoided by designing and detailing column to foundation connections as pin rather than fixed. The load path and possible locations of damage in an unbraced frame with pin bases is shown in Figure 6.1c. Later, it will be shown that an unbraced frame with pin bases satisfying "strong column-weak beam" design principles will exhibit soft-storey mechanism even for high column to beam capacity ratios. Because of change of the base fixity from fixed to pin, lateral strength and stiffness of an unbraced frame is reduced to varying extent depending on the geometric layout. In an unbraced frame with pin bases, because of lack of rotational fixity at the column bases, the lateral sway in the lower storeys is higher than the upper storeys, and the overall response of the frame is more of shear type deformation. On the other hand, full rotational fixity (fixed) at the column bases restricts the lateral sway at the first storey and thus induces initial flexural behaviour near the base, but the overall response of the frame is still of shear type deformation due to the flexural stiffness of the beams (which is further stiffened by the slab).

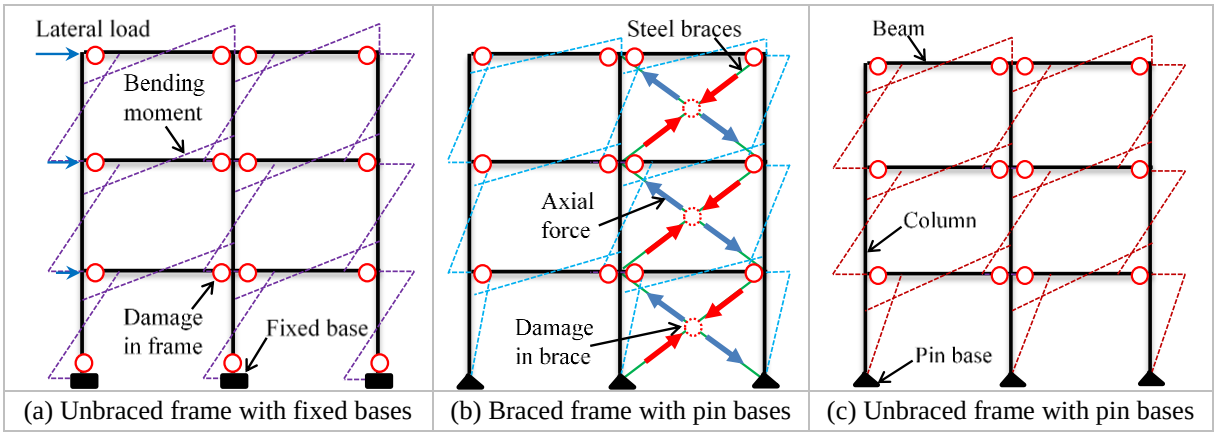

(a) Unbraced frame with fixed bases (b) Braced frame with pin bases (c) Unbraced frame with pin bases

Figure 6.1. Lateral load resisting frame options for the proposed demountable building system

The lateral strength and stiffness of an unbraced frame with pin bases can be increased to match with the capacity curve of the fixed base frame by adopting two different approaches. In the first approach, strength and stiffness of an unbraced concrete frame with pin bases can be increased by increasing the longitudinal rebar percentage or cross-sectional dimensions or

both. It is important to note that even if the strength and stiffness of unbraced frames with fixed and pin bases are about the same, an unbraced frame with pin bases is not robust and redundant as that of an unbraced frame with fixed bases. Also, the cyclic performance of an unbraced frame with pin bases will not be the same as that of the fixed base frame due to different levels of secondary and higher mode effects.

In the second approach, lateral strength and stiffness of an unbraced concrete frame with pin bases can be increased by the addition of steel braces (or buckling restrained braces). By properly designing the structural performance of a braced concrete frame, it can be better than that of an unbraced concrete frame with fixed bases. In braced concrete frames with rigid beam column connections, the lateral load is resisted by a combination of flexural resistance of frame elements and axial resistance of braces, whereas with pin beam column connections the lateral load is transferred to the foundation only through strut and tie action provided by the braces, which is schematically shown in Figure 6.1b. The damage in a braced frame with rigid beam column connections is limited to beams and braces, which are comparatively easier to replace than replacing the damaged columns of an unbraced frame with fixed bases. In a braced frame with pin beam column connections, the damage can be limited to braces only, which is even easier to replace compared to replacing the damaged beams. Schematic representation of possible locations of plastic hinges (i.e. damage) in a braced frame with rigid beam-column connections is shown in Figure 6.1b. It is important to note that a braced frame with rigid or pin beam-column connections is more redundant and robust compared to unbraced frame with pin bases. The options to increase the lateral strength and stiffness of an unbraced frame with pin bases to match with the capacity curve of an unbraced frame with fixed bases is schematically represented in Figure 6.2.

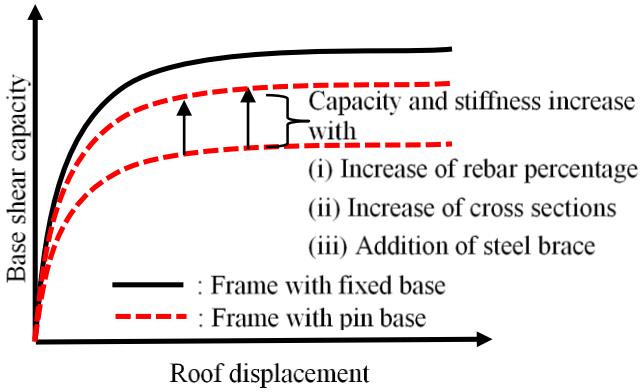

Figure 6.2. Options to increase the lateral strength and stiffness of an unbraced frame with pin bases

6.3 Nonlinear static/pushover analysis

To quantify the average range of reduction in the lateral strength (i.e. base shear capacity), initial lateral stiffness and seismic demand, and increase in fundamental period due to change of base fixity of an unbraced frame from fixed to pin, pushover analysis is carried out on a wide range of low to medium rise frames (i.e. up to 10 storeys) using the structural analysis software SAP2000 [6]. In the pushover analyses, a predefined triangular load pattern as per New Zealand design practice is applied to the frame as shown in Figure 6.3a and increased until any member of the frame reaches its yield limit state (as shown in Figure 6.3b), and then the frame is modified with reduced secant stiffness for the yielded member and the lateral load is further increased until the target displacement is reached [7]. Pushover capacity curve for a frame is obtained by plotting the base shear capacity against the roof displacement, which is schematically shown in Figure 6.3a.

6.3.1 *Macro modelling*

In the pushover analyses conducted in this study, to capture the material and geometric nonlinearity of the frame components under increasing lateral load, beams and columns are modelled as elastic elements with lumped plastic rotational springs at both ends along with P-Δ formulation. A typical backbone input curve required for the rotational spring is shown in Figure 6.3b, which can be developed from the first principles (i.e. from moment curvature to moment rotation assuming a plastic hinge length) or can be directly obtained from ASCE 41/FEMA 356 guidelines depending on the geometrical properties of member's cross-section and the axial load acting on it [8]. The capping rotation (θ_{cp}) and moment (M_{cp}) given in ASCE 41 are the conservative lower bound values used for the seismic capacity evaluation rather than the actual values for a particular member cross-section. As the aim of the study is to evaluate the base shear capacity rather than estimating the ultimate deformation capacity of a frame, the moment-rotation backbone curves obtained from ASCE41 are directly used as input for the rotational springs. It is important to note that the initial stiffness of the rotational spring has to be rigid so that the elastic behaviour of the overall element (elastic element plus rotational springs) is rightly captured. The effective moment inertias of the elastic elements are obtained from moment-curvature analysis.

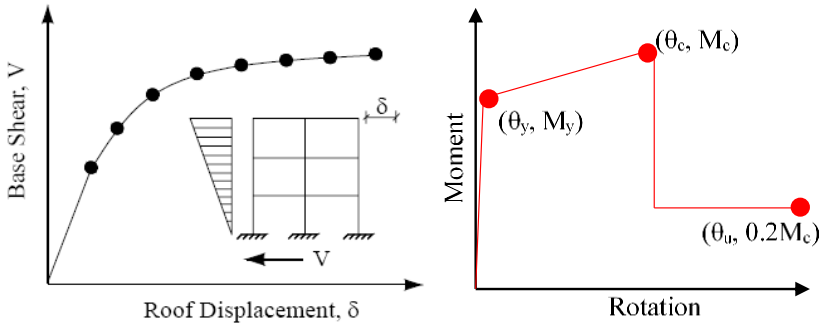

(a) Pushover capacity curve (b) Backbone (M-θ) input curve

Figure 6.3. Pushover capacity curve of a frame and backbone input envelope for rotational spring

6.3.2 *Variation of structural parameters*

The parameters that were varied to investigate the effect of base fixity on the structural performance of an unbraced frame are column to beam capacity ratio β, number of storeys n_s, number of bays n_b, and span length l. In total, around six to seven hundred pushover analyses were performed by varying the parameters listed in Table 6.1. Cross sectional properties of the beams and columns used in the parametric study can be identified from Tables 6.2 and 6.3, respectively. For calculation of the seismic mass, it was assumed that the frame building considered for the parametric analysis has 4 bays of 6 m width in the perpendicular direction with the same lateral stiffness and the floors are assumed to be rigid in plane.

Table 6.1. Variables used in the parametric study to investigate effect of base fixity

Building characteristics		**Material description**		**Beam dimensions**	
No of storeys	3-10	Grade of concrete	35 N/mm^2	Dimensions	0.4×0.4-0.6 m
Storey height	3.6 m	Grade of rebars	500 N/mm^2	Rebar percentage	0.38-0.92%
Span length	5-7 m	**Loading details**		**Column dimensions**	
No of bays	3-5	Dead load	Roof: 4.75 kN/m^2 Other: 4.25 kN/m^2	Dimensions	0.4×0.5-0.6 m, 0.5×0.7 m
Base boundary condition	Fix or pin	Live load	Roof: 2.5 kN/m^2 Other: 3.0 kN/m^2	Rebar percentage	0.8-3.44 %
Note: for further details of beam and column properties, refer Tables 6.2 and 6.3, respectively.					

It was realized that the most important parameter that dictates the base shear capacity of an unbraced frame is the column to beam moment capacity ratio ($i.e. \beta = M_c/M_b$). In reality, it is possible to have the same β for different combinations of beam and column moment capacities. Also, for a given β, the same frame can be designed to different levels of strength (i.e. base shear capacity) depending on the seismicity of the building location, occupancy class, and expected ductility. Also, because of uncertainty in the material properties, the actual column to beam capacity ratio (also referred as over-strength factor) of a frame can be

very different to the initial assumed design value. So, a matrix of column to beam capacity ratios is generated and reported in Table 6.4 by using different possible combinations of beam and column capacities obtained from Tables 6.2 and 6.3. Here, the capacities of beams and columns are actually the section moment capacities corresponding to concrete strain (ε_c) of 0.003 instead of the yield strain of the rebars.

Table 6.2. Beam cross sectional details along with moment capacities used in the parametric study

Beam identification	**Dimensions**		**No of bars**		**Rebar details**		**Moment**
	Breadth (m)	**Depth (m)**	**Bottom**	**Top**	**mm**	**%**	**(kN-m)**
B-0.4×0.4-3-Y16	0.4	0.4	3	3	16	0.38	110.89
B-0.4×0.4-3-Y20	0.4	0.4	3	3	20	0.59	164.19
B-0.4×0.4-3-Y25	0.4	0.4	3	3	25	0.92	246.71
B-0.4×0.5-3-Y16	0.4	0.5	3	3	16	0.30	147.12
B-0.4×0.5-3-Y20	0.4	0.5	3	3	20	0.47	217.56
B-0.4×0.5-3-Y25	0.4	0.5	3	3	25	0.74	323.80
B-0.4×0.6-3-Y16	0.4	0.6	3	3	16	0.25	184.43
B-0.4×0.6-3-Y20	0.4	0.6	3	3	20	0.39	272.93
B-0.4×0.6-3-Y25	0.4	0.6	3	3	25	0.61	406.99

Since, any modern frame building has to satisfy the capacity design principles (i.e. strong column-weak beam) and also most building codes recommend a minimum capacity ratio β around 1.5, in Table 6.4 any combinations with the capacity ratio β less than 1.5 are not considered in the parametric study. Similarly, any combination with the capacity ratio β more than 3.5 is also not considered, this is because it is not feasible (and meaningless) to have very unproportioned cross sections (very big columns and very small beams) in a real building. Therefore, only the column to beam capacity ratios between 1.5 and 3.5 are considered for the parametric study and this range has been divided in to four groups, as identified by different cell colours in Table 6.4 (i.e. β =1.5 to 2.0; β =2.0 to 2.5; β =2.5 to 3.0; β =3.0 to 3.5).

Table 6.3. Column cross sectional details along with moment capacities used in the parametric study

Column identification	Dimension		No of bars		Rebar details		Moment
	Breadth (m)	Depth (m)	Bottom &Top	Sides	(mm)	(%)	(kN-m)
C-0.4×0.5-3×3-Y16	0.4	0.5	3	3	16	0.80	184.70
C-0.4×0.5-3×3-Y20	0.4	0.5	3	3	20	1.26	275.33
C-0.4×0.5-3×3-Y25	0.4	0.5	3	3	25	1.96	418.60
C-0.4×0.5-4×5-Y16	0.4	0.5	4	5	16	1.41	304.21
C-0.4×0.5-4×5-Y20	0.4	0.5	4	5	20	2.20	447.35
C-0.4×0.5-4×5-Y25	0.4	0.5	4	5	25	3.44	660.46
C-0.4×0.6-3×3-Y16	0.4	0.6	3	3	16	0.67	229.90
C-0.4×0.6-3×3-Y20	0.4	0.6	3	3	20	1.05	342.71
C-0.4×0.6-3×3-Y25	0.4	0.6	3	3	25	1.64	516.79
C-0.4×0.6-4×6-Y16	0.4	0.6	4	6	16	1.34	417.28
C-0.4×0.6-4×6-Y20	0.4	0.6	4	6	20	2.09	620.27
C-0.4×0.6-4×6-Y25	0.4	0.6	4	6	25	3.27	904.17
C-0.5×0.7-5×5-Y16	0.5	0.7	5	5	16	0.92	519.69
C-0.5×0.7-5×5-Y20	0.5	0.7	5	5	20	1.44	782.21
C-0.5x0.7-5×5-Y25	0.5	0.7	5	5	25	2.24	1167.83
C-0.5x0.7-5×6-Y16	0.5	0.7	5	6	16	1.03	572.67
C-0.5x0.7-5×6-Y20	0.5	0.7	5	6	20	1.62	856.02
C-0.5x0.7-5×6-Y25	0.5	0.7	5	6	25	2.52	1282.47

Also, the column sizes used in different storey frames have been divided into three groups, which can also be identified in Table 6.4. The column to beam capacity ratios within the categorized group have been numbered in the increasing order from the left to right side of the table, and for better understanding of this numbering scheme, the assigned numbers have been shown in brackets for the 3 to 5 storeys group (refer Table 6.4). By using all these combinations of column to beam capacity ratios, numerical results are generated and reported in the following sections to explain the effect of base fixity on lateral strength and stiffness, fundamental period, and seismic demand of an unbraced frame.

Table 6.4. Column to beam capacity ratio (β) with different combinations of beams and columns capacities

Identification		*B-0.4×0.4-3-Y16*	*B-0.4×0.4-3-Y20*	*B-0.4×0.4-3-Y25*		*B-0.4×0.5-3-Y16*	*B-0.4×0.5-3-Y20*	*B-0.4×0.5-3-Y25*		*B-0.4×0.6-3-Y16*	*B-0.4×0.6-3-Y20*	*B-0.4×0.6-3-Y25*
3 to 4 storeys	*M (kN-m)*	*110.89*	*164.19*	*246.71*		*147.12*	*217.56*	*323.80*		*184.43*	*272.93*	*406.99*
C-0.4×0.5-3x3-Y16	*184.70*	*1.67 (1)*	*1.12*	*0.75*		*1.26*	*0.85*	*0.57*		*1.00*	*0.68*	*0.45*
C-0.4×0.5-3x3-Y20	*275.33*	*2.48 (1)*	*1.68 (2)*	*1.12*		*1.87 (4)*	*1.27*	*0.85*		*1.49 (6)*	*1.01*	*0.68*
C-0.4×0.5-3x3-Y25	*418.60*	*3.77*	*2.55 (1)*	*1.70 (3)*		*2.85 (2)*	*1.92 (5)*	*1.29*		*2.27 (2)*	*1.53 (7)*	*1.03*
C-0.4×0.5-4x5-Y16	*304.21*	*2.74 (3)*	*1.85 (8)*	*1.23*		*2.07 (3)*	*1.40*	*0.94*		*1.65 (10)*	*1.11*	*0.75*
C-0.4×0.5-4x5-Y20	*447.35*	*4.03*	*2.72 (4)*	*1.81 (9)*		*3.04 (1)*	*2.06 (4)*	*1.38*		*2.43 (6)*	*1.64 (11)*	*1.10*
C-0.4×0.5-4x5-Y25	*660.46*	*5.96*	*4.02*	*2.68 (5)*		*4.49*	*3.04 (2)*	*2.04 (5)*		*3.58 (3)*	*2.42 (7)*	*1.62 (12)*
5 to 7 storeys												
C-0.4×0.6-3x3-Y16	*229.90*	*2.07*	*1.40*	*0.93*		*1.56*	*1.06*	*0.71*		*1.25*	*0.84*	*0.56*
C-0.4×0.6-3x3-Y20	*342.71*	*3.09*	*2.09*	*1.39*		*2.33*	*1.58*	*1.06*		*1.86*	*1.26*	*0.84*
C-0.4×0.6-3x3-Y25	*516.79*	*4.66*	*3.15*	*2.09*		*3.51*	*2.38*	*1.60*		*2.80*	*1.89*	*1.27*
C-0.4×0.6-4x6-Y16	*417.28*	*3.76*	*2.54*	*1.69*		*2.84*	*1.92*	*1.29*		*2.26*	*1.53*	*1.03*
C-0.4×0.6-4x6-Y20	*620.27*	*5.59*	*3.78*	*2.51*		*4.22*	*2.85*	*1.92*		*3.36*	*2.27*	*1.52*
C-0.4×0.6-4x6-Y25	*904.17*	*8.15*	*5.51*	*3.66*		*6.15*	*4.16*	*2.79*		*4.90*	*3.31*	*2.22*
8 to 10 storeys												
C-0.5×0.7-5x5-Y16	*519.69*	*4.69*	*3.17*	*2.11*		*3.53*	*2.39*	*1.60*		*2.82*	*1.90*	*1.28*
C-0.5×0.7-5x5-Y20	*782.21*	*7.05*	*4.76*	*3.17*		*5.32*	*3.60*	*2.42*		*4.24*	*2.87*	*1.92*
C-0.5×0.7-5x5-Y25	*1167.83*	*10.53*	*7.11*	*4.73*		*7.94*	*5.37*	*3.61*		*6.33*	*4.28*	*2.87*
C-0.5×0.7-5x6-Y16	*572.67*	*5.16*	*3.49*	*2.32*		*3.89*	*2.63*	*1.77*		*3.11*	*2.10*	*1.41*
C-0.5×0.7-5x6-Y20	*856.02*	*7.72*	*5.21*	*3.47*		*5.82*	*3.93*	*2.64*		*4.64*	*3.14*	*2.10*
C-0.5×0.7-5x6-Y25	*1282.47*	*11.56*	*7.81*	*5.20*		*8.72*	*5.89*	*3.96*		*6.95*	*4.70*	*3.15*
Note: β < not feasible and not used in parametric study. Grouping of the capacity ratios can be identified by the color of the cell.					*β=*	*1.5 -2.0*			*β=*	*2.0 -2.5*		
					β=	*2.5 -3.0*			*β=*	*3.0 -3.5*		

6.4 Effect of base fixity on structural performance of unbraced frames

6.4.1 *Variation of base shear capacity (V) for a given Mc or Mb and varying β*

In this section, a mathematical relationship is developed between the base shear capacity V of an unbraced frame with either fixed or pin bases and the column to beam capacity ratio β by utilizing well known plastic analysis method. The lateral force F_i at any storey level i of a frame can be related to the total base shear capacity V as:

$$F_i = \frac{2i}{n_s(n_s+1)}V \tag{1}$$

For an unbraced frame with fixed base with assumption of beam sway mechanism, the external work done due to lateral force F_i is related to internal work done (due to rotation of plastic hinges) as;

$$\sum_{i=1}^{ns} F_i\Delta_i = \sum_{i=1}^{nb+1} M_c\theta_c + \sum_{i=1}^{nb}\sum_{i=1}^{ns} 2M_b\theta_b \tag{2}$$

Where M_c and M_b are plastic moment capacities of the beams and columns respectively, θ_b and θ_c are the plastic rotation capacities of the beams and columns respectively. By substituting Equation 1 in Equation 2 and summing Equation 2, and then introducing α and β into modified Equation 2 and dividing both sides by $M_b\theta_c$ or $M_c\theta_c$ will result in a mathematical relationship between the base shear capacity V of an unbraced frame with fixed bases and the column to beam capacity ratio β for a given M_b or M_c, which is given in Equation 3.

$$V = \frac{M_b((n_b+1)\beta+2n_bn_s\alpha)}{(0.67n_s+0.33)h};\ V = \frac{M_c((n_b+1)\beta+2n_bn_s\alpha)}{\beta(0.67n_s+0.33)h} \tag{3}$$

In Equation 3, h is storey height, and α is the ratio of the plastic rotation capacity of the beam to the column (i.e. $\alpha = \theta_b/\theta_c$). Equation 3 can also be applied to an unbraced frame with pin bases by setting the columns internal work done to zero (i.e. $(n_b+1)\beta = 0$). It is clear from Equation 3 that the base shear capacity V of an unbraced frame is a linear function of the column to beam capacity ratio β (α is assumed to be constant as it doesn't significantly influence the base shear capacity). To verify the accuracy of Equation 3 in predicting the base shear capacity V, a three storey frame with storey height of 3.6 m and three bays of 5 m span length, and with the parameters listed in Table 6.5 is chosen. The base shear capacity V of the frame with fixed or pin bases obtained from Equation 3 and the pushover analysis is reported in Table 6.5. It is clear that Equation 3 is able to capture the reduction in the base shear capacity of an unbraced frame due to change of base fixity from fixed to pin, but the

predicted base shear capacity is substantially greater than the base shear capacity obtained from pushover analysis. The reasons for this are; (i) in reality it is very unlikely that all ground storey column bases and all beams will reach their ultimate moment and rotation capacities at the same time, and most of the upper storey beams may not reach their yield moment capacity, (ii) beam sway mechanism is unlikely unless the column to beam capacity ratio β is high, whereas the mixed sway mechanism is the common mechanism which dictates the base shear capacity of a frame in the practical range of β, and (iii) a triangular load pattern was assumed in development of Equation 3, whereas the applied load pattern in the pushover analysis was as per New Zealand seismic code [7].

Table 6.5. Parameters used in Equations and verification predicted V with SAP 2000 results

Cases	Parameters used in Equation 3 and in SAP2000	V: Equation 3		V: Pushover analysis	
		Fixed base	Pin base	Fixed base	Pin base
Case-1: β =1.5 and 2.0	Mc=328.6; Mb=180.23; θc=0.02; θb=0.025; β=1.82; α=1.25	638	481	514	313
Case-2: β ≥3.5	Mc=675; Mb=180.23; θc=0.02; θb=0.025; β=3.74; α=1.25	801	481	698	360
Note: force, moment, rotation units are in kN, kN-m, and radians respectively.					

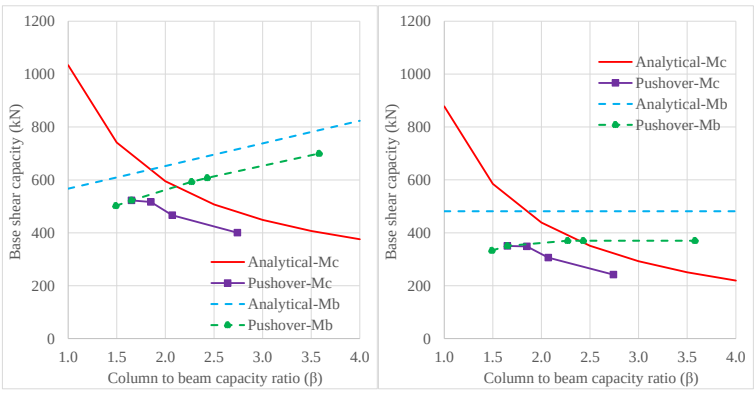

(a) Fixed base (b) Pin base

Figure 6.4. Comparison of lateral strength obtained from Equation 3 and pushover analysis (Case-1)

The variation of the base shear capacity V of a three storey frame with fixed or pin base for a given beam capacity M_b or column capacity M_c and varying column to beam capacity ratio β obtained from Equation 3 and pushover analysis is plotted in Figure 6.4. The base shear variation plots for other storeys (i.e. 5 to 10 storeys) are reported in Appendix J (refer Figures J.1 to J.6). The base shear capacity of an unbraced frame decreases with increase of the column to beam capacity ratio β for a given column capacity M_c. This decrease is due to decrease in beam moment capacity M_b which is the major contributor to overall base shear capacity. Also, by increasing the column to beam capacity ratio β for a given beam capacity M_b, the base shear capacity V of the frame increases. The increase is due to; (i)

increase in the internal work done because of shift in mechanism mode (i.e. from mixed sway to beam sway mechanism), and (ii) increase in contribution of the column moment capacity to the overall base shear capacity (applicable only for fixed base frames). It is also important to note that, for a pin base frame, Equation 3 is independent of β and only function of beam capacity M_b, whereas there is a slight variation in base shear capacity obtained from the pushover analysis with increasing β, this increment is due to change of mechanism mode (refer Figure 6.4b).

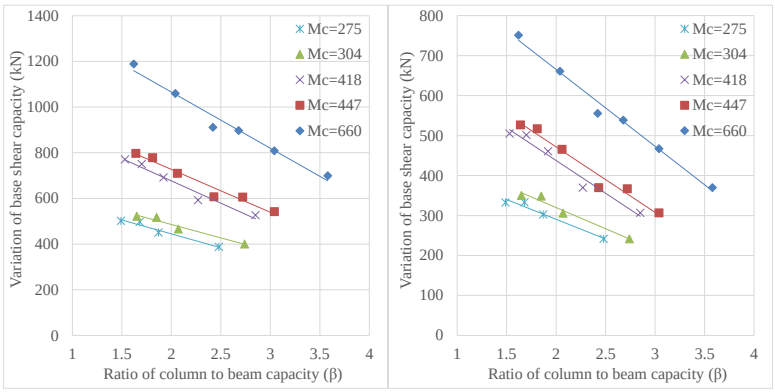

(a) Fixed base: M_c constant (b) Pin base: M_c constant

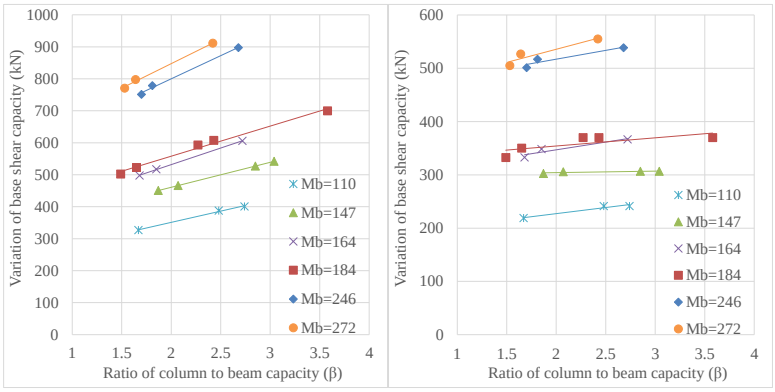

(c) Fixed base: M_b constant (d) Pin base: M_b constant

Figure 6.5. Variation of lateral strength obtained from pushover analysis with varying M_c, M_b, and β

The rate of decrease of base shear capacity V for given column capacity M_c and varying β is high compared to the rate of increase of base shear capacity V for a given beam capacity M_b and varying β. This is due to higher contribution of beam moment capacities to the internal work done compared to the column moment capacities. Also, variation of the base shear capacity V of an unbraced frame with fixed or pin bases for given different column or beam capacities and varying column to beam capacity ratio β is plotted in Figure 6.5. As expected by increasing the column and beam capacities for a constant β increases the overall base shear capacity of the frame. This is because the frame is getting stronger by the simultaneous increase of the beam and column capacities.

6.4.2 *Reduction in base shear capacity of an unbraced frame due to change of base fixity*

For a given building height, with increase of ratio of column to beam capacity β, the base shear capacity reduces more, which is pictorially shown in Figure 6.6a. This is due to the fact that the contribution of columns strength to the base shear capacity is limited in the pin base frame compared to the fixed base frame (in the pin base frame, main contribution to base shear capacity comes from the beams' flexural strength).

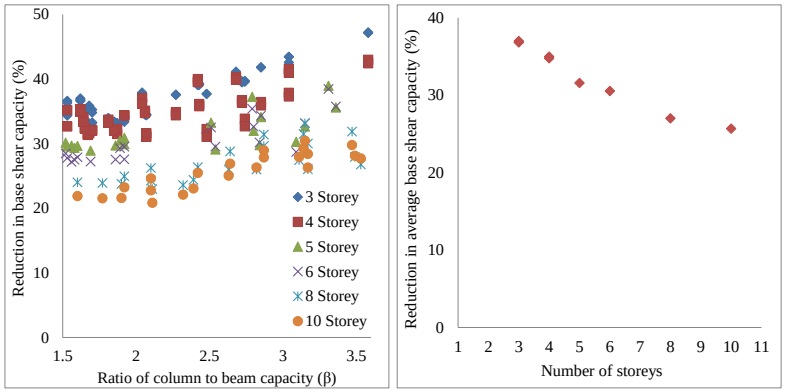

(a) As function of β (b) As function of n_s

Figure 6.6. Reduction in base shear capacity V of pin base frame compared to fixed base frame

Plots showing the variation of reduction in base shear capacity of a pin base frame compared to a fixed base frame for each storey are reported in Appendix J (refer Figure J.7). Also, the reduction in base shear capacity of pin base frames compared to the "*reference frame"* with varying number of storeys is shown in Figure 6.6b. It was observed that the reduction of average base shear capacity varies from 37% to 26% with increase in number of storeys from 3 to 10. The rate of reduction of base shear capacity with an increase in the number of storeys is mainly because of the less relative contribution of column base moment capacities to the overall base shear capacity as the number of beams increases in higher storey frames.

6.4.3 *Reduction in lateral stiffness of an unbraced frame due to change of base fixity*

The effect of change of base fixity (i.e. fixed to pin base) on reduction of initial lateral stiffness of an unbraced frame is considerably high; the variation as a function of column to beam capacity ratio β is pictorially shown in Figure 6.7. Plots showing the variation of reduction in initial lateral stiffness of pin base frame compared to a fixed base frame for each storey are reported in Appendix J (refer Figure J.8). It is clear that the reduction in initial lateral stiffness K is independent of column to beam capacity ratio β. This is because the initial lateral stiffness of a frame is function of the gross sectional properties of the beams and columns unlike the lateral secant stiffness of a frame which is function of both section

properties and yield strength of the members. It was found from the parametric study that the reduction in average initial lateral stiffness varies from 50% to 20% with increase in number of storeys from 3 to 10, which is shown graphically in Figure 6.7b.

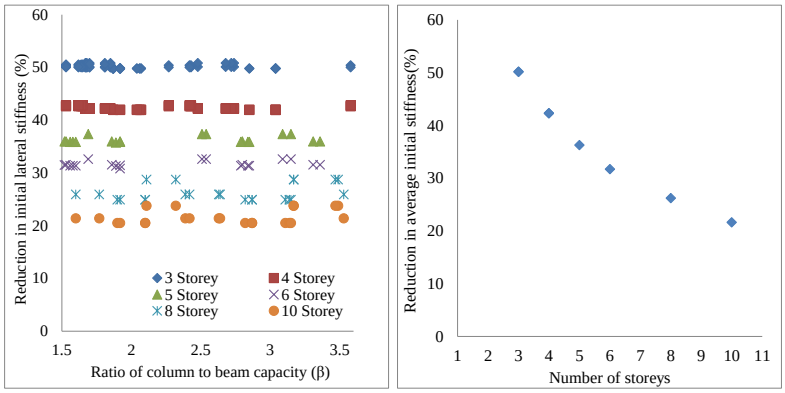

(a) Reduction as function of β (b) Reduction as function of n_s

Figure 6.7. Reduction in initial lateral stiffness of pin base frame compared to fixed base frame

6.4.4 *Reduction in seismic demand on unbraced frame due to change of base fixity*

From previous sections, it is clear that the base shear capacity and initial lateral stiffness of a pin base frame is less compared to a fixed base frame and the difference primarily depends on the column to beam capacity ratio β, and number of storeys n_s. Because of less initial lateral stiffness, the fundamental period of a pin base frame is higher compared to a fixed base frame. The average fundamental period of fixed and pin base frames with increasing storey numbers is plotted in Figure 6.8a and it appears that the average increase in period due to the change of base fixity is between 0.30 to 0.37 Sec. Also, the average increase in fundamental period in terms of percentage is shown in Figure 6.8b, and it is clear that fundamental period of the pin base frame is higher than the fixed base frame by 54% to 18% depending on the number of storeys.

Due to increase in fundamental period by changing the base boundary condition from fixed to pin, the seismic demand on a pin base frame will be less compared to a fixed base frame and the amount of reduction in seismic demand primarily depends on the actual period of the fixed base frame, soil condition, and number of storeys. It was found from the parametric study that the average seismic demand reduces by 27% to 15% with an increase in number of storeys from 3 to 10. Plots showing maximum and minimum reduction of the seismic demand with different soil conditions and varying number of storeys are reported in Appendix J (refer Figure J.9). Comparison of the average reduction in base shear capacity and seismic demand due to change of base fixity (i.e. fixed to pin) of an unbraced frame as a function of number of storeys is plotted in Figure 6.8d. It is clear that reduction in base shear capacity is more

than the reduction of seismic demand and this difference can be compensated with the options listed in the next section.

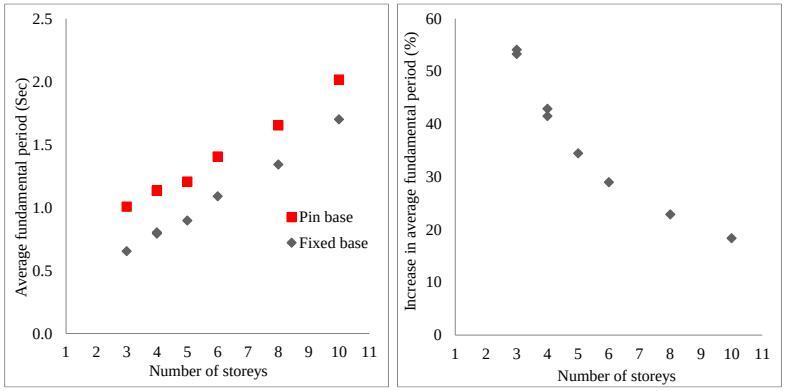

(a) Average fundamental period (Sec) (b) Average increase in period (%)

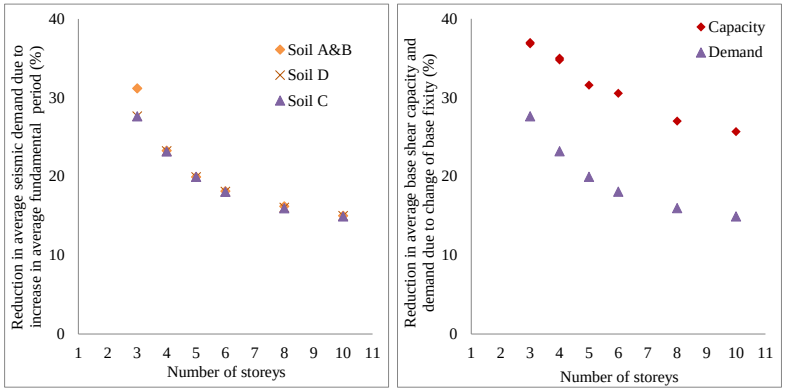

(c) Average reduction in demand (%) (d) Reduction in capacity and demand (%)

Figure 6.8. Increase in average period and reducton in average demand due to change of base fixity

6.5 Options to increase strength and stiffness of unbraced frame with pin bases

The lateral strength (i.e. base shear capacity) and stiffness of an unbraced frame with pin bases can be increased to match with those of the fixed base frame by; (i) increasing the rebar percentage without increasing members cross-section sizes, (ii) increasing beam and column cross sections without increasing the rebar percentage, (iii) simultaneous increase of both rebar percentage and members cross sections, and (iv) adding steel braces without modifying beams and columns properties.

6.5.1 *Increase of the rebar percentage*

Comparison of the capacity curves of the 3 storey frames with fixed and pin bases and varying the column to beam capacity ratios (i.e. β between 1.5 and 3.5) is shown in Figure 6.9. Pushover capacity curves for other storey frames (i.e. 4 to 10) are reported in Appendix J (refer Figure J.10). As mentioned before, the column to beam capacity ratios are divided into

four groups (i.e. β=1.5 to 2.0, β= 2.0 to 2.5, β=2.5 to 3.0, and β=3.0 to 3.5), and higher β indicates that columns are stronger compared to beam moment capacity. In Figure 6.9, legend "Fixed-β=1.5 to 2.0-1" indicates that the frame is with fixed bases and column to beam capacity ratio is between 1.5 and 2 and the number (1 to 3) indicates increasing rebar percentage both in beams and columns while keeping the same cross section sizes. The actual cross-section sizes and rebar percentages of the beams and columns in different cases can be identified from Table 6.4. A higher number indicates a stronger frame but with the designated range of column to beam capacity ratio β.

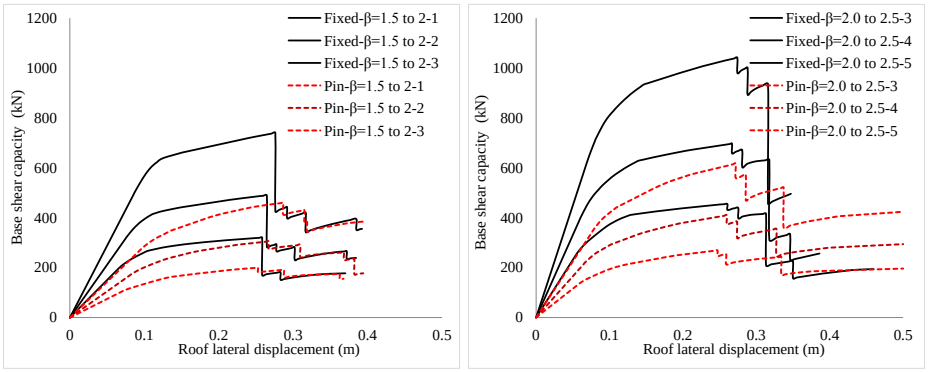

(a) β between 1.5 and 2.0 (b) β between 2.0 and 2.5

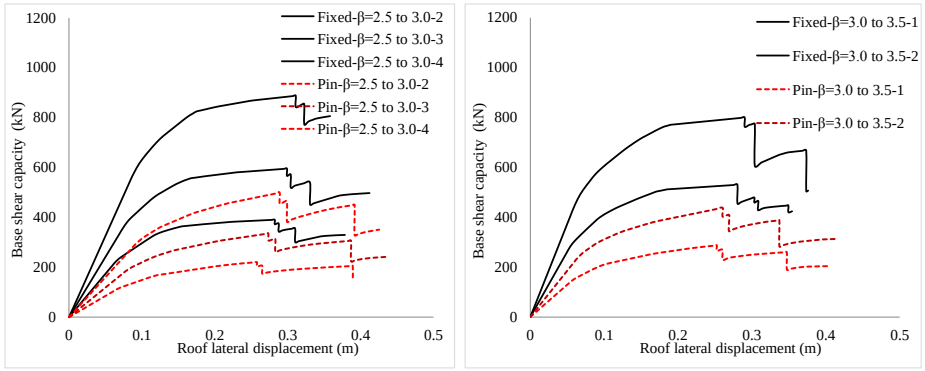

(c) β between 2.5 and 3.0 (d) β between 3.0 and 3.5

Figure 6.9. Comparision of capacity curves of 3 storey frames with same cross-sections and varying β

By comparing the pushover curve plots with legend "Fixed-β=1.5 to 2.0-1" and "Pin-β=1.5 to 2.0-3", "Fixed-β=2.0 to 2.5-3" and "Pin-β=2.0 to 2.5-5", and "Fixed-β=2.5 to 3.0-2" and "Pin-β=2.5 to 3.0-4", it is clear that the strength and stiffness of a pin base frame can be increased to match with those of relatively less reinforced fixed base frames (i.e. with less base shear capacity) by increasing rebar percentage without modifying the cross sectional dimensions. For high column to beam capacity ratio (i.e. β>=3.0) though, it is not possible for the pin base frame to achieve the strength and stiffness of the weaker fixed base frame (i.e. with less base shear capacity) even with higher rebar percentage, which is clearly shown

in Figure 6.9d. This is because the capacity of the pin base frame is limited by the capacity of the beams. Because of the practical limitation of the rebar percentage, strength and stifnness of a pin base frame cannot match with pushover capacity curve of the stronger fixed base frames (i.e. with high base shear capacity) for any column to beam capacity ratio.

6.5.2 *Increase of the cross-section sizes*

In the previous section, it was shown that pushover capacity curves of pin base frames cannot be matched to the stronger fixed base frames by increasing the rebar percentage alone. In those cases, lateral strength and stiffness can be significantly increased by increasing the cross sectional members and adjusting the rebar percentage such that column to beam capacity ratio is in the same range of the original pin base frame. To investigate this, the pushover capacity plots shown in Figure 6.9c were taken as reference. The capacity curves of a pin base frame with increased cross sections (i.e. column of 0.5×0.7 m and beam of 0.4×0.6 m) and increasing rebar percentage is obtained from the pushover analysis. Figure 6.10a shows the response of the fixed base frames, pin base frames with the same cross sections and pin base frames with bigger cross sections.

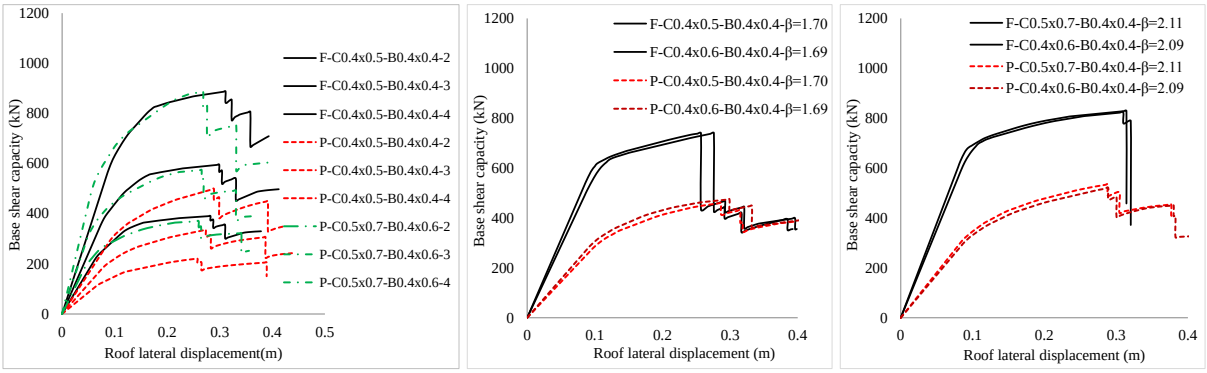

(a) Increasing cross sections (b) and (c) Similar strength and different stiffness

Figure 6.10. Increasing strength and stiffness of a pin base frame by increasing the dimensions, and two frame systems with similar strength but different stiffness

In Figure 6.10a, legend "F-C0.4×0.5-B0.4×0.4-2" indicates column dimensions are 0.4 m×0.5 m, beam dimensions are 0.4 m×0.4 m, and the final number (2 to 4) indicates increasing rebar percentage. It is clear that both strength and stiffness of a pin base frame can be increased to the level of a stronger fixed base frame by using bigger cross section sizes and more reinforcement while keeping similar range of column to beam capacity ratio β. It is important to note that the base shear capacities of the frames with different member cross sections will be similar as long as the capacities of the columns and beams are unchanged, which is not the case with the lateral secant stiffness, this difference is shown in Figures

6.10b and 6.10c. This is because lateral secant stiffness is a function of the cross sectional dimensions, rebar percentage, and capacities of the members.

6.5.3 *Addition of steel braces*

It was shown in the previous section that both strength and stiffness of the pin base frame can be increased by increasing cross sectional dimensions and rebar percentage to match with the pushover capacity curve of the stronger fixed base frames. This can also be achieved simply by adding steel braces to the pin base frame without modifying the original member properties. To investigate this, again the pushover capacity plots shown in Figure 6.9c were taken as the reference. X tube braces of 75 mm diameter were added to one bay (out of three bays) with varying thickness of 5 mm (b1), 7.5 mm (b2), and 10 mm (b3) in three different cases compared here in.

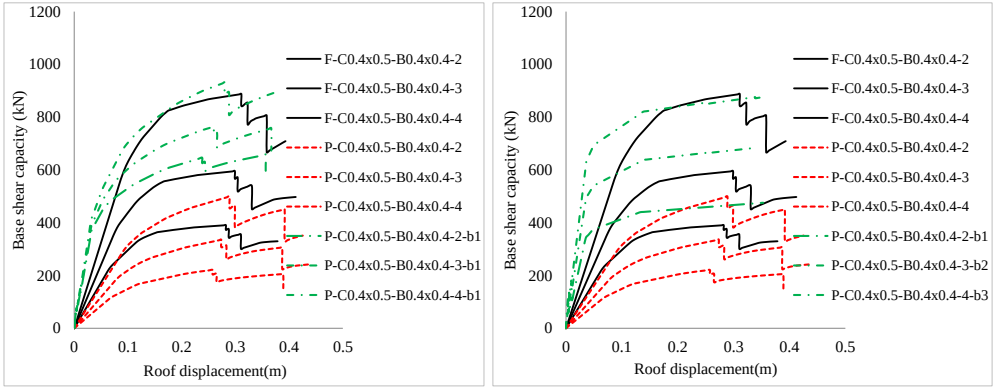

(a) Braced frames with rigid beam column connections (b) Braced frames with pin beam column connections

Figure 6.11. Increasing the strength and stiffness of a pin base frame by addition of steel braces

Figure 6.11 shows the pushover capacities of the upgraded pin base frames with braces. In Figure 6.11, "F-C0.4×0.5-B0.4×0.4-2" indicates column dimensions are 0.4 m×0.5 m, beam dimensions are 0.4 m×0.4 m, the number (2 to 4) indicates increasing rebar percentage, and "b" represents upgraded pushover capacity curve of a pin base frame with brace. In Figure 6.11a, braced frames have rigid beam column connections, whereas in Figure 6.11b braced frames have simple/pin beam column connections. It is clear that the lateral strength and stiffness of the pin base frames have been significantly increased with the addition of steel braces and even exceeded the pushover capacity curves of the stronger fixed base frames. The increase in base shear capacities of the braced frames with rigid beam column connections is due to an increase of the flexural resistance, whereas increase in base shear capacities of the braced frames with simple beam column connections is due to increase of braces strength (i.e. b1 to b3). It is important to note that a braced frame with pin bases with

strength and stiffness of an unbraced frame with pin bases is more redundant and robust and expected to perform better in seismic excitation. Also, in general a braced frame is categorized as “non-sway”, whereas an unbraced frame is a “sway frame” where secondary effects need to be explicitly considered in the design and capacity evaluation.

6.6 Soft storey mechanism in an unbraced frame with pin bases

It is very likely to form a soft storey mechanism in an unbraced frame with pin bases and column to beam capacity ratio β more than 1.5, this is due to high moment demand in the lower storey columns because of the pin bases. The soft storey mechanism (also referred as a column sway mechanism) may not be limited to the ground storey but can occur in the storeys above the ground floor. Plots showing soft storey mechanism in 2nd storey of a 3 storey frame with β between 1.5 and 2.0, and in 3rd storey of a 10 storey frame with β between 3.0 and 3.5 are shown in Figure 6.12. The soft storey mechanism in an unbraced frame with pin bases can be avoided by choosing column to beam capacity ratio β between 2.25 and 2.5 for 3 and 4 storey buildings, and β between 2.75 and 3.0 for 5 and 6 storey buildings. To avoid the soft storey mechanism in higher storey frames (i.e. $n_s \geq 7$), very high column to beam capacity ratio (i.e. $\beta \geq 3.5$) is required and it is not practical.

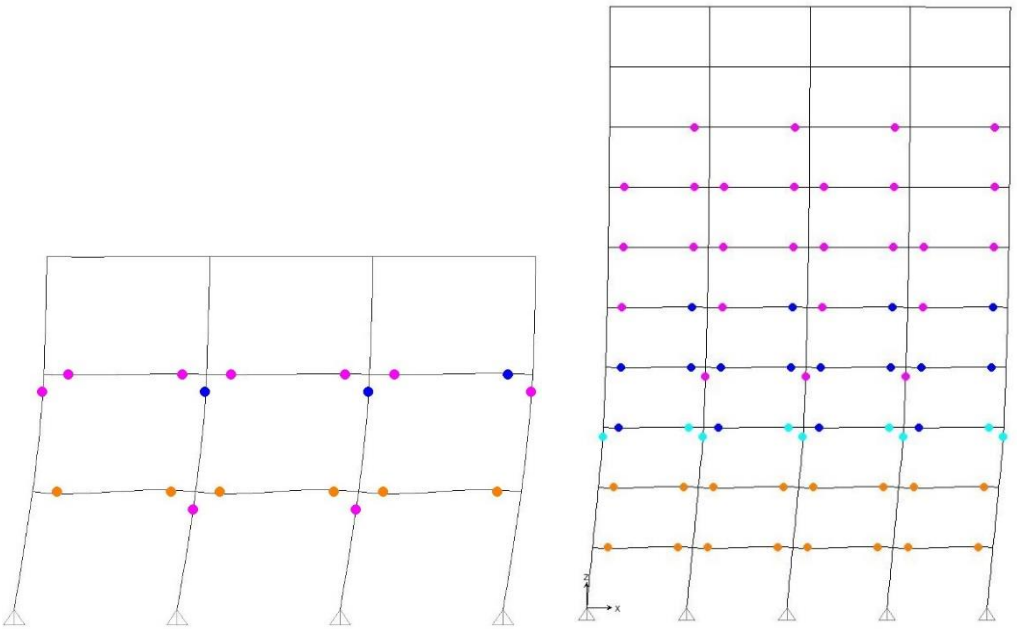

(a) 3 storey frame with β=1.5 to 2.0 (b) 10 storey frame with β=3.0 to 3.5

Figure 6.12. Soft storey mechanism in an unbraced frame with pin bases and different β

The main idea in changing the base fixity of an unbraced frame from fixed to pin is to avoid the damage to the columns within the first storey level, thereby eliminating the need to replace the damaged columns. It is evident from Figure 6.12 that by changing the base fixity from fixed to pin, the damage to the columns cannot be avoided unless the column to beam capacity ratio β is very high. Otherwise, it is very likely that the columns of an unbraced frame with pin bases will get damaged at different storey levels as shown in Figure 6.12. As it is not practically possible to avoid the damage to the columns even by changing the base fixity from fixed to pin, the best option for an unbraced moment resisting frame is to have demountable fixed bases as shown in Figure 6.13a. As mentioned before, in an unbraced frame with fixed bases, the column bases will be damaged. But, with the column to column connections at mid height of the first storey level as shown in Figure 6.13a will facilitate the replacement of only the damaged precast column elements between the column bases and mid height of first storey level rather than replacing entire columns (which is challenging).

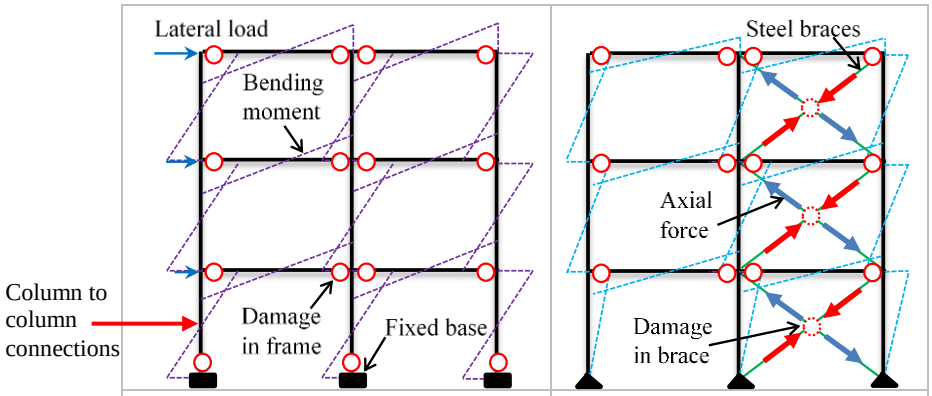

Figure 6.13. Final lateral load resisting frame options for the proposed demountable building system

If the pin bases are inevitable (in cases where damaged columns cannot be replaced/not feasible), the best option to avoid the column sway mechanism (damage to the columns) in an unbraced frame is to add the steel braces, thereby converting a "sway" unbraced frame with flexural mode of deformation to a "non-sway" braced frame with predominant strut and tie behaviour (refer Figure 6.13b). To make the proposed demountable building system structurally robust and flexible/adaptable (which allows replacement of its components), the following options with increasing order of structural flexibility/adaptability (i.e. less time to replace the damaged elements) can be considered; (i) an unbraced lateral load resisting frame with demountable fixed bases and column to column connections at mid height of first storey level, and in this case both damaged beams and column units (within first storey level) need to be replaced (refer Figure 6.13a), (ii) a braced lateral load resisting frame with removable pin bases and rigid beam column connections as shown in Figure 6.13b (damaged braces and

beams need to be replaced), and (iii) a braced lateral load resisting frame with removable pin bases and pin beam column connections (only braces need to be replaced).

6.7 Conclusions

Pros and cons of three types of lateral load resisting frames for the proposed demountable concrete frame building system are reported in this chapter. The damage to the ground storey columns (i.e. at the base) of an unbraced lateral load resisting frame can be avoided by having pin bases rather than fixed bases. Feasibility study is carried out to evaluate the effect of base fixity on structural performance of an unbraced frame. Pushover analysis is carried out to on a wide range of low to medium rise frames and it was found that by changing base fixity of an unbraced frame from fixed to pin and by increasing the number of storeys from 3 to 10; the average reduction in base shear capacity is 37% to 26%, average reduction in initial lateral stiffness is 50% to 20%, average increase in fundamental period is 54% to 18%, and the average reduction in seismic demand is 27% to 15%. Also, the variation of base shear capacity of an unbraced frame with either fixed or pin bases as a function of β is analytically captured and compared with pushover analysis results, and it was found that analytical equation predicts the upper bound value of the base shear capacity. It was shown that the lateral strength and stiffness of an unbraced frame with pin bases can be increased to match with the pushover capacity curve of a fixed base frame by; (i) increasing rebar percentage or cross section sizes or both, and (ii) adding steel braces. It was found that the soft storey mechanism (damage to the columns) is very likely in an unbraced frame with pin bases, even in frames with high column to beam capacity ratio because of high column moments. Based on the numerical investigation, it can be concluded that an unbraced frame with pin bases is not suitable for the proposed demountable building system because; (i) it is less redundant and robust, (ii) of large sway deformations, (iii) the reduction in base shear capacity is more than the reduction in demand (by changing the base fixity from fixed to pin), (iv) very high (which is not practical) column to beam capacity ratio is required to avoid the soft-storey mechanism (i.e. damage to the columns), and (v) secondary (i.e. P-Δ) and higher mode effects need to be explicitly evaluated and nonlinear time history analysis is required to capture these effects.

If pin bases are inevitable to avoid the damage to ground storey columns of an unbraced lateral load resisting frame of the proposed demountable building system, it appears that converting an unbraced frame with pin bases into a braced frame by adding steel braces is the

easiest option. To make the proposed demountable building system structurally robust and flexible (which allows replacement of its components), the following options with increasing order of structural flexibility/adaptability (i.e. less time to replace the damaged elements) can be considered; (i) an unbraced lateral load resisting frame with fixed bases and in this case both damaged beams and columns need to be replaced (a strategy to replace the damaged columns is reported in Chapter 2), and (ii) a braced lateral load resisting frame with pin bases and rigid beam column connections (damaged braces and beams need to be replaced) or pin beam column connections (only braces need to be replaced).

6.8 References

1. Eurocode, *3: Design of steel structures, Part 1.8: Design of joints*. 2005, EN-1993-1-8. Brussels: European Committee for Standardization.
2. Aninthaneni, P.K. and R.P. Dhakal, *Demountable concrete building system for seismic regions: conceptual development.* Journal of Architectural Engineering 2016. **(accepted)**
3. Aninthaneni, P.K. and R.P. Dhakal, *Conceptual development: Low loss precast concrete frame building system with steel connections*, in *NZSEE Conference*. 2014: Auckalnd, New Zealand. p. Paper No 44.
4. Aninthaneni, P.K. and R.P. Dhakal, *Demountable precast RC frame building system for seismic regions*, in *International Conference on Earthquake Engineering and Seismology (IZIIS-50).* 2015: Kiel, Germany.
5. Ariyaratana, C. and L.A. Fahnestock, *Evaluation of buckling-restrained braced frame seismic performance considering reserve strength.* Engineering Structures, 2011. **33**(1): p. 77-89.
6. SAP, *Computers and Structures Inc*. 2013: Berkeley, CA, USA.
7. NZS1170, *NZS1170: Structural design actions. Part 5: Earthquake actions - New Zealand*. 2004: Wellington, NZ.
8. ASCE41, *Seismic Evaluation and Retrofit of Existing Buildings*. 2014.

Chapter 7: Prediction of lateral stiffness and fundamental period of unbraced frame buildings with fixed bases

Aninthaneni, P. K., and Dhakal, R. P. (2016). "Prediction of fundamental period of regular frame buildings." Bulletin of the New Zealand Society for Earthquake Engineering, 49(2).

7.1 Introduction

7.1.1 *Overview*

In this chapter, a generic method to estimate the fundamental period of regular unbraced frame buildings with fixed bases is developed and a simple yet reliable equation is proposed. To verify the reliability and versatility of the developed equation, the predicted fundamental periods are compared with the periods obtained from Eigenvalue analysis for a large number of low to medium rise RC frame buildings. The fundamental period predicted using the proposed equation is also verified against the period obtained using the Rayleigh method and experimental tests. The fundamental period predicted using the developed equation and obtained from Eigenvalue analysis are used to study the limitations of the empirical equations prescribed in building codes. The applicability of the proposed equation to predict the fundamental period of low to medium rise frame buildings with minor irregularity is also investigated.

7.1.2 *Background*

One important parameter in the seismic design of a building is its period of fundamental mode of vibration, which controls the seismic demand on the building and subsequently its structural element sizes. The fundamental period of a building depends on the lateral stiffness and seismic mass and it cannot be precisely calculated for a building yet to be designed. In reality, it is very difficult to predict the actual period of vibration of a building under real earthquake shaking because of many uncertain parameters (i.e. actual material properties, seismic mass of a building during earthquakes, soil condition, contribution of secondary elements to the lateral stiffness of a building, etc.). Therefore, it is common practice to use

approximate empirical, analytical and experimental methods to estimate the fundamental period for the design of a new building as well as assessment of an existing building.

The empirical equations prescribed in most of the building codes to predict the fundamental period are developed using an actual database of recorded periods of real buildings in earthquakes [1, 2]. Most of the empirical equations relate the fundamental period of a building to the height of the building H; usually in the form $T_a = C_t H^x$[3]. In the Japanese building code [4], the fundamental period is a linear function of the building height which is given as $T_a = (0.02 + 0.01\varphi)H$ [5], where the value of φ for concrete and steel buildings are 0 and 1 respectively. The full compilation of existing empirical equations and seismic demand prediction using equivalent static procedure in different building codes can be found in literature [6-9]. The empirical equations prescribed in the building codes are simple, but they are very approximate. In most cases, they underestimate the fundamental period, which is conservative (hence acceptable) in the design of a new building, but are unsuitable for assessment of an existing building as they underestimate seismic displacement [10].

Building codes in different countries prescribe different empirical equations to estimate the fundamental period at ultimate and serviceability limit states. The values of the coefficients to be used in those empirical equations (i.e. $T_a = C_t H^x$) in the different building codes are shown in Table 7.1. Obviously, the different values of the coefficients result in different fundamental periods, and hence different seismic demands for the same building. It is important to note that some building codes (e.g. New Zealand) prescribe the periods at different limit states, whereas most of the other building codes define the period at only one limit state, and then the seismic demand for other limit state is scaled up or down [11]. The fundamental period of 3 and 10 storey RC and steel frame buildings calculated using empirical equations given in the Japanese, American and New Zealand building seismic design standards [4, 12, 13] are shown in Figure 7.1. It is clear that there is a lot of variation in the estimated fundamental periods from one building code to another.

Table 7.1. Values to be used in the empirical equation $T_a = C_t H^x$ in different building codes

Country	**Limit state**	**Concrete**		**Steel**		**Building code**
		C_t	x	C_t	x	
US/Chile	ULS	0.0466	0.9	0.0724	0.8	ASCE7-10 and NCh433-11
NZ	ULS & (SLS=ULS/1.25)	0.0937	0.75	0.1375	0.75	NZS1170.5-04
Europe/India	SLS	0.075	0.75	0.085	0.75	EN1998-1-04 and IS1893-02
Japan*	ULS	0.02	1	0.03	1	BLEO-1981
* Though the empirical equation in Japanese code is in a different form, the coefficient values given in the table are derived after converting the Japanese expression into the form $T_a = C_t H^x$, thereby resulting in the same period.						

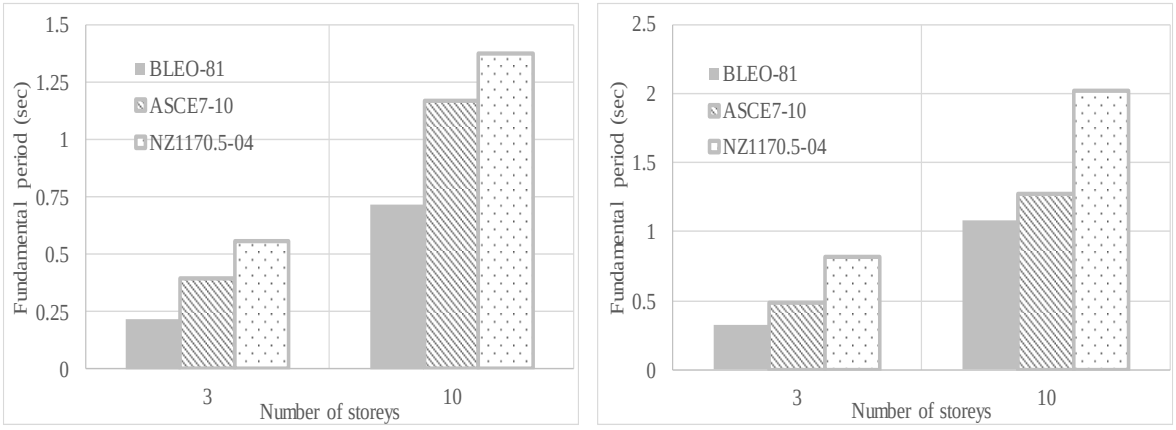

(a) RC moment resisting frame building (b) Steel moment resisting frame building

Figure 7.1. Fundamental period calculated using empirical equations in different standards.

The building codes allow to use any method of analysis (i.e. Eigenvalue, Rayleigh method, etc.) to calculate the fundamental period, but some codes limit the analytical predicted period to a value more than the period calculated using empirical equations prescribed in the codes [12, 13]. This upper bound limit is intended to avoid underestimating design base shear force due to unreasonable assumptions in analytical modelling. Some building codes specify the upper bound limit on the predicted period obtained from analytical methods only for capacity design (i.e. sizing the structural members), but not for calculating lateral displacements at serviceability limit state [12]. It is also important to note that some building codes do not impose any limit on period calculated from analytical methods in strength and displacement checks [11]. Also, building codes differ from each other in the calculation/use of the gross or effective section properties (i.e. moment of inertia) in the estimation of the fundamental period using analytical methods [14, 15]. There are some hand calculation equations available for estimation of the fundamental period of frame buildings [16, 17]. In these methods, a building frame is idealized as an equivalent cantilever column with separate flexural and shear modes of deformation. The periods of shear and flexural modes of vibration are then combined using Dunkerley's combination rule to obtain the period of the frame [17].

The existing analytical methods like Eigenvalue analysis and Rayleigh method take into account all parameters that affect the period of a building. These methods are able to predict the fundamental period of frame buildings with reasonable accuracy, but require considerable effort and expertise in using structural analysis software. In most cases, the periods predicted using analytical methods (e.g. Eigenvalue analysis and the proposed equation) using effective section properties will be higher than those predicted using empirical equations, which will

be proved in later sections. There is no simple and reliable analytical equation which accounts for all structural parameters that are likely to affect the period and can be used both in design of new building as well as in the assessment of an existing building.

7.1.3 *Objectives and scope*

The main objective of the research work is to theoretically derive a generic expression to predict the fundamental period of regular frame buildings with constant storey height and uniform mass along the building height which takes into account most structural parameters that are known to affect the period. The other objective of the research work is to modify and improve the accuracy of the original Macleod's equation in predicting the lateral deflection and the lateral stiffness of a moment resisting frame building under lateral seismic forces. Although the proposed equation can be used for any type of frame buildings, only reinforced concrete (RC) frame buildings are analysed in this chapter for validation. The equation developed in this chapter to predict the fundamental period of frame buildings, which has been simplified for design engineers' use in day to day projects, can be used for the following purposes:

1. To quickly (and much more accurately than the available empirical formulae) estimate the seismic demand in design of regular frame buildings.
2. To predict seismic demand and to estimate the seismic displacement for assessment of an existing frame building.
3. To verify stiffness and mass properties of finite element models by comparing the time periods obtained from finite element analysis and the proposed equation.
4. Handy tool for practicing structural engineers to understand change in seismic demand with change in cross sectional properties.

A flowchart that explains the use of the proposed equation in the design of a new frame building or assessment of an existing building is reported in Appendix K. Firstly, the basis for the proposed equation and brief details of Macleod's original model to estimate roof/top deflection of a frame building is discussed. Thereafter, the lateral stiffness of frames obtained with Macleod's modified equation are compared with initial lateral stiffness obtained from pushover analyses performed using the structural analysis software SAP 2000 [18]. The error in predicting the lateral stiffness with Macleod's original and modified equations is compared. Later, the fundamental periods predicted by the proposed equation are compared with those obtained from Eigenvalue analysis. The accuracy and reliability of the proposed

equations are thoroughly verified by comparing predicted results with those obtained from computer analysis for a wide range of low-medium rise RC frame buildings covering a wide range of bay widths, seismic mass and beam to column relative stiffness. Also, the fundamental period predicted using the proposed equation is compared with the period obtained using Rayleigh method and measured from experimental tests [19, 20]. This chapter also investigates the reliability of the empirical equations in predicting fundamental period of frame buildings for design or assessment purpose. The results obtained using the proposed equation and Eigenvalue analysis are used to scrutinize the limitations of the empirical equations; for example their inability to capture the effects of geometric configuration, seismic mass, and effective section properties. Finally, the ability of the proposed equation to predict fundamental period of slightly irregular buildings with varying bay lengths, storey heights and storey seismic mass is also investigated.

7.2 Derivation of theoretical/analytical model

The proposed analytical model/equation to predict the fundamental period is developed by modifying and extending Macleod's original method [21] which was originally developed to estimate top the displacement of a frame building. The basic philosophy of the Macleod's method is to condense multiple bays into an equivalent single bay frame. Because of symmetry, only a half of the frame is considered. Firstly, the lateral deflection of the beam-column subassembly in a single storey of the half bay frame is calculated using any standard analysis methods. To estimate the top deflection of a frame, thus the calculated inter-storey deflection is then integrated over the total building height assuming linear variation of deflection over storey height. Key features of the original Macleod's method are discussed again in the chapter; and interested readers can obtain its full details from the literature [21].

It is important to note that the Macleod's original model is developed to predict top deflection only, not to predict the fundamental period of a frame building. Two main assumptions in the original method are: (i) cross sections are un-cracked; and (ii) the point of contra-flexure is at the mid-height of a storey. Because of these assumptions, the original model cannot be directly used in estimating the lateral deflection and the lateral stiffness of a RC frame building in seismic regions. For these reasons the original model is modified and extended herein by incorporating factors to account for the above mentioned issues.

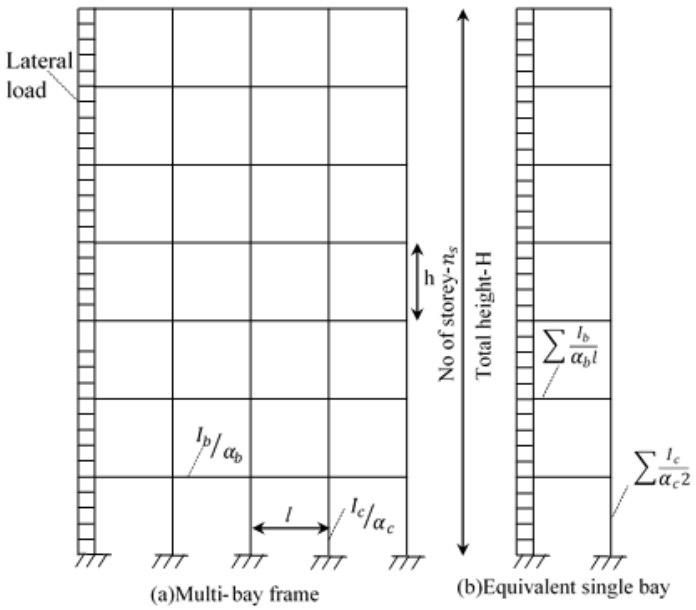

Figure 7.2. Condensation of a multi bay frame into an equivalent single bay frame

The modified model is generic and can predict the top deflection, the lateral stiffness under different lateral load profiles; such as a point load at the top of a frame, a uniformly distributed load over the whole building height to represent wind load or a triangular load which can be used to represent the lateral seismic force profile in frame buildings at different limit states. The modified expression for lateral deflection is further extended to predict the lateral stiffness and the fundamental period of frame buildings. In Figure 7.2, I_b and I_c represent the gross moment of inertia of the beams and columns respectively. The figure also shows the process of condensing a multi-bay frame into an equivalent single bay frame by taking into account the effective sectional properties of beams and columns through factors α_b and α_c, respectively. Note that the factors α_b and α_c are calculated as the ratio of gross to effective moments of inertia at corresponding limit states, hence the values of the factors are always greater than or equal to 1. These values are generally prescribed in the corresponding building codes or can be calculated using Table 7.2 which are taken from the New Zealand concrete structures standard [15]. Figure 7.3 shows the overall modified Macleod's model. Idealization of a single bay frame into a half bent is shown in Figure 7.3a; and the factors α and β in Figure 7.3b define the location of point of contra-flexure in the columns. It is assumed that the point of contra-flexure in beams is at mid length, which is a reasonable assumption. The linear variation of the sectional properties with height is kept the same as in the original Macleod's model, which is shown in Figure 7.3c. Most of the notations and symbols are kept the same as in the original Macleod's model, so that the readers can easily

identify the modifications and understand the extension of the original model from the estimation of top deflection to the prediction of the fundamental period.

Table 7.2. Effective moment of inertia of RC sections at different limit states [15]

Type of member	Ultimate limit state		Serviceability limit state		
	f_y = 300 MPa	f_y = 500 MPa	μ = 1.25	μ = 3	μ = 6
1 Beams					
(a) Rectangular ¶	0.40 I_g (use with E_{40}) §	0.32 I_g (use with E_{40}) §	I_g	0.7 I_g	0.40 I_g (use with E_{40})§
(b) T and L beams ¶	0.35 I_g (use with E_{40}) §	0.27 I_g (use with E_{40}) §	I_g	0.6 I_g	0.35 I_g (use with E_{40})§
2 Columns					
(a) $N^*/A_g f'_c > 0.5$	0.80 I_g (1.0 I_g)‡	0.80 I_g (1.0 I_g)‡	I_g	1.0 I_g	As for the ultimate limit state values in brackets
(b) $N^*/A_g f'_c = 0.2$	0.55 I_g (0.66 I_g)‡	0.50 I_g (0.66 I_g)‡	I_g	0.8 I_g	
(c) $N^*/A_g f'_c = 0.0$	0.40 I_g (0.45 I_g)‡	0.30 I_g (0.35 I_g)‡	I_g	0.7 I_g	

NOTES –
(§) With these values the E value should be the elastic modulus for concrete with a strength of 40 MPa regardless of the actual concrete strength.
(‡) The values in brackets apply to columns which have a high level of protection against plastic hinge formation in the ultimate limit state.
(¶) For additional flexibility, within joint zones and for conventionally reinforced coupling beams refer to the text.

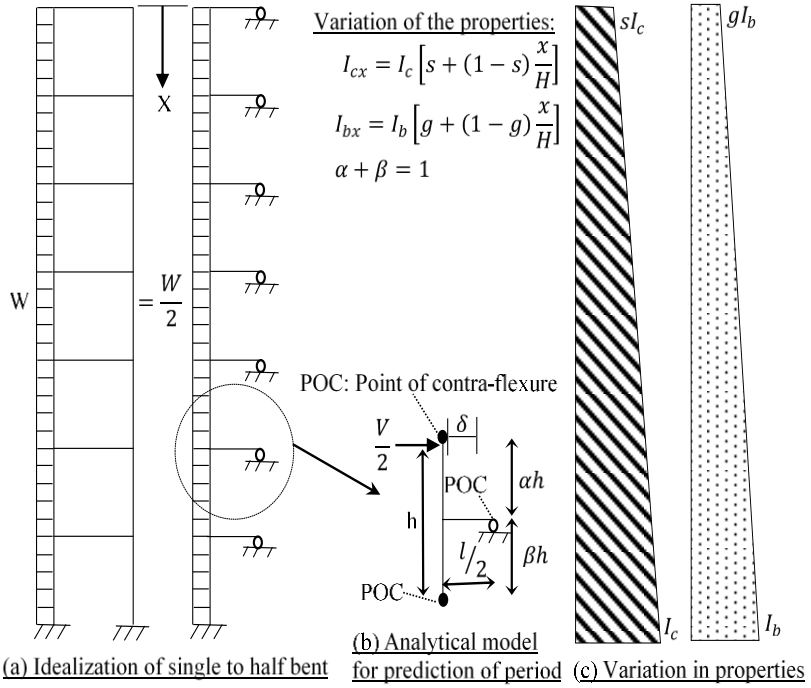

Figure 7.3. Modified Macleod's model to predict the fundamental period of a frame building

The lateral deformation of a single storey half bent shown in Figure 7.3b can be calculated using any standard analysis methods (e.g. moment area theorem); which is given by:

$$\delta = \frac{\alpha_c V h^3[\alpha^3+\beta^3]}{6E_c I_c} + \frac{\alpha_b V h^2 l}{12E_b I_b} \quad (1)$$

For the equivalent single frame, $I_c = \sum \frac{I_c}{2}$ and $\frac{I_b}{l} = \sum \frac{I_b}{l}$, by substituting these in Equation 1, Equation 1 turns into:

$$\delta = \frac{Vh^3}{12\sum E_c I_c}\left(4\alpha_c[\alpha^3+\beta^3] + \alpha_b \frac{\sum\frac{E_c I_c}{h}}{\sum\frac{E_b I_b}{l}}\right) \quad (2)$$

$$\delta = \frac{Vh^3}{12\sum E_c I_{cef}}(4\,[\alpha^3+\beta^3] + \lambda\,) \quad (3)$$

Where $\lambda = \frac{\sum\frac{E_c I_c}{h\alpha_c}}{\sum\frac{E_b I_b}{l\alpha_b}}$ is calculated as a ratio of the sum of column effective stiffness to sum of beam effective stiffness at the first storey level, n_b is number of bays, I_{cef} is the effective moment of inertia of the column, and *V* is the storey shear at the level of sub-assembly under consideration (as shown in Figure 7.3b). For the integration to be performed later, the deflection of the single storey half bent is converted to the differential form for the height dX (with the assumption of linear variation over storey height, which is reasonable for low-medium rise buildings).

$$d\delta = \frac{Vh^2}{12\sum E_c I_{cefx}}(4[\alpha^3+\beta^3] + \lambda\,)dx \quad (4)$$

Equation 4 is further modified by incorporating factors to account for variation of section properties, and finite size of the beam-column joint:

$$d\delta = \frac{Vh^2}{12\sum E_c I_{cef}}\left(\frac{4\,[\alpha^3+\beta^3](1-\beta_d)^3}{s+(1-s)\frac{x}{H}} + \frac{\lambda\,(1-\beta_c)^3}{g+(1-g)\frac{x}{H}}\right)dx \quad (5)$$

Where *s* and *g* are the ratio of the moment of inertias of column and beam at the top and bottom of the frame respectively. The factors $\beta_d = \frac{D}{h}$ (h to be measured between top of successive floors) and $\beta_c = \frac{C}{l}$ (l to be measured between centrelines of columns) are to account for the finite size of beam-column joint as mentioned before; *D* is beam depth and *C* is column depth. Note that the factor β_d should be calculated differently for low rise frames if *h* is measured to the centre of the beams. As frames do not have any beam at the base, for one storey frame the factor becomes $\beta_d = \frac{D}{2h}$. The term $[\alpha^3+\beta^3]$ in Equation 5 is replaced with a single factor $\frac{\gamma}{4}$, where the value of γ depends on the location of point of contra-flexure in the columns. The factor γ is evaluated by calculating the actual deflection of the sub-frame shown in Figure 7.3b by varying the parameters α and β (i.e. location of point of contra-flexure in columns) as defined. Thereafter, the calculated deflection is normalized with the deflection corresponding to point of contra-flexure at mid-height, which give the γ values shown in Table 7.3. Equation 5 is now integrated over the whole building height $H = n_s \times h$ for the different load profiles to predict the corresponding top deflection Δ, which is given by

Equation 6. Here, the additional top deflection contribution due to axial deformation of columns is neglected; this is a fair assumption for low to medium rise buildings.

$$\Delta = \frac{Vh^3 n_s}{12 \sum E_c I_{cef}} \left(\gamma F_s \, (1 - \beta_d)^3 + \lambda F_g \, (1 - \beta_c)^3 \right) \tag{6}$$

Table 7.3. Values of γ with variation of location of point of contra-flexure in columns

Location of POC in the columns	$\boldsymbol{\alpha}$	$\boldsymbol{\beta}$	**γ**
At 0.5h (i.e. mid height)	0.5	0.5	1
At 0.4h	0.4	0.6	1.12
At 0.35h	0.35	0.65	1.27
At 0.3h	0.3	0.7	1.48

The factors F_s and F_g in Equation 6 depend on the type of loading profile, and variation of section properties with the height of the building, these factors can be calculated using the equations given in Table 7.4.

Table 7.4. F_s and F_g values with variation of sectional properties and different load profiles [21]

Type of loading	$\boldsymbol{F_s}$ **(m=s) and** $\boldsymbol{F_g}$ **(m=g)**	**s=g=1**
Point load (F_{sp}, F_{gp})	$\frac{log_e m}{(m-1)}$	1
UDL (F_{su}, F_{gu})	$\frac{1}{(1-m)} + \frac{m log_e m}{(1-m)^2}$	0.5
Triangular load (F_{st}, F_{gt})	$\frac{log_e m}{(m-1)} + \frac{(-1.5+2m-0.5m^2-log_e m)}{(m-1)^3}$	0.67

Thereafter, the lateral stiffness of the frame is calculated as the ratio of total load (i.e. base shear) and top deflection as shown below:

$$K_{l1} = \frac{12 \sum E_c I_{cef}}{h^3 n_s (\gamma F_s \, (1-\beta_d)^3 + \lambda F_g \, (1-\beta_c)^3)} \tag{7}$$

As indicated by the Equation 7, the lateral stiffness of a frame predominantly depends on the relative flexural stiffness between its beams and columns. The relative stiffness is a function of moment of inertia of the beams and the columns, span length and storey height. To understand better the factors which affect the relative stiffness, here it is assumed that the storey height and the span length are constant. Then, the relative stiffness of beam to column can be increased either for a given column size by increasing the beam size or for a given beam size by decreasing the column size. The lateral stiffness of a frame can be increased by increasing the relative stiffness of beam to column (represented by 1/ λ) or by decreasing the column to beam relative stiffness (represented by λ) for a given column size and vice versa.

To clarify the difference between the two different ways of interpretation of the relative stiffness, Figure 7.4a plots the initial lateral stiffness of the frame as a function of beam-to-column and column-to-beam stiffness ratios. In this figure, for both cases the lateral stiffness

is calculated using Equation 7 but plotted as a function of beam-to-column and column-to-beam stiffness ratio respectively, and "SAP" represents the lateral stiffness values obtained from pushover analysis results performed using SAP 2000. For a given column size, very small beam to column relative stiffness $1/\lambda$ means that the overall frame behaviour is close to cantilever deformation mode (i.e. flexural response with single curvature throughout the building height) without any point of contra-flexure in the columns throughout the building height, which is illustrated in Figure 7.4b. As the relative stiffness $1/\lambda$ approaches a very large value, the building deforms in shear mode (i.e. columns within the floors deform in double curvature with point of contra-flexure at mid-height), which is shown in Figure 7.4c. For practical range of relative stiffness $1/\lambda$, the building frame deforms with a combination of flexural and shear deformation modes with no definite pattern of column curvature profiles along the building height (i.e. points of contra-flexure in the columns of different storeys are not at the same location), which is shown in Figure 7.4d. Generally, lower storeys of a frame deform in flexure dominated mode whereas upper storeys deform in shear dominated mode.

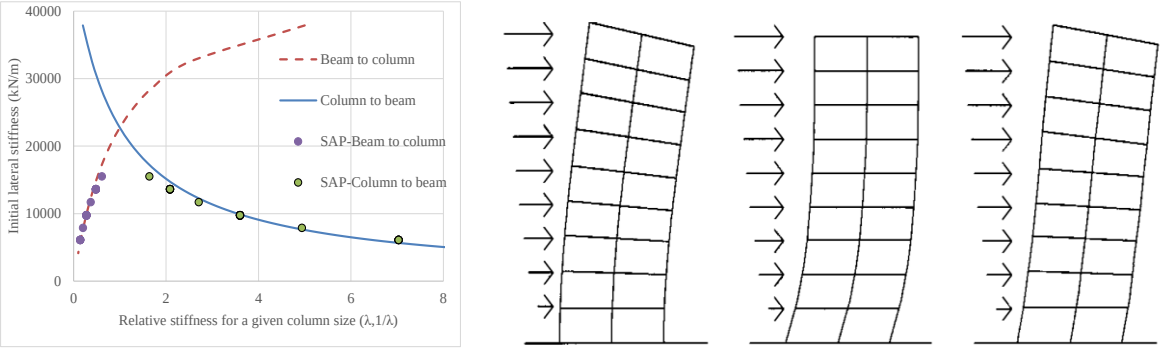

(a) Lateral stiffness vs $\lambda, 1/\lambda$ (b) Flexural deformation (c) Shear deformation (d) Flexural-shear deformation

Figure 7.4. Lateral stiffness vs beam-column, column-beam relative stiffness and lateral deformation of frame buildings [22]

To find the inaccuracy in prediction of the lateral stiffness with original Macleod's equation, the lateral stiffness of a wide range of frames predicted by using Equation 7 with the assumption of point of contra-flexure at mid height of the columns (i.e. γ=1) is compared with initial lateral stiffness obtained from the pushover analysis in Figure 7.5. Pushover analysis of the chosen frames is performed with triangular load pattern as per New Zealand Seismic Standard [12, 13]. In Figure 7.5a, "*n*S-Sap" represents an *n* storey frame whose lateral stiffness is calculated using SAP 2000, and "*n*S-predicted" represents the same frame but the lateral stiffness is calculated using Equation 7. It is observed from the plot that there is a discrepancy of ±25% between the lateral stiffness predicted by Equation 7 and the initial

lateral stiffness obtained from pushover analysis. This error is due to the fact that the point of contra-flexure is never at mid height in columns and not at the same location in the columns of all storeys. Moreover, Equation 7 is developed based on the assumption that the bending moment in a beam is equal to the sum of column moments at the top and bottom of the beam, which is not true for low beam-to-column relative stiffness ratio. Such frames deform in cantilever mode, which adds further to the error in the stiffness predicted using Equation 7 with γ=1. Although the ratio of beam to column stiffness is varied up to 1.5 for verification purpose, in modern frame buildings designed to capacity design principles and confirming to weak beam-strong column hierarchy the beam to column stiffness ratio ranges between 0.25 and 0.75, which is indicated in the figures as the shaded region. The horizontal lines in Figure 7.5b (and later in Figures 7.6b and 7.7b as well) define the upper and lower bound values used in the regression analysis to get a correction factor as described in the next paragraph.

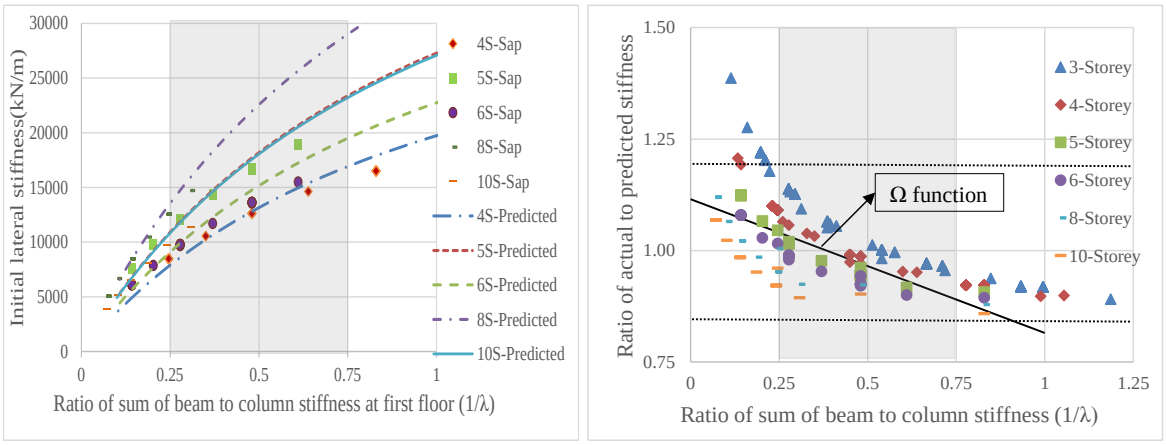

(a) Comparison of predicted and actual stiffness (b) Range of actual to predicted stiffness

Figure 7.5. Comparison of predicted and actual lateral stiffness with γ=1

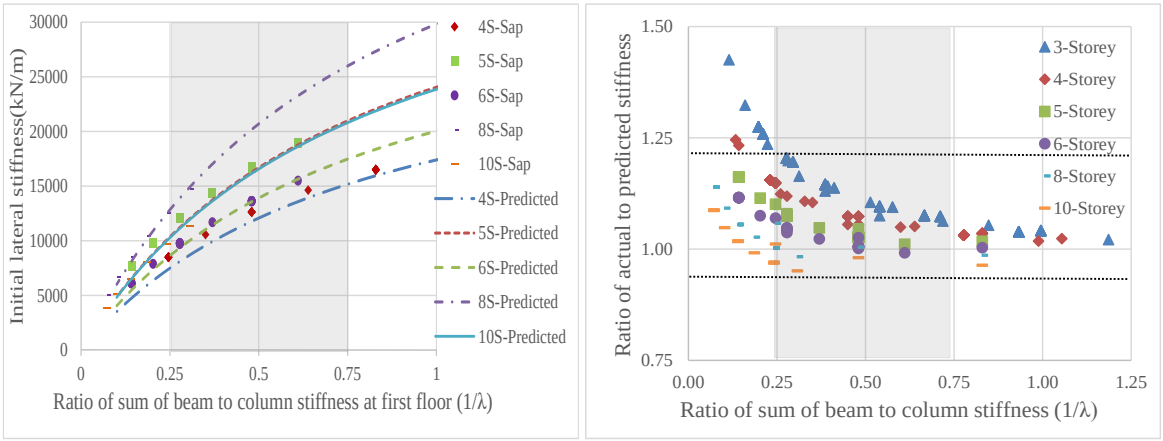

(a) Comparison of predicted with actual stiffness (b) Range of actual to predicted stiffness

Figure 7.6. Comparison of predicted and actual lateral stiffness with γ=1.27

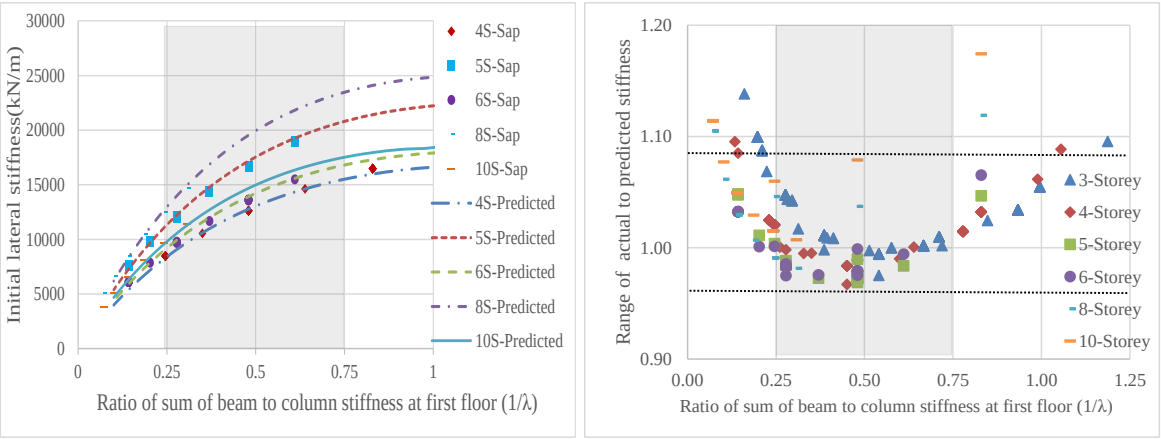

(a) Comparison of predicted with actual stiffness (b) Range of actual to predicted stiffness

Figure 7.7. Comparison of predicted and actual lateral stiffness with use of Ω factor

Strictly speaking, it is impossible to precisely locate the point of contra-flexure in columns in all storeys without the use of any structural analysis software. The error in the predicted lateral stiffness because of this can be corrected by a correction factor. Here, two approaches are adopted to arrive at a factor which corrects the error shown in Figure 7.5. In the first approach, the lateral stiffness of the frames is calculated using Equation 7 using different γ values (as listed in Table 7.3) and finding the value of γ such that Equation 7 results in the lateral stiffness close to the lower bound value. As can be seen in Figure 7.6, it is found from regression analysis that γ = 1.27 (which corresponds to the point of contra-flexure being at 0.35 times column height) predicts a lower bound lateral stiffness value for most of the cases. Any error resulting in the predicted fundamental period due to remaining discrepancy in the lateral stiffness predicted using Equation 7 with γ = 1.27 will be corrected later with another factor φ which is aimed to account also for the difference between the total seismic mass and the effective mass and between the top deflection based lateral stiffness and the effective lateral stiffness of an equivalent single degree of freedom (SDOF) system under the fundamental mode of vibration.

In the second approach, Equation 7 is used with $\gamma = 1$ and later modified with another factor Ω. As the factor Ω is aimed to correct the lateral stiffness predicted by Equation 7 with $\gamma = 1$, Equation 7 then turns into:

$$K_{l2} = \frac{12\Omega \sum E_c I_{cef}}{h^3 n_s \left(F_s\,(1-\beta_d)^3 + \lambda F_g\,(1-\beta_c)^3\right)} \qquad (8)$$

Multiple variable regression analyses are carried out to correct the error in predicted lateral stiffness shown in Figure 7.5. A linear relation between the correction factor Ω with the relative stiffness λ and the number of storeys n_s is developed using data shown in Figure

7.5b; and the resulting expression is given in Equation 9. After incorporating the correction factor Ω in Equation 8, the comparison of the predicted and actual lateral stiffness are shown in Figure 7.7a. It is clear from Figure 7.7b that the accuracy of the predicted lateral stiffness is within ±10% of actual lateral stiffness in the practical beam-to-column relative stiffness range between 0.25 and 0.75.

$$\Omega = 1.25 - \left(\frac{0.3}{\lambda}\right) - 0.027n_s \geq 0.67 \text{ with } R^2 = 0.86 \quad (9)$$

A multi-degree of freedom (MDOF) building frame system has many modes of vibration with different periods. Out of many periods, the period of the first (i.e. fundamental) mode of vibration is commonly used in estimation of seismic demand. The period of the first mode of vibration is generally calculated using Eigenvalue analysis or Rayleigh method by condensing a MDOF system into an equivalent SDOF system. The period of an equivalent SDOF system is given by Equation 10.

$$T = 2\pi\sqrt{\frac{M_{eff}}{K_{eff}}} \quad (10)$$

The effective mass M_{eff} in the first mode of vibration depends on the mass participation factor, which in turn depends on the mode shape and mass distribution along the building height. Generally, for low-medium rise frame buildings with uniform stiffness and mass distribution, the mass participation in the fundamental mode will be between 70%-100%. The effective stiffness of an equivalent SDOF system depends on the mode shape and the effective height of the equivalent SDOF system. The lateral stiffness calculated using Equation 7 or 8 is based on the top deflection of a frame, which needs to be modified at the effective height of the frame in the fundamental mode of vibration to get the effective stiffness K_{eff}. A factor φ is introduced herein to account for the effective mass and effective height (i.e. effective stiffness) in the first mode of vibration, which then turns Equation 10 into:

$$T = 2\pi\varphi\sqrt{\frac{M}{K_l}} \quad (11)$$

In Equation 11, M is replaced with $\frac{W_s}{g}$, where W_s is the seismic weight acting on the chosen frame and g is acceleration due to gravity. Here, the fundamental period of the equivalent SDOF is calculated in two ways; one using the lateral stiffness calculated using Equation 7 and another using lateral stiffness calculated using Equation 8. With the first approach, K_l in

equation 11 is replaced with K_{l1}; then the equation to predict the fundamental period can be written as Equation 12a.

$$T = 2\pi\varphi_1\sqrt{\frac{W_s\, h^3 n_s\left(F_{st}1.27\,(1-\beta_d)^3+\lambda F_{gt}\,(1-\beta_c)^3\right)}{g\;12\sum E_c I_{cef}}} \tag{12a}$$

With the second approach, K_l is replaced with K_{l2}; then the equation to predict the period turns into Equation 12b.

$$T = 2\pi\varphi_2\sqrt{\frac{W_s\, h^3 n_s\left(F_{st}\,(1-\beta_d)^3+\lambda F_{gt}\,(1-\beta_c)^3\right)}{g12\Omega\sum E_c I_{cef}}} \tag{12b}$$

To arrive at the values of factors φ_1 and φ_2, the fundamental periods computed using Equation 12a with $\varphi_1 = 1$ and using Equation 12b with $\varphi_2 = 1$ are compared with the periods obtained from Eigenvalue analysis using SAP 2000. The correction factors required to multiply the predicted periods to obtain the actual periods for a wide range of frames are plotted in Figure 7.8. Linear relations between the correction factor φ_1 or φ_2, the relative stiffness λ and the number of storeys n_s are developed to minimize the error in the predicted fundamental period. The correction factors are given as $\varphi_1 = 0.67 + 0.10/\lambda + 0.005n_s$ with $R^2 = 0.82$ and $\varphi_2 = 0.79 + \frac{0.01}{\lambda} - 0.005n_s$ with $R^2 = 0.63$. The overall variation of φ_1 and φ_2 is between 0.65 and 0.8, and 0.70 and 0.8 respectively. The variation of factor φ_2 with relative stiffness is negligible and can be further simplified to $\varphi_2 = 0.79 - 0.005n_s$. Though overall variation of φ_2 is very less, the linear fit is not good enough. Note that the above expressions have been derived using the F_{st} and F_{gt} values corresponding to a triangular load pattern, if any other load pattern is used to compute the lateral stiffness then these factors have to be recalibrated.

It is realized that both Ω and φ_2 in Equation 12b are functions of the relative stiffness λ and the number of storeys n_s, so a new period correction factor φ_3 $\left(\text{i. e. } \varphi_3(\lambda, n_s) = \frac{\varphi_2(\lambda,n_s)}{\sqrt{\Omega(\lambda,n_s)}}\right)$ is developed by calibrating against actual periods with $\Omega = 1$, then Equation 12b turns into:

$$T = 2\pi\varphi_3\sqrt{\frac{W_s\, h^3 n_s\left(F_{st}\,(1-\beta_d)^3+\lambda F_{gt}\,(1-\beta_c)^3\right)}{g12\sum E_c I_{cef}}} \tag{12c}$$

From regression analysis, φ_3 is related to λ and n_s as: $\varphi_3 = 0.66 + 0.19/\lambda + 0.008n_s \leq 1.0$ with $R^2 = 0.86$, which is shown in Figure 7.9a. Although not apparent from the data plotted in the figure, the maximum limit of φ_3 is decided as the ratio of the maximum value of φ_2 (about 0.8 as apparent in Figure 7.8b) and the square root of the minimum value of Ω

specified in Equation 9 (i.e. $\sqrt{0.67} \approx 0.8$). Note that the limiting maximum value is irrelevant in most normal frames and will only come into effect for frames with unusually high values of $1/\lambda$ (i.e. frames with very stiff beams and flexible columns). The ratio of actual to predicted periods for varying number of storeys is shown in Figure 7.9b, and it is clear that the predicted periods are within ±10% of the actual periods. The comparison of the fundamental periods calculated using Equations 12a, 12b and 12c for a four and ten storey frame with the parameters listed in Tables 7.5 and 7.6 are plotted as a function of relative stiffness in Figure 7.10. It can be observed that there is no major difference between the periods predicted by different equations.

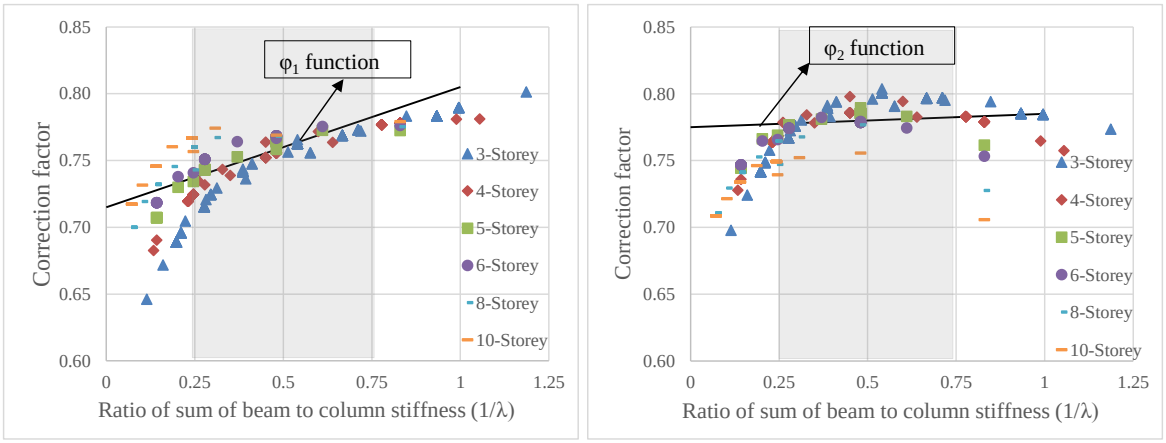

(a) Correction factor for $\varphi_1 = 1$ (b) Correction factor for $\varphi_2 = 1$

Figure 7.8. Correction factors to multiply the predicted period with $\varphi_1 = 1, \varphi_2 = 1$

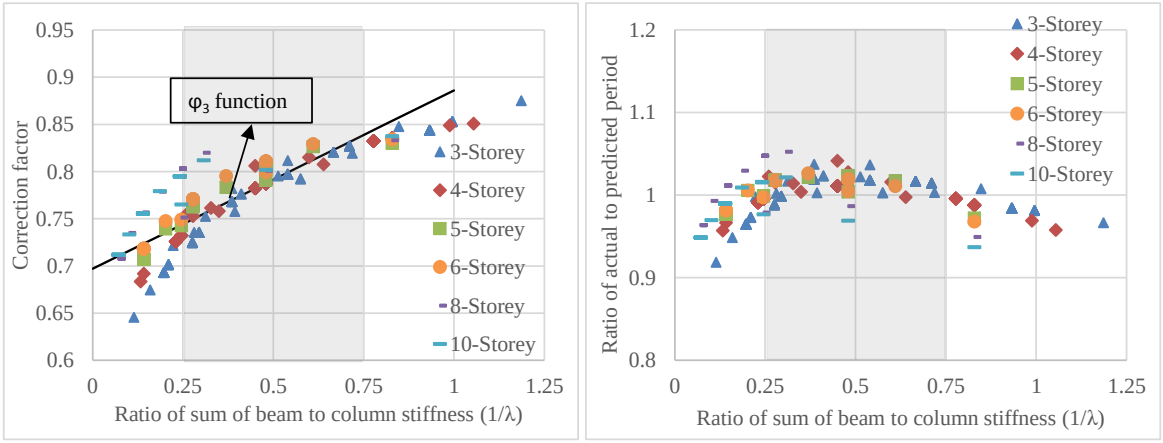

(a) φ_3 as function of λ and n_s (b) Range of actual to predicted period using Equation 12c

Figure 7.9. Correction factor φ_3 and ratio of actual to predicted period using Equation 12c

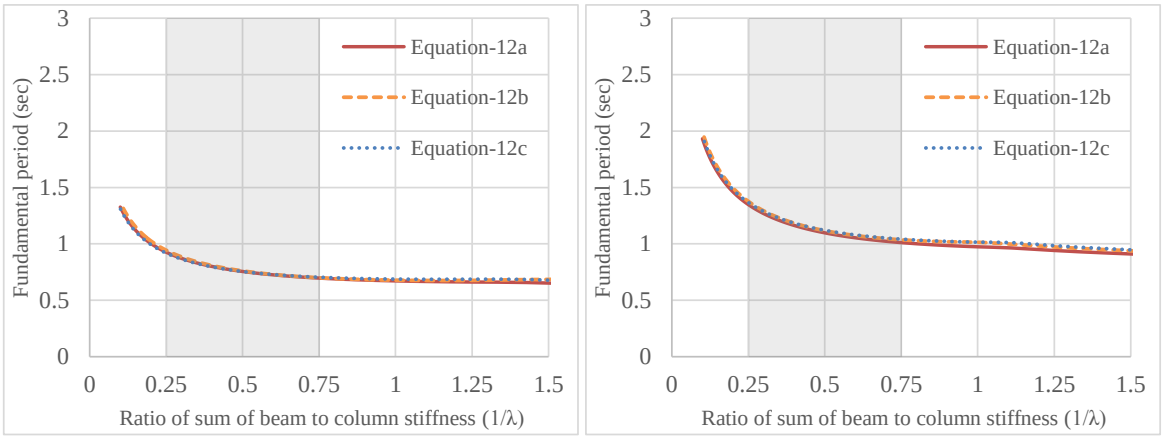

(a) 4 storey frame (b) 10 storey frame

Figure 7.10. Comparison period plots for a 4 and 10 storey frame using Equation 12a, 12b and 12c

As Equation 12c needs only one correction factor to be calculated and has high R^2 value compared to other equations, it is proposed for practical applications. The generic Equation 12c can be further simplified for a regular frame with sectional properties don't change with the height of the building (i.e. $F_{st} = F_{gt} = 0.67$ as shown in Table 7.4 for triangular lateral force distribution). The simplified expression is presented in Equation 13a, where n_b is the number of bays.

$$T = 0.47\varphi_3\sqrt{\frac{W_s\, h^3 n_s(\,(1-\beta_d)^3+\lambda\,(1-\beta_c)^3)}{(n_b+1)E_c I_{cef}}} \tag{13a}$$

When clear spans of beam length and column height are used (rather than centre to centre dimension of the frame), the effect of finite size of beam-column joint on the fundamental period can be neglected (i.e. $\beta_d = \beta_c = 0$). In such cases, Equation 13a turns into Equation 13b.

$$T = 0.47\varphi_3\sqrt{\frac{W_s\, h^3 n_s(\,1+\lambda\,)}{(n_b+1)E_c I_{cef}}} \tag{13b}$$

7.3 Results and discussion

As mentioned earlier, to verify and validate the developed analytical equation to estimate the fundamental period of frame buildings, Eigenvalue analysis is performed on a wide range of low-medium rise RC frame buildings using SAP 2000. The varied parameters and their ranges used in the verification are identified in Table 7.5. For calculation of the seismic weight on a chosen frame, it is assumed that the building has 4 bays of 6 m width in the perpendicular direction unless otherwise specifically mentioned. The tributary seismic weights on the chosen frame is calculated on the assumption that the floor is rigid in plane (i.e. rigid diaphragm) and are distributed proportional to the stiffness of the frames (here it is assumed all frames in a building have equal stiffness). The geometrical dimensions and the seismic weight of the frames used in the parametric investigation are shown in Table 7.6.

Note that the fundamental periods are calculated based on gross section properties and by neglecting the effect of finite beam-column joint (i.e. $\beta_d = \beta_c = 0$) unless otherwise specifically mentioned. To be consistent with this simplification, the lengths of the beams and columns in the SAP2000 model of the frame used for the Eigenvalue analysis are made equal to their centre to centre spans (without deducting for the joint dimension) and the rigidity provided by the beam-column joint panel is not accounted for. The fundamental periods predicted using the proposed equation are compared with the periods obtained by using Rayleigh method and measured from experimental tests. The periods predicted using the proposed equation are also used for scrutinizing the limitations of the empirical equations in predicting the fundamental periods. The applicability of the proposed equation to predict the fundamental period of low to medium rise frame buildings with minor irregularity is also investigated.

Table 7.5. Variables used in a parametric study

Building characteristics		**Material description**	
Number of storeys	3-10	Grade of concrete	35 N/mm^2
Storey height	3.6 m	Grade of rebar	500 N/mm^2
Span length	5-10 m	**Loading details**	
Number of bays	3-5	Dead load	Roof: 4.75 kN/m^2 Other:4.25 kN/m^2
Young's modulus	19641 N/mm^2	Live load	Roof: 2.5 kN/m^2 Other: 3.0 kN/m^2

Table 7.6. Seismic weights used in the parametric study

Number of storeys	Number of bays	Span length (m)	Column dimensions (m×m)	Seismic weight (kN)
3	3	5	0.4x0.5	1501
3	3	5	0.4x0.6	1539
3	3	7	0.4x0.5	2020
3	3	7	0.4x0.6	2057
3	4	5	0.4x0.5	1981
3	4	7	0.4x0.5	2672
4	3	6	0.4x0.5	2358
4	3	6	0.4x0.6	2409
4	4	6	0.4x0.5	3122
4	4	6	0.4x0.6	3185
5	4	6	0.4x0.5	3908
5	4	6	0.4x0.6	4010
6	4	6	0.4x0.5	4698
6	4	6	0.4x0.6	4821
8	4	6	0.4x0.5	6188
8	4	6	0.5x0.7	6484
10	4	6	0.4x0.5	7677
10	4	6	0.5x0.7	8359

7.3.1 *Fundamental period: Proposed equation vs Eigenvalue analysis*

For the verification of Equation 12c in predicting the fundamental period of a low-medium rise RC frame buildings, the period calculated using Equation 12c is compared with period calculated using Eigenvalue analysis. Initially a six storey and four bay frame building is chosen with the following properties: beam span of 6 m, column section of 0.4×0.6 m, beam section of 0.4×0.45 m, and seismic weight of 4731 kN. The predicted fundamental period using Equation 12c is 1.18 sec whereas the period obtained from Eigenvalue analysis using SAP 2000 is 1.19 sec. As mentioned before, for same frame it is possible to have different fundamental periods depending on the lateral stiffness, which in turn depends on the relative stiffness between beam and column. For a single storey frame, as the beam stiffness is increased from 0 to ∞, the lateral stiffness increases from $\frac{6E_cI_c}{h^3}$ to $\frac{24E_cI_c}{h^3}$ and the period is halved. The variation of the fundamental period of the single storey frame as a function of the relative stiffness of beam to column can be easily developed and understood. But, for a multi-storey, multi-bay frame the variation of the fundamental period by varying the relative stiffness is not easy to predict and understand. Here, variation of the fundamental period due to variation of the relative stiffness is quantified using the proposed Equation 12c.

To verify the proposed Equation 12c extensively, the fundamental periods are plotted against the beam-to-column relative stiffness ratio for a wide range of 3 to 10 storey frames. The periods predicted by the proposed Equation 12c are compared with those obtained from

Eigenvalue analysis; the comparisons are shown in Figures 7.10 to 7.12. In the legend of these figures, "C-0.4×0.5" represents the cases with column size 0.4×0.5 m, "S-5" represents the span length of 5 m, "3Bay" represents the frame of 3 bays, "predicted" represents that the periods are calculated using Equation 12c, "Eigen" indicates that the periods are calculated by performing Eigenvalue analysis using SAP 2000. It is important to note that in Figures 7.11 to 7.13, the fundamental periods predicted using Equation 12c are based on the seismic weights given in Table 7.6. Strictly speaking, there will be a slight change in the seismic weight due to change of beam cross-sections (i.e. with the change in relative stiffness between beams and columns), but here the average seismic weight is considered for the analysis and any minor error because of this is neglected.

It is clear from Figures 7.11 to 7.13 that as the ratio of beam to column stiffness increases for a given column size, the fundamental period of the frame decreases. This is because the lateral stiffness of the overall frame increases, which is inversely proportional to the period. For the same frame configuration and the same relative stiffness ratio of beam to column, increase in the column dimensions results in an increase in the lateral stiffness and as a consequence the natural period decreases, which can be clearly seen in Figures 7.11a to 7.11c, 7.12 and 7.13. As the span length of the frame increases for a given frame configuration for a given column size, the lateral stiffness decreases and the period consequently increases, which is evident in Figure 7.11c. As it can be observed in Figures 7.11d and 7.12b, the addition of extra bays of the same span length with given frame configuration does not change the period significantly, because both the lateral stiffness and seismic mass increase when an extra bay is added.

As mentioned before, the ratio of beam to column stiffness is varied up to 1.5 for verification purpose, but in modern frame buildings the beam to column stiffness ratio ranges between 0.25 and 0.75, which is indicated in the figures as the shaded region. The maximum error in the predicted fundamental periods when compared to Eigenvalue analysis results is less than 10% within the shaded zone. Nevertheless, the predicted values in general are very close to Eigenvalue analysis results; and the minor difference is acceptable considering the uncertainties and complexities involved.

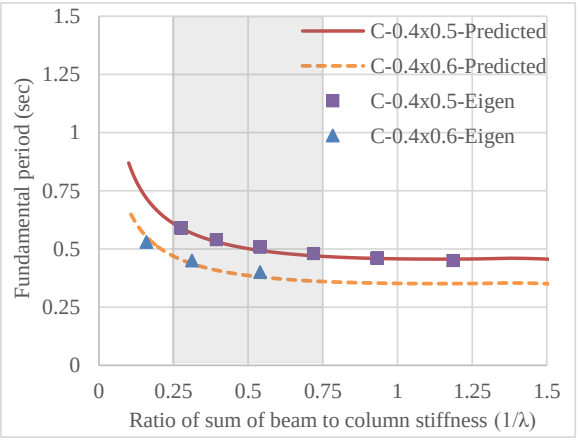

(a) 3 bays of 5 m span length

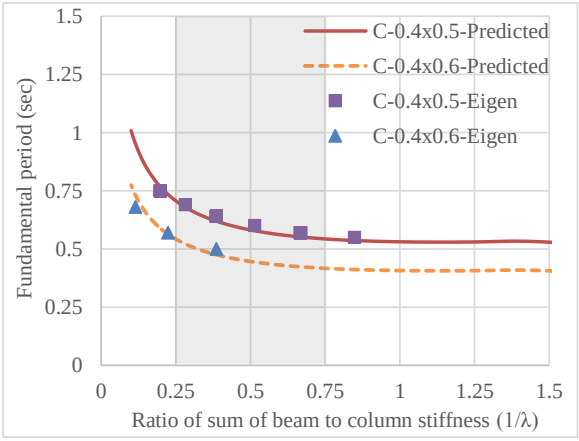

(b) 3 bays of 7 m span length

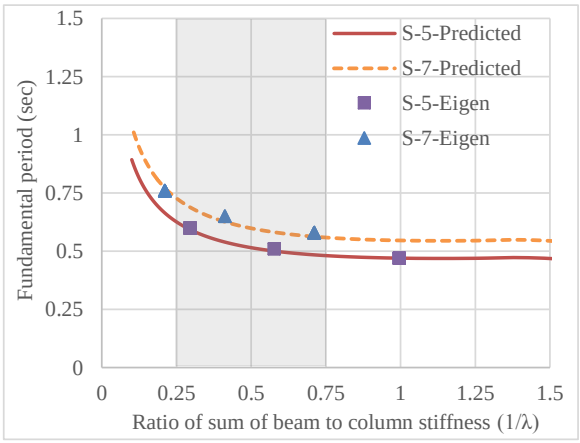

(c) 3 bays of 5 and 7 m span length

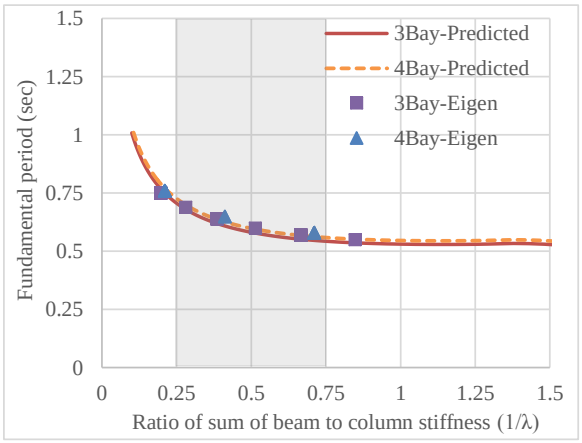

(d) 3 and 4 bays of 7 m span length

Figure 7.11. Comparison of periods using proposed equation and Eigenvalue analysis for a 3 storey frame

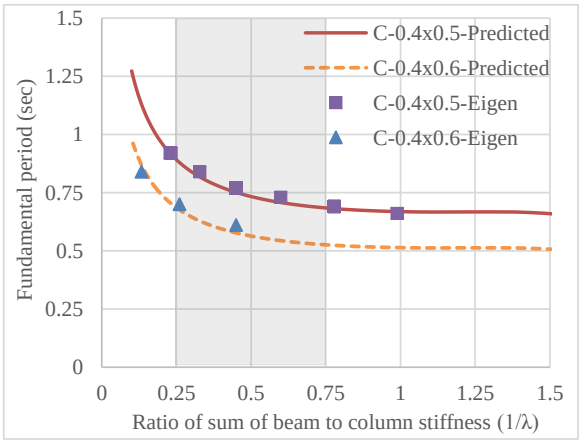

(a) 3 bays of 6 m span length

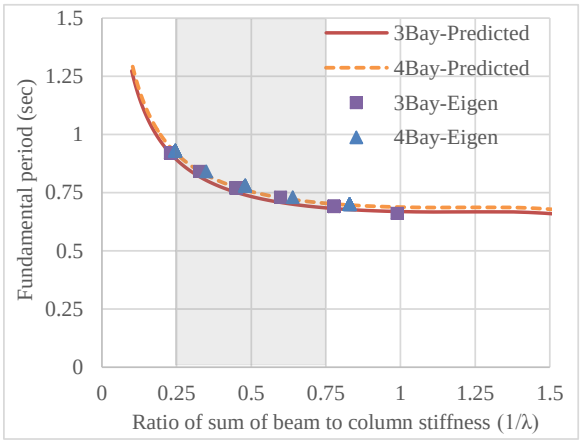

(b) 3 and 4 bays of 6 m span length

Figure 7.12. Comparison of periods using proposed equation and Eigenvalue analysis for a 4 storey frame

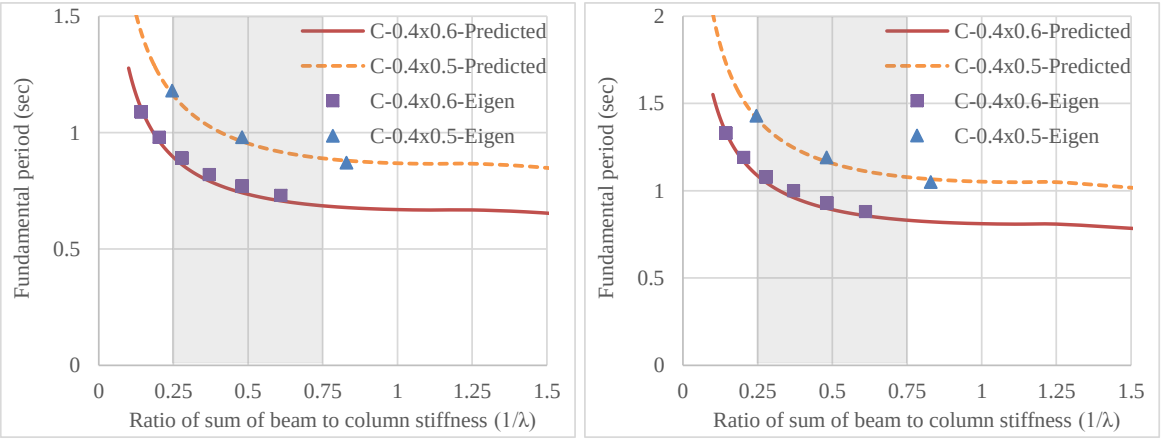

(a) 5 storey frame with 4 bays and 6 m span (b) 6 storey frame with 4 bays and 6 m span

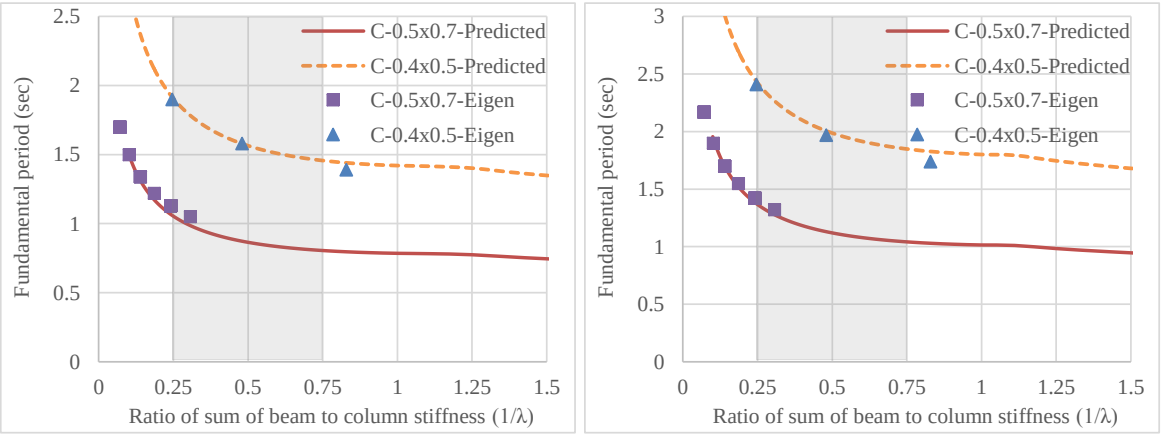

(c) 8 storey frame with 4 bays and 6 m span (d) 10 storey frame with 4 bays and 6 m span

Figure 7.13. Comparison of periods using proposed equation and Eigenvalue analysis for a 5 to 10 storey frames

7.3.2 *Fundamental period: Proposed vs Rayleigh method*

The fundamental period of a frame can be estimated using the Rayleigh equation, which is given in Equation 14, where W_i, δ_i and F_i represent the seismic weight, lateral defection and lateral force at the i^{th} storey level of a frame building.

$$T = 2\pi\sqrt{\frac{\sum_{i=1}^{n} W_i {\delta_i}^2}{g\sum_{i=1}^{n} F_i\delta_i}} \tag{14}$$

To compute fundamental period with the use of Rayleigh equation, the lateral defections at different storey levels under the triangular load profile need to be computed, for which a structural analysis software is required. If the deflections at different storey levels are computed assuming the building as shear frame building (i.e. storey stiffness$= \sum\frac{12E_cI_c}{h^3}$), the deflections are under predicted (i.e. lateral stiffness is over estimated) and consequently the period estimated will be less than the actual period.

For blind prediction of the fundamental period using the developed equations, a five bay seven storey frame (which is not from the original sample of frame buildings used earlier for calibration) is chosen with the following properties: storey height of 3 m, beam span of 6 m, column section of 0.6×0.6 m, beam section of 0.4×0.6 m, and seismic weight of 150 kN at each floor level. The lateral deflections at different storeys of the frame under a triangular lateral load profile are shown in Table 7.7. The fundamental period calculated using the Rayleigh method is 0.32 sec, which is shown in Equation 15.

$$T = 2\pi\sqrt{\frac{60442}{9810\times2369}} = 0.32 \text{ sec} \tag{14}$$

Table 7.7. Seismic weights, lateral force and displacements used in Rayleigh method to estimate fundamental period

Level	$W_i\ (kN)$	$F_i(kN)$	$\delta_i\ (mm)$	$W_i{\delta_i}^2$	$F_i\delta_i$
7	150	70	10.88	17775	762
6	150	60	10.18	15544	610
5	150	50	9.02	12214	451
4	150	40	7.44	8303	297
3	150	30	5.54	4605	166
2	150	20	3.41	1748	68
1	150	10	1.29	250	13
				∑=60442	∑=2369

On the other hand, as listed in Table 7.8, the fundamental period estimated using Equations 12a-12c and 13a vary between 0.30 and 0.32 sec. It is clear that for practical applications the fundamental period estimated using the developed equations are close enough to the fundamental period predicted using the Rayleigh method.

Table 7.8. Prediction of period using equations 12a-12c, 13a

Equation	**Lamda (λ)**	**Sigma (Ω)**	**Phi (φ)**	**Period (sec)**
12a	3.6	N/A	0.73	0.303
12b	3.6	0.98	0.76	0.308
12c, 13a	3.6	N/A	0.77	0.307

7.3.3 *Fundamental period: Effect of finite beam-column joint*

Note that the previous verifications were conducted for frames with no consideration to the rigid joint panel dimensions. In reality, the joint dimension to the member span ratio (i.e. β_d or β_c in Equations 12c and 13a) in typical frames varies between 0.05 and 0.2. As the flexural stiffness of a beam or column is inversely proportional to the third power of its length, these can result in substantial increase in the stiffness; and consequently noticeable reduction in period. In this section, the validity and accuracy of Equation 12c in predicting the fundamental period including the effect of finite beam-column joint is investigated. For this

purpose, a six storey and four bay frame building is chosen with the following properties: storey height of 3.6 m, beam centre to centre span of 6 m, column section of 0.4×0.6 m, beam section of 0.4×0.45 m, seismic weight of 4731 kN, $\beta_d = 0.12$ and $\beta_c = 0.1$. Eigenvalue analysis is conducted by modelling the frame with a combination of beam and column elements of lengths equal to their clear spans/heights and rigid blocks representing the half of the joint dimension at each end of the beam and column elements. The period obtained from Eigenvalue analysis is 1.03 sec (for the same frame, neglecting the effect of finite beam-column joint results fundamental period of 1.18 sec) whereas the predicted period using Equation 12c is 1.0 sec. The authors believe this extent of difference in prediction of fundamental period, which depends on several parameters, is acceptable.

7.3.4 *Fundamental period: Proposed vs Experimental results*

Fundamental period of two RC gravity frames obtained from experimental tests are compared with the fundamental period predicted using the proposed equation. First one is a two storey RC gravity frame with dimensional and cross sectional properties as follows [19]; two bays of 2.85 m c/c span in Y direction and one bay of 4.70 m c/c span in X direction, inter-storey height measured to the centre of the beams of 3.50 m and 3.6 m for the first and second levels, beam cross-section of 0.3×0.5 m, column cross-section of 0.3×0.3 m, modulus of elasticity of 26672 MPa, $\beta_d = 0.07$ in X and Y direction, $\beta_c = 0.06$ in X direction, $\beta_c = 0.1$ in Y direction, and seismic weight of 330 kN. The fundamental period of vibration measured in the experiment for the two storey un-retrofitted frame in X direction was 3.15 Hz (i.e. 0.32 sec) and in Y direction was 3.30 Hz (i.e. 0.31 sec) [19].

In the estimation of the fundamental period using the developed Equations 12c and 13a, storey height of 3.5 m is used even though there is slight difference in actual storey heights. It is important to note that the tested frame has stronger beams and weaker columns; and the relative column to beam stiffness (λ) is very small compared to a frame building that is designed using modern capacity design based building codes. Hence, the correction factor φ_3 value is dictated by the upper limit, which is expected to induce some error in the prediction. The fundamental periods predicted using the developed Equations 12c and 13a are shown in Table 7.9. Using the clear spans of beams and columns in Equation 13b also results in the same periods. It is clear from Table 7.9 the predicted fundamental periods are in comparable range and in reasonable agreement with the actual periods measured from the experimental test. The largest error in the prediction of fundamental period using the

proposed Equations in this case is around 20%. As mentioned earlier, this error is mainly due to the column to beam stiffness ratio λ being well outside the range for which φ_3 has been calibrated.

Table 7.9. Calculation of period using developed equations

Equation	**Lamda (λ)**		**Phi (φ_3)**	**Period (sec)**	
	X	**Y**		**X**	**Y**
12c, 13a	0.58	0.26	1.0	0.27	0.24

The comparison between the measured period and periods predicted by different code formulae is also reported by the experimenters [19]. They showed that there is a variation of 100% in the periods predicted by different code formulae, which supports the argument shown in Figure 7.1. Moreover, it is also obvious that all code formulae have a major shortcoming in their inability to recognize the difference in lateral stiffness (and hence the natural period of vibration) in the two directions whereas the equations proposed herein can capture the do.

The second experimental test used for verification of the proposed equation is a three storey RC gravity frame with following cross sectional and dimensional properties [20]; three bays of 6 ft c/c span in one direction and one bay of 6ft c/c span in another direction, inter-storey height of 4 ft, beam cross-section of 3×6 inch, column cross-section of 4×4 inch, modulus of elasticity of 24376 MPa, $\beta_d = 0.12$, $\beta_c = 0.05$, and seismic weight of 360 kN. The three storey frame was tested only in the long (3 bays) direction and the corresponding fundamental period of vibration obtained from white noise test was 0.56 sec [20]. The parameters calculated and used to predict the fundamental period in Equation 12c are $\lambda = 0.79$ and $\varphi = 0.92$. The fundamental period of the frame in the tested direction calculated using Equation 12c and 13a is 0.54 sec. In the other (single bay) direction, the frame should be slightly more flexible, and expectedly the proposed equations predict a longer period (i.e. 0.64 sec) in that direction. Note that some difference between the experimental test and the prediction is inevitable because of the inherent assumptions in the development of the proposed equations, e.g. contribution of slab to the lateral stiffness is not considered, any minor flexibility/slackness in the base connection is not accounted for, the correction factors are developed using data of periods with $1/\lambda$ between 0.25 and 0.75 (i.e. λ between 1.33 and 4), and decoupling of mass in transitional and rotational modes is not completely possible during experimental tests. Despite the above mentioned facts, the predicted periods are close enough to the periods measured in the two series of tests. These verifications prove that the

proposed equations can be relied on to predict the fundamental period provided the building properties are well established.

7.3.5 *Fundamental period: Proposed vs analytical method vs empirical equations*

Since the fundamental periods predicted by the proposed Equation 12c are in good agreement with Eigenvalue analysis results, these results are used to scrutinize the limitations of empirical equations in predicting natural period of frame buildings; mainly their inability to capture the change in natural period due to changes in actual seismic mass, lateral stiffness (i.e. effective section properties) at different limit states, and the geometric configuration of a frame building. Firstly, the effect of seismic mass variation, and then the effect of effective section properties on the fundamental period are studied in this section. The seismic mass of a building during seismic excitation is comprised of the dead weight of a building itself and variable imposed load. The imposed load on a building depends on the occupancy class and varies from 1.5 kN/m^2 to 7.5 kN/m^2. In this comparative parametric study, the imposed load is varied by changing the tributary span width from 5 m to 10 m, and the corresponding seismic weights for a 3 storey and a 10 storey frames are shown in Table 7.10.

Table 7.10. Seismic weights used to study the effect of mass variation on the fundamental period

Storeys	**Tributary span width = 5 m**		**Tributary span width = 10 m**	
	0.1xLL=1.5 kN/m^2	0.6xLL=7.5 kN/m^2	0.1xLL=1.5 kN/m^2	0.6xLL=7.5 kN/m^2
3	1347	1947	2492	3745
10	6866	10624	12251	19768

Building codes prescribe that seismic mass includes only a fraction of live load, generally 30% of characteristic live load. Here, periods are compared for cases including 10% and 60% of the live load to understand its effect on the period. In the legend of Figure 7.14, “S=5” indicates that the tributary span width is 5 m, and “LL=0.1x1.5” corresponds to live load of 0.1 times 1.5 kN/m^2. It is clear from Figure 7.14 that the empirical equations prescribed in different building codes do predict the period with reasonable accuracy for certain range of beam to column stiffness ratios and for low to medium range of imposed loads. For the frames with high imposed loads, the empirical equations under-predict the period. Moreover, it is already discussed and shown in the previous section that for different column size the natural period will be different, but the empirical equations account only for the overall building height.

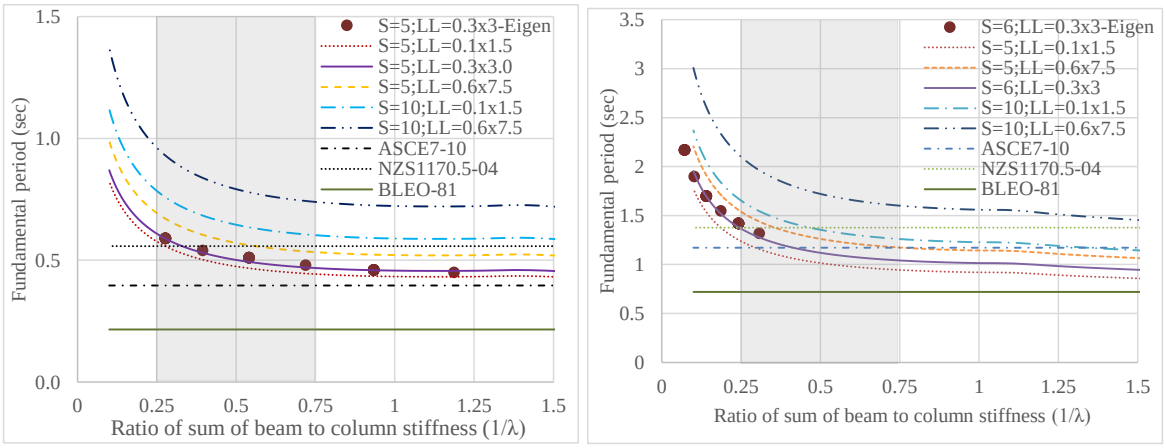

(a) 3 storey–live load variation (b) 10 storey-live load variation

Figure 7.14. Limitations of empirical equations in prediction of period (i.e. with mass variation)

As a case study, a six storey frame building is chosen to investigate the effect of effective section properties on the fundamental period. The periods are calculated using the effective section properties reported in Table 7.3 and using the proposed Equation 12c and compared with the periods calculated using empirical equations from different building codes. It is assumed that at the ultimate limit state (ULS) the effective moment of inertias are 0.5 and 0.32 times gross moment of inertia and at the serviceability limit state (SLS) the effective moment of inertias are 0.8 and 0.7 times gross moment of inertia for columns and beams respectively (i.e. $\alpha_c = 2; \alpha_b = 3.125$ at ULS, $\alpha_c = 1.25; \alpha_b = 1.43$ at SLS). It is observed that in most cases, the fundamental periods obtained using analytical methods (i.e. proposed equation and Eigenvalue analysis) with use of effective section properties (with the assumption that the cross sections chosen here are safe and adequate) are higher than the periods calculated using empirical equations at all limit states, which are shown in Figure 7.15. In legend of Figure 7.15, "I_g" and "I_{eff}" represent that the fundamental periods are calculated using gross and effective section properties respectively. It is clear from the plotted comparison in Figures 7.14 and 7.15 that empirical equations prescribed in the building codes significantly under predict the fundamental period; and cannot be used in assessment of an existing building. Hence, it can be concluded that the empirical equations are unable to capture the effect of lateral stiffness (i.e. wide range of combination of beam and column sizes) and imposed loads on a frame building's fundamental period. Since the proposed equation is simple, reasonably accurate, and considers all parameters known to affect the natural period, it can be reliably used in design or assessment of a building. As mentioned before, design engineers can also use the proposed equation for comparison with computer analysis results.

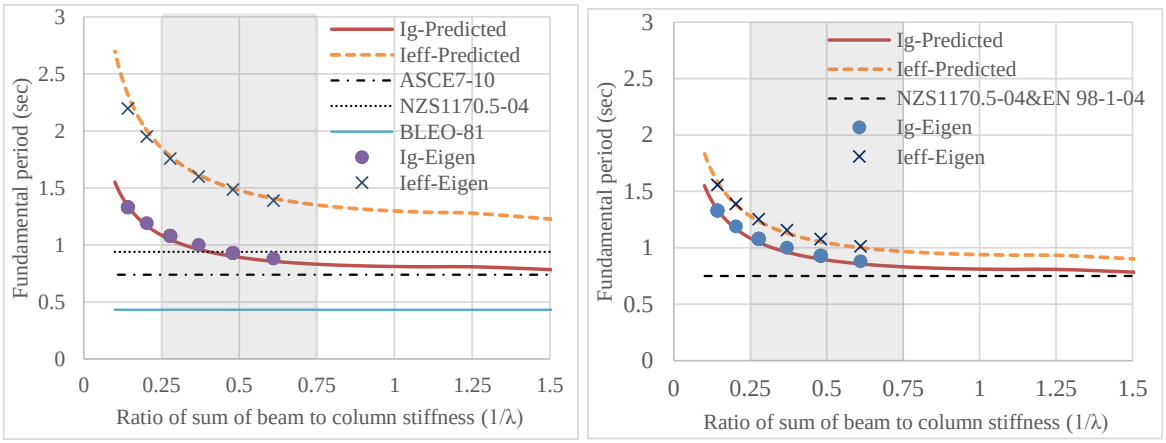

(a) 6 storey–ultimate limit state (ULS) (b) 6 storey–serviceability limit state (SLS)

Figure 7.15. Limitations of empirical equations in prediction of period (i.e. effective properties)

7.3.6 *Application to buildings with minor irregularity*

The applicability of the proposed equation in predicting the fundamental period for slightly irregular frame buildings is scrutinised herein. For this purpose, the bay lengths are assumed to differ through the building width, the bottom storey is assigned a greater height, and the seismic weight is assumed to vary across different storeys; but the variation is restricted to 15% to be within the limits posed by the New Zealand seismic loading standard [13] for buildings which do not need an advanced dynamic analysis to assess the design seismic actions. A six storey four bay frame building is selected with both beam and column cross-sections of 0.4×0.5 m but other properties varying as listed in Table 7.11. It is assumed that the bottom storey height is 1.15 times other storeys height of 3.6 m (i.e. all other storeys are of the same height). The effective height h_{ef} and λ to be used in Equation 12c to predict the period is given by $\frac{1.15h+(n_s-1)h}{n_s}$ and $\frac{\frac{(n_b+1)E_cI_c}{h_{ef}}}{\frac{E_bI_b}{l1}+\frac{E_bI_b}{l2}+\frac{E_bI_b}{l3}+\frac{E_bI_b}{l4}}$ respectively. In Table 7.11, "L1-4=6" represents the length of all four bays is 6 m and "S1-6=w" indicates the seismic weight of storeys 1 to 6 is "w" kN. The fundamental period from Eigenvalue analysis and Equation 12c and the prediction error are reported in Table 7.11. For this case, the error is less than 5%, and it is believed that the error for other low to medium rise irregular frame buildings will be of similar magnitude. Even though the proposed equation is developed based on the assumption of equal storey heights, it can used to estimate period of slightly irregular frame buildings using the effective storey height h_{ef}.

Table 7.11. Variation of bay lengths, seismic weights, and fundamental periods

Case	Bay length (m)	Seismic weight (kN)		Eigen value-period (sec)	Lamda (λ)	Correction factor (φ_3)	Equation 12c- period (sec)	Error (%)
1	L1-4=6	S1-6=w	4756.77	1.248	2.03	0.801	1.24	0.76
2	L1-2=6 L3-4=5	S1=1.15w S2-6=w	4485.31	1.172	1.85	0.811	1.18	0.60
3	L1-2=6 L3-4=7	S1-2=1.15w S3-6=w	5302.63	1.327	2.19	0.795	1.33	0.21
4	L1-2=6 L3-4=7	S1-3=1.15w S4-6=w	5399.03	1.337	2.19	0.795	1.34	0.36
5	L1-2=6 L3-4=7	S1-3=w S4-6=1.15w	5399.03	1.380	2.19	0.795	1.34	2.77
6	L1-2=6 L3-4=7	S1-4=w S5-6=1.15w	5302.63	1.365	2.19	0.795	1.33	2.58
7	L1-2=6 L3-4=7	S1-5=w S6=1.15w	5206.22	1.345	2.19	0.795	1.32	2.04

7.4 Conclusions

The original Macleod's model is modified to more accurately predict the top deflection and the lateral stiffness of regular frame buildings in seismic regions. The error in the predicted lateral stiffness is reduced from ±25% in the original equation to ±10% in the modified equation. A new approach to predict the fundamental period of regular frame buildings with constant storey height and uniform mass along the building height is developed and a versatile generic formula is proposed. According to this formula the fundamental period can be calculated as:

$$T = 0.47\varphi_3\sqrt{\frac{W_s\, h^3 n_s(\,(1-\beta_d)^3+\lambda\,(1-\beta_c)^3)}{(n_b+1)E_c I_{cef}}}$$

where W_s is the total seismic weight of the frame, h is the storey height (measured between top of successive floors), n_s is the number of storeys, n_b is the number of bays, I_{cef} is the average effective moment of inertia of the columns, l is the average bay length (measured between the column centre lines), φ_3 is the correction factor to account for effective mass and effective height (calculated as $\varphi_3 = 0.66 + 0.19/\lambda + 0.008n_s \leq 1.0$), $\lambda = \frac{\sum\frac{E_c I_c}{h\alpha_c}}{\sum\frac{E_b I_b}{l\alpha_b}}$ is the ratio of total effective stiffness of the columns to the total beam stiffness at the first floor level, E_b and E_c are elastic modulus of beam and column, $I_b$and I_c are gross moment of inertia of beam and column, and α_b and α_c are factors to account for effective section properties of beams and columns. The factors $\beta_d = \frac{D}{h}$ and $\beta_c = \frac{c}{l}$ are to account for the finite size of beam-column

joint; *D* and *C* are the beam and column depths, respectively. When clear spans of beam length and column/storey height are used (rather than centre to centre dimensions of the frame), the effect of finite size of beam-column joint on the fundamental period can be neglected (i.e. $\beta_d = \beta_c = 0$), then the fundamental period can be calculated as:

$$T = 0.47\varphi_3\sqrt{\frac{W_s\, h^3 n_s(\,1+\lambda\,)}{(n_b+1)E_c I_{cef}}}$$

The proposed equation captures the effect of all parameters that are known to affect the fundamental period of a frame building. As a distinct advantage over other existing empirical equations used in codes/standards throughout the world, the proposed equation recognises the difference between the periods of vibration in the two orthogonal directions of response of a frame building. It is shown to reliably capture the period of frame buildings with all configurations and characteristics. The fundamental periods predicted using the proposed equation are shown to be in good agreement with periods obtained from Eigenvalue analysis for a large number of frame buildings covering a wide range of building characteristics. Also, the predicted periods are found to be reasonably close to the periods obtained using Rayleigh method and those measured from experimental tests.

Although developed for regular frame buildings, the proposed equation has also been found to be able to predict the fundamental period of frame buildings with minor irregularity without inducing much additional error. It provides a viable tool to investigate the actual variation of the period with change in frame characteristics; e.g. number of bays and storeys, beam and column dimensions, bay length, storey height, seismic mass etc. Moreover, the proposed equation requires input parameters that are not difficult to determine, and is simple enough to be easily implemented into building design codes. Hence, this can be readily used by practicing engineers in designing new buildings as well as in the assessment of existing buildings.

7.5 References

1. Goel, R.K. and A.K. Chopra, *Period formulas for moment-resisting frame buildings.* Journal of Structural Engineering, 1997. **123**(11): p. 1454-1461.
2. Günaydın, E. and C. Topkaya, *Fundamental periods of steel concentrically braced frames designed to Eurocode 8.* Earthquake Engineering & Structural Dynamics, 2013. **42**(10): p. 1415-1433.
3. Crowley, H. and R. Pinho, *Period-height relationship for existing European reinforced concrete buildings.* Journal of Earthquake Engineering, 2004. **8**(spec01): p. 93-119.
4. JapanBLEO, *Part 1, Earthquake Resistant Design of Structures and Part 2, Earthquake Resistant*

Design of Buildings. 1981: Tokyo, Japan.

5. Aoyama, H., *Outline of earthquake provisions in the recently revised Japanese building code.* Tokyo University, Japan, 1981.
6. Bangash, M., *Earthquake resistant buildings: dynamic analyses, numerical computations, codified methods, case studies and examples*. 2011: Springer Science & Business Media.
7. Kelly, C.Y., *An Investigation of the Fundamental Period of Vibration of Irregular Steel Structures*. 2011, Master's Thesis, The Ohio State University.
8. Günaydn, E., *Natural periods of braced steel frames designed to EC8*. 2012, Master's Thesis, Middle East Technical University.
9. Shon, B.A., *Study on the fundamental period of vibration for buildings with different configurations*. 2015, Atilim University.
10. Chopra, A.K. and R.K. Goel, *Building period formulas for estimating seismic displacements.* Earthquake Spectra, 2000. **16**(2): p. 533-536.
11. EN1998, *Eurocode 8: Design of structures for earthquake resistance-Part 1: General rules, seismic actions and rules for buildings*, in *London: BSi*. 2004. p. 10-12.
12. ASCE, *Minimum Design Loads for Buildings and Other Structures*. Standards. 2013: American Society of Civil Engineers. -1.
13. NZS1170, *NZS1170: Structural design actions. Part 5: Earthquake actions - New Zealand*. 2004: Wellington, NZ.
14. ACI, *Building code requirements for structural concrete (ACI 318-08) and commentary*. 2008, American Concrete Institute.
15. NZS3101, *NZS3101: The Design of Concrete Structures*. 2006, Standards New Zealand Wellington.
16. Adeli, H., *Approximate formulae for period of vibrations of building systems.* Civil Engineering for practicing and design engineers, 1985. **4**(1): p. 93-128.
17. Chrysanthakopoulos, C., N. Bazeos, and D. Beskos, *Approximate formulae for natural periods of plane steel frames.* Journal of Constructional Steel Research, 2006. **62**(6): p. 592-604.
18. SAP, *Computers and Structures Inc*. 2013: Berkeley, CA, USA.
19. Di Sarno, L. and G. Manfredi, *Experimental tests on full-scale RC unretrofitted frame and retrofitted with buckling-restrained braces.* Earthquake Engineering & Structural Dynamics, 2012. **41**(2): p. 315-333.
20. Bracci, J.M., A.M. Reinhorn, and J.B. Mander, *Seismic resistance of reinforced concrete frame structures designed for gravity loads: performance of structural system.* ACI Structural Journal, 1995. **92**(5): p. 597-610.
21. Iain, A., *Simplified equations for deflection of multistory frames.* Building Science, 1971. **6**(1): p. 25-31.
22. Miranda, E., *Approximate seismic lateral deformation demands in multistory buildings.* Journal of Structural Engineering, 1999. **125**(4): p. 417-425.

Chapter 8: Prediction of lateral stiffness and fundamental period of concentrically braced frame buildings with either fixed or pin bases

Aninthaneni, P. K., and Dhakal, R. P. (2017). "Prediction of lateral stiffness and fundamental period of concentrically braced frame buildings." Bulletin of Earthquake Engineering, pp 1-30.

8.1 Introduction

8.1.1 *Overview*

In this chapter, a simple hand calculation method to predict lateral stiffness and fundamental period of concentrically braced frame buildings with either fixed or pin bases, which can also be used for unbraced frame buildings, is theoretically derived. To verify the reliability of the developed equations, the estimated lateral stiffness and fundamental periods are compared with the corresponding values obtained from pushover and Eigenvalue analyses for a wide range of low to medium rise buildings (i.e. up to 10 storeys) with varying geometrical configurations. Systematic investigation of parameters affecting the fundamental period of frame buildings is also carried out. The basic analytical formulation considers X and chevron brace configurations explicitly, but its applicability to other types of brace configurations is also investigated. The suitability of the proposed equation for the braced frames with linear variation of section properties along the building height and pin beam-column connections is also scrutinized. Reliability of the developed method is verified using the experimental test and numerical analysis results available in the literature. Finally, a flowchart and two worked examples are provided to explain the sequence of steps to calculate the fundamental period of concentrically braced frame buildings.

8.1.2 *Background*

Braces are quite common in frame buildings designed to resist earthquake induced lateral forces. With advent of buckling restraint braces (BRB), seismic performance of braced frame buildings has considerably improved compared to conventional braced frame buildings [1]. The addition of steel braces to an existing frame building (steel or concrete) is also considered as one of the primary retrofit/strengthening option [2]. The common types of brace configurations that are being used in frame building construction are shown in Figure 8.1. Generally, the type of brace configuration is selected for a particular building based on

the magnitude of lateral load, desired structural ductility, and architectural/aesthetic requirements [3]. The column to foundation connections of a braced frame building are classified as either fixed/rigid or semi-rigid or pin/simple depending on the rotational stiffness and moment carrying capacity [4]. In the analysis and design, pin base connections with low rotational stiffness are also considered as pin connections as long as they are able to transfer the internal forces to the base and the distribution of internal forces in the frame are not significantly altered because of the partial fixity at the base. With the use of pin base connections, the cost of the connections and the size of the foundations are substantially reduced. Building codes allow pin base connections as long as the overall structural system satisfies the strength and stability requirements at ultimate and serviceability limit states. Moreover, the authors are also working towards development of a demountable frame building system made of precast concrete elements and steel connections which can have either fixed or pin base connections [5]. Generally, the beam to column connections of a braced frame are simple connections, but in seismic regions braced frame buildings with rigid beam column connections are also being constructed in order to improve reserve strength and to reduce maximum and residual drift demands after an earthquake [6].

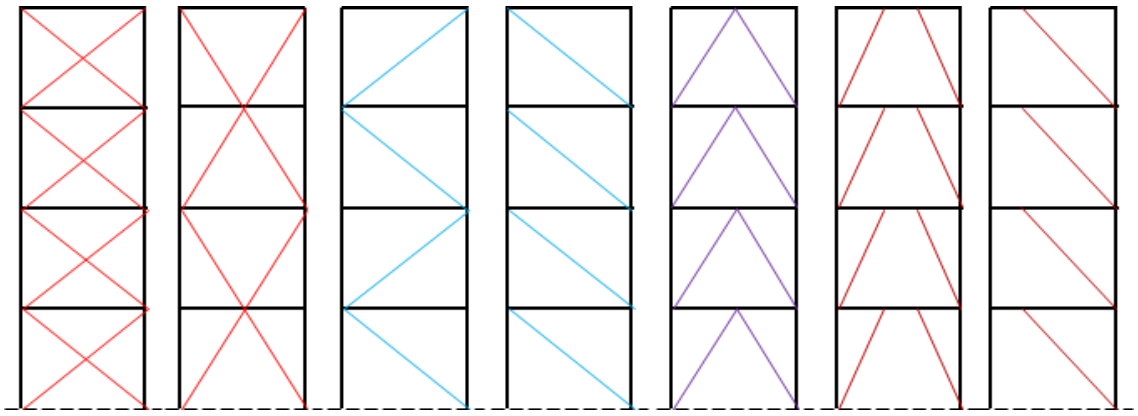

(a) X and split X (b) K and diagonal (c) Chevron (d) Eccentric chevron and diagonal

Figure 8.1.Typical layouts of concentric and eccentric brace configurations for a frame building

The most vital structural parameter required in seismic design of a frame building (braced or unbraced) is its period of fundamental mode of vibration, which controls the seismic demand and subsequently its structural member dimensions. The fundamental period of a frame building depends on the lateral stiffness and seismic mass and it cannot be precisely calculated for a building yet to be designed. A frame building lateral stiffness is a function of material properties, sectional properties, geometric configuration of its frames, and also the base boundary conditions. In reality, it is very difficult to predict the actual period of vibration of a building under real earthquake shaking because of many uncertain parameters

(i.e. actual material properties, seismic mass of a building during an earthquake shaking, soil condition, contribution of secondary elements such as infill walls to the lateral stiffness of a building, actual base fixity condition etc.). Therefore, it is a common practice to use approximate empirical and analytical methods to estimate the fundamental period for design of a new building as well in assessment of an existing building.

The empirical equations prescribed in most of the building codes to predict the fundamental period are developed by carrying out regression analysis using an actual database of recorded periods of a real building in earthquakes [7, 8]. Most of the empirical equations relate the fundamental period of a building to the height of the building *H*; usually in the form $T_a = C_t H^x$ [9-11]. In some building codes; e.g. the Japanese and Canadian building codes, the fundamental period of a building is a linear function of the building height which is given as $T_a = C_t H$ [12-14]. The fundamental period of braced frame buildings is also calculated by $T_a = C_t H/\sqrt{D}$, where D is the length of the braced bay [15]. The values of C_t and x differ from one building code to another, thereby resulting in different periods for the same building. The full compilation of existing empirical equations to predict fundamental periods and seismic demand prediction using an equivalent static procedure in different building codes can be found in the literature [15-18]. The empirical equations prescribed in the building codes are simple, but they are very approximate. In most cases, they underestimate the fundamental period, which is conservative (hence acceptable) in design of a new building, but are unsuitable for assessment of an existing building as they under estimate lateral displacement [19]. The empirical equations to predict the fundamental period developed using database from high seismic regions results in overly conservative seismic demand for the buildings in low to moderate seismic regions [20]. Also, the empirical equations prescribed in the building codes do not recognize the effect of base fixity (i.e. fixed or pin base) on the fundamental period [9, 10, 14].

The building codes allow to use analytical methods (Eigenvalue analysis, and Rayleigh method, etc.) to predict the fundamental period, but limits by a value more than the fundamental period calculated using empirical equations prescribed in the building code. This upper bound limit is to protect the buildings against un-conservative estimate of seismic demand because of unreasonable assumptions in finite element modelling. It is important to note that some building codes specify an upper bound limit on the predicted period obtained from analytical methods only for capacity design (i.e. sizing the structural members), but not for calculating lateral displacement at serviceability limit state [9]. On the other hand, some

building codes do not impose any upper limit on the period calculated from analytical methods in strength and displacement checks [11]. Building codes also differ from each other in the calculation/use of the gross or effective section properties (i.e. moment of inertia) in the estimation of the fundamental period by using analytical methods [21, 22]. Existing analytical methods take into account most of the parameters that affect the period of a building. Also, these methods are able to predict the fundamental period with reasonable accuracy, but require considerable effort in computer modelling of a building and expertise in using a structural analysis software. In most cases, the fundamental periods predicted using analytical methods will be higher than those predicted using empirical equations [23].

There has been little effort towards the development of hand calculation methods/simple theoretical equations to predict the fundamental period of a braced frame building which accounts for all structural parameters that are likely to affect and can be used both in design of new buildings as well as in the assessment of existing buildings. Approximate hand calculation methods for estimation of fundamental period of frame buildings reported so far in literature are derived by solving the fourth order differential equation of cantilever column under free vibration [24, 25]. In these methods, a frame building is idealized as an equivalent cantilever column with separate flexural and shear mode of deformation. The periods of shear and flexural mode of vibration are combined using Dunkerley's combination rule to obtain the period of a building [25].

8.1.3 *Objectives and scope*

The primary objective of the research work is to develop a simple yet versatile theoretical model and derive a generic equation to predict the lateral stiffness and the fundamental period of concentrically braced frame buildings with either fixed or pin bases. Applicability of the developed equation to unbraced frame buildings is also verified. In the basic formulation of the theoretical model, X and chevron brace configurations are explicitly considered, and its applicability to other types of brace configurations is also investigated. Firstly, the basis for the idealization of a multi bay braced frame into an equivalent single bay moment and braced frames and representation of a braced frame building as a parallel spring system is discussed. Also, the assumptions made in the derivation of theoretical model to estimate the lateral stiffness of braced frames are reported. Simple equations are derived to estimate the lateral stiffness and fundamental period. The predicted lateral stiffness and fundamental period values using developed equations are compared with actual lateral stiffness and fundamental periods obtained from pushover analyses and Eigenvalue analyses respectively for a wide

range of low to medium rise frame buildings. The range of errors with original equation is reported, reasons for the error are identified and a correction factor as a function of key structural parameters is introduced to neutralize the error. Thereafter, the predicted lateral stiffness and fundamental period in conjunction with the correction factor are again compared with the actual values, and the amount of reduction in error is reported. By utilizing the results obtained from the developed equation, systematic interpretation of the parameters affecting the fundamental period is carried out. Also, the fundamental periods predicted by the proposed method are compared with the fundamental periods obtained from experimental tests and numerical analysis reported in literature.

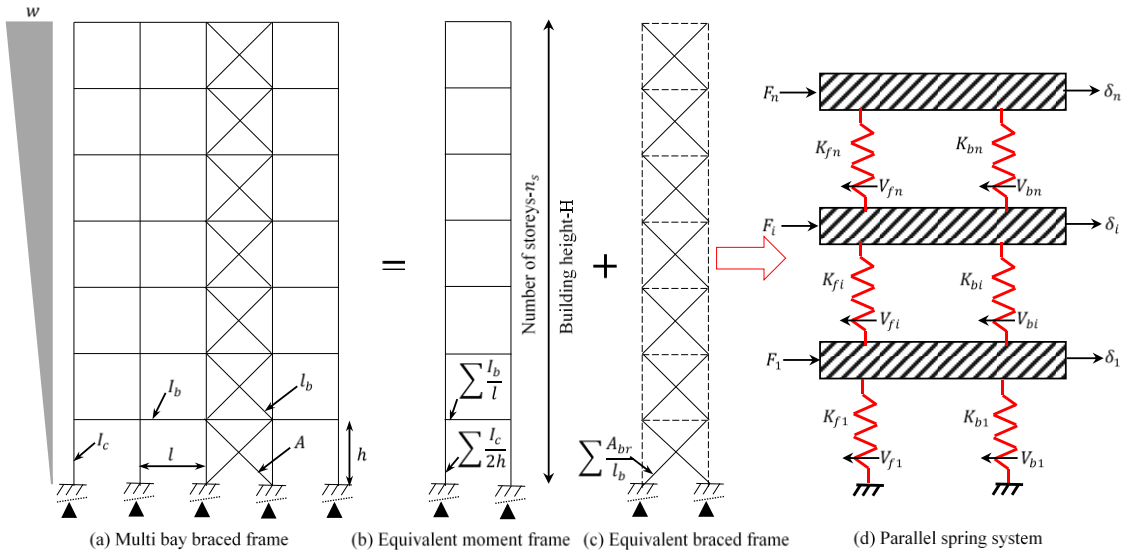

Figure 8.2.Condensation of a multi bay into an equivalent bays and representation as spring system

8.2 Development of the theoretical model

8.2.1 *Idealization of a braced frame*

The theoretical model to predict the lateral stiffness and the fundamental period is developed by condensing and separating a multi bay braced frame into an equivalent single bay moment and braced frames as shown in Figure 8.2. The proposed theoretical model is inspired by and developed based on the lines of Macleod's method [26], which was originally developed to estimate the top/roof lateral displacement of an unbraced frame building with fixed base. It is also important to note that some of the basic equations of original Macleod's method are reproduced and modified for its applicability to braced frame buildings with either fixed or pin base. The lateral load acting on the braced frame is represented as a continuous function in a triangular pattern as depicted in Figure 8.2a. In the Figure, w represents the magnitude of the lateral load at the top of the frame, h is the storey height, H is the building height, l is the

bay length, l_b is the brace length, n_s is the number of storeys, I_c and I_b are respectively the moment of inertia of the columns and beams at the first storey level, and A_{br} is the cross sectional area of the braces at the first storey level.

8.2.2 *Parallel spring system*

To enforce equilibrium and compatibility between the equivalent single bay moment and braced frames shown in Figures 8.2b and 8.2c, a multi bay braced frame shown in Figure 8.2a is represented as a parallel spring system as shown in Figure 8.2d. The total shear force V_i is shared between the equivalent moment and braced frames depending on the relative lateral stiffness. The total shear force V_i at any storey level i is equal to the sum of the shear force in the equivalent moment frame V_{fi} and the braced frame V_{bi} (i.e. equilibrium). Similarly, the lateral displacement at any storey level δ_i is equal to the lateral displacement of the equivalent moment frame δ_{fi} and braced frame δ_{bi} (i.e. compatibility). Mathematically, it can be expressed as shown in Equation 1.

$$V_i = V_{fi} + V_{bi};\ \delta_i = \delta_{fi} = \delta_{bi} \tag{1}$$

By using the force displacement relationship $V_i = K_i\delta_i$ of the equivalent single bay systems and Equation 1, the shear force shared among the equivalent singe bay frames in terms of the total shear force, and the relationship between the total lateral stiffness K_i and the lateral stiffness of the equivalent moment frame K_{fi} and the braced frame K_{bi} can be obtained, which is given in Equation 2.

$$\frac{V_i}{K_i} = \frac{V_{fi}}{K_{fi}} = \frac{V_{bi}}{K_{bi}};\ K_i = K_{fi} + K_{bi} \tag{2}$$

8.2.3 *Assumptions*

In the process of derivation of the lateral displacement and the lateral stiffness of a multi bay braced frame, the following assumptions are made to arrive at a simple closed form equation:

1. The point of contra-flexure (POC) is at the mid-height of the columns and at the same location in all storeys. Also, it is assumed that the POC is at mid-length in the beams and the effect of gravity loads in shifting the location of POC is neglected.
2. It is assumed that the lateral displacement due to axial shortening of columns comes only from the equivalent braced frame (i.e. columns of braced bays) whereas any minor contribution from the equivalent moment frame (i.e. columns of unbraced bays) is neglected.

3. The lateral displacement varies linearly within the storey height of the equivalent moment and braced frames. This assumption enables the use of principle of superposition.
4. All beam-column connections are rigid, and joint equilibrium of the equivalent moment frame is achieved by equating the sum of the bending moment in the beams at either side of the joint with the sum of column moments at the top and bottom of the joint.

8.2.4 *Lateral stiffness*

As mentioned before, the lateral load acting on the equivalent moment and braced frames is distributed as a continuous function as shown in Figure 8.3a and the magnitude of the lateral force at distance x from the top of the frame is given in Equation 3. Also, this method allows a linear variation of the section properties within the building height (also represented as a continuous function of height) to be incorporated in the derivation process. The values of section properties of columns, beams and braces at distance x from the top of the frame are given in Equation 4. Another method/approach to arrive at equations to estimate the lateral stiffness with lateral load represented as discrete point loads in a triangular pattern is reported in Appendix L.

$$w(x) = w\left[1 - \frac{x}{H}\right]; w_f(x) = w_f\left[1 - \frac{x}{H}\right]; w_b(x) = w_b\left[1 - \frac{x}{H}\right] \quad (3)$$

$$I_{cx} = I_c\left[s + (1-s)\frac{x}{H}\right]; I_{bx} = I_b\left[g + (1-g)\frac{x}{H}\right]; A_{brx} = A_{br}\left[r + (1-r)\frac{x}{H}\right] \quad (4)$$

where $w = w_f + w_b$, w_f and w_b represents the intensity of the load at the top of the equivalent moment and braced frames, respectively. The shear force acting on the equivalent moment frame V_{fx} and the braced frame V_{bx} at distance x from the top of the frame is obtained by integrating the lateral force intensity given in Equation 3 over distance x, which is given as:

$$V_{fx} = w_f\left[x - \frac{x^2}{2H}\right];\ V_{bx} = w_b\left[x - \frac{x^2}{2H}\right] \quad (5)$$

Because of symmetry of the equivalent moment frame, only a half of the frame is considered for the lateral displacement calculation, which is shown Figure 8.3a. Accordingly, the intensity of the lateral load, sectional properties and bay lengths are halved as shown in Figures 8.2b, 8.3b and 8.3c. Subassembly Models-A and B shown in Figures 8.3b and 8.3c are used for the lateral displacement estimation of the equivalent moment frame. The

procedure to predict the top/roof lateral displacement of the equivalent moment frame is as follows; first, the lateral displacement of the beam column subassembly in a single storey of the half bay frame is calculated and integrated over the building height assuming linear variation of displacement over the storey height. For the equivalent braced frame shown in Figure 8.3d, the lateral displacement is contributed by the axial deformation of braces δ_{bx1} and axial deformation of columns in the braced bay δ_{bx2}, and the total lateral displacement is the sum of these two contributions (i.e. $\delta_{bx} = \delta_{bx1} + \delta_{bx2}$). Sub-assembly Model-C (X and chevron braces shown in Figures 8.3e and 8.3f, respectively) and Model-D (braced bay columns shown in Figure 8.3g) are used in the lateral displacement calculation. For the estimation of the top lateral displacement of the equivalent braced frame contributed by braces, the axial deformation of the brace elements in local coordinates is converted into the global lateral displacement and then integrated over the building height. Top lateral displacement of the equivalent braced frame due to axial shortening of the columns of the braced bays is computed by equating the external work done by the lateral load and the internal axial strain energy of the columns.

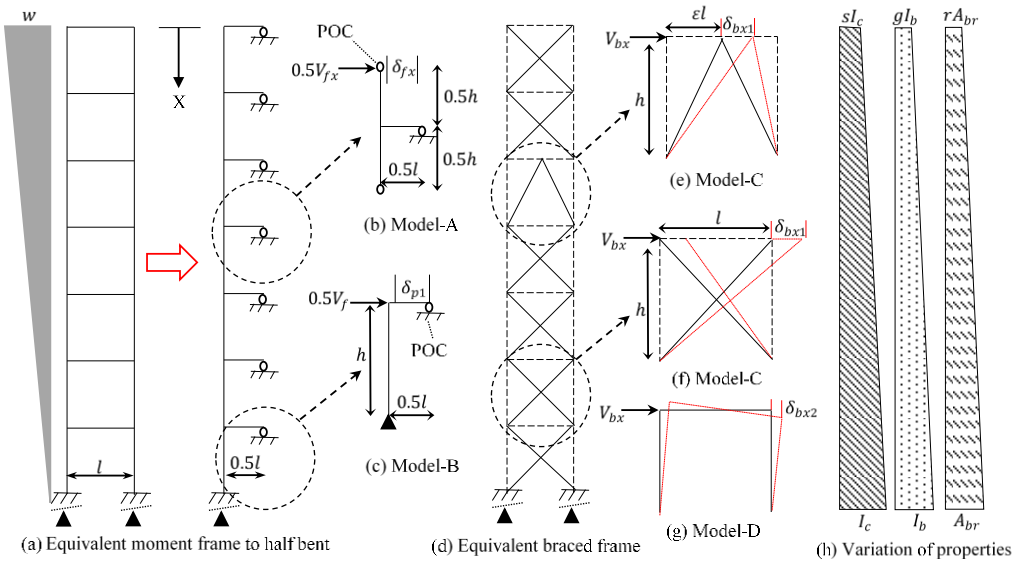

Figure 8.3. Analytical model with lateral load and section properties represented as continuous functions

The lateral displacement δ_{fx} of the subassembly Model-A shown in Figure 8.3b can be calculated using any standard analysis methods, which is given as:

$$\delta_{fx} = \frac{V_{fx}h^3}{12\sum E_c I_{cx}} + \frac{V_{fx}h^2 l}{12\sum E_b I_{bx}} \tag{6}$$

where E_c and E_b are modulus of elasticity of the columns and beams, respectively. By substituting for the storey shear V_{fx} acting on the equivalent moment frame from Equation 5

in Equation 6, the lateral displacement equation turns into:

$$\delta_{fx} = \frac{w_f\left[x-\frac{x^2}{2H}\right]h^3}{12\sum E_c I_c\left[s+(1-s)\frac{x}{H}\right]} + \frac{w_f\left[x-\frac{x^2}{2H}\right]h^2 l}{12\sum E_b I_b\left[g+(1-g)\frac{x}{H}\right]} \tag{7}$$

By utilizing the assumption of linear variation of lateral displacement within the storey height, Equation 7 can be converted into a differential form as given by:

$$d\delta_{fx} = \frac{w_f h^2}{12\sum E_c I_c}\left(\frac{\left[x-\frac{x^2}{2H}\right]}{\left[s+(1-s)\frac{x}{H}\right]} + \lambda\frac{\left[x-\frac{x^2}{2H}\right]}{\left[g+(1-g)\frac{x}{H}\right]}\right)dx \tag{8}$$

where $\lambda=\frac{\sum\frac{E_c I_c}{h}}{\sum\frac{E_b I_b}{l}}$ is calculated as a ratio of the sum of column stiffness to the sum of beam stiffness at the first storey level. Accounting for the finite size of the beam column joint, Equation 8 turns into:

$$d\delta_{fx} = \frac{w_f h^2}{12\sum E_c I_c}\left(\frac{\left[x-\frac{x^2}{2H}\right](1-\beta_d)^3}{\left[s+(1-s)\frac{x}{H}\right]} + \lambda\frac{\left[x-\frac{x^2}{2H}\right](1-\beta_c)^3}{\left[g+(1-g)\frac{x}{H}\right]}\right)dx \tag{9}$$

where $\beta_d = \frac{D}{h}$ and $\beta_c = \frac{C}{l}$; D is the beam depth and C is the column depth. It is important to note that h and l are center to center dimensions. The top storey lateral displacement of the equivalent moment frame with fixed base is calculated by integrating Equation 9 over the building height, which results in Equation 10.

$$\Delta_{ff} = \frac{V_f h^3 n_s}{12\sum E_c I_c}\left(F_s(1-\beta_d)^3 + \lambda F_g(1-\beta_c)^3\right) \tag{10}$$

In case of the equivalent moment frame with pin base, Equation 9 is integrated from the top of the frame to the top of the first storey to obtain cumulative lateral displacement over the $(n_s - 1)$ storeys, which gives Equation 11.

$$\Delta_{fp(n_s-1)} = \frac{V_f h^3\left(n_s{}^2-1\right)(n_s-1)}{12 n_s{}^2\sum E_c I_c}\left(F_s(1-\beta_d)^3 + \lambda F_g(1-\beta_c)^3\right) \tag{11}$$

The values of factors F_s and F_g in Equations 10 and 11 depend on the type of base fixity and variation of section properties with the height of the building, these factors can be calculated by using the equations given in Table 8.1 or from Figure 8.4. If the clear spans of bay length and storey height are used instead of the center to center dimensions, Equations 10 and 11 can be written as:

$$\Delta_{ff} = \frac{V_f h^3 n_s}{12 \sum E_c I_c} \left(F_s + \lambda F_g\right) \tag{12}$$

$$\Delta_{(fp)(n_s-1)} = \frac{V_f h^3 \left({n_s}^2 - 1\right)(n_s - 1)}{12 {n_s}^2 \sum E_c I_c} \left(F_s + \lambda F_g\right) \tag{13}$$

The lateral displacement δ_{f1} of Model-B representing the subassembly at the first storey level of the equivalent moment frame with pin base shown in Figure 8.3c is given by Equation 14. Note that in the calculation of λ, clear span lengths of the bay and storey height need to be used rather than the center to center dimensions.

$$\delta_{p1} = \frac{V_f h^3}{12 \sum E_c I_c} (4 + \lambda) \tag{14}$$

The top storey lateral displacement of the equivalent moment frame with pin base is obtained by adding Equation 13 and 14, which results in Equation 15.

$$\Delta_{fp} = \frac{V_f h^3}{12 {n_s}^2 \sum E_c I_c} \left(({n_s}^2 - 1)(n_s - 1)\left(F_s + \lambda F_g\right) + {n_s}^2 (4 + \lambda)\right) \tag{15}$$

The lateral displacement δ_{bx1} of the subassembly Model-C of the equivalent braced frame is calculated by converting the axial deformation along the brace length into global lateral direction, which is given as:

$$\delta_{bx1} = \frac{V_{bx} l_b^3}{2(\varepsilon l)^2 \sum A_{brx} E_{br}} \tag{16}$$

where the value of ε depends on the type of brace and is defined as the ratio of the horizontal projected length of brace to the span length of the braced bay (for example, $\varepsilon = 1$ for X brace, and $\varepsilon = 0.5$ for chevron brace), and E_{br} is the modulus of elasticity of the brace. Depending on the type of the brace configuration, the length of the brace is given as $l_b = \sqrt{h^2 + (\varepsilon l)^2}$. By substituting for the storey shear V_{bx} acting on the equivalent braced frame from Equation 5 and the cross sectional area of the brace A_{brx} from Equation 4 in Equation 16, and by assuming linear variation of the lateral displacement within the storey height, Equation 16 can be converted into a differential form as:

$$d\delta_{bx1} = \frac{w_b \left[x - \frac{x^2}{2H}\right] l_b^3}{2h(\varepsilon l)^2 \sum E_{br} A_{br} \left[r + (1-r)\frac{x}{H}\right]} dx \tag{17}$$

By integrating Equation 17 over the building height H, the top lateral displacement Δ_{b1} of the equivalent braced frame contributed by braces is given by Equation 18. The value of factor F_r in Equation 18 depends on the variation of the cross section area of brace with the height

of the building, and can be calculated by using the equation given in Table 8.1 or from Figure 8.4a.

$$\Delta_{b1}=\frac{V_b l_b^3 n_s F_r}{2(\varepsilon l)^2 \sum A_{br}E_{br}} \tag{18}$$

The lateral displacement δ_{bx2} of the subassembly Model-D of the equivalent braced frame due to axial shortening of columns of the braced bays is converted into differential form and then integrated over the whole building height to arrive at the top lateral displacement Δ_{b2}, which is given in Equation 19, where A_c is the cross sectional area of the braced bay columns.

$$\Delta_{b2}=\frac{0.31V_b h^3 n_s^3}{l^2 \sum A_c E_c} \tag{19}$$

The total top lateral displacement of the equivalent braced frame due to axial deformation of the braces and columns of the braced bays is given by Equation 20, where $\tau = 0.92(\varepsilon n_s)^2 \frac{\frac{E_{br}A_{br}}{l_b^3}}{\frac{E_c A_c}{h^3}}$ is a factor which accounts for the additional lateral displacement due to axial shortening of the columns.

$$\Delta_b=\frac{V_b l_b^3 F_r}{2(\varepsilon l)^2 A_{br}E_{br}}\frac{n_s}{n_r}(1+\tau) \tag{20}$$

The lateral stiffness of a multi bay braced frame is computed as the ratio of the total shear force V to the top storey lateral displacement Δ. It is already shown in Equation 3 that the total lateral stiffness is equal to the sum of the lateral stiffness of the equivalent moment and braced frames. By using the top storey lateral displacement from Equations 10 and 20 and the lateral stiffness relationship given in Equation 2, the lateral stiffness of a multi bay braced frame with fixed base is given as:

$$K_f = \frac{12E_c I_c \chi_f}{h^3} \tag{21}$$

where $\chi_f = \left[\frac{(n_b+1)}{n_s(F_s+\lambda F_g)} + \frac{(\varepsilon l)^2 \vartheta}{6F_r(1+\tau)}\frac{n_r}{n_s}\right]$ is a factor and depends on the geometric configuration of the braced frame with fixed base, $\vartheta = \frac{\frac{E_{br}A}{l_b^3}}{\frac{E_c I_c}{h^3}}$ is the pseudo relative stiffness of the brace to the column, n_b is the total number of bays, and n_r is the total number of braced bays. The factor χ_f can be further simplified for the case with uniform sectional properties along the building height by using $F_s = F_g = F_r = 0.67$. In the equations used to compute the lateral stiffness

and fundamental period, subscripts with f and p represent the corresponding values for fixed and pin base frames respectively. By adopting a similar approach, the lateral stiffness of a multi bay braced frame with a pin base can be derived as given in Equation 22.

$$K_p = \frac{12E_cI_c\chi_p}{h^3} \tag{22}$$

where $\chi_p = \left[\frac{{n_s}^2(n_b+1)}{({n_s}^2-1)(n_s-1)(F_s+\lambda F_g)+{n_s}^2(4+\lambda)} + \frac{(\varepsilon l)^2\vartheta}{6F_r(1+\tau)}\frac{n_r}{n_s}\right]$ is a factor and depends on the geometric configuration of the braced frame with pin base, and the factor χ_p can be further simplified for uniform sectional properties by substituting $F_s = F_g = \frac{0.67n_s+0.33}{(n_s+1)}; F_r = 0.67$. While using Equation 21 or 22 to predict the lateral stiffness, the first part of χ_f or χ_p has to be eliminated for braced frames with pin beam-column connections and the second part of χ_f or χ_p has to be eliminated for unbraced frames. It is important to note that the lateral stiffness of a braced frame building in the direction of interest is the summation of all individual frames' lateral stiffness.

Table 8.1. $F_s,\ F_g, and\ F_r$ factor values with variation of sectional properties

Element	**Fixity**	**General cases : $F_s; F_g; F_r (m = s = g = r)$**	**$(s = g = r = 1)$**
Frame	Fixed	$\frac{1.5(1-m)^2+(1-m)m(2\,log_e\,m+1)+m^2\,log_e\,m}{(1-m)^3}$	0.67
	Pin	$\frac{2((1-m)^2+(1-m)\,mlog_e\,m)+(n_s-1)(1.5(1-m)^2+(1-m)m(2\,log_e\,m+1)+m^2\,log_e\,m)}{(1-m)^3(n_s+1)}$	$\frac{0.67n_s+0.33}{(n_s+1)}$
Brace	Both	$\frac{1.5(1-m)^2+(1-m)m(2\,log_e\,m+1)+m^2\,log_e\,m}{(1-m)^3}$	0.67

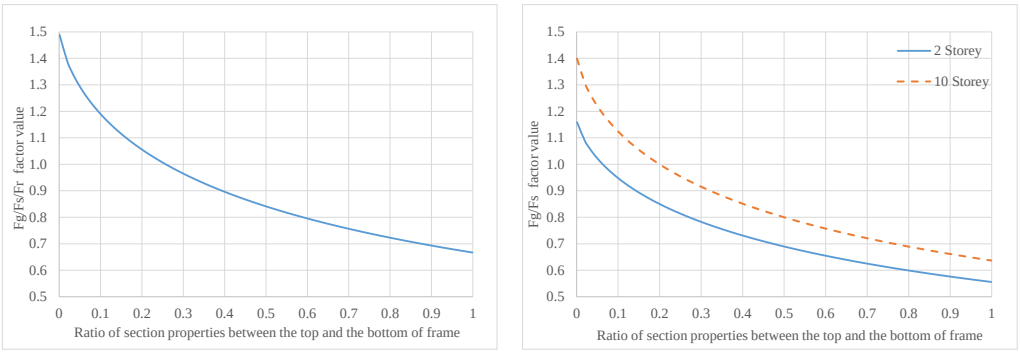

(a) For a fixed base frame and brace element (b) For a pin base frame

Figure 8.4. Variation of $F_s,\ F_g, and\ F_r$ factors with variation of sectional properties

8.2.5 *Fundamental period*

A multi degree of freedom (MDOF) frame building has many possible modes of vibration, out of which the period of the fundamental/first mode of vibration in orthogonal directions are used in the estimation of seismic demand. As mentioned before, the period of the first

mode of vibration is generally calculated using Eigenvalue analysis by condensing the MDOF system into an equivalent single degree of freedom (SDOF) system. The fundamental period of the equivalent SDOF system is given as:

$$T = 2\pi\sqrt{\frac{M_{eff}}{K_{eff}}} \tag{23}$$

The modal mass M_{eff} in the first mode of vibration depends on the mass participation factor, which in turn depends on the mode shape and mass distribution along the building height. The lateral stiffness K_{eff} of the equivalent SDOF system depends on the mode shape, stiffness distribution along the building height, and the effective height of the SDOF system. By substituting lateral stiffness K_f or K_p values and replacing M with $\frac{W_s}{g}$ in Equation 23, then it turns into Equation 24, where W_s is the seismic weight, and g is the acceleration due to gravity.

$$T_f = 2\pi\sqrt{\frac{W_s h^3}{12g\sum E_c I_c \chi_f}};\ T_p = 2\pi\sqrt{\frac{W_s h^3}{12g\sum E_c I_c \chi_p}} \tag{24}$$

8.3 Results and discussion

To verify and validate the developed equation to estimate the lateral stiffness and fundamental period, pushover analysis and Eigenvalue analysis are performed on a wide range of low to medium rise frames (i.e. up to 10 storeys) by using SAP2000 [27]. The varied parameters and their ranges of values used can be identified in Table 8.2. For calculation of the seismic weight, it is assumed that the building considered for the parametric analysis has 4 bays of 6 m width in the perpendicular direction and floor is rigid in plane. The seismic weight of the floor is distributed to the lateral load resisting frames depending on their relative stiffness (here all frames are assumed to have equal stiffness). The seismic weights of the chosen frames with varying geometric configurations used in the developed equation to predict the fundamental period are reported in Table 8.3. Typical layout of the braced frame is provided in Appendix N. It is important to note that the fundamental periods calculated are based on gross section properties and the effect of axial shortening of the braced bay columns on the fundamental period is ignored in the verification process (i.e. $\tau = 0$), unless otherwise explicitly mentioned.

Table 8.2. Variables and their values used in the parametric verification study (refer Figure N.1 for layout)

Frame building characteristics			**Material properties**	
	Braced	**Unbraced**	Grade of concrete	35 N/mm^2
No of storeys	3, 6 and 10	3-6,8 and 10	Grade of reinforcement	500 N/mm^2
Storey height	3.6 m	3.6 m	Grade of steel brace	345 N/mm^2
Span length	6 m	5-7 m	Grade of structural steel	345 N/mm^2
Total bays	3 - 5	3- 4	Young's modulus of concrete	19641 N/mm^2
Braced bays	1 - 2	N/A	Young's modulus of steel	200000 N/mm^2
Type of brace	X and Chevron	N/A	**Cross sectional dimensions**	
Loading details			Concrete columns	0.4-0.5×0.5-0.7 m
Dead load	4.25 kN/m^2	Roof: 4.75 kN/m^2 Other: 4.25 kN/m^2	Concrete beams	0.4×0.4-0.65 m
Live load	3.0 kN/m^2	Roof: 2.5 kN/m^2 Other: 3.0 kN/m^2	Steel tube braces	100×100×3-9 mm

8.3.1 *Comparison between the calculated lateral stiffness and the lateral stiffness predicted by pushover analysis*

Comparison between the calculated lateral stiffness and the lateral stiffness obtained from pushover analysis for braced frames with fixed and pin base is shown in Figure 8.5. Although the main objective of the chapter is to develop a simple method for braced frames, its applicability to unbraced frames is also investigated. Hence, comparison of the predicted lateral stiffness with actual values for unbraced frames with pin base is shown in Figure 8.6a, whereas for unbraced frames with fixed base, the results are available in Chapter 7 [28]. The range of error in predicting lateral stiffness for braced frames with fixed and pin base is between 10% and 20% depending on the relative stiffness of the column to the beam λ and pseudo relative stiffness of the brace to the column ϑ. Similarly, for unbraced frames with pin base the error ranges from 15% to 25% depending on the column to beam relative stiffness λ. The reason for the deviation of predicted lateral stiffness from the pushover analysis based lateral stiffness is because of the assumptions made in the theoretical formulation (as listed in the previous section). It is not possible to address the assumptions explicitly as it will not lead to a simple closed form solution. Therefore, a correction factor is sought to neutralize the error in the predicted lateral stiffness. A correction factor Ω is introduced into Equations 21 and 22, which results in the following equation for predicting lateral stiffness of the frames with fixed or pin base.

$$K_f = \Omega_f \frac{12E_c I_c \chi_f}{h^3}; K_p = \Omega_p \frac{12E_c I_c \chi_p}{h^3} \quad (25)$$

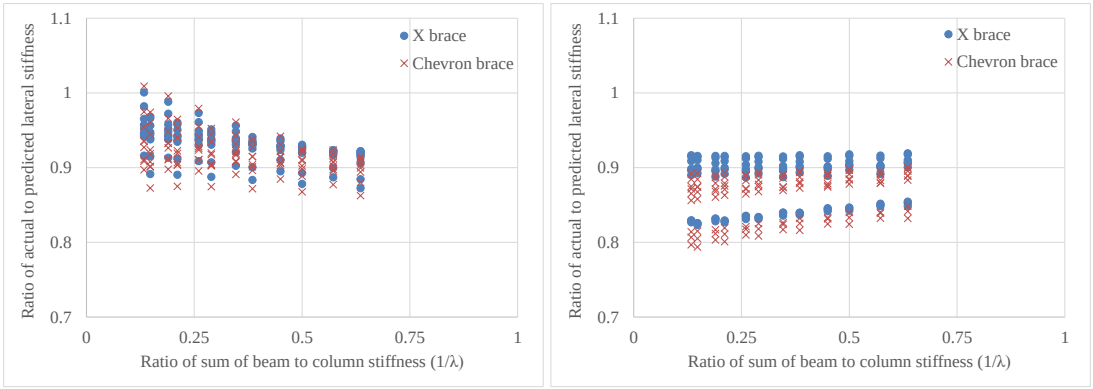

(a) Braced frames with fixed base (b) Braced frames with pin base

Figure 8.5. Comparison of predicted and actual stiffness for braced frames without correction factor

Table 8.3. Seismic weights used in the parametric study

Storeys	Bays	Bay length (m)	Column size (m×m)	Seismic weight (kN)
Braced frames				
3	3	6	0.4×0.6	1851
3	5	6	0.4×0.6	3048
6	3	6	0.4×0.6	3703
6	5	6	0.4×0.6	6095
10	3	6	0.4×0.6	6172
10	5	6	0.4×0.6	10159
Unbraced frames				
3	3	5	0.4×0.5/0.6	1501/1539
3	3	7	0.4×0.5/0.6	2020/2057
3	4	5/7	0.4×0.5	1981/2672
4	3	6	0.4×0.5/0.6	2358/2409
4	4	6	0.4×0.5/0.6	3122/3185
5	4	6	0.4×0.5/0.6	3908/4010
6	4	6	0.4×0.5/0.6	4698/4821
8	4	6	0.4×0.5/0.5×0.7	6188/6484
10	4	6	0.4×0.5/0.5×0.7	7677/8359

A multiple variable regression analysis is carried out to relate the correction factor Ω with the relative stiffness of the column to the beam λ, pseudo relative stiffness of the brace to the column ϑ, and the number of storeys n_s, which is given by Equation 26 for both fixed and pinned bases. The correction factor Ω is obtained by relating the predicted lateral stiffness with the target lateral stiffness obtained from pushover analysis with load pattern as per New Zealand seismic code [10]. The values of the constants to be used in Equation 26 can be obtained from Table 8.4.

$$\Omega_f = A + \frac{B}{\lambda} + C\varepsilon\vartheta + Dn_s; \Omega_p = A + \frac{B}{\lambda} + C\varepsilon^2\vartheta + Dn_s \quad (26)$$

Table 8.4. Coefficients to correct the lateral stiffness depending on type of frame and base fixity

Frame	Fixity	*A*	*B*	*C*	*D*
Braced	Fixed	0.98	-0.08	-0.08	0.00
	Pin	0.80	0.00	0.00	0.009
Unbraced	Fixed [28]	1.27	0.30	0.00	-0.027
	Pin	0.74	0.03	0.00	0.007

The values of the constants have been determined for low to medium rise buildings and their application to high rise buildings may not result in realistic lateral stiffness. After incorporating the correction factor Ω in Equation 25, the error in the predicted lateral stiffness greatly reduces and the maximum error becomes less than 7%, which can be observed in Figure 8.7 for braced frames with fixed and pin base and in Figure 8.6b for unbraced frames with pin base.

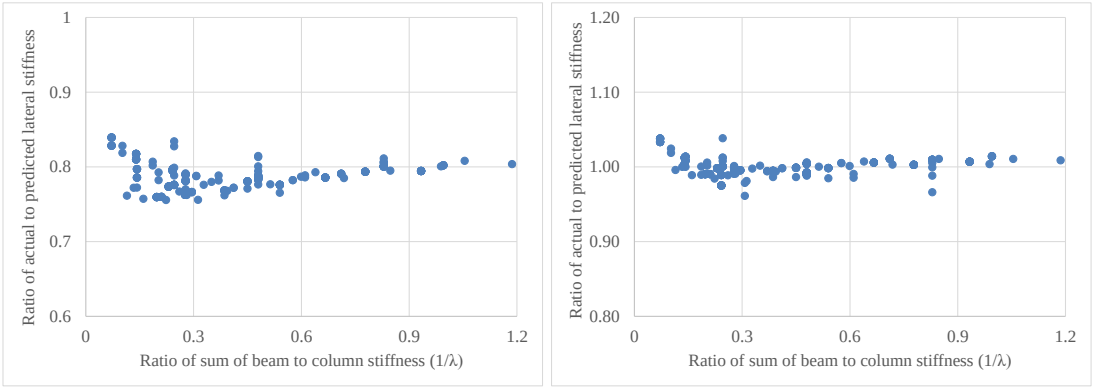

(a) Uncorrected lateral stiffness (b) Corrected lateral stiffness

Figure 8.6. Comparison of predicted and actual lateral stiffness for unbraced frames with pin base

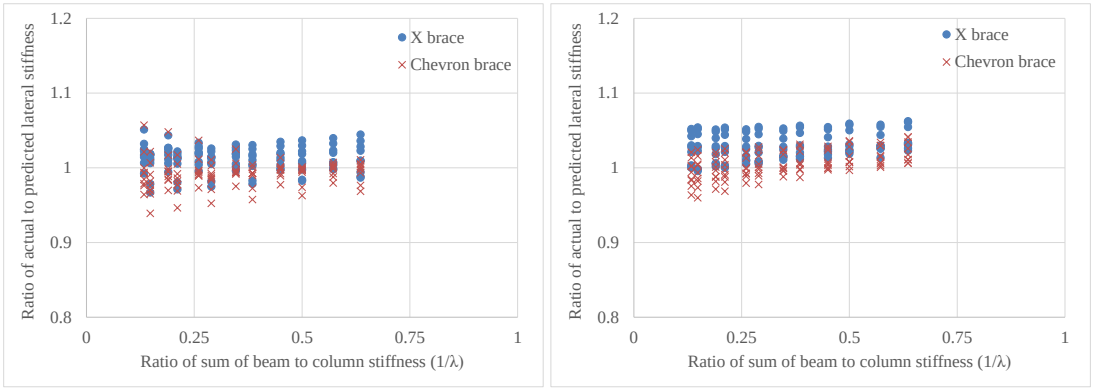

(a) Braced frames with fixed base (b) Braced frames with pin base

Figure 8.7. Predicted lateral stiffness for braced frames in conjunction with correction factor

8.3.2 *Comparison between the calculated fundamental period and the fundamental period obtained from Eigenvalue analysis*

Comparison between the fundamental periods calculated using the developed formula and the fundamental periods obtained from Eigenvalue analysis for a wide range of low to medium rise braced frames with fixed and pin base is shown in Figure 8.8. The developed equation can also be used for prediction of fundamental period of unbraced frames by setting the second term in χ_f or χ_p to zero. The ratio of actual to predicted fundamental periods for the unbraced frames with pin base is shown in Figure 8.9a and the results for the unbraced

frames with fixed base are reported in Chapter 7 [28]. It is clear that Equation 24 predicts fundamental periods with similar order of error when compared to the fundamental periods given by Eigenvalue analysis, as can be seen in Figures 8.8 and 8.9a. The error in the predicted fundamental periods for braced frames with fixed and pin bases range between 20% to 10% depending on the relative stiffness of the column to the beam λ and the pseudo relative stiffness of the brace to the column ϑ, whereas for unbraced frames with pin base the error is in between 15% and 5% depending on the relative column to beam stiffness λ. The range of error in prediction of the fundamental period is less than the range of error in prediction of lateral stiffness because the error in lateral stiffness is square rooted when computing the fundamental period.

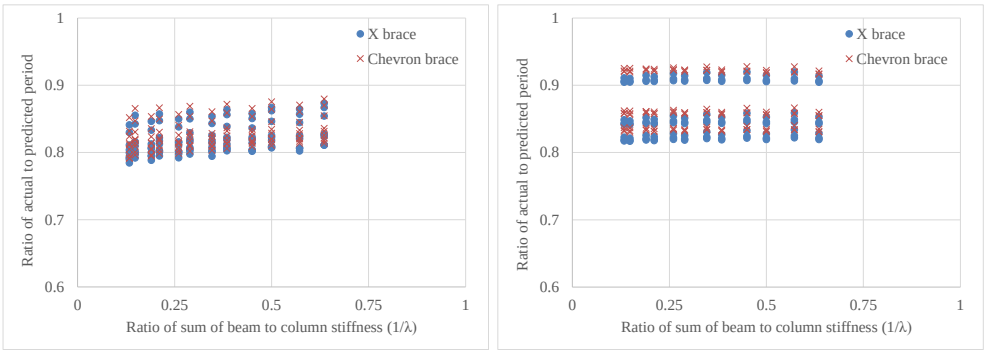

(a) Braced frames with fixed base (b) Braced frames with pin base

Figure 8 8. Comparison of predicted and actual fundamental period for braced frames

The identified reasons for the remaining error in prediction of fundamental period are; (i) the assumptions used in developing the equation for prediction of lateral stiffness, (ii) the lateral stiffness estimated is based on the top storey lateral displacement, which needs to be modified to obtain the effective stiffness K_{eff} depending on the mode shape corresponding to the fundamental mode of vibration, and (iii) total seismic weight/mass is used instead of effective mass in the first mode of vibration. To neutralize the error, a correction factor φ is introduced into Equation 24 to account for both the effective mass and effective stiffness. After introducing the correction factor φ, Equation 24 now turns into Equation 27.

$$T_f = 2\pi\varphi_f\sqrt{\frac{W_s h^3}{12g\sum E_c I_c \chi_f}};\ T_p = 2\pi\varphi_p\sqrt{\frac{W_s h^3}{12g\sum E_c I_c \chi_p}} \qquad (27)$$

A multiple variable regression analysis is carried out to relate the correction factor φ with the relative stiffness of the column to the beam λ, pseudo relative stiffness of the brace to the column ϑ, and the number of storeys n_s, which is given by Equation 28 for both fixed and pin base frames. The values of the constants to be used in Equation 28 can be obtained from Table 8.5.

$$\varphi_f = A + \frac{B}{\lambda} + C\varepsilon\vartheta + Dn_s; \varphi_p = A + \frac{B}{\lambda} + C\varepsilon^2\vartheta + Dn_s \quad (28)$$

Table 8.5. Coefficients to correct the fundamental period depending on type of frame and base fixity

Frame	Fixity	*A*	*B*	*C*	*D*
Braced	Fixed	0.82	0.05	0.04	-0.006
	Pin	0.95	0.00	-0.03	-0.012
Unbraced	Fixed [28]	0.66	0.19	0.00	0.008
	Pin	1.00	0.02	0.00	-0.014

The values of the constants have been determined for low to medium rise buildings and their application to high rise buildings may not result in realistic fundamental period. After incorporating the correction factor in Equation 27, the error in the predicted fundamental period decreases significantly. The maximum error is less than 5%, which can be seen in Figure 8.10 for braced frames with fixed and pin bases and in Figure 8.9b for unbraced frames with pin base. A flow chart which helps to quickly identify different parameters and constant values to be used in Equation 27 to calculate the fundamental period is given in Appendix M. Also, two example problems showing step by step calculation to arrive at the fundamental period is also given in Appendix N.

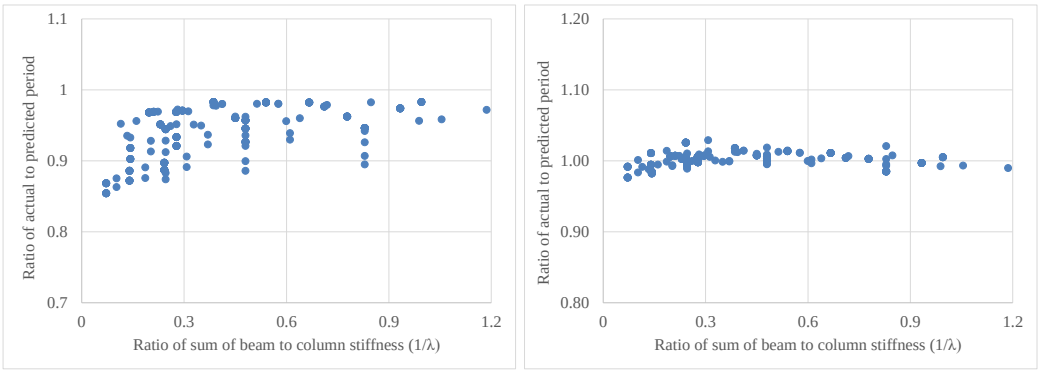

(a) Uncorrected fundamental period (b) Corrected fundamental period

Figure 8 9. Comparison of predicted and actual period for unbraced frames with pin base

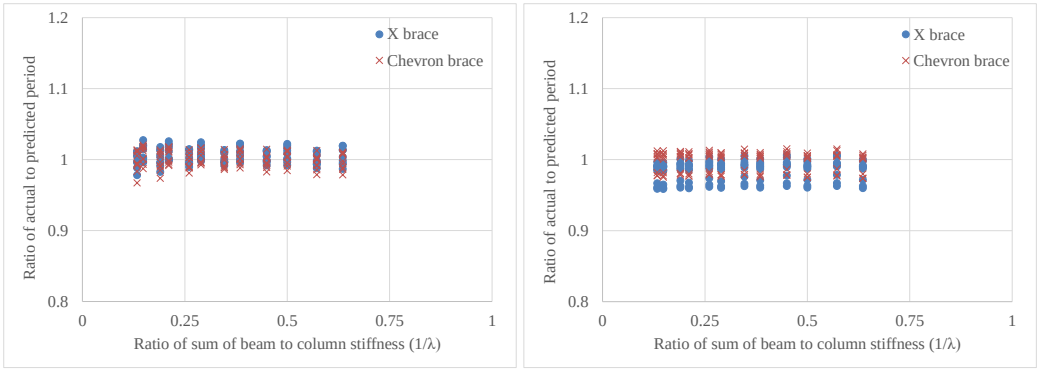

(a) Braced frames with fixed base (b) Braced frames with pin base

Figure 8.10. Predicted fundamental period of braced frames in conjunction with the correction factor

8.3.3 *Systematic interpretation of the parameters affecting the fundamental period*

In this section, systematic interpretation of the structural parameters affecting the fundamental period is studied by utilizing the results obtained from Equation 27 and Eigenvalue analysis. The variation of the fundamental period with the following geometrical parameters is investigated; (i) relative stiffness of the beam to the column $1/\lambda$, (ii) pseudo relative stiffness of the brace to the column ϑ, (iii) number of storeys n_s, (iv) base fixity (i.e. fixed or pin), and (v) type of brace (X and chevron). The results are plotted in Figures 8.11 to 8.17, where "P" represents that the fundamental periods are predicted using Equation 27, "E" indicates that the fundamental periods are obtained from Eigenvalue analysis, "C-0.4x0.5" represents the cases with column size 0.4×0.5 m, "S=5" represents the span length of 5 m, and "B=3" represents the frame of 3 bays. It is important to note that in Figures 8.11 to 8.17, the fundamental periods predicted using Equation 27 are based on the seismic weights given in Table 8.5. Strictly speaking, there will be a slight change in the seismic weight due to the change of beam and brace cross-sections (i.e. with the change of $1/\lambda$ and ϑ), but the error induced because of this will be negligible.

It is clear from Figures 8.11 to 8.17 that as the ratio of the beam to the column stiffness $1/\lambda$ for a given column dimension increases, the fundamental period of the frame decreases. This is because the lateral stiffness of the overall frame increases, which is inversely proportional to the fundamental period. For a braced frame, the dependency of the fundamental period on the relative stiffness of the beam to the column $1/\lambda$ decreases as pseudo relative stiffness of the brace to the column ϑ increases, which is shown in Figure 8.11. This is because as ϑ increases, the major portion of the overall lateral frame stiffness is contributed by the brace components rather than frame elements. For the same frame configuration and the same relative stiffness ratio of the beam to the column $1/\lambda$, increase in the column dimensions results in an increase in the lateral stiffness and as a consequence the fundamental period decreases, which can be clearly seen in Figures 8.12a, 8.12b and 8.14. As the span length of the frame increases for a given frame configuration with given column dimensions, the lateral stiffness decreases and the period consequently increases, which is evident in Figure 8.12c. As it can be observed in Figure 8.12d, the addition of extra bays of the same span length to a pin base frame with given configuration will not change the period significantly, because both the lateral stiffness and seismic mass increase proportionally when an extra bay is added.

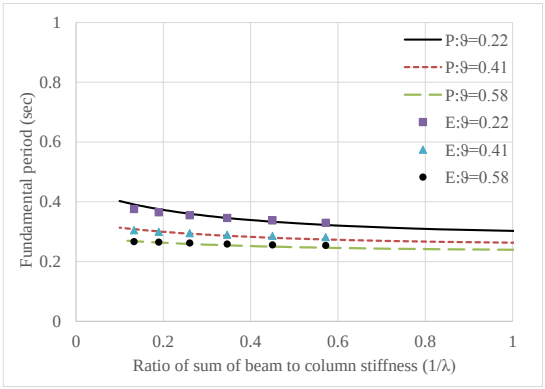

(a) X braced frames with fixed base

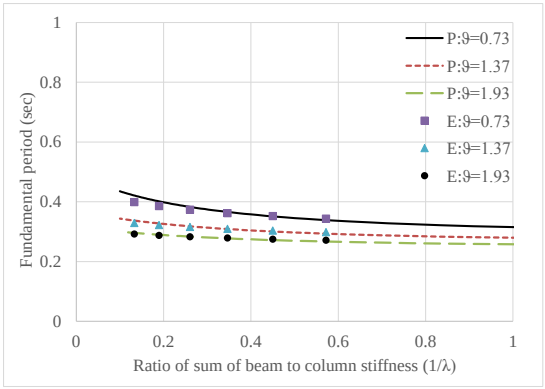

(b) Chevron braced frames with fixed base

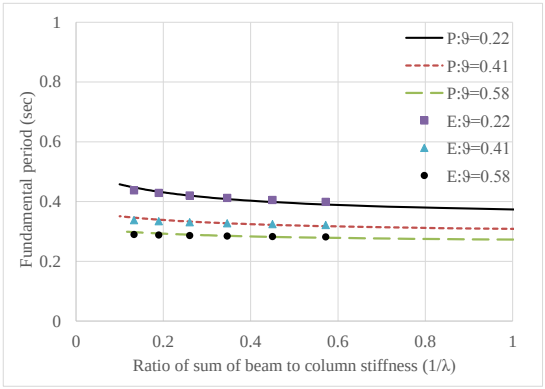

(c) X braced frames with pin base

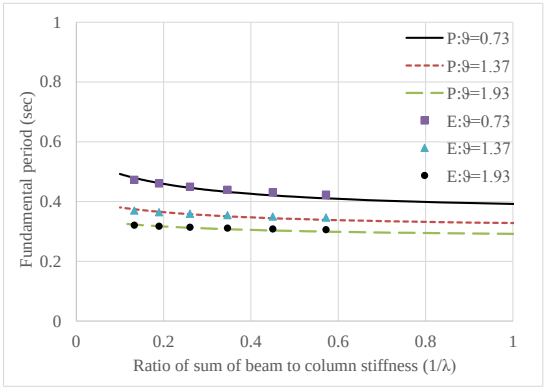

(d) Chevron braced frames with pin base

Figure 8.11. Fundamental periods of 3 storey braced frame of 3 bays with varying λ and ϑ

As the number of storeys n_s increases for a frame (braced or unbraced) the overall lateral stiffness of the frame decreases. As a result, the fundamental period increases, which is shown in Figures 8.13 and 8.14. The fixity of the column to the foundation (i.e. fixed or pin) significantly contributes to the lateral stiffness of the frame, which in turn affects the period of vibration. In Figures 8.15 and 8.16, the comparison of the fundamental periods of braced and unbraced frame with fixed and pin base is shown. It is obvious that the period of a pin base frame is longer than the period of a fixed base frame, because a pin base frame is more flexible than if its bases are fixed. Also, the difference in periods between fixed and pin base frames reduces with increase in the number of storeys, because the contribution of base fixity to the overall lateral stiffness decreases with an increase in the number of storeys, which is evident in Figure 8.16. It is obvious that the lateral stiffness of a chevron brace is less than an X brace (with the same cross sectional area) because of the sharper inclination angle. As a result, fundamental period of a chevron braced frame is longer than that of it X braced counterpart, which is evident in Figure 8.17.

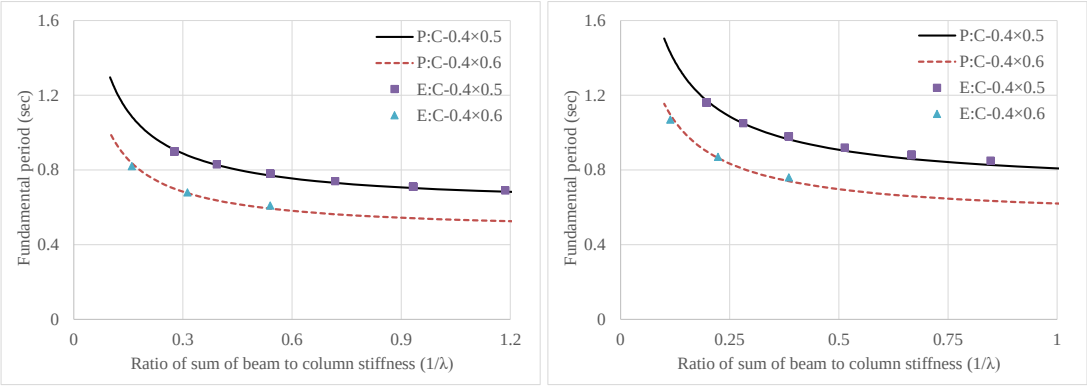

(a) 3 bays of 5 m span length

(b) 3 bays of 7 m span length

(c) 3 bays of 5 and 7 m span length

(d) 3 and 4 bays of 7 m span length

Figure 8.12. Fundamental periods of 3 storey unbraced frames with pin base with varying λ

The effect of base fixity (fixed or pin) on the fundamental period of braced frames is less pronounced compared to unbraced frames, which can be seen by comparing Figures 8.15 and 8.16. This is because the overall lateral stiffness of the braced frame comes from predominantly brace elements through axial resistance which is less sensitive to base fixity. As mentioned before, the maximum error in the predicted fundamental period values when compared to Eigenvalue analysis results is less than 5%. Nevertheless, the predicted values in general are very close to the Eigenvalue analysis results; and the minor difference is acceptable considering the uncertainties and complexities involved. As Equation 27 predicts the fundamental period of braced or unbraced frame building with good accuracy, this equation can be easily used in the design of new frame buildings or assessment of existing frame buildings.

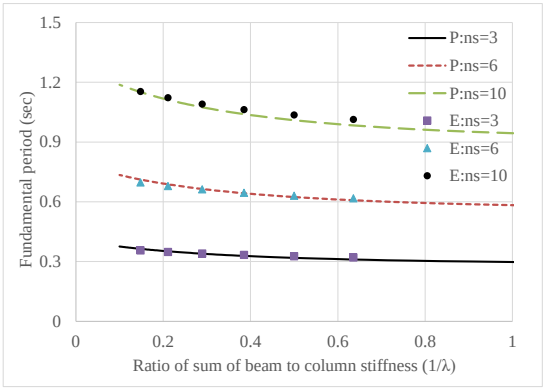

(a) X braced frames with ϑ=0.22 and fixed base

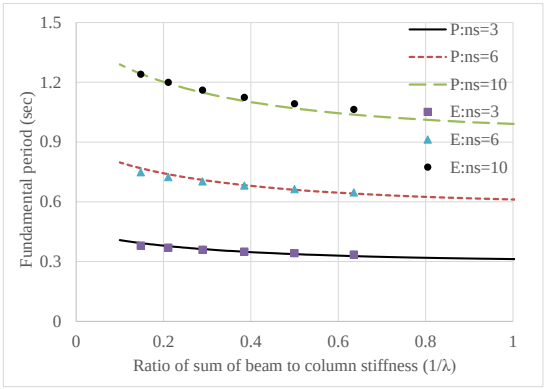

(b) Chevron braced frames with ϑ=0.73 and fixed base

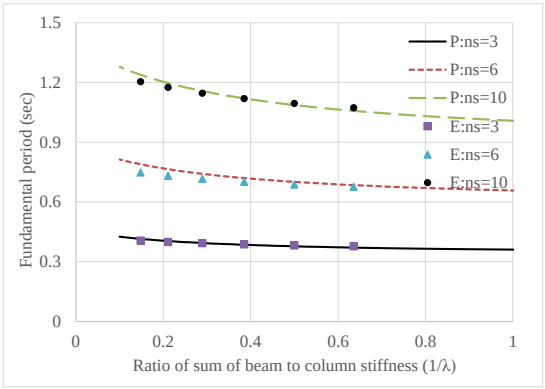

(c) X braced frames with ϑ=0.22 and pin base

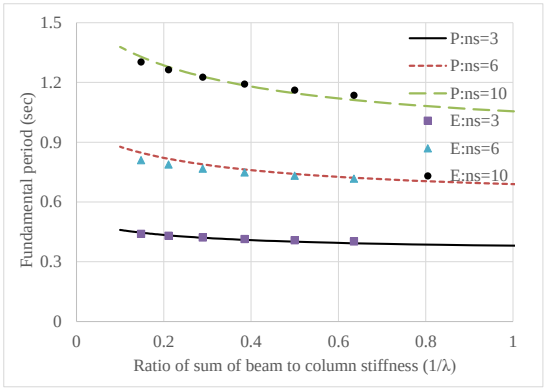

(b) Chevron braced frames with ϑ=0.73 and pin base

Figure 8.13. Variation of period of braced frames with 5 bay with varying number of storeys n_s

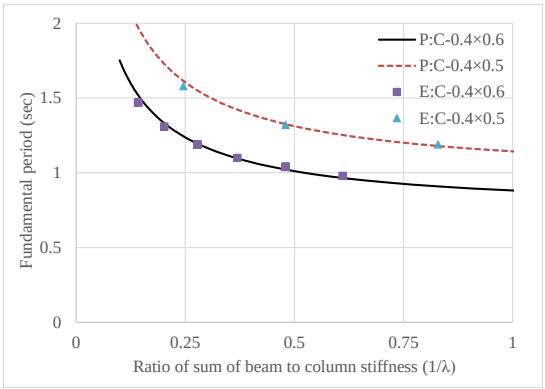

(a) 5 storey frame with 4 bays and 6 m span

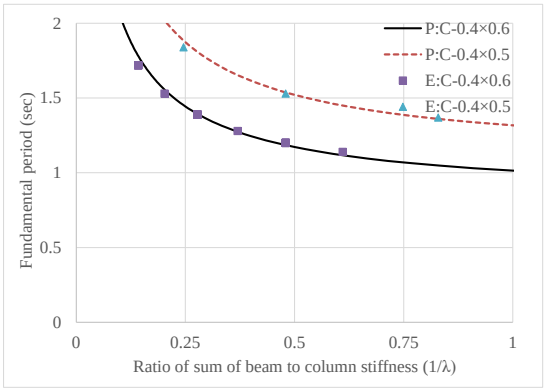

(b) 6 storey frame with 4 bays and 6 m span

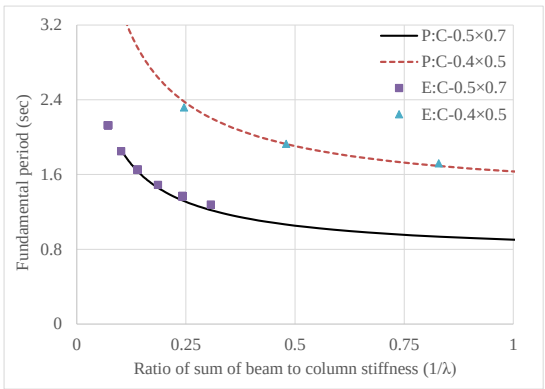

(c) 8 storey frame with 4 bays and 6 m span

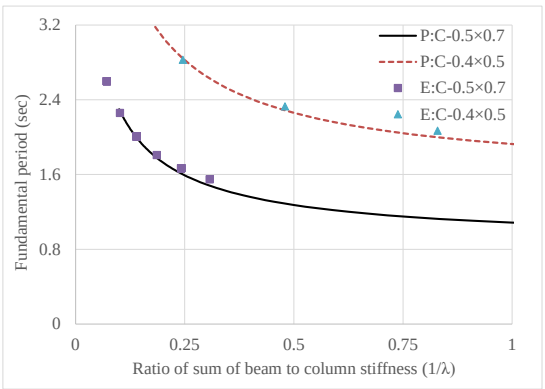

(d) 10 storey frame with 4 bays and 6 m span

Figure 8.14. Variation of fundamental period of unbraced frames with varying number of storeys n_s

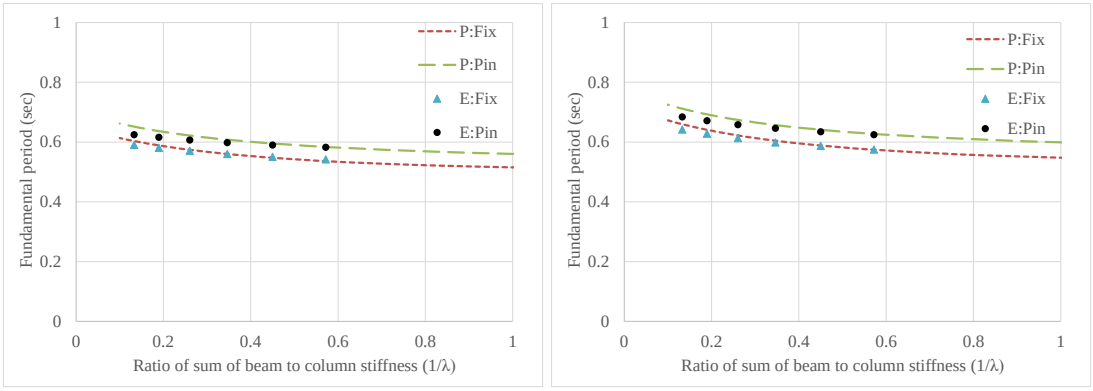

(a) X braced frames with ϑ=0.41 (b) Chevron braced frames with ϑ=1.37

Figure 8.15. Fundamental periods of 6 storey braced frame with 3 bays with fixed and pin base

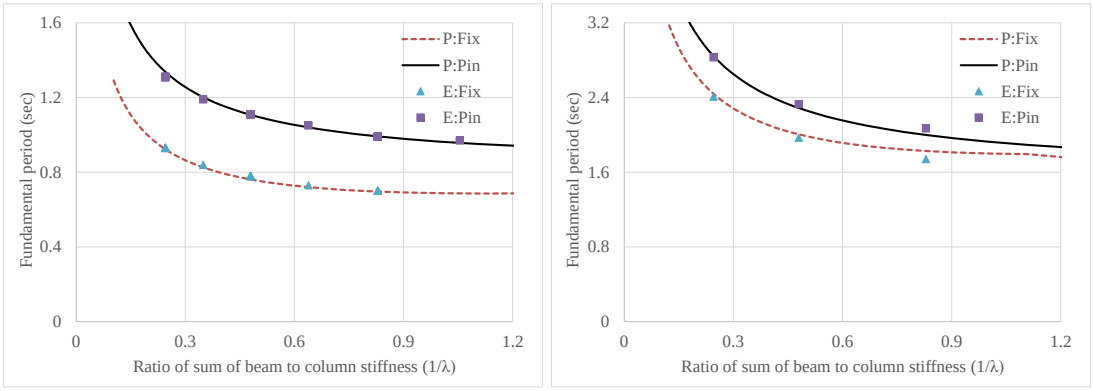

(a) 4 storey frame (b) 10 storey frame

Figure 8.16. Fundamental periods of 4 bayed unbraced frame of 6 m span length with fixed and pin base

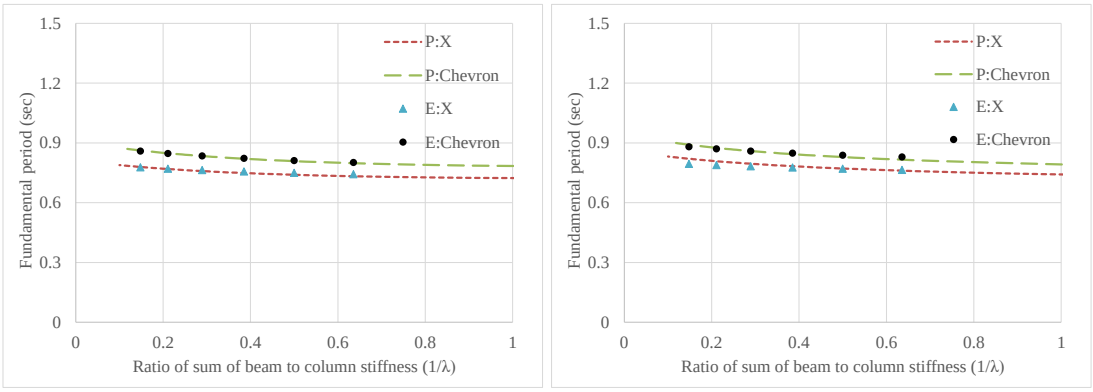

(a) 5 bayed frame with fixed base (b) 5 bayed frame with pin base

Figure 8.17. Fundamental periods of 10 storey frame with X (ϑ=0.58) and Chevron braces (ϑ=1.93)

8.3.4 *Application to braced frames with pin beam-column connections*

The basic formulation in development of Equation 27 to predict the fundamental period of braced frame buildings assumes that beam column connections are rigid, whereas in braced frames it is common to have simple/pin beam column connections to economize the building

cost. So, the applicability of the developed Equation 27 for a braced frame with pin beam column connections is also studied herein. A seven storey braced frame with span length of 6 m, column size of 0.4×0.6 m, beam size of 0.4×0.65 m, and with varying pseudo relative stiffness of the brace to the column ϑ (as shown in Table 8.6) is chosen for the verification. It is important to note that the first term in χ_f and χ_p and the second term in φ_f and φ_p which represent the contribution of frame stiffness through flexural resistance will have to be set to zero when computing the fundamental period for such pin jointed frames. By comparing the predicted values with those obtained from Eigenvalue analysis shown in Table 8.6, it can be concluded that Equation 27 can be used to predict the fundamental period of braced frames with pin beam-column connections.

Table 8.6. Comparison between the calculated and analytically predicted period of braced frame with pin beam-column connections

Brace		**Weight (kN)**	**Fixed base period (Sec)**		**Pin base period (Sec)**	
	ϑ		**Eigenvalue**	**Calculated**	**Eigenvalue**	**Calculated**
X brace	0.22	7344	0.95	0.96	0.99	1.05
	0.41	7359	0.71	0.70	0.73	0.75
	0.58	7372	0.60	0.59	0.62	0.63
Chevron brace	0.73	7338	1.03	1.04	1.09	1.13
	1.37	7348	0.78	0.77	0.81	0.82
	1.93	7357	0.66	0.66	0.68	0.69

8.3.5 *Investigation on effect of axial shortening of columns on fundamental period*

To investigate the reliability of the proposed equation in capturing the effect of axial shortening of columns on the fundamental period of braced frames, an eight storey frame with pin base and simple beam column connections is chosen. The cross sections of the frame members were taken from a similar eight storey frame available in steel tips manual; column size of W14×132, beam size of W24×103, X-brace size of 2L-5×5×3/4, and chevron brace size of W10×45 [29]. Seismic weight of a three bay frame with one bay braced with X brace and chevron brace is 4076 kN and 4047 kN respectively, and that of a five bay frame with two bays braced with X brace and chevron brace is 6782 kN and 6725 kN respectively. The cross sectional area of the columns is varied by multiplying by a factor rather than changing the actual column section size and the moment of inertia of the columns is assigned the same value in all cases. The comparison of the predicted and analytically calculated fundamental period of the eight storey frame with varying cross section of columns (and consequently different values of factor τ) is shown in Figure 8.18. In the figure, abscissa is the ratio of the cross section area of the column in that particular case to the actual cross section area of the column, "3" and "1b" represent the total number of bays and number of braced bays

respectively. It is evident that the proposed equation is able to incorporate the effect of axial shortening of columns through factor τ and the level of accuracy in prediction of fundamental period is of the same order as other cases. It is important to note that the factor τ depends on designed cross sectional area of the column, and if capacity design principle (i.e. weak brace-strong column) is adopted then τ approaches towards zero, which actual means columns are axially rigid. Also, the axial shortening of columns is more prominent in braced frames because significant portion of the lateral load demand is resisted by the braced bays.

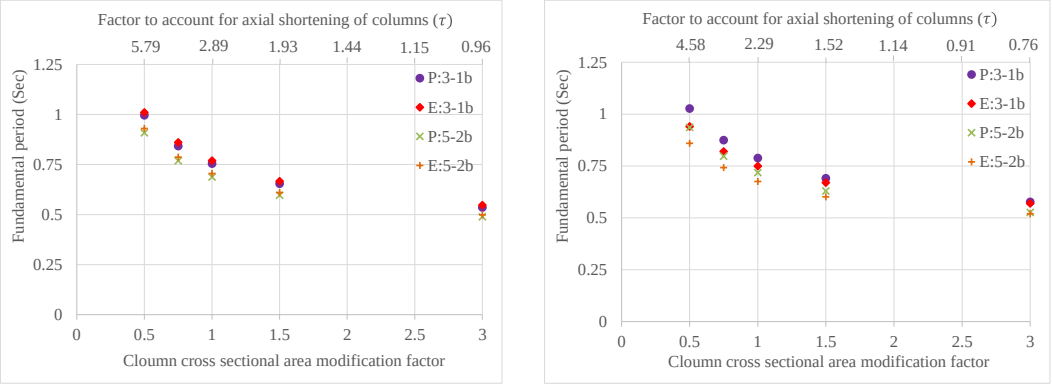

(a) X braced frames (b) Chevron braced frames

Figure 8.18. Fundamental periods of 8 storey braced frames with varying column cross section area

8.3.6 *Application to other types of brace configurations*

The model has been developed explicitly for X and chevron brace configurations. In this section, the applicability of Equation 27 to other types of brace configurations (i.e. split X, K, diagonal, eccentric chevron, and eccentric diagonal) is investigated. An eight storey frame with 3 bays of 6 m span length, column size of 310UC158 and beam size of 310UB110 resulting in λ of 3.65, and brace size of L150×150×16 mm is chosen for the analysis. When applying Equation 27 to other types of brace configurations, the second term of χ_f and χ_p has to be multiplied by a factor; (i) for X braces split over two storeys the factor is 2, and (ii) for K, diagonal, and eccentric diagonal braces the factor is 0.5. It is important to note that ε is the ratio of the horizontal projected length of brace to span length of braced bay. As can be seen in Table 8.7, Equation 27 in general predicts the fundamental period with reasonable accuracy for concentric brace frame configurations, whereas it underestimates for eccentric brace frame configurations. This is because in eccentric braced frames, the actual flexural moment variation in the beams is very different from the assumed bending moment variation in the derivation. Also, Equation 27 does not distinguish a K braced frame from a diagonal braced frame, which is evident in Table 8.7, which is the limitation of the proposed equation.

Table 8.7. Comparison between the calculated and analytically predicted period of braced frame with different brace configurations

Brace	ε	l_b(m)	ϑ	Weight (kN)	Fixed base period (Sec)		Pin base period (Sec)	
					Eigenvalue	Calculated	Eigenvalue	Calculated
X	1	7.00	1.59	3932	0.52	0.54	0.53	0.52
Split X	1	9.37	0.66	3919	0.57	0.56	0.58	0.58
K	1	7.00	1.59	3912	0.71	0.74	0.73	0.70
Diagonal	1	7.00	1.59	3912	0.76	0.74	0.78	0.70
Chevron	0.5	4.69	5.28	3919	0.59	0.62	0.6	0.57
E-Chevron	0.42	4.39	6.41	3917	*0.78*	*0.66*	*0.81*	*0.61*
E-Diagonal	0.75	5.76	2.84	3909	*0.9*	*0.75*	*0.94*	*0.70*

8.3.7 *Application to frames with varying section properties*

To validate the applicability of Equation 27 in predicting the fundamental period of frame buildings (braced or unbraced) with linear varying section properties along the building height, a nine storey frame with 3 bays of 6 m span length is chosen. At the first storey level, columns made of 310UC158 and beams of 310UB110 resulting in λ of 3.65, and brace section of L100×100×10 mm are used in the analysis. The section properties for the 1st to 3rd storeys are same as the first storey section properties, for the 4th to 6th storeys the section properties are 2/3rd of the first storey section properties, and for the 7th to 9th storeys the section properties are 1/3rd of the first storey section properties. In Equation 27, F_s, F_g, and F_r values corresponding to *s=g=r=0.33* can be obtained from Figure 8.4 or Table 8.1. It is obvious that depending on the extent of variation of section properties, the fundamental period of the frame building will be affected. It can be seen from Table 8.8 that the fundamental period considerably increases with *s=g=r=0.33*. Also, it is clear that Equation 27 is able to predict the fundamental period of frame with varying section properties with reasonable accuracy as long as the variation is close to linear fit.

Table 8.8. Comparison between the calculated and analytically predicted period with and without variation of section properties

Brace	ε	l_b(m)	ϑ	Weight (kN)	Fixed base period (Sec)		Pin base period (Sec)	
					Eigenvalue	Calculated	Eigenvalue	Calculated
No variation of properties (Fixed base: $F_s = F_g = F_r = 0.67$ and pin base: $F_s = F_g = 0.64; F_r = 0.67$)								
X	1	7.00	0.64	4397	0.88	0.86	0.90	0.89
Chevron	0.5	4.69	2.11	4391	0.95	0.94	0.98	0.96
Variation of properties (Fixed base: $F_s = F_g = F_r = 0.94$ and pin base: $F_s = F_g = 0.89; F_r = 0.94$)								
X	1	7.00	0.64	4397	1.00	1.02	1.02	1.05
Chevron	0.5	4.69	2.11	4391	1.09	1.12	1.12	1.13

8.3.8 *Verification using experimental and numerical results*

In this section, reliability of Equation 27 in predicting the fundamental period of frame buildings is verified by comparing with experimental and numerical analysis results

published in the literature. The parameters which are taken from the literature and used in Equation 27 along with the predicted and reported values are given in Tables 9 and 10. It is clear that the predicted fundamental periods are in close agreement with the reported/measured values. The discrepancies in some cases are due to the following identified reasons; (i) section properties do not vary in a linear way, (ii) combination of rigid and pin beam column connections in the same frame, (iii) lack of detailed geometrical and base fixity information.

Table 8.9. Comparison between the calculated fundamental periods with published numerical results

Reference		**Parameters used in Equation 27 (** Note: In the below table, all units are in SI units (m, kN))		**Period (Sec)**	
				Reported	**Calculated**
[6]	BRBF7: MR	$n_s = 7;$ $n_b = 1;$ $n_{br} = 1;$ $l = 7.6$; $h = 3.6;$ $l_b = 5.24;$ $W_s = 13191$	$\lambda = 17; \vartheta = 2.1; \varphi_f = 0.82;$ $F_s = 0.96; F_g = 0.67; F_r = 0.99$	0.93	0.92
	DS7: MR		$\lambda = 6.28; \vartheta = 1.39; \varphi_f = 0.81$ $F_s = 0.83; F_g = 0.94; F_r = 0.99$	0.89	0.89
	BRBF7:NMR		$\lambda = 17; \vartheta = 2.1; \varphi_f = 0.82$ $F_s = 0.96; F_g = 0.67; F_r = 0.99$	0.94	0.93
	DS7:NMR		$\lambda = 6.28; \vartheta = 1.39; \varphi_f = 0.81$ $F_s = 0.83; F_g = 0.94; F_r = 0.99$	0.90	0.92
[23]	MRF	$n_s = 9;$ $n_b = 5;$ $n_{br} = 2;$ $l = 9.14;$ $h = 4.13;$ $l_b = 10.03;$ $W_s = 45070$	$\lambda = 2.08; \varphi_f = 0.82;$ Fixed base. $F_s = 0.83; F_g = 0.94$	2.05	2.14
	SCBF		$\lambda = 2.08; \vartheta = 0.52; \varphi_f = 0.82;$ Pin base; Rigid beam column joint. $F_s = 0.79; F_g = 0.85; F_r = 0.81$	1.08	0.98
			$\vartheta = 0.52; \varphi_p = 0.82;$ Pin base; Pin beam column joint; $F_r = 0.81$		1.07
Note: "BRBF", "DS", "MR", NMR", "MRF", and "SCBF" represent buckling restrained braced frame, dual system, moment resisting, nominal moment resisting, moment resisting frame, and concentric brace frame, respectively.					

Table 8.10. Comparison between the calculated fundamental periods with experimental test results

Reference		**Parameters used in Equation 27 (** Note: In the below table, all units are in SI units (m, kN))		**Period (Sec)**	
				Reported	**Calculated**
[30]	BRB Specimen	$n_s = 3;$ $n_b = 3;$ $n_{br} = 1;$ $l = 7; h = 4;$ $l_b = 5.32;$ $W_s = 4350$	$\lambda = 2.48; \vartheta = 3.57; \varphi_f = 0.89;$ Fixed base; Rigid beam column joint. $F_s = 0.67; F_g = 0.78; F_r = 0.84$	0.68	0.55
			$\vartheta = 3.57; \varphi_p = 0.87;$ $F_r = 0.84$ Fixed base; Pin beam column joint.		0.59
[31]	6 Storey	$n_s = 6;$ $n_b = 2;$ $n_{br} = 1;$	$l = 7.5; h = 3.58; l_b = 5.18; \varphi_f = 0.9$ $W_s = 5647; \lambda_o = 4.57; \lambda_i = 4.80$ $F_s = 1.08; F_g = 0.79; F_r = 1.00$	0.61	0.62
[32, 33]	Prototype	$n_s = 4;$ $n_b = 1;$ $n_{br} = 1$	$l = 9.14; h = 4; l_b = 6.07; F_r = 0.74$ $W_s = 14772; \vartheta = 1.28; \varphi_p = 0.89$	0.92	0.97
	Tested		$l = 5.49; h = 2.4; l_b = 3.64; F_r = 0.74$ $W_s = 5317; \vartheta = 3.53; \varphi_p = 0.88$	0.71	0.75

8.4 Conclusions

A simple yet versatile hand-calculation method to predict lateral stiffness and fundamental period of concentrically braced frame buildings with fixed or pin base, which can also be used for unbraced frame buildings, has been developed in this chapter. First, equations are derived for lateral stiffness and fundamental period of frames by incorporating established theories of structural mechanics and making approximations and assumptions whenever necessary to retain simplicity. By comparing the lateral stiffness and fundamental period predicted by the theoretically derived equations with the corresponding values obtained from computer analysis, correction factors are established to neutralize the error inherently induced by the simplifications used in the theoretical derivation. By applying these correction factors, generic and versatile equations are obtained for practical applications. According to the findings of this study, the lateral stiffness and fundamental period of a braced or unbraced frame building (with fixed or pin base) can be reliably estimated as:

$$Lateral\ stiffness\ (K) = \Omega \frac{12 \sum E_c I_c \chi}{h^3}; Fundamental\ period\ (T) = 2\pi\varphi \sqrt{\frac{W_s h^3}{12 g \sum E_c I_c \chi}}$$

where Ω is a correction factor to neutralize the error in predicted lateral stiffness and can be determined using Equation 26, φ is a correction factor to neutralize the error in predicted fundamental period and can be evaluated using Equation 28, χ is a geometric configuration factor and can be determined using Equations 21 or 22 depending on the base fixity, W_s is the seismic weight, h is the storey height, E_c is the Young's modulus of the column, I_c is the gross or effective moment of inertia of the column, and g is the acceleration due to gravity. A flowchart showing the sequence of steps involved in calculating the lateral stiffness and the fundamental period of a braced frame building is provided in Appendix M along with two worked examples. The validity of the proposed equations to predict the fundamental period of braced frames with fixed or pin base, with and without variation of section properties along the building height, and with rigid or pin beam-column connections is thoroughly checked by comparing with the fundamental periods obtained from Eigenvalue analysis for a wide range of low to medium rise frame buildings (i.e. up to 10 storeys). Also, the proposed equation is found to reliably capture the effect of axial shortening of the columns on the fundamental period of braced frame buildings. Although the proposed equations are explicitly developed for X and chevron brace configurations, their applicability to other brace configurations is also investigated. It can be concluded that the proposed equations can predict the lateral stiffness and the fundamental period of braced frames within ± 5% of the actual values. To

conclude, the proposed method is simple, captures the effect of all parameters that are known to affect the fundamental period of frame buildings, requires input parameters that are not difficult to determine, and can be easily implemented in analysis and design tools. The proposed equation can reliably capture the fundamental period of braced frame buildings with all configurations and characteristics, and it can be readily used by practicing engineers in designing new buildings as well as in the assessment of existing buildings.

8.5 References

1. Sabelli, R., S. Mahin, and C. Chang, *Seismic demands on steel braced frame buildings with buckling-restrained braces.* Engineering Structures, 2003. **25**(5): p. 655-666.
2. Di Sarno, L. and G. Manfredi, *Experimental tests on full-scale RC unretrofitted frame and retrofitted with buckling-restrained braces.* Earthquake Engineering & Structural Dynamics, 2012. **41**(2): p. 315-333.
3. Sabelli, R., *Research on improving the design and analysis of earthquake-resistant steel-braced frames*. 2001: EERI.
4. Eurocode, *3: Design of steel structures, Part 1.8: Design of joints*. 2005, EN-1993-1-8. Brussels: European Committee for Standardization.
5. Aninthaneni, P.K. and R.P. Dhakal, *Conceptual development: Low loss precast concrete frame building system with steel connections*, in *NZSEE Conference*. 2014: Auckalnd, New Zealand. p. Paper No 44.
6. Ariyaratana, C. and L.A. Fahnestock, *Evaluation of buckling-restrained braced frame seismic performance considering reserve strength.* Engineering Structures, 2011. **33**(1): p. 77-89.
7. Goel, R.K. and A.K. Chopra, *Period formulas for moment-resisting frame buildings.* Journal of Structural Engineering, 1997. **123**(11): p. 1454-1461.
8. Tremblay, R., *Fundamental periods of vibration of braced steel frames for seismic design.* Earthquake Spectra, 2005. **21**(3): p. 833-860.
9. ASCE, *Minimum Design Loads for Buildings and Other Structures*. Standards. 2013: American Society of Civil Engineers. -1.
10. NZS1170, *NZS1170: Structural design actions. Part 5: Earthquake actions - New Zealand*. 2004: Wellington, NZ.
11. EN1998, *Eurocode 8: Design of structures for earthquake resistance-Part 1: General rules, seismic actions and rules for buildings*, in *London: BSi*. 2004. p. 10-12.
12. Aoyama, H., *Outline of earthquake provisions in the recently revised Japanese building code.* Tokyo University, Japan, 1981.
13. NBCC, *National Building Code of Canada*. 2005, National Research Council of Canada: Ottawa, Canada.
14. JapanBLEO, *Part 1, Earthquake Resistant Design of Structures and Part 2, Earthquake Resistant Design of Buildings*. 1981: Tokyo, Japan.
15. Bangash, M., *Earthquake resistant buildings: dynamic analyses, numerical computations, codified methods, case studies and examples*. 2011: Springer Science & Business Media.
16. Kelly, C.Y., *An Investigation of the Fundamental Period of Vibration of Irregular Steel Structures*. 2011, Master's Thesis, The Ohio State University.

17. Günaydn, E., *Natural periods of braced steel frames designed to EC8*. 2012, Master's Thesis, Middle East Technical University.
18. Shon, B.A., *Study on the fundamental period of vibration for buildings with different configurations*. 2015, Atilim University.
19. Chopra, A.K. and R.K. Goel, *Building period formulas for estimating seismic displacements.* Earthquake Spectra, 2000. **16**(2): p. 533-536.
20. Günaydın, E. and C. Topkaya, *Fundamental periods of steel concentrically braced frames designed to Eurocode 8.* Earthquake Engineering & Structural Dynamics, 2013. **42**(10): p. 1415-1433.
21. ACI, *Building code requirements for structural concrete (ACI 318-08) and commentary*. 2008, American Concrete Institute.
22. NZS3101, *NZS3101: The Design of Concrete Structures*. 2006, Standards New Zealand Wellington.
23. Di Sarno, L. and A.S. Elnashai, *Bracing systems for seismic retrofitting of steel frames.* Journal of Constructional Steel Research, 2009. **65**(2): p. 452-465.
24. Adeli, H., *Approximate formulae for period of vibrations of building systems.* Civil Engineering for practicing and design engineers, 1985. **4**(1): p. 93-128.
25. Chrysanthakopoulos, C., N. Bazeos, and D. Beskos, *Approximate formulae for natural periods of plane steel frames.* Journal of Constructional Steel Research, 2006. **62**(6): p. 592-604.
26. Iain, A., *Simplified equations for deflection of multistory frames.* Building Science, 1971. **6**(1): p. 25-31.
27. SAP, *Computers and Structures Inc*. 2013: Berkeley, CA, USA.
28. Aninthaneni, P.K. and R.P. Dhakal, *Prediction of fundamental period of regular frame buildings.* Bulletin of the New Zealand Society for Earthquake Engineering, 2016. **49**(2).
29. Becker, R., *Seismic design of special concentrically braced steel frames*. 1996: Structural Steel Educational Council.
30. Tsai, K.-C., et al., *Pseudo-dynamic tests of a full-scale CFT/BRB frame-Part I: Specimen design, experiment and analysis.* Earthquake Engineering and Structural Dynamics, 2008. **37**(7): p. 1081-1098.
31. Foutch, D.A., S.C. Goel, and C.W. Roeder, *Seismic testing of full-scale steel building-Part I.* Journal of Structural Engineering, 1987. **113**(11): p. 2111-2129.
32. Fahnestock, L.A., J.M. Ricles, and R. Sause, *Experimental evaluation of a large-scale buckling-restrained braced frame.* Journal of structural engineering, 2007. **133**(9): p. 1205-1214.
33. Fahnestock, L.A., R. Sause, and J.M. Ricles, *Analytical and large-scale experimental studies of earthquake-resistant buckling-restrained braced frame systems*, in *ATLSS Report No. 06-01*. 2006, Lehigh University.

Chapter 9: Conclusions and scope for future research work

In this research, a "demountable" and "structurally flexible" concrete building system which can be built in seismic regions is developed by utilizing the layout of a conventional frame building system (i.e. perimeter frames resisting lateral loads and internal frames resisting predominantly gravity loads). To address the key issues related to the concept and to assess the suitability of the proposed demountable building system in seismic regions, this research focused into four different stages as set out earlier in Chapter 1; (i) conceptual development, (ii) experimental test programme, (iii) numerical analysis, and (iv) analytical methods. The specific objectives associated with each of these stages were thoroughly investigated as described in different chapters. The key findings and the overall conclusions of this research are presented herein, and more specific conclusions related to different stages of the research are reported at the end of each chapter. Also, the scope and possible areas for future research work related to the proposed demountable building system is reported towards the end of this chapter.

9.1 Key findings/conclusions

9.1.1 *Conceptual development*

The main concluding remarks that can be drawn based on the research carried out on the conceptual development of a seismically robust demountable building system are;

- The proposed building system is comprised of standard precast concrete elements/components and "strong" steel connections. The schematic layout of the structural system and the possible types of "dry" and removable connections between different building components are presented in Chapter 2.
- The perimeter frames of the proposed building system can be designed to achieve the desired level of lateral load resistance (against the seismic demand) either through moment resisting frames or truss actions (i.e. strut and tie forces) provided by braced frames or a combination of both, depending on the desired damage mechanism in earthquake shaking.
- The proposed building system satisfies all technical requirements of a next generation building (NGB) system. A building with the proposed system does not need to be demolished when a building is obsolete in function, instead the building can be

sequentially dismantled (from top to bottom) and its components can be reused; thereby saving non-renewable building materials and energy associated with the demolition.

- The structural flexibility/adaptability of the proposed building system is demonstrated through different case scenarios. Following a damaging earthquake, the building system can be quickly repaired (compared to a monolithic concrete frame building) to the satisfaction of all stakeholders either by replacing the damaged building components with new ones of the same (or higher) capacity or by adding the steel braces to the existing lateral load resisting frames (by utilizing existing beam-column steel connections). This significantly reduces the building downtime and makes it a low downtime/loss building system in terms of earthquake induced losses.
- Compared to "wet jointed" precast concrete or monolithic concrete buildings and existing NGB systems, the proposed building system offers several additional advantages in seismic regions. In addition to its quick construction/erection, the system is demountable (not needing demolition), is quickly repairable to the satisfaction of all stakeholders and complying to the common insurance policy "like for like as when new", and can be upgraded/strengthened whenever needed.

9.1.2 *Experimental test programme*

The structural behaviour of a lateral load resisting frame of the proposed demountable building system predominantly depends on the type of the beam-column connections. The main objective of the experimental test programme is to identify the most suitable beam-column connection type among the three different "dry" and removable connection types, namely; (i) Type-1: end plate connection, (ii) Type-2: angle connection, and (iii) Type-3: tube connection. The connection types which result in the seismic performance of the proposed demountable frame system to be similar to that of a "wet jointed" precast concrete or monolithic concrete frame building system are identified and their overall seismic performance and system level performance are compared. The structural behaviour of a frame sub-assembly with Type-1 connections is found to be very different compared to a frame sub-assembly with Type-2 or 3 connections, and this is due to the different load transfer mechanism. The major identified differences between a frame sub-assembly with the Type-1 connections and a frame sub-assembly with Type-2 or 3 connections are;

- In Type-1 connection, the bolts on the column side are pre-tensioned to generate the frictional force to resist the vertical shear demand, whereas in other connection types,

the bolts on the beam side are also pre-tensioned to generate the frictional force to resist the horizontal shear demand (generated due to the bending moment) along with the bolts on the column side.

- In the end plate connection, tensile/compressive forces from the rebars directly transfer to the connection plates (embedded into the beam) which is not the case with other connection types, hence they need to rely on some other load transfer mechanisms (i.e. such as friction and beam end/edge breakout resistance).
- Load displacement characteristics (i.e. initial stiffness, nominal lateral strength, ductility, and energy dissipation) of a frame sub-assembly with the Type-1 connection is dictated by the structural properties of the frame members (as long as the connections are designed using capacity design principles), whereas with other connection types it is governed by a combination of structural properties of the connections (associated with beam edge failure mechanism) and frame members.
- The Type-1 connection is categorized as "non-sliding" connection (as long as the vertical slip between the connection and the column is eliminated by ensuring the frictional resistance is more than the over-strength shear demand), whereas Type-2 and 3 connections are the "sliding hinge" (i.e. slip critical) connections (practically the slip between the connection and the beam cannot be eliminated).

Based on the experimental test results reported in Chapters 3, 4, and 5, the following conclusions are drawn with regard to the cyclic behaviour of the frame sub-assemblies with the proposed three types of "dry" beam-column connections;

- The initial lateral stiffness and nominal lateral strength of a frame sub-assembly with "dry" end plate connection is about the same as that of a "wet jointed" precast concrete or monolithic concrete frame sub-assembly, whereas with the angle and tube connections, it may or may not reach that level of resistance depending on the available frictional and beam edge breakout moment capacity of the connection. The frictional moment capacity depends on the frictional shear resistance (between the connection and the beam) which in turn depends on the total pre-tension in the bolts and frictional coefficient, and the beam edge breakout moment capacity depends on the level of confinement (i.e. number of horizontal stirrups in the connection region).
- The cyclic behaviour of a frame sub-assembly with the end plate connection is similar to that of a monolithic concrete frame system with a "fat" hysteresis loop, and has better energy dissipation characteristics compared to a precast concrete frame sub-

assembly with “ductile connectors”. It can be concluded that emulation of structural behaviour (in every aspect) of a “wet jointed” precast concrete frame system can be definitely achieved by a precast concrete frame system developed using proposed “dry” end plate beam column connections.

- Hysteresis behaviour of the sub-assemblies with either angle or tube connections can be categorized as “pinching” type due to slip of the connection and concentrated beam edge failure. The extent of pinching and the rate of strength and stiffness degradation depends on the type of infill material (i.e. rubber sheet, non-shrink grout, epoxy, and dental plaster) between the connection plates and the member surfaces, the beam edge distance, the gap between beam end face and column face, and the amount of pre-tension in the bolts. The condition of the ducts on the beam side (i.e. un-grouted or grouted) has no significant effect on the overall hysteresis behaviour, this is because in both cases the ultimate mode of failure is the beam edge failure.
- A frame sub-assembly with either Type-2 or 3 connection underperforms in-terms of ductility, energy dissipation, and strength and stiffness degradation when compared to “wet jointed” precast concrete sub-assembly if the beam edge failure mechanism is not delayed until full yielding of the beam (which was the case in all tested sub-assemblies). Comparison of the tested sub-assemblies’ cyclic performance with existing precast concrete sub-assemblies with “wet joints” and “ductile connectors” proved that the performance of the sub-assemblies with these two connection types can be very uncertain depending on design and detailing of the beam edge, infill material properties, and strength hierarchy.
- The sequence of damage and the modes of failure in a precast concrete beam with the end plate connection is similar to the damage that will occur in the beam of a wet jointed precast concrete or monolithic concrete frame system; i.e.cracking of concrete, spread of flexural cracks, yielding of longitudinal rebars, spread of flexural-shear cracks, spalling of concrete, and bucking of rebars.
- The initial damage to the precast concrete beam with either Type-2 or 3 connection is due to the spread of flexural cracks until the slip of the connection is minimal (i.e. no contact between the bolts and the ducts). Thereafter, when the slip of the connection exceeds the clearance between the bolts and ducts, the bolts bear against the steel ducts, which induces bearing stress (i.e. bursting stress) into the beam edge resulting in bursting cracks and spalling of the concrete.

- The structural performance of the original sub-assembly can be regained after the beam is damaged and replaced with a new beam of the same capacity (provided the column and the steel connection components are undamaged), and this has been demonstrated with all three connection types.
- Upgrading a frame sub-assembly by replacing the damaged beam with a new beam of higher capacity is investigated only with the angle connection type, and this was not achieved due to alteration in the strength hierarchy (connection strength corresponding to beam edge failure turned out to be less than yield moment capacity of the beam). The strength hierarchy of a frame with the end plate connections can be easily be controlled (i.e. strong column/connection-weak beam) by the applying capacity design principles because of the direct load transfer from the rebars to the connection. As a result, upgradation of a frame by replacing weak beams with the strong beams and maintain intended strength hierarchy is possible with the end plate connection type.
- Assembly of a precast concrete beam with the Type-1 connection requires alignment of the bolts in one direction (i.e. along the beam length) which is comparatively easier compared to Type-2 and 3 connections where the bolts need to be aligned in both directions. Also, Type-2 and 3 connections require infill material to fill the uneven gaps between the precast concrete member surfaces and the connection surfaces which is an additional task that need to be carried out compared to Type-1 connection.
- A damaged beam from a frame sub-assembly with the Type-1 connection can be easily dismantled by unbolting the bolts and replaced with new one without much effort, whereas with Type-2 and 3 connections, because of the sliding of the connection the bolts on the beam side had moved away from their initial position, which resulted in some difficulty in removing the bolts and the steel components.
- By comparing all structural performance parameters, it can be concluded that the performance of a frame sub-assembly with the Type-1 (end plate) connection is superior compared to a frame sub-assembly with either Type-2 (angle) or Type-3 (tube) connection. Also, based on the subjective and qualitative comparative analysis, it can be concluded that the Type-1 connection ranks first in terms of ease of erection and dismantling when compared to the other two connection types. So, the recommended beam-column connection for a lateral load resisting frame of the proposed demountable precast concrete building system is the “end plate” connection.

9.1.3 *Analytical investigation and numerical analysis of the tested sub-assemblies*

Based on the analytical and numerical results reported in Chapters 5, 6, and 7, the following conclusions are drawn regarding simulation/prediction of structural performance parameters of a frame sub-assembly with the proposed "dry" beam column connections;

- Existing analytical equations developed originally for monolithic frames can reliably predict the initial or secant lateral stiffness and nominal lateral strength of a precast concrete frame with the end plate connection (connection can be treated as continuous and rigid). The only difference in the analytical formulation for a frame with the end plate connection is the increased finite joint length (half of the column depth plus the gusset length) when compared to a monolithic frame (half of the column depth).

- For Type-2 or 3 connections, the developed analytical model is able to reliably estimate the ultimate moment capacity of the connection on beam side corresponding to beam edge failure. By incorporating the connection's ultimate capacity into a strength hierarchy of the sub-assembly (i.e. strong column-weak beam or connection), the developed analytical equations could predict the nominal lateral strength of the frame sub-assembly with either angle or tube connections to a reasonable accuracy, and the predicted values matched well with the experimental test results. Also, the predicted initial lateral stiffness of the sub-assemblies are in close agreement with experimentally obtained values for the cases where the slip of the connection is minimal until the yielding of beam's longitudinal rebars.

- Existing numerical models developed for monolithic concrete frames, such as "Pivot" and "IMK peak oriented" reliably capture the hysteresis behaviour of a precast concrete frame sub-assembly with the end plate connection. The strength degradation of a frame (either end plate connection or wet joints) can only be captured with the right input backbone curve, and the construction of the right input backbone depends on the right combination of material models and plastic hinge length. The only difference in the numerical modelling of a frame with the end plate connections compared to wet/jointed monolithic concrete frame system is that the location of nonlinear rotational spring is shifted from the face of the column to in front of the connection.
- The cyclic behaviour of the sub-assemblies (with either Type-2 or Type-3 connections) associated with the slip of the connection can be simulated by using two macro modelling approaches; (i) approach-1; two parallel translation connection springs in series with beam rotational spring, and (ii) approach-2: connection rotational spring in

series with beam spring. In this study, “hysteretic material” and “IMK peak-oriented” hysteresis models available in structural analysis software “OpenSees” were utilized to model the behaviour of the connection and beam springs respectively. In general, the simulated overall hysteresis behaviour of the sub-assemblies with angle and tube connection were in close agreement with the experimental test results. The developed method to obtain the input backbone curve of the connection spring is simple to understand and captures the nonlinearity of the connection associated with the slip to a reasonable extent.

- Based on the numerical investigation, it can be concluded that an unbraced moment resisting frame with pin bases is not suitable for the proposed demountable building system because; (i) it is less redundant and robust, (ii) of large sway deformations, (iii) the reduction in base shear capacity (by changing the base fixity from fixed to pin) is more than the reduction in demand, (iv) very high (which is not practical) column to beam capacity ratio is required to avoid the soft-storey mechanism (i.e. damage to the columns), and (v) secondary (i.e. P-Δ) and higher mode effects need to be explicitly evaluated and a nonlinear time history analysis is required to capture these effects.

- To make the proposed demountable building system structurally robust and flexible (which allows replacement of its components), the following options with increasing order of structural flexibility/adaptability (i.e. less time to replace the damaged elements) can be considered; (i) an unbraced lateral load resisting frame with demountable fixed bases and column to column connections at mid height of first storey level, in this case both the damaged beam and column units (within first storey level) need to be replaced rather than replacing entire column units (which is challenging), and (ii) a braced lateral load resisting frame with removable pin bases and demountable rigid beam-column connections (damaged braces and beams need to be replaced) or removable pin beam-column connections (only braces need to be replaced).

9.1.4 *Analytical equation to estimate lateral stiffness and fundamental period of a frame*

Based on the analytical and numerical results reported in Chapters 7 and 8, the following conclusions are drawn with regards to the developed analytical framework to estimate the lateral stiffness and fundamental period of a frame;

- A simple yet versatile hand-calculation method/equation to estimate the lateral stiffness and fundamental period of concentrically braced or unbraced frame buildings is developed, which is given as:

  $Lateral\ stiffness\ (K) = \Omega \frac{12 \sum E_c I_c \chi}{h^3}$; $Fundamental\ period\ (T) = 2\pi\varphi \sqrt{\frac{W_s h^3}{12 g \sum E_c I_c \chi}}$

  where Ω is a correction factor to neutralize the error in predicted lateral stiffness, φ is a correction factor to neutralize the error in predicted fundamental period, χ is a geometric configuration factor, W_s is the seismic weight, h is the storey height, E_c is the Young's modulus of the column, I_c is the gross or effective moment of inertia of the column, and g is the acceleration due to gravity. A flowchart showing the sequence of steps involved in calculating the lateral stiffness and the fundamental period of a frame building is provided in Appendix M.
- The validity of the developed equation in predicting the fundamental period of a frame with fixed or pin bases, with and without variation of section properties along the building height, and with rigid or pin beam-column connections is thoroughly checked by comparing with the fundamental periods obtained from Eigenvalue analysis for a wide range of low to medium rise frame buildings (i.e. up to 10 storeys). Also, the predicted periods are found to be reasonably close to the periods obtained using the Rayleigh method and those measured from experimental tests, and the proposed equation is found to reliably capture the effect of axial shortening of the columns on the fundamental period of braced frame buildings.
- The proposed equations can predict the lateral stiffness and the fundamental period of braced frames within ± 5% of the actual values (obtained from computer analysis). To conclude, the proposed equation is simple, captures the effect of all parameters that are known to affect the fundamental period of frame buildings, requires input parameters that are not difficult to determine, and can be easily implemented in analysis and design tools. As the proposed equation is simple, it can be readily used by practicing engineers in designing new frame buildings as well as in the assessment of existing frame buildings.

9.2 Scope for future research work

9.2.1 *Optimization of the proposed dry steel connections*

As the main aim of the test programme was to demonstrate that it is possible to achieve the cyclic performance of a "wet jointed" precast concrete or monolithic concrete frame system by a precast concrete frame system with the proposed "dry" connections, the steel connections were designed by applying capacity design principles (i.e. strong column/connection-weak beam). For this test programme, the steel connections were designed with a high factor of safety (between 2 and 3) so that any unexpected mode of failure in the connections are eliminated. In reality, the size of the connections can be optimized by reducing thickness of the steel plates, and the number and thickness of gussets. The cost of the connections can be substantially reduced by standardizing the connections for different beam capacities.

9.2.2 *Possible improvements to enhance the performance of the Type-2 and 3 connections*

It is realized that the following improvements can be made to improve the performance of a frame sub-assembly with Type-2 or 3 connections (i.e. angle and tube) and delay the beam edge failure until full yielding of the beam.

- The provided horizontal stirrups (i.e. bursting reinforcement) in the connection zone are effective to a certain extent in resisting the bursting stresses because of the bolts bearing onto the steel ducts and beam edge. To further improve the performance, U shaped steel bars can be placed around the steel ducts along with the bursting stirrups and can be welded to the longitudinal rebars.
- The use of U-shaped longitudinal rebars as top and bottom reinforcement instead of separate bent-up rebars provides additional resistance to the bearing of the bolts (due to slip of the connection).
- Thin steel plates can be embedded around the beams and columns in the connection zone, so that the contact surface will be more level. This will increase the contact area and induce uniform contact pressure, thereby increasing the frictional shear resistance.
- Instead of using less number and large diameter bolts, use of more number and smaller diameter bolts will induce uniform contact pressure, thereby increasing frictional resistance.

9.2.3 *Micro modelling of the tested sub-assemblies with different connection configurations*

In this research, nonlinearity of the connection and the beam under quasi-static cyclic loading was simulated using nonlinear springs connected to the elastic line elements (i.e. macro modelling). With the macro modelling of a frame sub-assembly, it is not possible to simulate the propagation of cracks, bond-slip between the rebars and concrete, interaction of shear with flexural response, and nonlinear contact behaviour between the steel connection plates and precast concrete member surfaces. Nevertheless it is possible to simulate these mechanisms using micro-modelling (i.e. finite element solid modelling) and this can be the scope of a future research work. Also, micro modelling can be very useful to clearly understand the internal load transfer mechanism from the beam to the connection, and from the connection to the column.

9.2.4 *Experimental test programme at building system level*

The experimental tests carried out in this research were on the frame sub-assemblies, where it is not possible to evaluate and study the load transfer mechanism between other building component connections (i.e. floor to floor, floor to beam, column to column, and column to foundation). Also, the ease of erection and assembly of different building components, and difficulties in replacing any damaged components with new ones cannot be experimentally evaluated from a frame sub-assembly test. So, future research work can be aimed to investigate the seismic performance of a demountable precast concrete frame system by utilizing the best “dry” beam-column moment connection (i.e. end plate connection) found in this research. Also, the future research can be targeted to assess the specific objectives such as; (i) identify the challenges involved in assembly and dismantle of the precast concrete building components using the proposed dry connections, (ii) arrive at the erection and deconstruction time required for the different building components and estimate overall project completion time/downtime and compare against conventional monolithic systems, (iii) investigate the seismic performance of the proposed demountable precast concrete frame building system by conducting shake table tests, (iv) enforce the damage to occur in the selected components (say beams and column bases) and replace them with new ones to demonstrate that the building can regain its intended structural performance objective, and (v) numerically and analytically simulate the cyclic behaviour of the demountable precast concrete frame building system and compare with the wet jointed precast concrete or monolithic concrete frame buildings.

Appendix A: Downtime assessment framework for the proposed demountable precast concrete frame building system

A.1 Introduction

The damage state of a building after an earthquake is predominantly characterized by the residual drift in any storey level. In general, a building with the residual drift less than 0.5% in any storey is considered be in a reparable damage state [1]. The guidelines for assessing the damage state of a building post-earthquake can be found in ATC document [2]. The Caltech damage assessment model [3] is also handy in deciding the condition of a building after an earthquake, and the framework is shown in Figure A.1. A building after an earthquake is either green or yellow or red tagged depending on the damage state (i.e. condition of structural and non-structural components). A green tagged building means the damage to structural and non-structural elements is minor, and if egress paths are undamaged, re-occupancy can be immediately after the inspection. A yellow tagged building indicates that the building experienced a moderate level of structural damage (which may not necessarily indicate deterioration of strength) and re-occupancy occurs only after the necessary repair or retrofit/strengthening. A red tagged building is the one which experienced severe structural damage (i.e. spalled concrete, and buckled rebars, etc.) and the building may not feasible to bring back to re-occupancy state by applying any existing repair/retrofit techniques.

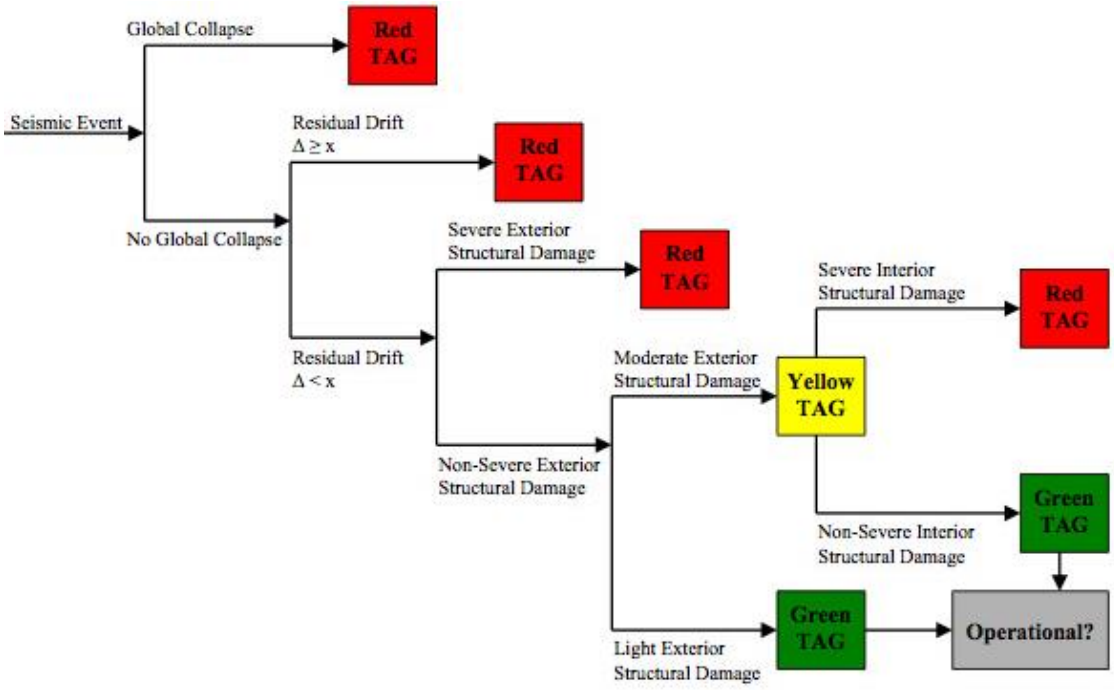

Figure A.1. Caltech damage assessment model to decide the condition of a building [3]

A.2 Retrofit/Strengthening techniques

A.2.1 *Conventional monolithic concrete buildings*

The type of repair/retrofit/strengthening technique that can be applied to an existing building after an earthquake depends on the damage state, available residual seismic capacity and ductility, and cost/benefit analysis of different options [4]. Different retrofit techniques are applied to increase either the lateral strength or ductility or both of a conventional monolithic concrete building. The typical strengthening techniques adopted in Japan are shown in Figure A.2. The most common retrofit techniques to strengthen a concrete building are by; (i) adding new shear walls connected to the new foundations, (ii) jacketing of existing columns and beams, and (iii) addition of steel braces, whereas the ductility capacity is increased by (i) carbon or fibre wrapping of critical regions of non-ductile frame components, and (ii) steel encasement/strapping. Because of many available retrofit techniques, the decision making time to finalize the retrofit option is influenced by many factors such as (i) evaluation of the residual lateral strength and ductility capacity of an existing building, (ii) identification of an appropriate strategy for that particular damaged building so that the repaired/retrofitted building meets the target, and (iii) assessment of economic feasibility. This is one "impending factor" that contributes significantly to downtime (i.e. time to re-occupy the repaired/retrofitted building) in case of conventional monolithic concrete frame buildings.

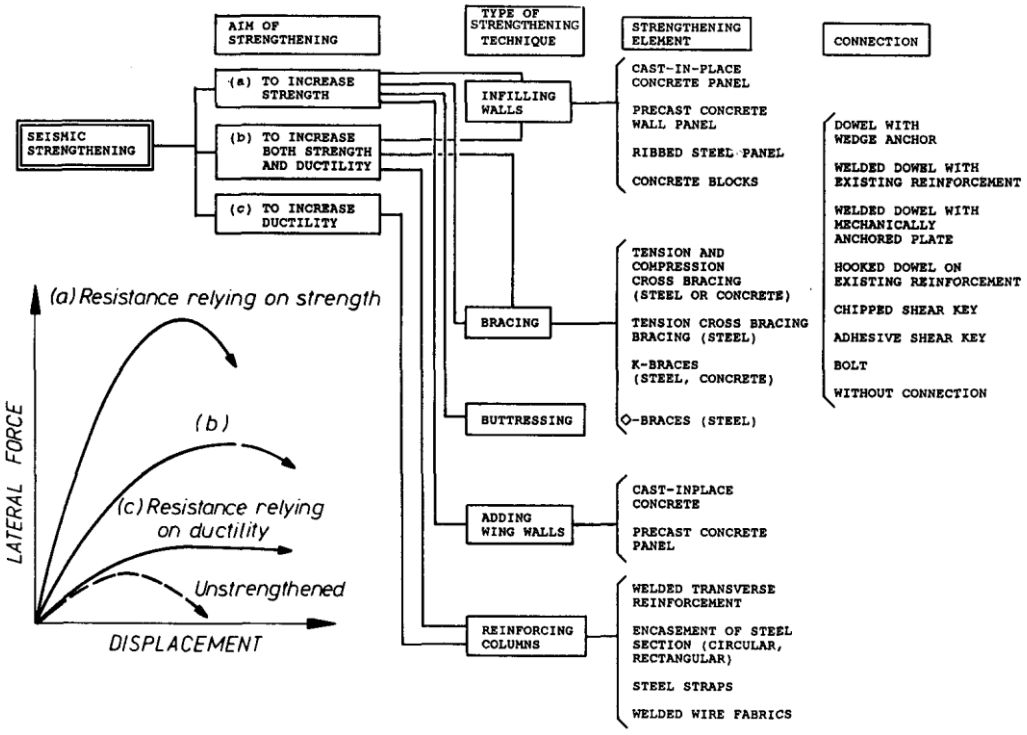

Figure A.2. Typical retrofit techniques adopted to strengthen the concrete buildings [4]

A.2.2 *Proposed demountable concrete building*

The repair/retrofit strategy for the proposed demountable building system damaged in an earthquake shaking is a straight forward process; replace the damaged building components with new ones. It is important to note that the replacement strategy may not be feasible in the following cases; (i) the majority (say more than 50%) of internal frame components (i.e. beams and columns) are damaged, (ii) many slab components (in the proposed building system damage to the slabs is avoided by providing slotted connections but when the demand exceeds a particular limit there is a possibility of damage to the slabs) along with frame components are also damaged (replacement of damaged slabs is not possible because of heavy weight and constrained degree of movement in a building), and (iii) if the building site has no space for the tower cranes and other lifting vehicles (to remove the damaged components).

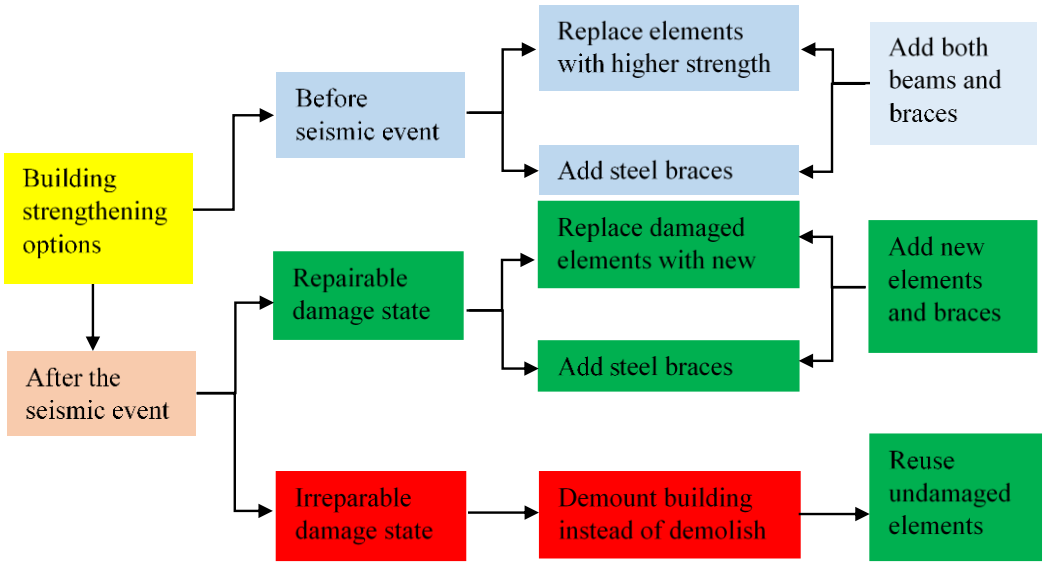

Figure A.3. Strengthening options for the proposed demountable building system

The proposed building system can be strengthened/upgraded at any time to resist high seismic demand by replacing weaker beams with stronger beams while maintaining the "strong column-weak beam" strength hierarchy. The building system can also be upgraded by addition of steel braces to the lateral load resisting frames, which is easy because the beam-column connections are steel connections with gussets to which the braces can be connected (with initial planning the upgrading process can be simple and easy). A building which is in repairable damage state can be brought to functional state either by replacing the damaged components with new components or by addition of new components (steel braces) or both. A building which is in irreparable damage state can be deconstructed and undamaged components can be reused (the reuse is only possible if the precast concrete components are

in standard sizes like steel sections). The process of strengthening/upgrading of a building either before or after a seismic event is shown in Figure A.3.

A.3 Downtime assessment/estimation for a damaged building/structure

A.3.1 *Downtime framework*

Downtime in the seismic context is defined as the time required to bring the damaged building/structure to the desired recovery state (i.e. re-occupancy, functional recovery, and full recovery) after an earthquake. Downtime for a particular damaged building depends on the desired recovery state. The major factors that need to be considered in downtime assessment of a structure are shown in Figure A.4 [1]; (i) impending factors such as post-earthquake inspection, decision making time (repair or demolition), engineering mobilization and review/re-design, financing, contractor mobilization and bid process, permitting, and procurement of long-lead time components, (ii) utilities such as pipelines, transmission towers, roads, and bridges etc., and (iii) damage state of the structure itself (i.e. repair class 1: cosmetic damage to structural or non-structural components, repair class 2: severe damage to non-structural components and minor damage to structural components, and repair class 3: heavy damage to structural and non-structural components).

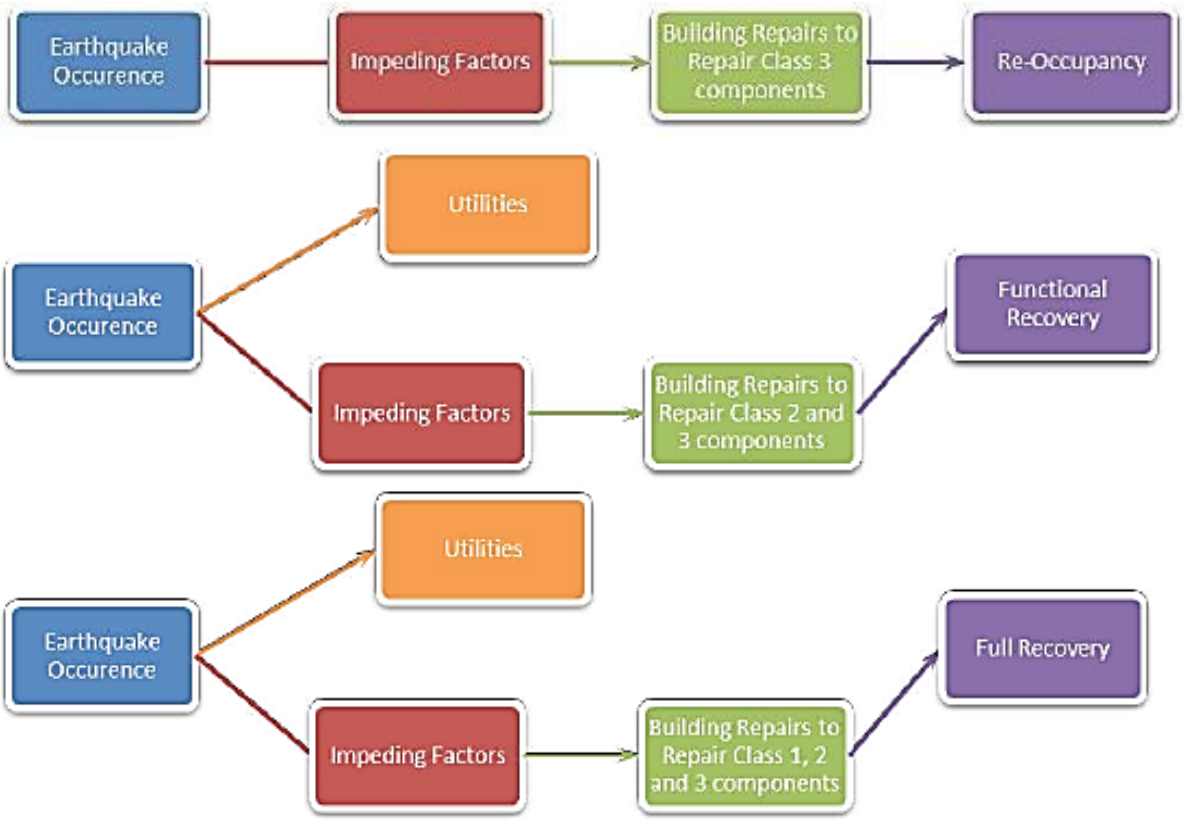

Figure A.4. Downtime framework to achieve different recovery states [1]

It is important to realize that the repair/replacement time of a damaged building is only a subset of overall downtime. In many cases, the repair time is only a small fraction of recovery process time and the impending factors are major contributors to the overall downtime. The repair time depends on the damage state of the building and the adopted repair/retrofit strategy. Some retrofit techniques are economical but require more time to repair (for example, addition of new shear walls and foundations), whereas some retrofit techniques are costly but the building can be repaired in quickly (such as the addition of viscous dampers or bucking restrained braces to the lateral load resisting frames) [4]. Because of interaction of many complex and uncontrolled activities, it is not possible to assess/estimate the actual downtime required to achieve the desired recovery state. But, a qualitative downtime assessment can be made by utilizing the data from past earthquakes. In conventional monolithic concrete buildings, "repair time" is referred as the actual time required to repair/retrofit the damaged structural components, whereas for the proposed demountable concrete building system, it is appropriate to use "replacement time" rather than "repair time", which is defined as the actual time required to replace the components.

Table A.1. Different scenarios considered for the downtime assessment

Case	Scenario	Retrofit strategy
1	A MC building is structurally damaged and requires redesign/review to identify appropriate retrofit strategy.	Addition of new braces and foundations.
2	A DC building is structurally damaged and requires redesign of new braces to fit to existing connections and foundations.	Addition of new braces.
3	Perimeter frames of a DC building are structurally damaged and require the components to be replaced (4 columns and 24 beams).	Replace the damaged beams and columns.
4	Perimeter and internal frames of a DC building are structurally damaged and require the components to be replaced (4 perimeter and 4 interior columns, 24 perimeter and 20 interior beams).	Replace the damaged beams and columns.
5	Steel braces of a braced DC building are structurally damaged and require the braces to be replaced (12 brace units damaged).	Replace the damaged braces.
MC: Monolithic concrete; DC: Demountable concrete		

A.3.2 *Downtime assessment for different damage state scenarios*

In this section, an approximate downtime assessment is carried out for different damage state scenarios for the proposed demountable building system and a comparison is made with conventional monolithic concrete frame building. The time required to decide (i.e. decision making time) whether a conventional monolithic building can be repaired or needs to be demolished is considerably higher (because of many uncertainties as listed before) compared to the proposed demountable building system (because of well-defined repair/retrofit and dismantling strategy), and this time will be even longer if the building is insured (which was the

common case for the buildings located in Christchurch). It is important to note that in the estimation of downtime, impending factors related to review/re-design of a damaged building and repair/replacement time are variable, but it is assumed here that all other impending factors and utility disruption are same for all cases. The different cases considered for the downtime assessment are reported in Table A.1. In all cases, the building is a five storey frame provided with moment resisting frames in both directions with internal frames resisting predominantly gravity loads, and perimeter frames resisting lateral forces. The building is square in plan with four bays in both directions, with each bay of span length 6 m and storey height of 3.6 m.

Table A.2. Important activities in the redesign/review, and retrofit process of a MC building

Activity	**Major activities in the redesign and review process of damaged building**
1	Stage-1:Junior engineer -assess the capacity of the damaged building, redesign and review
2	Stage-1:Senior engineer-review the redesign of the damaged building/ retrofit strategy
3	Stage-1:Drafting of structural drawings of the retrofitted building
4	Stage-1:Peer review of structural design/drawings of the retrofitted building
5	Stage-2:Junior engineer –revise and redesign of the building by incorporating comments
6	Stage-2:Senior engineer-review of the revised design of the retrofitted building
7	Stage-2:Finalizing of structural drawings of retrofitted building
8	Stage-2:Peer review process /approval for construction
	Major activities in retrofit process of structural components only
A	Setting up of the formwork around the building
B	Installation of new foundations to which braces are to be connected
C	Location of the rebar in beams and columns of the bays that are to be braced
D	Drilling of the anchor holes to set up the connection (for each joint)
E	Fabrication of the connection plates
F	Fabrication of the braces
G	Setting up of anchor connection plates, aligning, and curing time
H	Erection of each brace unit

Case-1: A MC building is structurally damaged and requires redesign/review to identify the appropriate retrofit strategy. To estimate the downtime required to retrofit the damaged building, it is very important to identify all the activities that need to be either sequentially or simultaneously carried out along with the optimistic time, most likely time, and pessimistic time to complete each activity. For the chosen damaged building, the final retrofit option was to add X steel braces to one bay of the lateral load resisting frames in both directions. It was found that the new foundations are required as the existing foundations were not strong enough. The cracks of the damaged building components will be epoxied. The important activities in the redesign and retrofit process of MC building with addition of braces as final retrofit option are listed in Table A.2. As per this sequence, time for each activity in the rede-

sign/review process is assigned as shown in Table A.3. Also, the time for each activity in retrofit process is assigned based on the author understanding of the building construction (this can differ from person to person) as reported in Table A.3.

A Gantt chart is constructed by using the estimated time for each activity (in terms of days), which is shown in Figure A.5. The time required for the complete redesign/review process and to identify the appropriate retrofit strategy for the damaged monolithic concrete building is approximately 22 weeks. This time estimation to redesign/review process is in line with the time reported in REDi guideline, which is approximately 20 weeks (assuming that the building is in repair class-3) as shown in Figure A.6 [1]. The approximate time to complete structural retrofit for the monolithic concrete building is 30 weeks.

Table A.3. Time for each activity in review/redesign and retrofit process

Activity	Quantity	OT	MT	PT	ET (for each quantity)		ET (for total quantity)	
1	1	4	6	8	6.0	weeks	42.00	days
2	1	1	2	3	2.0	weeks	14.00	days
3	1	2	2.5	3	2.5	weeks	17.50	days
4	1	2	3	4	3.0	weeks	21.00	days
5	1	3	4	6	4.17	weeks	29.17	days
6	1	1	1.5	2	1.50	weeks	10.50	days
7	1	1	1.5	2	1.50	weeks	10.50	days
8	1	1	1.5	2	1.50	weeks	10.50	days
A	4	1	1.5	2	1.5	weeks	42.00	days
B	4	2	4	6	4.0	weeks	112.00	days
C	4	0.28	0.57	1	0.6	weeks	16.61	days
D	40	0.07	0.14	0.28	0.2	weeks	42.47	days
E	80	0.07	0.14	0.21	0.1	weeks	78.40	days
F	80	0.07	0.14	0.28	0.2	weeks	84.93	days
G	40	0.14	0.21	0.28	0.21	weeks	58.8	days
H	40	0.07	0.14	0.28	0.2	weeks	42.47	days
OT: optimistic time; MT; most likely time; PT: pessimistic time; ET: estimated time								

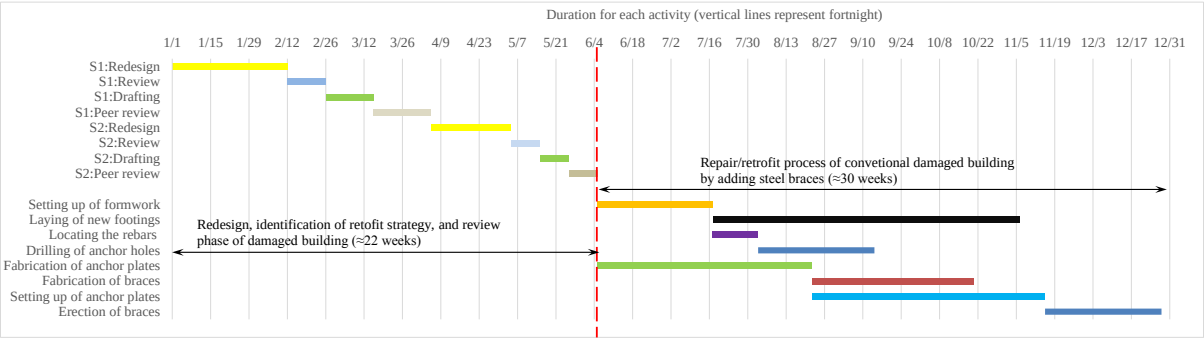

Figure A.5. Gantt chart showing the time to complete redesign and retrofit process for the damaged monolithic concrete building

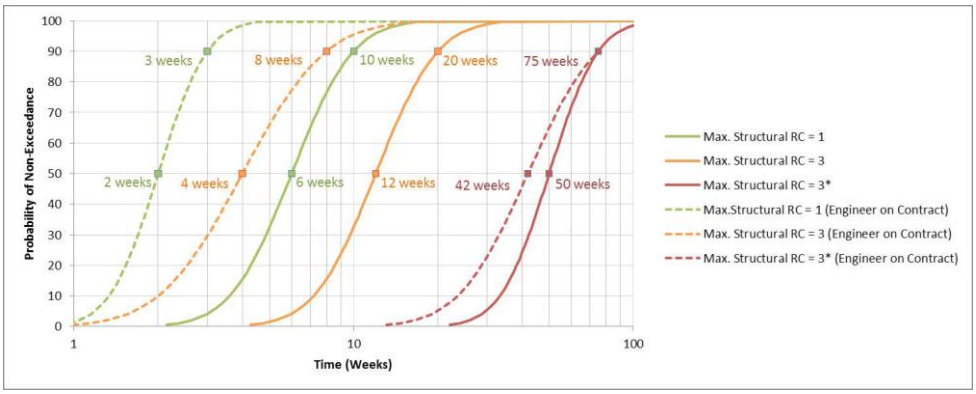

Figure A.6. Probable time required for re-design/review of building in different repair class (RC)

Case-2: A demountable concrete building is damaged and the identified retrofit strategy is to add new steel braces (similar to case-1) to the lateral load resisting frames. In this case, the foundations and beam-column connections were pre-designed to accommodate new braces. The major activities involved in redesign/review and retrofit for this case are listed in Table A.4 and the time required to complete each activity are reported in Table A.5.

Table A.4. Important activities in the redesign/review, and retrofit process of a DC building (Case-2)

Activity	**Major activities in the redesign and review process of damaged building**
1	Stage-1:Junior engineer -design the braces that fit to the existing connections and foundations
2	Stage-1:Senior engineer-review the redesign of the damaged building/ retrofit strategy
3	Stage-1:Drafting of structural drawings of the retrofitted building
4	Stage-1:Peer review of structural design/drawings of the retrofitted building/approval
	Major activities in retrofit process of structural components only
A	Setting up of the formwork around the building
B	Fabrication of the braces
C	Erection of each brace unit

Table A.5. Time for each activity in review/redesign and retrofit process (Case-2)

Activity	Quantity	OT	MT	PT	ET (for each quantity)		ET (for total quantity)	
1	1	2	3	4	3.0	weeks	21.00	days
2	1	1	1.5	2	1.5	weeks	10.50	days
3	1	1	1.5	2	1.5	weeks	10.50	days
4	1	1	2	3	2.0	weeks	14.00	days
A	4	1	1.5	2	1.5	weeks	42.00	days
B	40	0.14	0.21	0.28	0.21	weeks	58.80	days
C	40	0.07	0.14	0.28	0.2	weeks	42.47	days
OT: optimistic time; MT; most likely time; PT: pessimistic time; ET: estimated time								

The approximate times required to complete redesign/review process and retrofit process is 8 and 15 weeks, respectively. A Gantt chart showing duration for each activity is shown in Figure A.7.

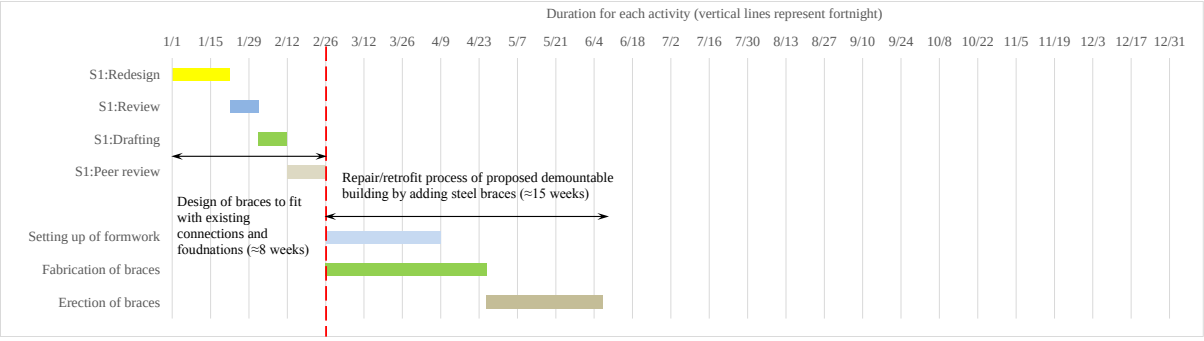

Figure A.7. Gantt chart showing the time to complete redesign and retrofit process for the damaged demountable concrete building (Case-2)

Case-3: A demountable concrete building is damaged and the damage is concentrated to the perimeter frame beams and columns, and it was found that 4 columns and 24 beams were damaged. The identified retrofit strategy is to replace the damaged components with new ones of same strength. The major activities involved in redesign/review and retrofit for this case are listed in Table A.6 and the time required to complete each activity are reported in Table A.7.

Table A.6. Important activities in the redesign/review, and retrofit process of a DC building (Case-3)

Activity	**Major activities in the redesign and review process of damaged building**
1	Junior engineer -Identification of drawings of damaged components
2	Senior engineer-review of damaged components drawings
3	Peer review of replacement strategy
	Major activities in retrofit process of structural components only
A	Shore the damaged components and floors
B	Fabrication of new components
C	Remove damaged columns and replace with new ones
D	Remove damaged beams and replace with new ones

Table A.7. Time for each activity in review/redesign and retrofit process (Case-3)

Activity	Quantity	OT	MT	PT	ET (for each quantity)		ET (for total quantity)	
1	1	1	1.5	1.5	1.4	weeks	9.92	days
2	1	0.5	1	1.5	1.0	weeks	7.00	days
3	1	0.5	1	1.5	1.0	weeks	7.00	days
A	4	1	1.5	2	1.5	weeks	42.00	days
B	28	0.42	0.21	0.28	0.26	weeks	50.3	days
C	4	1	1.5	2	1.5	weeks	42.00	days
D	24	0.28	0.42	0.57	0.42	weeks	70.84	days
OT: optimistic time; MT; most likely time; PT: pessimistic time; ET: estimated time								

The approximate time required to complete redesign/review process and to replace the damaged components with new ones is 4 and 24 weeks, respectively. A Gantt chart showing the duration for each activity is shown in Figure A.8.

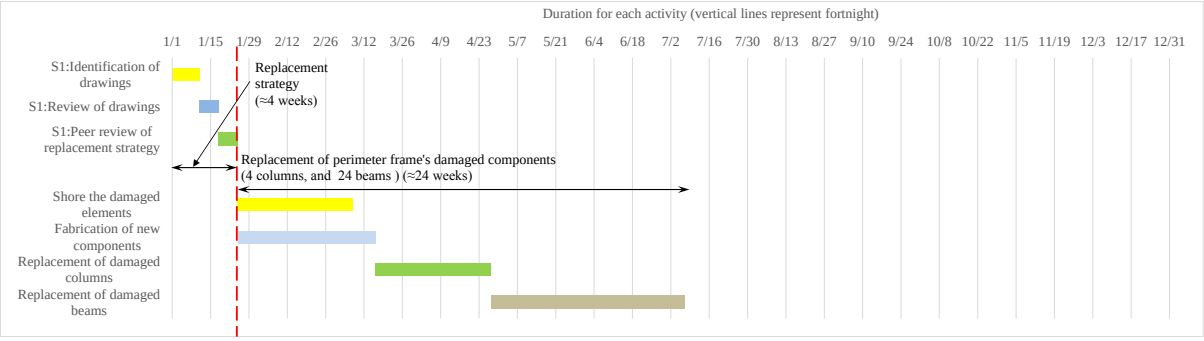

Figure A.8. Gantt chart showing the time to complete redesign and retrofit process for the damaged demountable concrete building (Case-3)

Case-4: A demountable concrete building is damaged and the damage is spread across perimeter and internal frames. It was found that 4 columns and 24 beams of perimeter frames and 4 columns and 20 beams of internal frames were damaged. The identified retrofit strategy is to replace the damaged components with new ones of same strength. The major activities involved in redesign/review and retrofit for this case are listed in Table A.8 and the time required to complete each activity are reported in Table A.9.

Table A.8. Important activities in the redesign/review, and retrofit process of a DC building (Case-4)

Activity	**Major activities in the redesign and review process of damaged building**
1	Junior engineer -Identification of drawings of damaged components
2	Senior engineer-review of damaged components drawings
3	Peer review of replacement strategy
	Major activities in retrofit process of structural components only
A	Shore the damaged components and floors
B	Fabrication of new components
C	Remove damaged perimeter columns and replace with new ones
D	Remove damaged perimeter beams and replace with new ones
E	Remove damaged interior columns and replace with new ones
F	Remove damaged interior beams and replace with new ones

Table A.9. Time for each activity in review/redesign and retrofit process (Case-3)

Activity	Quantity	OT	MT	PT	ET (for each quantity)		ET (for total quantity)	
1	1	1	1.5	1.5	1.4	weeks	9.92	days
2	1	0.5	1	1.5	1.0	weeks	7.00	days
3	1	0.5	1	1.5	1.0	weeks	7.00	days
A	4	1	1.5	2	1.5	weeks	42.00	days
B	28	0.42	0.21	0.28	0.26	weeks	50.3	days
C	4	1	1.5	2	1.5	weeks	42.00	days
D	24	0.28	0.42	0.57	0.42	weeks	70.84	days
E	4	1.5	2	3	2.1	weeks	58.33	days
F	20	0.42	0.57	1	0.62	weeks	86.33	days
OT: optimistic time; MT; most likely time; PT: pessimistic time; ET: estimated time								

The approximate times required to complete redesign/review process and to replace the damaged components with new ones is 4 and 44 weeks, respectively. A Gantt chart showing the duration for each activity is shown in Figure A.9.

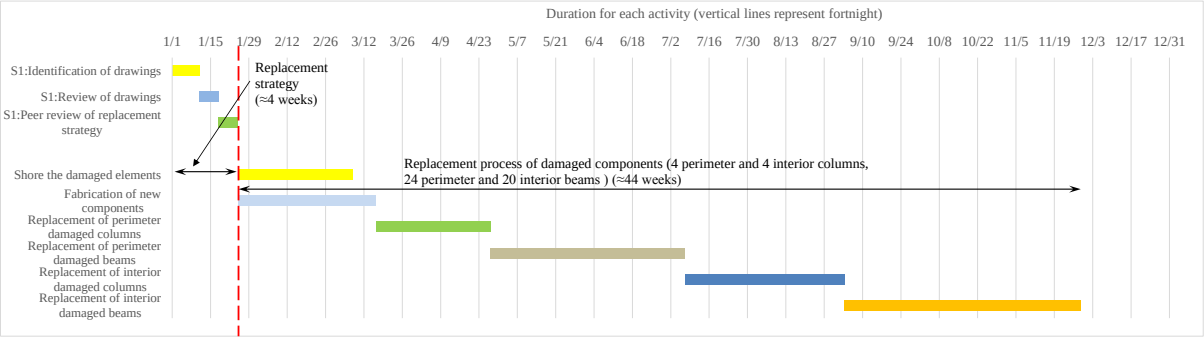

Figure A.9. Gantt chart showing the time to complete redesign and retrofit process for the damaged demountable concrete building (Case-4)

Case-5: A braced demountable concrete building is damaged and the damage is concentrated only to the braces, and it was found that a total of 12 brace units were damaged. The identified retrofit strategy is to replace the damaged braces with new ones of same capacity. The major activities involved in redesign/review and retrofit for this case are listed in Table A.10 and the time required to complete each activity are reported in Table A.11.

Table A.10. Important activities in the redesign/review, and retrofit process of a DC building (Case-3)

Activity	**Major activities in the redesign and review process of damaged building**
1	Junior engineer -Identification of drawings of damaged components
2	Senior engineer-review of damaged components drawings
3	Peer review of replacement strategy
	Major activities in retrofit process of structural components only
A	Removal of damaged braces
B	Fabrication of new braces
C	Time required to set up each brace unit

Table A.11. Time for each activity in review/redesign and retrofit process (Case-3)

Activity	Quantity	OT	MT	PT	ET (for each quantity)		ET (for total quantity)	
1	1	1	1.5	1.5	1.4	weeks	9.92	days
2	1	0.5	1	1.5	1.0	weeks	7.00	days
3	1	0.5	1	1.5	1.0	weeks	7.00	days
A	12	0.07	0.14	0.28	0.2	weeks	12.74	days
B	12	0.14	0.21	0.28	0.21	weeks	17.6	days
C	12	0.07	0.14	0.28	0.2	weeks	12.74	days
OT: optimistic time; MT; most likely time; PT: pessimistic time; ET: estimated time								

The approximate times required to complete redesign/review process and to replace the damaged components with new ones is 4 and 4 weeks, respectively. A Gantt chart showing the duration for each activity is shown in Figure A.10.

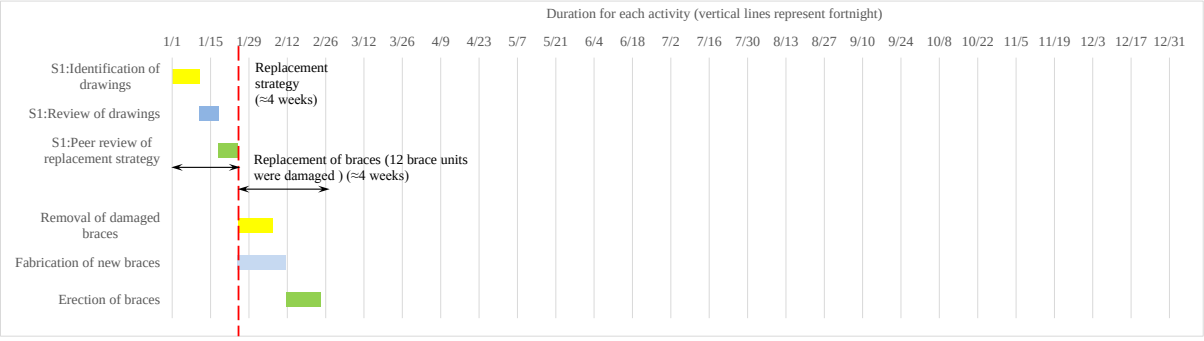

Figure A.10. Gantt chart showing the time to complete redesign and retrofit process for the damaged demountable concrete building (Case-4)

A.3.3 *Comparison of downtime*

The summary of time required to complete the redesign and review, and retrofit the damaged monolithic and demountable concrete buildings with different damage state scenarios are reported in Table A.12. By utilizing the downtime assessment framework and results reported in Table A.12, the following important observations can be made regarding downtime; (i) downtime is a function of both number of activities and the time required to complete activity, (ii) downtime depends on number of simultaneous and sequential activities, and (iii) downtime depends on the accuracy of estimated time (i.e. most likely time).

Table A.12. Comparison of review/redesign time, and repair/retrofit time for different scenarios

Case	Scenario	Repair/Retrofit	Redesign time	Retrofit time	Total time
1	Monolithic concrete building damaged	Addition of new braces and foundations	22 weeks	30 weeks	52 weeks
2	Demountable concrete building damaged	Addition of new braces	8 weeks	15 weeks	23 weeks
3	Demountable concrete building damaged	Replacement of perimeter frame elements	4 weeks	24 weeks	28 weeks
4	Demountable concrete building damaged	Replacement of perimeter and internal frame elements	4 weeks	44 weeks	48 weeks
5	Braced demountable concrete building damaged	Replacement of braces	4 weeks	4 weeks	8 weeks

It is clear that the monolithic concrete building requires more time in redesign/review because of uncertainty in identification of retrofit strategy and process. Also, it requires more time to retrofit because of many activities to be performed to bring the damaged building to usable state. In case of the proposed demountable concrete building system, the

redesign/review time is considerably less as compared to the MC building, this is because of well-defined repair/retrofit strategy; i.e. replacement of damaged components. The time required to replace the damaged components can vary a lot depending on the number of damaged components, location of damaged components, number of activities that need to be performed before the replacement of damaged components, and time required to replace each component type. It is clear from Table A.12, replacement of damaged braces requires the least amount of time, whereas replacement of internal frame components along with the perimeter frame components needs maximum time.

A.4 Concluding remarks

Downtime assessment of a damaged building is a complex process as it involves the interrelation of many uncertain activities and uncertain time associated with each activity. It can be concluded that the decision making time (although this cannot be explicitly quantified) about the condition of the building and the nature of action that be performed (i.e. repair or demolition), and the time required to redesign/review a damaged demountable concrete building system is less compared to that of a monolithic concrete building because of the well-defined retrofit strategy. The repair/replacement time required for the proposed demountable concrete building system can vary a lot depending on the number and location of damaged components, and other activities that need to be performed before the actual replacement.

A.5 References

1. Almufti, I. and M. Willford, *REDiTM Rating System: Resilience-based Earthquake Design Initiative for the Next Generation of Buildings.* ARUP Co, 2013.
2. ATC-20, *Procedures for Postearthquake Safety Evaluation of Buildings*. 1989, Applied Technology Council: San Francisco.
3. Beck, J.L. *Loss Modeling for Downtime, Deaths and Decision-Making*. 2006; Available from: http://peer.berkeley.edu/research/funded_projects_1/project_1362005.html.
4. Rodriguez, M. and R. Park, *Repair and strengthening of reinforced concrete buildings for seismic resistance.* Earthquake Spectra, 1991. **7**(3): p. 439-459.

Appendix B: Analysis and design details of the benchmark building

B.1 Summary of the analysis results

It was assumed that concrete slab of thickness 150 mm is sufficient to resist the combination of factored loads. The summary of calculations to arrive at the seismic weight of the benchmark building is given in Table B.1. Also, the combinations of the loads considered for the analysis and design at ultimate and serviceability limit states is reported in Table B.1. The summary of fundamental periods of the building with and without consideration of slab contribution to the lateral stiffness in the orthogonal directions at ULS and SLS is given in Table B.2. It can be observed that 100% change in the fundamental period of building by comparing with gross and effective section properties. Also, the slab stiffness also contributes significantly to the overall lateral stiffness of the frame and thereby to the fundamental period of the building. The identification numbers for the beams and columns of the perimeter frame to be used in analysis and the design is shown in Figure B.1. The un-factored demands on the members of the perimeter frame is shown in Figure B.1.

Table B.1. Seismic weight calculation and load combinations for the analysis and design

Dead load (DL)		**Load combinations**		
DL on floors	Roof: 4.75 kN/m^2 ;Other: 4.25 kN/m^2	**Reference**	**ULS**	**ULS**
Column:C1	0.6×0.6×18×16×23.5=2436.48 kN	DCON1	1.35D	D
Column:C2	0.4×0.4×18×9×23.5=609.12 kN	DCON2	1.2D+1.5L	D+0.7L
Beam:B1 & B2	0.3×0.4×24×5×23.5=3384 kN	DCON3	D+0.3L+E_{ux}	D+0.3L+E_{sx}
Total DL	18957.6 kN	DCON4	D+0.3L-E_{ux}	D+0.3L-E_{sx}
Reduced live load (RLL)		DCON5	D+0.3L+E_{uy}	D+0.3L+E_{uy}
Roof	(0.3+3/√576=0.425≥0.5)×2.5×576=748.8 kN	DCON6	D+0.3L-E_{uy}	D+0.3L-E_{sy}
Other floors	(0.3+3/√576=0.425≥0.5)×3×4×576=3456 kN	DCON7	D+E_{ux}	D+E_{sx}
Total RLL	748.8+3456=4204.8 kN	DCON8	D-E_{ux}	D-E_{sx}
Seismic weight (SW)		DCON9	D+E_{uy}	D+E_{uy}
DL +0.3×RLL	18957.6+0.3×4204.8=20219 kN	DCON10	D-E_{uy}	D-E_{sy}

Table B.2. Summary of fundamental period at different limit states

Section properties and slab contribution	**Fundamental period (sec)**	
	ULS	**SLS**
Effective section properties and without slab	1.97	1.44
Effective section properties and with slab	1.34	1.14
Gross section properties and without slab	1.23	
Gross section properties and with slab	1.03	

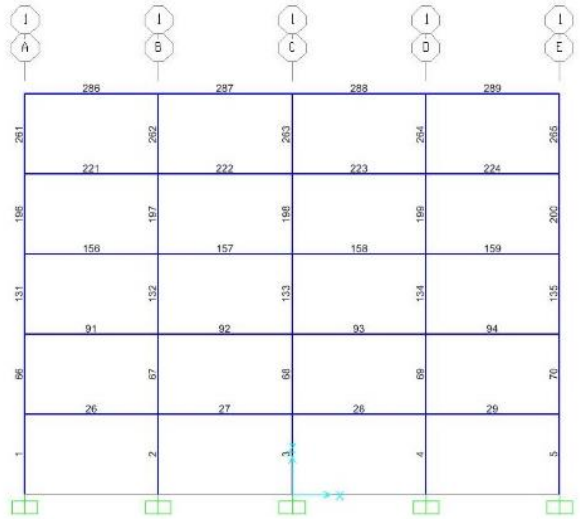

(a) Identification number

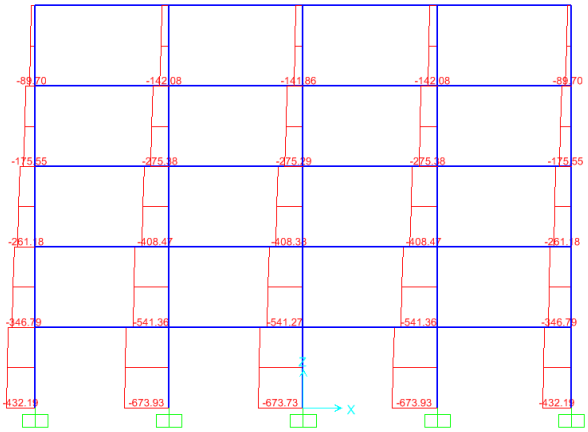

(b) AFD-Dead load

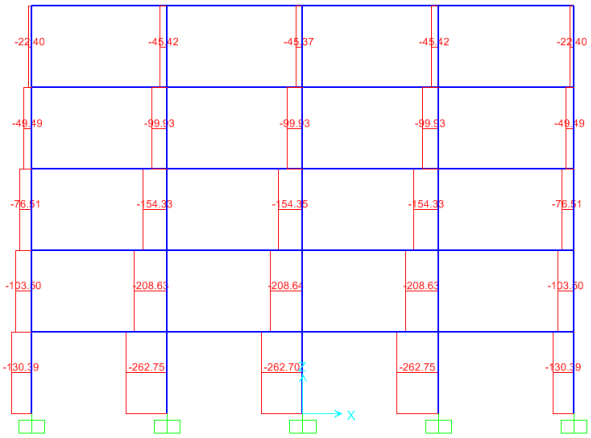

(c) AFD-Live load

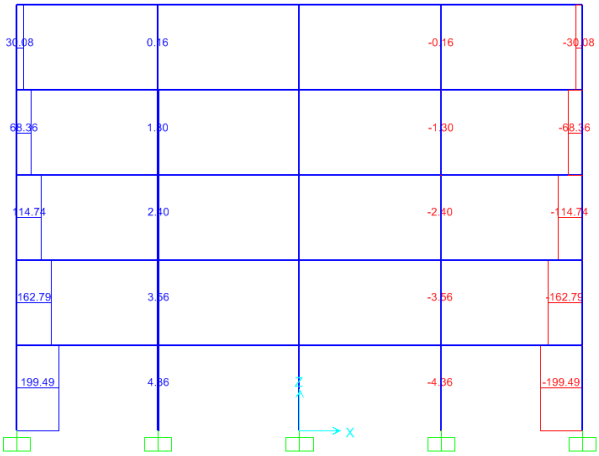

(d) AFD-Earthquake load

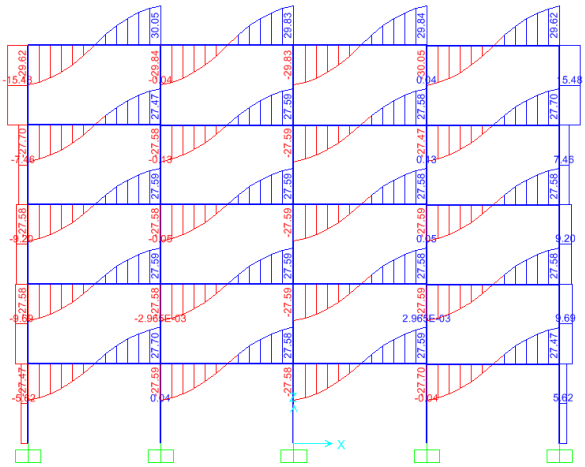

(e) SFD-Dead load

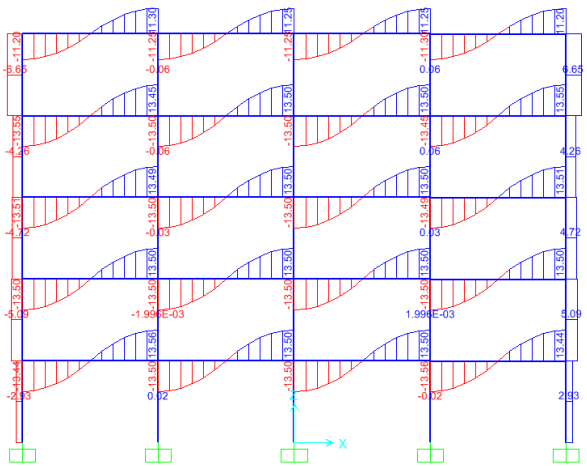

(f) SFD-Live load

Figure B.1. Demands on perimeter frame under unfactored loads (continuded)

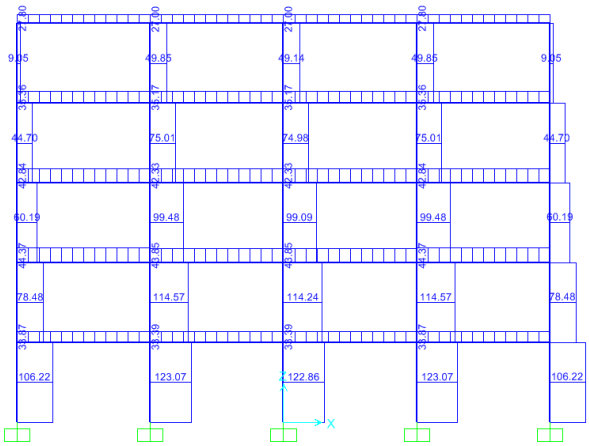

(g) SFD-Earthquake load

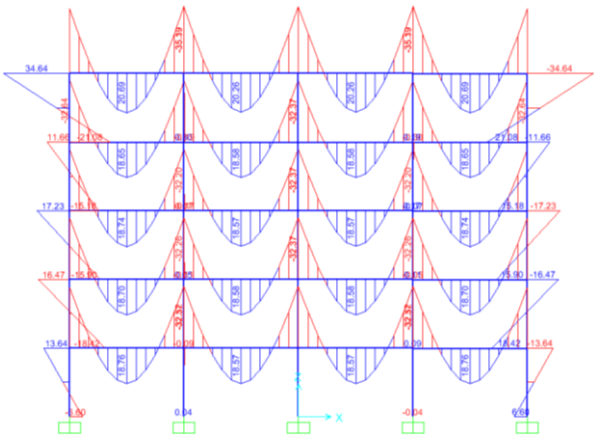

(h) BMD-Dead load (DL)

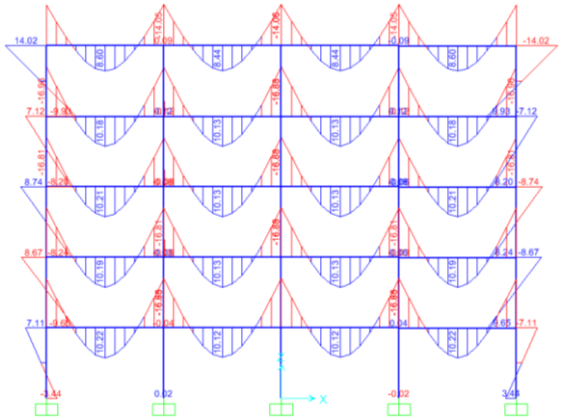

(i) BMD-Live load (LL)

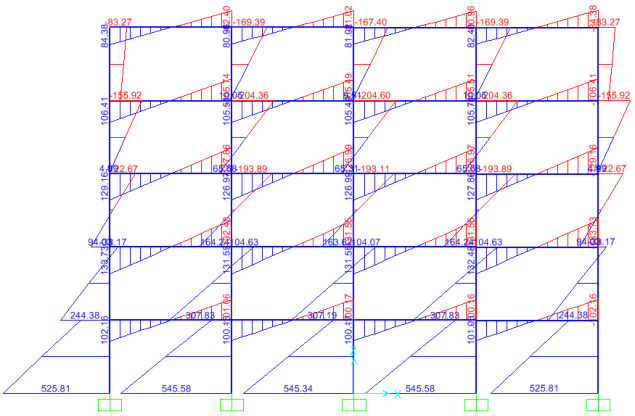

(j) BMD-Earthquake load (Eu)

Figure B.1. Demands on perimeter frame under unfactored loads

B.2 Inter-storey drift check including P- Δ effects

The summary of the calculations showing inter-storey lateral deformation including P- Δ is reported in Table B.3.

Table B.3. Inter-storey deformation calculation including P- Δ

Storey no	Storey shear (kN)	Seismic weight (kN)	Deformation (mm)	Deformation×μ×k_{dm} (mm)	Stability coefficient
1	2,426.28	3,993.12	11.00	33.26	0.08
2	2,280.56	3,993.12	32.43	98.07	0.13
3	1,989.10	3,993.12	55.00	166.32	0.12
4	1,551.91	3,993.12	74.20	224.38	0.09
5	968.99	4,246.56	88.65	268.08	0.05
P-Δ storey shear (kN)	**P-Δ force (kN)**	**P-Δ deflection (mm)**	**P- Δ deflection ×μ×β (mm)**	**Total deformation (mm)**	**Inter-storey drift (%)**
186.82	-105.26	1.64	6.73	39.99	1.11
292.09	60.17	5.24	21.50	119.57	2.21
231.92	99.03	8.91	36.57	202.89	2.31
132.89	81.34	11.67	47.89	272.27	1.93
51.54	51.54	13.46	55.24	323.32	1.42

B.3 Concrete design results

The detailed calculation for a column and beam of the perimeter frame is reported below. The summary of required rebar percentage, shear area per unit length, and capacity to demand ratios for the column are shown in Figure B.2.

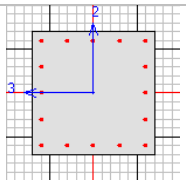

NZS 3101:2006 COLUMN SECTION DESIGN Type: Limited Units: KN, m, C
Element: 5
Station Loc 0.000
Section ID C1
Combo ID DCON9
Understrength Factors
Bending/Tension=0.85 Shear=0.75
Compression=0.85
L=3.600
B=0.600 D=0.600 dc=0.043
E=20997000.00 fy=500000.000 fc=40000.000 Light Wt. Shr. Fac.=1.000 fys=500000.000
RLLF=1.000

AXIAL FORCE & BIAXIAL MOMENT CHECK FOR PU, M2, M3

Capacity Ratio	Design Pu	Design M2	Minimum M3	Minimum M2	M3
0.878	232.704	760.043	63.767	0.000	0.000

AXIAL FORCE & BIAXIAL MOMENT FACTORS

	Cm Factor	Delta_b Factor	Delta_s Factor	K Factor	L Length
Major Bending(M3)	0.582	1.000	1.000	1.000	3.600
Minor Bending(M2)	0.718	1.000	1.000	1.000	3.600

SHEAR DESIGN FOR V2,V3

	Design Rebar	Shear Vu	Shear phi*Vc	Shear phi*Vs	Shear Vp
Major Shear(V2)	0.003	762.456	155.903	606.553	762.45
Minor Shear(V3)	0.003	762.456	155.903	606.553	762.456

NZS 3101:2006 BEAM SECTION DESIGN Type: Limited Units: KN, m, C
Element: 91
Station Loc 0.000
Section ID B1
Combo ID DCON4
Understrength Factors
Bending/Tension=0.85 Shear=0.75
Compression=0.85
L=6.000
B=0.300 D=0.400 bf=0.300 ds=0.000 dct=0.020 dcb=0.020
E=20997000.00 fy=500000.000 fc=40000.000 Light Wt. Shr. Fac.=1.000 fys=500000.000
DESIGN MOMENTS, M3

Positive Moment	Negative Moment	Special +Moment	Special -Moment
0.000	-170.977	64.116	-170.977

FLEXURAL REINFORCEMENT FOR MOMENT, M3

	Required Rebar	+Moment Rebar	-Moment Rebar	Minimum Rebar
Top (+2 Axis)	0.001	0.000	0.001	3.605E-04
Bottom (-2 Axis)	4.077E-04	4.077E-04	0.000	3.605E-04

SHEAR REINFORCEMENT FOR SHEAR, V2

Design Rebar	Shear Vu	Shear phi*Vc	Shear phi*Vs	Shear Vp
8.688E-04	177.875	54.075	123.800	146.250

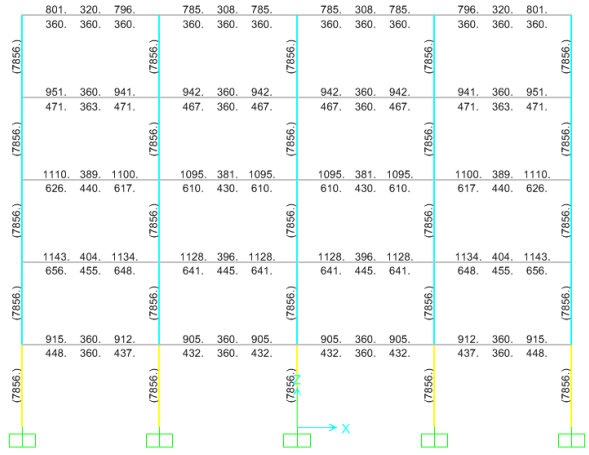

(a) Rebar area (mm^2)

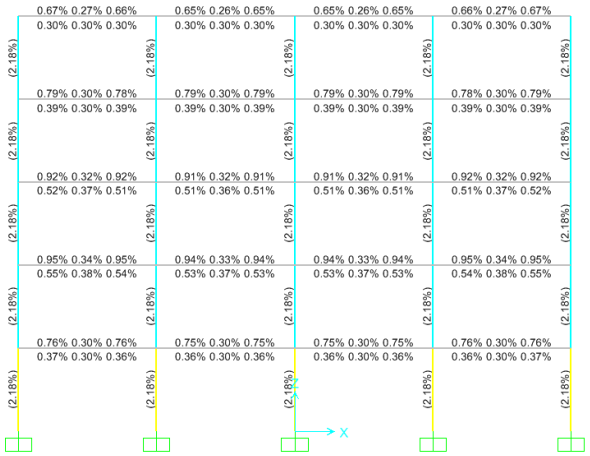

(b) Rebar percentage (%)

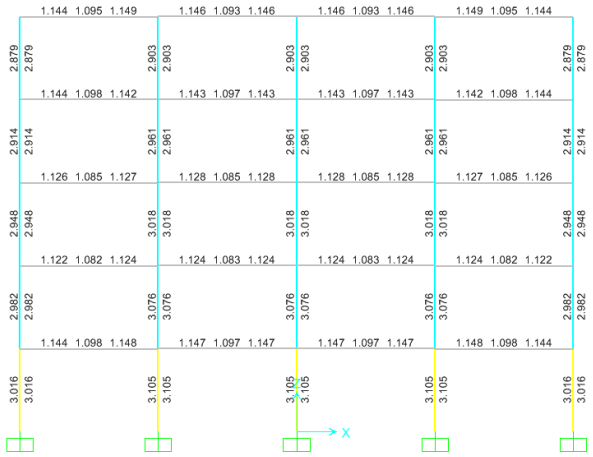

(c) Shear area per unit length (mm^2/mm)

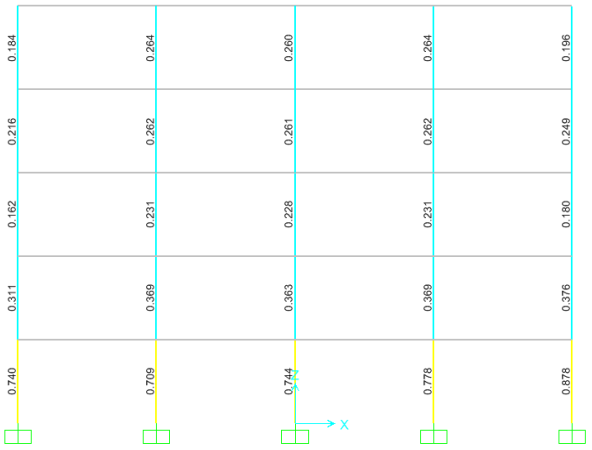

(d) Column-PMM demand/capacity ratio

Figure B.2. Summary of design results of perimeter frame

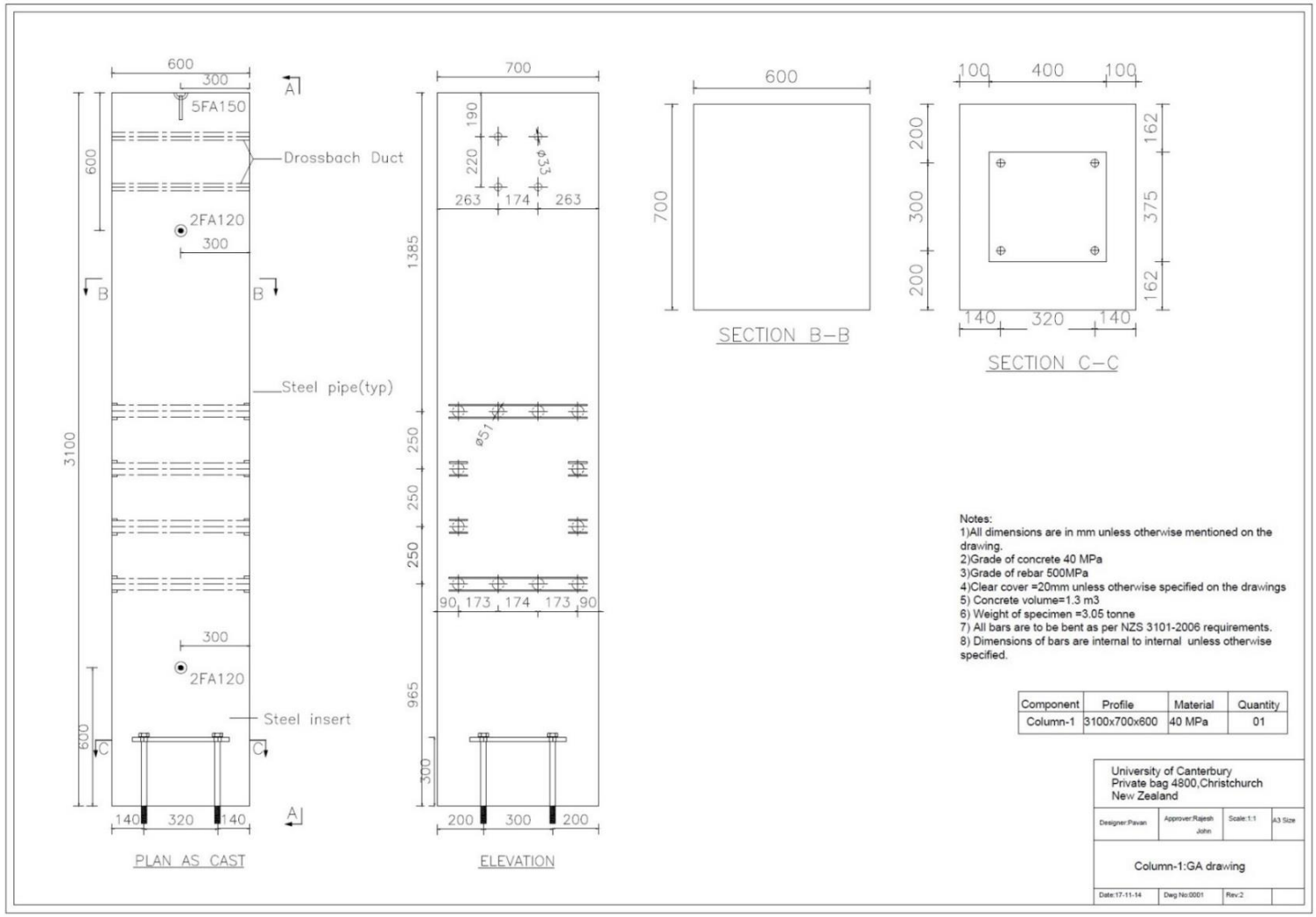
600
300
A
5FA150
Drossbach Duct
600
2FA120
300
B
B
Steel pipe(typ)
3100
300
2FA120
Steel insert
600
C
C
140
320
140
A
PLAN AS CAST
700
190
220
263
174
263
1385
250
250
250
90
173
174
173
90
965
300
200
300
200
ELEVATION
600
700
SECTION B–B
100
400
100
200
300
200
162
375
162
140
320
140
SECTION C–C
Notes:
1)All dimensions are in mm unless otherwise mentioned on the drawing.
2)Grade of concrete 40 MPa
3)Grade of rebar 500MPa
4)Clear cover =20mm unless otherwise specified on the drawings
5) Concrete volume=1.3 m3
6) Weight of specimen =3.05 tonne
7) All bars are to be bent as per NZS 3101-2006 requirements.
8) Dimensions of bars are internal to internal unless otherwise specified.
Component
Profile
Material
Quantity
Column-1
3100x700x600
40 MPa
01
University of Canterbury
Private bag 4800,Christchurch
New Zealand
Designer:Pavan
Approver:Rajesh John
Scale:1:1
A3 Size
Column-1:GA drawing
Date:17-11-14
Dwg No:0001
Rev:2

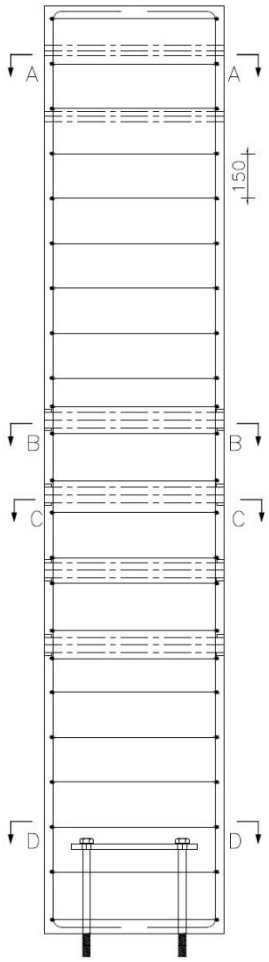

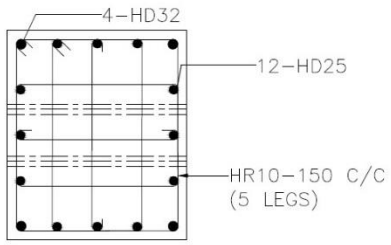

SECTION A–A

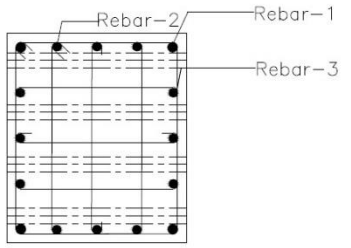

SECTION B–B

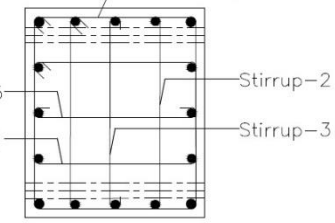

SECTION C–C

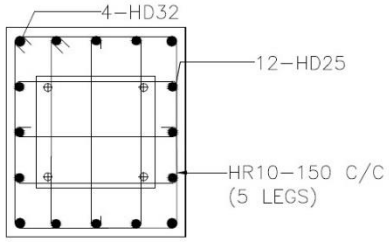

SECTION D–D

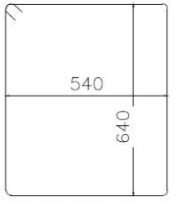

STIRRUP–1

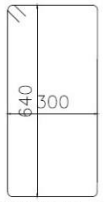

STIRRUP–2

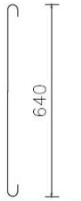

STIRRUP–3

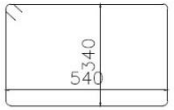

STIRRUP–4

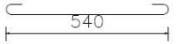

STIRRUP–5

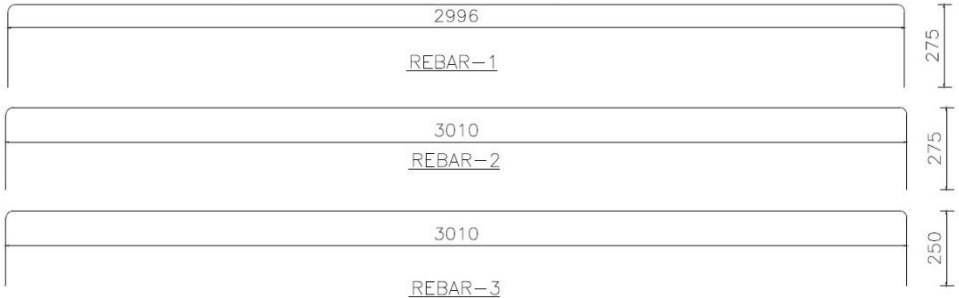

Notes:
1)All dimensions are in mm unless otherwise mentioned on the drawing.
2)Grade of concrete 40 MPa
3)Grade of rebar 500MPa
4)Clear cover =20mm unless otherwise specified on the drawings
5) All bars are to be bent as per NZS 3101-2006 requirements.
6) Minimum diameter of bend for stirrups is 4d and rebar's is 6d
7) Dimensions of rebar/stirrup specified are internal to internal unless otherwise specified.
8) Corner bars are 32dia, internal are 25 dia

University of Canterbury
Private bag 4800,Christchurch
New Zealand

Designer:Pavan	Approver:Rajesh John	Scale:1:1	A3 Size

Column-1:Reinforcement drawing

Date:17-11-14	Dwg No:002	Rev:2	

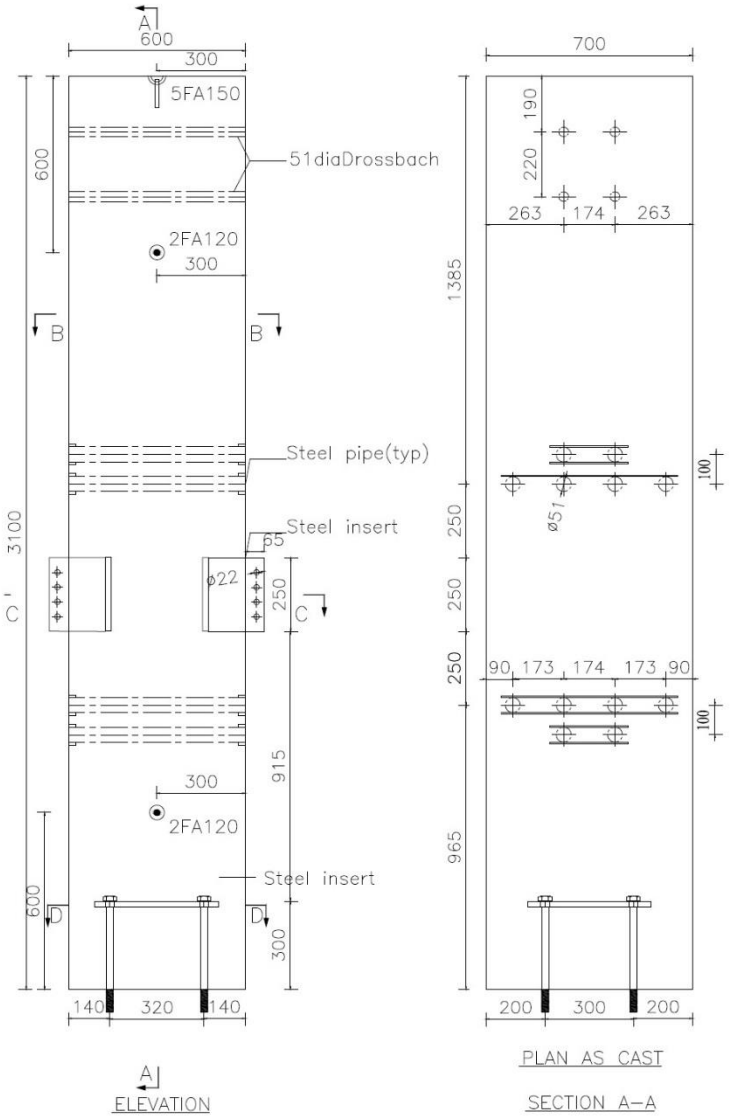

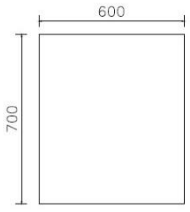

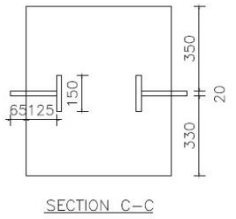

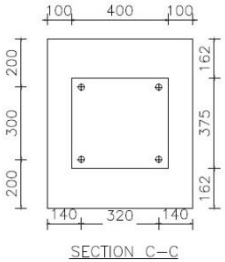

Notes:
1)All dimensions are in mm unless otherwise mentioned on the drawing.
2)Grade of concrete 40 MPa
3)Grade of rebar 500MPa
4)Clear cover =20mm unless otherwise specified on the drawings
5) Concrete volume=1.3 m3
6) Weight of specimen =3.05 tonne
7) All bars are to be bent as per NZS 3101-2006 requirements.
8) Dimensions of bars are internal to internal dimensions unless otherwise specified.

Component	Profile	Material	Quantity
Column-2	3100x700x600	40 MPa	01

University of Canterbury
Private bag 4800,Christchurch
New Zealand

Designer:Pavan	Approver:Rajesh John	Scale:1:1	A3 Size

Column-2:GA drawing

Date:28-11-14	Dwg No:0003	Rev:3	

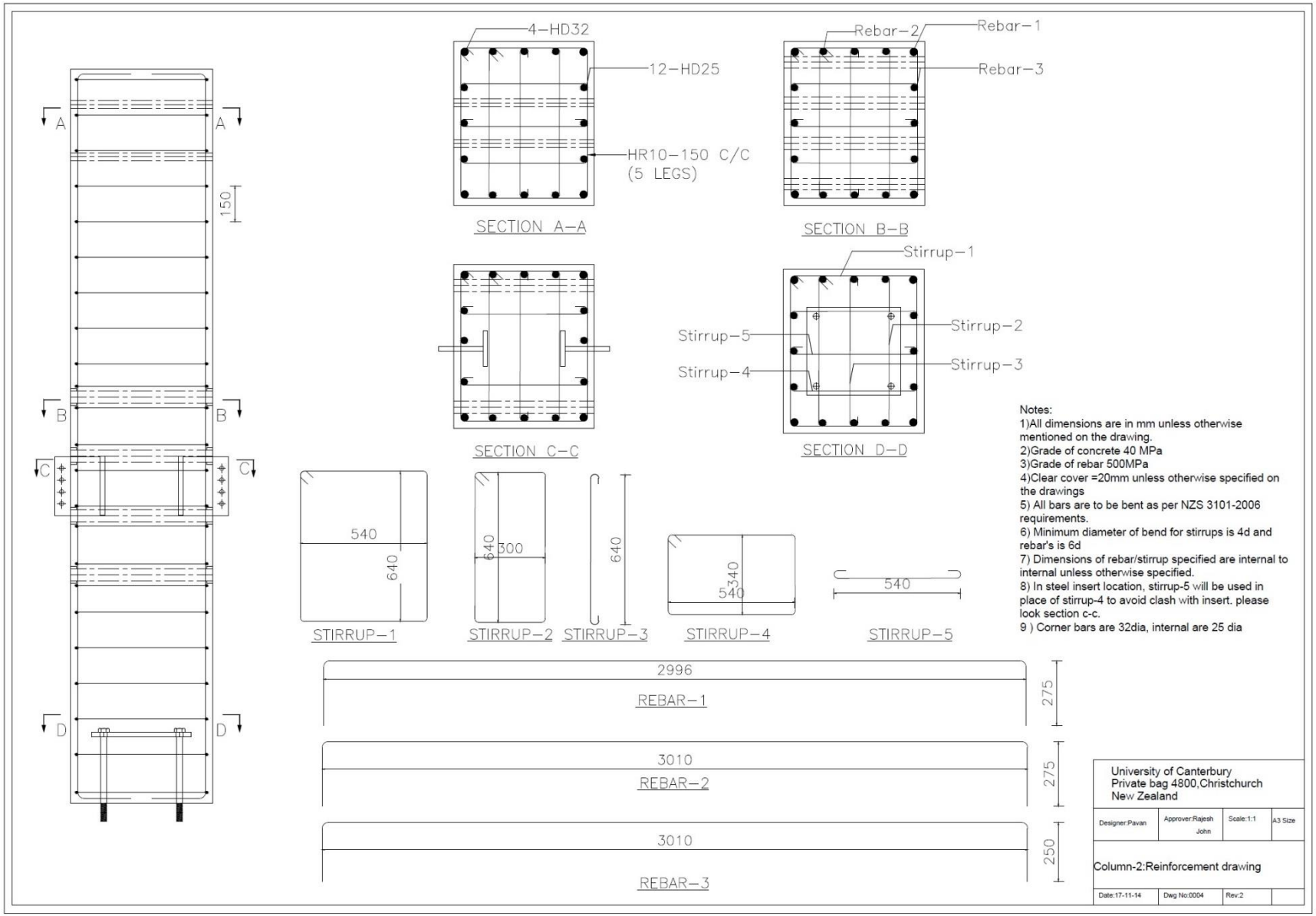
A
A
150
B
B
C
C
D
D
4–HD32
12–HD25
HR10–150 C/C
(5 LEGS)
SECTION A–A
Rebar–2
Rebar–1
Rebar–3
SECTION B–B
SECTION C–C
Stirrup–1
Stirrup–5
Stirrup–2
Stirrup–4
Stirrup–3
SECTION D–D
540
640
STIRRUP–1
640
300
STIRRUP–2
640
STIRRUP–3
340
540
STIRRUP–4
540
STIRRUP–5
Notes:
1)All dimensions are in mm unless otherwise mentioned on the drawing.
2)Grade of concrete 40 MPa
3)Grade of rebar 500MPa
4)Clear cover =20mm unless otherwise specified on the drawings
5) All bars are to be bent as per NZS 3101-2006 requirements.
6) Minimum diameter of bend for stirrups is 4d and rebar's is 6d
7) Dimensions of rebar/stirrup specified are internal to internal unless otherwise specified.
8) In steel insert location, stirrup-5 will be used in place of stirrup-4 to avoid clash with insert. please look section c-c.
9) Corner bars are 32dia, internal are 25 dia
2996
REBAR–1
275
3010
REBAR–2
275
3010
REBAR–3
250
University of Canterbury
Private bag 4800,Christchurch
New Zealand
Designer:Pavan
Approver:Rajesh John
Scale:1:1
A3 Size
Column-2:Reinforcement drawing
Date:17-11-14
Dwg No:0004
Rev:2

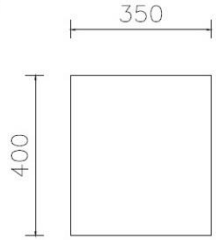

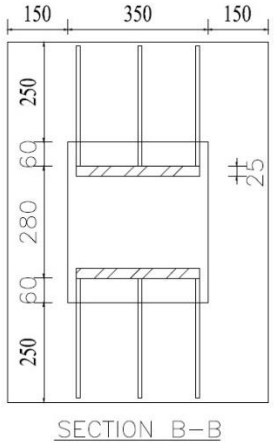

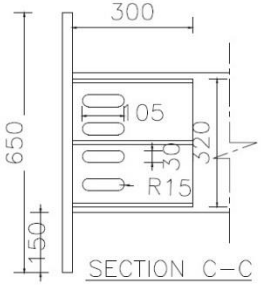

Notes:
1)All dimensions are in mm unless otherwise mentioned on the drawing.
2)Grade of concrete 40 MPa
3)Grade of rebar 500MPa
4)Clear cover =20mm unless otherwise specified on the drawings
5) Concrete volume=0.43 m3
6) Weight of specimen =1.01 tonne
7) All bars are to be bent as per NZS 3101-2006 requirements.
8) Dimensions of bars are internal to internal dimensions unless otherwise specified.

Component	Profile	Material	Quantity
Beam-1	3100x400x350	40 MPa	02

University of Canterbury
Private bag 4800,Christchurch
New Zealand

Designer:Pavan	Approver:Rajesh John	Scale:1:1	A3 Size

Beam-1:GA drawing

Date:17-11-14	Dwg No:005	Rev:2	

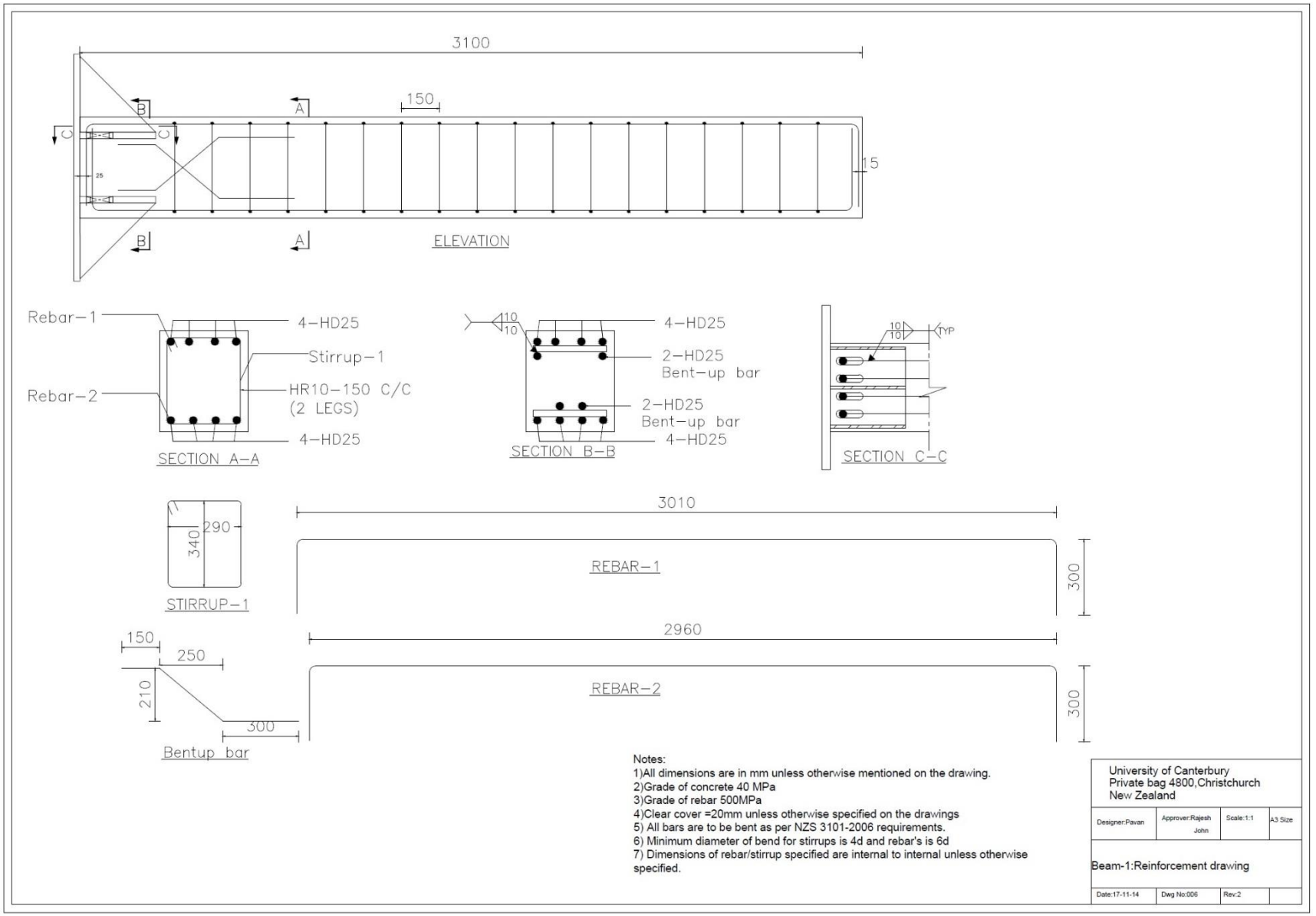
3100
150
B
A
C
C
25
15
B
A
ELEVATION
Rebar–1
4–HD25
Stirrup–1
Rebar–2
HR10–150 C/C
(2 LEGS)
4–HD25
SECTION A–A
10
10
4–HD25
2–HD25
Bent–up bar
2–HD25
Bent–up bar
4–HD25
SECTION B–B
10
10
TYP
SECTION C–C
340
290
STIRRUP–1
3010
REBAR–1
300
2960
REBAR–2
300
150
250
210
300
Bentup bar
Notes:
1)All dimensions are in mm unless otherwise mentioned on the drawing.
2)Grade of concrete 40 MPa
3)Grade of rebar 500MPa
4)Clear cover =20mm unless otherwise specified on the drawings
5) All bars are to be bent as per NZS 3101-2006 requirements.
6) Minimum diameter of bend for stirrups is 4d and rebar's is 6d
7) Dimensions of rebar/stirrup specified are internal to internal unless otherwise specified.
University of Canterbury
Private bag 4800,Christchurch
New Zealand
Designer:Pavan
Approver:Rajesh John
Scale:1:1
A3 Size
Beam-1:Reinforcement drawing
Date:17-11-14
Dwg No:006
Rev:2

ELEVATION

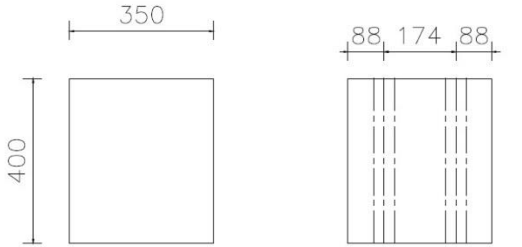

SECTION A–A

SECTION B–B

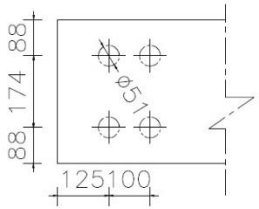

SECTION C–C

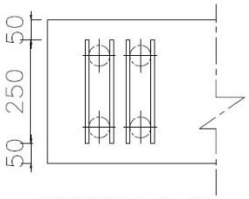

SECTION D–D

Notes:
1)All dimensions are in mm unless otherwise mentioned on the drawing.
2)Grade of concrete 40 MPa
3)Grade of rebar 500MPa
4)Clear cover =20mm unless otherwise specified on the drawings
5) Concrete volume=0.43 m3
6) Weight of specimen =1.01 tonne
7) All bars are to be bent as per NZS 3101-2006 requirements.
8) Dimensions of bars are internal to internal dimensions unless otherwise specified.
Special note:
9) For two beams out of six beams, location of the first duct will be at 165 mm from beam end, all others remain same.

Component	Profile	Material	Quantity
Beam-2	3100x400x350	40 MPa	06

University of Canterbury
Private bag 4800,Christchurch
New Zealand

Designer:Pavan	Approver:Rajesh John	Scale:1:1	A3 Size

Beam-2:GA drawing

Date:17-11-14	Dwg No:007	Rev:2	

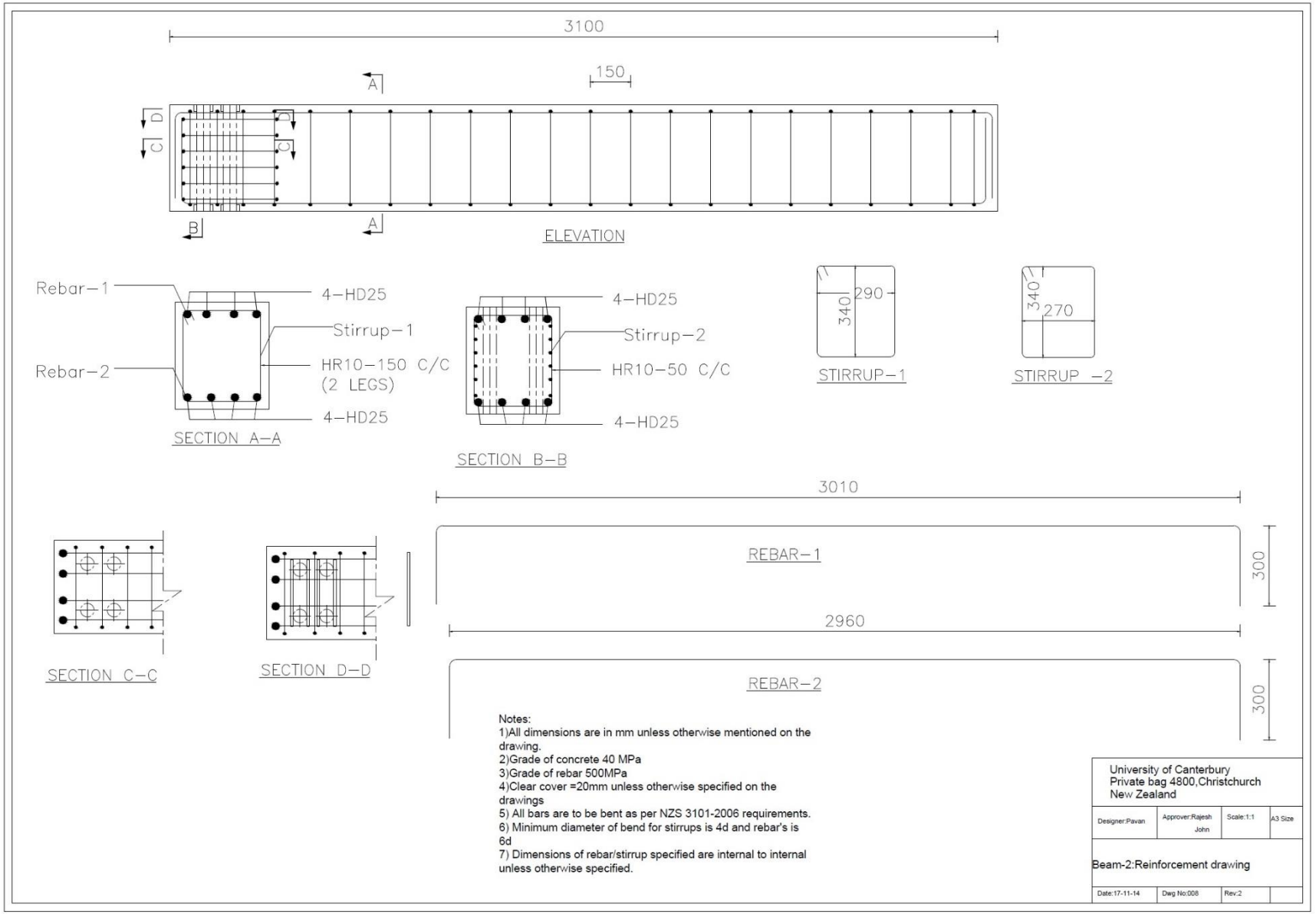
3100
150
A
B
C
D
ELEVATION
Rebar–1
Rebar–2
4–HD25
Stirrup–1
HR10–150 C/C
(2 LEGS)
4–HD25
SECTION A–A
4–HD25
Stirrup–2
HR10–50 C/C
4–HD25
SECTION B–B
340
290
STIRRUP–1
340
270
STIRRUP –2
3010
REBAR–1
300
2960
REBAR–2
300
SECTION C–C
SECTION D–D
Notes:
1)All dimensions are in mm unless otherwise mentioned on the drawing.
2)Grade of concrete 40 MPa
3)Grade of rebar 500MPa
4)Clear cover =20mm unless otherwise specified on the drawings
5) All bars are to be bent as per NZS 3101-2006 requirements.
6) Minimum diameter of bend for stirrups is 4d and rebar's is 6d
7) Dimensions of rebar/stirrup specified are internal to internal unless otherwise specified.
University of Canterbury
Private bag 4800,Christchurch
New Zealand
Designer:Pavan
Approver:Rajesh John
Scale:1:1
A3 Size
Beam-2:Reinforcement drawing
Date:17-11-14
Dwg No:008
Rev:2

ELEVATION

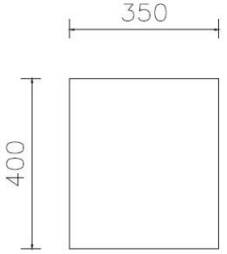

SECTION A–A

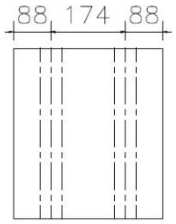

SECTION B–B

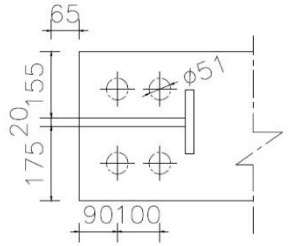

SECTION C–C

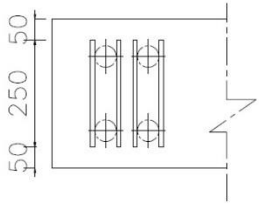

SECTION D–D

Component	Profile	Material	Quantity
Beam-3	3100x400x350	40 MPa	02

Notes:
1)All dimensions are in mm unless otherwise mentioned on the drawing.
2)Grade of concrete 40 MPa
3)Grade of rebar 500MPa
4)Clear cover =20mm unless otherwise specified on the drawings
5) Concrete volume=0.43 m3
6) Weight of specimen =1.01 tonne
7) All bars are to be bent as per NZS 3101-2006 requirements.
8) Dimensions of bars are internal to internal dimensions unless otherwise specified.

University of Canterbury
Private bag 4800,Christchurch
New Zealand

Designer:Pavan	Approver:Rajesh John	Scale:1:1	A3 Size

Beam-3:GA drawing

Date:17-11-14	Dwg No:009	Rev:2	

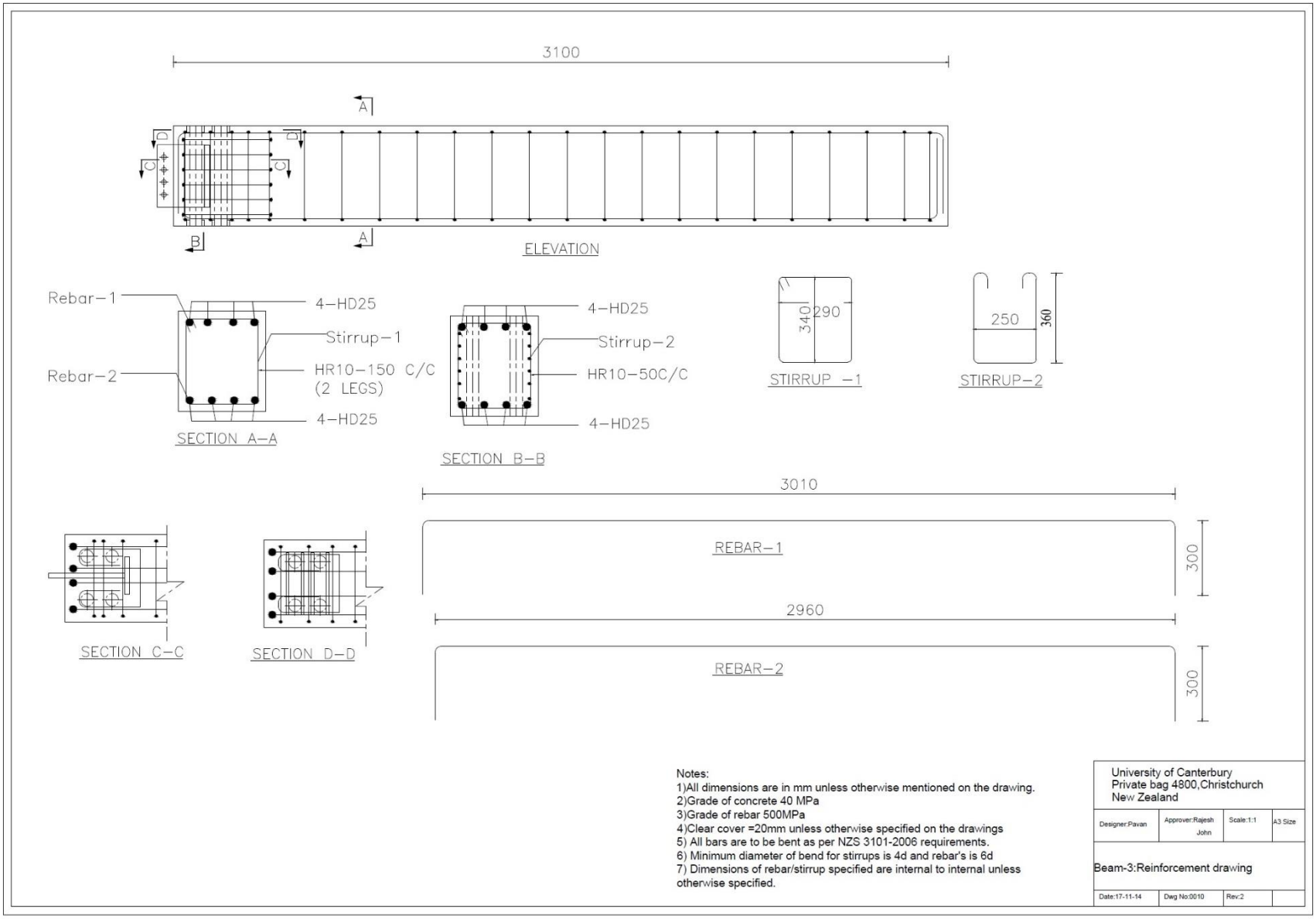
3100
A
B
C
D
ELEVATION
Rebar–1
Rebar–2
4–HD25
Stirrup–1
HR10–150 C/C
(2 LEGS)
4–HD25
SECTION A–A
4–HD25
Stirrup–2
HR10–50C/C
4–HD25
SECTION B–B
340
290
STIRRUP –1
250
360
STIRRUP–2
3010
REBAR–1
300
2960
REBAR–2
300
SECTION C–C
SECTION D–D
Notes:
1)All dimensions are in mm unless otherwise mentioned on the drawing.
2)Grade of concrete 40 MPa
3)Grade of rebar 500MPa
4)Clear cover =20mm unless otherwise specified on the drawings
5) All bars are to be bent as per NZS 3101-2006 requirements.
6) Minimum diameter of bend for stirrups is 4d and rebar's is 6d
7) Dimensions of rebar/stirrup specified are internal to internal unless otherwise specified.
University of Canterbury
Private bag 4800,Christchurch
New Zealand
Designer:Pavan
Approver:Rajesh John
Scale:1:1
A3 Size
Beam-3:Reinforcement drawing
Date:17-11-14
Dwg No:0010
Rev:2

ELEVATION

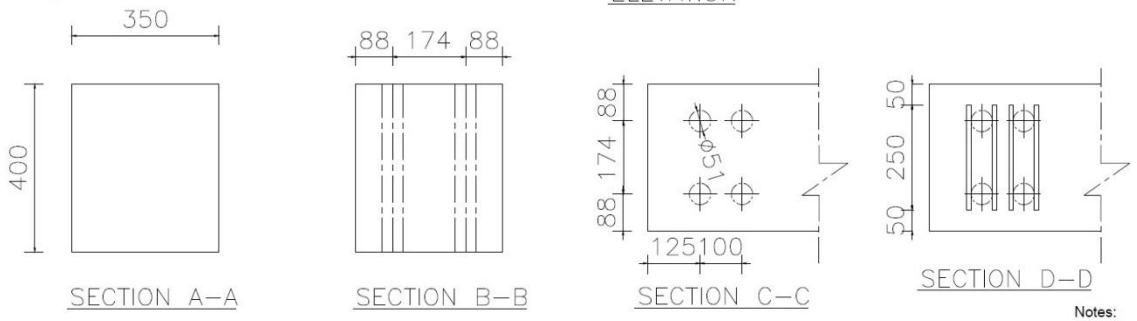

SECTION A–A

SECTION B–B

SECTION C–C

SECTION D–D

Notes:
1)All dimensions are in mm unless otherwise mentioned on the drawing.
2)Grade of concrete 40 MPa
3)Grade of rebar 500MPa
4)Clear cover =20mm unless otherwise specified on the drawings
5)Side clear cover=15 mm
6) Concrete volume=0.43 m3
7) Weight of specimen =1.01 tonne
8) All bars are to be bent as per NZS 3101-2006 requirements.
9) Dimensions of bars are internal to internal dimensions unless otherwise specified.

Component	Profile	Material	Quantity
Beam-4	3100x400x350	40 MPa	02

University of Canterbury
Private bag 4800,Christchurch
New Zealand

Designer:Pavan	Approver:Rajesh John	Scale:1:1	A3 Size

Beam-4:GA drawing

Date:17-11-14	Dwg No:0011	Rev:2	

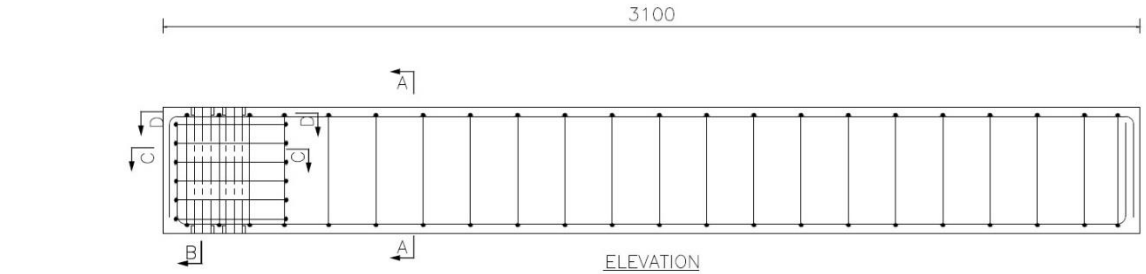

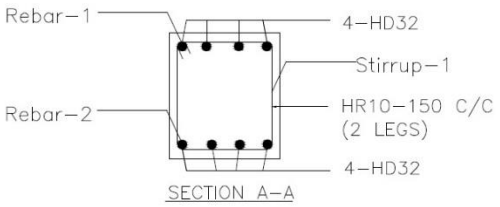

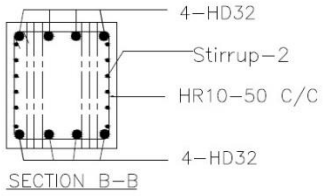

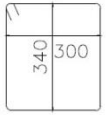

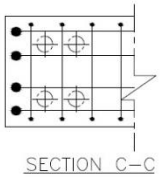

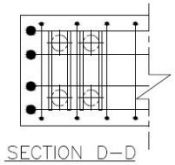

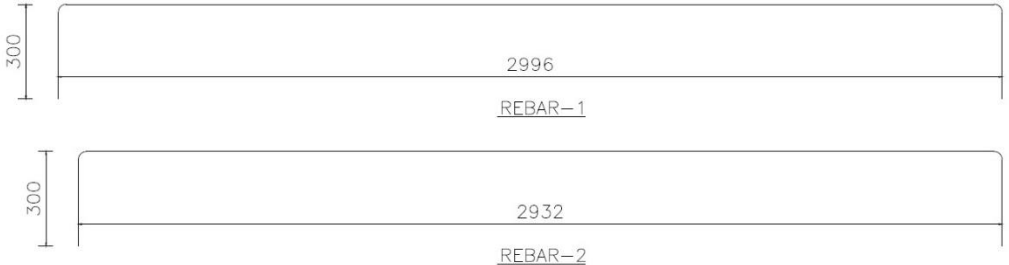

Notes:
1)All dimensions are in mm unless otherwise mentioned on the drawing.
2)Grade of concrete 40 MPa
3)Grade of rebar 500MPa
4)Clear cover =20mm unless otherwise specified on the drawings
5) All bars are to be bent as per NZS 3101-2006 requirements.
6) Minimum diameter of bend for stirrups is 4d and rebar's is 6d
7) Dimensions of rebar/stirrup specified are internal to internal unless otherwise specified.

University of Canterbury
Private bag 4800,Christchurch
New Zealand

Designer:Pavan	Approver:Rajesh John	Scale:1:1	A3 Size

Beam-4:Reinforcement drawing

Date:17-11-14	Dwg No:0012	Rev:2	

Appendix D: Evaluation of capacities of the steel connections

D.1 Type-1: Steel end plate connection

D.1.1 *Connection capacity on the beam side*

The ultimate moment capacity of the Type-1 connection on the beam side is dictated by the strength of the embedded steel plate, the strength of the weld between the rebars and the embedded plate, and strength of the weld between the embedded plate and the end plate. As there will not be a significant shift in the position of neutral axis within the connection region compared to a neutral axis location next to the connection region, the ratio of the ultimate moment capacity of the connection to over strength beam demand is equal to the ratio of the ultimate tensile capacities of the embedded plate and rebars.

Tensile demand on the embedded steel plate $T_d = f_{ur}A$ =625×6×0.78×25^2=1828 kN

Tensile capacity of the embedded steel plate $T_p = f_{up}bt$ =480×(320-120)×25=2400 kN

The ratio of ultimate capacity of the connection to over-strength moment demand on the beam side is (T_p/T_d) = 2400/1828=1.31

To avoid the failure of the weld, the capacity of the weld has to be more the tensile demand on the embedded plate. Weld capacity between the rebars and the embedded steel plate is calculated as $T_w = \left(\frac{f_{yw}}{\sqrt{3}}\right) t_w l_{eff}$=4×480/(√3)×10/(√2)×150×2=2351 kN (T_w>T_d, OK).

The weld between the embedded steel plate and the end plate is a full penetration T-butt weld. As the grade of the weld is more than the grade of the steel components, the capacity of the weld is more than the capacity of steel plates and rebars.

D.1.2 *Connection capacity on the column side*

The moment capacity of the connection on the column side is governed by the thickness of the endplate, number, diameter and arrangement of threaded rods. It is important to note that threaded rods/bolts on the column side are pre tensioned to 200 kN before loading of the specimens, so only reserve tensile capacity of 412 kN was available for the capacity calculation. Conservatively, it was assumed only top two rows of bolts are assumed to resist the moment and bottom two rows of bolts (which are in full compression) were designed explicitly to resist shear force. As the distance between the bolt rows is large enough to avoid the combined mode of failure of bolt rows, the capacity of the individual bolt row will govern the design. Moment of resistance of the connection on column side is evaluated using yield

line theory, and the summary of the calculations is reported below.

For the top/first bolt row:-

m_x=175 mm ; e_x=75 mm ; n_x= min (e_x, 1.25 m_x)= 75 mm ; m1=175 mm; e= 75; m2l=m2u=82 mm; λ1= (ml/(m2l+e)); λ2=(m21or m2u/(m2u+e)); λ1=0.7; λ2=0.32 results in α= α'= 5.25.

Effective length for the top row L_{eff} is min (max (αm_{1+} $\alpha' m_1$-(4m_1+1.25e), αm_1, $\alpha' m_2$, 4m+1.25e), 2πm); L_{eff}= min (max(1043, 430, 430,793), 1099)= 1043 mm

Plastic moment capacity of the equivalent T-stub M_p=1043×25^2×480×0.25= 78.22 kN-m

For Mode-1 failure, $P_{r1} = \frac{4M_p}{m}$ = 4×78.22/0.175=1787 kN

For Mode-2 failure, $\frac{2M_p+n\sum P_t'}{m+n}$= 2×78.22+0.075×4×412/ (0.175+0.075) =1120 kN

For Mode-3 failure, $\sum P_t'$ =4×412= 1648 kN

Probable capacity of the bolt row T_{ci} = min (1787, 1120, 1648) =1120 kN

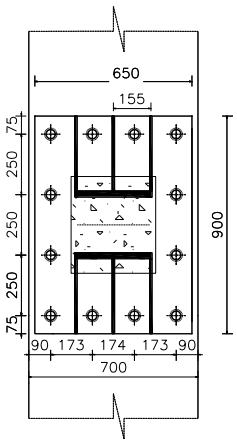

For second bolt row:-

m=85 mm; e=65 mm; n= min (e, 1.25m) = 65 mm

Calculation of effective length for second row L_{eff} = min (4m+1.25e, 2πm); = min (425, 534) = 421 mm

Plastic moment capacity of T-stub M_p =421×25^2×480×0.25= 31.57 kN-m

For Mode 1, $P_{r1} = \frac{4M_p}{m}$ = 4×31.87/0.085=1485 kN

For Mode 2, $\frac{2M_p+n\sum P_t'}{m+n}$= 2×31.57+0.065×2×412/(0.085+0.065)=778 kN

For Mode 3, $\sum P_t'$ =2×412= 824 kN

Probable capacity of second row bolts T_{ci} = min (1485, 778, 824) =778 kN

If the thickness of the plate Tp< (33/1.9)×√900/350= 27.85 mm, then no need to limit bolt force distribution to a triangular pattern.

Location of the neutral axis from extreme compression/bearing stress; $\sum T_{ci} = \left(\alpha f_c'\right) b(\beta a)$

1120000+778000=0.85×40×650×0.85×a; a= 101 mm

Without much significant error in the calculation, it was assumed that center of compression force is at the bottom row of bolts. Accordingly, the moment of resistance of the connection is calculated as M_c= 778×0.5+1120×0.75=1230 kN-m. Ratio of the ultimate moment capacity

of connection to over strength beam demand on the column side= 1230/565 =2.17.

Tensile force demand in the bolts due to bending moment M can also be estimated based on the elastic analysis as $Fi=(M_o \times d)/\sum d^2$, where $\sum d^2=0.25^2+0.50^2+0.75^2=0.875$.

Additional tension force in top row bolts = 565×0.75/(4×0.875)= 121 kN <275 kN (Ok)

Additional tension force in second row bolts = 565×0.5/(2×0.875)= 161 kN <275 kN (Ok)

Additional tension force in third row bolts = 565×0.25/(2×0.875)= 80 kN <275 kN (Ok)

D.1.3 *Shear capacity on the column side*

For the calculation of shear resistance of the connection, only bottom two rows of bolts which are in compression are considered to be fully effective. The assumed static coefficient of friction between the steel plate and concrete surface was 0.4. Total pretension force (P) applied to bottom two rows of bolts is = 6×200= 1200 kN. The frictional shear resistance of the connection is calculated as V_f =0.4×1200= 480 kN. Ratio of frictional shear capacity to over strength shear demand of the beam is 480/188=2.55. As there was no expected slip under the ultimate load condition, bolts were not going to engage into the shear and bearing against the steel ducts, hence calculations are not reported.

D.2 Type-2 and 3: Steel angle and tube connections

D.2.1 *Connection capacity on beam side*

The behaviour of the connection on the beam side is a two stage process; (i) no slip until frictional resistance is more than longitudinal shear, (ii) final resistance through the bearing of threaded rods against the beam edge. The frictional resistance of the connection is governed by the total pre-tension force in the bolts, coefficient of friction between the connection and the member or infill material (grout, dental plaster, epoxy resin and rubber). For Beams-2 and 3, the amount of pre-tension applied to the bolts is such that slip is avoided before the beam reaches its 2/3rd yield moment capacity, whereas for the Beam-4 before it achieves it half of yield moment capacity. Also, the amount of pre-tension in each bolt should not exceed 70% of its yield tensile capacity for Beams-2 and 3, and for the Beam-4, it should not exceed 80% of yield tensile capacity. Also, the bearing pressure induced to the beams and columns due to pre-tensioning of the bolts should not exceed 25% of grade of concrete and infill material (if any). The length and breadth of the connections are dictated by the location of the ducts and minimum required beam edge distance. The capacities of the connections with 25 mm thickness plate, varying dimensions, pre-tension in the bolts and number of bolts

is checked against the beam's yield and over strength moment demand.

Slip critical moment of resistance

The slip critical moment of resistance of the connection is the moment at which slip initiates between the connection and beam and is calculated as μ×P×d, where μ is friction coefficient, P is a total pre-tension force, and d is the beam's depth.

Case 1: Rubber sheet as infill material (Test -1)

The slip critical moment of resistance of the connection with total pre-tension force (P) of 960 kN and rubber as infill material (μ=0.6) is 0.6×960×0.4= 230 kN-m. Accordingly, the ratio of slip critical moment of resistance of the connection to yield moment capacity of the beam = 230/319 =0.72.

Case 2: Rubber and dental plaster as infill material (Test-2)

The moment of resistance of the connection with rubber and dental as infill materials (μ=0.6) and total pre-tension force of 1200 kN is 0.6×1200×0.4= 288 kN-m, and the ratio of slip critical moment of resistance of the connection to yield capacity of the beam = 288/319 =0.90

Case 3: Dental plaster, grout, and epoxy as infill material (Test-3 to 6, and 9 to 12)

For Tests 3 to 6, the total pre-tension force was 1360, so the slip critical moment of resistance of the connection was =0.4×1360×0.4= 218 kN-m, and the ratio of slip critical moment of resistance of the connection to yield moment of resistance of the beam = 218/319 =0.68.

For Tests-9 and 10, the total pre-tension force is 1200, so the slip critical moment of resistance was =0.4×1200×0.4= 192 kN-m, and the ratio of slip critical moment of resistance of the connection to yield moment of resistance of the beam = 192/319 =0.60.

For Tests-11 and 12, the total pre-tension force is 1500, so slip critical moment of resistance is =0.4×1500×0.4= 240 kN-m, and the ratio of slip critical moment of resistance of the connection to yield moment of resistance of the beam = 240/487 =0.50.

Ultimate moment of resistance of the connection on the beam side

The ultimate moment of resistance of the connection on the beam side depends on the beam edge breakout strength which depends on the edge distance (i.e. distance between beam end face to the location of the first row of ducts/bolts), grade of concrete, and ultimate strength of the horizontal stirrups in the connection zone (which depends on the number of stirrups above the pivot point of rotation of threaded rods). Accordingly, the ultimate moment of resistance of the connection on beam side is M_c= Fd+(V_c+T_s)×(d-d*0.33), where V_{cbr} is the concrete

breakout strength in shear, T_s is the yield strength of stirrups and it is assumed to act at a distance of d/3 from the beam top surface.

Case 1: No horizontal stirrups in the connection zone

For Test-1, the beam edge distance was 90 mm, and no stirrups were provided in the connection zone. In this case, the ultimate resistance after the slip comes from the beam edge break out strength only and calculated as M_c=0.6×960×0.4+45×(0.4-0.33×0.4)= 242 kN-m, and the ratio of ultimate moment of resistance of the connection to yield moment of resistance of the beam = 242/319 =0.76.

Case 2: Horizontal stirrups in the connection zone

In this case, the resistance after the slip between the connection and the beam is from the concrete breakout and horizontal stirrups.

For Test-2, the ultimate moment of resistance of the connection on the beam side M_c=0.6×1200×0.4+503×(0.4-0.33×0.4)= 423 kN-m, and the ratio of ultimate moment of resistance of the connection to yield moment of resistance of the beam = 423/319 =1.33.

For Tests-3, ultimate moment of resistance of the connection on beam side is M_c=0.4×1360×0.4+503×(0.4-0.33×0.4)= 352 kN-m and the ratio of ultimate moment of resistance of the connection to yield moment of resistance of the beam = 352/319 =1.10.

For Tests-5, and 6 ultimate moment of resistance of the connection on beam side is M_c=0.4×1360×0.4+499×(0.4-0.33×0.4)= 351 kN-m and the ratio of ultimate moment of resistance of the connection to yield moment of resistance of the beam = 351/319 =1.10.

For Tests-9 and 10, ultimate moment of resistance of the connection on beam side M_c=0.4×1200×0.4+499×(0.4-0.33×0.4)= 326 kN-m, and the ratio of ultimate moment of resistance of the connection to yield moment of resistance of the beam = 326/319 =1.03.

For Tests-11 and 12, ultimate moment of resistance of the connection on beam side M_c=0.4×1500×0.4+499×(0.4-0.33×0.4)= 374 kN-m, and the ratio of ultimate moment of resistance of the connection to yield moment of resistance of the beam = 374/487 =0.77

Case 3: Repaired beam of test-1 by encasing with steel tube and welding rebars to tube

For Test-4, the ultimate moment of resistance of the connection on the beam side cannot be directly estimated by using the developed analytical model. As the rebars are welded to the armoured tube, it can be ensured that beam can develop its yield moment of resistance.

With Type-2 and 3 connections, if the beam edge beyond the bolts is infinitely stiff and strong the failure mode in the connection region will be shearing of the bolts. Then, the ultimate moment of resistance of the connection on beam side with a shear mode of failure of threaded rods is calculated as = $(f_{ub}/\sqrt{3})A_sd = (900/\sqrt{3})\times4\times0.78\times0.8\times33^2\times400$= 565 kN-m.

The other possible modes of failure such as; tearing and bearing failure of the horizontal leg of the steel angle need to be avoided before yielding of the beam. The maximum longitudinal shear demand that can be generated between the beam and the connection is (V_{sd}) = 680/0.4= 1700 kN. Tensile capacity of the horizontal leg of the angle (without stiffeners) is calculated as $T_c = 480\times(350-2\times40)\times25$ = 3240 kN. Bearing strength of the horizontal leg of the angle is (T_b) = 480×40×25×4 =1920 kN (T_c, T_b> V_{sd}, OK).

D.2.2 *Connection capacity on column side*

For the connection's capacity evaluation on the column side, in all cases it was assumed that bolts are stressed to 340 kN, so only 272 kN of reserved tensile capacity was used for moment capacity estimation.

Case 1: Vertical leg of 350 mm and 2 rows of bolts (Test 1, 2, 3, 4 and 12)

For top row of bolts:-

m_x=275 mm ; e_x=75 mm ; n_x= min (e_x, 1.25 m_x)= 75 mm ; m1=275 mm; e= 75; m2l=m2u= 82 mm; λ1= (ml/(m2l+e)); λ2=(m21or m2u/(m2u+e)); λ1=0.78; λ2=0.23 results in α= α'= 5.0

Calculation of effective length for top/first row L_{eff}= min (max (αm_{1+} $\alpha' m_1$-(4m_1+1.25e), αm_1, $\alpha' m_2$, 4m+1.25e), 2πm); L_{eff}= min (max(1556, 410, 410, 1193), 1727)= 1556 mm

Plastic moment capacity of T-stub M_p=1556×25^2×480×0.25= 116 kN-m

For Mode 1, $P_{r1} = \frac{4M_p}{m}$ = 4×116/0.275=1687 kN

For Mode 2, $\frac{2M_p+n\sum P_t'}{m+n}$= 2×88+0.075×2×272/ (0.275+0.075) =779 kN

For Mode 3, $\sum P_t'$ =2×272= 544 kN

Probable capacity of row 1 T_{ci} = min (1687, 779, 544) =544 kN

For second row of bolts:-

m_x=175 mm; e_x=175 mm; n_x= min (e_x, 1.25 m_x)= 175 mm; m1=175 mm; e= 175; m2l=m2u= 82 mm; λ1= (ml/(m2l+e)); λ2=(m21 or m2u/(m2u+e)); λ1=0.5; λ2=0.23 results in α= α'= 6.28

Calculation of effective length for second row L_{eff} = min (max (αm_{1+} $\alpha'm_1$-($4m_1$+1.25e), αm_1, α'm2, 4m+1.25e), $2\pi m$); L_{eff}= min (max(1279, 515, 515,918), 1099)= 1099 mm

Plastic moment capacity of T-stub M_p=1099×25^2×480×0.25= 82.46 kN-m

For Mode 1, $P_{r1} = \frac{4M_p}{m}$ = 4×82.46/0.175=1884 kN

For Mode 2, $\frac{2M_p+n\sum P_t'}{m+n}$= 2×82.46+0.175×2×272/ (0.175+0.175) =743 kN

For Mode 3, $\sum P_t'$ =2×272= 544 kN

Capacity of row 2 T_{ci} = min (1884, 743, 544) =544 kN

First and second row of bolts together:-

m_x=175 mm ; e_x=75 mm ; n_x= min (e_x, 1.25 m_x)= 75 mm; m1=175 mm; e= 75; m2l=m2u= 82 mm; λ1= (m2l/(m2l+e)); λ2=(m2u/(m2u+e)); λ1=0.7; λ2=0.32 results in α= α'= 5.25

Calculation of effective length of yield line for second and first row together L_{eff}= min (max (αm_{1+} $\alpha'm_1$-($4m_1$+1.25e)+p, αm_1+p, $\alpha'm_2$+p, 4m+1.25e+p), $2\pi m$); L_{eff}= min (max(1143, 530, 530, 893), 1099)= 1099 mm

Plastic moment capacity of T-stub Mp=1099×25^2×480×0.25= 82.42 kN-m

For Mode 1, $P_{r1} = \frac{4M_p}{m}$ = 4×82.42/0.175=1884 kN

For Mode 2, $\frac{2M_p+n\sum P_t'}{m+n}$= 2×82.42+0.075×4×272/ (0.175+0.075) =985 kN

For Mode 3, $\sum P_t'$ =4×272= 1088 kN

Probable capacity of row 1 T_{ci} = min (1787, 985, 1088) =985 kN

Minimum probable bolts force for second row of bolts = min (544, 985-544) =441

By using translation equilibrium; $\sum T = 0.85f'cb0.85\,c$ = 985000=0.85×40×350×0.85×a

Location of neutral axis from extreme compressive stress a= 97 mm

Ultimate moment of resistance of the connection on column side is $Mc = \sum Td'$

=544× (0.315+0.4+0.275) +445×(0.315+0.4+0.175) =944 kN-m

Case 2: Vertical leg of 250 mm and 1 row of 2 bolts (Test 6, 9 and 11)

m_x=175 mm ; e_x=75 mm ; n_x= min (e_x, 1.25 m_x)= 75 mm ; m1=175 mm; e= 75; m2l=m2u= 82 mm ;λ1= (ml/(m2l+e)); λ2=(m21or m2u/(m2u+e)); λ1=0.7; λ2=0.32 results in α= α'= 5.25

Effective length for top/first row L_{eff} = min (max (αm_{1+} $\alpha'm_1$-($4m_1$+1.25e), αm_1, $\alpha'm_2$,

4m+1.25e), 2πm); L_{eff}= min (max(1043, 430, 430,793), 1099)= 1043 mm

Plastic moment capacity of T-stub M_p=1043×25^2×480×0.25= 78.22 kN-m

For Mode 1 failure, $P_{r1} = \frac{4M_p}{m}$ = 4×78.22/0.175=1787 kN

For Mode 2 failure, $\frac{2M_p+n\sum P_t'}{m+n}$= 2×78.77+0.075×2×272/ (0.175+0.075) =783 kN

For Mode 3 failure, $\sum P_t'$ =2×272= 544 kN

Probable capacity of bolt row T_{ci} = min (1787, 783, 544) =544 kN

By using translation equilibrium; $\sum T = 0.85f'cb0.85\,a$ =544000=0.85×40×350×0.85×a

Location of neutral axis from extreme compressive stress a= 54 mm

Ultimate moment of resistance of the connection on column side is $\sum Td'$

=544× (0.175 +0.4+0.175) =408 kN-m

Case 3: Vertical leg of 250 mm and 1 row of 4 bolts (Test 5):

m_x=175 mm ; e_x=75 mm ; n_x= min (e_x, 1.25 m_x)= 75 mm ; m1=175 mm; e= 75; m2l=m2u= 82 mm ; λ1= (ml/(m2l+e)); λ2=(m21 or m2u/(m2u+e)); λ1= 0.7; λ2=0.32 results in α= α'= 5.25

Effective length for first row L_{eff} = min (max (αm_{1+} α'm_1-(4m_1+1.25e), αm_1, α'm_2, 4m+1.25e), 2πm); Leff= min (max(1043, 430, 430, 793), 1099)= 1043 mm

Plastic moment capacity of T-stub M_p=1043×25^2×480×0.25= 78.22 kN-m

For Mode 1 failure, $P_{r1} = \frac{4M_p}{m}$ = 4×78.22/0.175=1787 kN

For Mode 2 failure, $\frac{2M_p+n\sum P_t'}{m+n}$= 2×78.22+0.075×4×272/ (0.175+0.075) =952 kN

For Mode 3 failure, $\sum P_t'$ =4×272= 1088 kN

Probable capacity of bolt row T_{ci} = min (1884, 985, 1088) =952 kN

By using translation equilibrium; $\sum T = 0.85f'cb0.85\,a$ = 952000=0.85×40×650×0.85×a

Location of neutral axis from extreme compressive stress a= 51 mm

Ultimate moment of resistance of the connection on column side is $\sum Td'$

=952× (0.175 +0.4+0.175)

=693 kN-m

D.2.3 *Shear capacity on the column side*

Shear capacity of Type-2 and 3 connection is evaluated by using only the bottom row of bolts which are in compression are considered to be fully effective in resisting shear by utilizing the frictional resistance. The static coefficient of friction between the steel plate and concrete surface is 0.4. Of all tests with Type-2 and 3 connections, Test 11 has only 2 bolts resisting shear against over-strength shear demand of 225 kN is calculated below and shear capacity for remaining tests can be estimated in a similar manner.

Total pretension force in the bottom two row of bolts (P) = 2×375= 750 kN.

Friction shear resistance of the connection V_c = 0.4×750= 300 kN.

Ratio of frictional shear capacity to over strength shear demand of beam = 300/225= 1.33

As there is no expected slip under the ultimate load condition, bolts are not going to engage into the shear and bearing against the steel ducts, hence calculations are not reported. On similar lines, calculation has been performed for other cases.

D.3 Beam edge breakout strength

Beam breakout strength strength in shear (TEST-1)

Input

Grade of concrete (f'c)		40	N/mm^2
Beam details			
Width of beam (B)		350	mm
Depth of beam (D)		400	mm
Threaded bar details			
Number of threaded rods		4	
Diameter (da)		33	mm
Embedded depth (hef)		200	mm
Yield strength (fya)		640	N/mm^2
Ultimate strength (fua)		800	N/mm^2
Steel duct diameter (sdd)		50	mm
Horizontal reinforcement details			
Yield strength of stirrup (fys)		586	N/mm^2
Diameter of the stirrup (ds)		10	mm
Number of stirrups in upper half of beam depth		0	
Provided length of the stirrup (ls)		300	mm
Location of threaded rods			
Beam edge distance in X-direction (X1)		90	mm
Spacing of ducts in X-direction (X2)		100	mm
Beam edge distance in Y-direction (Y1)		88	mm
Spacing of ducts in Y-direction (Y2)		174	mm

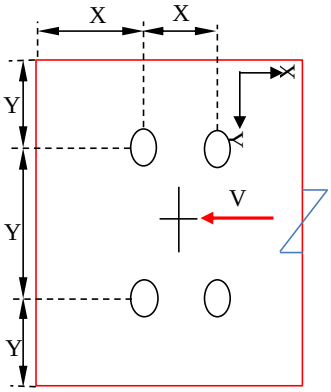

Concrete breakout strength in shear

ACI318M-08 (Section D 6.2)

Half of the depth of beam	ha	200	mm
Load bearing length of the anchor	le	200	mm
Diameter of the threaded rod	da	33	mm
factor for normal or light weight concrete	λ	1	
Eccentricity of applied shear	ev	0	mm
distance from the edge to farthest anchor	Ca1	65	mm
Breakout strength of single anchor	Vb	16379.91	N
Factor to account for eccentric shear	$\Psi_{ec,V}$	1	
Factor to account for edge effect	$\Psi_{ed,V}$	0.970769	
Factor to account for uncracked concrete	$\Psi_{c,V}$	1.4	
Factor for short embedded anchors	$\Psi_{h,V}$	1	
Unaffected Projected area of single anchc	Avco	19012.5	mm^2
Actual projected area of group of anchors	Avc	34125	mm^2
Concrete breakout strength in shear	Vc	40.0	kN

$Vb=0.\{(l_e/d_a)^{0.2} d_a^{1/2} \lambda f'_c{}^{1/2} C_{a1}{}^{1.5}$

$V_c = \frac{A_{vc}}{A_{vco}} \Psi_{ec,V}\Psi_{ed,V}\Psi_{c,V}\Psi_{h,V}V_b$

PCI Design handbook /7th Edition

See adjacent figure	SED	10.31	inch
See adjacent figure	BED	6.50	inch
Corner beam failure	SED/BED	1.59	
Breakout strength of single anchor	Vb	15.13823	kip
Factor to account for front edge failure	cx3	1.201515	
Factor for short embedded anchors	ch3	0.825723	
Factor to account for eccentric shear	cev3	1	
Factor to account for corner failure	Cc3	0.815394	
Factor to account for uncracked concrete	Cvr	1	
Corner edge breakout strength in shea	Vc3	45.25	kN
Front edge breakout strength in shear	Vc3	66.684	kN
Govering breakout strength in shear	Vc3	45.25	kN

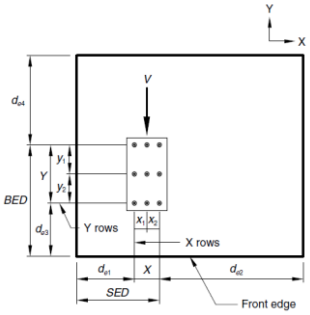

$V_{c3}=V_{co3}\, C_{x3}\, C_{h3}\, C_{ev3}\, C_{vcr}$

Vb=16.5λ√fc (BED)^1.33

Beam breakout strength strength in shear (TEST 2 and 3)

Input

Grade of concrete (f'c)		40	N/mm^2
Beam details			
Width of beam (B)		350	mm
Depth of beam (D)		400	mm
Threaded bar details			
Number of threaded rods		4	
Diameter (da)		33	mm
Embedded depth (hef)		200	mm
Yield strength (fya)		640	N/mm^2
Ultimate strength (fua)		800	N/mm^2
Steel duct diameter (sdd)		50	mm
Horizontal reinforcement details			
Yield strength of stirrup (fys)		720	N/mm^2
Diameter of the stirrup (ds)		10	mm
Number of stirrups in upper half of beam depth		4	
Provided length of the stirrup (ls)		300	mm
Location of threaded rods			
Beam edge distance in X-direction (X1)		165	mm
Spacing of ducts in X-direction (X2)		100	mm
Beam edge distance in Y-direction (Y1)		88	mm
Spacing of ducts in Y-direction (Y2)		174	mm

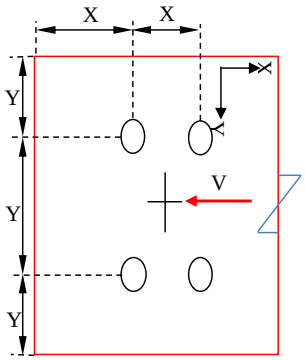

Concrete breakout strength in shear

ACI318M-08 (Section D 6.2)

Half of the depth of beam	ha	200	mm
Load bearing length of the anchor	le	200	mm
Diameter of the threaded rod	da	33	mm
factor for normal or light weight concrete	λ	1	
Eccentricity of applied shear	ev	0	mm
distance from the edge to farthest anchor	Ca1	133.3333	mm
Breakout strength of single anchor	Vb	48122.65	N
Factor to account for eccentric shear	$\Psi_{ec,V}$	1	
Factor to account for edge effect	$\Psi_{ed,V}$	0.832	
Factor to account for uncracked concrete	$\Psi_{c,V}$	1.4	
Factor for short embedded anchors	$\Psi_{h,V}$	1	
Unaffected Projected area of single anch	Avco	80000	mm^2
Actual projected area of group of anchors	Avc	70000	mm^2
Concrete breakout strength in shear	Vc	49.0	kN

$Vb=0.(l_e/d_a)^{0.2}d_a^{1/2}\lambda f'_c{}^{1/2}C_{a1}{}^{1.5}$

$V_c = \frac{A_{vc}}{A_{vco}} \Psi_{ec,V}\Psi_{ed,V}\Psi_{c,V}\Psi_{h,V}V_b$

PCI Design handbook /7th Edition

See adjacent figure	SED	10.31	inch
See adjacent figure	BED	9.45	inch
Corner beam failure	SED/BED	1.09	
Breakout strength of single anchor	Vb	24.91738	kip
Factor to account for front edge failure	cx3	1.091667	
Factor for short embedded anchors	ch3	0.684653	
Factor to account for eccentric shear	cev3	1	
Factor to account for corner failure	Cc3	0.720556	
Factor to account for uncracked concrete	Cvr	1	
Corner edge breakout strength in shea	Vc3	54.58	kN
Front edge breakout strength in shear	Vc3	82.68869	kN
Govering breakout strength in shear	Vc3	54.58	kN

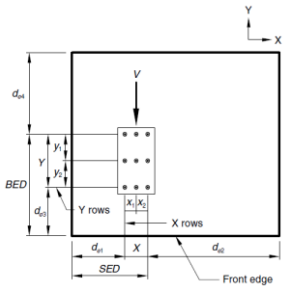

$V_{c3}=V_{co3}\,C_{x3}\,C_{h3}\,C_{ev3}\,C_{vcr}$

$Vb=16.5\lambda\sqrt{fc}\,(BED)^{1.33}$

Shear resistance of horizontal stirrups

Required development length (ld)	437	mm
Yield strength of each stirupp	112.32	kN
Total yield strength of stirrup (Ts)	449.28	kN
Total yield resistance after slip (Vc+Ts)	503.86	kN

Beam breakout strength strength in shear (TEST-5,6,9,10, 11 and 12)

Input

Grade of concrete (f'c)		40	N/mm^2
Beam details			
Width of beam (B)		350	mm
Depth of beam (D)		400	mm
Threaded bar details			
Number of threaded rods		4	
Diameter (da)		33	mm
Embedded depth (hef)		200	mm
Yield strength (fya)		640	N/mm^2
Ultimate strength (fua)		800	N/mm^2
Steel duct diameter (sdd)		50	mm
Horizontal reinforcement details			
Yield strength of stirrup (fys)		720	N/mm^2
Diameter of the stirrup (ds)		10	mm
Number of stirrups in upper half of beam depth		4	
Provided length of the stirrup (ls)		300	mm
Location of threaded rods			
Beam edge distance in X-direction (X1)		125	mm
Spacing of ducts in X-direction (X2)		100	mm
Beam edge distance in Y-direction (Y1)		88	mm
Spacing of ducts in Y-direction (Y2)		174	mm

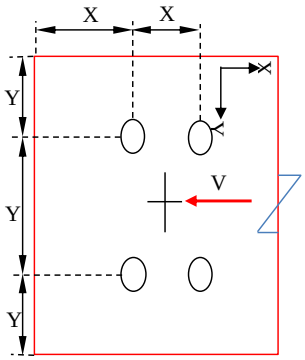

Concrete breakout strength in shear

ACI318M-08 (Section D 6.2)

Half of the depth of beam	ha	200	mm
Load bearing length of the anchor	le	200	mm
Diameter of the threaded rod	da	33	mm
factor for normal or light weight concrete	λ	1	
Eccentricity of applied shear	ev	0	mm
distance from the edge to farthest anchor	Ca1	100	mm
Breakout strength of single anchor	Vb	31256.58	N
Factor to account for eccentric shear	$\Psi_{ec,V}$	1	
Factor to account for edge effect	$\Psi_{ed,V}$	0.876	
Factor to account for uncracked concrete	$\Psi_{c,V}$	1.4	
Factor for short embedded anchors	$\Psi_{h,V}$	1	
Unaffected Projected area of single anch	Avco	45000	mm^2
Actual projected area of group of anchors	Avc	52500	mm^2
Concrete breakout strength in shear	Vc	44.7	kN

$Vb=0.(l_e/d_a)^{0.2}d_a^{1/2}\lambda f'_c{}^{1/2}C_{a1}{}^{1.5}$

$V_c = \frac{A_{vc}}{A_{vco}} \Psi_{ec,V}\Psi_{ed,V}\Psi_{c,V}\Psi_{h,V}V_b$

PCI Design handbook /7th Edition

See adjacent figure	SED	10.31	inch
See adjacent figure	BED	7.87	inch
Corner beam failure	SED/BED	1.31	
Breakout strength of single anchor	Vb	19.55201	kip
Factor to account for front edge failure	cx3	1.14	
Factor for short embedded anchors	ch3	0.75	
Factor to account for eccentric shear	cev3	1	
Factor to account for corner failure	Cc3	0.76524	
Factor to account for uncracked concrete	Cvr	1	
Corner edge breakout strength in shea	Vc3	49.82	kN
Front edge breakout strength in shear	Vc3	74.22334	kN
Govering breakout strength in shear	Vc3	49.82	kN

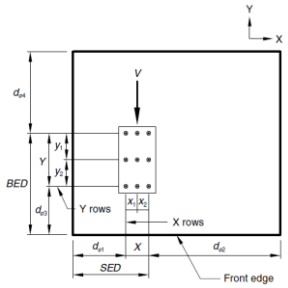

$V_{c3}=V_{co3}\,C_{x3}\,C_{h3}\,C_{ev3}\,C_{vcr}$

$Vb=16.5\lambda\sqrt{fc}\,(BED)\text{^}1.33$

Shear resistance of horizontal stirrups

Required development length (ld)	437	mm
Yield strength of each stirupp	112.32	kN
Total yield strength of stirrup (Vs)	449.28	kN
Total yield resistance after slip (Vc+Ts)	499.10	kN

Appendix E: Modes of failure of the sub-assemblies with end plate connections

E.1 Test EP1: Damage state of the precast concrete beam

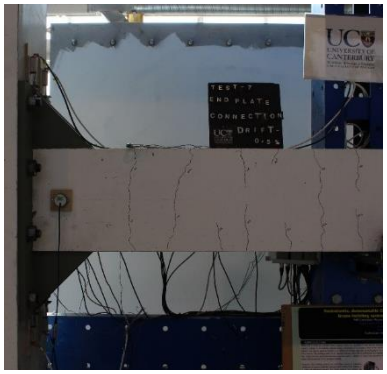

(a) 0.75% lateral drift: spread of flexural cracks

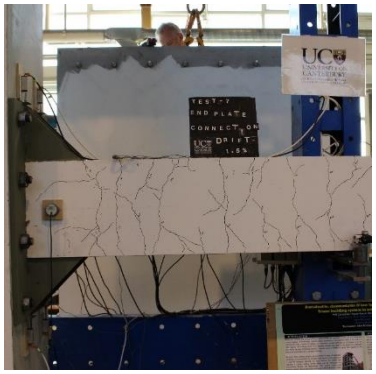

(b) 1.5% lateral drift: Initiation of cracks in connection region

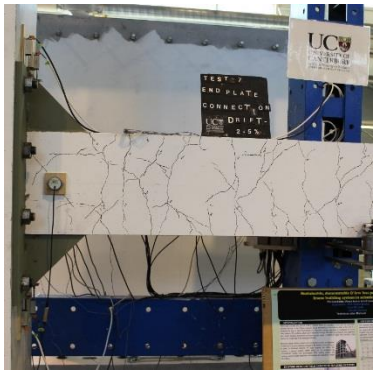

(c) 2.5% lateral drift: Spread of flexural shear cracks

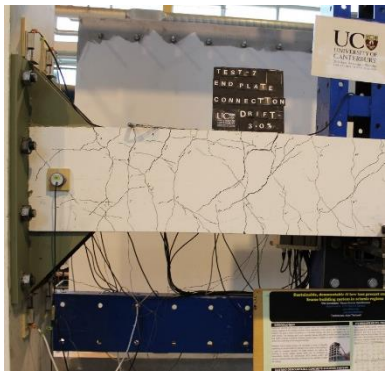

(d) Close up view of flexural shear cracks

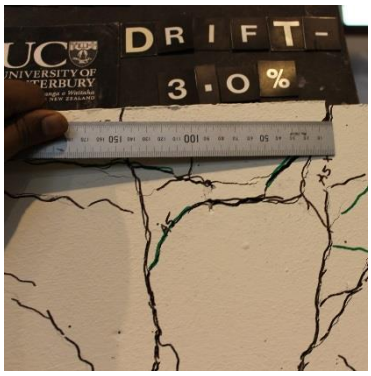

(e) 3.0% lateral drift: Cracks more than 4 mm width

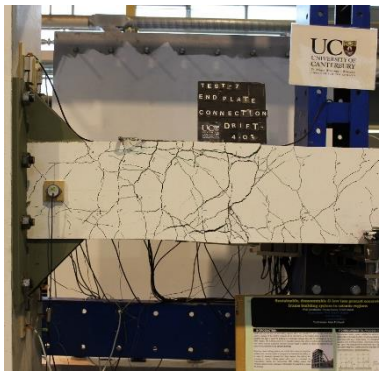

(f)4.0% lateral drift: damage state of beam

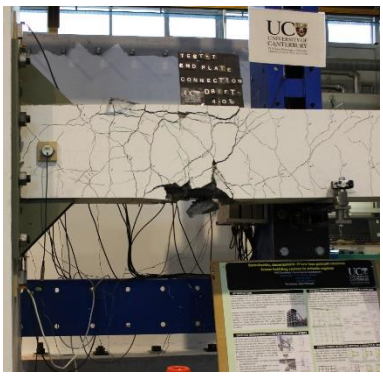

(g) 4.0% lateral drift: Spalling of cover concrete

(h) 5.0% lateral drift: Rebar buck-ing

(i) Close up view of rebar buckling

Figure E.1. Damage state of the precast concrete beam with end plate connection at different drifts

E.2 Test EP2: damage state of the precast concrete beam

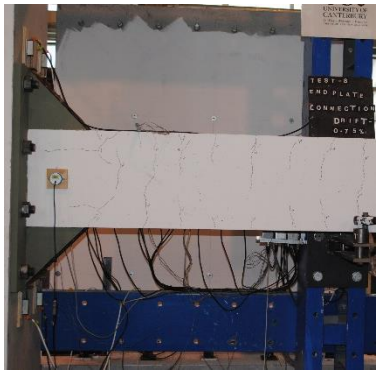

(a) 0.75% lateral drift: spread of flexural cracks

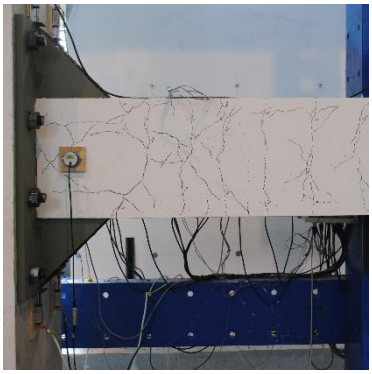

(b) 1.5% lateral drift: Initiation of cracks in connection region

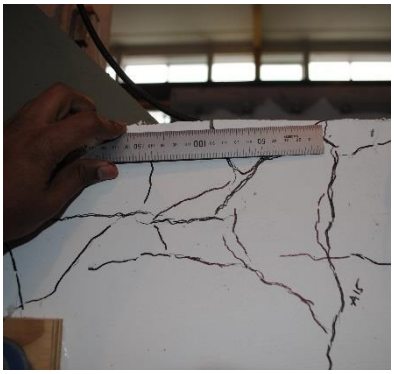

(c) Cracks more than 3mm width in front of gussets

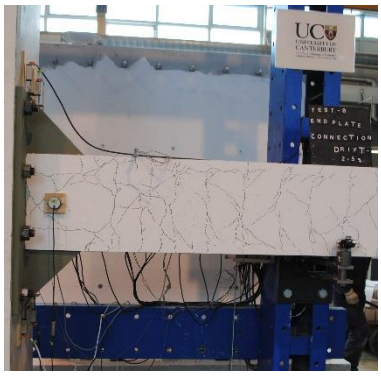

(d) 2.5% lateral drift: Damage state of beam

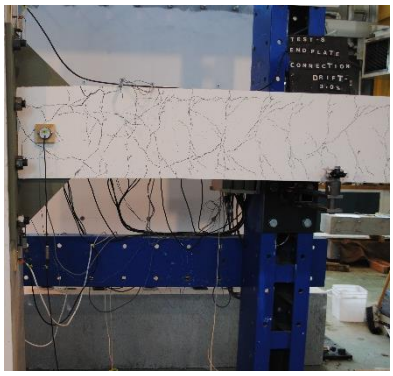

(e) 3.0% lateral drift: Damage state of beam

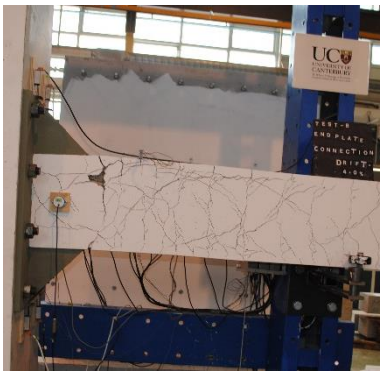

(f)4.0% lateral drift: Spalling of concrete

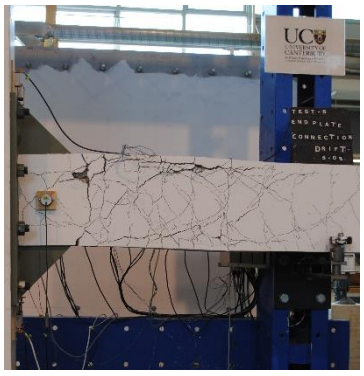

(g) 5.0% lateral drift: Initiation of rebar bucking

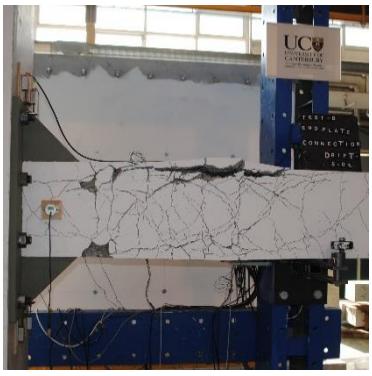

(h) 5.0% lateral drift: Rebar buck-ing

(i) Close up view of rebar buckling

Figure E.2. Damage state of the precast concrete beam with end plate connection at different drifts

Appendix F: Slip/movement plots of the sub-assemblies with angle and tube connections

F.1 Relative slip/movement of the angle connection

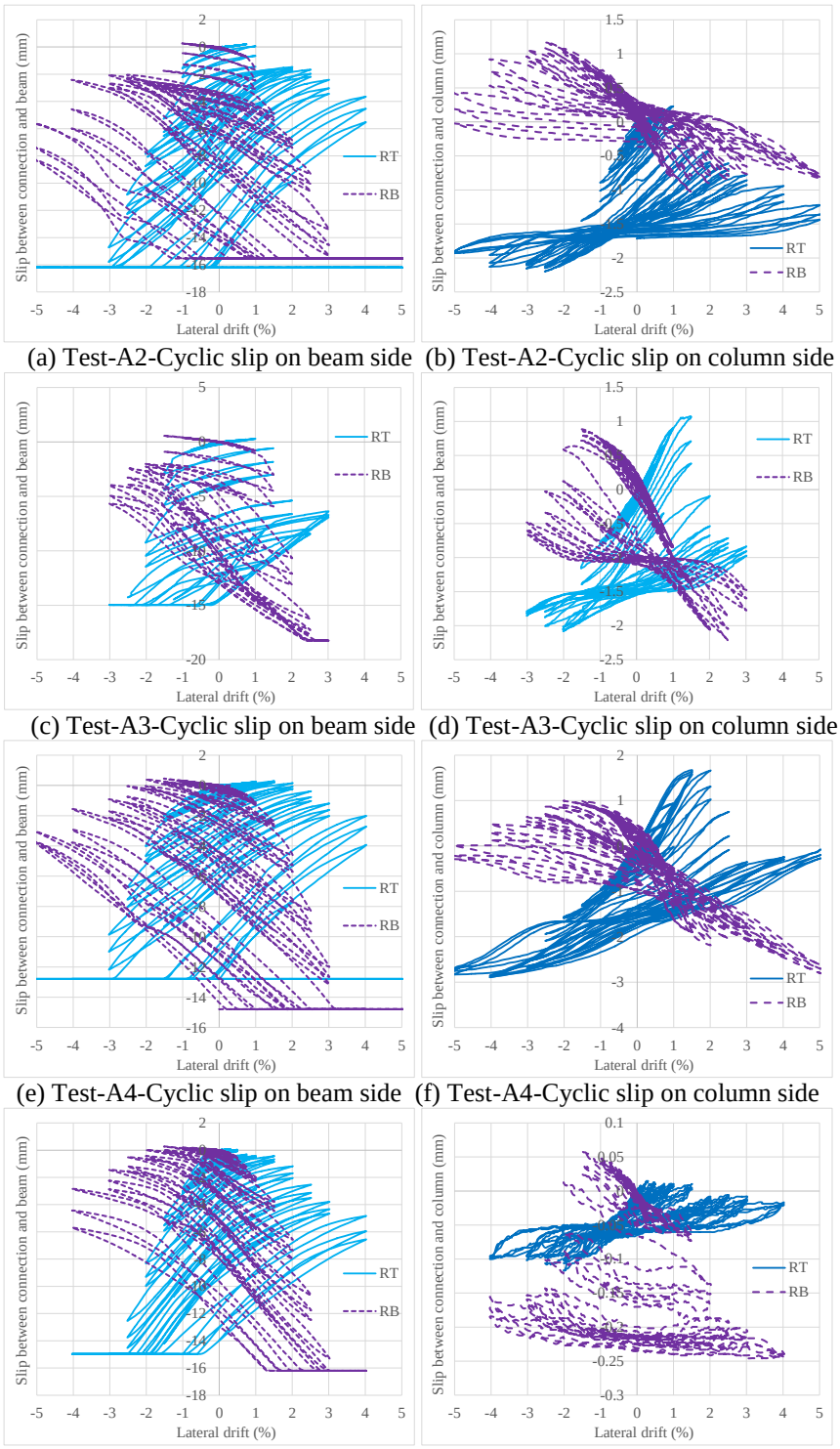

(a) Test-A2-Cyclic slip on beam side (b) Test-A2-Cyclic slip on column side

(c) Test-A3-Cyclic slip on beam side (d) Test-A3-Cyclic slip on column side

(e) Test-A4-Cyclic slip on beam side (f) Test-A4-Cyclic slip on column side

(g) Test-A5-Cyclic slip on beam side (h) Test-A5-Cyclic slip on column side

Figure F.1. Slip of the angle connection on beam and column sides obtained from Tests-A2 to A5

F.2 Relative slip/movement of the tube connection

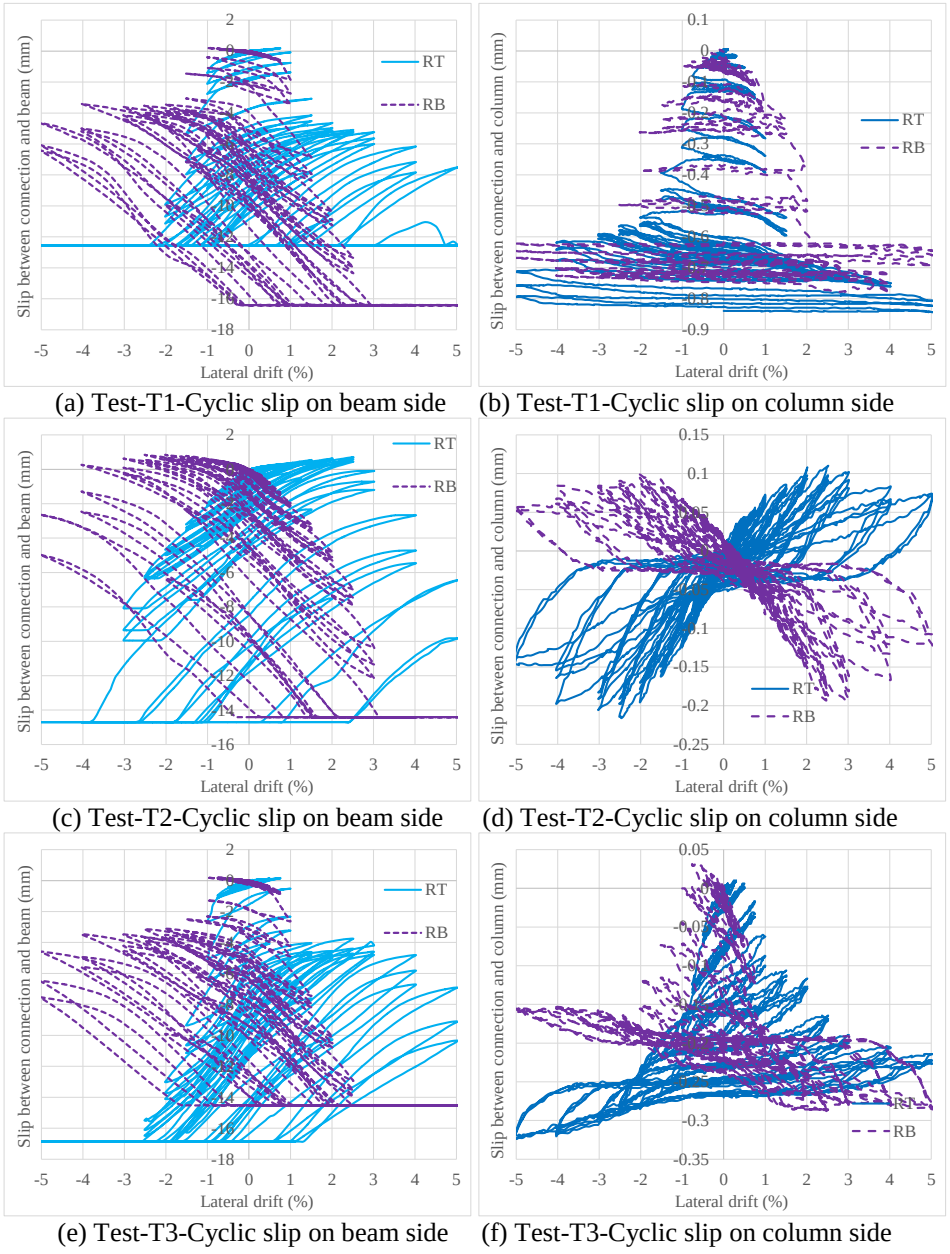

(a) Test-T1-Cyclic slip on beam side (b) Test-T1-Cyclic slip on column side

(c) Test-T2-Cyclic slip on beam side (d) Test-T2-Cyclic slip on column side

(e) Test-T3-Cyclic slip on beam side (f) Test-T3-Cyclic slip on column side

Figure F.2. Slip of tube connection on beam and column sides obtained from Tests-T1 to T3

Appendix G: Modes of failure of the sub-assemblies with angle and tube connections

G.1 Test A1: damage state of the precast concrete beam

(a) 0.5% drift: spread of flexural cracks along the beam length

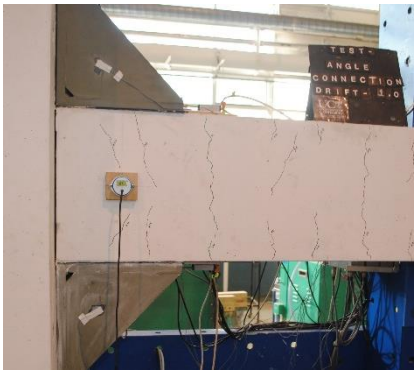

(b) 1.0% drift: initiation of beam edge cracks due to slip of connection

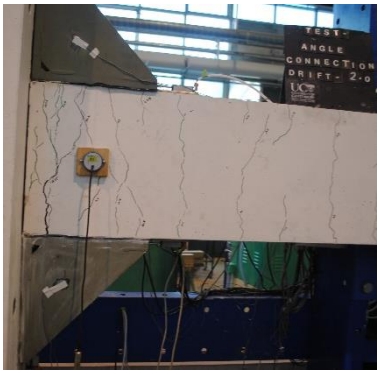

(c) Close-up view of the bursting cracks in the connection region

(d) Squeezing of the rubber sheet due to sliding of the connection

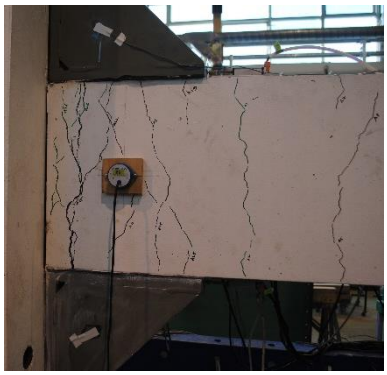

(e) 2% drift: wider bursting cracks beyond the 2nd row of steel ducts

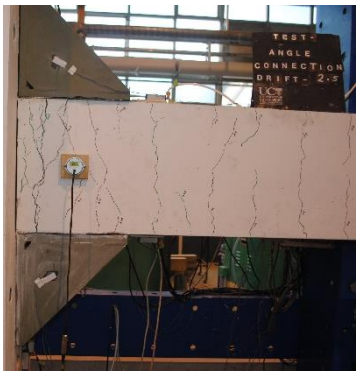

(f) 2.5% drift: ≥0.3 mm cracks in the connection region

(g) 5.0% drift: 300 mm length of spalled concrete and damage zone

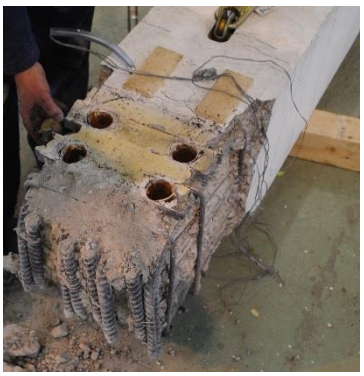

(h) Top view of the damaged beam removed after the test

(i) Elongated steel ducts due to bearing of the bolts

Figure G.1. Damage state of the beam with angle connection at different drifts obtained from Test-A1

G.2 Test A2: damage state of the precast concrete beam

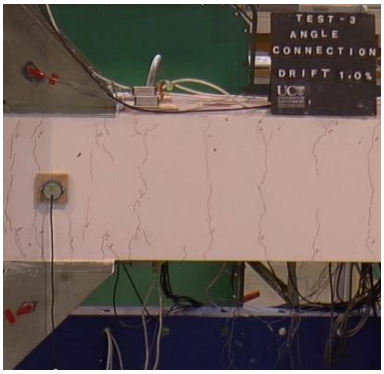

(a) 1% drift: spread of flexural cracks

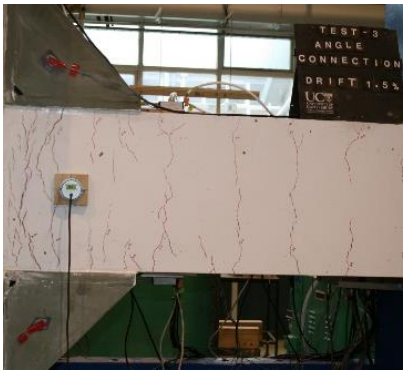

(b) 1.5% drift: initiation of beam edge/bursting cracks

(c) Close-up view of beam edge cracks

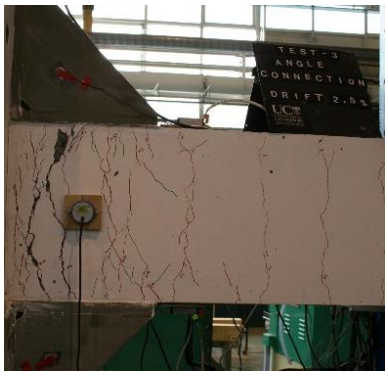

(d) 2.5% drift: concrete spalled near edge due to bearing of bolts

(e) 3% drift: close up view of the beam edge failure

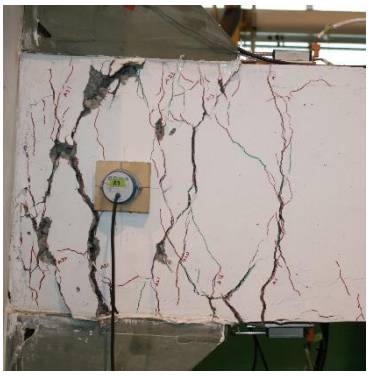

(f) 4.0% drift: severe damage to the beam in connection region

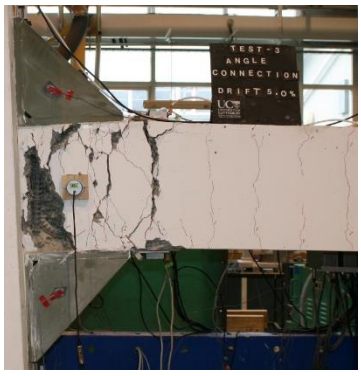

(g) 5.0% drift: spalled concrete and damage zone

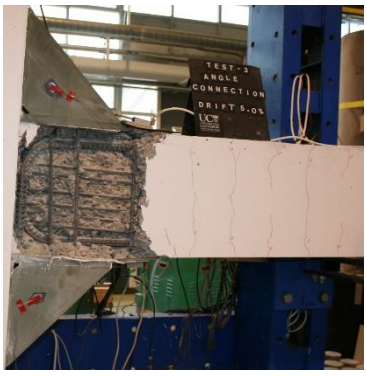

(h) Final damage state of the beam in the connection region

(i) Elongated steel ducts due to bearing of the bolts

Figure G.2. Damage state of the beam with angle connection at different drifts obtained from Test-A2

G.3 Test A3: damage state of the precast concrete beam

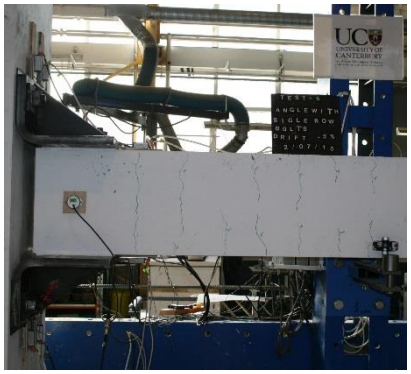

(a) 0.5% drift: spread of flexural cracks along the beam length

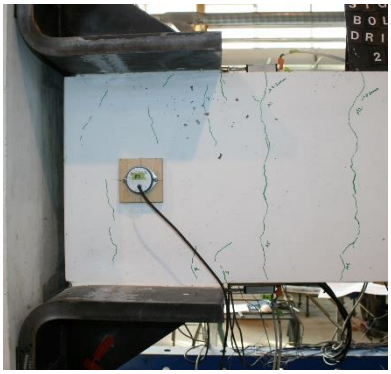

(b) 0.75% drift: initiation of beam edge/bursting cracks

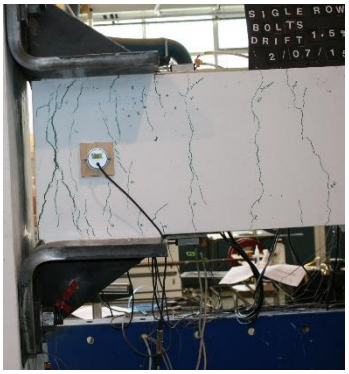

(c) Close-up view of beam edge cracks

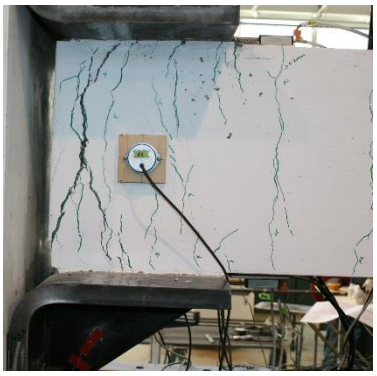

(d) 1.5% drift: big edge cracks due to bearing of the bolts

(e) 2.0% drift: 10 mm slip of the connection

(f) 2.0% drift: severe damage to the beam in connection region

(g) Close up view of damage to the beam in the connection region

(h) Spalled beam edge concrete

(i) 3.0% drift: damage state of the beam at the end of the test

Figure G.3. Damage state of the beam with angle connection at different drifts obtained from Test-A3

G.4 Test A4: damage state of the precast concrete beam

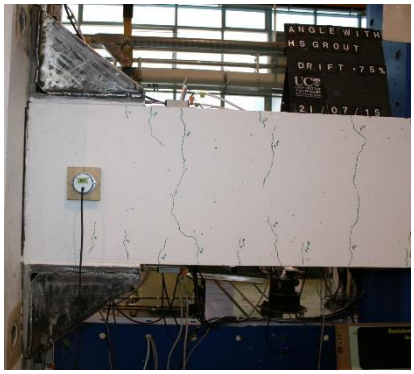

(a) 0.75% drift: spread of flexural cracks

(b) 1.0% drift: initiation of beam edge/bursting cracks

(c) 1.5% drift: spread of beam edge/bursting cracks

(d) 1.5% drift: close-up view of beam edge cracks

(e) 2.0% drift: spalled concrete in front of the bolts

(f) 2.0% drift: severe damage to the beam in connection region

(g) Close up view of damage to the beam in connection region

(h) Spalled beam edge concrete

(i) 5.0% drift: damage state of the beam at end of the test

Figure G.4. Damage state of the beam with angle connection at different drifts obtained from Test-A4

G.5 Test A5: damage state of the precast concrete beam

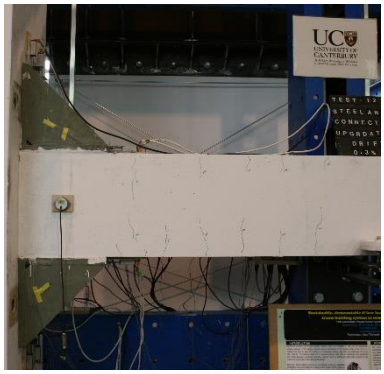

(a) 0.75% drift: spread of flexural cracks

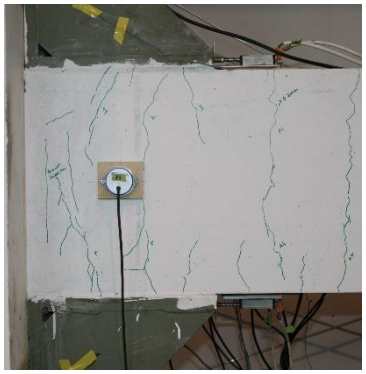

(b) 1.0% drift: initiation of beam edge/bursting cracks

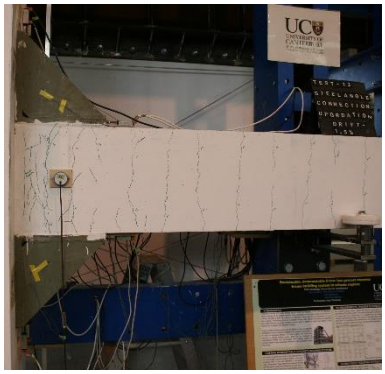

(c) 1.5% drift: spread of beam edge/bursting cracks

(d) 1.5% drift: close-up view of beam edge cracks

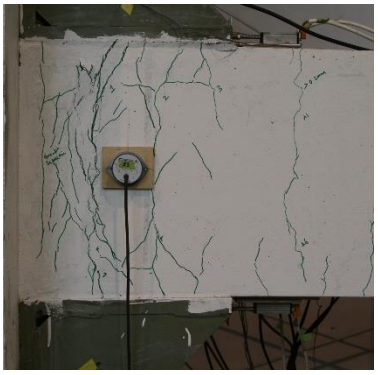

(e) 2.0% drift: spalled concrete in front of the bolts

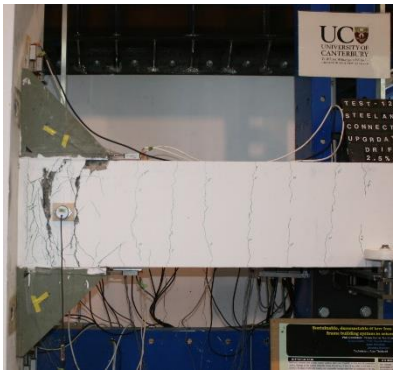

(f) 2.0% drift: severe damage to the beam in connection region

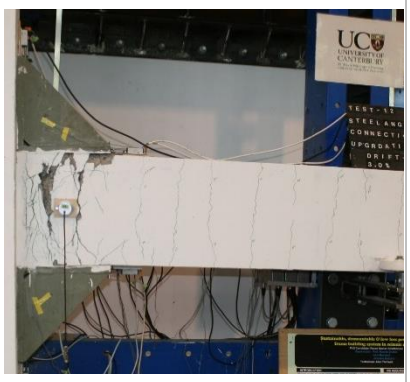

(g) Close up view of damage to the beam in connection region

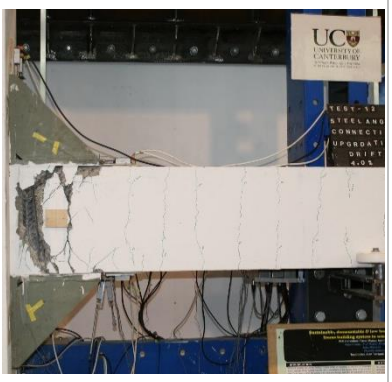

(h) Spalled beam edge concrete

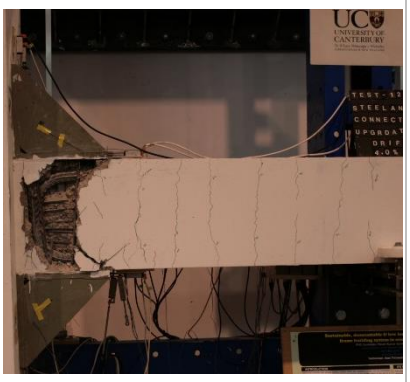

(i) 5.0% drift: damage state of the beam at end of the test

Figure G.5. Damage state of the beam with angle connection at different drifts obtained from Test-A5

G.6 Test T1: damage state of the precast concrete beam

(a) 1.0% drift: spread of flexural cracks

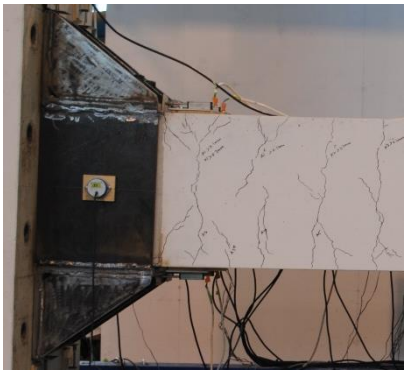

(b) 1.0% drift: initiation of beam edge/bursting cracks

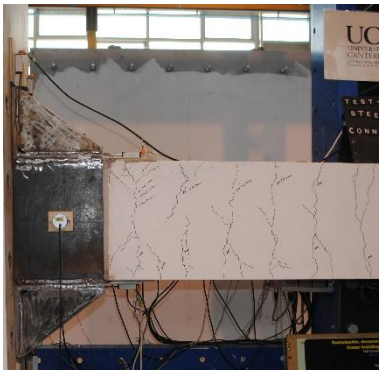

(c) 1.5% drift: damage state of beam

(d) 2.5% drift: diagonal cracks more than 5 mm near tube

(e) 3.0% drift: clear view of beam edge failure in front of the tube

(f) 2.0% drift: severe damage to the beam in connection region

(g) Close up view of damage to the beam in connection region

(h) Displaced threaded rods due to slip of the tube

(i) Spalled beam end concrete due to slip of the steel tube

Figure G.6. Damage state of the beam with angle connection at different drifts obtained from Test-T1

G.7 Test T2: damage state of the precast concrete beam

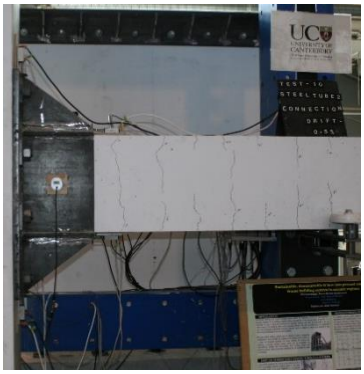

(a) 1.0% drift: spread of flexural cracks

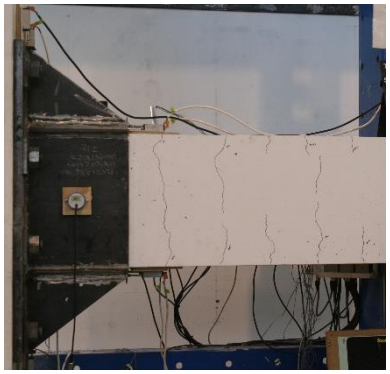

(b) 1.0% drift: close up view of cracks

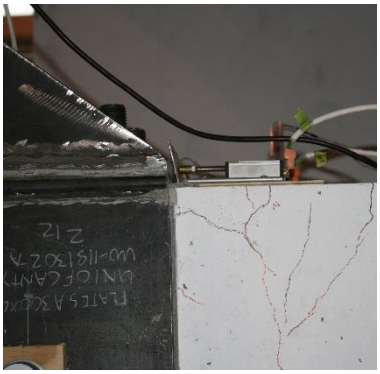

(c) Initiation of diagonal cracks due ingress of gusset plates

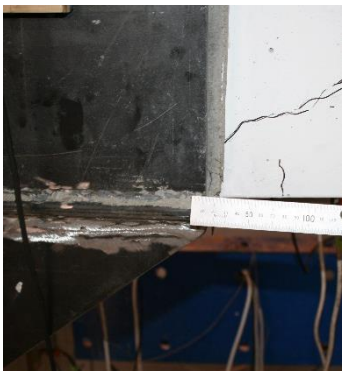

(d) Close up view of slip of the steel tube connection

(e) Diagonal cracks of more than 4 mm width

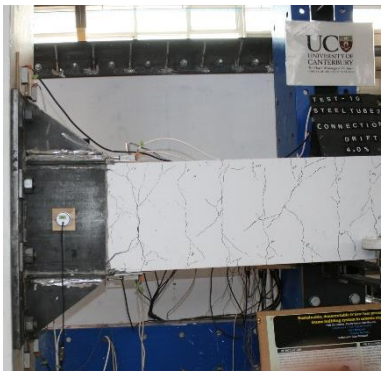

(f) 2.0% drift: damage state of beam in connection region

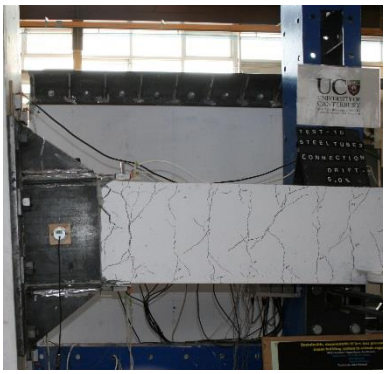

(g) 4.0% drift: severe damage to beam near connection

(h) 5.0% drift: spalled concrete in front of the tube

(i) Final damage state of the beam

Figure G.7. Damage state of the beam with angle connection at different drifts obtained from Test-T2

G.8 Test T3: damage state of the precast concrete beam

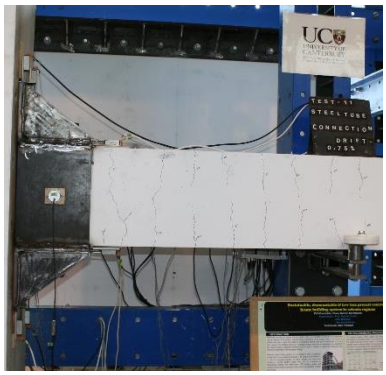

(a) 0.75% drift: spread of flexural cracks

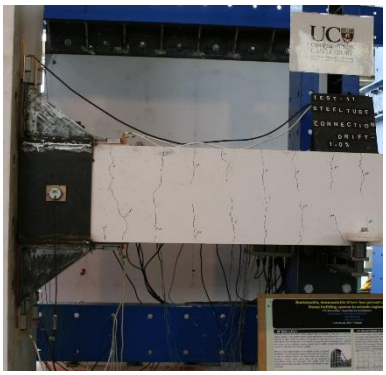

(b) 0.75% drift: close up view of cracks

(c) Close up view of early slip of the tube because of smooth epoxy

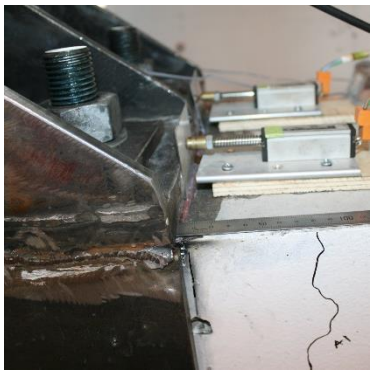

(d) Top view of slip of the connection

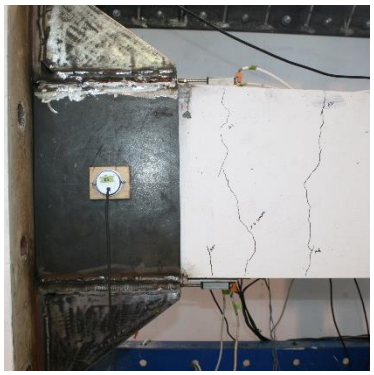

(e) Clear view of relative rotation of the beam in relation to column

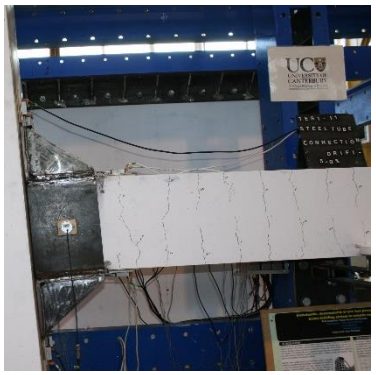

(f) 3.0% drift: damage state of beam in connection region

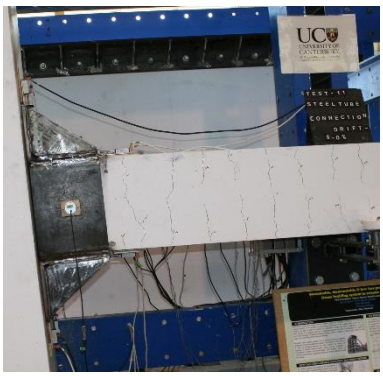

(g) 4.0% drift: minor damage to beam

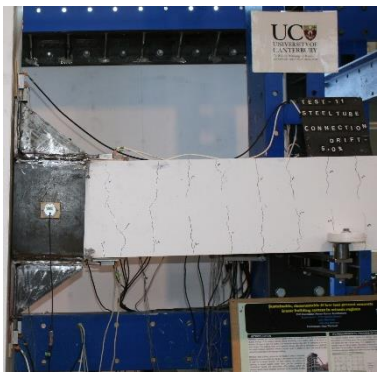

(h) 5.0% drift: no severe damage to the beam

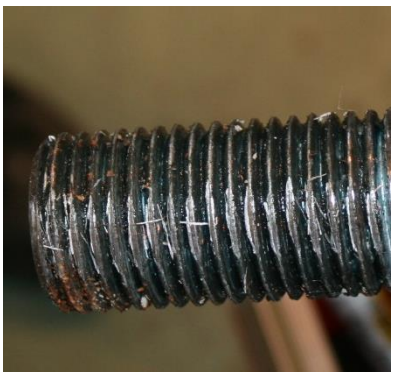

(i) Damaged threads of the bolt due to bearing on to steel ducts

Figure G.8. Damage state of the beam with angle connection at different drifts obtained from Test-T3

Appendix H:Nonlinear response of the connection and beam springs of the sub-assemblies with angle and tube connections

H.1 Monolithic system (MS) beam spring's nonlinear cyclic behaviour

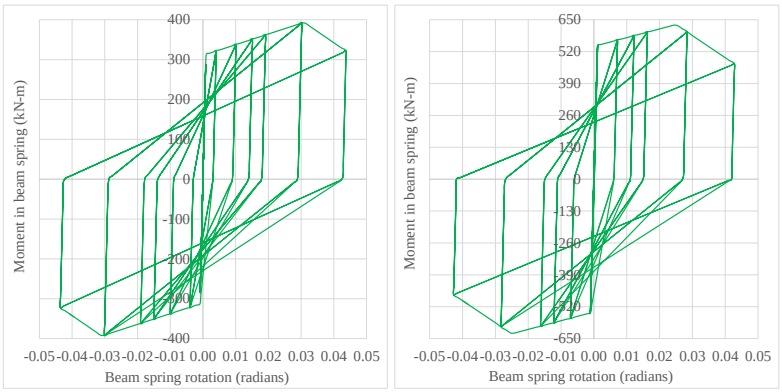

(a) Beam -1 (b) Beam-2

Figure H.1. Nonlinear response of beam springs of Beam-1 and 2 of monolithic sub-assembly system

H.2 Approach 1: Two parallel connection springs in series with the beam spring

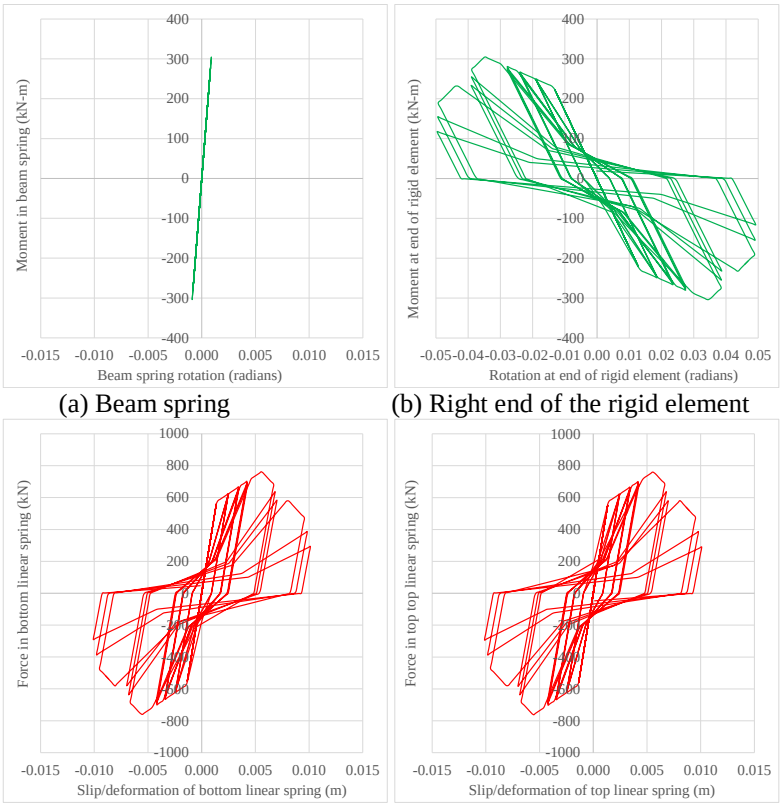

(a) Beam spring (b) Right end of the rigid element

(c) Bottom linear connection spring (d) Top linear connection spring

Figure H.2. Non-linear response of connection and beam springs of Test-A1sub-assembly

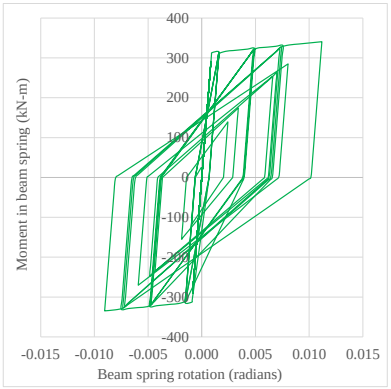

(a) Beam spring

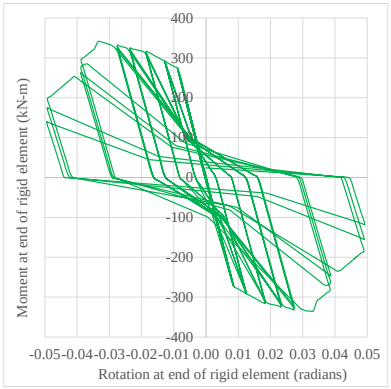

(b) Right end of rigid element

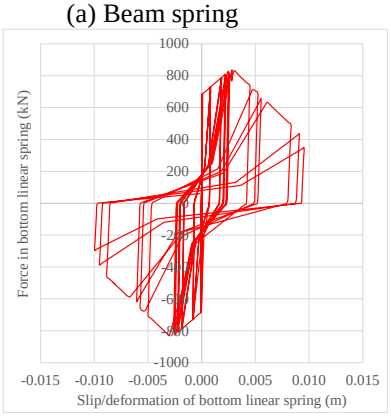

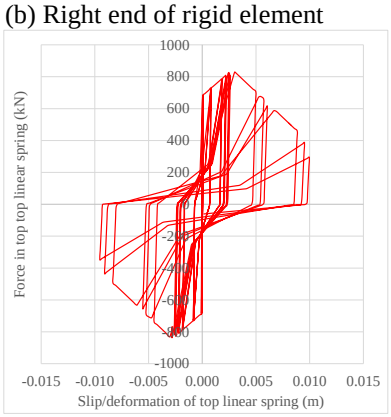

(c) Bottom linear connection spring (d) Top linear connection spring

Figure H.3. Non-linear response of connection and beam springs of Test-A2/A4 sub-assembly

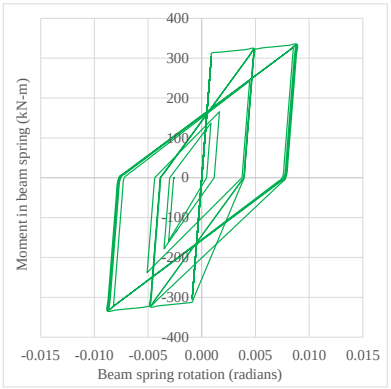

(a) Beam spring

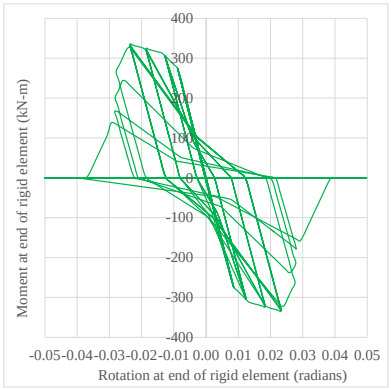

(b) Right end of rigid element

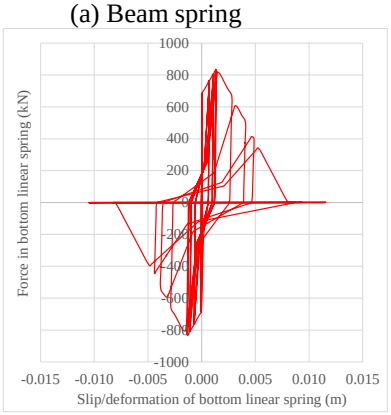

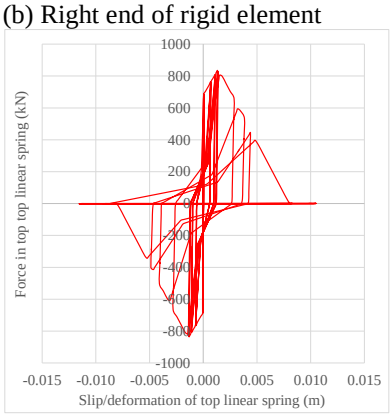

(c) Bottom linear connection spring (d) Top linear connection spring

Figure H.4. Nonlinear response of connection and beam springs of Test-A3 sub-assembly

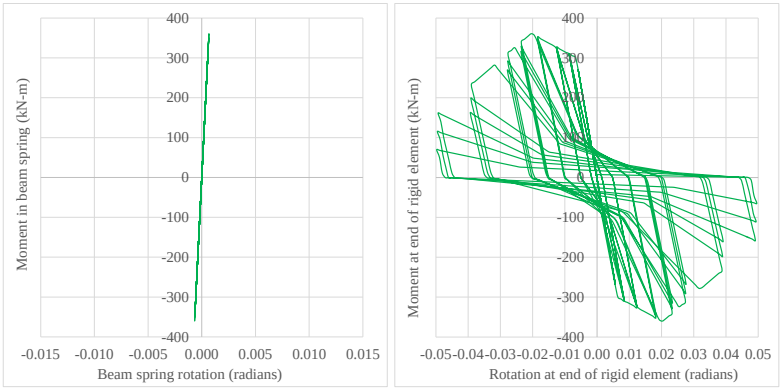

(a) Beam spring (b) Right end of rigid element

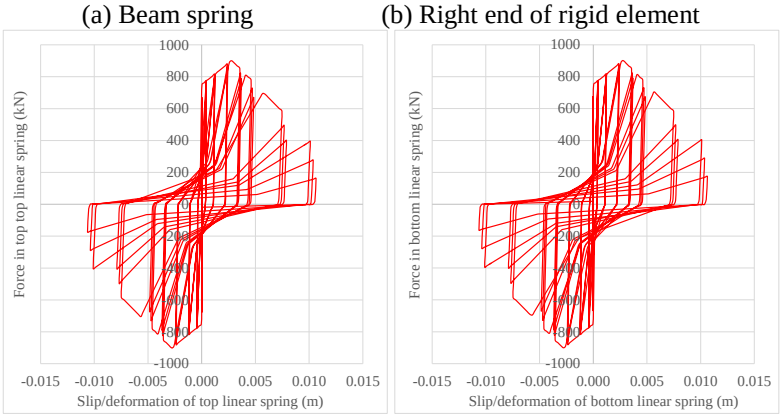

(c) Bottom linear connection spring (d)Top linear connection spring

Figure H.5. Nonlinear response of connection and beam springs of Test-A5 sub-assembly

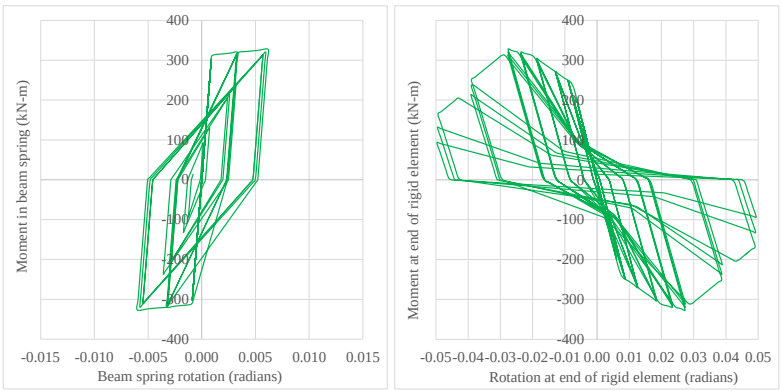

(a) Beam spring (b) Right end of rigid element

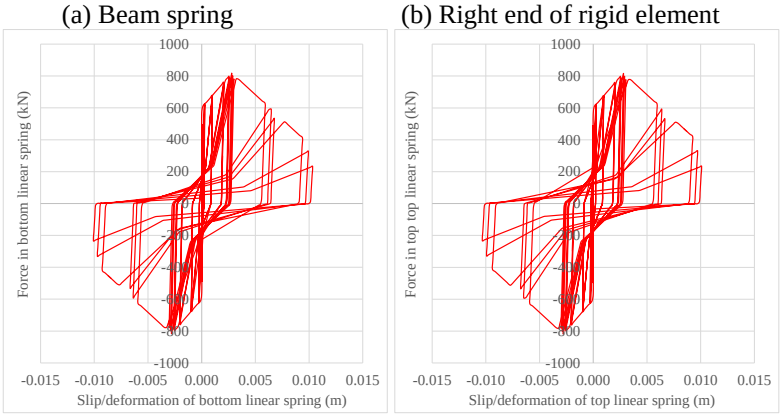

(c) Bottom linear connection spring (d) Top linear connection spring

Figure H.6. Non-linear response of connection and beam springs of Test-T1/T2 sub-assembly

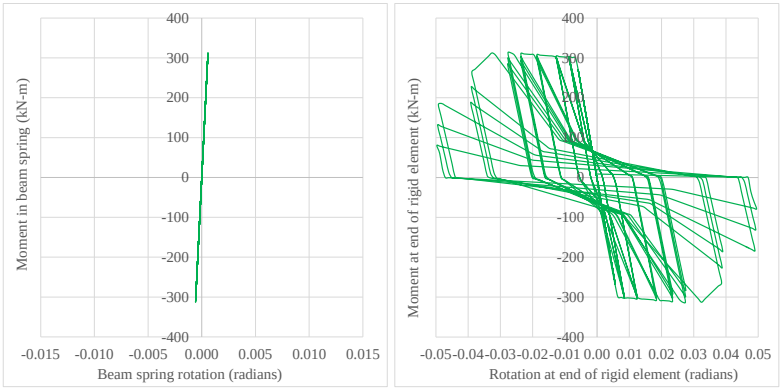

(a) Beam spring (b) Right end of rigid element

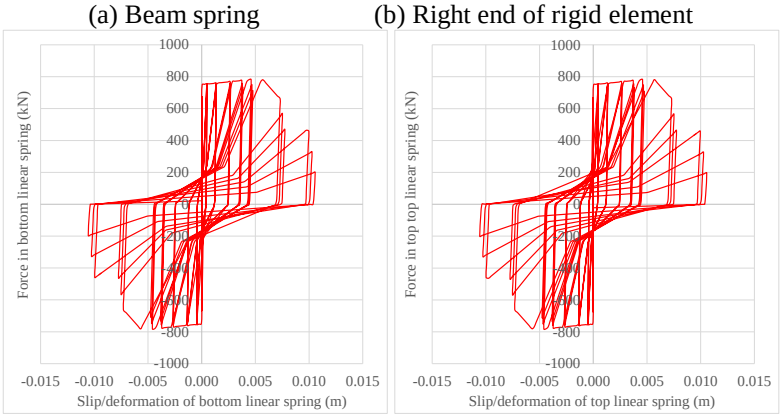

(c) Bottom linear connection spring (d) Top linear connection spring

Figure H.7. Non-linear response of connection and beam springs of Test-T3 sub-assembly

H.3 Approach 2: connection spring in series with beam spring

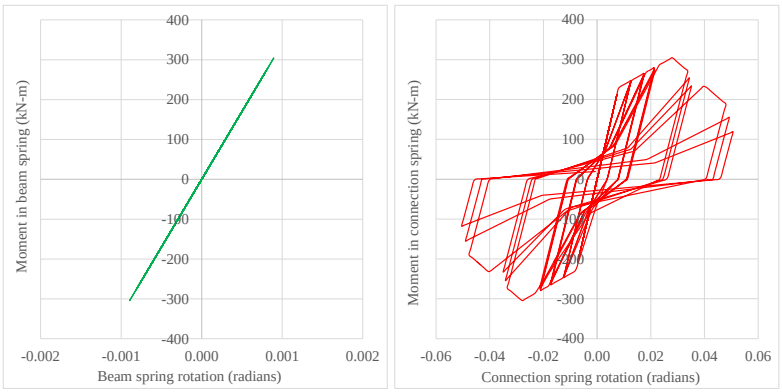

(a) Beam spring (b) Connection spring

Figure H.8. Nonlinear response of connection and beam springs of Test-A1 sub-assembly

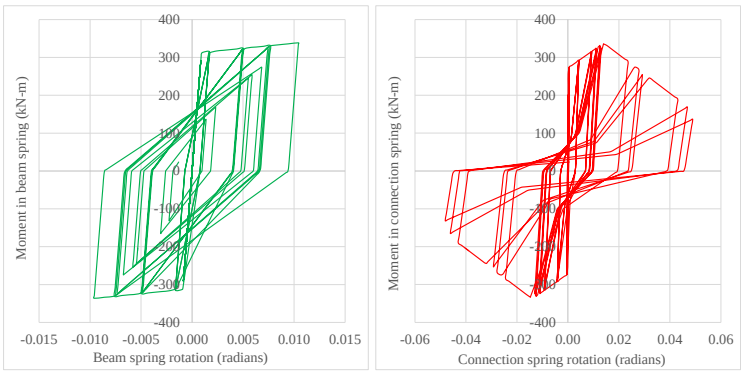

(a) Beam spring (b) Connection spring

Figure H.9. Nonlinear response of connection and beam springs of Test-A2/A4 sub-assembly

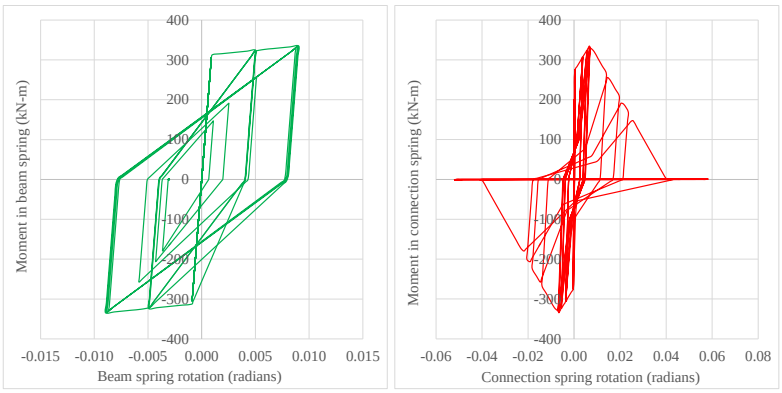

(a) Beam spring (b) Connection spring

Figure H.10. Nonlinear response of connection and beam springs of Test-A3 sub-assembly

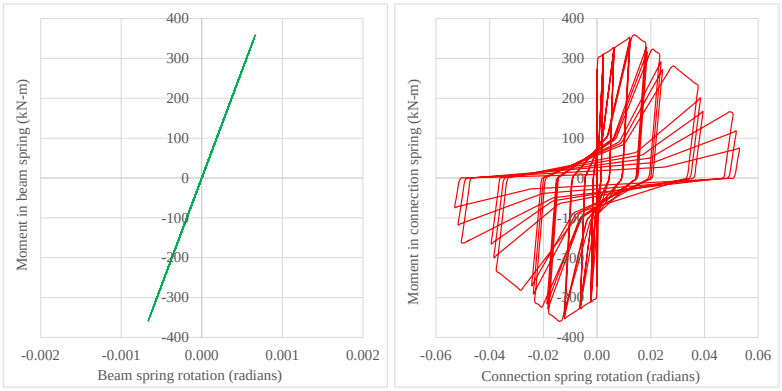

(a) Beam spring (b) Connection spring

Figure H.11. Nonlinear response of connection and beam springs of Test-A5 sub-assembly

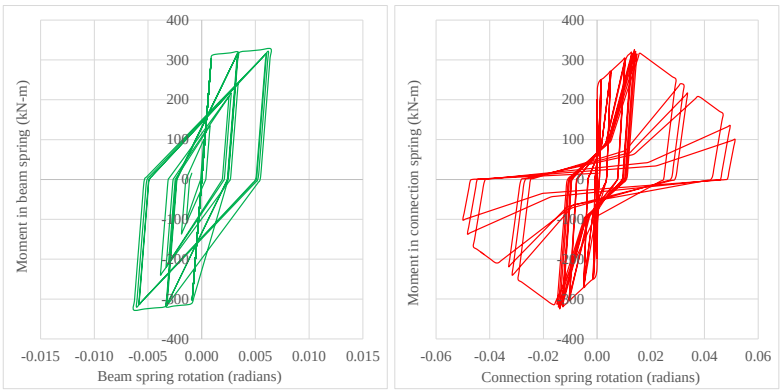

(a) Beam spring (b) Connection spring

Figure H.12. Nonlinear response of connection and beam springs of Test-T1/T2 sub-assembly

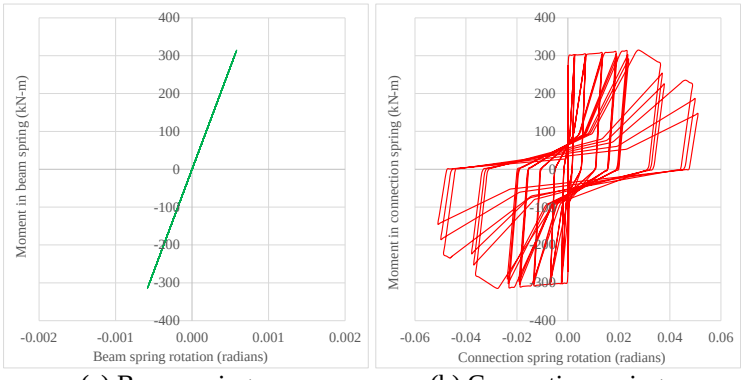

(a) Beam spring (b) Connection spring

Figure H.13. Non-linear response of connection and beam springs of Test-T3 sub-assembly

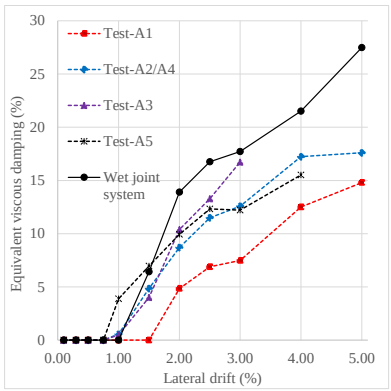

(a) Damping ξ_{eq} of Tests:A1-A5

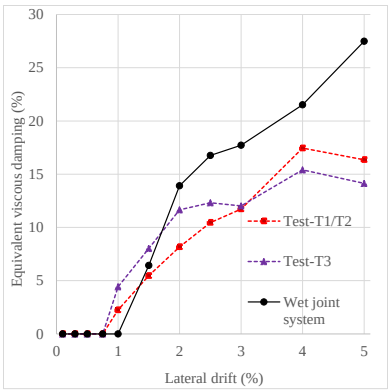

(b) Damping ξ_{eq} of Tests:T1-T3

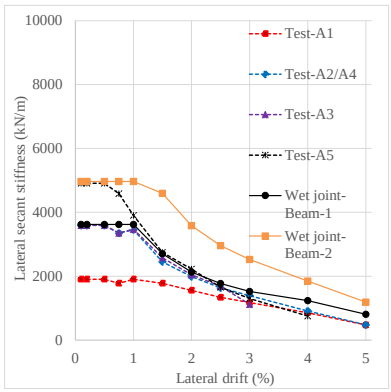

(c) Stiffness degradation K_l of Tests:A1-A5

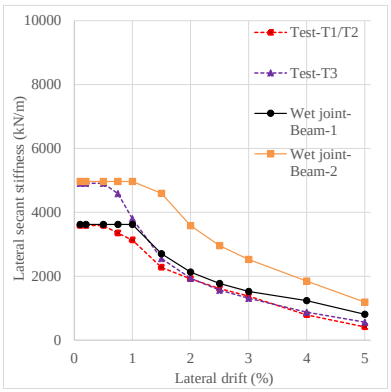

(d) Stiffness degradation K_l of Tests:T1-T3

Figure H.14. Damping and stiffness degradation of sub-assemblies (Appraoch-2)

Appendix I: Modes of failure of the sub-assemblies with angle and web plate connection and nonlinear behaviour of element springs

I.1 Test-AWP1: internal frame sub-assembly

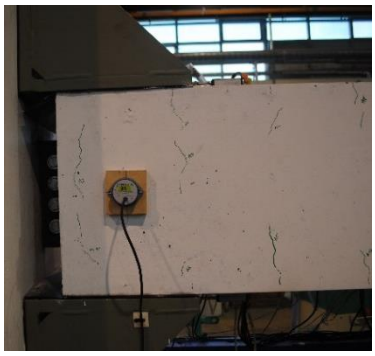

(a) 0.5% drift: spread of flexural cracks

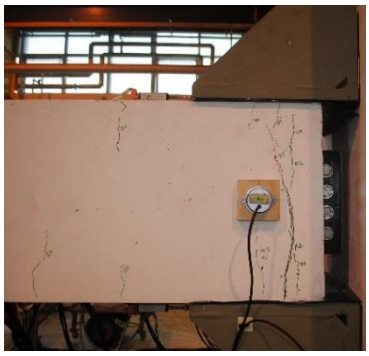

(b) 0.75% drift: initiation of beam edge cracks due to early slip

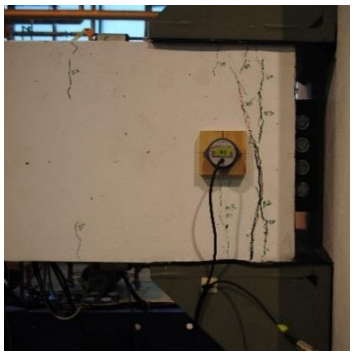

(c) Close-up view of the bursting cracks beyond first duct location

(d) 1.5% drift: another view of full depth beam edge failure

(e) 2% drift: initiation of cracks beyond the 2nd row of steel ducts

(f) 2.5% drift: spalled concrete due to high relative slip of connection

(g) Complete damage to the infill rubber sheet

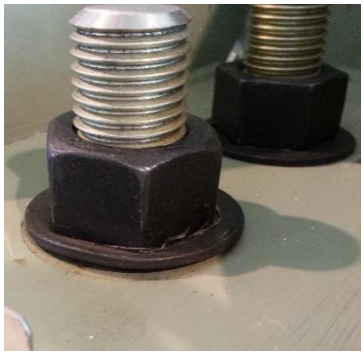

(h) Damage to the steel washers

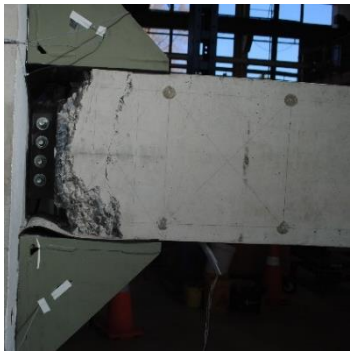

(i) 4.0% drift: complete beam edge failure due to slip of connection

Figure I.1. Damage state of the precast concrete beam at different drifts obtained from Test-AWP1

I.2 Test-AWP2: frame sub-assembly with repaired beam from Test-AWP1

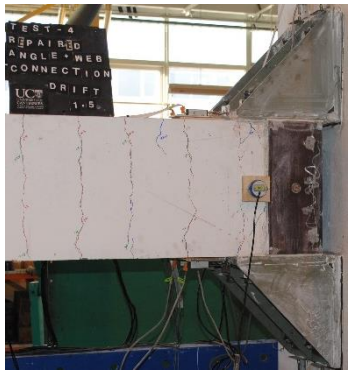

(a) 1.5% drift: formation of new cracks

(b) 2.0% drift: bulging of side plates

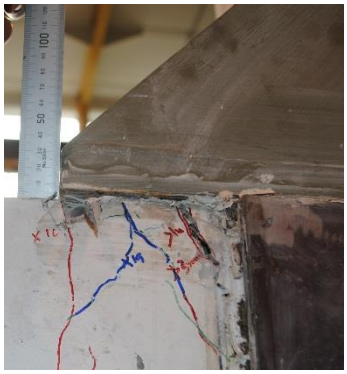

(c) Lift up of connection from beam due to prying

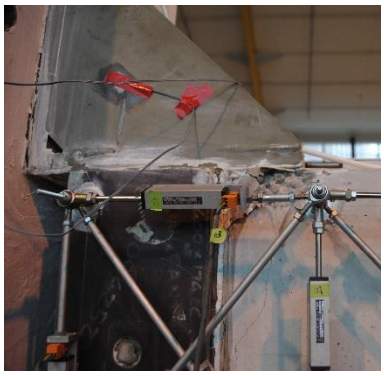

(d) 2.5% drift: spalled concrete due to ingress of the angle

(e) 3.0% drift: slide of the armored side plates

(f) spalled concrete in-front of the connection

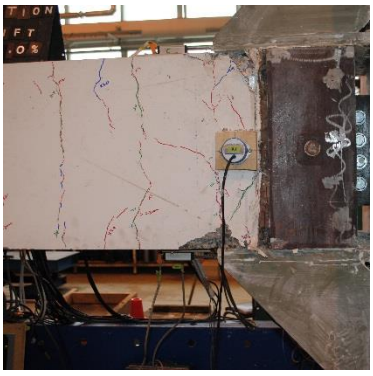

(g) 4.0% drift: high slip of the connection

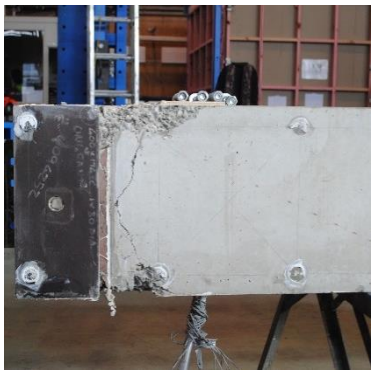

(h) Final damage state of the beam after the test

(i) Sliding marks on the beam top surface

Figure I.2. Damage state of the beam with angle and web plate connection at different drifts

I.3 Test-AWP2: nonlinear behaviour of element springs of the sub-assembly

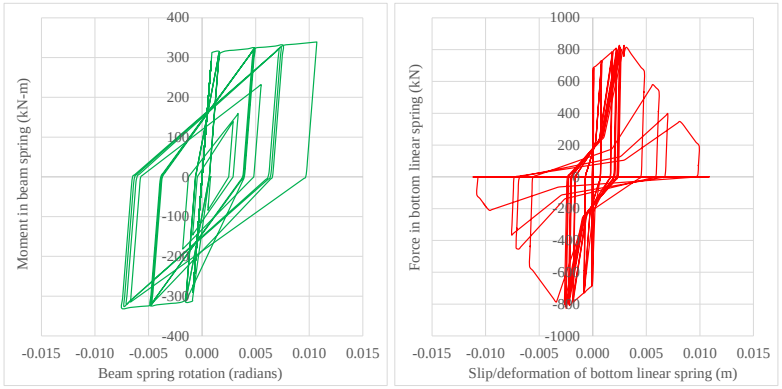

(a) Beam spring (b) Right end of rigid element

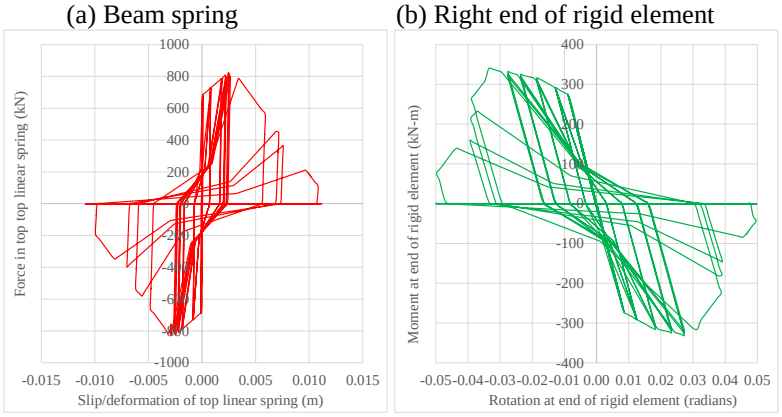

(c) Bottom linear connection spring (d) Top linear connection spring

Figure I.3. Approach-1: response of connection and beam springs of Test-AWP2 sub-assembly

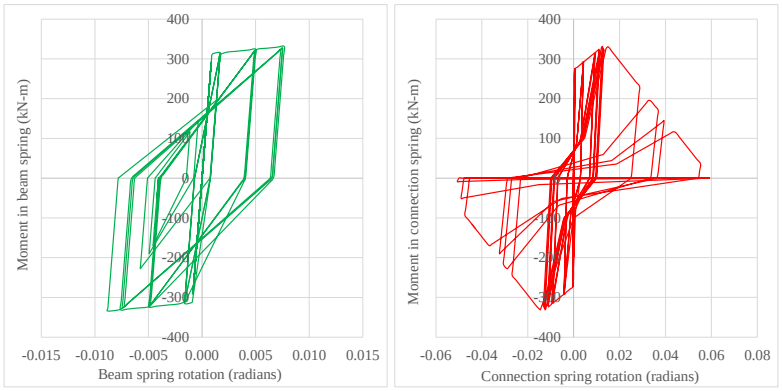

(a) Beam spring (b) Connection spring

Figure I.4. Approach-2: response of connection and beam springs of Test-AWP2 sub-assembly

Appendix J: Feasibility assessment of pin base connections for the lateral load resisting frame of proposed demountable building system

J.1 Variation of the base shear capacity with varying β for given Mc or Mb

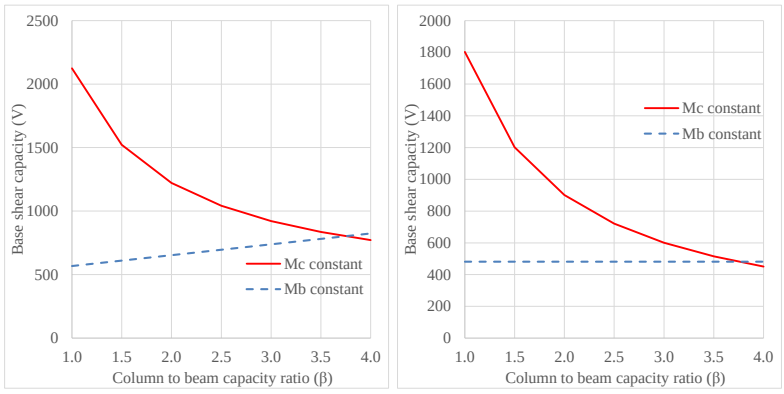

(a) Fixed base; Mc=675; Mb=180.23 (b) Pin base; Mc=675; Mb=180.23

Figure J.1. Variation of base shear capacity obtained from Equation 3 with varying β (Case-2)

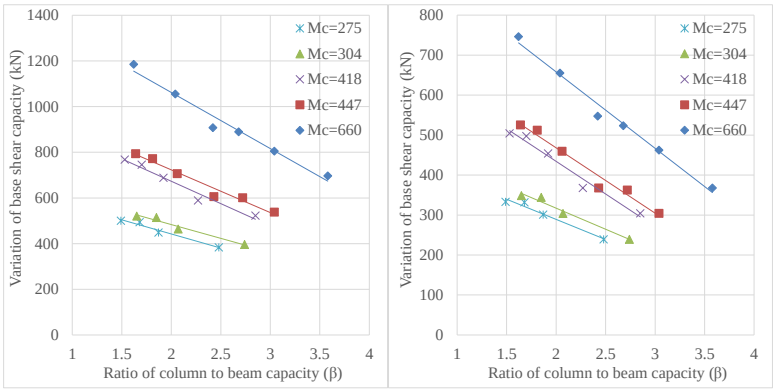

(a) 3s-3b-s=7-Fixed base (b) 3s-3b-s=7-Pin base

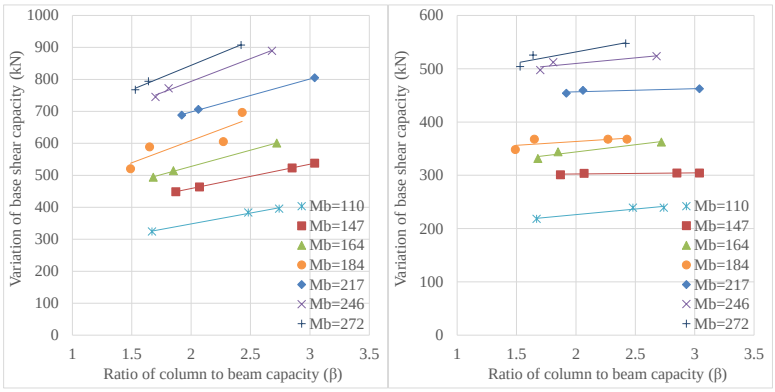

(c) 3s-3b-s=7-Fixed base (d) 3s-3b-s=7-Pin base

Figure J.2. Variation of base shear capacity of 3 storey frame for given Mc or Mb and varying β

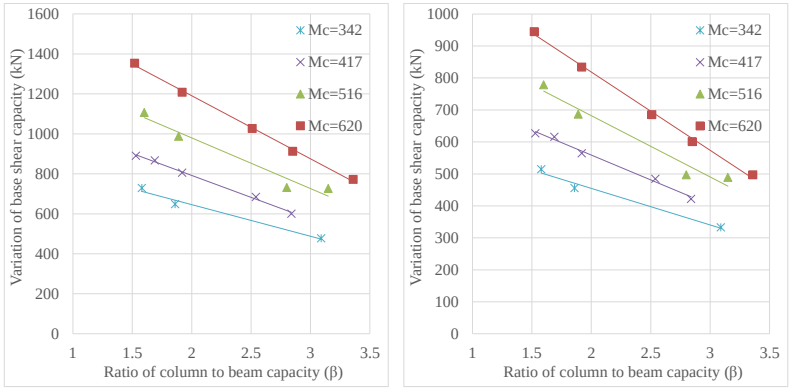

(a) 5s-4b-s=6-Fixed base (b) 5s-4b-s=6-Pin base

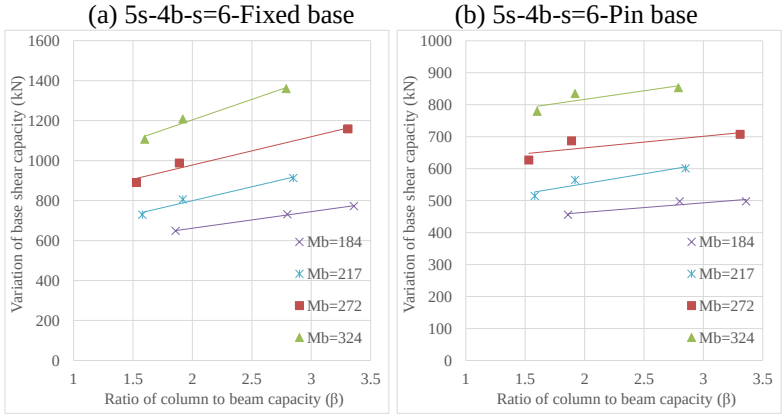

(c) 5s-4b-s=6-Fixed base (d) 5s-4b-s=6-Pin base

Figure J.3. Variation of base shear capacity of 5 storey frame for given Mc or Mb and varying β

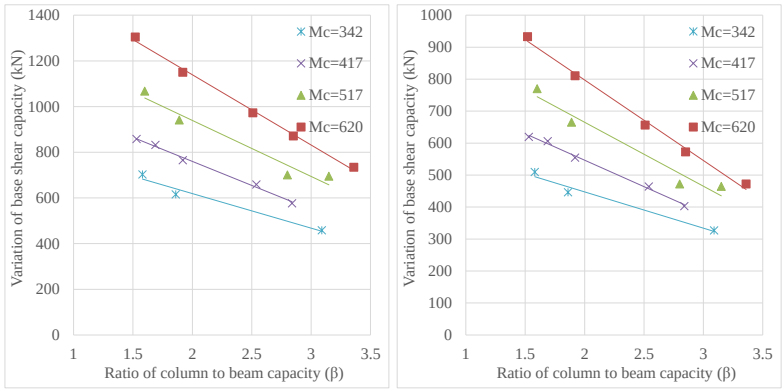

(a) 6s-4b-s=6-Fixed base (b) 6s-4b-s=6-Pin base

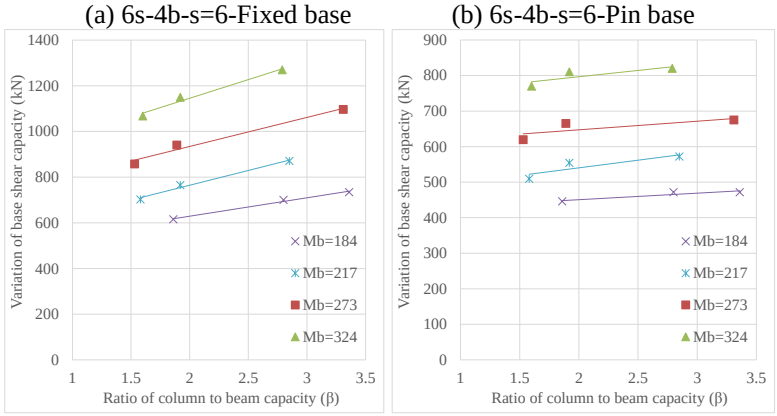

(c) 6s-4b-s=6-Fixed base (d) 6s-4b-s=6-Pin base

Figure J.4. Variation of base shear capacity of 6 storey frame for given Mc or Mb and varying β

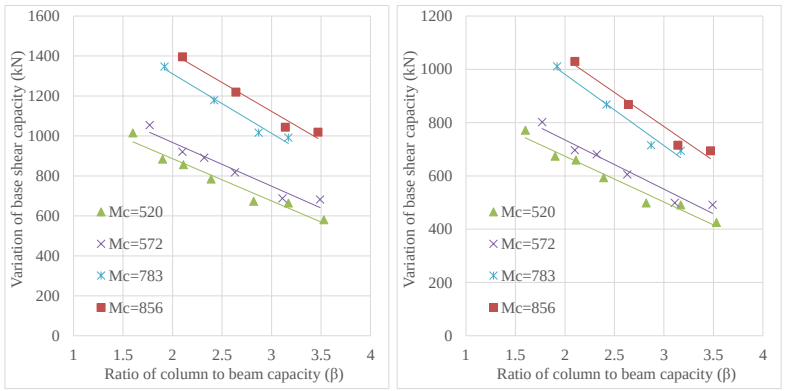

(a) 8s-4b-s=6-Fixed base (b) 8s-4b-s=6-Pin base

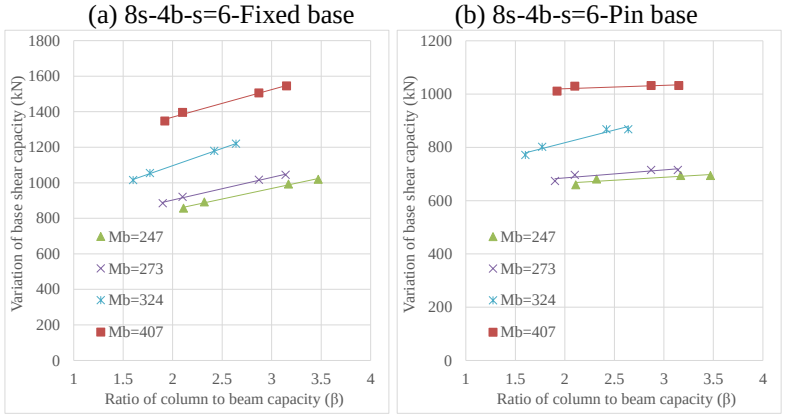

(c) 8s-4b-s=6-Fixed base (d) 8s-4b-s=6-Pin base

Figure J.5. Variation of base shear capacity of 8 storey frame for given Mc or Mb and varying β

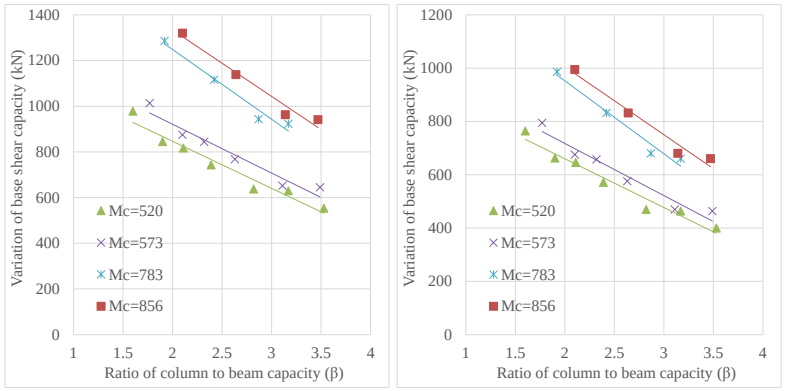

(a) 10s-4b-s=6-Fixed base (b) 10s-4b-s=6-Pin base

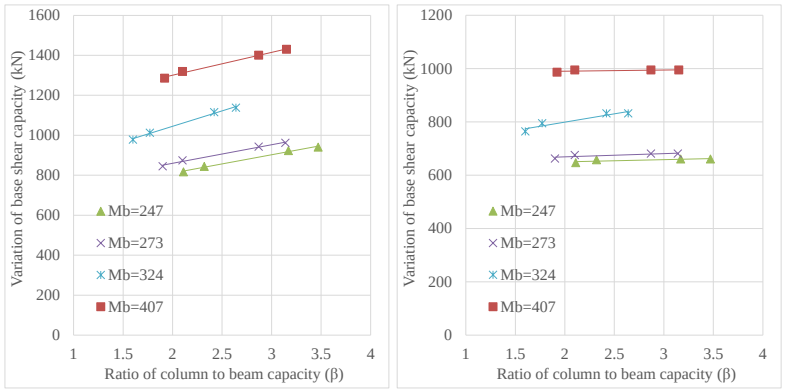

(c) 10s-4b-s=6-Fixed base (d) 10s-4b-s=6-Pin base

Figure J.6. Variation of base shear capacity of 10 storey frame for given Mc or Mb and varying β

J.2 Reduction in base shear capacity due to change of base fixity as function of β

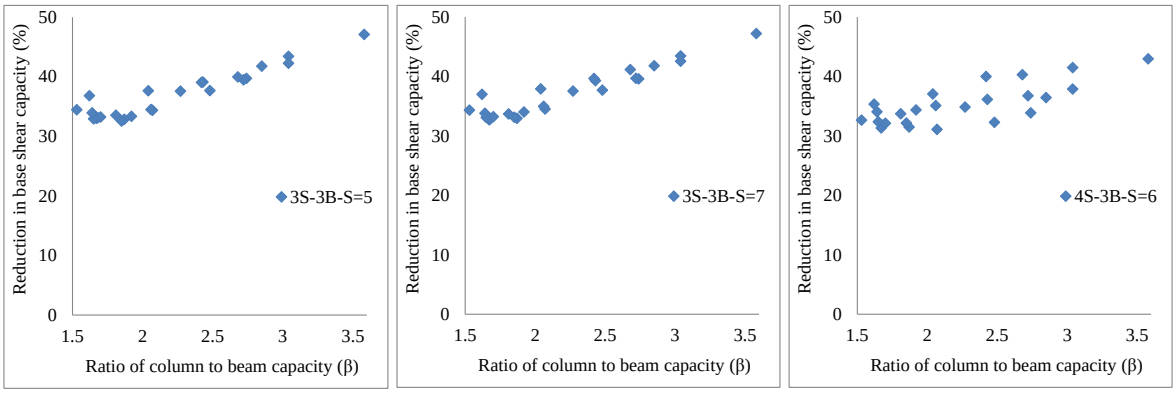

(a) 3 storey frame with 3 bays of 5 m span (b) 3 storey frame with 3 bays of 7 m span (c) 4 storey frame with 3 bays of span 6 m

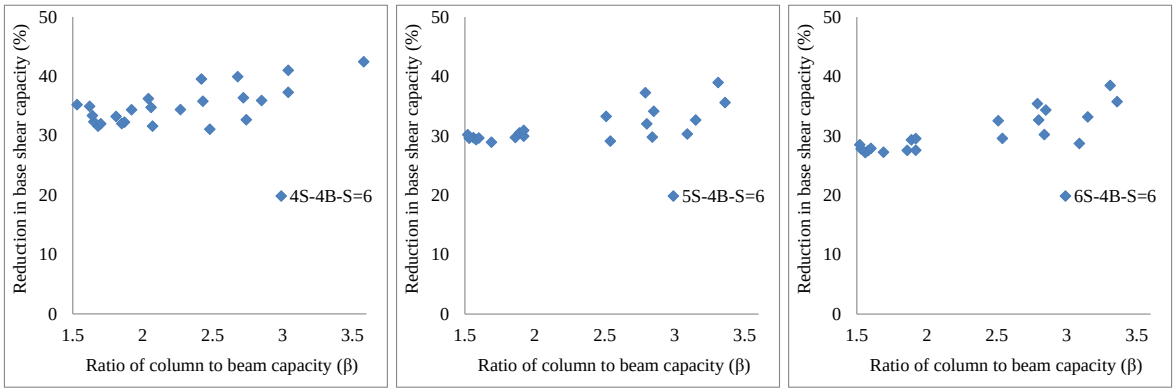

(d) 4 storey frame with 4 bays of span 6 m (e) 5 storey frame with 4 bays of span 6 m (f) 6 storey frame with 4 bays of span 6 m

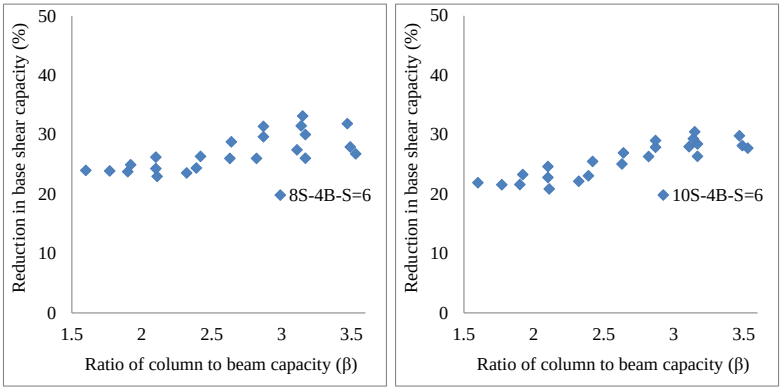

(f) 8 storey frame with 4 bays of span 6 m (f) 8 storey frame with 4 bays of span 6 m

Figure J.7. Variation of reduction of base shear capacity with varying β

J.3 Reduction in initial lateral stiffness due to change of bases as function of β

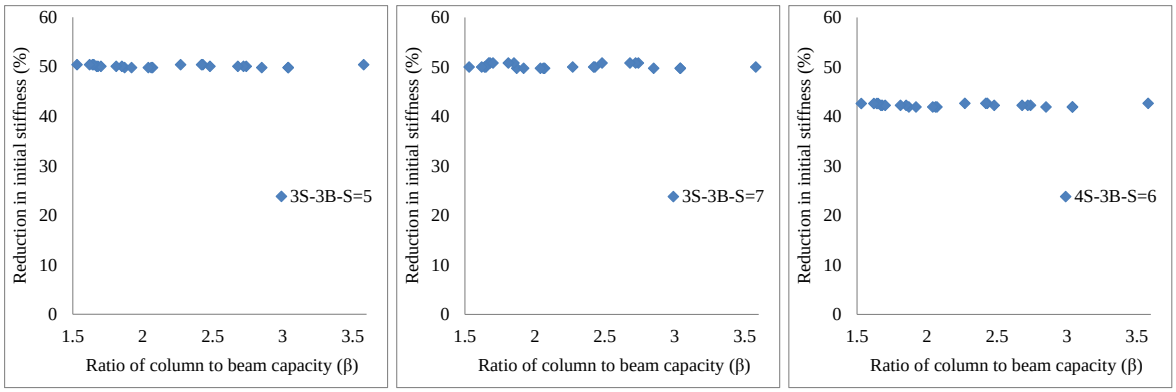

(a) 3 storey frame with 3 bays of 5 m span (b) 3 storey frame with 3 bays of 7 m span (c) 4 storey frame with 3 bays of span 6 m

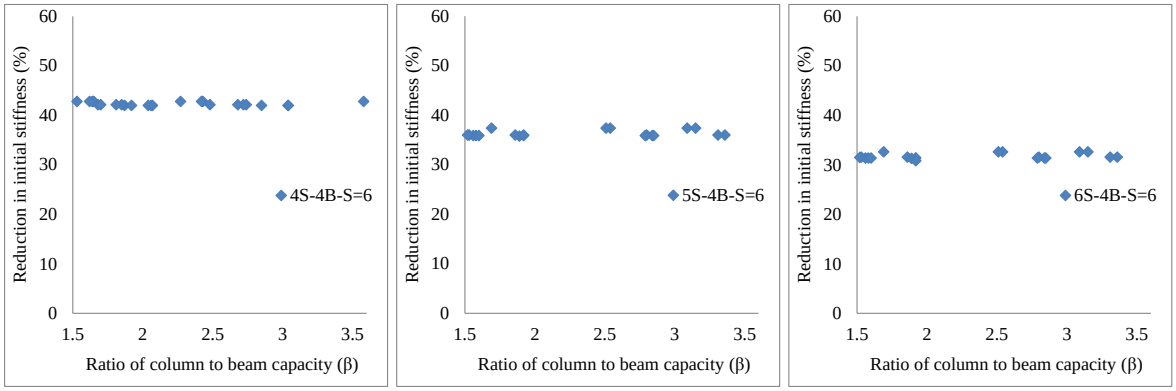

(d) 4 storey frame with 4 bays of span 6 m (e) 5 storey frame with 4 bays of span 6 m (f) 6 storey frame with 4 bays of span 6 m

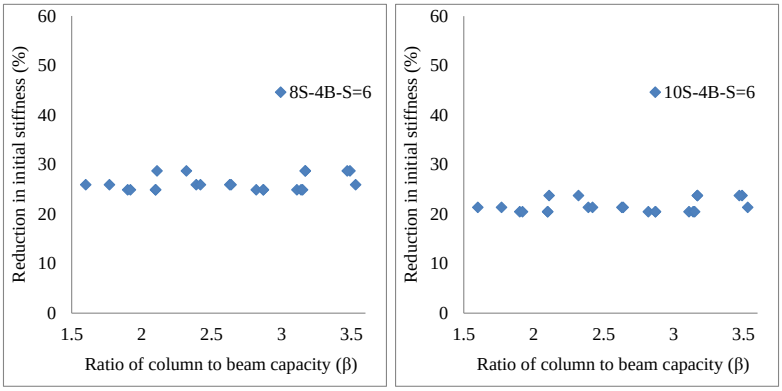

(f) 8 storey frame with 4 bays of span 6 m (f) 8 storey frame with 4 bays of span 6 m

Figure J.8. Variation of reduction of intial lateral stiffness with varying β for each storey

J.4 Reduction in seismic demand due to change of base fixity as function of n_s

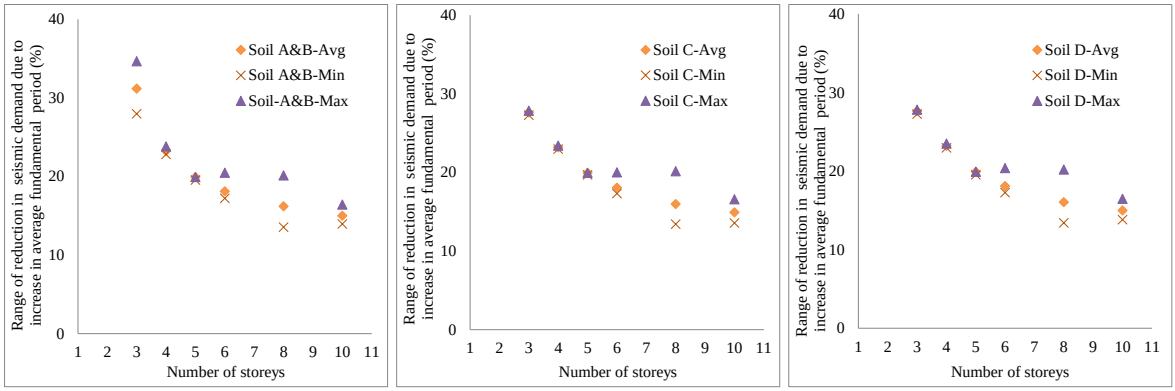

(a) Soil-A and B (b) Soil-C (c) Soil-D

Figure J.9. Maximum, minimum, and average reduciton of demand with varying number of storeys

J.5 Capacity of an unbraced frame with pin bases by increasing rebar percentage

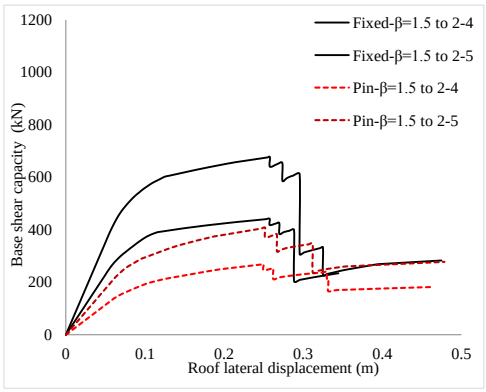

(a) β between 1.5 and 2.0

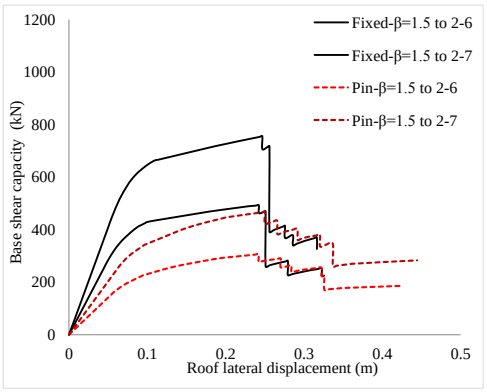

(b) β between 1.5 and 2.0

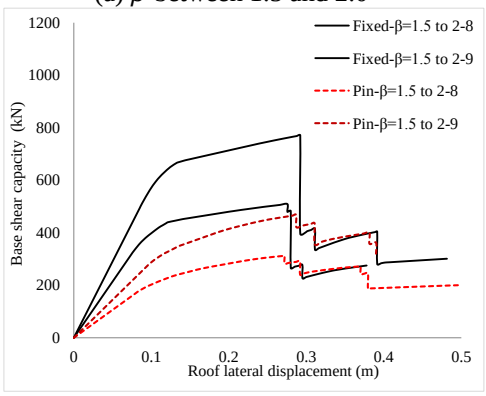

(c) β between 1.5 and 2.0

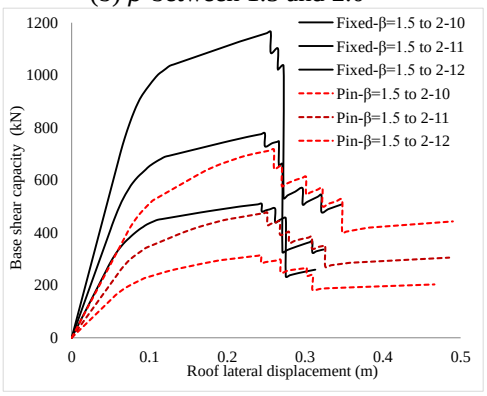

(d) β between 1.5 and 2.0

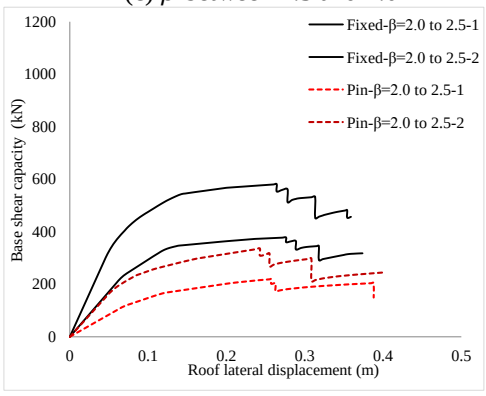

(e) β between 2.5 and 3.0

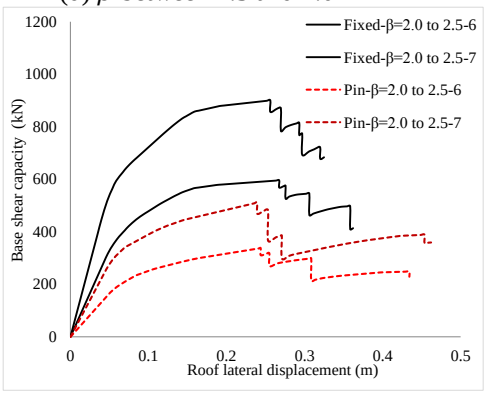

(f) β between 2.5 and 3.0

Figure J.10. Capacity curves of 3 storey frames with same cross sections and varying β

Appendix K:Flow chart explaining the use of proposed equation in design or assessment of a frame building.

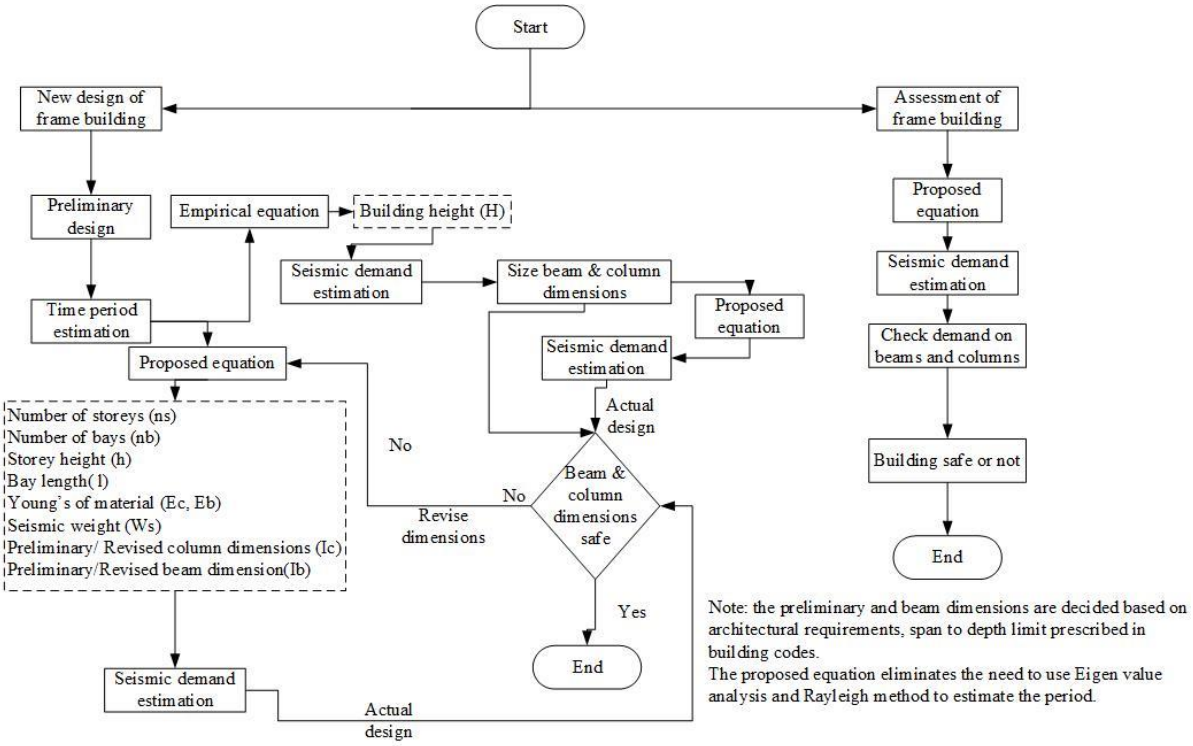

Figure K.1. Flow chart explaining the use of proposed equation in design or assessment of a frame.

Appendix L: Theoretical model to evaluate lateral stiffness with lateral load represented as a discrete function

In this approach (referred as Method 2), the lateral load acting on the equivalent moment and braced frames is represented as a discrete function in a triangular pattern as shown in Figure L.1. To arrive at the top storey lateral displacement the process of derivation is the same as that for method with lateral load represented as a continuous function (i.e. Method 1, refer Chapter 8 for theoretical derivation), hence only important steps are reported. Also, in this method the section properties are assumed to be uniform along the building height. This is because, linear variation of section properties need to be represented as a step function, which creates a singularity for which it is not possible to arrive at a simple closed form solution.

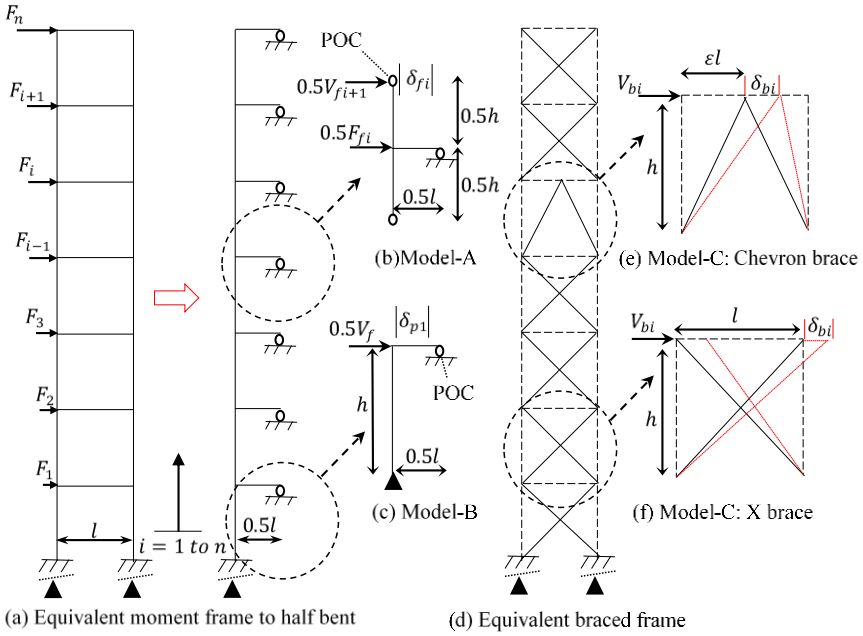

Figure L.1. Analytical model with lateral load represented as discrete function

The lateral force F_i acting at any storey level i from the base of the frame can be expressed in terms of total shear force V as

$$F_i = \frac{2i}{n_s(n_s+1)}V;\ F_{fi} = \frac{2i}{n_s(n_s+1)}V_f; F_{bi} = \frac{2i}{n_s(n_s+1)}V_b \tag{1}$$

where $F_i = F_{fi} + F_{bi}$, F_{fi} and F_{bi} represent the lateral forces acting at any storey level i of the equivalent moment and braced frames, respectively. The shear force at any storey level i from the base of the equivalent moment frame V_{fi} and the braced frame V_{bi} is expressed in terms of total shear force as:

$$V_{fi} = \sum_{i=1}^{n} F_i - \sum_{i=1}^{i-1} F_i \quad (2)$$

$$V_{fi} = \left[1 - \frac{i(i-1)}{n_s(n_s+1)}\right] V_f; V_{bi} = \left[1 - \frac{i(i-1)}{n_s(n_s+1)}\right] V_b \quad (3)$$

L.1 Lateral displacement

The lateral displacement δ_{fi} of the subassembly Model-A shown in Figure L.1b is given in Equation 4.

$$\delta_{fi} = \left(\frac{V_{fi+1}h^3}{12\sum E_c I_c} + \frac{V_{fi+1}h^2 l}{12E_b I_b}\right) + \left(\frac{F_{fi}h^3}{24\sum E_c I_c} + \frac{F_{fi}h^2 l}{24E_b I_b}\right) \quad (4)$$

By substituting the values of F_{fi} from Equation 1 and V_{fi} from Equation 3 in Equation 4 results in:

$$\delta_{fi} = V_f \left[1 - \frac{i(i+1)}{n_s(n_s+1)}\right]\left(\frac{h^3}{12\sum E_c I_c} + \frac{h^2 l}{12E_b I_b}\right) + V_f \frac{2i}{n_s(n_s+1)}\left(\frac{h^3}{24\sum E_c I_c} + \frac{h^2 l}{24E_b I_b}\right) \quad (5)$$

Equation 5 can be further simplified by combining common terms and introducing λ term, which results in Equation 6.

$$\delta_{fi} = \frac{V_f h^3(1+\lambda)}{12\sum E_c I_c}\left[1 - \frac{i^2}{n_s(n_s+1)}\right] \quad (6)$$

For an equivalent moment frame with fixed base, Equation 6 is summed over n_s storeys, which results in the top storey lateral deformation as given by Equation 7.

$$\Delta_{ff} = \frac{V_f h^3(0.67n_s - 0.17)(1+\lambda)}{12\sum E_c I_c} \quad (7)$$

For an equivalent moment frame with pin base, Equation 6 is summed over $n_s - 1$ storeys resulting in cumulative lateral displacement over $n_s - 1$ storeys, which is given as:

$$\Delta_{(fp)(n_s-1)} = \frac{V_f h^3(n_s(n_s+1)(0.67n_s - 1.17)+1)(1+\lambda)}{12n_s(n_s+1)\sum E_c I_c} \quad (8)$$

The lateral displacement δ_{p1} of subassembly Model-B shown in Figure L.1c is given as:

$$\delta_{p1} = \frac{V_f h^3}{12\sum E_c I_c}(4+\lambda) \quad (9)$$

For an equivalent moment frame with pin base, the lateral displacement at the top storey is

obtained by summing Equation 8 and 9, which is given in Equation 10.

$$\Delta_{fp}=\frac{V_f h^3}{12n_s(n_s+1)\sum E_c I_c}((n_s(n_s+1)(0.67n_s-1.17)+1)(1+\lambda)+n_s(n_s+1)(4+\lambda)) \quad (10)$$

The lateral displacement of the sub assembly Model-C of the equivalent braced frame shown in Figures L.1e and L.1f is given by Equation 11.

$$\delta_{bi}=\frac{V_{bi}l_b^3}{2(\varepsilon l)^2\sum A_{br}E_{br}} \quad (11)$$

Substituting the shear force V_{bi} from Equation 3 in Equation 1 results in the lateral displacement in terms of total shear force V_b, which is given in Equation 12.

$$\delta_{bi}=\left[1-\frac{i(i-1)}{n_s(n_s+1)}\right]\frac{V_b\, l_b^3}{2(\varepsilon l)^2\sum A_{br}E_{br}} \quad (12)$$

By summing up Equation 12 over n_s storeys results in the top storey lateral displacement of the equivalent braced frame, which is given in Equation 13.

$$\Delta_b=\frac{V_b l_b^3(0.67n_s+0.33)}{2(\varepsilon l)^2\sum A_{br}E_{br}} \quad (13)$$

L.2 Lateral stiffness

By using lateral displacements given by Equations 7 and 13, the lateral stiffness of a multi bay braced frame with fixed base is given by Equation 14, where $\chi_f=\left[\frac{(n_b+1)}{(0.67n_s-0.17)(1+\lambda)}+\frac{(\varepsilon l)^2\vartheta}{6}\frac{n_r}{(0.67n_s+0.33)}\right]$.

$$K_{f2}=\frac{12E_cI_c\chi_f}{h^3} \quad (14)$$

Similarly, by using Equations 10 and 13, the lateral stiffness of a braced frame with pin base is given by Equation 15.

$$K_{p2}=\frac{12E_cI_c\chi_p}{h^3} \quad (15)$$

where $\chi_p=\left[\frac{(n_b+1)n_s(n_s+1)}{(n_s(n_s+1)(0.67n_s-1.17)+1)(1+\lambda)+n_s(n_s+1)(4+\lambda)}+\frac{(\varepsilon l)^2\vartheta}{6}\frac{n_r}{(0.67n_s+0.33)}\right]$.

L.3 Comparison of predicted lateral stiffness with actual lateral stiffness

The comparison of predicted lateral stiffness by using Methods 1 and 2 with actual lateral stiffness obtained from pushover analysis for braced frames with fixed and pin base is shown in Figure L.2. Although the main objective is to develop a simple method for braced frames, its applicability to unbraced frames is also investigated. Hence, comparison of the predicted lateral stiffness with actual values for unbraced frames with pin base is shown in Figure L.3a, whereas for unbraced frames with fixed base, the results are available in Chapter 7.

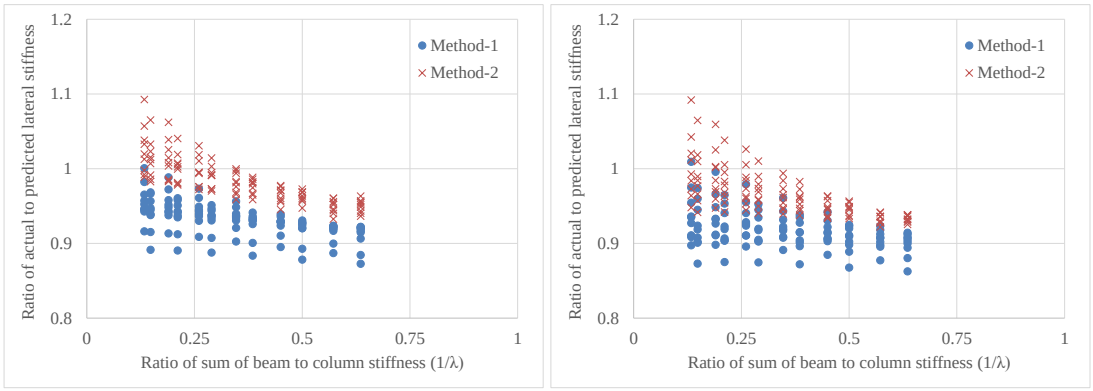

(a) X braced frames with fixed base (b) Chevron braced frames with fixed base

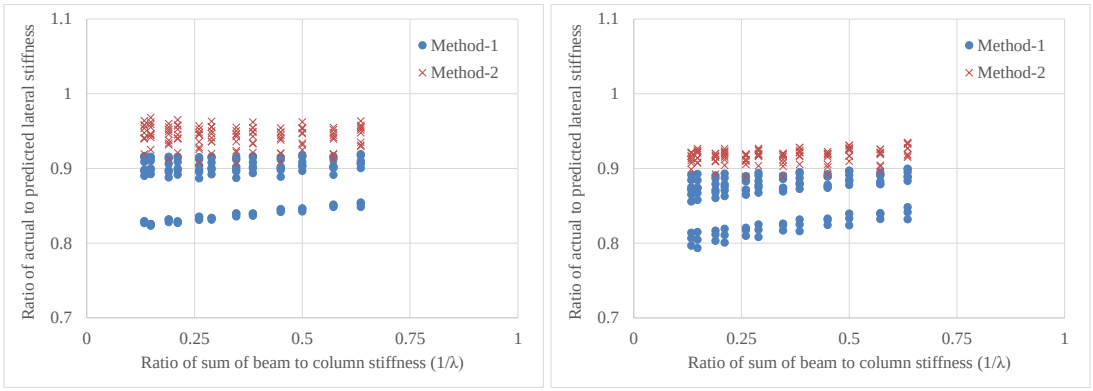

(c) X braced frames with pin base (d) Chevron braced frames with pin base

Figure L.2. Comparison of predicted and actual lateral stiffness for braced frames without correction factor

Even though Methods 1 and 2 differ in representation of lateral load, it is clear from the Figures L.2 and L.3 that both methods predict the lateral stiffness with the same order of accuracy (or error). This is because, the final form of the equation in both methods is very much similar and have similar magnitudes of error in predicting lateral stiffness when compared to the actual lateral stiffness. The range of error in predicting lateral stiffness for braced frames with fixed and pin base is between 10% and 20% depending on the relative stiffness of the column to the beam λ and pseudo relative stiffness of the brace to the column ϑ. Similarly, for unbraced frames with pin base both methods predict lateral stiffness with an error of 15% to 30% depending on the column to beam relative stiffness λ. The

reason for the deviation of predicted lateral stiffness from actual lateral stiffness is because of the assumptions made in the theoretical formulation (as listed in Chapter 8). It is not possible to address the assumptions explicitly as it will not lead to a simple closed form solution. Therefore, a correction factor is sought to neutralize the error in the predicted lateral stiffness. A correction factor Ω is introduced, then the final equation for predicting lateral stiffness in conjunction with the correction factor is given as:

$$K_f = \Omega_f \frac{12E_c I_c \chi_f}{h^3}; K_p = \Omega_p \frac{12E_c I_c \chi_p}{h^3} \tag{16}$$

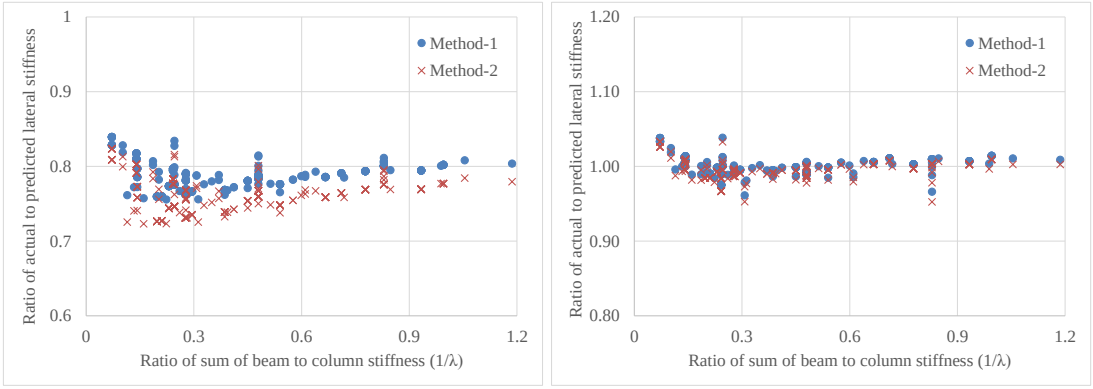

(a) Uncorrected lateral stiffness (b) Corrected lateral stiffness

Figure L.3. Comparison of predicted and actual lateral stiffness for unbraced frames with pin base

The multiple variable regression analysis is carried out to relate the correction factor Ω with the relative stiffness of the column to the beam λ, pseudo relative stiffness of the brace to the column ϑ, and the number of storeys n_s, which is given by Equation 17 for both fixed and pinned bases. The correction factor Ω is obtained by relating the predicted lateral stiffness with the actual lateral stiffness obtained from pushover analysis with load pattern as per New Zealand seismic code [10]. The values of the constants to be used in Equation 17 can be obtained from Table L.1. The values of the constants have been determined for low to medium rise buildings and their application to high rise buildings may not result in realistic lateral stiffness. After incorporating the correction factor Ω in Equation 37, the error in the predicted lateral stiffness greatly reduces and the maximum error becomes less than 10%, which can be observed in Figure L.4 for braced frames with fixed and pin base and in Figure L.3b for unbraced frames with pin base.

$$\Omega_f = A + \frac{B}{\lambda} + C\varepsilon\vartheta + Dn_s; \Omega_p = A + \frac{B}{\lambda} + C\varepsilon^2\vartheta + Dn_s \tag{17}$$

Table L.1. Factor values to correct the lateral stiffness depending on type of frame and base fixity

Frame	Fixity	Method	*A*	*B*	*C*	*D*
Braced	Fixed	1	0.98	-0.08	-0.08	0.00
		2	1.07	-0.15	0.00	-0.006
	Pin	1	0.80	0.00	0.00	0.009
		2	0.90	0.00	0.08	0.00
Unbraced	Fixed [28]	1	1.27	0.30	0.00	-0.027
	Pin	1	0.74	0.03	0.00	0.007
		2	0.70	0.04	0.00	0.01

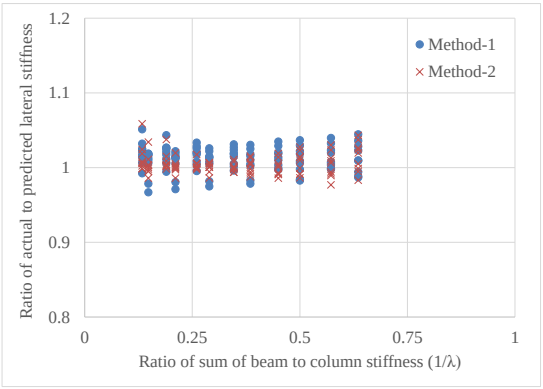

(a) X braced frames with fixed base

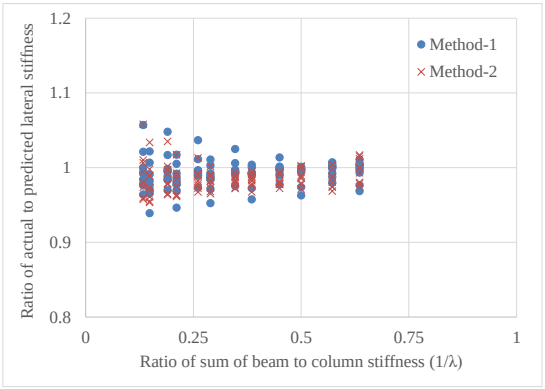

(b) Chevron braced frames with fixed base

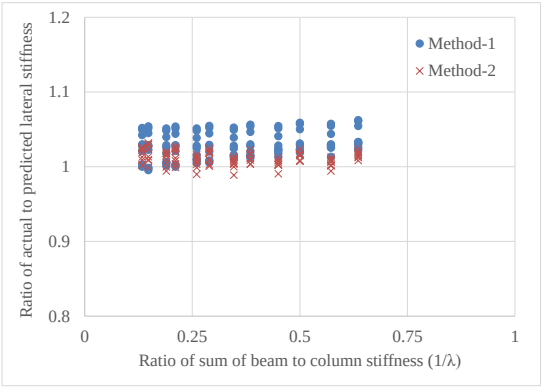

(c) X braced frames with pin base

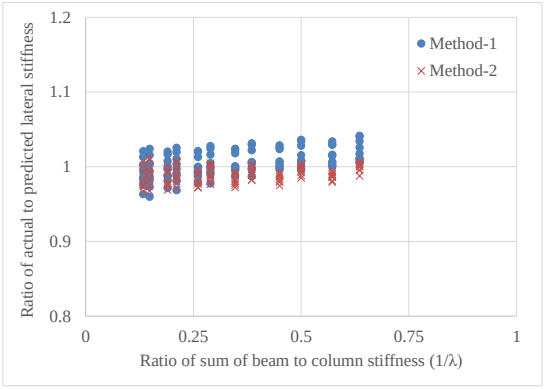

(d) Chevron braced frames with pin base

Figure L.4. Predicted lateral stiffness for braced frames in conjunction with correction factor

L.4 Comparison of predicted fundamental period with actual fundamental period

Comparison of the predicted fundamental periods based on Methods 1 and 2 with actual fundamental periods obtained from Eigenvalue analysis for a wide range of low to medium rise braced frames with fixed and pin base is shown in Figure L.5. The developed equation can also be used for prediction of fundamental period of unbraced frames by setting the second term in χ_f or χ_p to zero. The ratio of actual to predicted fundamental periods for the unbraced frames with pin base is shown in Figure L.6 and the results for the unbraced frames with fixed base are reported in Chapter 7. It is clear that Methods 1 and 2 predict fundamental periods with similar order of error when compared to the actual fundamental periods, as can be seen in Figures L.6 and L.7a. It can be seen that the error in the predicted fundamental

periods for braced frames with fixed and pin bases range between 25% to 10% depending on the relative stiffness of the column to the beam λ and the pseudo relative stiffness of the brace to the column ϑ, whereas for unbraced frames with pin base the error is in between 15% and 5% depending on the relative column to beam stiffness λ. The range of error in prediction of the fundamental period is less than the range of error in prediction of lateral stiffness because the error in lateral stiffness is square rooted when computing the fundamental period.

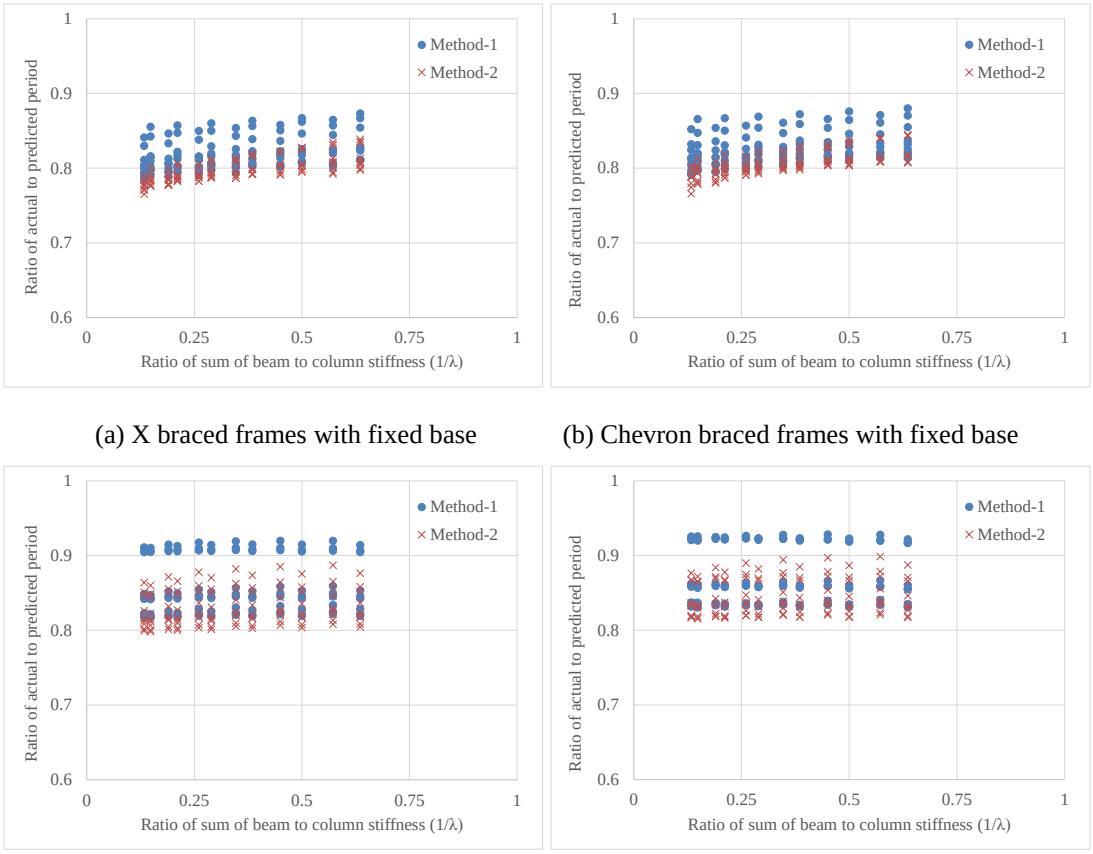

(a) X braced frames with fixed base (b) Chevron braced frames with fixed base

(c) X braced frames with pin base (d) Chevron braced frames with pin base

Figure L.5. Comparison of predicted and actual fundamental period for braced frames

The identified reasons for the remaining error in prediction of fundamental period are; (i) the assumptions used in developing the equation for prediction of lateral stiffness, (ii) the lateral stiffness given by Methods 1 and 2 are based on the top storey lateral displacement, which needs to be modified to obtain the effective stiffness K_{eff} depending on the mode shape corresponding to the fundamental mode of vibration, and (iii) total seismic weight/mass is used instead of effective mass in the first mode of vibration. To neutralize the error, a correction factor φ is introduced to account for both the effective mass and effective stiffness, then the final equation turns into:

$$T_f = 2\pi\varphi_f\sqrt{\frac{W_s h^3}{12 g n_l E_c I_c \chi_f}};\ T_p = 2\pi\varphi_p\sqrt{\frac{W_s h^3}{12 g n_l E_c I_c \chi_p}} \tag{18}$$

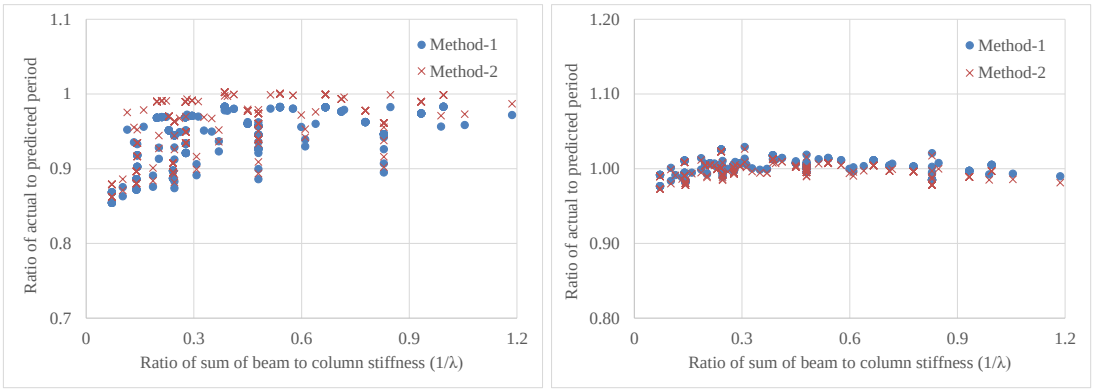

(a) Uncorrected fundamental period (b) Corrected fundamental period

Figure L.6. Comparison of predicted and actual fundamental period for unbraced frames with pin base

A multiple variable regression analysis is carried out to relate the correction factor φ with the relative stiffness of the column to the beam λ, pseudo relative stiffness of the brace to the column ϑ, and the number of storeys n_s, which is given by Equation 19 for both fixed and pinned based frames. The values of the constants to be used in Equation 19 can be obtained from Table L.2. The values of the constants have been determined for low to medium rise buildings and their application to high rise buildings may not result in realistic fundamental period. After incorporating the correction factor in Equation 18, the error in the predicted fundamental period decreases significantly. The maximum error is less than 5%, which can be seen in Figure L.7 for braced frames with fixed and pin bases and in Figure L.6b for unbraced frames with pin base.

$$\varphi_f = A + \frac{B}{\lambda} + C\varepsilon\vartheta + Dn_s;\ \varphi_p = A + \frac{B}{\lambda} + C\varepsilon^2\vartheta + Dn_s \tag{19}$$

Table L.2. Factor values to correct the fundamental period depending on type of frame and base fixity

Frame	Fixity	Method	*A*	*B*	*C*	*D*
Braced	Fixed	1	0.82	0.05	0.04	-0.006
		2	0.79	0.07	0.00	-0.003
	Pin	1	0.95	0.00	-0.03	-0.012
		2	0.90	0.00	-0.05	-0.008
Unbraced	Fixed [28]	1	0.66	0.19	0.00	0.008
	Pin	1	1.00	0.02	0.00	-0.014
		2	1.03	0.02	0.00	-0.016

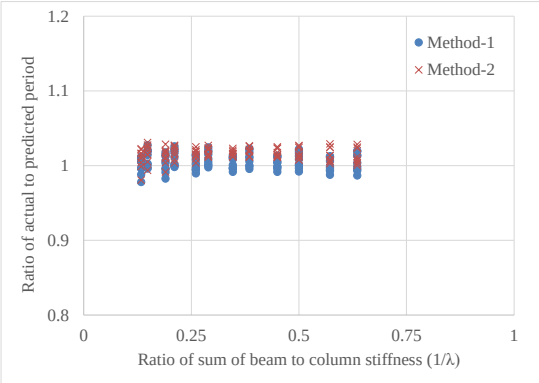

(a) X braced frames with fixed base

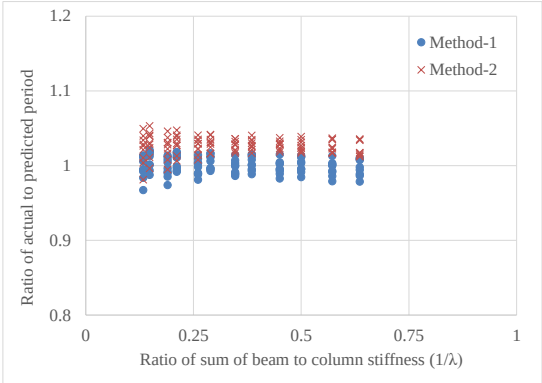

(b) Chevron braced frames with fixed base

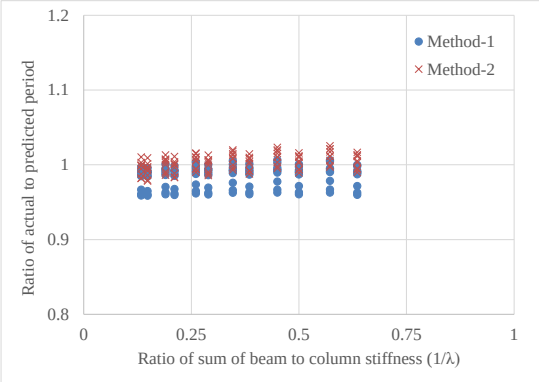

(c) X braced frames with pin base

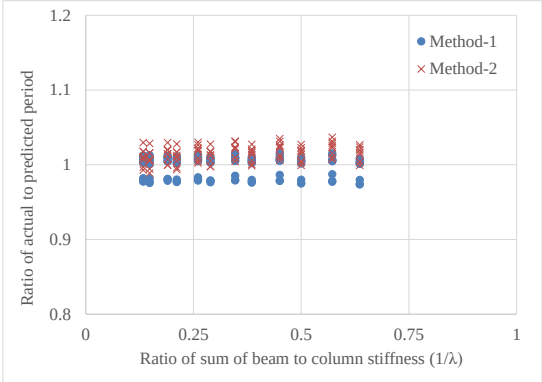

(d) Chevron braced frames with pin base

Figure L.7. Predicted fundamental period of braced frames in conjunction with the correction factor

It is clear from Figures L.5 to L.7 that Methods 1 and 2 predict the lateral stiffness and fundamental period with a similar range of accuracy, but Method 1 (which is reported in Chapter 8) has a distinct advantage over Method 2 as it can be applied to frame buildings with varying section properties and also the form of the equation is relatively simpler. So, Method 1 is recommended for practical use.

Appendix M: Flow chart to calculate the fundamental period of braced frames with fixed and pin bases

The sequence of steps in the application of the proposed method to calculate the fundamental period of a braced frame building with either fixed or pin base is shown below. For the definitions of symbols, refer the paper or Appendix M.

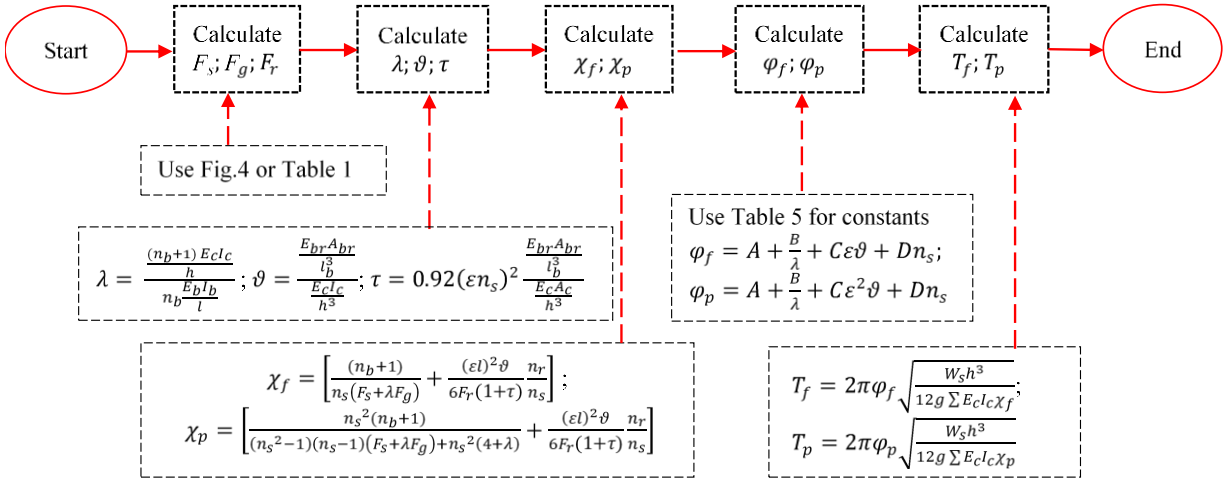

Figure M.1. Flow chart of the fundamental period calculation process

Appendix N: Step by step calculation to arrive at fundamental period

Description: A six storey frame (n_s equal to 6) with five bays (n_b equal to 5) in each direction is used to show the calculation process. Two cases are considered for the demonstration purpose; (i) a reinforced concrete (RC) frame building with X brace and fixed base, (ii) a steel frame with chevron brace and pin base as shown in Figure N.1. Both buildings have a storey height h of 3.6 m and span length l of 6 m. In the two buildings, it is assumed that braces are provided in respectively two and three bays (out of the five bays) only in the two perimeter frames, resulting in n_r equal to 2 and 3. It is assumed that all beam column connections of the RC frame building are rigid, whereas for the steel frame building the perimeter frames have rigid beam column connections and the internal frames are provided with pin beam column connections. The material and cross section properties of the RC and steel frame buildings considered for the demonstration purpose are reported in Table N.1. The step by step calculation for both cases is shown in Table N.2; note the formulas for each step implemented in Table N.2 are given above in Figure N.1. Eigenvalue analyses are also performed for the two example buildings and the analytically obtained natural periods are listed in the last row of Table N.2 for comparison. The subscripts "o" and "i" in Table N.1 and N.2 represent the corresponding variable for the perimeter (outer) and internal frames. It is important to note that in both cases, it is assumed that the effect of axial shortening of columns is neglected (i.e.$\tau = 0$).

Table N.1. Cross sectional and material properties of case study buildings

Building details	**Case 1: RC frame building**	**Case 2: Steel frame building**
Perimeter columns	0.4×0.6 m ($I_{co}\ of\ 7.2 \times 10^{-3}\ m^4$)	310UC158 ($I_{co} = 3.88 \times 10^{-4}\ m^4$)
Perimeter beams	0.4×0.5 m ($I_{bo}\ of\ 4.12 \times 10^{-3}\ m^4$	310UB110 ($I_{bo} = 2.36 \times 10^{-4}\ m^4$)
Internal columns	0.4×0.4 m ($I_{ci}\ of\ 2.13 \times 10^{-3}\ m^4$)	200UC59.5 ($I_{ci} = 6.13 \times 10^{-5}\ m^4$)
Internal beams	0.3×0.4 m ($I_{bi}\ of\ 1.60 \times 10^{-3}\ m^4$)	150UB37.5 ($I_{bi} = 2.22 \times 10^{-5}\ m^4$)
Steel angle brace	102×102×6.4 mm ($A_b = 1.25 \times 10^{-3}\ m^2$)	50×50×8 mm ($A_b = 7.23 \times 10^{-4}\ m^2$)
Brace -E_{br}	200 GPa	200 GPa
Frame- $E_c; E_b$	19.6 GPa	200 GPa
Floor load	5 kN/m^2	5 kN/m^2
Total mass	38275	29208

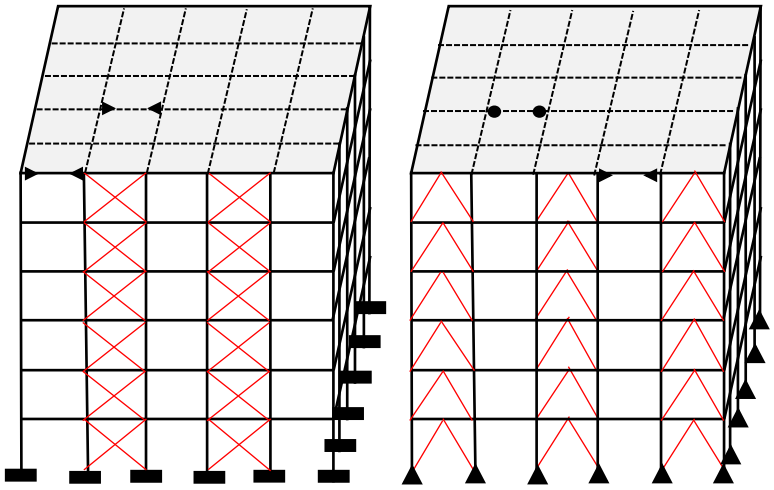

(a) Case 1: RC frame building with X brace (b) Case 2: Steel frame building with chevron brace

Figure N.1. Building frame configurations considered for detailed calculation as examples

Table N.2. Step by step calculation of fundamental period of the two example buildings

Steps	**Case 1**	**Case 2**
Calculation of λ_o; λ_i	$\lambda_o = \frac{\frac{6\times7.2\times10^{-3}}{3.6}}{\frac{5\times4.12\times10^{-3}}{6}} = 3.46;\ \lambda_i = \frac{\frac{6\times2.13\times10^{-3}}{3.6}}{\frac{5\times1.60\times10^{-3}}{6}} = 2.67$	$\lambda_o = \frac{\frac{6\times3.88\times10^{-4}}{3.6}}{\frac{5\times2.36\times10^{-4}}{6}} = 3.29$
Calculation of ϑ	$\frac{\frac{2\times10^{8}\times1.25\times10^{-3}}{7.0^3}}{\frac{1.96\times10^{7}\times7.2\times10^{-3}}{3.6^3}} = 0.24$	$\frac{\frac{7.23\times10^{-4}}{4.68^3}}{\frac{3.88\times10^{-4}}{3.6^3}} = 0.84$
Calculation of χ_o; χ_i	$\chi_o = \frac{6}{6\times0.67\times(1+3.46)} + \frac{6^2\times0.24\times2}{6\times0.67\times6} = 1.06$ $\chi_i = \frac{6}{6\times0.67\times(1+2.67)} = 0.41$	$\chi_o = \frac{6^2\times6}{5^2\times(0.67\times6+0.33)\times(1+3.29)+5^2\times(4+3.29)} + \frac{0.25\times6^2\times0.84\times3}{6\times0.67\times6} = 1.25$
Calculation of φ	$0.82 + \left(\frac{0.05}{3.46}\right) + 0.04\times0.24 - 0.006\times6 = 0.81$	$0.95 - 0.03\times0.25\times0.84 - 0.012\times6 = 0.87$
Calculation of T	$2\times\pi\times0.81\times\sqrt{\frac{38275\times3.6^3}{12\times9.81\times1.96\times10^{7}\times(2\times7.2\times10^{-3}\times1.06+3\times2.13\times10^{-3}\times0.41)}} =$ 1.06 Sec	$2\times\pi\times0.87\times\sqrt{\frac{29209\times3.6^3}{12\times9.81\times2\times10^{8}\times2\times3.88\times10^{-4}\times1.25}} =$ 1.34 Sec
Eigenvalue analysis-T	1.07 Sec	1.36 Sec